**15th International Symposium
on Column Liquid Chromatography
Basel, June 3–7, 1991
Part I**

Period.

JOURNAL OF
CHROMATOGRAPHY
INCLUDING ELECTROPHORESIS AND OTHER SEPARATION METHODS

SYMPOSIUM VOLUMES

JOURNAL OF CHROMATOGRAPHY

Call for nominations for

The 1992 Elsevier Chemometrics Award

This award will be presented for the first time in 1992 at the 5th International Conference on Chemometrics in Analytical Chemistry in Montreal, Canada. The award has been established to stimulate careers of young scientists who have achieved noteworthy accomplishments in Chemometrics.

The award consists of a US$ 2000 cash amount and will be presented at the conference (14-17 July 1992) by the chairman of an international committee of leading scientists in chemometrics.

In the selection procedure the committee will consider the accomplishments of nominees mainly on the basis of one or more scientific publications, but contributions to the field of Chemometrics in another form will be considered as well.

There are no restrictions of nationality, or professional affiliation, but nominees should be younger than 40 years old. Deadline for nominations for the 1992 award is 1 May 1992.

Nominations can be made by sending five copies of a nomination letter and a complete resumé of the nominee to the Committee secretariat:

Dr. Hans Laeven
Elsevier Science Publishers B.V.
P.O.BOX 330
1000 AH Amsterdam
The Netherlands
Fax (+31-20) 5862 459

JOURNAL

of

CHROMATOGRAPHY

INCLUDING ELECTROPHORESIS AND OTHER SEPARATION METHODS

Basel; view of the bridge over the River
Rhine from the Small Town, 1761

SYMPOSIUM VOLUME

15TH INTERNATIONAL SYMPOSIUM
ON
COLUMN LIQUID CHROMATOGRAPHY

PART I

Basel (Switzerland), June 3–7, 1991

Guest Editor

F. ERNI
(Basel)

The proceedings of the *15th International Symposium on Column Liquid Chromatography, Basel, June 3–7, 1991*, are published in two consecutive volumes of the *Journal of Chromatography*: Vols. 592 and 593 (1992). The Foreword to the proceedings only appears in Vol. 592. A combined Author Index to both Vols. 592 and 593 only appears in Vol. 593.

CONTENTS

VIII

****

In articles with more than one author, the name of the author to whom correspondence should be addressed is indicated in the article heading by a 6-pointed asterisk (*).

****

Foreword

The *15th International Symposium on Column Liquid Chromatography* (HPLC '91) was held from June 3 to 7, 1991, in the heart of Europe, Basel, Switzerland. HPLC '91 is the latest symposium in this series, which alternates between Europe and the USA. About 1200 chromatographers from 32 countries worldwide came to Basel to learn about the newest developments in liquid chromatography and related techniques.

HPLC '91 was sponsored by the Swiss Association of Chemists (Schweizer Chemikerverband) and was held in the excellent facilities of the "Convention Center Basel". More than 500 contributions were accepted in 60 lectures and approximately 450 posters. Three discussion sessions and a large exhibition of commercial products showcased the latest trends in techniques and instrumentation. All posters were exhibited for 2 days, and this greatly facilitated an intensive exchange of information and discussions in small groups in the poster and exhibition area.

The symposium showed that of all the separation techniques HPLC is still the most important tool in the hands of the analytical chemist. Highlights from the scientific programme included the application of separation techniques to biotechnology, high-performance capillary electrophoresis as a technique complementary to HPLC, miniaturization by means of capillary systems for high-resolution separations, and innovative approaches from microchip technology.

The symposium showed not only that "small is beautiful" but also that process-scale chromatography is playing an increasing role in production. Other highlights of the symposium were the separation of enantiomers, the use of expert systems for method development, and supercritical fluid chromatography.

Apart from the science, the social programme will be well remembered by all participants. There was an excellent, stimulating atmosphere from the Welcome Party to the Farewell Drink. Everybody will remember the pleasant evenings at the reception in the "Kunstmuseum", the concert, and the Three Countries Evening at the Zoo.

Planning and organizing a huge international symposium such as HPLC '91 could only succeed through the excellent cooperation of the organizing committee, the scientific committee, the permanent scientific committee, and the professional organization of the staff of the convention centre. I would like to thank all members of these committees for their contributions to the success of HPLC '91, and I wish to express my special thanks to the core team of Mariette Hirschi, Doris Abdel'Al and Peter Kiechle, who made HPLC '91 run so smoothly.

Now we are looking forward to the next meeting, HPLC '92, in Baltimore, with Professor Fred Regnier as Chairman. All of us expect HPLC '92 to continue the success of the series of these symposia and to highlight further developments in liquid chromatography.

Basel (Switzerland)   Fritz Erni

Separation techniques for biotechnology in the 1990s

Mark Roman and Phyllis R. Brown*

Department of Chemistry, University of Rhode Island, Kingston, RI 02881 (USA)

ABSTRACT

Scientists are constantly looking for better and cheaper separation techniques to replace or complement the current technology. Over the past few decades, and in particular the last 10 years, new separation techniques or modifications of existing techniques have become available for separating compounds from complex sample matrices. There are many areas, however, where the separation technology is not sufficient to achieve high purity and yield while remaining cost effective. In the area of biotechnology, separation techniques are urgently needed to meet demands for ultra-high purity and yield. Thus, a variety of techniques are being developed to address these needs. Generally, biological compounds for the pharmaceutical and biotechnology industries must be obtained at greater than 99.9% purity (sometimes >99.99%) while maintaining high yield. In any area of chemistry this degree of purity would cause problems; in biotechnology it is even more difficult to achieve because of the complex sample matrices. In addition, the compounds of interest may be very similar to impurities or contaminants in the sample matrix, and the compounds could be denatured (or even destroyed) by certain solvents and/or high temperature. In particular, three areas of biotechnology have presented scientists with problems in separations: cell separations, DNA–RNA separations, and protein–peptide separations. The current technology available and possible future trends in these areas are discussed, and also problems to be solved in the future.

CELL SEPARATIONS

Cell separations are unique and challenging. As cells are living organisms, separation conditions are required which ensure the continued activity and function(s) of the cells. The conditions which may affect the viability of the cell include analysis time, temperature, pH and salt content of the sample solution and the presence of organic solvents.

There are may applications for cell separations. Cells which have been genetically altered by recombinant DNA must be separated from the unaltered host cells in order to propagate the genetically engineered cells and study their behavior. In cancer and AIDS research, the diseased cells must be separated from the healthy cells to investigate the abnormal behavior of the diseased cells. In addition, for treatments such as bone-marrow transplants, the red blood cells from the donor must be purified and transplanted within 2 h of removal. Other applications exist for cell separations, and novel techniques have been developed to separate various types of cells.

Two problems are encoutered with cell separations. First, cells are large and bulky, and have about the same diameter. Therefore, it is difficult to separate them by traditional high-performance liquid chromatography (HPLC) or size-exclusion chromatography (SEC). Second, because the cells must be intact and functioning after they have been separated, neither organic solvents nor extremes in pH can be used in the separation process. Hence the mobile phase must consist of aqueous buffer solutions in a narrow pH range. Nevertheless, several techniques have been developed to address the problem of cell separations [1].

As cells generally have densities ranging from 1.005 to 1.110 g/ml [2], one class of separation techniques takes advantage of different cell densities. These techniques include sedimentation at unit gravity, centrifugation, elutriation and field-flow fractionation separations.

Centrifugation methods are the most common methods of separating cells. In this method, the sedimentation rate of the cell is largely dependent on its size; however, the system will reach equilibrium

when the cell density and the surrounding solution density are the same. Therefore, each cell will migrate to its respective solution density. This technique, in which the cells are allowed to migrate to their respective densities in the density gradient, is called isopycnic centrifugation. Because cell densities are often close to one another, and because of non-uniform density gradients, density isopycnic centrifugation is not a very selective technique and usually can only be used as a preliminary step in cell separations.

Velocity sedimentation at unit gravity works on the same basic principles as centrifugation, but no centrifugal force is applied to the cells. Instead, a constant cell velocity due to gravity is attained for each type of cell depending on the size and density of the cell, in addition to the density and viscosity of the medium. When the force of gravity is balanced by the resistance to movement, constant velocity is reached [3]. Other related techniques, such as centrifugation elutriation [4] and buoyant density centrifugation [5], work on similar principles; all these methods, however, provide enrichment of the cells and not complete purification. Thus, cell separation techniques based on centrifugation or sedimentation are often not adequate to isolate cells of extremely high purity.

Field-flow fractionation (FFF) is another technique used to separate particles based on size [6]. There are many different types of fields which can be utilized in FFF, such as thermal, electric, magnetic and gravitational. When cells are being separated, cross-flow field-flow fractionation (CFFF) is usually used. In this technique, a thin column is sandwiched between two membranes. Solvent molecules can penetrate this membrane but large macromolecules cannot. The cells are transported along the column while a cross-flow acts perpendicular to the column. The cells separate according to their weight, and the separation is governed by their diffusion coefficients. An interesting phenomenon is that zone broadening decreases with increasing retention, hence longer run times are used to achieve adequate resolution. Increasing the amount of time the solute spends in the field prior to initiation of the flow allows the solutes to reach equilibrium in the channel.

Another method developed to complement cell separations based on size and density is the partitioning of the cells between two aqueous polymer solutions [7]. Polyethylene glycol (PEG) has been used as one aqueous polymer and dextran as the other. The upper phase was 5–10% PEG in water and the lower phase was 10–20% dextran in water. In addition, salts, simple sugars and low-molecular-weight compounds which distribute equally between the two phases can be added to optimize the separation. The separation of the cells takes place according to the surface properties of the cells. These properties include surface charge, hydrophobicity and specific receptors. The type and molecular weights of the polymers used can affect the separation, as does pH and the overall composition of the phase system. Because the separation is based on the surface properties of cells, the results obtained are complementary to those of centrifugation; combining the two methods can result in highly selective separations. The main drawbacks of partitioning between two polymer phases are that it is difficult to optimize the separation and sometimes repeated phase separations are necessary to isolate the cells of interest.

A promising technique for cell separation is free-flow electrophoresis (FFE) [8]. This method is used to separate cells on the basis of their surface charge to size ratio. Because each type of cell has a fairly unique surface charge to size ratio, FFE has the potential of being a very selective technique (Fig. 1). As it is a continuous process, potentially large-scale separations can be carried out. The major disadvantage thus far has been that scale-up to the preparative scale is not yet possible owing to the size limitation of the instrument. This limit is imposed by the thermal convection arising from Joule heating of the solution when high voltages and currents are used.

DNA

The separation and purification of deoxyribonucleic acids (DNA), both on an analytical scale and on a preparative scale, is of extreme importance in biotechnology. With the explosive growth in recombinant DNA technology, the massive undertaking of the human genome project and the research being performed on genetic diseases, the need for pure DNA strands (such as recombinant DNA or defective genomic DNA) and accurate DNA sequences
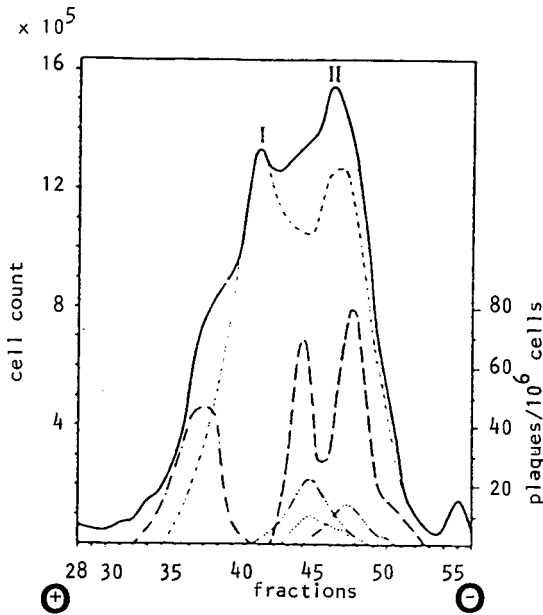
Fig. 1. Electrophoretic separation of lymph node cells. Cell isolation was carried out 82 h after injecting Wistar rat with sheep red blood cells. (—) Cell counts in the various fractions; (- - -) haemolysin-producing cells; (- - -) lymphocytes (I is the T cell region; II is the B cell region); (- - - - -) erythrocytes; (- - - - · · -) plasma cells; (- · · - - · · -) blast cells; (······) plasmocytes. Separation medium, 15 mM triethanolamine–4 mM potassium acetate–240 mM glycine–11 mM glucose, adjusted to pH 7.2 with acetic acid and 310 mOsm with sucrose; conductivity, 900 μmho; Electrode medium, 75 mM triethanolamine–20 mM potassium acetate; voltage gradient, 100 V/cm. From ref. 8.

has increased tremendously over the past few years.

Two types of DNA separations are needed in biotechnology: (1) the separation of whole DNA strands (or large fragments) from the serum matrix, and (2) the analysis of the individual deoxyribonucleotides which make up DNA. Strands of pure DNA, free from foreign DNA and RNA, are needed for the study of recombinant DNA and for gene mapping. The analyses of nucleotides are used in gene sequencing, the study of nucleic acid metabolism and investigations of disease processes.

Separating DNA stands from blood serum is not difficult. A number of chemical precipitation techniques can be used to accomplish this task in high yield and fairly high purity [9]. In the past, serum was deproteinized with undesirable organic solvents such as phenol or chloroform. To avoid the use of these solvents, proteins may be precipitated by

treatment with a saturated NaCl solution, followed by centrifugation at 2500 rpm for 15 min. The proteins precipitate as a pellet at the bottom of the centrifuge tube, leaving the DNA in the supernatant [10]. Another technique utilizes the enzyme proteinase K, which digests protein. When incubated at 65°C, the enzyme digests the proteins and then becomes inactivated after 2 h [11].

Chemical precipitation methods are only useful, however, for bulk precipitation of DNA. The technique cannot be used to precipitate certain DNA strands of interest selectively. The DNA obtained by chemical precipitation must then be further purified if it is to be used in biomedical investigations. For example, several types of DNA may be present in the matrix solution; if the DNA of interest is a recombinant DNA, it may be only a small fraction of the total DNA present. Because DNA molecules are often very large, the separation of different types of DNA is difficult. A recombinant DNA strand may differ from the bulk DNA by only a few nucleotides; thus the two different kinds of DNA possess very similar chemical properties.

Electrophoresis is probably the most common technique for separating DNA on an analytical scale. Gel electrophoresis is commonly used to separate DNA molecules and to determine their size and conformation. Conventional gel electrophoresis on polyacrylamide gels (PAGE) in a static electric field is only suitable for DNA molecules up to 1000 base pairs; however, DNA molecules of very similar sizes can be separated. Very large polynucleotides are not separated easily in gels, because their radius of gyration is often larger than the pore size of the gel [12]. Much larger DNA molecules (up to $3 \cdot 10^7$ base pairs) can be separated on agarose gels, but poorer resolution is obtained [13].

A very active area of research in gel electrophoresis is pulsed-field gel electrophoresis (PFGE). In PFGE, the electric field is alternately applied in different directions, resulting in a two-dimensional separation [14]. This technique extends the size range of the technique to several million base pairs [15]. Variations of this technique exist that differ in the manner in which the alternating electric field is applied; however, all of these techniques work on the same basic principle. The main advantage of these techniques is the high resolution of DNA. The complex instrumentation and long separation times
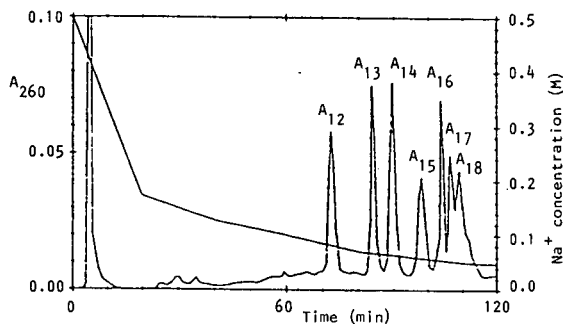
Fig. 2. Separation of oligoadenine mixture by high-performance affinity chromatography. Chromatographic conditions: column, 30 mm × 4.6 mm I.D.; stationary phase, octadecamer of thymidylic acid with primary amino group on the 5′-terminal phosphate group covalently coupled to 300 Å pore macroporous silica; temperature, 35°C. Buffer A, 0.01 M sodium phosphate (pH 6.5)–0.49 M sodium chloride; buffer B, 0.01 M sodium phosphate–0.09 M sodium chloride; buffer C, water. The gradient, shown on the right-hand ordinate, was linear between the following times and percentages: 0 min, 100% A; 20 min, 18% A–82% B; 40 min, 7% A–93% B; 60 min, 100% B; 80 min, 70% B–30% C; 100 min, 60% B–40% C; 140 min, 50% B–50% C. From ref. 17.

are disadvantages. As an analytical tool, PFGE and related techniques work very well. Because of heat dissipation problems in addition to problems with sample recovery from the gel, large-scale separations cannot yet be achieved with this type of system.

Whereas low-pressure open-column affinity chromatography has been used for many years to separate DNA polynucleotides [16], HPLC has rarely been used in the separation of whole DNA molecules because of the large size of DNA. Recent innovations in affinity packings may make high-performance affinity chromatography (HPAC) a very attractive solution for large-scale DNA separations, as it is reported that DNA molecules differing by only one base pair can be separated with good selectivity [17] (Fig. 2).

Nucleotide mapping of DNA molecules is now a vital area of study. Nucleotide mapping involves enzymatic degradation of DNA by either the Sanger method [18] or the Maxam–Gilbert method [19], and then separation and analysis of the individual fragments which are created. The separations can be obtained with two-dimensional PAGE [20] or HPLC [21]. Two-dimensional gel electrophoresis
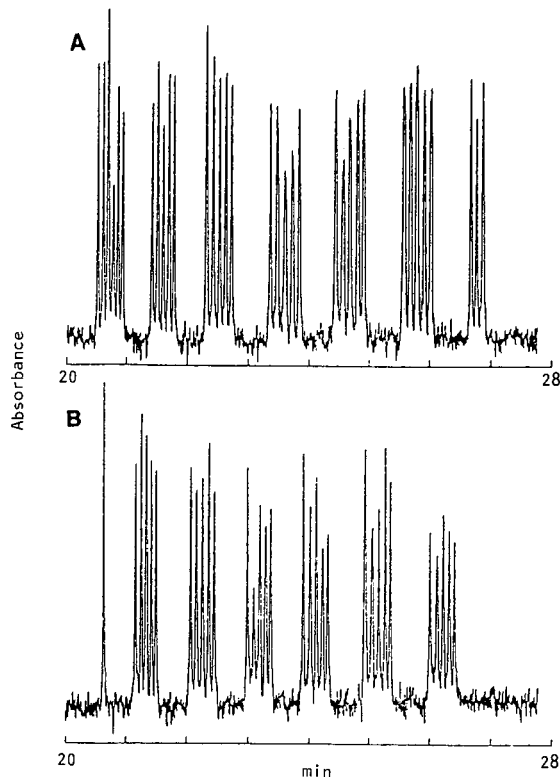
Fig. 3. Electropherogram of chain-termination sequencing reaction products. Template, TEM80.2 = 5′-T₃A₅T₅A₅T₅A₅T₅A₅-T₅A₅T₅A₅T₅ACAACGTCGTGACTGGG-3′. Primer, JOE-PRM18.1 = 5′-JOE-TCCCAGTCACGACGTTGT-3′. (A)dA reaction: primer was extended by Sequenase 2.0 in the presence of ddATP. (B) dT reaction: primer was extended by Sequenase 2.0 in the presence of ddTTP. Sequence reaction and electrophoretic conditions: column, fused-silica capillary packed with polyacrylamide gel, 75 μm I.D., 375 μm O.D., effective length = 540 mm. Injection was performed by dipping the cathodic end of the capillary tube into the sample and applying 10 kV for 10 s. Applied field, 300 V/cm; buffer, 0.1 M Tris–borate–2.5 mM EDTA–7 M urea (pH 7.6); analysis time, 30 min. From ref. 25.

gives a unique fingerprint for each type of DNA, which can then be used in forensic chemistry for positive or negative identification of a suspect. HPLC has also been used for analytical- and preparative-scale separations of nucleotides and nucleosides [22] and of derivatives of these compounds, which are being investigated as possible anti-AIDS drugs [23].

Capillary electrophoresis (CE) is being extensively studied as a method for separating DNA and RNA. The main advantages of CE over HPLC or

gel electrophoresis include its phenomenal resolving power (potentially up to 10^6 plates/m), rapid analysis time and the use of simple buffer solutions as a carrier fluid. CE has been used for the separation of nucleotides, oligonucleotides and polynucleotides with over 10^3 base pairs [24]. Capillary gel electrophoresis coupled with laser-induced fluorescence detection has been used to determine DNA sequence reaction products [25] (Fig. 3). There is currently a great deal of research on separating long-chain DNA and DNA reaction products by CE [26] (Fig. 4). The drawbacks with CE are that it is difficult to detect the extremely small amounts of analytes and that injection techniques are not routinely reliable and reproducible; however, when these problems are overcome, CE will be a valuable analytical research tool in biotechnology.

At present, the best method for the large-scale purification of small DNA molecules is HPLC. In addition, it is a very good analytical technique for nucleotides and oligonucleotides. Oligonucleotides up to 500 base pairs can be readily separated by HPLC. The DNA which is frequently made by synthesis of restriction fragments is usually separated on ion-exchange columns. High throughput is the major advantage of HPLC over capillary and gel electrophoresis. Although HPLC can achieve a similar resolution as electrophoresis of similar DNA fragments, extremely large DNA molecules are difficult to work with in HPLC because they tend to clog the column frits. Nevertheless, at present HPLC is the only method available for high-purity, large-scale separations.
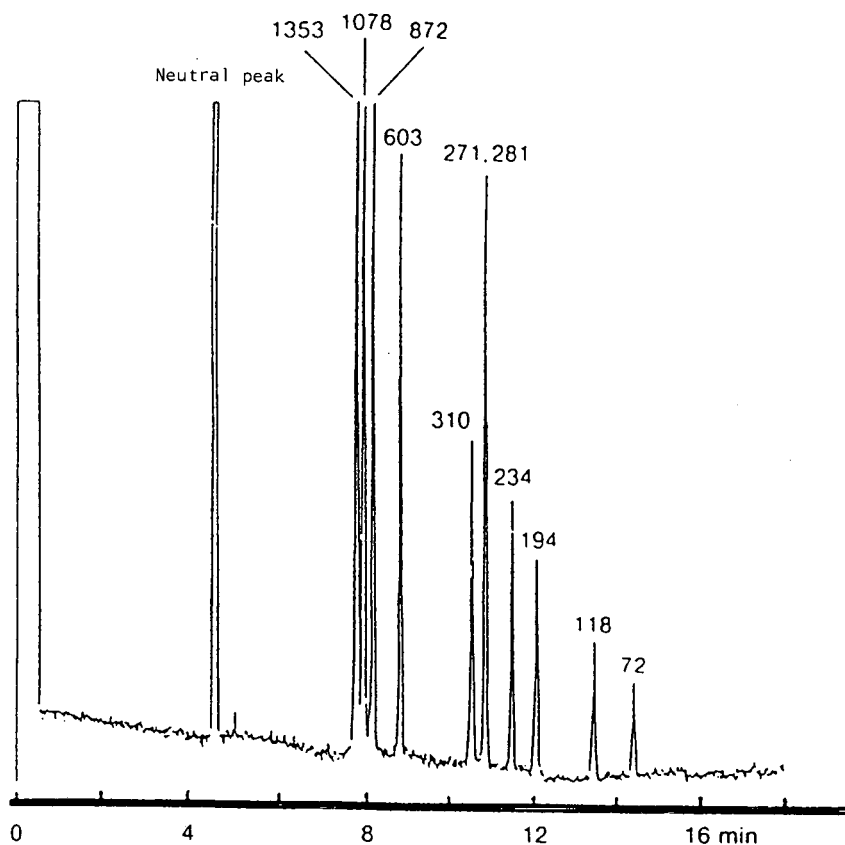
Fig. 4. HPCE (counter-migration) separation of double-stranded DNA fragments (Phi X174/Hae III fragments). Capillary, 42 cm × 50 μm I.D.; effective length, 21 cm; field 140 V/cm; detection, $\lambda = 260$ nm; buffer, Sepragene 500. From ref. 26.

PROTEINS AND PEPTIDES

As with DNA, the separation of proteins and peptides is a challenging problem. Protein–peptide separations also fall into two categories: (1) the separation and purification of entire proteins or peptides for either analytical purposes or for use in biotechnology and (2) the identification of protein–peptide amino acid sequences. Because of the large number of possible protein products, such as interleukins, interferons and antibodies, a great deal of effort has been expended on developing methods

for purifying proteins in high yield [27]. Like DNA, proteins exist in a complex matrix, making high-purity, high-yield separations difficult.

HPLC has been used extensively in protein separations. Several different modes can be used for protein–peptide separations. Traditionally, SEC and ion-exchange chromatography (IEC) have been used, often in sequence. Thus, the proteins can be separated first according to size by SEC and then according to ionic species by IEC. A new size-exclusion technique based on the use of aligned fibers made of porous silica has been developed for work
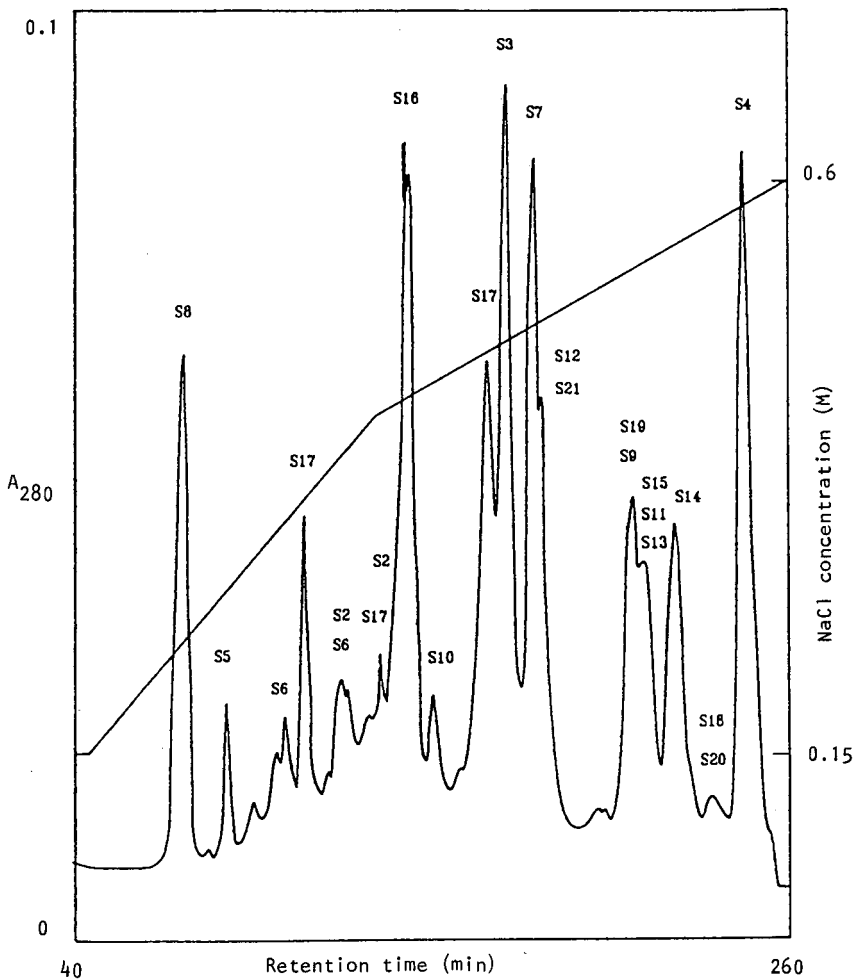
Fig. 5. HPIEC on LKB Ultropac TSK CM-3SW (150 × 7.5 mm I.D.) of TP30 under non-denaturing conditions. 50–200 μg of TP30 in 5–10 ml of 0.05 M ammonium acetate (buffer A)–0.15 M NaCl were applied to the column. Following a 30-min equilibration time with buffer A–0.15 M NaCl, gradients were applied from 0.15 to 0.4 M NaCl over 30 min and from 0.4 to 0.6 M over 140 min. Note that the absorbance scale was changed to 0.2 a.u.f.s. after 145 min (elution time of S16). From ref. 30.

with proteins and polymers [28]. This technique could increase the efficiency of size separations. Although SEC–IEC often requires multiple separations, good separations can be achieved in a single experiment with new higher performance (HP) high-pressure ion-exchange columns [29]. Because the conditions of HPIEC may denature the proteins, ion-exchange separations under non-denaturing conditions utilizing salt gradients have been developed [30] (Fig. 5). The disadvantages of this technique are that a prefractionation step is needed to separate a large number of proteins and the run times are very long, sometimes over 4 h.

Affinity chromatography, reversed-phase chromatography (RP-HPLC) and hydrophobic-interaction chromatography (HIC) are gaining popularity in protein separations. In affinity chromatography, a ligand which binds strongly but selectively to a certain protein (or group of proteins) is covalently attached to the solid support in the column. The sample is then passed through the column with buffer as the mobile phase. Only those proteins which selectively bind to the ligands will be retained on the column. All other components are washed off the column with the mobile phase. After all unwanted components have been removed, the column is treated with another solution (often a salt or acidic solution), which then releases the desired protein from the stationary phase and elutes it [27]. These columns are expensive, but the purity of the desired protein is usually ⩾99.99% after dialysis has been used to remove the buffer salts. Unfortunately, if the concentration of the protein of interest is low, as is usually the case, the solution must be passed through the column several times for high adsorption efficiency, making affinity chromatography very time consuming. A method in which the analyte is adsorbed in a batch mode in a slurry tank and eluted through a fixed-bed column has been developed which greatly reduces the time for a complete separation [31].

In RP-HPLC the separations are based on the hydrophobic character of proteins [32]. Selective separations are possible, but sometimes no separation will occur if the hydrophobic areas of the proteins are not accessible to the stationary phase. In addition, denaturation of proteins can occur if there is too much organic modifier in the stationary phase or as a result of the interaction of proteins with the stationary phase. Therefore, both the stationary phase and the mobile phase must be carefully selected and controlled to ensure good separation, purification and maintenance of biological activity of the proteins. The proteins must be soluble in the mobile phase; as a result, the mobile phase is usually a water–acetonitrile gradient.

HIC is similar to RP-HPLC in that both utilize differences in the hydrophobic nature of the solutes to achieve separation. Whereas the stationary phase is usually dense and very hydrophobic in RP-HPLC, HIC utilizes less dense, less hydrophobic stationary phases so that the adsorption of proteins to the stationary phase is more gentle. The mobile phase is an aqueous solution, usually of high ionic strength at the beginning and gradually decreasing in the applied gradient, and very little if any organic modifier is used. Therefore, denaturation due to stationary phase and mobile phase interactions is minimized, while the mode of retention is essentially the same. PEG-bonded stationary phases are now available which preserve the full biological activity of proteins while yielding a mass recovery of >90% for some proteins [33].
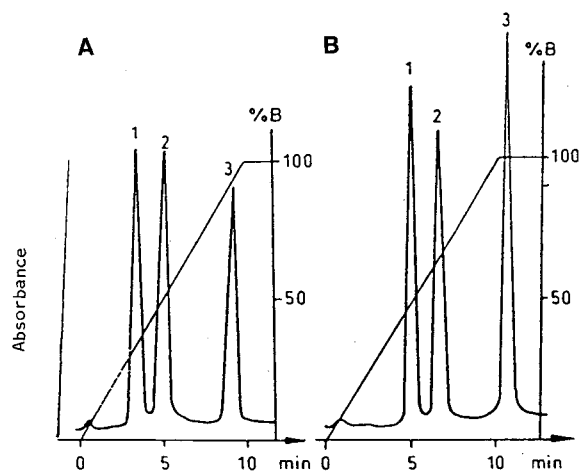
Fig. 6. Protein separation by HPLC on short capillary columns. (1) Trypsinogen, (2) chymotrypsinogen and (3) lysozyme separated by means of microcolumn cation-exchange HPLC. Column, 150 × 9.5 mm I.D.; flow rate, 10 μl/min. (A) Mono S sorbent (Pharmacia); (B) sorbent MPG-350 polyol-sulfopropyl (Lenchrom, USSR). Sample mass, 10 ng of each protein; detection, fluorescence (excitation wavelength 230 nm, emission wavelength 375 nm). From ref. 34.

Capillary HPLC columns have been developed for protein analyses where the proteins of interest are present in very low concentrations (<10 ng/ml). These columns are made of PTFE and have an inner diameter of 500 μm. In addition to the ability to separate and detect much lower concentrations of proteins, separations on these columns require considerably less solvent than standard 4.6 mm I.D. columns. These columns can be used in the ion-exchange, RP-HPLC or HIC mode [34] (Fig. 6). The use of fast atom bombardment mass spectrometry (FAB-MS) for detection in capillary HPLC could prove to be a very powerful technique for protein and peptide analyses [35]. With conventional HPLC columns, time-of-flight mass spectrometry (TOF-MS) is a useful detection method [36].

Both gel and capillary electrophoresis are used for analytical-scale separations of proteins and for protein mapping. The methods utilized are very similar to electrophoretic separations of DNA–RNA; in fact, proteins have been analysed simultaneously with DNA–RNA [37]. CE is rapidly gaining popularity in protein separations because of its speed and resolving power. In addition, CE is much less labor intensive than gel electrophoresis [38]. Mass spectrometry has been coupled to CE for the analysis of proteins and peptides, resulting in an extremely powerful analytical technique. This technique (CE–MS) can provide not only quantitation of amino acids after enzymatic digestion, but also on-line peptide sequencing [35,39] (Fig. 7). FFE, which is a continuous process, has potential for preparative-scale separations of proteins. A major problem in FFE is the conductive heating which prevents scale-up of the technique. On a small scale, in which the bed thickness is between 0.5 and 2 mm, FFE has been used to separate proteins continuously [40]. Hoffstetter-Kuhn and Wagner [41] have achieved a sample throughput of 2.75 g/h of crude yeast extract protein and a 4.7-fold purification of alcohol dehydrogenase from crude protein by FFE (Fig. 8).

Immunoglobulins

Immunoglubulins are a special class of proteins which are of extreme importance in biotechnology. Five classes of immunoglobulin antibodies are produced by the body. Immunoglobulin G (IgG) is the most abundant of all immunoglobulins; it has mo-
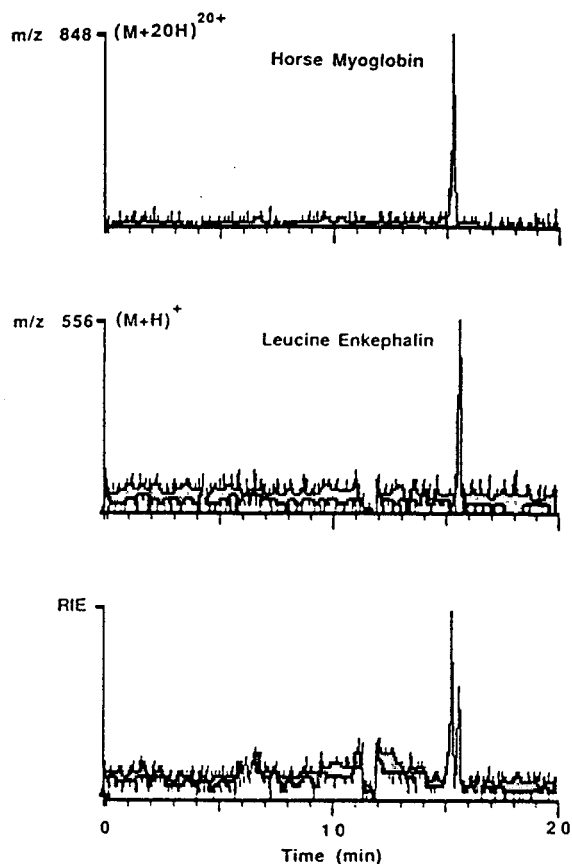
Fig. 7. CZE–ESI-MS separation–detection of horse myoglobin and leucine enkephalin (Tyr–Gly–Gly–Phe–Leu) in a 125 cm × 50 μm I.D. fused-silica capillary at 30 kV (17 μA). Buffer, 20 mM Tris solution adjusted to pH 8.25 with HCl–KCl solution. Electromigration injection for 10 s at 15 kV. From ref. 39.

lecular weight of about 150 000 dalton. Immunoglobulins are composed of four chains. Two chains are heavy chains (called "H" chains) and two are light chains (called "L" chains). These four chains, which are held together by –S–S– bridges, comprise three different areas or domains on the antibody: two antigen-binding sites and one non-antigen-binding site is called the Fc part. Enzymatic cleavage and fractionation of immunoglobulin into its three separate domains does not deactivate the binding sites but greatly reduces the ability of the antibody to remove foreign antigens [42].

As immunoglobulins are being extensively studied as possible cancer therapeutic agents, good separation and purification techniques are urgently
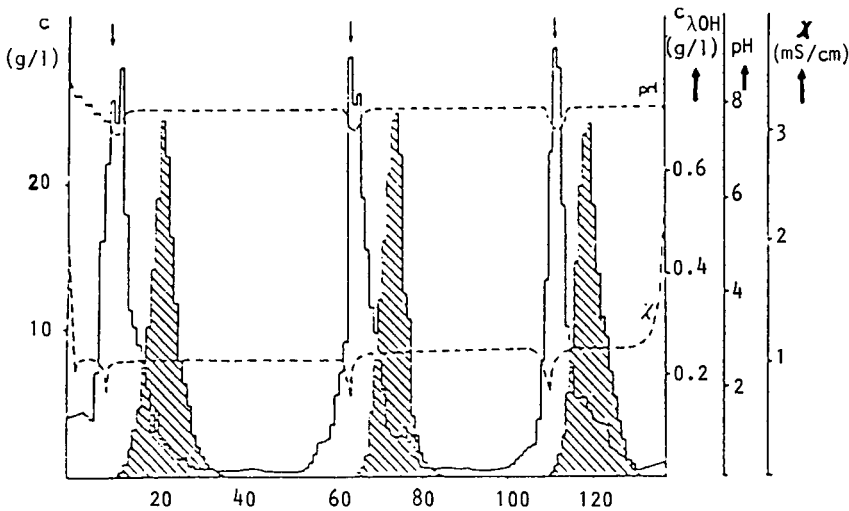
Fig. 8. Free-flow zone electrophoresis of yeast extract with a simultaneous threefold sample dosing in 0.02 M Tris, adjusted to pH 8.0 with HCl. Sample dialyzed yeast extract, containing 45.8 g/l of total protein and 1.53 g/l of ADH. Conditions 1000 V; residence time, 5 min; sample flow-rate, 20 ml/h; electrode solution, 0.2 M Tris, adjusted to pH 8.0 with HCl; electrophoretic apparatus, ElphorVap 22 (Bender and Hobein), 100 cm length × 15 cm width × 1 mm thick. From ref. 41.

needed to obtain extremely pure (>99.99%) products. It has been estimated that between 40% and 90% of the overall cost of processing immunoglobulins is in the separation and purification steps [43].

The most common method of purification of immunoglobulins is by precipitation with ammonium sulfate, followed by anion-exchange chromatography on a DEAE-cellulose column [44]. This procedure results in an IgG purity of >90%; to achieve higher purity, a high-performance ion-exchange column must be used. In either case, at least two steps are necessary to achieve the purification of IgG. A third method of purification involves coupling RP-HPLC with anion-exchange chromatography, further purifying the IgG, but adding another step to the purification process [40].

In a non-chromatographic technique, albumin and other serum proteins were precipitated by octanoic acid, leaving IgG in the solution. IgG was then precipitated by addition of ammonium sulfate. About 80% of rabbit serum IgG was recovered by this method, in high purity (comparable to that obtained by anion-exchange chromatography) and at low cost. Increased purity was obtained by repeating both steps, but the IgG yield was decreased to about 50% [45].

One of the most promising methods of IgG sep-
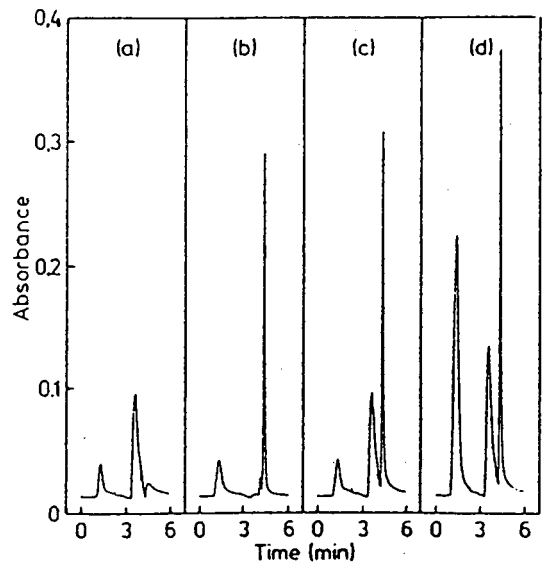
Fig. 9. Dual-column determination of human serum albumin (HSA) and immunoglobulin G (IgG) in serum by high-performance affinity chromatography. (a) HSA; (b) IgG; (c) HSA plus IgG; (d) normal serum in the dual-column system. Chromatographic conditions: column 1 protein A column (protein A coupled diol-bonded LiChrospher Si-500), 6.4 mm × 4.1 mm ID; column 2, anti-HSA column (anti-HSA antiserum coupled to LiChrospher Si-4000), 12.8 mm × 4.6 mm I.D. Sequence of events: 0 min, switch from pH 3.0 phosphate buffer to pH 7.0 phosphate buffer; 0.50 min, sample injection; 2.25 min, protein A column switched off-line, switch to pH 3 buffer; 4.00 min, protein A column switched on-line. From ref. 46.

aration is HPAC. Hage and Walters [46] separated albumin and IgG simultaneously from serum by using dual columns (Fig. 9). One column contained albumin-specific antibodies, immobilized on the stationary phase, and the other column contained IgG-specific protein A. This technique has been used for the determination of IgG and albumin, and it is widely used for preparative and semi-preparative purifications.

A new technique geared towards large-scale purification is affinity cross-flow filtration (ACFF). This technique combines aspects of biospecific adsorption with cross-flow filtration. The antibody of interest is reversibly bound to an adsorbent coated with antigen "ligands". When the antibody is bound to the adsorbent, the molecular size is greatly increased, making separation by filtration possible. Washing with buffer removes the antibody from the adsorbent. A drawback to this technique is the low recovery of IgG (about 50%) [44].

Gel electrophoresis has been used a great deal for the qualitative determination of IgG. A method of continuous free-film electrophoresis has been developed which can overcome the problems of heat dissipation associated with the scale-up of electrophoresis. Its major disadvantage is that it introduces a 40-fold dilution into the fractionation [47].

REFERENCES

1 K. Shortman, *Annu. Rev. Biophys. Bioeng.*, 1 (1972) 93.
2 T. G. Pretlow and T. P. Pretlow, *Methods Enzymol.*, 171 (1989) 462.
3 T. G. Pretlow and T. P. Pretlow (Editors), Cell Separation: Methods and Selected Applications, Vol. 1, Academic Press, San Diego, CA, 1982, p. 41.
4 M. J. Sanders and A. H. Soll, *Methods Enzymol.*, 171 (1989) 482.
5 J. Wells, *Methods Enzymol.*, 171 (1989) 497.
6 H. M. Widmer and L. Koch-Kellner, *Chimia*, 43 (1989) 388.
7 P. Albertsson, *Methods Enzymol.*, 171 (1989) 532.
8 H. G. Heiddrich and K. Hannig, *Methods Enzymol.*, 171 (1989) 513.
9 J. K. Karlinset, G. Stamatoyannopoulos and T. Enver, *Anal. Biochem.*, 180 (1989) 303.
10 S. A. Miller, D. D. Dykes and H. F. Polesky, *Nucleic Acid Res.*, 16 (1988) 1215.
11 J. Grimberg, S. Nawoschik, L. Belluscio, A. Turck and A. Eisenberg, *Nucleic Acid Res.*, 17 (1989) 8390.
12 J. Noolandi, *Makromol. Chem., Rapid Commun.*, 10 (1989) 207.
13 S. Tas, *Anal. Biochem.*, 188 (1990) 33.
14 M. V. Olson, *J. Chromatogr.*, 470 (1989) 377.
15 R. W. Whitcomb and G. Holzwarth, *Nucleic Acids Res.*, 18 (1990) 6331.
16 P. T. Gilham, *J. Am. Chem. Soc.*, 86 (1964) 4982.
17 T. A. Goss, M. Bard and H. W. Jarret, *J. Chromatogr.*, 508 (1990) 279.
18 F. Sanger, S. Nicklen and A. R. Coulson, *Proc. Natl. Acad. Sci. U.S.A.*, 74 (1977) 5463.
19 A. M. Maxam and W. Gilbert, *Proc. Natl. Acad. Sci. U.S.A.*, 74 (1977) 560.
20 B. W. Birren, M. I. Simon and E. Lai, *Nucleic Acids Res.*, 18 (1990) 1481.
21 P. R. Brown (Editor), *HPLC in Nucleic Acid Research*, Marcel Dekker, New York, 1984.
22 R. A. Hartwick and P. R. Brown, *J. Chromatogr.*, 126 (1976) 679.
23 J. G. Turcotte, P. E. Pivarnik, S. S. Shirali, H. K. Singh, R. K. Sehgal, P. Macbride, N.-I. Jang and P. R. Brown, *J. Chromatogr.*, 499 (1990) 55.
24 V. Dolnik, J. Liu, J. F. Banks and M. V. Novotny, *J. Chromatogr.*, 480 (1989) 321.
25 A.S. Cohen, D. R. Najarian and B. L. Karger, *J. Chromatogr.*, 516 (1990) 49.
26 Y. Baba, M. Tsuhako, S. Enomoto, A. M. Chin and R. S. Dubrow, *J. High Resolut. Chromatogr.*, 14 (1991) 204.
27 L. A. Haff, *Chromatography*, March (1987) 25.
28 M. Czok and G. Guiochon, *J. Chromatogr.*, 506 (1990) 303.
29 A. M. Tsai and D. Englert, *J. Chromatogr.*, 504 (1990) 89.
30 C. Cachia, P.-J. Flamion and J.-P. Schreiber, *J. Chromatogr.*, 539 (1991) 343.
31 B. Yang, M. Goto and S. Goto, *J. Chem. Eng. Jpn.*, 22 (1989) 532.
32 B. L. Karger, F. E. Regnier and T. C. Wehr (Editors), *High Performance Liquid Chromatography of Proteins and Peptides*, Academic Press, New York, 1983.
33 N. Cooke, P. Shieh and N. Miller, *LC · GC*, 7 (1989) 954.
34 V. G. Mal'tsev, D. G. Nasledov, S. A. Trushin, T. B. Tennikova, L. V. Vinogradova, I. N. Volokitina and V. N. Zgonnik, *J. High Resolut. Chromatogr.*, 13 (1990) 185.
35 M. A. Moseley, L. J. Deterding, K. B. Tomer and J. W. Jorgenson, *J. Chromatogr.*, 480 (1989) 197.
36 R. C. Simpson, W. B. Emary, I. Lys, R. J. Cotter and C. C. Fenselau, *J. Chromatogr.*, 536 (1991) 143.
37 R. G. Hatch, *J. Chromatogr. Sci.*, 28 (1990) 210.
38 F.-T. Chen, C.-M. Liu, Y.-Z. Hsieh and J. C. Sternberg, *Clin. Chem.*, 37 (1991) 14.
39 R. D. Smith, J. A. Loo, C. J. Barinaga, C. G. Edmonds and H. R. Udseth, *J. Chromatogr.*, 480 (1989) 211.
40 J. Chmelík, M. Deml and J. Janca, *Anal. Chem.*, 61 (1989) 914.
41 S. Hoffstetter-Kuhn and H. Wagner, *Electrophoresis*, 11 (1990) 451.
42 L. Stryer, *Biochemistry*, W. H. Freeman & Co., New York, 1981, Ch. 33.
43 D. C. Herak and E. W. Merrill, *Biotechnol. Prog.*, 6 (1990) 33.
44 F. E. Regnier, *LC · GC*, 5 (1987) 962.
45 M. McKinney and A. Parkinson, *J. Immunol. Methods*, 96 (1987) 271.
46 D. S. Hage and R. R. Walters, *J. Chromatogr.*, 386 (1987) 37.
47 D. E. Austen, T. Cartwright and C. H. Dickerson, *Vox Sang.*, 44 (1983) 151.

CHROMSYMP. 2442

Increasing data precision in reversed-phase liquid chromatography leads to new information level

U. Dreyer, H. Melzer and H. J. Möckel*

Hahn-Meitner Institut Berlin GmbH, Abteilung S 3, Glienicker Strasse 100, W-1000 Berlin 39 (Germany)

ABSTRACT

Reversed-phase liquid chromatographic systems as commonly used yield retention time data at a precision and reproducibility level of 0.05 to, at best, 0.01 standard deviation units within a set of several (typically 5–10) runs. This corresponds to a time resolution of some hundredths to some tenths of a minute. Improving the apparatus can reduce the data standard deviation to 0.001. At this precision level, several effects usually hidden in the data scatter band become clearly visible. This is demonstrated for the column dead volume determination via the $t(n+1)/t(n)$ method using n-alkane solutes in a octadecylsilane–methanol system. Whereas standard precision data yield erratically scattering results, improved precision data show an apparently linear decrease in the effective dead volume with increasing solute size. This observation can be explained by steric exclusion effects, which seem to have a far greater influence on retention data than is commonly assumed.

INTRODUCTION

The number of studies on the determination of kinetic and thermodynamic parameters from reversed-phase liquid chromatographic retention data is increasing continuously. The determination of partition coefficients, similar to the octanol–water partition coefficient or other solvophobicity parameters, is only one example. The desired information cannot be taken directly from the primary chromatographic results but must be calculated from the gross retention values. A prerequisite for this calculation is the column dead volume, V_m.

The determination and definition of the column dead volume are the subject of incessant discussion, manifested in more than 100 publications [1,2]. Our point of view is that V_m is the volume that is accessible to non-sorbed and partly excluded solutes during a chromatographic run [3]. The determination according to the method of Berendsen *et al.* [4] is the most effective and yields results with the highest precision if based on high-quality retention data. Insufficient comparability and reproducibility of kinetic and thermodynamic data found in the litera-

ture seem often to be based on two factors: first, the level of data precision is low, and second, the size-exclusion effect of solutes of normal size is not taken into account. The intention of this paper is to show that the first factor influences reproducibility and comparability to a high degree.

EXPERIMENTAL

The influence of the quality of the high-performance liquid chromatographic (HPLC) apparatus used on the level of data precision is shown by comparing the results from two different experimental set-ups.

Standard precision apparatus

The apparatus consisted of a Varian Model 5000 pump (flow-rate 1 ml/min), a Waters Rad PAK 10-μm C_{18} cartridge in a non-thermostated RCM 100 compression module, an air-driven Rheodyne Model 7010 six-port valve, a Melz LCD 201 refractive index detector and a Trio integrator (retention time in minutes to 2 decimals places). Methanol was used as the eluent and was not degassed. The Rheo-

dyne valve and integrator were switched simulaneously. The extra-column dead volume, V_{extra}, of the apparatus was 150 μl.

Improved precision apparatus

The higher precision apparatus consisted of a Knauer C64 pump, an empty column (250 × 4.6 mm I.D.) connected via a T-fitting as a pulse damper, a helium-driven piloted Valco C6W valve (switching time <20 ms) [5], a Nucleosil 5-μm C_{18} column (250 × 4.6 mm I.D.) from Macherey-Nagel, which was thermostated in a water-bath (35 ± 0.03°C), a Melz LCD 201 refractive index detector and a Nelson Model 960 analogue-to-digital converter (ADC) operated with the Nelson software on a Melchers CMC 2000E computer (retention time in minutes to 3 decimal places). Methanol was used as the eluent and was degassed with helium and prewarmed in the water-bath before flowing through the column. Valve switching and the ADC start were controlled electronically. V_{extra} of the apparatus was 60 μl.

RESULTS AND DISCUSSION

The dead-volume calculation was performed according to the method of Berendsen *et al.* [4]. This method is based on the assumption that selectivity

(α) between neighbouring members of a homologous series is constant (k' = capacity factor):

$$\alpha = k'(n+1)/k'(n) = \text{constant} \tag{1}$$

Transformation of eqn. 1 yields

$$V_{ms}(n+1) = \alpha V_{ms}(n) + (1-\alpha)V_m \tag{2}$$

which yields V_m from the intercept $(1-\alpha)V_m$ and slope α of a linear regression of $V_{ms}(n+1)$ against $V_{ms}(n)$.

The dead-volume calculation was performed in two ways. First, it was done for the whole set of C_5 to C_{17}. The mean column dead volume found for the Rad PAK cartridge is $V_{m,av.} = 2.487$ ml and for the Nucleosil C_{18} column $V_{m,av.} = 2.700$ ml. Second, sub-sets of six members, *e.g.*, C_5–C_{10}, C_6–C_{11}, ..., C_{12}–C_{17}, were subjected to the same calculation [6]. With the standard precision apparatus three runs were performed and with the improved apparatus fifteen runs, as the probability of finding "mavericks" increases with the number of experiments performed. In Table I, standard precision data are shown. The data quality would normally be regarded as good. Table II gives the results obtained with the improved apparatus. It is seen that the data scatter is unusually low.

The sub-set dead-volume calculation with the standard precision data is shown in Fig. 1. C_{start} is

TABLE I

RETENTION VOLUMES OF *n*-ALKANES ON THE RAD PAK C_{18} CARTRIDGE

n_C, Number of carbon atoms; $V_{msr,run\ x}$, gross retention volume (including V_{extra}) of three runs; $V_{msr,av.}$, average of the gross retention volumes; $V_{ms,av.}$, mean net retention volume (excluding V_{extra}); S.D., standard deviation; R.S.D. relative standard deviation referred to $V_{msr,\ av.}$:

n_C	$V_{msr,run\ 1}$ (min)	$V_{msr,\ run\ 2}$ (min)	$V_{msr,\ run\ 3}$ (min)	$V_{msr,\ av.}$ (min)	$V_{ms,av.}$ (min)	S.D. (min)	R.S.D. (%)
5	4.40	4.40	4.40	4.40	4.25	0	0
6	4.77	4.78	4.77	4.77	4.62	0.01	0.23
7	5.25	5.25	5.25	5.25	5.10	0	0
8	5.83	5.83	5.83	5.83	5.68	0	0
9	6.57	6.57	6.57	6.57	6.52	0	0
10	7.43	7.47	7.45	7.45	7.30	0.02	0.27
11	8.57	8.57	8.57	8.57	8.42	0	0
12	9.90	9.92	9.92	9.91	9.77	0.01	0.1
13	11.57	11.58	11.57	11.57	11.42	0.01	0.09
14	13.60	13.60	13.60	13.60	13.45	0	0
15	16.12	16.10	16.10	16.11	15.96	0.01	0.06
16	19.13	19.18	19.18	19.16	19.01	0.03	0.16
17	22.88	22.87	22.88	22.88	22.73	0.01	0.04

TABLE II

RETENTION VOLUMES OF n-ALKANES ON THE NUCLEOSIL C_{18} COLUMN

n_C, Number of carbon atoms; $V_{msr,max}$ and $V_{msr,min}$, maximum and minimum gross retention volumes (including V_{extra}) of 15 runs; $V_{msr,av.}$ average of the gross retention volumes (including V_{extra}); $V_{ms,av.}$, average of the net retention volumes (excluding V_{extra}); S.D., standard deviation; R.S.D. relative standard deviation referred to $V_{msr,av.}$.

n_C	$V_{msr,max}$ (min)	$V_{msr,\ min}$ (min)	$V_{msr,\ av.}$ (min)	$V_{msr,\ av.}$ (min)	S.D. (min)	R.S.D. (%)
5	4.160	4.158	4.159	4.099	0.001	0.025
6	4.390	4.387	4.388	4.328	0.001	0.022
7	4.663	4.658	4.660	4.600	0.001	0.021
8	4.985	4.982	4.983	4.923	0.001	0.016
9	5.365	5.362	5.363	5.303	0.001	0.018
10	5.812	5.808	5.810	5.750	0.002	0.034
11	6.337	6.333	6.335	6.275	0.001	0.016
12	6.952	6.948	6.950	6.890	0.001	0.014
13	7.673	7.667	7.671	7.611	0.002	0.026
14	8.515	8.508	8.512	8.452	0.002	0.023
15	9.498	9.490	9.493	9.433	0.002	0.021
16	10.647	10.637	10.641	10.581	0.003	0.028
17	11.983	11.975	11.980	11.920	0.003	0.025

the carbon number of the first member of a sub-set. V_m found for the various sub-sets show a strong scatter around a linear regression line of V_m against C_{start}:

$$V_m = 2.819 - 3.9 \cdot 10^{-2} C_{start} \quad (r = 0.769) \quad (3)$$

The correlation coefficient is so poor that a linear dependence is not really justified.

The results obtained with the improved precision data are shown in Fig. 2. The scatter of data points around the regression

$$V_m = 2.990 - 3.4 \cdot 10^{-2} C_{start} \quad (r = 0.987) \quad (4)$$

is greatly reduced, and the correlation coefficient is acceptable, although nopt entirely satisfactory.

It can be seen that the dead volume is not constant, but decreases almost linearly from $V_m = 2.825$ ml for the C_5–C_{10} subset to $V_m = 2.593$ ml for the C_{12}–C_{17} subset. The moderate scatter around the Nucleosil C_{18} curve indicates that the data precision achieved with the improved apparatus is still not high enough to allow a decision about
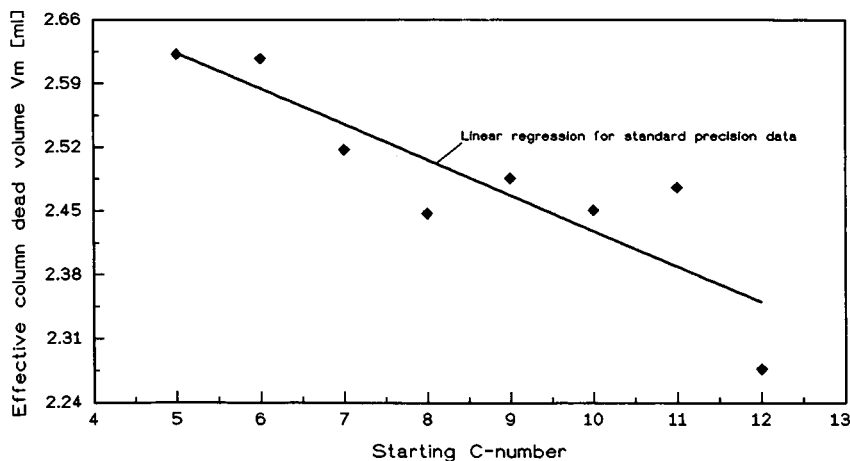
Fig. 1. Effective column dead volume as a function of the starting carbon number of the sub-set with standard precision apparatus.
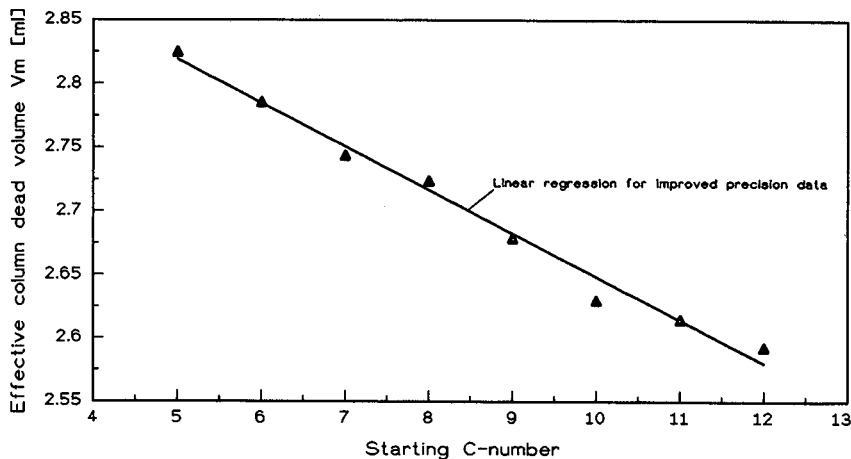
Fig. 2. Effective column dead volume as a function of the starting carbon number of the sub-set with improved precision apparatus.

an actually linear dependence of V_m on carbon number to be made.

In order to differentiate between influences of columns and apparatus, the Nucleosil C_{18} column and several others (Intersil ODS, LiChrospher ODS) were run under the same conditions as the standard precision apparatus. In all instances the same large data scatter as with the Rad PAK column was found.

CONCLUSIONS

It has been shown that the "effective" dead volume decreases with increasing solute size. This decrease is probably caused by a partial size exclusion of solutes. Solute size and ability to penetrate into the pores are directly related. To a first approximation, only those solutes whose effective diameter is smaller than the pore diameter can enter. Among the solutes fulfilling this condition, smaller ones have a higher probability per unit time than larger ones of actually finding the pore opening. These effects have to be evaluated over the pore-size distribution of the column used. A detailed report on this subject will be. published elsewhere.

From the results presented, it is obvious that the

data precision commonly attained in HPLC is not sufficient for a reliable dead-volume determination [7]. Our attempt to improve the apparatus led to the conclusion that commercially available HPLC pumps do not reach the required level of flow constancy. In order to solve this problem, we are working on a high-precision flow meter which monitors the actual flow at the detector exit continously on a ± 0.001 ml level. The flow-rate–time function allows the measured retention times to be converted into *true* retention volumes. We shall report on this principle later.

REFERENCES

1 H. Engelhardt, H. Mueller and B. Dreyer, *Chromatographia*, 19 (1984) 240, and references cited therein.
2 R. J. Smith, C. S. Nieass and M. S. Wainright, *J. Liq. Chromatogr.*, 9 (1986) 1387, and references cited therein.
3 Cs. Horváth and H.-J. Lin, *J. Chromatogr.*, 126 (1976) 401.
4 G. E. Berendsen, P. J. Schoenmakers, L. de Galan, G. Vigh, Z. Varga-Puchony and J. Inczedy, *J. Liq. Chromatogr.*, 3 (1980) 1669.
5 M. C. Harvey and S. D. Stearns, *Anal. Chem.*, 56 (1984) 837.
6 H. J. Möckel and T. Freyholdt, *Chromatographia*, 17 (1983) 215.
7 R. J. Smith and J. K. Haken, M. S. Wainright and B. G. Madden, *J. Chromatogr.*, 328 (1985) 11.

CHROMSYMP. 2399

Peak purity, yield and throughput in preparative liquid chromatography with self-displacement

Veronika R. Meyer

Institute of Organic Chemistry, University of Berne, Freiestrasse 3, CH-3012 Berne (Switzerland)

ABSTRACT

A cyclohexanone–cyclopentanone mixture was separated on silica with an average particle diameter of 5 or 25 μm using mobile phases of three different mixtures of hexane and *tert.*-butyl methyl ether. Two fractions were collected with the cut made at the lowest point between the two peaks. With increasing load the width of the first peak decreased, *i.e.*, the second compound began to displace the first. Under all conditions of high load the purity of the first fraction was markedly higher than that of the second; therefore, its recovery yield decreased because part of the compound was lost as an impurity in the second one. An equation for the calculation of the amount of collected fraction in milligrams is given; this amount depends on the purities of both fractions. Because the width of the fractions is known, it is then possible to calculate the yield, throughput and concentration of the fractions of interest, usually the first one. Of the three parameters purity, yield and throughput, it is possible to find conditions where two are kept high at the expense of the third by using a particular combination from the two stationary and three mobile phases.

INTRODUCTION

Preparative liquid chromatography, which is used to obtain pure compounds from a mixture, can be performed in various modes: analytical-scale separations with fraction collection, scaled-up elution chromatography under conditions of mass and/or volume overload, displacement chromatography [1] or frontal chromatography [2]. The frontal technique has not yet been investigated thoroughly but at least for special separation problems it could be useful. Displacement chromatography is gaining increasing interest because the throughpt is high; its drawback is the necessity to remove the displacer from the column after each separation. However, displacement effects are not uncommon in scaled-up elution chromatography if the mass overload is high enough. Under these circumstances the peak shapes of the individual compounds usually become triangular [3] (depending on the type of adsorption isotherm) and neighbouring peaks not only overlap but the later eluted compound can displace the less retained compound [4]. This phenomenon is not uncommon, as was shown recently [5,6], and can be used advantageously for the separation of two-component mixtures.

In this study, the behaviour of a mixture of two ketones when separated on silica under conditions of increasing mass overload was studied. Two columns of identical size but packed with stationary phases of 5 and 25 μm, thus giving different plate numbers, were used in combination with three mobile phases of differing elution strength.

EXPERIMENTAL

The columns used were stainless steel tubes of 25 cm × 10 mm I.D. When packed properly, such columns contain almost exactly 10 g of silica. Two batches of LiChrospher SI 100 (Merck, Darmstadt, Germany) were chosen by the manufacturer in order to use silicas with an as close matching of physical properties as possible: the 5-μm phase had a specific surface area of 393 m^2 g^{-1} and a pore volume of 1.29 ml g^{-1}, whereas these values for the 25-μm phase were 406 m^2 g^{-1} and 1.27 ml g^{-1}. Also, the nitrogen adsorption isotherms were almost identical. Packing of the columns was done in both instances by a
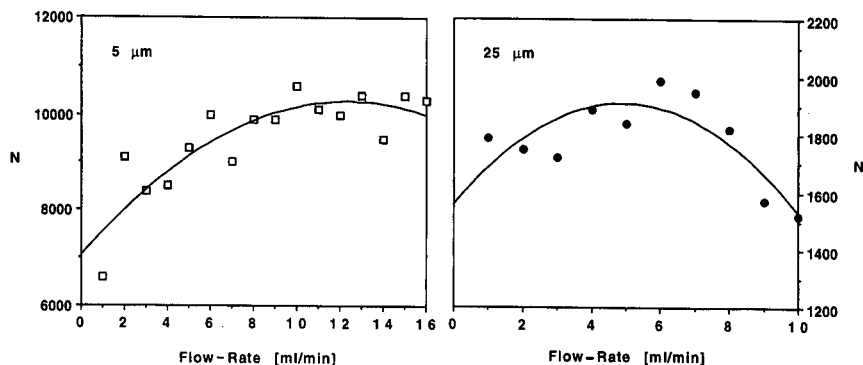
Fig. 1. Plate number, N, vs. flow-rate characteristics of the two columns used. Sample, 0.1 mg of cyclohexanone; mobile phase, hexane–*tert.*-butyl methyl ether (1:1). In both graphs a second-order polynomial is overlaid; however, for the 25-μm phase the maximum efficiency is at a higher flow-rate than the maximum of this curve. The data points are means of three measurements.

slurry method because no satisfactory results were obtained by dry packing of the coarse silica.

In Fig. 1, plots of plate number (N) vs. mobile phase flow-rate (kinds of van Deemter plots) of the two columns are shown. From previous studies it could be expected that under conditions of mass overload the column efficiency will be drastically lowered if the flow-rate is far from the Van Deemter optimum [7]. For the fine stationary phase no obvious optimum of the flow-rate (maximum N) was found and it was used at 14 ml min^{-1}. This corresponds to a reduced flow velocity v [8] of 4.4, where $v = (ud_p)/D_m$, u = volume flow-rate, d_p = particle diameter of the stationary phase and D_m = diffusion coefficient of the solute in the mobile phase, which can be calclated with the Wilke–Chang equation [9]. The value $v = 4.4$ is the reduced velocity calculated for cyclopentanone in hexane–*tert.*-butyl methyl ether (1:1). The coarse phase was used at 7 ml min, which is in the region of its optimum (see Fig. 1) and which corresponds to $v = 11$. Although the reduced velocities are not the same in both instances, the two columns are of equal quality if this is defined by the minimum reduced plate height, h [8], where $h = L/(Nd_p)$ and L = column length: $h_{5 \mu m} = 5.0$ (with $N = 10\ 000$) and $h_{25 \mu m}$ 5.0 (with $N = 2000$). The plate height (and reduced plate height) is responsible for the purity of fractions and therefore for the yield, whereas the flow-rate (and reduced velocity) determines the throughput.

As mobile phase mixtures of hexane (hexane fraction) and *tert.*-butyl methyl ether, both of HPLC quality (Romil, Shepshed, UK), in volume ratios of 1:1, 3:1 and 9:1 were used.

The two-component mixture studied was cyclohexanone (first peak) and cyclopentanone (second peak), both of purum quality from Fluka (Buchs, Switzerland). These ketones have low UV absorptivity and therefore detector overload caused by too high a signal when large amounts of sample are injected is avoided; they also have almost identical molar absorptivities at the wavelength chosen (280 nm), which is advantageous when the shape of overlapping peaks has to be judged. They are separated with a low separation factor with the chromatographic system used here (if the separation factor were larger, separation by flash chromatography would be possible). They are cheap and non-toxic and can be analysed by gas chromatography. The sample was a 1:1 mixture (both by mass and by volume as the densities are identical) of the two ketones dissolved in the same volume of mobile phase (with the exception of "analytical" runs, where 0.1 mg of each was dissolved in 20 μl of mobile phase).

The following liquid chromatographic equipment was used: pump, Model 100 with preparative head (Altex, Berkeley, CA, USA); sampling valve, Model 7120 with various loop sizes (Rheodyne, Berkeley, CA, USA); detector, Uvikon LCD 725 at 280 nm (Kontron, Zürich, Switzerland); and recorder,

Tarkan 600 (W + W Electronic, Basle, Switzerland).

The touching and overlapping peaks were manually collected as two fractions. The fractionation was always made at the lowest point between the bands. For overlapping peaks this collection strategy is not backed by theoretical considerations but by the fact that the peak valley is the only criterion useful for simple laboratory-scale preparative separations. These samples were then analysed by capillary gas chromatography with the following equipment: stationary phase, OV-1701; column, Duran glass, 30 mm × 0.5 mm I.D.; film thickness, 1 μm; carrier gas, helium; flow-rate, 3.5 ml min^{-1}; chromatograph, Perkin-Elmer (Überlingen, Germany) Sigma 3; temperature programme, from 50 to 91°C at 2°C min^{-1}; injector, 250°C, splitless; detector, flame ionization, 250°C; and integrator, HP 3390 A (Hewlett-Packard, Palo Alto, CA, USA). Results were obtained by means of a calibration graph.

All data presented in the tables are means of two experiments.

RESULTS

Table I shows the behaviour of the chromatographic systems studied when used under analytical conditions, i.e., without overload. The amount of sample is 0.1 mg of each of the ketones, giving a load of 0.01 mg of each compound per gram of silica. Capacity factor, k', plate number, N, and tailing, T (the ratio of the distances from peak maximum to peak end and peak front, respectively, measured at

10% of the peak height), are given for cyclohexanone (the first peak), whereas the sample mixture is represented by the separation factor α and the resolution R. It should be noted that the separation factor decreases with decreasing mobile phase polarity, i.e., decreasing content of tert.-butyl methyl ether.

Tables II–VII present the results with increasing load for each of the two stationary and three mobile phases. Because the first fraction, from peak front to the valley between the peaks, is of higher purity than the second one, especially with increasing load, the calculations refer to the first compound. The question is always what purity, recovery yield and throughput of this substance can be obtained. The second fraction is of markedly lower purity and recycling would be necessary anyway if it was required to be obtained in pure form. It is clear from the results that conditions should be chosen in such a way that the compound of interest is eluted first.

By using the given sample mass and the experimentally found values of purities and fraction widths (in units of time or elution volume), it is possible to perform the calculations of interest, i.e., to determine the yield as a percentage of the injected amount of cyclohexanone, the throughput in milligrams per minute and the concentration of the solute in the collected fraction in milligrams per millilitre.

The load per component in milligrams per gram is ten times lower than the mass injected in milligrams because the columns contain 10 g of stationary

TABLE I

CAPACITY FACTOR, PLATE NUMBER, TAILING, SEPARATION FACTOR, AND RESOLUTION OF THE DIFFERENT CHROMATOGRAPHIC SYSTEMS UNDER ANALYTICAL CONDITIONS

Columns: 25 cm × 10 mm I.D.; mobile phase flow-rate: 14 and 7 ml min^{-1} for the 5- and 25-μm phase, respectively. Ether is tert.-butyl methyl ether. Sample: 0.1 mg each of cyclohexanone and cyclopentanone in 20 μl of mobile phase.

Stationary phase (μm)	Mobile phase hexane–ether	k'_1	N_1	T_1	α	R
5	1:1	0.46	12 800	1.4	1.26	2.16
	3:1	0.76	13 000	1.6	1.21	2.50
	9:1	1.56	10 700	1.8	1.16	2.43
25	1:1	0.44	2390	2.2	1.26	0.86
	3:1	0.96	1860	2.2	1.20	0.98
	9:1	1.52	1840	2.3	1.16	1.00

TABLE II

PURITY OF FRACTIONS, AMOUNT OF FIRST FRACTION[a], RECOVERY YIELD OF FIRST COMPOUND[a], WIDTH OF BOTH FRACTIONS, THROUGHPUT OF FIRST COMPOUND[a], WIDTH OF FIRST FRACTION AND CONCENTRATION OF FIRST COMPOUND[a] WITH 5-μm STATIONARY PHASE, AND MOBILE PHASE HEXANE-*tert.*-BUTYL METHYL ETHER (1:1)

Chromatographic conditions as given in Table I with the exception of sample size.

Mass injected per compound (mg)	Load per compound (mg g^{-1})	Purity fraction 1 (%)	Purity fraction 2 (%)	Amount fraction 1 (mg)	Yield compound 1 (%)	Width both fractions (min)	Throughput compound 1 (mg min^{-1})	Width fraction 1 (ml)	Concentration compound 1 (mg ml^{-1})
0.1	0.01	100	100	0.1	100	0.32	0.31	1.63	0.061
1	0.1	99.3	96.5	0.971	97.1	0.325	2.99	1.63	0.61
3	0.3	98.9	95.4	2.89	96.3	0.367	7.88	1.63	1.77
10	1	96.9	92.7	9.53	95.3	0.383	24.9	1.40	6.81
30	3	99.6	61.2	11.1	36.8	0.417	26.6	1.05	10.6
100	10	83.1	55.6	28.9	28.9	0.517	55.9	1.22	23.7

[a] With purity as given in "purity fraction 1".

TABLE III

RESULTS OBTAINED WITH 5-μm STATIONARY PHASE AND MOBILE PHASE HEXANE-*tert.*-BUTYL METHYL ETHER (3:1)

Details as in Table II.

Mass injected per compound (mg)	Load per compound (mg g^{-1})	Purity fraction 1 (%)	Purity fraction 2 (%)	Amount fraction 1 (mg)	Yield compound 1 (%)	Width both fractions (min)	Throughput compound 1 (mg min^{-1})	Width fraction 1 (ml)	Concentration compound 1 (mg ml^{-1})
0.1	0.01	100	100	0.1	100	0.433	0.231	2.33	0.043
1	0.1	100	98.1	0.981	98.1	0.458	2.14	2.75	0.357
3	0.3	99.6	97.6	2.938	97.9	0.500	5.88	2.56	1.15
10	1	99.2	95.9	9.65	96.5	0.600	16.1	2.56	3.76
30	3	99.8	83.0	23.9	79.7	0.767	31.2	2.10	11.4
100	10	93.4	70.5	64.2	64.2	0.933	68.8	1.81	35.5

TABLE IV

RESULTS OBTAINED WITH 5-μm STATIONARY PHASE AND MOBILE PHASE HEXANE-*tert.*-BUTYL METHYL ETHER (9:1)

Details as in Table II.

Mass injected per compound (mg)	Load per compound (mg g^{-1})	Purity fraction 1 (%)	Purity fraction 2 (%)	Amount fraction 1 (mg)	Yield compound 1 (%)	Width both fractions (min)	Throughput compound 1 (mg min^{-1})	Width fraction 1 (ml)	Concentration compound 1 (mg ml^{-1})
0.1	0.01	100	100	0.1	100	0.700	0.143	4.67	0.021
1	0.1	100	98.4	0.984	98.4	0.867	1.14	4.67	0.211
3	0.3	99.5	98.0	2.95	98.5	1.03	2.86	4.90	0.602
10	1	100	90.1	8.90	89.0	1.38	6.45	4.67	1.91
30	3	97.6	78.6	22.5	75.1	1.77	12.7	4.44	5.07
100	10	79.0	69.5	80.4	80.4	2.43	33.1	5.70	14.1

TABLE V

RESULTS OBTAINED WITH 25-μm STATIONARY PHASE AND MOBILE PHASE HEXANE-*tert.*-BUTYL METHYL ETHER (1:1)

Details as in Table II.

Mass injected per compound (mg)	Load per compound (mg g^{-1})	Purity fraction 1 (%)	Purity fraction 2 (%)	Amount fraction 1 (mg)	Yield compound 1 (%)	Width both fractions (min)	Throughput compound 1 (mg min^{-1})	Width fraction 1 (ml)	Concentration compound 1 (mg ml^{-1})
0.1	0.01	100	84.5	0.0817	81.7	0.833	0.0981	1.98	0.041
1	0.1	99.0	80.9	0.773	77.3	0.967	0.800	2.10	0.368
3	0.3	98.7	78.5	2.21	73.8	0.983	2.25	1.75	1.26
10	1	99.1	71.0	5.99	59.9	1.07	5.60	1.52	3.94
30	3	99.5	62.2	11.9	39.5	1.13	10.5	1.28	9.30
100	10	90.7	55.7	24.6	24.6	1.17	21.0	1.40	17.6

TABLE VI

RESULTS OBTAINED WITH 25-μm STATIONARY PHASE AND MOBILE PHASE HEXANE–*tert.*-BUTYL METHYL ETHER (3:1)

Details as in Table II.

Mass injected per compound (mg)	Load per compound (mg g⁻¹)	Purity fraction 1 (%)	Purity fraction 2 (%)	Amount fraction 1 (mg)	Yield compound 1 (%)	Width both fractions (min)	Throughput compound 1 (mg min⁻¹)	Width fraction 1 (ml)	Concentration compound 1 (mg ml⁻¹)
0.1	0.01	100	88.0	0.0864	86.4	1.43	0.0604	3.38	0.0256
1	0.1	100	85.4	0.829	82.9	1.37	0.605	3.03	0.274
3	0.3	99.4	82.4	2.38	79.2	1.57	1.51	3.03	0.785
10	1	99.3	79.1	7.42	74.1	1.73	4.29	2.68	2.77
30	3	98.4	76.1	21.0	70.1	1.90	11.1	1.98	10.6
100	10	96.4	61.1	38.6	38.6	2.20	17.5	1.86	20.8

TABLE VII

RESULTS OBTAINED WITH 25-μm STATIONARY PHASE AND MOBILE PHASE HEXANE–*tert.*-BUTYL METHYL ETHER (9:1)

Details as in Table II.

Mass injected per compound (mg)	Load per compound (mg g⁻¹)	Purity fraction 1 (%)	Purity fraction 2 (%)	Amount fraction 1 (mg)	Yield compound 1 (%)	Width both fractions (min)	Throughput compound 1 (mg min⁻¹)	Width fraction 1 (ml)	Concentration compound 1 (mg ml⁻¹)
0.1	0.01	100	75.6	0.0677	67.7	1.83	0.037	5.13	0.013
1	0.1	100	82.6	0.789	78.9	2.20	0.359	4.89	0.161
3	0.3	99.4	82.1	2.36	78.8	2.53	0.933	4.66	0.506
10	1	99.3	80.8	7.69	76.9	2.78	2.78	4.31	1.78
30	3	99.1	76.0	20.8	69.2	3.50	5.94	3.61	5.76
100	10	98.1	62.2	40.5	40.5	4.40	9.20	2.80	14.5

phase. The fractions of less than 100% purity are contaminated by the other ketone, and because the two solutes are always injected as a 1:1 mixture the absolute amount of fraction 1 in milligrams is given by

$$A + b = M \cdot \frac{2P_2 - 1}{P_1 + P_2 - 1}$$

where A = mass of compound 1 in fraction 1; a = mass of compound 1 in fraction 2 (see below); B = mass of compound 2 in fraction 2; b = mass of com-

pound 2 in fraction 1; M = injected mass of each compound, with $M_{cyclohexanone} = M_{cyclopentanone} = M$; and P = purity of fraction 1 or 2.

The expression for $A + b$ is found by a combination of the four equations $A + a = M$, $B + b = M$, $A/(A + b) = P_1$ and $B/(B + a) = P_2$. The total amount of fraction 2, $B + a$, could be calculated by an analogous equation. If the sample were not a 1:1 mixture of the two ketones, the equation for the calculation of $A + b$ would be much more complicated.
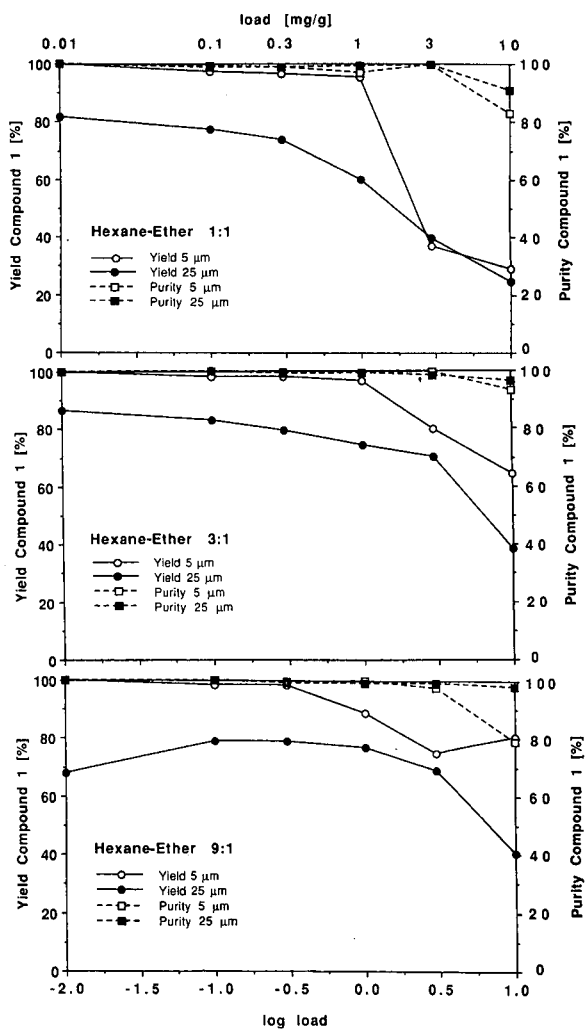
Fig. 2. Recovery yield and purity of compound 1 (cyclohexanone) vs. increasing load on 5- and 25-μm silica with hexane–tert.-butyl methyl ether mixtures of various compositions as mobile phase.
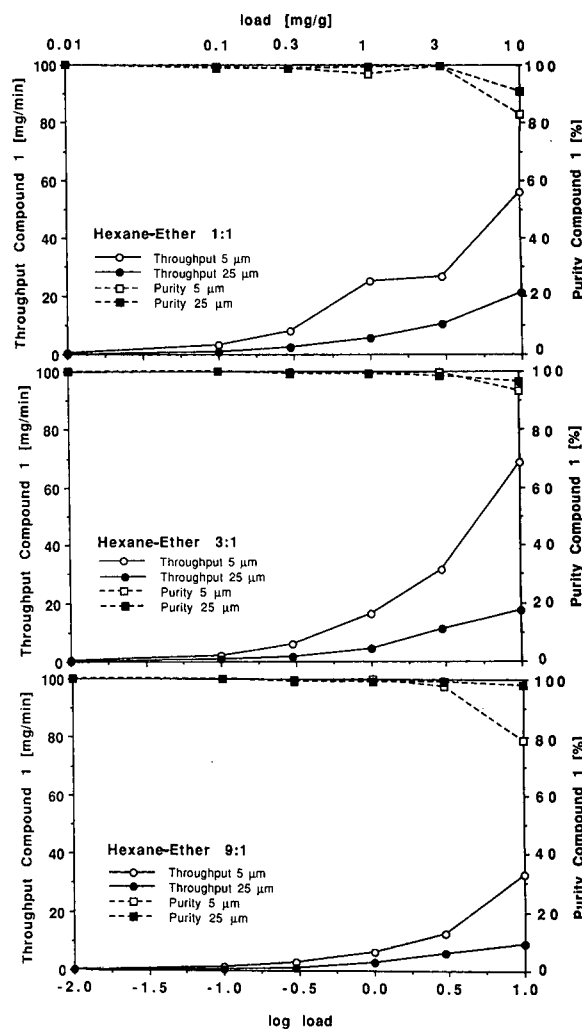
Fig. 3. Throughput and purity of compound 1 (cyclohexanone) vs. increasing load on 5- and 25-μm silica with hexane–tert. butyl methyl ether mixtures of various compositions as mobile phase.

The calculation of the recovery yield of compound 1 (with purity as given in the third column of the tables) is obvious. Its throughput is given by dividing the amount of fraction 1 by the width of both fractions in minutes. This approach presupposes that consecutive injections are nested in order to give touching peak pairs, *i.e.*, peaks other than those for the two ketones are absent. For a correct calculation of throughput, the retention time of the first injection should also be considered, which is not the case in the tables.

In the last column of the tables the concentration of compound 1 is listed, which can easily be

Fig. 4. Elution profiles of the individual compounds and of a 1:1 mixture of the two ketones. Sample, 100 mg of each component, *i.e.*, 200 mg of mixture, dissolved in the same amount of mobile phase; stationary phase, 25-μm silica; mobile phase, hexane–*tert.* butyl methyl ether (3:1); flow-rate, 7 ml min^{-1}.

calculated if the width (volume) of fraction 1 is known.

Fig. 2 summarizes the recovery yield and purity of compound 1 and Fig. 3 shows the throughput and purity.

DISCUSSION

The displacement effect manifests itself by the fact that the width of fraction 1 decreases with increasing load (with the exception of the 5-μm silica and 9:1 mobile phase composition). Without a displacement effect, the volume of this fraction would be constant and any shifting of retention times of the two ketones would be expected to be parallel. Fig. 4 shows that cyclohexanone is eluted earlier and as a narrower peak (of 96% purity) when injected as a mixture in comparison with the peak profiles of the individual compounds. A similar result was found by Newburger and Guiochon [5] for the diethyl phthalate–β-tetralone pair. For effective self-displacement, they stated that the amount of the second-eluted compound should be higher than of the first-eluted compound.

With increasing load, the purity of both fractions decreases, *i.e.*, a certain amount of compound is "lost" as an impurity in the fraction of the other ketone. Therefore, the recovery yield of compound 1 decreases. Note that its yield can be low, although its purity is high. The purity of fraction 1 is always markedly higher than that of fraction 2. As already mentioned, this approach is not economical if the second-eluted compound, cyclopentanone, needs to be obtained in pure form.

Regarding the throughput of compound 1, this increases with increasing load at the expense of purity and recovery yield. The concentration of compound 1 also increases, which is desirable because the isolation of the product by evaporation of the mobile phase is easier and possible contamination from eluent impurities is lower.

Influence of mobile phase composition

As can be seen from Table I, decreasing the ether content and therefore the polarity of the mobile phase entails higher capacity factors, k', and, as expected, better resolution, R, of the peaks. However, this latter effect is less pronounced, as would be expected owing to the observed decrease in the
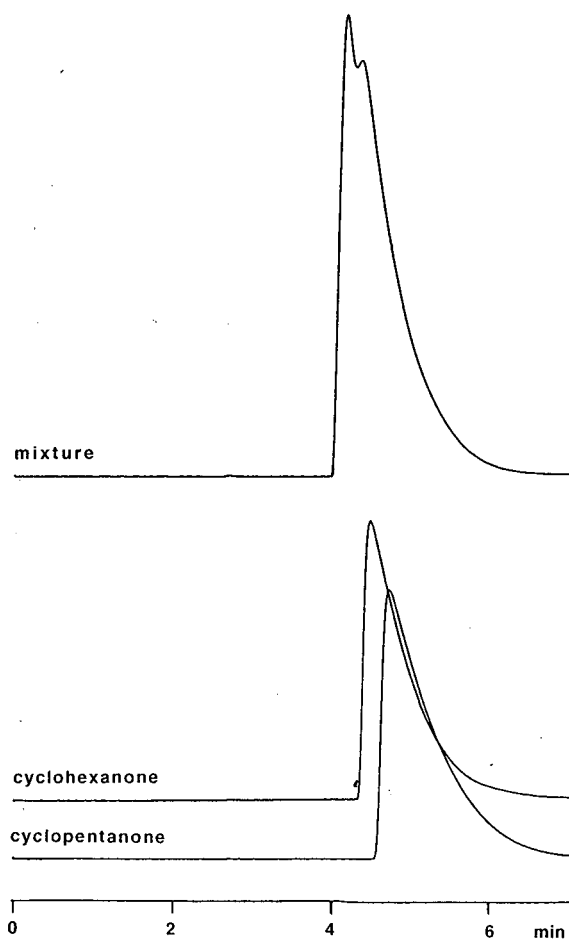
separation factor, α. Also, the tailing, T, increases with decreasing mobile phase polarity, a feature typically found with normal-phase separations on silica. For preparative separations it is highly desirable to find conditions where the separation factor and resolution (under analytical conditions) are high whereas tailing would be low. This is not possible here, and therefore Fig. 2 shows no clear trend that the purity and yield of compound 1 increase with decreasing ether content. It seems as if the mobile phase of medium polarity would be the best compromise. Concerning throughput, the results are clearer. Owing to increased peak widths with lower polarity, the throughput decreases. Any effect of mobile phase strength on capacity factors (retention times) has no influence on throughput if this is calculated by the method given above, i.e., with consecutive and nested injections. Concerning the sample concentration in the eluate, the mobile phase of medium strength is best for both types of stationary phase.

Influence of stationary phase particle size

The 25-μm silica gives a higher purity of fraction 1 whereas with the 5-μm phase the purity of fraction 2 is higher (or its impurity is lower). This is the reason why the yield of compound 1 is higher with the fine silica (but with lower purity). Also, the throughput of compound 1 is higher on the 5-μm phase (again with lower purity). The throughput on the coarse stationary phase is only *ca.* 30% of that on the fine material. If the 25-μm column were also used at a flow-rate of 14 ml min^{-1}, its throughput could be expected to be *ca.* 60% but perhaps with lower purity, considering the earlier studies on van Deemter plots at mass overload [7]. In contrast, Guiochon and co-workers found that the conditions for maximum productivity are far from the van Deemter optimum [5,10].

CONCLUSIONS

This study provides further confirmation that of purity, yield and throughput, only two parameters can be kept high at the expense of the third. The calculation of the amount of fraction mass presented here, which is possible from the amount injected and the fraction purities, is the key for the determination of yield, throughput and product concentration. Concerning the size of the stationary phase, no general recommendations can be given but as the mobile phase hexane and *tert.*-butyl methyl ether (3:1) is often the best compromise.

REFERENCES

1 J. Frenz and C. Horváth, in C. Horváth (Editor), *HPLC, Advances and Perspectives*, Vol. 5, Academic Press, New York, 1988, p. 211.
2 D. A. Hill, P. Mace and D. Moore, *J. Chromatogr.*, 523 (1990) 11.
3 S. Golshan-Shirazi and G. Guiochon, *Anal. Chem.*, 61 (1989) 462.
4 S. Golshan-Shirazi and G. Guiochon, *J. Chromatogr.*, 536 (1991) 57.
5 J. Newburger and G. Guiochon, *J. Chromatogr.*, 523 (1990) 63.
6 J. Newburger, B. DeLange and G. Guiochon, poster presented at the *15th International Symposium on Column Liquid Chromatography, Basle, 1991*.
7 V. R. Meyer, *Sep. Sci. Technol.*, 22 (1987) 1909.
8 P. A. Bristow and J. H. Knox, *Chromatographia*, 10 (1977) 279.
9 C. R. Wilke and P. Chang, *AIChE J.*, 1 (1955) 264.
10 S. Golshan-Shirazi and G. Guiochon, *Anal. Chem.*, 61 (1989) 1368.

Assessment of chromatographic peak purity by means of multi-wavelength detection and correlation-based algorithms

J. B. Castledine and A. F. Fell*

Pharmaceutical Chemistry, University of Bradford, Bradford BD7 1DP (UK)

R. Modin and B. Sellberg

Analytical Chemistry, Kabi Pharmacia AB, Therapeutics, Uppsala (Sweden)

ABSTRACT

Dual-wavelength UV detection is widely employed to generate absorbance ratios as a relatively non-specific method for characterizing peak purity in liquid chromatography. The sensitivity of this method is largely dependent on the pair of wavelengths chosen. An alternative technique, correlation of the spectral information, proposed primarily to overcome this constraint, has been investigated. The implications for the application of correlation coefficients to peak purity and homogeneity determination are examined. Particular attention is focused on the successful use of correlating multiple chromatographic peak-area data (peak areas calculated from the absorbance values at various detection wavelengths) for the reliable assessment of both peak identity and peak homogeneity. Using a model system, 1% of a putative related compound of sulphasalazine in a mixture with sulphasalazine could be detected regardless of the chromatographic resolution between the two compounds.

INTRODUCTION

One of the key requirements for the validation of chromatographic methods is to determine the purity of the analyte peaks. The establishment of the purity of a chromatographic peak is in essence a negative concept, requiring that the absence of impurity be demonstrated and as such is not directly measurable [1]. Consequently, the identity and purity of a pharmaceutical compound are often determined by comparison of the results obtained from several tests with those acquired under similar conditions from a standard of known and accepted quality [2,3].

In addition to comparing the chromatographic retention characteristics of the compound of interest with a reference sample, it was first recognized in a theoretical analysis by Ostojic [4] that multiple sets of detection data could be used to enhance solute identification and facilitate peak deconvolution.

Prior to the development of the now widely used diode-array detectors (DAD) [5–21], application of this theory based on UV absorbance data required repeated analysis using two detectors in series; alternatively, stopped-flow conditions were used [6,7]. The identity or purity of individual peaks can be confirmed when absorbance ratios (usually calculated from the chromatographic peak apex spectrum, as proposed by White and Catterick [17]) are compared with those from reference samples. Moreover, by comparing absorbance ratios calculated at points through the chromatographic peak, it is possible in principle to determine the presence of partially overlapping species, provided that there are sufficient differences between the spectra involved and their respective elution times.

Although the advent of DAD has reduced many of the problems that affected the overall precision of absorbance ratio measurements, as discussed by

early workers [6], the sensitivity of the method remains largely dependent on the wavelengths chosen and the consequent differences in absorptivity of the overlapping solutes. If several wavelength pairs are selected, as is possible with the DAD, the selectivity of the absorbance ratio method and its sensitivity to interfering impurities can be increased [6,9,16,18]. Multiple absorbance ratio correlation (MARC) is an alternative approach to enhancing peak purity detection, as proposed by Marr *et al.* [22], based on the correlation between five-point absorbance ratio vectors at points through the chromatographic peak. A competitive approach, recently advocated for the assessment of protein and peptide purity [23,24], is based on calculating the correlation coefficient directly between pairs of UV–visible absorption spectra.

This paper examines the use of correlation coefficients to compare spectral data for the assessment of peak purity, as data at all wavelengths of detection can be utilized for the comparison. Moreover, mathematical transformation of the correlation coefficients obtained is possible, giving rise to an approximately normal distribution of results. This makes the data generally applicable for Student's *t*-test evaluation, rather than relying on an empirically based descriminatory factor [18].

Monitoring an absorbance ratio continually through a chromatographic peak can provide two separate pieces of information. The appearance of the function as a square waveform may give an indication of peak homogeneity, within the constraints applied due to noise, resolution, peak tailing and wavelength choice. Second, the average value of the square waveform may be used to establish the peak's purity and, if pure, its identity. In analogous fashion, correlation coefficients may be used to assess peak homogeneity and identity [22].

Although most work reported using absorbance ratios utilizes the ratio between absorbance values at two wavelengths at a given time point in the chromatographic peak [5–21], it is possible to generate such ratios from a comparison of chromatographic peak areas, calculated from integrating the chromatographic peaks generated at different wavelengths of detection [17,25]. The principles and the relative advantages and disadvantages of this method are similar to those involved in ratioing single absorbance values. White *et al.* [17] found that, for

peak identification, better precision was obtained with ratios derived from peak-height measurements. This may be attributed, at least in part, to the integration algorithm employed.

An advantage of ratios calculated from peak areas is that they assess peak homogeneity in addition to peak identity, giving a single figure assessment of purity. Given that the sensitivity of this method is dependent on the wavelength pair used, this paper re-examines this technique using correlation of the chromatographic peak areas at several detection wavelengths.

EXPERIMENTAL

Reagents

Methanol [high-performance liquid chromatographic (HPLC) grade, Rathburn Chemicals, Walkerburn, UK], sodium dihydrogenphosphate monohydrate and anhydrous sodium acetate (Merck, Darmstadt, Germany) were used as received. All buffer salts were dissolved in distilled water and filtered using HVLP 0.45-μm filters (Waters–Millipore, Milford, MA, USA). Sulphasalazine (USP reference material, Batch 408641) and potential related compounds were obtained from Kabi Pharmacia Therapeutics (Uppsala, Sweden).

Apparatus

The chromatographic system used consisted of a Series 400 chromatograph with an SEC-4 solvent environment controller and an ISS-101 autosampler (all from Perklin-Elmer, Norwalk, CT, USA), and an HP 1040A diode-array detector (Hewlett-Packard, Waldbron, Germany). Data collection and evaluation were performed using an HP-85 computer, HP-9000 Series Workstation (with HPLC Chemstation software), HP-7470 plotter and a Model 9121 dual-disk drive (all from Hewlett-Packard). The original HP-85A specifications were enhanced through the addition of read-only memory modules for input–output, printer–plotter communications and available memory (expanded by 16K) (Hewlett-Packard).

LC conditions

A stainless steel column (250 mm × 4.6 mm I.D.) packed with 7-μm Nucleosil C_{18} (Macherey, Nagel & Co., Düren, Germany) was used. The

mobile phase, pumped at 1.0 ml/min, was a mixture of methanol and phosphate–acetate buffer.

Computation

Programs were written in BASIC to correlate the chromatographic peak apex spectra and also the sets of peak-area data using an HP-85 microcomputer (Hewlett-Packard). Correlation coefficients were calculated using the equation [26]

$$r = \frac{\sum A_{1i} \cdot A_{2i}}{(\sum A_{1i}^2 \cdot \sum A_{2i}^2)^{\frac{1}{2}}}$$

where A_{1i} and A_{2i} are the absorbance values or peak areas at i nm for spectra or chromatograms 1 and 2, respectively.

As correlation coefficients are not normally distributed, the confidence limits were calculated after transformation of the data to give the normalized correlation, Z, using

$$Z = 0.5 \ln[(1 + r)/(1 - r)]$$

The values of Z are approximately normally distributed [27].

Statistical evaluation was performed using Student's t-test. As it was found that the sample standard deviations varied significantly and were dependent, in part, on the absolute value of the correlation coefficient, it was considered that the population standard deviations could not be assumed to be equal. Hence the appropriate equation used was [28]

$$t = (x_1 - x_2)/(s_1^2/n_1 + s_2^2/n_2)^{\frac{1}{2}}$$

where x_1 = mean, s_1 = standard deviation and n_1 = number of normalized correlation coefficients calculated between sample and reference data and x_2 = mean, s_2 = standard deviation and n_2 = number of normalized correlation coefficients calculated between two sets of reference data.

The number of degrees of freedom (d.f.) was calculated thus [28]:

$$d.f. = \left[\frac{(s_1^2 n_1 + s_2^2/n_2)^2}{\dfrac{(s_1^2/n_1)^2}{n_1 + 1} + \dfrac{(s_2^2/n_2)^2}{n_2 + 1}} \right] - 2$$

the results being rounded to the nearest whole number.

RESULTS AND DISCUSSION

An LC system was developed, as described above, using sulphasalazine and potential-related compounds, such that one of these compounds, A, could be made to elute simultaneously with sulphasalazine ($R_s = 0$). By varying the composition of the mobile phase, three different degrees of chromatographic peak overlap between sulphasalazine (10 μg on-column) and compound A were obtained and investigated. In addition to the simultaneous elution conditions ($R_s = 0$), separations of the respective retention times for sulphasalazine and compound A of +0.25 min and +0.45 min were established. This corresponds to R_s values of ca. 0.2 and 0.3, when calculated with reference to sulphasalazine (10 μg on-column) and compound A (1 μg on-column), chromatographed individually.

Visual examination of spectra

Sulphasalazine is prepared by diazotizing sulphapyridine and coupling the diazotized intermediate with salicylic acid [29]. Compound A contains an additional sulphapyridine moiety attached to the sulphasalazine molecule via the central benzene ring. Consequently, the UV–visible absorption spectrum of compound A (which thus contains two additional chromophores) differs significantly from that of sulphasalazine (Fig. 1b). Nevertheless, the presence of a minor proportion of this potential-related compound in a mixture with sulphasalazine results in a combined spectrum that closely resembles that of the unadulterated sulphasalazine. Although visual examination of the overlaid normalized apex spectra, obtained using $R_s = 0$ data, revealed detectable differences for 10% of compound A added to the sample of sulphasalazine, the presence of 1% or less of related compound A could not be detected in this way (Fig. 1).

Evaluation of correlation-based methods

Solutions of sulphasalazine (0.5 mg/ml), in the linear response range of the LC system (measured at 320 nm), were spiked with 10%, 1% and 0.1% of compound A. The chromatographic peak apex spectra obtained for $R_s = 0$ conditions were compared with those acquired for the USP reference sulphasalazine by (i) single absorbance ratios and (ii) correlation of the UV–visible absorption spectra.
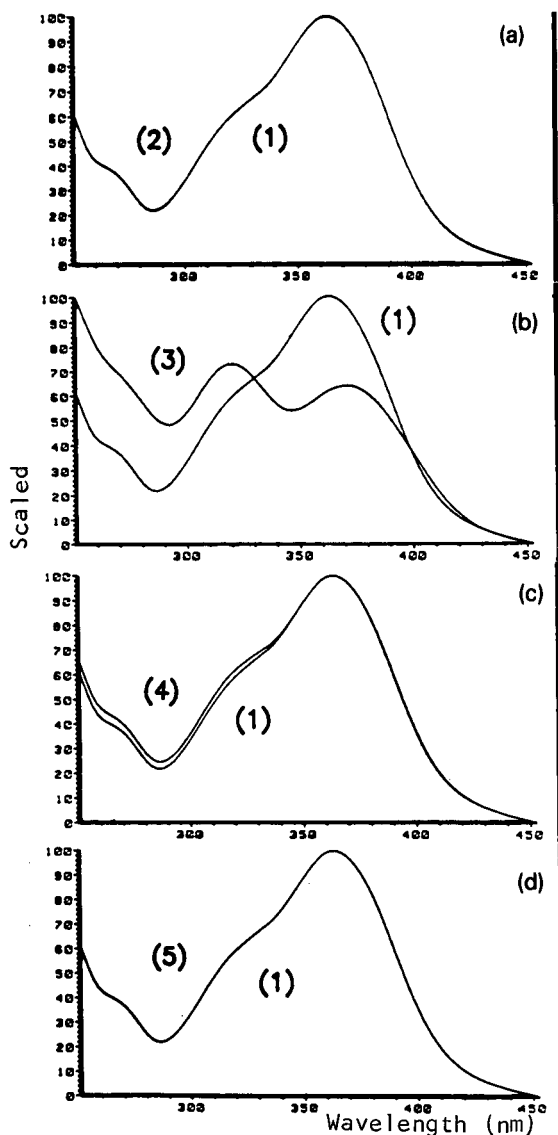
Fig. 1. Overlaid normalized spectra: comparison of the sulpha-salazine chromatographic peak apex spectrum with the apex spectra of (a) sulphasalazine, (b) compound A, (c) sulphasalazine + 10% A and (d) sulphasalazine + 1% A. Spectra: 1 and 2 = sulphasalazine; 3 = compound A; 4 = sulphasalazine + 10% A; 5 = sulphasalazine + 1% A.

From the data in Table I, the sensitivity of the absorbance ratio (AR) algorithm and its dependence on the wavelength pair selected can be observed. For the model system described, it was found possible to detect 1% of the simultaneously eluted compound A

in a mixture with sulphasalazine when the chromatographic peak apex AR, calculated from data at 280 and 360 nm, was compared with a similar AR for sulphasalazine alone. These results, when compared with the visual examination of overlaid normalized spectra (Fig. 1), illustrate the potentially high sensitivity that the AR technique can provide in the assessment of peak purity under well defined conditions. Moreover, the dependence of the AR method on the wavelength pair selected is illustrated by the ratios generated using data at 340 and 380 nm, as the presence of relatively high concentrations of the related compound cannot be detected.

The comparable sensitivity of the correlation coefficient to that of a well chosen AR and the application of Student's t-test to the data generated are shown in Table I.

The ability of multi-wavelength LC detectors to generate large amounts of data necessitates a reduction of the data set interrogated for efficient application of peak-purity algorithms. Data reduction may be effected in the wavelength and/or time domain.

In the case of non-continuous use of the time data set, as used by the Hewlett-Packard Chemstation Data Editor peak-homogeneity correlation-based assessment algorithm [25,30], when the partially overlapping "impurity" peak elutes at a retention time that corresponds closely with a sampling point in the time domain (*e.g.*, downslope inflection), the presence of a heterogeneous peak may be reliably detected. Thus, in the system described above with an interval of 0.25 min between the retention times, corresponding to elution of compound A coincident with the downslope inflection of the sulphasalazine peak, the sensitivity of detection of compound A is at a maximum (Table II). If this is not the case, then such algorithms can fail, as also shown in Table II.

Further experiments were therefore initiated to examine the alternative approach of reducing the number of data points in the wavelength domain.

Fig. 2 illustrates graphically the relationship between the spectral correlation coefficient (SCC) and the number of data points used. By comparing spectra collected at a similar time point on the downslope of the chromatographic peak, obtained from the injection of *ca.* 1 μg of the samples, the signal-to-noise ratio of the data selected was such that 1% of compound A mixed with sulphasalazine could only be detected after careful choice of the

TABLE I

COMPARISON OF CHROMATOGRAPHIC PEAK APEX SPECTRA USING ABSORBANCE RATIOS AND THE CORRELATION BETWEEN SAMPLE AND REFERENCE SOLUTES APEX SPECTRA

Triplicate injections (10 μg on-column) of each sample. Spectral correlations calculated from 250 to 450 nm at 4-nm intervals.

Sample	Absorbance ratio		Normalized spectral correlation			
	280/360 nm	340/380 nm	Mean ($n = 9$)	t-Value	Tabulated t ($P = 0.01$ one-tailed)	
Reference sulphasalazine	0.313	0.941				
	0.314	0.940	7.92			
	0.313	0.940				
Sulphasalazine + 10% A	0.342^a	0.941				
	0.342^a	0.941	4.40	23.4^a	2.90	
	0.341^a	0.941				
Sulphasalazine + 1% A	0.316^a	0.940				
	0.316^a	0.941	6.55	8.24^a	2.68	
	0.317^a	0.941				
Sulphasalazine + 0.1% A	0.314	0.941				
	0.313	0.941	7.92	0	2.55	
	0.313	0.941				

^{a} Denotes reliable detection of simultaneously eluted impurity.

TABLE II

ASSESSMENT OF PEAK HOMOGENEITY USING THE HEWLETT-PACKARD CHEMSTATION, DATA EDITOR, PEAK-PURITY ALGORITHM

Triplicate injections (10 μg on-column) of each sample.

Sample	Retention of compound A relative to sulphasalazine	
	+0.25 min.	+0.45 min
Reference sulphasalazine	1000	1000
	1000	1000
	1000	1000
Sulphasalazine + 10% A	989^a	1000
	996^a	998^a
	997^a	1000
Sulphasalazine + 1% A	1000	1000
	1000	1000
	1000	1000
Sulphasalazine + 0.1% A	1000	1000
	1000	1000
	1000	1000

^{a} Denotes that the presence of the impurity could be detected.

number of data points used in the correlation.

Surprisingly, the data show that, in this instance, as few as four spectral data points (distributed equally through the spectra) are sufficient to give a reliable correlation coefficient. This may be explained by observations from overlaying the normalized spectra (Fig. 1). These show that the spectra differ by a small amount over a wide range of wavelengths, rather than display large differences over a very limited number of wavelengths. This, in turn, may be explained by the nature of UV–visible absorption, as electronic transitions are also accompanied by vibrational and rotational transitions within the molecules. The additive effect of these transitions cause UV–visible absorption bands to be broader than if only electrons were involved.

While the data presented are for one pair of related compounds only, a similarly small number of data points (six) was found to be necessary by Marr et al. [22] in order to characterize the difference between theophylline and the spectrally similar paraxanthine. This is further supported by recent work investigating protein purity [23]. Examination
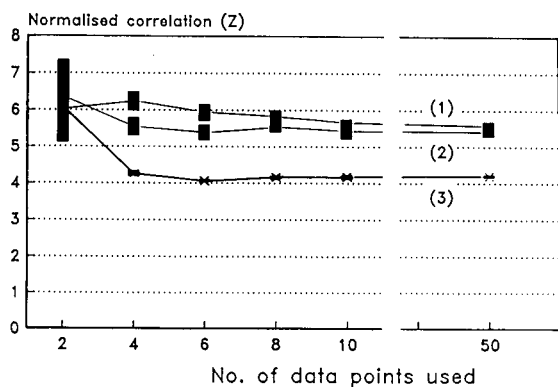
Fig. 2. Spectral correlation: comparison of the number of data points used in the correlation and the ability to identify the presence of a simultaneously eluted compound. 1 = Sulphasalazine; 2 = sulphasalazine + 1% A; 3 = sulphasalazine + 10% A. ■ = 95% confidence interval; × = mean (n = 9).

of the literature reveals that small spectral differences over a wide wavelength range are common for closely related compounds [31]. Hence it may be postulated that simultaneously eluted "impurities" will be efficiently detected using the SCC with a

relatively small number of data points.

Fig. 2 also demonstrates that the number of data points in excess of this critical threshold figure determines, in part, the sensitivity of the correlation methods. This may be attributed to the nature of the correlation algorithm, as all variations (both positive and negative) between both of the two spectra compared will reduce the degree of correlation between them. Thus every data point (each incorporating experimental error, i.e., signal noise), in excess of the threshold figure, will reduce the degree of correlation between spectra from the same sample and thus affect the discriminatory ability of the algorithm.

Peak identity and homogeneity assessment

The above observations gives rise to several implications for the use of correlation coefficients to assess the identity and homogeneity of a chromatographic peak. To examine this further, the LC model system was used. Evaluation of the purity of the complete chromatographic peak involves examination of the apparent peak identity coupled with assessment of peak homogeneity. Thus the apical spectral data can be compared with reference data,

TABLE III

ASSESSMENT OF PEAK PURITY BASED ON CORRELATION OF CHROMATOGRAPHIC PEAK APEX SPECTRA WITH SULPHASALAZINE APEX SPECTRA OF SIMILAR CONCENTRATION

Wavelengths used: 300, 320, 340, 360, 380, 400 and 420 nm. Triplicate injections (10 μg on-column) of each sample were correlated with triplicate injections of pure sulphasalazine.

Retention of compound A relative to sulphasalazine	Sample	Normalized spectral correlation		
		Mean (n = 9)	t-Value	Tabulated t (P = 0.01 one-tailed)
0 min	Reference sulphasalazine	8.09		
	Sulphasalazine + 10% A	4.84	16.5[a]	2.90
	Sulphasalazine + 1% A	7.00	4.96[a]	2.65
	Sulphasalazine + 0.1% A	8.15	−0.22	2.55
+0.25 min	Reference sulphasalazine	8.19		
	Sulphasalazine + 10% A	6.91	7.43[a]	2.76
	Sulphasalazine + 1% A	7.63	3.23[a]	2.76
	Sulphasalazine + 0.1% A	8.24	−0.23	2.55
+0.45 min	Reference sulphasalazine	8.85		
	Sulphasalazine + 10% A	7.74	6.65[a]	2.55
	Sulphasalazine + 1% A	8.15	3.42[a]	2.60
	Sulphasalazine + 0.1% A	8.67	0.95	2.58

[a] Denotes reliable detection of the presence of the impurity.

and the homogeneity of the peak can be assessed by comparing spectral data through the peak with the apex spectrum.

Table III shows, as would be expected, that the ability to determine the presence of a co-eluted analyte by comparing spectral data at the apex of the chromatographic peak diminishes as the degree of resolution of an overlapping peak increases. This is shown by a general increase in the mean normalized correlation coefficient and reduction of the *t*-value obtained, for similar levels of adulteration, with increasing chromatographic resolution. Thus a sensitive peak-homogeneity assessment algorithm may also be required in cases of partial resolution between the two compounds, to detect the presence of an impurity.

A common approach to the assessment of peak homogeneity, using continuous data in the time domain, is to express the data graphically using absorbance ratio plots. Fig. 3, where a single absorbance ratio, with a well selected wavelength pair, is used for the model system with a 0.45-min difference in retention time between the two mixture components, highlights a major drawback of this method, namely the deviations from the square waveform when assessing homogeneous peaks caused by noise. This is particularly significant at the front and trailing edges of the chromatographic peak due to the variation of the signal-to-noise ratio across the peak. Moreover, as operator involvement is required to interpret the plot, this approach is not suitable for the automation required to facilitate future incorporation in an expert system.

In developing a potentially operator-independent technique to take advantage of the foregoing results, it was decided to explore the use of correlating multiple chromatographic peak areas (Fig. 4). This could overcome many of the problems such as noise, peak tailing and spectral skewing.

Previously, the peak-area approach has been applied using chromatograms at two wavelengths of detection [13], with limited success owing to shortcomings in the peak-integration software then available, together with the disadvantages that affect all forms of *AR* algorithm. As it has been shown that a reduced wavelength data set with data points spread equally over the whole spectrum of interest maintains spectral discrimination, the collection and integration of the chromatographic signal at a

representative number of wavelengths is possible using the detection system described. Hence the
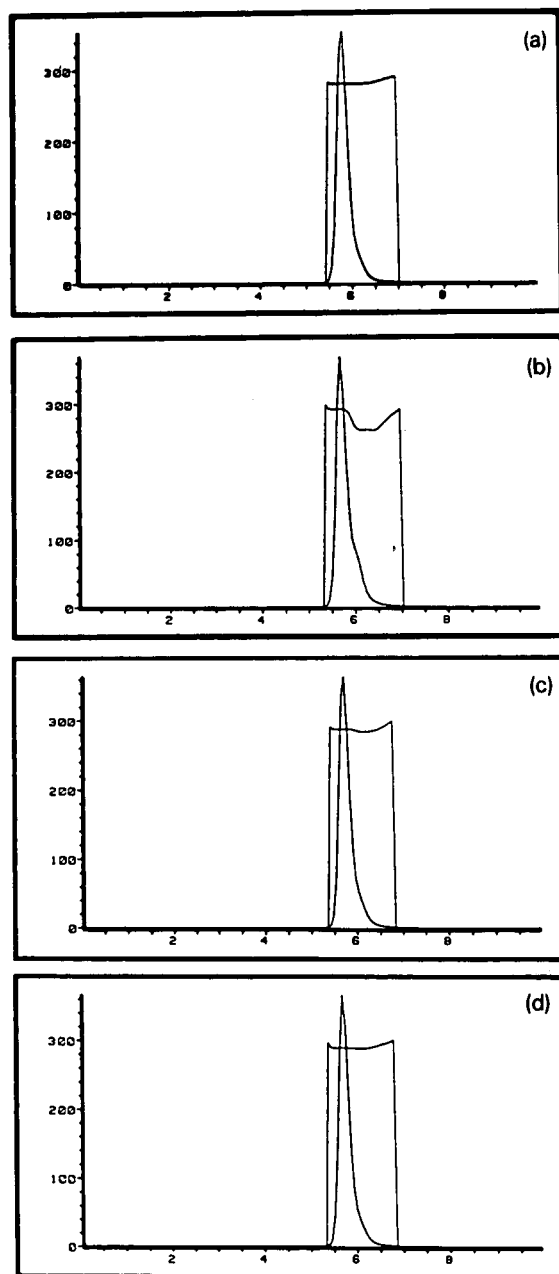
Fig. 3. Comparison of the absorbance ratio plot for (a) sulphasalazine with those obtained from partially co-eluted mixtures consisting of (b) sulphasalazine + 10% A, (c) sulphasalazine + 1% A and (d) sulphasalazine + 0.1% A. In all instances compound A elutes 0.45 min after sulphasalazine.
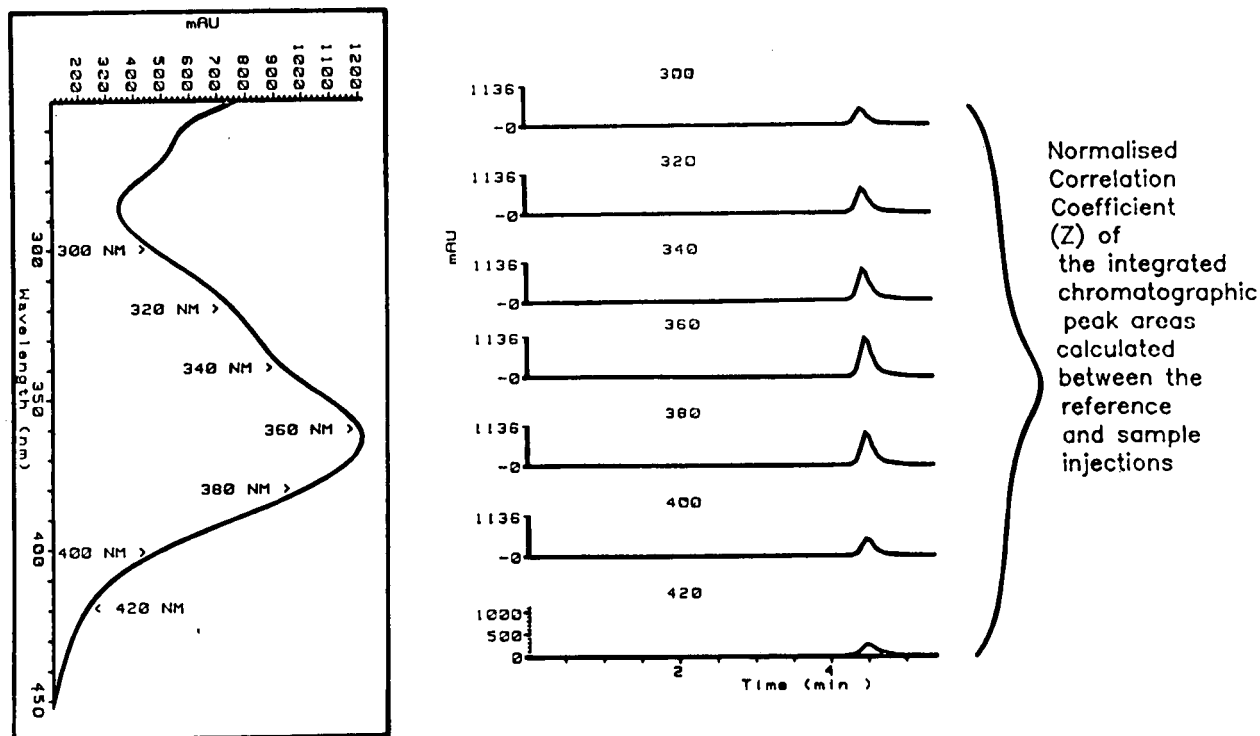
Fig. 4. The multiple peak area correlation technique.

TABLE IV

ASSESSMENT OF PEAK PURITY/HOMOGENEITY BASED ON CORRELATION OF CHROMATOGRAPHIC PEAK AREAS WITH THOSE FOR SULPHASALAZINE OF SIMILAR CONCENTRATION

Wavelengths used: 300, 320, 340, 360, 380, 400 and 420 nm. Triplicate injections (10 μg on-column) of each sample were correlated with triplicate injections of pure sulphasalazine.

Retention of compound A relative to sulphasalazine	Sample	Normalized spectral correlation		
		Mean ($n = 9$)	t-Value	Tabulated t ($P = 0.01$ one-tailed)
0 min	Reference sulphasalazine	9.45		
	Sulphasalazine + 10% A	4.77	39.9[a]	2.90
	Sulphasalazine + 1% A	7.05	22.3[a]	2.90
	Sulphasalazine + 0.1% A	9.29	1.41	2.72
+0.25 min	Reference sulphasalazine	8.26		
	Sulphasalazine + 10% A	4.74	20.7[a]	2.90
	Sulphasalazine + 1% A	6.88	8.10[a]	2.90
	Sulphasalazine + 0.1% A	8.82	−2.69	2.58
+0.45 min	Reference sulphasalazine	8.71		
	Sulphasalazine + 10% A	4.71	49.7[a]	2.82
	Sulphasalazine + 1% A	6.92	18.7[a]	2.65
	Sulphasalazine + 0.1% A	8.45	2.59[a]	2.55

[a] Denotes veliable detection of the presence of the impurity.

problems of wavelength selection can be overcome and consequently this allows operator-independent implementation. Further, high precision is now available in the integration algorithms used; indeed, a higher degree of correlation is observed between peak-area data than between apex data for many of the standards (Tables III and IV). This is analogous to the use of peak areas in analyte quantification.

It should be noted that, in the HP-1040 diode-array detector used, up to eight signal data collection channels exist, independent of spectra collection. The signal absorbance values are more accurate than spectral absorbances, as they are stored as three rather than two byte values. The use of other diode-array detectors, many of which rely on spectral data to reconstruct chromatographic plots at wavelengths other than that of the single wavelength at which the data was originally monitored, will clearly affect the implementation and the sensitivity of the peak-purity algorithm proposed.

In fact, a reliable single figure assessment of peak purity is obtained when multiple chromatographic peak area data are correlated with chromatographic data obtained from a reference sample, as shown in Table IV. Using the model system described, 1% of compound A in a mixture with sulphasalazine could be detected, regardless of the resolution between the two compounds, with quick and efficient use of the data collected, and without the need for prior knowledge of the impurity to maximize spectral discrimination. The general applicability of the t-test to this data is also shown in Table IV (and Tables I and III), although it is unlikely that the multiple peak-area correlation technique is truly detecting the presence of 0.1% of compound A at a 0.45-min difference in retention times. This highlights the approximate nature of the mathematical transformation and the probability-based statistical test used. In practice, such "borderline" samples could simply be re-tested. In addition, for a higher degree of confidence in the purity of a chromatographic peak, the confidence interval of the null hypothesis (i.e., that the sample peak and reference peak spectral characteristics are indistinguishable) could be lowered.

CONCLUSION

The use of the multiple peak-area correlation

technique minimizes the effects of variations in the signal-to-noise ratio of the data across the chromatographic peak, is not susceptible to the potential effects of spectral skewing and does not necessitate a knowledge of the spectral characteristics of possible simultaneously eluting species. Moreover, it gives a single figure purity parameter suitable for routine statistical analysis. Further work in this area is continuing.

ACKNOWLEDGEMENT

REFERENCES

1 J. Van Rompay, J. Pharm. Biomed. Anal., 4 (1986) 725–732.
2 British Pharmacopoeia 1988, HM Stationary Office, London, 1988.
3 The United States Pharmacopeia, United States Pharmacopeial Convention, Rockville, MD, 21st Revision, 1984.
4 N. Ostojic, Anal. Chem., 46 (1974) 1653–1659.
5 A. Bylina, D. Sybilska, Z. R. Grabowski and J. Koszewski, J. Chromatogr., 83 (1973) 357–362.
6 R. N. Smith and M. Zetlein, J. Chromatogr., 130 (1977) 314–317.
7 R. Yost, J. Stoveken and W. MacLean, J. Chromatogr., 134 (1977) 73–82.
8 P. C. White, J. Chromatogr., 200 (1980) 271.
9 A. F. Fell, H. P. Scott, R. Gill and A. C. Moffat, Chromatographia, 16 (1982) 69–78.
10 P. A. Webb, D. Ball and T. Thornton, J. Chromatogr. Sci., 21 (1983) 447.
11 A. F. Fell, H. P. Scott, R. Gill and A. C. Moffat, J. Chromatogr., 273 (1983) 3–17.
12 P. C. White and T. J. Catterick, J. Chromatogr., 280 (1983) 376.
13 A. F. Fell, H. P. Scott, R. Gill and A. C. Moffat, J. Chromatogr., 282 (1983) 123–140.
14 A. C. J. H. Drouen, H. A. H. Billiet and L. de Galan, Anal. Chem., 56 (1984) 971–978.
15 G. B. Marcelle, M. S. Ahmed, J. M. Pezzuto, G. A. Cordell, D. P. Waller, D. D. Soejarto and H. H. S. Fong, J. Pharm. Sci., 73 (1984) 396–398.
16 K. H. Law and N. P. Das, J. Chromatogr., 388 (1987) 225–233.
17 P. C. White and T. J. Catterick, J. Chromatogr., 402 (1987) 135.
18 P. C. White, Analyst (London), 113 (1988) 1625–1629.
19 A. F. Fell, T. P. Bridge and M. H. Williams, Anal. Chim. Acta, 223 (1989) 175–182.
20 E. L. Inman, M. D. Lantz and M. M. Strohl, J. Chromatogr. Sci., 28 (1990) 578–583.

21 A. F. Fell, J. B. Castledine, B. Sellberg, R. Modin and R. Weinberger, *J. Chromatogr.*, 535 (1990) 33–39.

22 J. G. D. Marr, G. G. R. Seaton, B. J. Clark and A. F. Fell, *J. Chromatogr.*, 506 (1990) 289–301.

23 J. Frank, Jzn, A. Braat and J. A. Duine, *Anal. Biochem.*, 162 (1987) 65–73.

24 H. J. P. Sievert, S. L. Wu, R. Chloupek and W. S. Hancock, *J. Chromatogr.*, 499 (1990) 221–234.

25 L. Huber, *Applications of Diode-Array Detection in HPLC*, Report 12-5953-2330, Hewlett-Packard, Avondale, PA, 1989.

26 J. C. Reid and E. C. Wong, *Appl. Spectrosc.*, 20 (1966) 320–325.

27 G. M. Clark and D. Cooke, *A Basic Course in Statistics*, Arnold, London, 2nd ed., 1983, pp. 333–337.

28 J. C. Miller and J. N. Miller, *Statistics for Analytical Chemistry*, Ellis Horwood, Chichester, Ellis Horwood, 1988, 57.

29 E. E. A. Askelof, N. Svartz and H. C. Willstaedt, *U.S. Pat.*, 2 396 145 (1946); *C.A.*, 40 (1946) 3472.

30 *HPLC Chemstation, Fact File*, Report 79994-90007, Hewlett-Packard, Avondale, PA, 1987.

31 A. C. Moffat (Editor), *Clarke's Isolation and Identification of Drugs*, Pharmaceutical Press, London, 2nd ed., 1986.

CHROMSYMP. 2473

Optimization of the separation of (6R)- and (6S)-leucovorin and evaluation of the robustness of the optimum

C. Vandenbosch, C. Vannecke and D. L. Massart*

Department of Pharmaceutical Analysis, Vrije Universiteit Brussel, Laarbeeklaan 103, B-1090 Brussels (Belgium)

ABSTRACT

The variable-size simplex approach was used to optimize the separation of (6R)- and (6S)-leucovorin diastereoisomers. The experimental parameters optimized were pH, ionic strength and percentage of propanol in the mobile phase. The optimization criterion was the valley-to-peak-ratio. Fourteen experiments were performed to obtain the optimum. The ruggedness of the optimum was evaluated by means of a partial factorial design for three factors.

INTRODUCTION

Leucovorin is a reduced folate that is used in combination with 5-fluorouracil for the treatment of colorectal and gastric carcinoma. Leucovorin contains two asymmetric carbon atoms. As L-glutamic acid is used for the chemical synthesis, racemic leucovorin consists of an equimolar mixture of 6R and 6S diastereoisomers. The 6S isomer is the biologically active form [1]. High-performance liquid chromatography (HPLC) can be used for the separation of stereoisomers, but stereoselective agents are necessary to perform these separations. Leucovorin diastereoisomers can be separated by means of a bovine serum albumin (BSA) chiral stationary phase [1]. An application to the analysis of plasma using column switching was reported by Wainer and Stiffin [2]. One of the columns was also a BSA column.

As the composition of the mobile phase influences the selectivity of the chromatographic system, it is important to optimize the different mobile phase parameters. Fell *et al.* [3] described the optimization of the enantioseparation of oxamniquine using a simplex design. Optimization procedures can be divided into two groups, sequential and simultaneous. Simultaneous optimization creates models for the chromatographic retention behaviour. In sequential optimization, one optimizes in a stepwise fashion without developing a model. The mobile phase composition in an experiment with such a procedure is determined from the results of the previous experiments. The simplex algorithm is a sequential optimization procedure. The rules for performing this algorithm have been fully described elsewhere [4].

This paper describes the optimization of the separation of (6R)- and (6S)-leucovorin on a BSA stationary phase by means of the simplex algorithm. The robustness of the optimum was evaluated by means of a saturated fractional factorial design.

EXPERIMENTAL

Apparatus

A Merck Hitachi L-6000 chromatograph with a Rheodyne loop injector (volume 100 μl) and a Merck Hitachi L-4000 variable-wavelength UV detector were used. The flow-rate of the mobile phase was 0.5 ml min^{-1} for all experiments. The detection

wavelength was 290 nm. Chromatograms were re-corded and integrated by a Shimadzu C-R6A Chromatopac.

The BSA column was a Resolvosil BSA-7 (150 mm × 4 mm I.D.), obtained from Macherey-Nagel (Düren, Germany).

Standards and reagents

1-Propanol was of HPLC quality and was supplied by Merck (Darmstad, Germany). Sodium dihydrogenphosphate monohydrate, disodium hydrogenphosphate dihydrate and phosphoric acid were of analytical-reagent grade (Merck) and were used for the preparation of the phosphate buffers. Milli-Q-purified water was used for the preparation of the buffer solutions. These solutions were filtered through a membrane filter (0.2 μm) before being used for chromatography.

Racemic leucovorin and (6R)- and (6S)-leucovorin (as sodium salts) were obtained from Lederle Labs.

Computer program

A computer program for the simplex optimization procedure is available [5]. It is written in BASIC and runs on an IBM-PC computer.

RESULTS AND DISCUSSION

The influence of pH, ionic strength (phosphate buffer) and percentage of 1-propanol in the mobile phase on the separation of (6R)- and (6S)-leucovorin was evaluated. 1-Propanol is recommended as an organic modifier by the manufacturer of the BSA phase. A variable-size simplex was used to optimize these parameters. As three parameters were
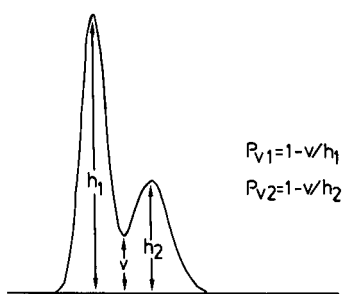
optimized, the resulting simplex contained four vertices and was thus a tetrahedron [4]. The algorithm is based on the rejection of the vertex giving the worst result. For a variable-size simplex, the search space is contracted or expanded [4]. To perform the optimization procedure, a criterion has to be chosen that expresses the quality of the separation. Therefore the expert system CRISE [6] was consulted. CRISE advises the valley-to-peak ratio (P_v) as a criterion. The calculation of P_v is illustrated in Fig. 1 [7]. If a complete resolution between two peaks is obtained, P_v becomes 1 as the height of the valley is zero. Fig. 1 shows that two P_v values can be calculated for a pair of peaks. Here, P_{v2} was calculated for each experiment, i.e., the valley height is divided by the height of the second peak.

The computer program calculated the experiments of the start simplex from the start and step values for each factor [5]. These values are shown in Table I. The start values represent a first guess, determined on the basis of preliminary experiments concerning the evaluation of the enantioselectivity of the BSA phase. The step values were chosen in order to make the search space as large as possible. For each factor, one also has to set the boundaries of the experimental domain. These can be determined from the advice of the column manufacturer (Table I). One should not exceed these limits in order to avoid denaturation of the protein.

Based on the P_v values of the first four experiments, the computer program calculated the mobile phase composition for the fifth experiment. Fourteen experiments were performed. The results of the experiments are summarized in Table II. Fig. 2 illustrates the movement of the simplex. The separate diastereoisomers were injected in each mobile phase: (6S)-leucovorin was the first-eluting diastereoisomer for each experiment. The optimization

Fig. 1. Calculation of the valley-to-peak ratio, P_v [7].

$P_{v1} = 1 - v/h_1$

$P_{v2} = 1 - v/h_2$

TABLE I

START AND STEP VALUES AND LIMITS FOR EACH MOBILE PHASE PARAMETER

Factor	Start value	Step value	Limits
pH	6	2	5–8
Ionic strength	0.1	0.1	0.05–0.20
1-Propanol (%)	0	0.5	0–5

TABLE II

RESULTS OF THE SIMPLEX OPTIMIZATION

Experiment No.	pH	Ionic strength	1-Propanol (%)	Valley-to-peak ratio, P_v	Capacity factor of second peak
1	6.00	0.10	0	0.05	5.44
2	8.00	0.10	0	0	0.97
3	6.00	0.20	0	0.09	3.31
4	6.00	0.10	0.5	0.17	4.69
5	7.00	0.12	0.10	0.05	2.39
6	6.70	0.18	0.40	0	1.65
7	6.20	0.12	0.10	0.09	4.45
8	5.10	0.16	0.30	0.81	12.3
9	5.50	0.06	0.61	0.66	21.7
10	5.85	0.11	0.28	0.16	5.76
11	5.75	0.11	0.45	0.13	6.19
12	5.06	0.10	0.63	0.86	21.4
13	5.49	0.11	0.48	0.62	13.4
14	5.10	0.16	0.30	0.81	12.3
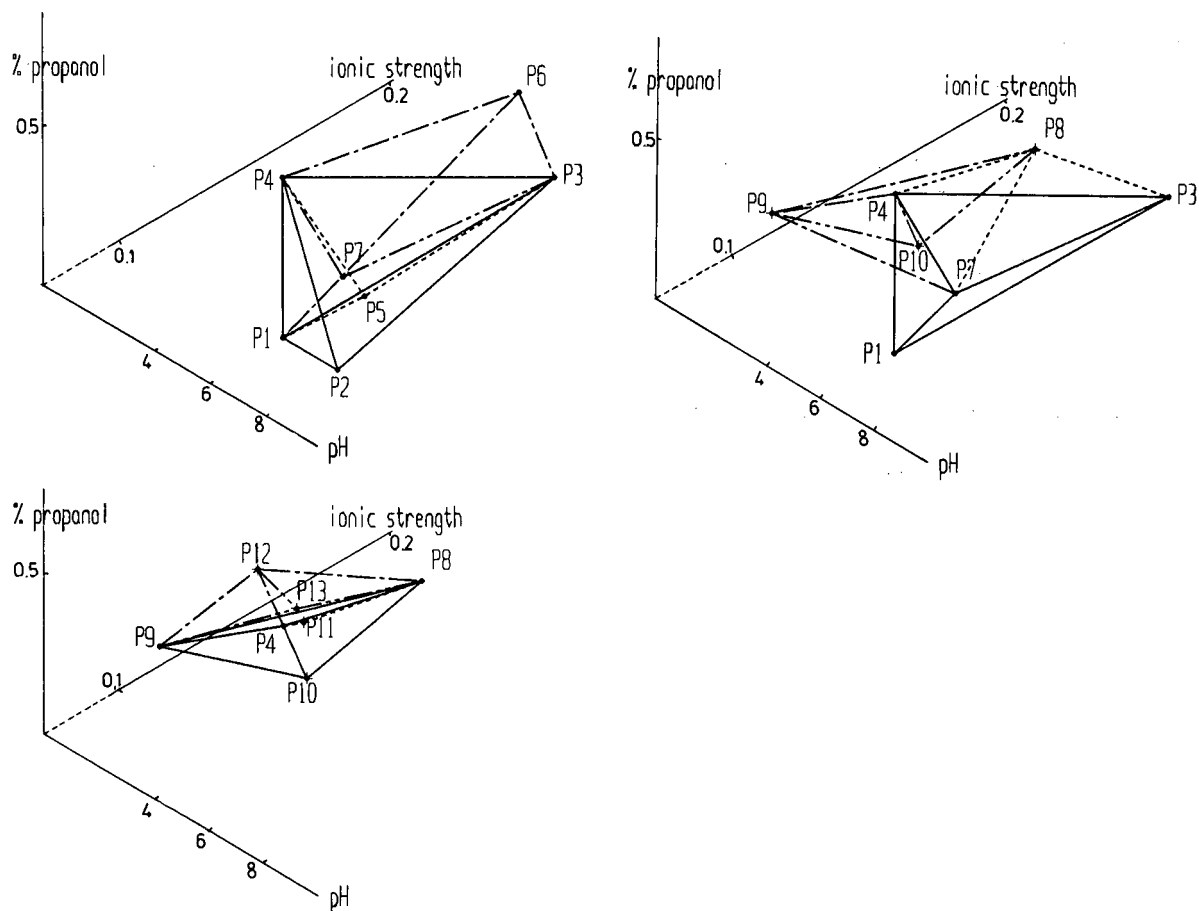
Fig. 2. Movement of the simplex.
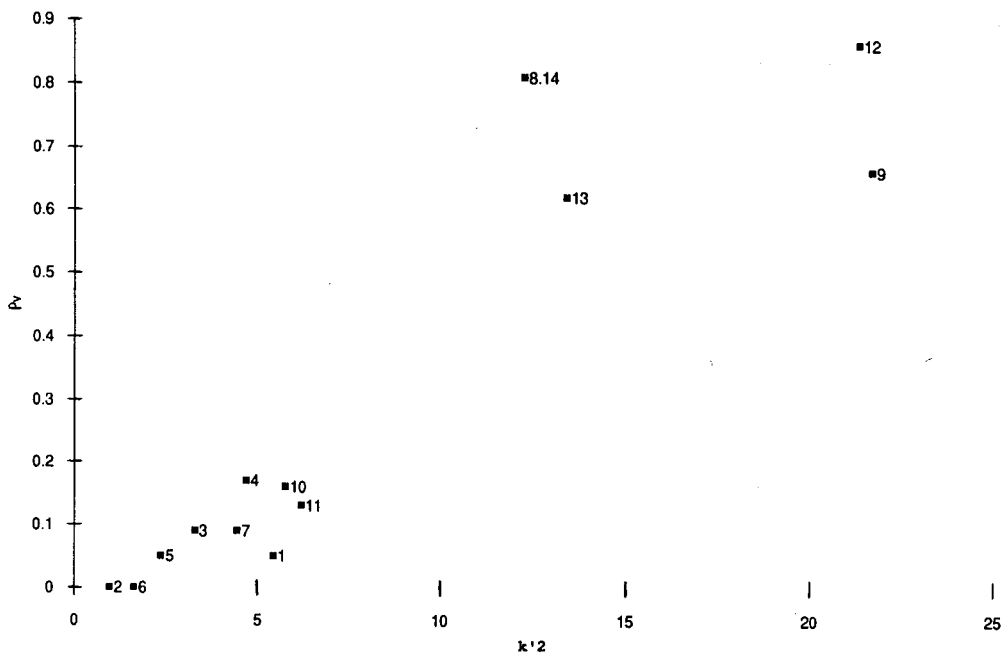
Fig. 3. Plot of P_v versus k'_2.

procedure was stopped as the mobile phase parameters for experiment fourteen were the same as those for experiment eight. The P_v value obtained for these experiments is 0.80 and approaches the maximum value of 1. Experiment 12 seems to give the best separation quality ($P_v = 0.86$). Resolutions calculated for these experiments are 1.29 and 1.33, respectively. The resolution of the separation described in the literature [1] was 1.65, but was achieved by coupling two BSA columns in series.

As the criterion P_v only measures chromatographic selectivity and takes no account of analysis time, the P_v values are plotted against the retention time of the second peak in Fig. 3. The purpose of this pareto-optimality plot [8,9] is to find the experiment with optimum separation versus analysis time characteristics. From Fig. 3, one can conclude that experiment 8 represents this optimum: the P_v value approaches unity and the time required for analysis does not become too long. The mobile phase parameters used in experiment 8 are pH 5.10, ionic strength 0.16 and 0.30% 1-propanol. The chromatogram in Fig. 4 illustrates the separation obtained with these mobile phase conditions.

The robustness of this optimum was evaluated by means of a fractional factorial design [4]. This was done to evaluate the influence of small changes in experimental conditions on the optimum. In this way, one can determine how accurately the different mobile phase parameters have to be set to obtain reproducible results (P_v values).
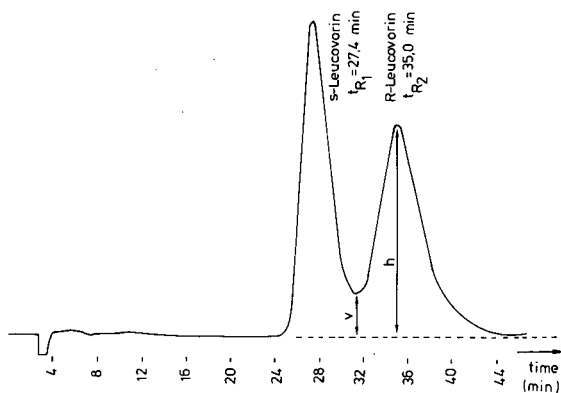
Fig. 4. Separation of (6S)- and (6R)-leucovorin with the optimum mobile phase (phosphate buffer pH 5.10, ionic strength 0.16, 0.30% 1-propanol).

TABLE III

TWO-LEVEL PARTIAL FACTORIAL DESIGN FOR THREE FACTORS

Experiment	Factor A	Factor B	Factor C
1	+	+	+
2	−	+	−
3	+	−	−
4	−	−	+

TABLE IV

PARTIAL FACTORIAL DESIGN TO EVALUATE THE ROBUSTNESS OF THE OPTIMUM

Experiment No.	Factor pH	Factor ion strength	Factor 1-propanol (%)	P_v
1	5.00	0.14	0.25	0.89
2	5.20	0.14	0.35	0.79
3	5.00	0.18	0.35	0.87
4	5.20	0.18	0.25	0.72

Here, a two-level partial factorial design in three factors was used to study the effect of small changes in mobile phase pH, ionic strength and percentage of 1-propanol on the P_v values. Each of the factors has two levels in the design, as indicated by + and − in Table III. Here, these levels were chosen so that the nominal value, *i.e.*, the exact value at which the optimum was obtained, was situated between them. The results of the experiments are shown in Table IV. The effect of factor A (D_A), for instance, was calculated as $[(P_{v1} + P_{v3})/2 - (P_{v2} + P_{v4})/2]$.

The main effect for each of the three factors was calculated and were as follows:

$$D_{pH} = \frac{(0.89 + 0.87)}{2} - \frac{(0.79 + 0.72)}{2} = 0.125$$

$$D_\mu = \frac{(0.89 + 0.79)}{2} - \frac{(0.87 + 0.72)}{2} = 0.045$$

$$D_{prop.} = \frac{(0.89 + 0.72)}{2} - \frac{(0.79 + 0.87)}{2} =$$

$$|-0.025| = 0.025$$

If changing the value of A has no effect on the results P_{vi}, one expects D_A to be close to zero. Factor A is regarded as significant if D exceeds $2s_D$ (s_D is the standard deviation of the difference between two averages, *i.e.*, the difference that expresses the effect of factor A) [4]. As the standard error of the mean of two measurements is $s/\sqrt{2}$, where s is the standard deviation of replicate measurements at the nominal level, s_D is equal to s.

The standard deviation s was determined by calculating the P_v values of eight experiments, performed at the exact nominal level for each factor. This standard deviation is 0.028. From the D values given above, on can conclude that only D_{pH} exceeds $2s = 0.056$. This means that the factor pH has to approach the nominal level more accurately than is the case with the two levels chosen here.

REFERENCES

1 K. E. Choi and R. L. Schilsky, *Anal. Biochem.*, 168 (1988) 398.
2 I. W. Wainer and R. M. Stiffin, *J. Chromatogr.*, 424 (1988) 158.
3 A. F. Fell, T. A. G. Noctor, J. E. Mama and B. J. Clark, *J. Chromatogr.*, 434 (1988) 377.
4 D. L. Massart, B. N. G. Vandeginste, S. N. Deming, Y. Michotte and L. Kaufman, *Chemometrics: a Textbook*, Elsevier, Amsterdam, 1988.
5 S. M. Deming and S. L. Morgan, *Instrumentune Up, IBM PC Version*, Elsevier Scientific Software, Amsterdam, 1984.
6 A. Peeters, L. Buydens, D. L. Massart and P. J. Schoenmakers, *Chromatographia*, 26 (1988) 101.
7 P. J. Schoenmakers, *Optimization of Chromatographic Selectivity: a Guide to Method Development*, Elsevier, Amsterdam, 1986, Ch. 4, p. 121.
8 H. R. Keller and D. L. Massart, *Trends Anal. Chem.*, 9 (1990) 251.
9 A. K. Smilde, A. Knevelmann and P. M. J. Coenegracht, *J. Chromatogr.*, 369 (1986) 1.

CHROMSYMP. 2450

Use of solvent selectivity optimization procedures for high-performance liquid chromatographic method development

S. D. Patterson

BP Research Centre, Chertsey Road, Sunbury-on-Thames, Middlesex TW16 7LN (UK)

ABSTRACT

Solvent optimization procedures for high-performance liquid chromatography (HPLC) method development have been used in the past, but have never become routinely established owing to the complexity of the task involved. A unique solvent optimization software package has been developed by Philips Research that reduces the complexity of the problem. The optimization software utilizes four solvents and data from a UV diode-array system, and requires only eleven experiments in order to produce an optimized isocratic method. It has proved to be a powerful tool for solvent optimization in HPLC method development, and has proved its ability to resolve complex chromatographic problems, reducing method development time considerably. The system produces isocratic methods which, when compared with similar gradient methods, have analysis times reduced typically by a factor of 3–4. The fact that isocratic rather than gradient methods are produced leads to the production of more robust methods that can be easily transferred to other HPLC laboratories for routine testing or quality control purposes.

INTRODUCTION

High-performance liquid chromatography (HPLC) has developed into one of the most useful and widely used analytical techniques. The range and variety of compounds that can be analysed by HPLC, coupled with its relative ease of use, have led to applications in fields ranging from industrial chemistry to biological science.

Chromatographers often spend a considerable amount of effort on method development, which can be a time-consuming and costly procedure, owing to the number of interactive variables involved. The composition of the mobile phase is the most influencial parameter with respect to solute selectivity, and is therefore highly significant in maximizing resolution for complex samples. It was thought that a mobile phase (solvent) optimization procedure would be of valuable assistance in reducing method development time and providing quicker, more robust HPLC methods [1].

The optimization of the mobile phase for HPLC separations can be classified into three main groups [1]: (1) grid search methods, in which a large number of experiments (typically between 50 and 100) are carried out and the best is chosen; (2) sequential methods, where the results of previous experiments are used to select a subsequent set of conditions, an example of this approach being the simplex method [2], in which typically between 25 and 30 chromatograms are required, but often local (and not global) optima are found; and (3) interpretive methods, where a model of retention data with varying solvent compositions is set up. Computer modelling of this data provides the optimum solvent composition. Only 7–10 chromatograms are required, and global optima are achieved.

This paper describes the use of an interpretive optimization software package developed by Philips Research. The use of reversed-phase separations of positional isomers and the analysis of aromatic carboxylic acids and amines will be demon-
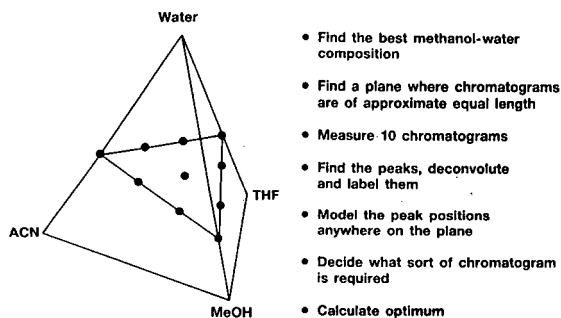
Fig. 1. Outline of the optimization procedure.

strated. The system was also used in a number of different modes of HPLC, including ion-pair, ion-suppression and normal-phase chromatography.

DESCRIPTION OF SOLVENT OPTIMIZATION SOFTWARE

The solvent optimization software package ("Diamond") has been specifically written by Philips Research for use on a diode-array detector. A brief outline of the procedure used by the solvent optimization system is given in Fig. 1.

The corners of the tetrahedron represent pure solvents, water, acetonitrile, methanol and tetrahydrofuran. For these solvents it is possible to define a plane which joins points of equal solvent strength. This is called the isoeluotropic plane, on which the total run time of the chromatograms will remain constant. The initial software calculates the location of the plane using data from a methanol–water gradient and solvent strength rules [3]. Once the plane has been located, the ten chromatograms (whose compositions are selected by the optimization software) are then run and the diode-arry data collected. After data collection, each chromatogram is processed; this involves (i) peak detection (using the second-derivative chromatogram) followed by deconvolution of any overlapping peaks using principal component analysis (PCA), (ii) reconstruction of chromatograms and spectra, using iterative target transformation factor analysis (ITT-FA) [4] and (iii) spectral matching against a reference set (both peak spectra and peak concentrations can be used for peak tracking and subsequent labelling, with a least-squares fit being applied for spectral matching).

For each peak, a mathematical retention model is fitted to the ten points on the plane. This is done using a piece-wise quadratic model. The end result of this process is that a "retention surface" is generated, which maps the movement of a peak with changing solvent composition. From the retention surfaces for all of the components, response functions can be calculated (and a response surface generated), which measure the quality of the chromatograms anywhere on the plane.

The global optimum solvent composition can be selected from this response surface and chromatograms at these points can be predicted. A number of response functions can be calculated depending on the criteria used to define a good chromatogram. The response functions available are described in detail elsewhere [5]. The response function can be adapted for all of the peaks or for a group of peaks which may be of interest. Thus, an optimum could be selected specifically for analytes of interest. Previous work [6] has shown that comparisons of predicted with actual data can be made, with typical errors of 1–2% being obtained.

EXPERIMENTAL

Chromatographic apparatus

The HPLC apparatus consisted of a Philips PU 4100 quaternary pump and a Philips PU 4021 diode-array detector. The samples were injected using a Valco C6W injection valve fitted with a 20-μl loop.

Software packages used for this work were the Philips PU 6003 diode-array detector software and Philips PU 6100 solvent optimization software. These packages were run on a Philips PU 3203 computer.

The HPLC columns used were 250 mm × 4.6 mm I.D. stainless-steel columns packed with (i) 5-μm octadecylsilane (ODS) packing material (Phase Separations, Clwyd, UK), (ii) 5-μm base-deactivated silica (BDS) packing material (Shandon, Runcorn, UK) and (iii) 5-μm cyanopropyl-bonded-silica (S5-CN) packing material (Phase Separations).

Chemicals and reagents

The solvents used included acetonitrile (ACN) (Romil Chemicals, Loughborough, UK) of far-UV

grade, methanol (MeOH), (Hichrom, Reading, UK) of HPLC grade. Tetrahydrofuran (THF), hexane, dichloromethane, 2-propanol and pentanesulphonic acid (all of HPLC grade) were from Fisons, Loughborough, UK. Water was purified by means of a Millipore Milli-Q system. Sample and standard materials were supplied by Aldrich (Gillingham, Dorset, UK), and BP Chemicals (Hythe and Hull, UK).

Solvent optimization

The solvent optimization package has been used in a number of different application areas to solve particular problems. The performance of the system was tested with different chromatographic modes, varying from the use of reversed-phase HPLC to ion-pair, ion-suppression and normal-phase chromatography.

RESULTS AND DISCUSSION

Positional isomers

The separation of two positional isomers was optimized using reversed-phase HPLC, and the results were compared with an initial gradient method which was developed previously [7]. This proved to

be a particularly testing example as the polarity and UV spectra of the isomers were very similar. The UV spectra differed by only 2 nm, but nevertheless were sufficiently different to allow accurate peak tracking of the two components.

The response function, S_{min}, was used for the optimization in order that the maximum resolution could be obtained between the two components. The response map or "solvent triangle" is produced, which is shown in contour form in Fig. 2. From this, the resolution of the two components can be observed at any given solvent composition. The optimum solvent composition is shown (cursor position, bottom right), with the chromatogram represented by a stick diagram showing the resolution obtained between the two components.

A comparison of the initial gradient method with the optimized isocratic method is demonstrated in Fig. 3. It can be seen that the resolution is significantly improved and the analysis time reduced by a factor of three using the optimized isocratic method.

Ion-pair HPLC

An initial gradient HPLC method was developed for the determination of aromatic amines. The gra-
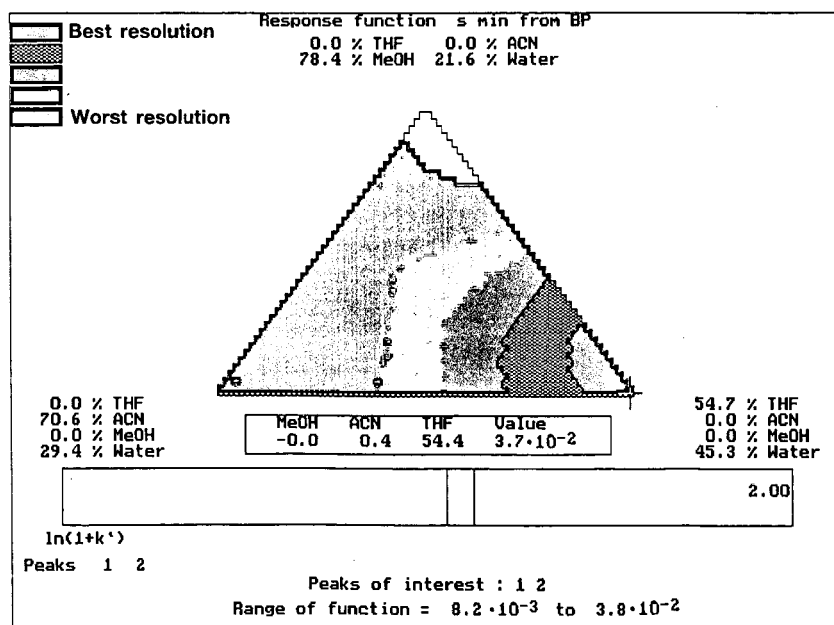
Fig. 2. Contour plot of the response function S_{min}.

dient method was subsequently optimized to produce a simpler isocratic method.

The response function R^* was chosen for the optimization in order to produce an even separation of all components. A comparison of the optimized method with the gradient method (Fig. 4) shows a reduction by a factor of three in the total analysis time. The original gradient method also suffers from solvent background peaks from the sulphonic acid ion-pairing agent, which were visible at the detection wavelength used. This was later overcome

by using the purer sodium salt (Fig. 5A), which was not available for this analysis. The isocratic method however, did not suffer from solvent background effects.

Ion-pair suppresion HPLC

The technique used for the analysis of a mixture of aromatic amines and acids has been termed ion-
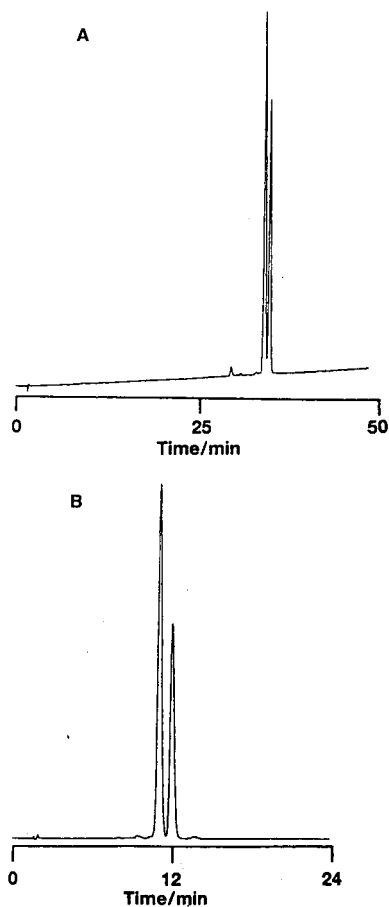
Fig. 3. Comparision of the initial gradient method with the optimized isocratic method. (A) Initial gradient method. Chromatographic conditions: mobile phase, (A) water–acetonitrile (80:20), (B) water–acetonitrile (20:80); gradient, 50–100% B in 50 min; column, 250 × 4.6 mm I.D. ODS; injector, Valco C6W, 10-μl loop; flow-rate, 1 ml/min; detector, UV, 280 nm. (B) Optimized isocratic method. Chromatographic conditions as in (A) except mobile phase, water–acetonitrile–methanol–THF (43:2:6:49).
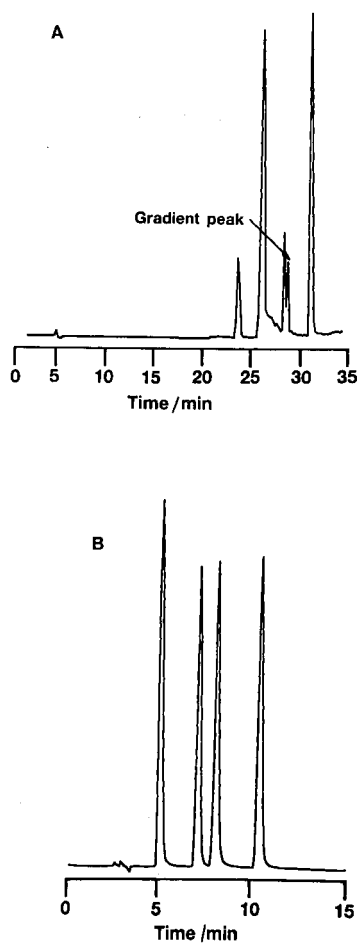
Fig. 4. Comparison of the initial gradient method with the optimized isocratic method. (A) Initial gradient method. Chromatographic conditions: mobile phase, (A) Aqueous 5 mM pentanesulphonic acid (pH 2), (B) methanol–water (60:40)–5 mM pentanesulphonic acid (pH 2); gradient: 0% B, 0–15 min, 0–20% B, 15–30 min, 20–100% B, 30–35 min, 100% B, 35–40 min; column, 250 × 4.6 mm I.D. BDS; flow-rate, 1 ml/min; injector, Valco C6W, 20-μl loop; detector, UV, 225 nm. (B) Optimized isocratic method. Chromatographic conditions as in (A) except mobile phase, water–acetonitrile (97:3)–5 mM pentanesulphonic acid (pH 2).
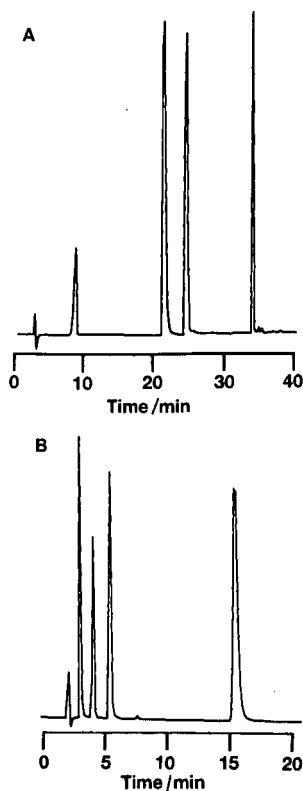
Fig. 5. Comparison of the initial gradient method with the optimized isocratic method. (A) Initial gradient method. Chromatographic conditions: mobile phase, (A) aqueous 5 mM sodium pentanesulphonate, (B) acetonitrile–water (70:30)–5 mM sodium pentanesulphonate; gradient: 5% B, 0–5 min, 5–15% B, 5–20 min, 15–100% B, 20–25 min; column, 250 × 4.6 mm I.D. BDS; flow-rate, 1.3 ml/min; injector, Valco C6W, 10-μl loop; detector, UV, 230 nm. (B) Optimized isocratic method. Chromatographic conditions as in (A) except mobile phase, water–THF (69:31)–5 mM sodium pentanesulphonate.

pair suppression. This uses sodium pentanesulphonate, which acts as an ion pair towards amines and a suppressor towards acidic functional groups.

The optimization procedure using the response function S_{min} predicted an optimum for the four-component separation in the "THF corner". A comparison of the initial gradient method with the optimized method (Fig. 5) again demonstrates the significantly reduced analysis time achieved.

Another important aspect of the optimization software is its value when used in conjunction with preparative chromatography, where only certain components may be of interest. Optimization for selected components can be performed, which may allow purer fractions to be collected.

Ion-suppression HPLC

The use of ion-suppression reversed-phase chromatography enabled a mixture of phthalate components to be analysed. When this method was optimized using the response function, S_{min} the optimum was again to be found in the "THF corner". This is shown in Fig. 6 as a response surface, which is an alternative view to the contour map display. Most of the methods developed within our laboratory are gradient elution methods with acetonitrile or methanol as the organic modifier. These solvents have a low UV absorbance, which is essential in gradient elution chromatography, particularly with low-wavelength UV detection. However, it has been observed that in the examples demonstrated here, THF is often the best solvent in terms of analyte selectivity, and as isocratic methods are produced the higher UV absorbance of THF is immaterial. This demonstrates the particular use of solvent selectivity optimization, whereby the best solvent for the component separation is selected.

Normal-phase HPLC

The optimization software was primarily developed to be used with reversed-phase chromatography. It can, however, be used to optimize separations for temperature, pH, buffer concentration or for normal-phase chromatography. Care is needed, however, when using these other modes, especially when applying this to normal-phase chromatography.

The reversed-phase solvents water, acetonitrile, methanol and THF were replaced with hexane, 2-propanol, dichloromethane and THF. The initial location of the isoeluotropic plane has to be done manually, as there are no solvent strength rules for normal-phase solvents programmed into the software. However, this can be done using a knowledge of the solvent strengths and, after location of the plane, the optimization procedure is the same as that outlined previously.

A method was developed originally to separate a five-component test mixture (2-nitrophenol, bromoacetophenone, dinitrobenzene, 4-butylphenol and 4-bromophenol) using a normal-phase gradient system. The solvent system was then optimized,
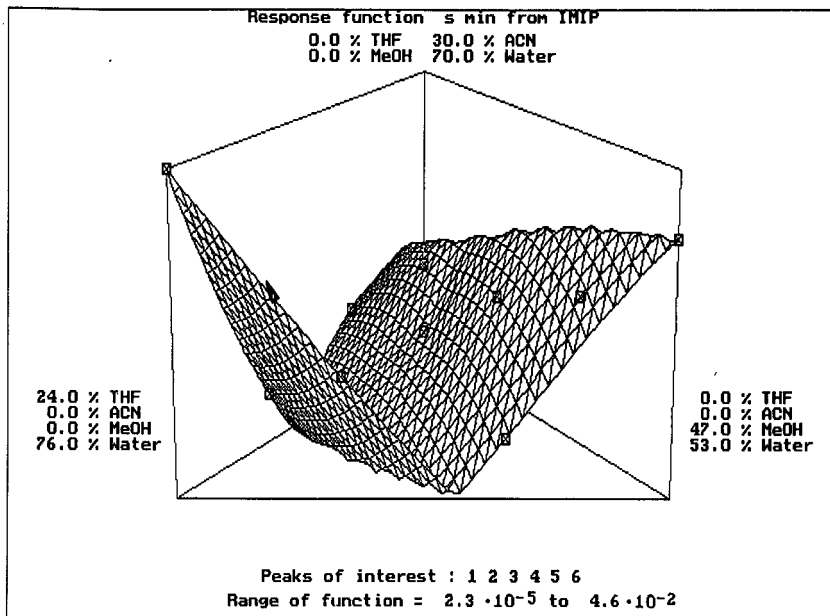
Fig. 6. Response surface of the S_{min} function.

producing an isocratic method with an analysis time of one third of the gradient method.

The effect of three different response functions (S_{min}, St_{min} and R^*) on the position of the optima were studied. A comparison of the chromatograms obtained at each optimum is shown as a stick diagram in Fig. 7. The S_{min} function produced an optimum to provide maximum resolution of the two least resolved peaks. The St_{min} function produced an optimum using the same criteria but biased for minimum retention time, thus providing reduced analysis time. If the most even spacing of peaks is required, the R^* function is used, and a more even distribution of peaks is observed.

CONCLUSIONS

The solvent optimization software package described here provides a unique optimization facility which allows methods to be optimized for resolution and analysis times. It provides a user-friendly environment where parameters can be readily modified, unlike "black box" systems in which optima are produced without user consultation. Optima are produced according to criteria which are manually selected, and the user can inspect and modify data at each stage. The optimization software does have its limitations; it can only be used for analytes with a UV response and the software itself is expensive. However, approximately 80% of the work we carry out utilizes UV detectors and, in a busy laboratory,
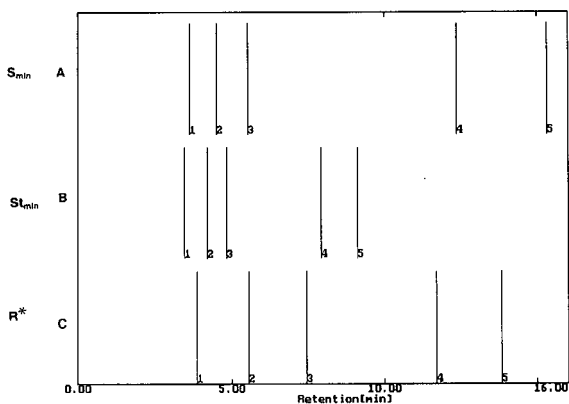
Fig. 7. Chromatograms obtained using the response functions (A) S_{min}, (B) St_{min} and (C) R^*. (A) Mobile phase: 2-propanol–dichloromethane–hexane (0.7:11.4:87.9); (B) mobile phase: 2-propanol–dichloromethane–THF–hexane (0.4:18.4:0.9:80.3); (C) mobile phase: 2-propanol–hexane (1.1:98.9). Components: 1 = 2-nitrophenol; 2 = bromoacetophenone; 3 = dinitrobenzene; 4 = 4-butylphenol; 5 = 4-bromophenol.

the software could pay for itself within 1–2 years on savings in analysis time alone.

It has already proved an invaluable tool for HPLC method development and has proved a significant benefit within our laboratory, reducing analysis times typically by one third. It has the capability to optimize on selected components, which should prove useful in preparative chromatographic applications. It has proved to be a highly beneficial chromatographic tool for developing HPLC methods and in reducing method development time. The optimized methods are generally more robust than existing gradient methods and are therefore readily transferable to other HPLC laboratories for routine analysis or quality control purposes.

REFERENCES

1 P. J. Schoenmakers, *Optimization of Chromatographic Selectivity*, Elsevier, Amsterdam, 1986.
2 J. C. Berridge, *J. Chromatogr.*, 244 (1982) 1.
3 L. R. Snyder and J. J. Kirkland, *Introduction to Modern Liquid Chromatography*, Wiley, New York, 1979.
4 P. J. Naish, R. J. Lynch and T. Blaffert, *Chromatographia*, 27 (1989) 343.
5 P. J. Schoenmakers, *J. Liq. Chromatogr.*, 10 (1987) 1865.
6 G. Measures and R. J. Lynch, *Lab. Pract.*, 39, Jan. (1990) 61.
7 S. D. Patterson, R. E. A. Escott and R. J. Lynch, *LC · GC Int.*, 9 (1990) 54.

CHROMSYMP. 2498

CRISEBOOK, a Hypermedia version of an expert system for the selection of optimization criteria in high-performance liquid chromatography

B. Bourguignon, P. Vankeerberghen and D. L. Massart*

Vrije Universiteit Brussel, Farmaceutisch Instituut, Laarbeeklaan 103, B-1090 Brussels (Belgium)

ABSTRACT

Expert systems built in shells such as KES suffer from a lack of easy maintenance, prototyping and a user-friendly man–machine interface. To solve these problems, the feasibility of using a Hypermedia approach was investigated. The reimplementation of the expert system CRISE, an object-oriented decision tree, in Toolbook was promising as a first application. The structure and features of the reimplemented system are described and similarities and differences with the KES version are discussed.

INTRODUCTION

Our laboratory has been involved in the development of several stand-alone expert systems for chromatographic method development [1–5], which were subsequently integrated in a complex expert system [6,7]. Both the stand-alone systems and the integrated system were developed with the aid of a shell. It was found that such expert systems present some problems [8].

One of these problems is the lack of easy maintenance. Expert systems must be easy to maintain. Especially in "first-guess" expert systems (systems that recommend the first mobile phase to be tried out [3,4], the user should be able to add new information and delete redundant knowledge as much as possible by himself. Indeed, technology changes and expert systems that are not updated would rapidly become obsolete. With the conventional present shells, it is difficult for the user to make changes owing to the way rules are connected to each other by such a system. Adding or changing rules could have repercussions all over the system. Moreover, some shells require advanced skills of knowledge engineering. This also implies that it is not easy to build a prototype without investing

significant resources. Another problem concerns the man–machine or user interface, the part of the expert system that guides the user through the various steps of the consultation. Because most often the expert system functions as a dynamic information source for inexperienced occasional users, a user-friendly man–machine interface is very important. In KES, little attention is paid to the presentation and one must write a front end in C to make this more acceptable.

To solve these problems, we decided to examine Hypermedia tools. One of the first applications of Hypermedia tools in the domain of chemical analysis was proposed by Farkas *et al.* [8]. They developed SpecTool, a software package having Hypermedia features, as a help for the interpretation of NMR, MS, IR and UV–VIS spectra. Their system functions primarily as an information source and not as an expert system because it does not make decisions.

HYPERMEDIA

Hypermedia is the combination of multimedia and hypertext. In a hypertext document the user does not have to read all information in a sequential

way, but is guided, according to his needs and interests, to pieces of information that are linked to each other. Multimedia is a collection of tools producing graphics, sound and animation, to present data in a more flexible way. The prototype of a software construction set with Hypermedia features is Hypercard, which runs on a MacIntosh PC. Hypercard combines the properties of both the relational database and an authoring system. By applying the relational capabilities, links can be created between individual files so that one can access from one file related information in another file. The distinction between Hypercard and a traditional database management system is the way of displaying information, which is provided by the authoring system. This system includes many kinds of tools such as painting, creating fields and buttons which are fundamental to build an efficient user interface. Hypermedia applications use object-oriented languages, such as Hypertalk in the Hypercard environment. In such a language, the author writes instructions to alter the behaviour of created objects (*e.g.*, Hypercard's stacks, collections of cards). In our experience, first-guess expert systems are really decision trees, at least in some instances, and Hypermedia can be used to create such trees. Therefore, it was decided to investigate their use for knowledge-based systems in this application area.

As a first application, we investigated the suitability of Toolbook [9], an IBM version of Hypercard, to reimplement an expert system called CRISE [5] that was built in a traditional expert system shell. The choice of the software was dictated by our IBM hardware. The reimplementation is called CRISE-BOOK.

Toolbook features two distinct working levels, namely an author and a reader level. It allows the author to create applications for readers for various purposes, such as information management, entertainment and education [10]. Applications are composed of one or more "books" (which are similar to stacks in Hypercard). Books contain "pages". A page is made up of a background and a foreground. Whereas the former is a template shared by a certain number of pages, the latter is unique to that page. Background and foreground may both contain objects such as buttons, fields and graphical objects. All those objects are part of the object hierarchy (Fig. 1), which determines the order in which
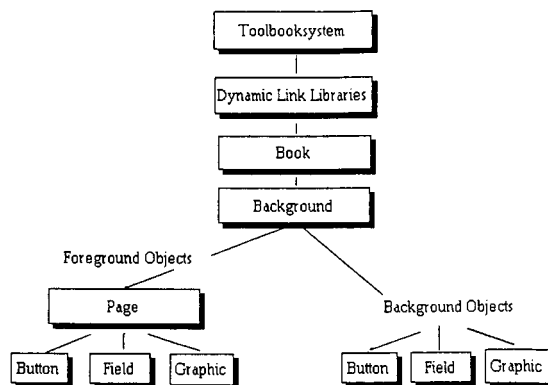
Fig. 1. CRISEBOOK's object hierarchy.

messages pass from one object to another. For each object, the author can write a script, a series of instructions, called statements, in Toolbooks's object-oriented programming language OpenScript [11,12]. As in Hypertalk, scripts may link all kinds of objects, which was most important to us in the reimplementation of CRISE. It may also show a hidden text or a button, do calculations, play sounds or modify pictures to introduce some animation and to customize the user interface to the needs of the end-user.

THE EXPERT SYSTEM

CRISE (*Cri*terion *Se*lection), was an expert system developed to assist the chromatographer in the selection of suitable optimization criteria [5]. As it was built in KES (Knowledge Engineering System, release 2.5), it suffers from the previously described problems. KES is a mid-sized expert system building tool that is mainly rule-based, but also supports frame-like structures and backward and forward chaining. A KES knowledge base is structured into an attribute section, for defining the characteristics of the problem, a rule section and an action section that guides the expert system to seek appropriate information.

CRISE consists of four modules. In the first module the most suitable elemental criterion is selected to quantify the extent of separation between two adjacent peaks in the chromatogram. Resolutions (R_s), separation factors (S), separation factors corrected for plate counts (S_N) but also expressions

such as peak–valley ratios (P, P_v, P_m) can be used. As R_s, S_N and S do not take into account a possible loss in resolution due to non-ideal situations (*e.g.*, large matrix or solvent peaks), corrections may be required and this is investigated in module 2. Module 3 assists the user in the selection of weighting factors to make a difference between peaks according to their relevance or relative importance. In the last module, the elemental criteria are incorporated in the global optimization criterion that is best suited to quantify the separation quality of the entire chromatogram taking into account the purpose of the separation.

Organization

It was decided to keep all the associated information together and thus to create one book. In a book, information can be organized in different ways, such as a series of pages, object networks or a hierarchical form, depending on the content of that information and on the way the reader is expected to use it. We decided to organize CRISEBOOK as a hierarchy and more precisely as a decision tree, first because this kind of organization fits in best with the hierarchical structure of the knowledge and also because it offers advantages for both the user and the author. The user, by choosing between different options, is guided to a particular piece of information, whereas for the author it will be easier to "write" the book. In Toolbook, the representation of knowledge is supported by object-oriented programming and rules. Those, representation facilities are perhaps more limited than in shells such as KES, where also framelike structures can be built [3], but appeared to be powerful enough to implement the knowledge base without problems. The ruleset is subdivided into scripts, smaller rulesets, which is impossible in KES and results in a better structured knowledge base.

The authoring is made easier by preprocessing, which means that a great deal of the programming has already been done. Consider, for instance, the creation of an object such as a button. The author only has to click the button tool, drag a button on the screen and adjust its size with the cursor. For the linking of pages, instead of writing a script, one can use the "link to" or "link with" function of buttons. Toolbook automatically creates a script and for the latter function even a return button is created on the

Script for button "a" of page "page 15".

```
To handle buttonUp
        if button a is false then
                go to page "page Rs"
        else
                go to page "page 30"
        end if
end buttonUp
```

Fig. 2. Example of a button script for two mutually exclusive options.

destination page. If one wants to perform unpreprocessed events and needs to write a script, this can be done in a very English-like syntax, as shown in Fig. 2. This syntax is one of the strengths of object-oriented languages such as Hypertalk and OpenScript and allows one to write scripts that are entirely readable even for those unfamiliar with programming. As in the knowledge engineer interface of most expert system building tools [13], tracing facilities allow the author to investigate the order in which statements in a script are executed. Scripts can also be checked on syntax and runtime errors by using the Script window (check syntax command) or the Debug window, respectively.

As an example, let us consider the structure and the way of executing a buttonscript in Fig. 2. The aim of this script is to display the page named "page thirty" if button a is clicked, or else to display the page with a message concerning the resolution. The if/then/else control structure tells Toolbook to execute a specific statement if a specific condition is true. In conditions, functions and logical operators (*e.g.*, or, is not, and) can be called. If the user clicks the button, Toolbook will send the message "buttonUp" to that button. On condition that the button contains one or more statements to be executed on arrival of that message, Toolbook will do so and thus display page 30. If the object's script does not contain such statements, the message will be sent to the object that is the next higher level in the object hierarchy (Fig. 1), which in this example would be the page that contains the button.

To answer most of the questions the user has to select only one of two mutually exclusive options (for instance, yes/no) and an example of such a buttonscript is given in Fig. 2. If there are more than two options and they are not mutually exclusive, a

Script for button "answer" of page 1".

```
To handle buttonUp
        step i from 1 to 4
                if the hilite of button i is false then
                        put "x" after answer
                else
                        put "0" after answer
                end if
        end step
        put "page"&space&quote&answer&quote into comment page
        go to comment page
end buttonUp
```

Fig. 3. Example of a checkbox button script.

different kind of buttons, namely checkbox buttons, is applied. Consider, for instance, the question "Which descriptive parameters can you determine in the chromatogram?" Four options are offered to the user, which means that he can answer one of sixteen possible combinations. In addition to the four buttons with possible answers, a fifth button was created ("this is my answer") which the user has to click after he has clicked one or more of the other buttons. In the script of the fifth button (see Fig. 3), a "loop" with the "step" command was applied. With this command the author can instruct Toolbook to execute one or more statements a certain number of times. "Highlight" is one of the several button properties that can be changed by the author. It

means that a button will flash when a reader clicks it, and hence that a visual signal will be shown. The "quote" constant and the "&" operator are used to include quotation marks as part of a string. With the "go to" command the user is referred to the page with the name "answer". All buttons are thus checked in a certain order and the answer is put in the variable "answer" in the form of a binary code, for instance 00xx if buttons 3 and 4 out of buttons 1, 2, 3 and 4 are clicked. The principle of this method is the translation of a number of clicked buttons into a binary number that is the name of the page to which the user has to go.

Altogether, CRISEBOOK includes 195 pages. Creating pages for each possible combination of answers does not necessarily result in a larger total development time and offers the important advantage that conflicting selections are error trapped. Consider, for instance, the selection of the required corrections to the elementary criteria R_s, S_N or S. If one or more corrections are selected together with the option "no correction", the user is informed of his conflicting answers. The question is asked again to determine with more certainty whether "some" or "no" corrections are required.

Presentation
        Compared with the end-user interfaces of, *e.g.*,
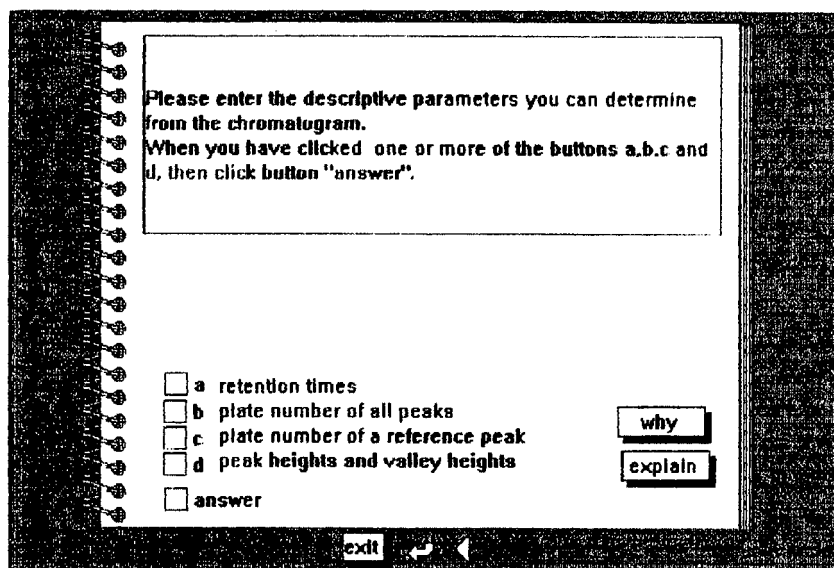
Fig. 4. Example of a page with a question.

Delfi-2, Apes and KES [13], Toolbook's interface is not standardized and hence can be customized to the needs of the user. It was decided to display on each page one question with the possible answers or a message. For each question, a number of buttons are created, equal to the number of possible answers to that question (Fig. 4). The user answers by clicking with the mouse on the button(s) next to the correct answer(s) and the result is that a following page appears with a new question. For pages with a question, the same background with three navigation buttons was always applied. The buttons allow the reader to go back through the pages that have been accessed one at a time (and thus to recall previous questions and change given answers) (arrow in Fig. 4), to go to the first page (and thus to restart the consultation) (triangle) or to leave the system (exit). In the end-user interface of KES it is not possible to recall previous questions. Consider, for instance, the case that the user has changed his mind after answering a question that is nearly at the end of the consultation. In the KES version he has to stop the consultation and start again by answering all previous questions, whereas in CRISEBOOK he only has to click the correct navigation button. Those buttons will appear in the same position and size on each page that shares that background. This enhances the conformity and hence also the user-friendliness of the system. If necessary, "explain" and "why" buttons are provided in addition to answers buttons. Questions and messages are typed in fields, most often record fields, with a scrollbar if not all of the text can be shown in the field. Pull-down menus allow the user, for instance, to print pages or to use the History command (see further). These additional features obviously represent an important advantage compared with the KES version. Another improvement of the man–machine interface was obtained by the introduction of graphics, by applying drawing tools, to explain p-type criteria, which cannot be explained well by definition alone (Fig. 5). Graphics cannot be provided in KES. With Toolbook's various representation facilities such as pattern-, drawing-, tool- and line-palettes and windows, a greatly improved overall representation of CRISE was achieved. As Toolbook runs in Windows, its preprocessed screen layouts (windows, menus, etc.) are in accordance with Extended CUA (Common Usser Access), IBM-

defined standard rules to regulate preprocessed screen layouts, among other things [14]. This offers the important advantage that one can switch from one CUA software tool to another because similar icons and menus will always appear at the same place.

An important feature, difficult to achieve with shells, is that at the end of the consultation an overview of intermediate results can be provided with system variables. Their values remain available in the variables while an instance is running and are changed in accordance with the statements in the scripts of CRISEBOOK's objects that are open in that instance. Although the overview was restricted to intermediate suggestions (selected elementary criterion, required corrections, use of weighting factors and selected global criterion), by using system variables it also is possible to provide a kind of "tracer window". Such a window could correspond to a page where all answers of the consultation process are represented so that the user can follow the reasoning process more easily. A list of the names of the last 100 pages accessed in a session can be displayed selecting the History command in a pull-down menu. If all pages are given a descriptive name related to the content of the message or to the question, the reader can also have in this way an overview of the path he has followed.

A validation of CRISEBOOK was accomplished by applying simulated test cases. All possible combi-
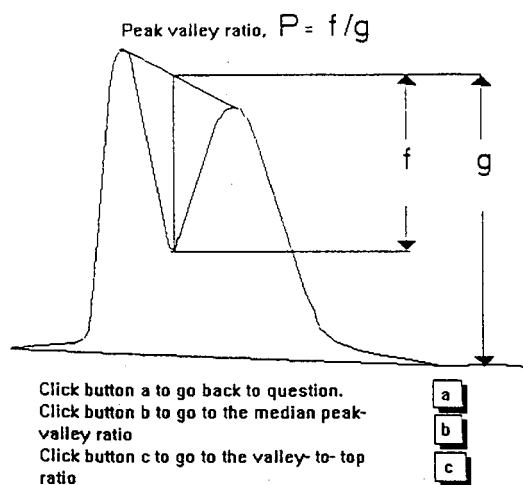
Fig. 5. Example of a graphic: the peak–valley ratio.

nations of answers were tried out and each time it was checked whether the script of the clicked button(s) referred to the correct page. This allowed us to fine-tune and optimize the system further and to test the ease of adding or deleting pages and thus of updating the system. To update one has to change only the previous script that leads to the new page; all following pages are renumbered automatically. This ease of updating is considered to be an important advantage, as explained in the Introduction. Suppose, for instance, that an additional question should be included. In CRISEBOOK one has to create a new page with buttons and with fields for the question and possible answers. The scripts of the buttons on the page that is just before have to be changed. Expanding the KES version with the same question requires a much more detailed and thus time-consuming analysis of the whole program. Changing a rule migth have consequences not only in the part that follows immediately, as is the case in CRISEBOOK, but also in rules that are elsewhere in the program and for which consequence seem much less evident. How easy it is to maintain a hypertext program in the long run is not clear yet. However, as for all types of programs, a good analysis of the system before starting the actual programming is certainly needed.

The system also has some disadvantages. One is that a full listing of all screen displays of the whole knowledge base is not possible unless a program is written, such as Hyperreporter on the MacIntosh, to print out the scripts of all objects in an application. The slow running of CRISEBOOK is not considered to be an important drawback. However, speed probably would become a real problem when external programs (see further) are added.

Algorithmic tools and external programs

CRISE and CRISEBOOK are restricted to the selection of the criterion. Therefore, they do not need any calculations and it is not yet clear how good Hypermedia will be in applications that do require computations. It is possible to perform calculations in Toolbook by means of arithmetic functions, such as average, log, tan. OpenScript has 40 of such built-in functions, each representing a particular operation that returns a value based on the values the user gives it. The author can add capabilities that are not provided in Toolbook, by

applying Dynamic Link Libraries (DLL). DLL functions as an interface between Toolbook and any non-Windows application. These are separate programs the author can create with Microsoft C, Pascal or Assembler language to add new functions to OpenScript. To perform tasks that require other Windows applications, one can use Dynamic Data Exchange (DDE), a set of rules that defines communication between Toolbook and any other Windows application. Programming under windows is not easy and this might create problems.

For the practical use of the expert system, a runtime version of Toolbook was created which allows a user who has Microsoft Windows 3 to use CRISEBOOK without having the development version of Toolbook.

CONCLUSIONS

By applying Toolbook to reimplement CRISE, a system was obtained with an attractive user interface that is easy to update. Toolbook has also most of the other essential features desired in the implementation of the knowledge base such as ease of prototyping, the possibility to add external programs, a runtime version on a PC computer, "why" and "history" facilities and a way of dividing the knowledge base into subdomains. The main drawbacks are the lack of speed and the large amount of memory required (2–8 MB, depending on whether sample and help books are also installed). Hypermedia certainly is a convenient way of implementing knowledge that is in the form of or that can be translated to if/then rules, as is the case in CRISE. It is to be expected that further developments in the field of hypermedia will eliminate some of the still existing drawbacks and make it a generally valid alternative to expert system shells. It is our intention to apply this approach to several other applications in the near future.

REFERENCES

1 M. De Smet, G. Musch, A. Peeters, L. Buydens and D. L. Massart, *J. Chromatogr.*, 485 (1989) 237.

2 M. De Smet, A. Peeters, L. Buydens and D. L. Massart, *J. Chromatogr.*, 457 (1988) 25.
3 R. Hindriks, F. Maris, J. Vink, A. Peeters, M. De Smet, D. L. Massart and L. Buydens, *J. Chromatogr.*, 485 (1989) 25.
4 F. Maris, R. Hindriks, J. Vink, A. Peeters, N. Vanden Driessche and D. L. Massart, *J. Chromatogr.*, 506 (1990) 211.
5 A. Peeters, L. Buydens, D. L. Massart and P. J. Schoenmakers, *Chromatographia*, 26 (1988) 101.
6 T. Hamoir, M. De Smet, H. Piryns, P. Conti, N. Vanden Driessche, D. L. Massart, F. Maris, H. Hindriks and P. J. Schoenmakers, *J. Chromatogr.*, in press.

7 P. Conti, T. Hamoir, M. De Smet, H. Piryns, N. Vanden Driessche, F. Maris, H. Hindriks, P. J. Schoenmakers and D. L. Massart, *Chemometr. Intell. Lab. Syst.*, 11 (1991) 27–35.
8 M. Farkas, M. Cadish and E. Pretsch, *Scientific Computing and Automation*, Elsevier, Amsterdam, 1990.
9 *TOOLBOOK*, Asymmetrix, Washington, DC, 1989.
10 *Using TOOLBOOK*, Asymmetrix, Washington, DC, 1989.
11 *Using OpenScript*, Asymmetrix, Washington, DC, 1990.
12 J. M. Pierce, *Toolbook Companion*, Microsoft Press, Washington, DC, 1990.
13 J. A. van Leeuwen, *Ph. D. Thesis*, University of Nijmegen, 1990.
14 D. Bartels, *DOS*, 5 (1990) 66.

Chromatographic separation and molecular modelling of triazines with respect to their inhibition of the growth of L1210/R71 cells

Klára Valkó*

Central Research Institute for Chemistry, Hungarian Academy of Sciences, P.O. Box 17, H-1525 Budapest (Hungary)

Péter Slégel

EGIS Pharmaceuticals, P.O. Box 100, H-1475 Budapest (Hungary)

ABSTRACT

The potential anti-cancer activity of triazines was characterized by the inhibition of the growth of L1210/R71 cells. The retention times for fifteen triazine derivatives were measured by high-performance liquid chromatography on octyl silica and silica gel columns. The slope and intercept values of the plot of the logarithmic capacity factor *versus* acetonitrile concentration were calculated from the reversed-phase retention measurements. The adsorption properties of the compounds were characterized by the retention data obtained on silica gel columns using high and low concentrations of ammonium salts in the hydro-organic mobile phase. The non-polar, non-polar unsaturated and polar surface areas, the surface energies, the dipole moments and the Van der Waals radii of the molecules were calculated from their chemical structures after energy minimization on the basis of molecular mechanics. Correlation analysis of these parameters showed that the inhibitory effect is dependent on the polar and non-polar surface areas of the molecules. The reversed-phase slope showed a significant correlation with the difference between the accessible and the total non-polar surface areas of the compounds, whereas the intercept values correlated with the non-polar accessible surface area. The adsorption properties of the triazines on silica gel cannot be described by the molecular parameters investigated here.

INTRODUCTION

Triazine derivatives are potential anti-cancer agents as they can inhibit the dihydrofolate reductase enzyme [1]. The inhibitory effect of 62 triazine derivatives on the growth of L1210/R71 cells has been studied with respect to the hydrophobic parameter (π) and the molar refractivity (MR) index of the substituents [2]. The general structure of the molecules is shown in Fig. 1. The quantitative structure–
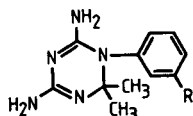
Fig. 1. General structure of the triazine derivatives investigated.

activity relationship (QSAR) study of Hansch and Fujita [3] suggested the presence of a hydrophobic pocket on the enzyme surface into which the R substituents can be fitted. The theoretical basis of using chromatographic retention data in drug design has been discussed previously [4]. For QSAR purposes the chromatographic behaviour of fifteen derivatives selected from a total of 62 was investigated by high-performance liquid chromatography on reversed-phase and silica gel stationary phases [5]. The measured reversed-phase retention data could be used to characterize the hydrophobicity of the compounds instead of the π values. Although the retention data obtained on the silica gel stationary phase did not correlate with the size of the molecules (*i.e.*, to the MR index of the R substituents), they

could be used to explain the variance of the inhibition of leukaemia cell growth [5].

The investgation of the three-dimensional structure of molecules and their fit to receptor sites is another approach to drug design. Many methods have been devised for the determination of molecular structures. It is now possible to determine molecular structures accurately by computational methods, typically by *ab initio* calculations for small molecules and by molecular mechanics [6] for large molecules.

This work investigated the relationship between molecular parameters calculated on the basis of molecular mechanics and the chromatographic retention and biological activity of triazines.

EXPERIMENTAL

The triazines used in this study were synthesized by the method of Selassie *et al.* [2] and were a kind gift of Professor C. Hansch (Pomona College, Claremont, CA, USA). The structure of the compounds is given in Table I. The data for the inhibition of the growth of L1210/R71 cells given in Table I were obtained from Selassie *et al.* [1].

The experimental conditions for the determination of the chromatographic retention data have been described in detail by Valkó *et al.* [5]. Table I gives the slope and intercept (log k'_0) values of the compounds obtained by plotting the log k' values against the acetonitrile concentration of the mobile phase in reversed-phase chromatography. The log k'_n values were measured as the difference between the log k'_a and log k'_b values, which were obtained on the same silica stationary phase using 95% (v/v) methanol and 5% (v/v) of a 0.25% (w/v) and a 1% (w/v) aqueous ammonium chloride solution [5], respectively. The retention data obtained on silica gel columns [5] are also given in Table I.

The three-dimensional structure of the compounds was determined based on energy minimization. After setting up the geometries of the molecules with the smallest molecular mechanics (mmx) energy, the non-polar (nopol), non-polar unsaturated and polar surface areas and surface energies were calculated. The water solvation shell was also considered in the calculations of the accessible polar (polac) and non-polar (npac) surface areas. The dipole moment values and Van der Waals radii of the molecules were also calculated.

The correlations of these parameters were investigated by stepwise linear regression analysis using the

TABLE I

INHIBITORY ACTIVITY [LOG(1/C)] AND CHROMATOGRAPHIC RETENTION DATA OF TRIAZINES OBTAINED FROM SELASSIE *et al.* [1] AND VALKÓ *et al.* [5], RESPECTIVELY

The serial numbers of the compounds are the same as in ref. 1. The log k'_0 and the slope values refer to the reversed-phase chromatographic retention and log k'_n refers to the retention data obtained on silica gel. All of the data are from ref. 5.

Compound No.	R	Log(1/C)	Slope	Log k'_0	Log k'_n
1	H	4.49	−0.00643	0.831	0.431
2	SO_2NH_2	3.57	−0.00388	0.385	0.569
3	$CONH_2$	3.52	−0.00270	0.188	0.490
5	OH	4.41	−0.00507	0.589	0.364
12	CN	4.89	−0.00691	0.814	0.297
14	CH_2CH_3	5.27	−0.01225	1.436	0.350
20	OCH_3	4.42	−0.00734	0.970	0.388
21	OCH_2CH_3	4.96	−0.01075	1.285	0.352
23	$O(CH_2)_3CH_3$	5.09	−0.01215	1.672	0.419
25	$O(CH_2)_5CH_3$	5.62	−0.02107	2.458	0.256
40	$CH_2OC_6H_5$	5.12	−0.01778	1.897	0.412
42	$CH_2OC_6H_4$-3'-CN	4.67	−0.01253	1.546	0.387
43	$CH_2OC_6H_4$-3'-OCH_3	5.20	−0.01237	1.601	0.351
44	$CH_2OC_6H_4$-3'-CH_2OH	4.76	−0.01672	1.502	0.322
49	$CH_2OC_6H_4$-3'-C_6H_5	5.62	−0.02538	2.707	0.402

TABLE II

CALCULATED MOLECULAR PARAMETERS FOR THE TRIAZINES ON THE BASE OF MOLECULAR MODELLING

Compound No.	nopol	npac	δnp\npc[a]	polac	tscal
1	229.8	216.8	13.0	121.8	−3.2
2	184.1	173.4	10.7	235.5	−14.6
3	179.6	168.9	10.7	216.8	−12.8
5	194.4	183.1	11.3	164.7	−8.0
12	197.9	186.5	11.4	167.5	−8.4
14	293.8	276.7	17.1	124.7	−2.3
20	270.3	253.9	16.3	134.9	−3.5
21	313.2	295.0	18.2	129.6	−2.0
23	371.2	349.8	21.4	129.1	−0.5
25	431.6	406.9	24.7	127.7	1.2
40	340.4	321.2	19.2	121.9	0.5
42	304.3	287.1	17.2	167.1	−4.8
43	379.4	357.3	22.1	131.1	0.3
44	344.3	324.7	19.6	160.1	−2.8
49	402.5	379.6	22.9	126.8	2.4

[a] δnp\npc = difference between the non-polar and non-polar accessible surface areas.

Drugidea program system developed for drug design (Chemicro, Budapest, Hungary). All the calculations were performed on an IBM AT compatible personal computer.

RESULTS AND DISCUSSION

The chemical structure, inhibitory activity and chromatographic retention data of the investigated triazine derivatives are given in Table I. The calculated molecular parameters are presented in Table II. The correlation coefficients between each pair of investigated parameters are given as a correlation matrix in Table III.

The reversed-phase retention data which showed a significant correlation with the hydrophobicity of the compounds ($r = 0.982$ from Valkó et al. [5]) could also be described as a function of the calculated molecular parameters. The log k_0' values showed the best correlation with the non-polar accessible surface area of the molecules, as formulated in eqn. 1:

$$\log k_0' = 8.53 \, (\pm 0.84) \cdot 10^{-3} \cdot \text{npac} - 1.05 \quad (1)$$

where $n = 15$, $r = 0.942$, $s = 0.249$ and $F = 102.9$ stand for the number of compounds, the correlation coefficient, the standard error of the estimate and the Fisher test value, respectively.

Eqn. 1 indicates that the larger the non-polar accessible surface area of the molecule, the higher the reversed-phase retention of the compounds.

The dependence of the retention of the compounds on the organic phase concentration of the mobile phase in reversed-phase chromatography can be expressed by the slope of the straight line obtained by plotting the log k' values against the concentration of the organic phase. As was emphasized previously [7], the slope values do not necessarily show a good correlation with the intercept (log k_0') values for structurally unrelated compounds and they can be expressed by the contact hydrophobic surface area of the molecules.

For the triazine derivatives investigated, the log k_0' and slope values showed a high correlation ($r = 0.85$), proving that they are similar with respect to their reversed-phase retention behaviour. Similar to results obtained previously [8], where structurally

TABLE III

CORRELATION COEFFICIENTS FOR THE PARAMETERS LISTED IN TABLES I AND II

	Log(1/C)	Slope	Log k_0'	Log k_n'	nopol	npac	δnp\npc	polac	tscal
Log(1/C)	1.00	−0.73	0.88	−0.75	0.84	0.84	0.83	−0.75	0.84
Slope	−	1.00	−0.85	0.37	−0.76	−0.76	−0.88	0.41	−0.65
Log k_0'	−	−	1.00	−0.49	0.94	0.94	0.93	−0.68	0.88
Log k_n'	−	−	−	1.00	−0.49	−0.49	−0.49	0.59	−0.57
nopol	−	−	−	−	1.00	0.99	0.99	−0.67	0.90
npac	−	−	−	−	−	1.00	0.99	−0.67	0.90
δnp\npc	−	−	−	−	−	−	1.00	−0.68	0.89
polac	−	−	−	−	−	−	−	1.00	−0.92
tscal	−	−	−	−	−	−	−	−	1.00

Fig. 2. Plot of the slope values against the difference between the non-polar and non-polar accessible surface areas (δnp\npc) of the molecules according to eqn. 3.

unrelated compounds were investigated, the variance of the slope values can be described by the difference of the non-polar and non-polar accessible surface areas of the molecules. For the triazine derivatives, eqn. 2 was obtained:

$$\text{slope} = 5.75\ (\pm 2.21) \cdot 10^{-3} \cdot \text{nopol} -$$
$$6.17\ (\pm 2.34) \cdot 10^{-3} \cdot \text{npac} + 6.65 \cdot 10^{-3} \quad (2)$$
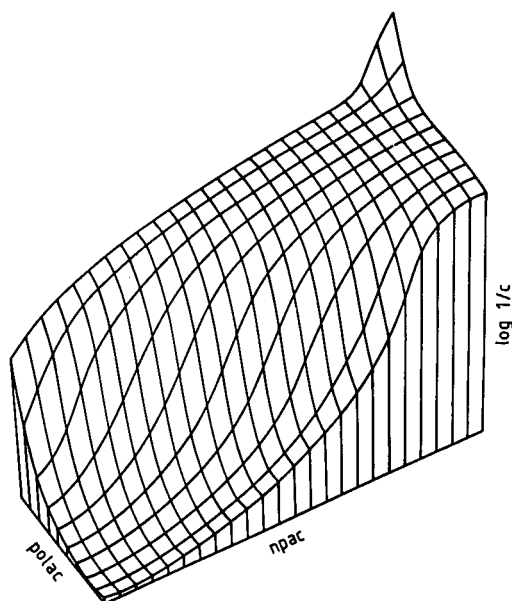
Fig. 3. Three-dimensional plot of eqn. 4, which represents the correlation between the inhibition activity log(1/C) and the polar (polac) and non-polar (npac) accessible surface areas of the molecules.

where $n = 15$, $r = 0.936$, $s = 0.0025$ and $F = 42.1$.

Although the two independent variables in eqn. 2 show a high cross-correlation (Table III), neither alone shows as high a correlation to the slope values as they show together. Therefore the correlation of the difference between the two variables, δnp\npc, (δnp\npc = nopol − npac) and the slope values was also investigated. The relationship between the slope values and the δnp\npc values can be described by eqn. 3:

$$\text{slope} = 1.21\ (\pm 0.18) \cdot 10^{-3} \cdot \delta\text{np\npc} +$$
$$9.122 \cdot 10^{-3} \quad (3)$$

where $n = 15$, $r = 0.878$, $s = 0.0032$ and $F = 43.8$.

This relationship is illustrated in Fig. 2.

An possible explanation of eqn. 3 is that it describes the slope as a function of the difference between the non-polar surface area of the molecules and the accessible non-polar surface area by the hydrophobic surface of the stationary phase and by the organic solvent molecules.

The log k'_n values, which are the differences between the logarithmic capacity ratio measured at low (log k'_a) and high (log k'_b) salt concentrations in the eluent are significant in the correlation of triazines with the inhibition of cell growth [5]. The log k'_n values cannot be described by any combination of the investigated molecular parameters. As was suggested previously [5], the log k'_n values reflect the electronic interactions of the compounds because at high salt concentrations the retention occurs predominantly by hydrophobic interactions and at low salt concentrations both the electronic and the hydrophobic interactions affect the retention behaviour.

A significant linear regression equation can be derived for the inhibitory effect of the compounds on L1210/R71 cell growth [log(1/C)] and the investigated molecular parameters:

$$\log(1/C) = 3.994\ (\pm 1.265) \cdot 10^{-3} \cdot \text{npac} -$$
$$8.794\ (\pm 2.836) \cdot 10^{-3} \cdot \text{polac} + 4.985 \quad (4)$$

where $n = 15$, $r = 0.913$, $s = 0.276$ and $F = 30.1$.

Fig. 3 shows the three-dimensional plot of eqn. 4. A relatively wide range of polar and non-polar surfaces provides a medium inhibitory activity for the compounds and only a narrow range of properties can be attributed to a strong inhibitory effect.

The inhibitory effect of the compounds on the

growth of L1210/R71 cells can also be mathematically described by the total surface energy (tscal) of the compounds and the electronic and adsorptive properties (log k'_n) obtained from adsorption chromatography:

$$\log(1/C) = 0.0913 \ (\pm 0.0149) \ \text{tscal} - 2.514 \ (\pm 0.983) \ \log k'_n + 6.100 \quad (5)$$

where $n = 15$, $r = 0.940$, $s = 0.231$ and $F = 45.3$.

The statistical characteristics of eqn. 5 indicate the importance of the electronic and adsorptive properties of the compounds which cannot be correlated with the calculated molecular parameters. It underlines the need to understand better the chromatographic retention mechanisms on silica stationary phases.

In conclusion, this work has illustrated the applicability of molecular modelling to the understanding of the chromatographic retention behaviour and the anti-cancer activity data of triazines. The reversed-phase retention data are related to the non-polar surface areas of the molecules.

The adsorption chromatographic retention behaviour of the compounds cannot be described by the molecular parameters investigated because none of these parameters characterizes the electronic or electrostatic properties of the compounds.

The inhibitory effect of the triazines on the growth of leukaemia cells is correlated to their accessible polar and non-polar surface areas.

REFERENCES

1 C. D. Selassie, C. D. Strong, C. Hansch, T. J. Delcamp, J. H. Freisheim and T. A. Khwaja, *Cancer Res.*, 46 (1986) 744.
2 C. D. Selassie, C. Hansch, T. A. Khwaja, C. B. Dias and S. Pentecost, *J. Med. Chem.*, 27 (1984) 347.
3 C. Hansch and T. J. Fujita, *J. Am. Chem. Soc.*, 86 (1964) 1616.
4 K. Valkó, *Trends Anal. Chem.*, 6 (1987) 214.
5 K. Valkó, I. Fellegvári, A. Katti and L. Ötvös, *J. Liq. Chromatogr.*, 11 (1988) 833.
6 U. Burkert and N. L. Allinger, *Molecular Mechanics*, American Chemical Society, Washington, DC, 1982.
7 K. Valkó, *J. Liq. Chromatogr.*, 10 (1987) 1663.
8 K. Valkó and P. Slégel, *J. Liq. Chromatogr.*, 14 (1991) in press.

CHROMSYMP. 2424

Correlations between high-performance liquid chromatographic retention, X-ray structural and ^{13}C NMR spectroscopic data of flavonoid compounds

Maria Chiara Pietrogrande*, Pierluigi Reschiglian and Francesco Dondi

Analytical Chemistry Laboratory, Department of Chemistry, University of Ferrara, Via L. Borsari 46, 44100 Ferrara (Italy)

Yassin Duale Kahie

Analytical Chemistry, Faculty of Industrial Chemistry, Somali National University, P.O. Box 1081, Mogadishu (Somalia)

Valerio Bertolasi

Centro Strutturistica Diffrattometrica, University of Ferrara, Via L. Borsari 46, 44100 Ferrara (Italy)

ABSTRACT

The retention behaviour of selected flavonoid compounds was analysed and correlated with structural properties, as elucidated by X-ray crystallographic and ^{13}C NMR spectroscopic studies. A detailed analysis of group retention contribution (Δlog k') makes it possible to establish how the introduction of an OH group in the molecule affects the overall solute polarity and, therefore, its retention, in relation to the position of the OH group and the molecular environment. X-ray structural information and ^{13}C NMR chemical shifts show the formation of strong intramolecular hydrogen bonding (HB) in 5-hydroxy-flavones and a weaker intramolecular HB in 3-hydroxy-substituted compounds. Δlog k' values may be explained in terms of these intramolecular HB properties; moreover a quantitative relationship between Δlog k' values and chemical shifts was found.

INTRODUCTION

The flavonoids are one of the most diverse and widespread groups of natural constituents; as many as 400 different compounds have been reported to exist and their practical relevance is increasingly described [1,2]. The systematic identification of flavonoid compounds was first well established by coupling the selectivity properties of classical chromatographic separation techniques (paper and column chromatography) with spectroscopic measurements [3,4]. ^{13}C NMR spectroscopy has been successively employed to establish the environment and nature of the carbon and hydrogen atoms and the information gained by this technique is fundamental for flavonoid structure determination. Modern reversed-phase high-performance liquid chromatographic (HPLC) methods are now the most commonly used techniques in the separation and analysis of flavonoid mixtures owing to their greater selectivity, sensitivity and speed [4,5]. The use of HPLC retention values in elucidating flavonoid structures has also been suggested and its potential role as an aid in systematic identification has been demonstrated [6–10].

This topic was further investigated in this work. The specific effects of the introduction of hydroxyl groups on structural features and therefore on HPLC retention were studied in relation to substituent position and number. The relationship

between HPLC retention values, NMR spectro-
scopic data and flavonoid molecular structure was
investigated. The structural information gained by
this comparative approach was examined by com-
parison with X-ray structural data.

EXPERIMENTAL

Materials

The selected flavonoid standards were obtained
from Sarsyntex (Merignac, France) and used as
received. Standard solutions in ethanol had a con-
centration of 10–100 ppm.

HPLC measurements

Capacity factors (k') for various fixed organic
solvent compositions were determined for standard
compounds with a Waters Model 600 multi-solvent
system, equipped with a Rheodyne injection valve
(20-μl sample loop) and a Waters Model 990 photo-
diode-array detector, coupled with an APC III
personal computer (NEC, Boxborough, MA, USA).
The mobile phases were mixtures of water, purified
with a Norganic system (Millipore, Bedford, MA,
USA) and HPLC-grade methanol (Rudi-Pont, He-
talab Chemical, USA). The aqueous phase was
buffered at pH 2–3 in 80 mM acetic acid–8 mM

TABLE I

MOLECULAR STRUCTURES OF COMPOUNDS STUDIED
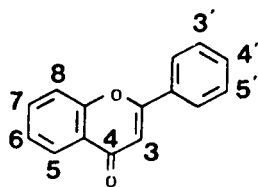
No.	Compound	Substituent position							
		3	5	6	7	8	3'	4'	5'
1	Acacetin		OH		OH			OCH$_3$	
2	Apigenin		OH		OH			OH	
3	Chrysin		OH		OH				
4	Chrysoeriol		OH		OH		OCH$_3$	OH	
5	Fisetin	OH			OH	OH	OH		
6	Flavone								
7	3-Hydroxyflavone	OH							
8	5-Hydroxyflavone		OH						
9	6-Hydroxyflavone			OH					
10	7-Hydroxyflavone				OH				
11	6,7-Dihydroxyflavone			OH	OH				
12	7,8-Dihydroxyflavone				OH	OH			
13	Galangin	OH	OH		OH				
14	Isorahmnetin	OH	OH		OH		OCH$_3$	OH	
15	Kaempferid	OH	OH		OH			OCH$_3$	
16	Kaempferol	OH	OH		OH		OH		
17	Luteolin		OH		OH		OH	OH	
18	Myricetin	OH	OH		OH		OH	OH	OH
19	Quercetin	OH	OH		OH		OH	OH	
20	Rhamnetin	OH	OH		OCH$_3$		OH	OH	
21	Robinetin	OH			OH		OH	OH	OH
22	Scutellarein		OH	OH	OH			OH	

disodium hydrogenphosphate (Carlo Erba, Milan, Italy). Solvent mixtures were filtered through 0.2-μm Millipore filters. All the data were obtained on a 30 cm $\times$ 3.9 mm I.D. 10-μm μBondapak C_{18} column (Waters Assoc., Milford, MA, USA) by following the experimental procedure described previously [8,9].

NMR study

The ^{13}C NMR spectra of compounds **1, 3, 8–11, 15** and **22** were all obtained at 300 MHz on a Varian Gemini spectrometer in [$^2H_6$]dimethyl sulphoxide (DMSO-d_6) or $C^2H_3O^2H$ solutions. All the chemical shifts (δ ^{13}C) are reported in ppm with DMSO-d_6 at 35.5 ppm and $C^2H_3O^2H$ at 49 ppm as references.

RESULTS AND DISCUSSION

The selected compounds represent the classes of flavones and flavonols. The structures reported in Table I illustrate the hydroxylation pattern. Standard compounds were chosen on the basis of structure in order to test the effect of substituent introduction into the molecule; some occur naturally and others are synthetic products.

Table II reports the measured log k' values for the extended series of compounds, while other retention data have been reported previously [6–10]. When retention values were correlated with mobile phase composition (as methanol volume fraction, φ) a linear fit was obtained (Table III). The statistical goodness of the fit confirmed the linearity of log k'–φ correlation when methanol is the organic modifier and acetic acid is the acid modifier [11]. For various substituents in the benzopyran ring the group contribution to retention was calculated as Δlog k' (*i.e.*, the difference between the retention of one molecule containing a particular substituent and that of a molecule which does not contain that group);

$$\Delta\log k' = \log k'_2 - \log k'_1 \qquad (1)$$

where k'_2 is retention of the solute with the added group and k'_1 is that of the molecule without the substituent. The values reported in Table IV were calculated employing only log k' data roughly in the range 0–1 (k' = 1–10) where the experimental accuracy is assumed to be $\pm 5\%$.

The group retention contributions obtained were largely independent of eluent volume fraction when methanol was the strong solvent, as shown in Fig. 1, where Δlog k' values are plotted as a function of mobile phase composition for a 3-OH substituent.

TABLE II

RETENTION VALUES LOG k' MEASURED FOR SELECTED FLAVONOID COMPOUNDS WITH DIFFERENT METHANOL CONCENTRATIONS IN THE MOBILE PHASE

Compound[a]	Methanol concentration (%)							
	30	40	45	50	55	60	70	80
5	1.52	0.96	0.69	0.48	0.19	0.09	−0.39	
6				1.29	0.99	0.85	0.35	0.02
7				1.40	1.10	0.95	0.45	0.07
8				1.58	1.26	1.11	0.60	0.21
9				1.12	0.82	0.67	0.18	−0.16
10				1.07	0.77	0.64	0.14	−0.24
11				0.92	0.60	0.46	−0.01	−0.33
12				0.68	0.40	0.28	−0.15	−0.44
15					1.16	1.01	0.47	0.00
16				0.98	0.65	0.53	0.01	−0.34
18	1.45	0.89	0.63	0.41	0.13	0.02	−0.46	
20				1.16	0.86	0.72	0.19	−0.21
21	1.18	0.64	0.37	0.18	−0.09	−0.18	−0.66	
22				0.51	0.30	0.05	−0.30	

[a] See Table I.

TABLE III

STATISTICAL PARAMETERS OF LINEAR FIT OF LOG k' VERSUS METHANOL CONCENTRATION IN THE MOBILE PHASE

Compound[a]	Intercept	Slope	R^b	S.E.[c]
5	2.93 ($\pm$0.13)	-4.89 ($\pm$0.26)	0.99	0.06
6	3.56 ($\pm$0.19)	-4.57 ($\pm$0.32)	1.00	0.05
7	3.69 ($\pm$0.18)	-4.63 ($\pm$0.30)	1.00	0.04
8	3.93 ($\pm$0.20)	-4.76 ($\pm$0.33)	1.00	0.05
9	3.39 ($\pm$0.17)	-4.58 ($\pm$0.29)	1.00	0.04
10	3.31 ($\pm$0.20)	-4.51 ($\pm$0.34)	0.99	0.05
11	3.11 ($\pm$0.20)	-4.46 ($\pm$0.33)	0.99	0.05
12	2.66 ($\pm$0.18)	-4.02 ($\pm$0.31)	0.99	0.05
15	3.79 ($\pm$0.37)	-4.71 ($\pm$0.59)	0.99	0.06
16	3.29 ($\pm$0.25)	-4.68 ($\pm$0.42)	0.99	0.06
18	2.86 ($\pm$0.12)	-4.87 ($\pm$0.25)	0.99	0.06
20	3.51 ($\pm$0.20)	-4.73 ($\pm$0.34)	0.99	0.05
21	2.52 ($\pm$0.13)	-4.65 ($\pm$0.28)	0.99	0.07
22	2.82 ($\pm$0.13)	-4.60 ($\pm$0.23)	1.00	0.02

[a] See Table I.
[b] R = correlation coefficient.
[c] S.E. = standard error of regression.

TABLE IV

EFFECT OF HYDROXY SUBSTITUTION ON RETENTION, EXPRESSED AS GROUP CONTRIBUTION TO RETENTION (ΔLOG k'), AND ON C-4 CHEMICAL SHIFT ($\Delta\delta^{13}$C)

Group	Compounds[a]	Δlog k'^b	$\Delta\delta^{13}$C[c]	$\Delta\delta^{13}$C[d]
3-OH	19–17	-0.13 ± 0.06	-6.3	-6.5
3-OH	16–2	-0.07 ± 0.02	-5.9	
3-OH	15–1	-0.04 ± 0.01	-5.8	
3-OH	14–4	-0.02 ± 0.01	-5.5	
3-OH	13–3	0.01 ± 0.01	-5.4	-6.3
3-OH	7–6	0.11 ± 0.01	-4.2	-5.3
5-OH	19–5	0.20 ± 0.02		
5-OH	18–21	0.20 ± 0.02		
5-OH	3–10	0.25 ± 0.02	5.9	
5-OH	8–6	0.27 ± 0.02	4.5	
6-OH	9–6	-0.17 ± 0.01	-0.6	
6-OH	11–10	-0.17 ± 0.01	-0.1	
6-OH	22–2	-0.34 ± 0.03	1.0	
7-OH	10–6	-0.22 ± 0.01		
7-OH	3–8	-0.22 ± 0.01		
7-OH	11–9	-0.21 ± 0.01		

[a] See Table I.
[b] Average value for three or four different solvent compositions.
[c] Determined in DMSO-d_6 solvent.
[d] Determined in $C^2H_3O^2H$ solvent.
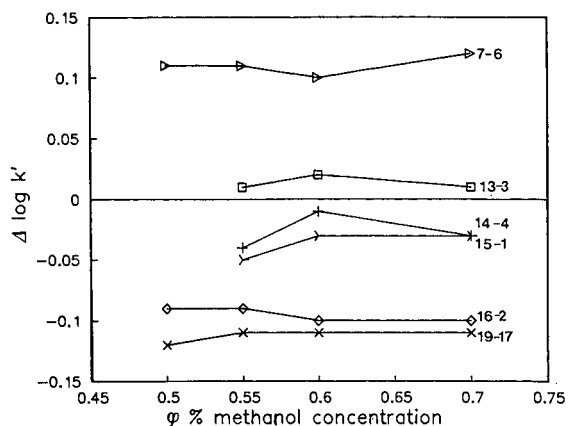
Fig. 1. Dependence of 3-OH retention contribution, Δlog k', on methanol concentration in the mobile phase (φ, %). Pairs of numbers represent compounds listed in Table I.

This peculiar behaviour of methanol as organic modifier was previously found with different HPLC and thin-layer chromatographic systems for different flavonoid compounds [9,10]. Owing to this peculiarity, methanol seems to be the solvent of choice for the systematic study of the retention behaviour of these compounds related to their molecular structure. An average of three or four different mobile phase compositions can be taken to obtain the retention contributions (Table IV; see the reported small standard deviations).

The retention of a molecule is determined by various intermolecular solute-mobile-stationary phase interactions, such as dispersive, inductive, orientative and charge transfer, including hydrogen bonding [12]. A detailed analysis of the group retention contributions makes it possible to single out the specific interactions controlling chromatographic behaviour. The data in Table IV show that the position of hydroxylation affects the retention in different ways, depending on the molecular environment. On introducing an OH group in positions 6 and 7 the retention value decreases, whereas substitution in position 5 results in an increase in retention. All these effects, with the exception of the 6-OH substitution, are independent of the presence of other substituents in the molecule. On the other hand, substitution in position 3 results in a very different behaviour: the Δlog k' value ranges from positive to negative values and is strongly dependent

on the molecular environment [10] (see Table IV and Fig. 1).

The introduction of a polar, hydrogen-bonding OH group normally increases solvation of the flavonoid molecules with an aqueous solvent and/or decreases hydrophobic interactions with the C_{18} stationary phase. This effect is valid for all 6- and 7-substituted compounds and some of the 3-OH derivatives, whereas for the other flavones introduction of an OH group results in a decrease in solute polarity (see all of the 5-OH and some of the 3-OH substitutions in Table IV). This behaviour shows that substituent retention contributions are not strictly constant and additive, but are a complex result of intramolecular interactions.

In order to obtain further insight into these intermolecular effects, the information on molecular structure obtained by ^{13}C NMR spectroscopic and X-ray crystallographic studies was investigated and correlated with the chromatographic data.

The usefulness of ^{13}C NMR spectroscopy for flavonoid structure analysis is well established and there is good agreement between different workers on the assignment of signals [13–15]. The ^{13}C chemical shift directly reflects the total charge density at the particular carbon nucleus and is therefore a sensitive probe for the structural characterization of the molecule. Many surveys have been published summarizing the results of ^{13}C NMR studies on flavonoids [13]. When not available in the literature, NMR spectra were measured for the flavonoid compounds and the results are reported in Table V. In the flavone derivatives the

lowest field carbon resonances are generally those of carbonyl and oxygenated aromatic carbons (due to the lower electron density on ^{13}C), and the highest field resonances are shown by non-oxygenated aliphatic carbons. In particular, the ^{13}C NMR data show the different effects of the introduction of an OH group in position 3 or 5 on the chemical shift of the C-4 carbon according to the different electron density on the carbon (Table V) [13]. The ^{13}C NMR chemical shift of the C-4 nucleus may be selected as a descriptor of electronic density on the carbonyl group, and therefore of the strength of hydrogen bonding (HB) involving this part of the flavonoid molecule. The group contribution to the chemical shift can be calculated in the same way as the group retention contribution:
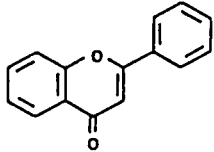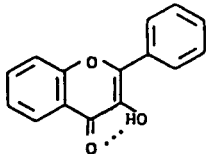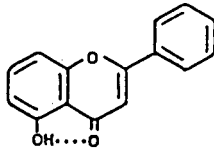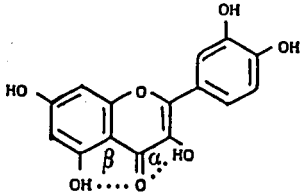
$$\Delta\delta \ ^{13}C = \delta_2{}^{13}C - \delta_1{}^{13}C \qquad (2)$$

where $\delta_2{}^{13}C$ represents the chemical shift of the molecule with the added hydroxyl group and $\delta_1{}^{13}C$ that for the compound without the substituent. The values obtained are reported in Table IV.

X-ray crystallographic information on flavonoids is summarized in Table VI, where the available literature data are grouped into four classes: (i) flavones unhydroxylated in positions 3 and 5 [16–20], (ii) flavonols unsubstituted in position 5 [21,22], (iii) 5-hydroxyflavones [22–34] and (iv) quercetin, the only 5-hydroxyflavonol whose crystallographic structure has been determined [35,36]. The reported data are average values calculated from the various measured data available in the literature. The molecular parameters most affected by intramolecular HB with the carbonyl group are shown in Table VI. The summarized structural data demonstrate that the HB between C-4 keto and C-3 hydroxyl groups has no significant effect on carbonyl bond strength, because C-4=O-4 bond length in the flavonols is not statistically different from that in flavones [cf., $d_{C-4-O-4} = 1.235(9)$ for flanones vs. 1.234(2) for flavonols]. Table VI also shows that the HB between the carbonyl oxygen (as a proton acceptor) and the 5-OH group, thus closing a six-membered ring (β-ring), is sterically and energetically more favoured than that of flavonols unsubstituted in position 5, where the HB closes a five-membered ring (α-ring) (compare flavones).

Let us now consider in detail the hydroxylation pattern effects.

TABLE V

SOME $\delta^{13}C$ NMR CHEMICAL SHIFTS (PPM IN DMSO-d_6) OF FLAVONOID MEASURED SPECTRA

Compound[a]	C-3	C-4	C-5
1	104.2	182.7	161.4
3	105.3	182.0	161.4
8	105.6	182.9	159.8
9	106.3	177.8	129.6
10	107.0	177.2	129.5
11	106.4	177.1	129.6
15	136.7	176.9	161.3
22	104.4	182.8	150.3

[a] See Table I.

TABLE VI

BOND LENGTHS (Å) AND ANGLES (°) FROM X-RAY CRYSTALLOGRAPHIC DATA

Compounds	$d_{C\text{-}4\text{-}O\text{-}4}$	$d_{O\text{-}3\text{-}H}/$ $d_{O\text{-}5\text{-}H}$	$d_{O\text{-}3\cdots O\text{-}4}/$ $d_{O\text{-}4\cdots O\text{-}5}$	$d_{O\text{-}4\cdots H}$	$\alpha_{O\text{-}3\text{-}H\cdots O\text{-}4}/$ $\alpha_{O\text{-}5\text{-}H\cdots O\text{-}4}$
(i) Flavones $(n = 6)^a$	1.235(9)				
(ii) Flavonols $(n = 4)$	1.234(2)	0.88(6)	2.72(4)	2.27(9)	122(8)
(iii) 5-Hydroxyflavones $(n = 5)$	1.255(9)	1.00(9)	2.60(3)	1.69(14)	151(11)
(iv) Quercetin $(n = 2)$ α-Ring:	1.268(1) 0.91[b]		2.795(2)		105[b]
β-Ring:	0.94[b]		2.581(8)	1.85[b]	133[b]

[a] n = Number of available structures.
[b] The only data reported in the literature [35,36].

C-3 hydroxylation

The introduction of a 3-OH group causes an upfield shift of about 5.5 ppm (on average) in the C-4 signal of differently substituted flavones (Table IV). Taking into account that the *ortho* effect of the OH substituent on the ^{13}C chemical shift of benzene is upfield of 12.7 ppm, the net effect on the C-4 resonance of the introduction of a 3-OH group into the unsubstituted flavone (compound 1) could corre spond to a net 7.2 ppm downfield shift. This result has been ascribed to the existence of the intramolecular HB interaction between C-4 keto and C-3 hydroxyl groups. The probable decrease in the HB strength between the C-4 keto and 3-OH, when

other hydroxyl groups are also present (see, *e.g.*, the mean distances $d_{O-3...O-4}$ in quercetin and in flavonols in Table VI), may be the reason why the net deshielding effect on the C-4 chemical shift decreases in the series going from the pair 3-hydroxyflavone–flavone to the pair quercetin–luteolin. In fact, when hydroxyl groups are also present on C-5 and C-7 atoms, the introduction of a further OH group in position 3 also causes a net downfield effect, but lower than the above, ranging from $+7.3$ to $+6.4$ ppm (corresponding to $\Delta\delta^{13}C$ values of -5.4 and -6.3 in Table IV). This behaviour may be considered to be a complex result of the inductive effect of the electron-withdrawing O atoms introduced and of the intramolecular HBs present in the molecule.

X-ray structural data provide another important insight into flavone structure [35,36]: it was observed that, in the crystal, quercetin exists in the dihydrated form. The HB formed by the 3-OH group is so weak that the hydroxyl proton is able to form a second bifurcated bond with an acceptor water molecule. The existence of this hydrated form may further justify the increased affinity of 3,5-OH derivatives to water and therefore their decreased retention values in reversed-phase chromatography ($\Delta\log k' = -0.13$ in Table IV for the pair quercetin–luteolin).

A quantitative description of this behaviour was attempted by linearly relating retention with molecular structure descriptors, expressed as group contribution to retention ($\Delta\log k'$) or with chemical shift ($\Delta\delta^{13}C$). The calculated linear relationship is expressed by the following equation:

$$\Delta\log k' = 0.58\ (+0.059) + 0.11\ (+0.011)\ \Delta\delta^{13}C$$

$$n = 6; \quad R = 0.981; \quad \text{S.E.} = 0.017 \qquad (3)$$

where R is the correlation coefficient and S.E. is the standard error of the regression (Fig. 2). This result shows that both ^{13}C NMR spectroscopy and reversed-phase HPLC retention values are equally affected by the same electronic properties: the increase in retention follows the increase in deshielding of the C-4 atom as a result of complex electronic rearrangements due to intramolecular HBs. The correlation between two independent measures of solute electronic interactions may be very promising for the structural characterization of molecules and solute retention prediction purposes.

The $\Delta\log k'$ *vs.* $\Delta\delta$ ^{13}C correlation may contain
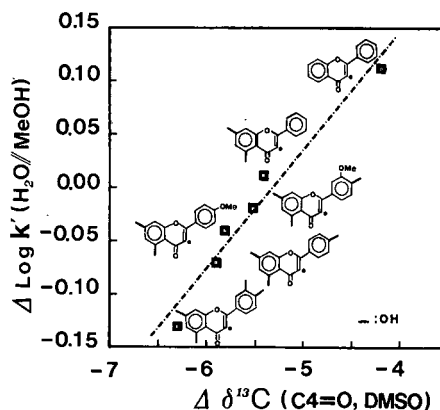
Fig. 2. Linear relationship between retention ($\Delta\log k'$) and chemical shift ($\Delta\delta$ ^{13}C in DMSO). Me = methyl.

some uncertainty due to the solvent effect, as the retention data were measured in methanol–water mixtures whereas the NMR spectra were determined in DMSO. In order to estimate solvent effects on the ^{13}C chemical shifts, the NMR spectra of some flavonoid compounds were determined using $C^2H_3O^2H$ as solvent. A downfield shift of the ^{13}C resonance for the solvent was observed; the solvent effect reflects the major ability of methanol to form a HB complex with the solute, particularly with the basic carbonyl group [37–39]. Moreover, the trend between $\Delta\delta^{13}C$ and $\Delta\log k'$ values is close to that observed in DMSO. Because of solubility problems, only a few spectra could be determined in $C^2H_3O^2H$ (Table IV), and the lack of experimental data prevents a better elucidation of specific solvent effects.

C-5 hydroxylation

The presence of a C-5 hydroxyl group causes, on average, a downfield shift of the C-4 resonance of about 5.2 ppm (see Table IV). A comparison with the *meta*-OH substituent effect on the benzene molecule [2] ($+1.4$ ppm) shows that an intramolecular HB between C-4 keto and C-5 hydroxyl groups overrides the substituent effect of the 5-OH group to produce a greater downfield shift. The internuclear distance lengths reported in Table VI for 5-hydroxyflavone and quercetin show the intramolecular HB between C-4 keto and C-5 hydroxy groups, forming a six-membered ring (β-ring), has a strong effect on the molecular structure. This intramolecular HB is

surprisingly strong owing to a synergistic mechanism similar to that found in β-diketones and called resonance-assisted hydrogen bonding (RAHB) through which π-bond delocalization strengthens and shortens the intramolecular HB [40–42]. This specific type of HB is characterized by a strong correlation between the bond strength (measured by the $d_{O\cdots O}$ contact distance) and the delocalization of the π-system of the conjugated double bonds. In quercetin, for example, the C-3 hydroxyl group, which forms an additional intramolecular HB, further strengthens the 5-OH hydrogen bond with consequent slight shortening of $d_{O\text{-}4\cdots O\text{-}5}$ and more pronounced lengthening of $d_{C\text{-}4\text{-}O\text{-}4}$ in the β-ring (Table VI). Accordingly, the chemical shifts of the C-4 carbon nucleus are strongly downfield. The group retention increments (Table IV) may be explained in terms of the above-reported structural information: the positive $\Delta \log k'$ values may be considered as the net effect of intramolecular HB in masking polar groups in solute molecules and therefore in making the whole molecule less polar.

The degree of resonance through the HB fragment affects the ^{13}C NMR chemical shifts: as the degree of π-bond delocalization increases, C-5 should become less shielded whereas C-4 becomes more shielded. Therefore, the greater the degree of resonance, the smaller is the $\Delta\delta_{C\text{-}4\text{-}C\text{-}5} = \delta_{C\text{-}4} - \delta_{C\text{-}5}$ difference is. The chemical shift differences for 5-hydroxy-substituted flavones and flavonols were calculated from the data available in the literature and reported in Table VII. The $\Delta\delta_{C\text{-}4\text{-}C\text{-}5}$ values obtained, ranging from 14.2 to 23.2 ppm, agree with the previously reported data for β-diketones where

the formation of RAHB was verified [41,42]. Large $\Delta\delta_{C\text{-}4\text{-}C\text{-}5}$ values (20.1–23.2) are found for 5-hydroxyflavones and smaller values (14.2–15.3) for 5-hydroxyflavonols; this behaviour indicates that the presence of a 3-OH substituent further increases the delocalization of the π-system. This may be one reason for the lower 5-OH contribution to retention in the flavonoid molecules whenever a 3-OH group is present (see the pairs quercetin–fisetin and myricetin–robinetin in Table IV).

C-6 hydroxylation

The introduction of a hydroxyl group in position 6 always leads to a negative $\Delta \log k'$ increment. The same values were obtained when 6-OH was added to flavone or to 7-hydroxyflavone (Table IV). A study of NMR spectra shows that the introduction of a 6-OH group produces a slight upfield shift of *ortho*-related C-5 and C-7 nuclei and a slight shielding effect on the C-4 keto group (Table V). A major perturbation of the electron distribution in the ^{13}C NMR spectra is evident when the scutellarein-apigenin pair is considered, where a 5-OH group is present: the signal of the C-4 keto nucleus shifts downfield of 1 ppm. The reason for this effect may be ascribed to the strong interaction of the three vicinal hydroxyl groups with consequent weakening of the HB in the β-ring. The same reasoning may apply to the greater increase in molecule polarity and therefore may explain the more negative $\Delta \log k'$ value.

TABLE VII

$\Delta\delta_{C\text{-}4\text{-}C\text{-}5}$ CHEMICAL SHIFT VALUES FOR VARIOUSLY SUBSTITUTED FLAVONES AND FLAVONOLS

Compound[a]	$\Delta\delta_{C\text{-}4\text{-}C\text{-}5}$ (ppm)	Compound[a]	$\Delta\delta_{C\text{-}4\text{-}C\text{-}5}$ (ppm)
1	20.1	**14**	15.1
2	20.7	**15**	15.3
3	20.3	**16**	15.2
4	23.2	**17**	20.1
8	23.1	**19**	15.1
13	14.2		

[a] See Table I.

REFERENCES

1 J. B. Harborne and T. J. Mabry, *The Flavonoids: Advances in Research*, Chapman and Hall, London, 1982, p. 1.
2 J. B. Harborne in V. Cody, E. Middleton and J. B. Harborne (Editors), *Plant Flavonoids in Biology and Medicine*, Alan R. Liss, New York, 1986, p. 243.
3 K. R. Markham, *Techniques of Flavonoid Identification*, Academic Press, New York, 1982.
4 J. B. Harborne, *Phytochemical Methods*, Chapman and Hall, London, 1984.
5 J. B. Harborne, in H. Heftmann (Editor), *Chromatography, Part B, Applications* (*Journal of Chromatography Library*, Vol. 22B), Elsevier, Amsterdam, 1986, p. B407.
6 F. Dondi, Y. D. Kahie, G. Lodi, P. Reschiglian, C. Pietrogrande, C. Bighi and G. P. Cartoni, *Chromatographia*, 23 (1987) 844.
7 F. Dondi, Y. D. Kahie, G. Lodi, G. Blo, C. Pietrograndе and P. Reschiglian, *Chromatographia*, 25 (1988) 423.
8 F. Dondi, Y. D. Kahie, G. Lodi, G. Blo, C. Pietrograndе and P. Reschiglian, *J. Chromatogr.*, 461 (1989) 281.

9 F. Dondi, G. Grassini-Strazza, Y. D. Kahie, G. Lodi, C. Pietrogrande, P. Reschiglian and C. Bighi, *J. Chromatogr.*, 462 (1989) 205.

10 Y. D. Kahie, C. Pietrogrande, M. I. Mendez, P. Reschiglian and F. Dondi, *Chromatographia*, 30 (1990) 447.

11 E. D. Katz, C. H. Lochmuller and R. P. W. Scott, *Anal. Chem.*, 61 (1989) 349.

12 P. T. Ying, J. C. Dorsey and K. A. Dill, *Anal. Chem.*, 61 (1989) 2540.

13 P. K. Agrawal, R. S. Thakur and M. C. Bansal, in P. K. Agrawal (Editor), *Carbon-13 NMR of Flavonoids*, Elsevier, Amsterdam, 1989, p. 95.

14 B. Ternai and K. R. Markham, *Tetrahedron*, 32 (1976) 565.

15 K. R. Markham and B. Ternai, *Tetrahedron*, 32 (1976) 2607.

16 H.-Y. Ting, W. H. Watson and X. A. Dominguez, *Acta Crystallogr., Sect. B*, 28 (1972) 1046.

17 J. S. Cantrell and R. A. Stalzen, *Acta Crystallogr., Sect. B*, 38 (1982) 983.

18 J.-C. Wallet, E. M. Gaydon, A. Fadlane and A. Baldy, *Acta Crystallogr., Sect. C*, 44 (1988) 357.

19 J.-C. Wallet, E. M. Gaydon and A. Baldy, *Acta Crystallogr., Sect. C*, 45 (1989) 512.

20 M. Hariharan and S. S. Rajan, *Acta Crystallogr., Sect. C*, 46 (1990) 437.

21 T. Hayashi, S. Kawai, T. Ohno, Y. Iitaka and T. Akimoto, *Chem. Pharm. Bull.*, 22 (1974) 1219.

22 M. C. Etter, Z. Urbanczyk-Lipkowska, S. Baer and P. F. Barbara, *J. Mol. Struct.*, 144 (1986) 155.

23 T. L. Lee, T. H. Lu and S. H. Zee, *Tetrahedron Lett.*, 24 (1974) 2081.

24 H. W. Schmalle, O. H. Jarchou, B. M. Hausen and R.-H. Schulz, *Acta Crystallogr., Sect. B*, 38 (1982) 3163.

25 J. Vijayalakshmi, S. S. Rajan, R. Srinivasan and A. G. Ramachandran Nair, *Acta Crystallogr., Sect. C*, 42 (1986) 1752.

26 I. R. Castleden, S. R. Hall, S. Nimgirawath and A. H. White, *Aust. J. Chem.*, 38 (1985) 1177.

27 M. A. Al-Yaha, M. S. Hifnawy, J. S. Mossa, F. S. El-Feraly, D. R. McPhail and A. T. McPhail, *Phytochemistry*, 26 (1987) 2648.

28 M. D. Estrada, A. Conde, R. Marquez and R. Jimenez-Garay, *Acta Crystallogr., Sect. C*, 43 (1987) 1826.

29 J. Vijayalakshmi, S. S. Rajan and R. Srinivarsan, *Acta Crystallogr., Sect. C*, 43 (1987) 1998.

30 M. Shoja, *Acta Crystallogr., Sect. C*, 46 (1990) 517.

31 K. A. Abboud, S. H. Simonsen, T. J. Mabry and N. Fang, *Acta Crystallogr., Sect. C*, 45 (1989) 1788.

32 N. H. Paradi and N. H. Fischer, *Acta Crystallogr., Sect. C*, 45 (1989) 1827.

33 M. Gajhade, R. Encarnacian, G. C. Leal, J. C. Patino, C. Christophersen and P. H. Nielsen, *Acta Crystallogr., Sect. C*, 45 (1989) 2012.

34 M. Breton, G. Precigoux, C. Canseille and M. Hospital, *Acta Crystallogr., Sect. B*, 31 (1975) 921.

35 M. Rossi, L. F. Rickles and W. A. Halpin, *Biorg. Chem.*, 14 (1986) 55.

36 G. Jin, Y. Yamagata and K. Tomita, *Acta Crystallogr., Sect. C*, 46 (1990) 310.

37 G. E. Marciel and J. J. Natterstad, *J. Phys. Chem.*, 42 (1965) 2752.

38 R. G. Wilson, J. H. Bowie and D. H. Williams, *Tetrahedron*, 24 (1968) 1407.

39 R. L. Lichter and J. D. Roberts, *J. Phys. Chem.*, 74 (1970) 912.

40 G. Gilli, F. Bellucci, V. Ferretti and V. Bertolasi, *J. Am. Chem. Soc.*, 111 (1989) 1023.

41 M. C. Etter and G. M. Vojta, personal communication.

42 J. B. Stothers and P. C. Lauterbur, *Can. J. Chem.*, 42 (1964) 1563.

CHROMSYMP. 2423

Retention behaviour of some ring-substituted phenol derivatives on a porous graphitized carbon column

Esther Forgács*, Tibor Cserháti and Klára Valkó

Central Research Institute for Chemistry, Hungarian Academy of Sciences, P.O. Box 17, H-1525 Budapest (Hungary)

ABSTRACT

The retentions of 24 ring-substituted phenol derivatives were determined on a graphitized carbon column using unbuffered acetonitrile–water and methanol–water eluent mixtures at various organic phase concentrations. Principal component analysis calculated from both the correlation and covariance matrices was used to detect the similarities and dissimilarities between the retention behaviours of phenol derivatives. Each phenol derivative showed narrow and symmetrical peaks in each eluent. The high percentage of variance explained in the first principal component suggests that the eluents have common elution characteristics; however, according to the second principal component they showed slightly different selectivities. Calculations demonstrated that the number and not the type of substituents exerts the highest impact on the retention. Both calculation methods (based on correlation and covariance matrices) gave similar results.

INTRODUCTION

The application of silica or silica-based supports in high-performance liquid chromatography (HPLC) is limited by the low stability of silica at alkaline pH values [1] and by the undesirable electrostatic interactions between the polar substructures of solutes and the free silanol groups not covered by the hydrophobic ligand [2,3]. To decrease or eliminate the effect of residual acidic silanol group, the eluent has to be buffered or various additives have to be added to the eluent to mask the effect of silanol groups [4]. The drawbacks mentioned above necessitated the search for suitable supports other than silica, such as alumina [5], octadecyl-coated alumina [6], zirconia [7,8] and various polymer-based supports [9].

The porous graphitic carbon support (PGC) has been developed in the last decade [10,11]. PGC is characterized by the following: sufficient hardness to withstand high pressures; a well defined, reproducible and stable surface that shows no change during chromatographic work or storage; a specific surface area in the range 50–500 m^2/g to give adequate retention of solutes and maintain a reasonable linear sample capacity; a mean pore size > 10

nm and the absence of micropores to ensure rapid mass transfer of solutes into and out of the particles; and uniform surface energy to give linear adsorption isotherms [12].

Until now PGC, has been mainly used to separate basic compounds [13,14]. The effect of various physico-chemical parameters of solutes on their retention behaviour has been studied in detail and the importance of electronic interactions between solutes and stationary phase on PGC has been emphasized [15]. A much greater influence of structural planarity of solutes on selectivity was observed on carbon than on C_{18} columns, presumably because the solute planarity emphasizes the interaction with the graphitic surface based on charge transfer and dispersion forces [16].

The evaluation of the performance of a new type of support generally involves the application of numerous eluents and solutes. The evaluation of such complicated data matrices is hardly possible without the application of computer-assisted multivariate mathematical–statistical methods. These methods make possible the simultaneous evaluation of an almost unlimited number of variables (chromatographic parameters), which greatly facilitates the solution of theoretical and practical problems.

Multivariate methods have been applied in chromatography to identify basic factors that influence solute–solvent interactions and to classify solutes and solvents into groups having similar characteristics.

Principal component analysis (PCA) has frequently been applied to the evaluation of chromatographic data matrices [17]. The advantages of PCA are that it allows a reduction in the number of variables, that is, instead of the measured variables, artificial variables can be calculated that the explain the highest possible ratio of the change of the phenomenon observed (principal component variables); and it is suitable not only for the calculation of two–two variables relationship (PC variables), but also for the study of all variables of a linear correlation system. Therefore, it was assumed that PCA can be used when more solutes and more eluent systems are involved and we are interested in the similarities or dissimilarities between solutes and eluent systems.

The objectives of this investigation were to determine the retentions of 24 ring-substituted phenol derivatives on a PGC column in various eluent systems, to assess the separation power of the column without buffering the eluent and to evaluate the results with multivariate mathematical–statistical methods.

EXPERIMENTAL

A porous graphitic carbon column (Shandon Hypercarb, 100 × 4.7 mm I.D., particle diameter 7 μm) was purchased from Shandon Scientific (Runcorn, UK). The HPLC system consisted of a Liquopump Model 312 pump (LaborMIM, Budapest, Hungary), a Cecil (Cambridge, UK) CE-212 variable-wavelength UV detector, a Valco (Houston, TX, USA) injector with a 20-μl sample loop and a Waters Model 740 integrator (Waters-Millipore, Milford, MA, USA). The flow-rate was 1 ml/min and the detection wavelength was 254 nm. Mixtures of methanol–water and acetonitrile–water were used as eluents. The methanol and acetonitrile concentrations ranged from 90 to 97.5 (in steps of 2.5%, v/v) and from 70 to 85% (v/v) (in steps of 5%, v/v) respectively. The use of these narrow concentration ranges was motivated by the high dependence of the retention of solutes on the organic mobile phase concentration. Buffers were not used.

The structures of the ring-substituted phenol derivatives are shown in Table I. The phenol derivatives were dissolved in methanol or in acetonitrile at a concentration of 0.05 mg/ml. The retention time of each compound in each eluent was determined with three consecutive determinations.

To compare the performance of PGC with that of the traditional reversed-phase column, the retentions of compounds **14**, **17** and **18** were determined on a 150 × 4 mm I.D. Hypersil ODS (5 μm) column in water–methanol (4:6, v/v) and 0.025 M KH_2PO_4–methanol (4:6, v/v) (pH adjusted to 1.75 with orthophosphoric acid) eluents. The asymmetry factor and the plate number for each derivative were calculated as described [18]. The plate number for toluene as a non-polar compound was also determined on both columns. The performance of the column was characterized by the ratio of the plate number for the phenol derivative to the plate number for toluene. We assume that this ratio reflects the influence of solute polarity on the column performance.

Principal component analysis was used to find the similarities and dissimilarities between the retention characteristics of the various eleuents and solutes. The mean retention times ± two standard deviations for phenol derivatives determined with the eight eluents formed the original data matrix for PCA. The various acetonitrile–water (four) and methanol–water (four) eluents were considered as variables, and the mean retention times ± two standard deviations for phenol derivatives were the observations. The calculation was carried out on both the correlation and covariance matrices. The calculation of the correlation matrix requires the normalization of the original data whereas the covariance matrix uses them without normalization. The explained variance was set to 99.9% in both instances. As the significance test of PCA loadings and variables is not yet known, we assumed that inserting the mean ± two standard deviations in PCA may help the elucidation of this problem. Linear correlations were calculated between PCA variables and loading calculated from the two different matrices. Dependent variables were always those calculated from the covariance matrix. Only the PCA variables and loadings with the same serial number were correlated:

TABLE I

STRUCTURES OF RING-SUBSTITUTED PHENOL DERIVATIVES
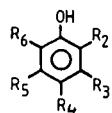
No.	R_2	R_3	R_4	R_5	R_6
1	CH_3	H	H	H	H
2	H	CH_3	H	H	H
3	H	H	CH_3	H	H
4	CH_3	H	H	H	CH_3
5	H	$N(CH_3)_2$	H	H	H
6	H	OH	CH_2CH_3	H	H
7	H	OCH_3	OCH_3	H	H
8	$C(CH_3)_3$	H	H	H	$C(CH_3)_3$
9	OCH_3	OCH_3	H	H	H
10	OCH_3	H	$CH_2CH=CH_2$	H	H
11	H	H	CH_2CN	H	H
12	CH_2OCH_3	H	H	H	H
13	CL	H	H	H	H
14	H	H	Cl	H	H
15	Cl	H	H	H	CL
16	H	Cl	H	Cl	H
17	H	Br	H	H	H
18	H	H	Br	H	H
19	Br	H	Br	H	H
20	H	F	H	H	H
21	H	H	F	H	H
22	H	H	CN	H	H
23	H	NO_2	H	H	H
24	H	H	NO_2	H	H

$$A_{cov} = a + b A_{corr} \tag{1}$$

where A = PCA loadings and

$$Z_{cov} = a + b Z_{corr} \tag{2}$$

where Z = PCA variable, corr = calculated from correlation matrix and cov = calculated from co-variance matrix.

The two-dimensional non-linear (nl) map of PCA variables was also calculated [19,20]. Linear correlations were also calculated between the coordinates of the nl maps calculated from the covariance and correlation matrices:

$$X_{cov} = a + b X_{corr} \tag{3}$$

$$Y_{cov} = a + b Y_{corr} \tag{4}$$

where X and Y are the coordinates of nl maps.

The aim of the determination of correlations listed above was the comparison of the information content of PCA methods. It was motivated by the fact that the normalization needed for the calculation of the correlation matrix may cause information loss and may lead to distorted conclusions in the evaluation of retention data [21].

RESULTS AND DISCUSSION

Each phenol derivative showed narrow and symmetric peaks in each eluent system (Figs. 1 and 2), that is, the carbon column can be successfully used for the separation of ring-substituted phenol derivatives without buffering the eluent. The *ortho, meta*

Absorption
254 nm
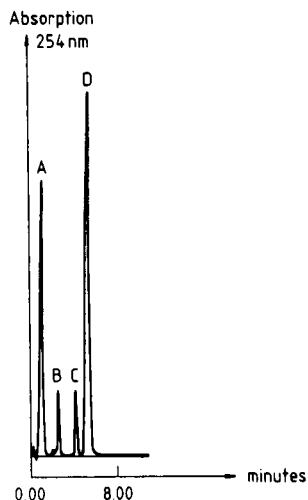
Fig. 1. Separation of phenol derivatives on the porous graphitic carbon column. Eluent, acetonitrile–water (7:3, v/v); flow-rate, 1 ml/min; detection, 254 nm. (A) 3-fluorophenol; (B) 3-bromophenol; (C) 4-nitrophenol; (D) 3-nitrophenol.

Absorption
254 nm
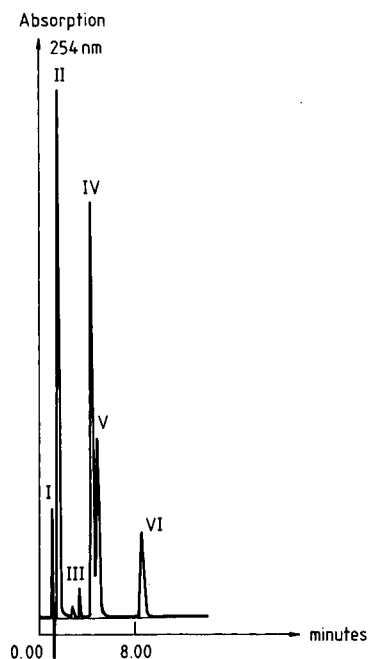
Fig. 2. Separation of phenol derivatives on the porous graphitic carbon column. Eluent, methanol–water (95:5, v/v); flow-rate, 1 ml/min; detection, 254 nm. (I) Dead time; (II) 2,3-dimethoxyphenol; (III) 3,5-dichlorophenol; (IV) 2,6-di-*tert.*-butylphenol; (V) 2,6-dichlorophenol; (VI) 2,4-dibromophenol.

and *para* isomers could be well separated on the column, which indicates the good separation capacity of PGC. The retention order of solutes does not follow the retention order expected according to their lipophilicity [22]. The more hydrophilic nitro derivatives elute after the more hydrophobic bromo and fluoro derivatives (Fig. 1) and di-*tert.*-butylphenol shows a lower retention than the corresponding dichloro derivative (Fig. 2), however, its lipophilicity is higher. These findings indicate that the retention behaviour of the PGC column differs from that of the common reversed-phase columns.

The retention times of phenol derivatives are compiled in Table II. The retention of each compound decreases with increasing concentration of organic modifier, and no anomalous retention behaviour was observed. The data support our previous qualitative conclusions that the lipophilicity of solutes does not determine their retention on a PGC column, but the eluents are typical reversed-phase eluents. The retention increases with increase in the number of substituents, which indicates the involvement of steric parameters in the retention mechanism. We are well aware that in general the molecular size is related to the lipophilicity, and therefore the influence of lipophilicity of solutes on the retention cannot be excluded. However, the relationship between the lipophilicity and molecular size is a loose one and our data rather support the hypothesis that molecular parameters other than lipophilicity govern the retention.

The data on peak symmetry and column performance are complied in Table III. The data indicate that the peak symmetry is similar on PGC in an unbuffered eluent and on an ODS column in a buffered eluent, but the relative performance of PGC column is markedly better than that of the ODS column even with a buffered eluent.

The results of PCA carried out on the covariance and correlation matrices are summarized in Tables IV and V, respectively. In both instances the fist principal component explained most of the variance, hence the main retention characteristics of the eight eluent systems applied can be expressed by only one hypothetical eluent system. PCA does not prove the existence of such an eluent system, but only indicates its mathematical possibility. Comparing the ratio of variance explained by the individual principal components, both calculation

TABLE II

RETENTION TIMES OF PHENOL DERIVATIVES (min)

Compound	Methanol (%, v/v)				Acetonitrile (%, v/v)			
	90	92.5	95	97.5	70	75	80	85
1	$3.23 \pm {<}10^{-3}$	$2.73 \pm {<}10^{-3}$	$2.29 \pm {<}10^{-3}$	$1.99 \pm 7.1{\cdot}10^{-3}$	$2.10 \pm {<}10^{-3}$	$1.92 \pm {<}10^{-3}$	$1.80 \pm {<}10^{-3}$	$1.71 \pm {<}10^{-3}$
2	$3.21 \pm {<}10^{-3}$	$2.70 \pm {<}10^{-3}$	$2.25 \pm {<}10^{-3}$	$1.97 \pm 7.1{\cdot}10^{-3}$	$2.11 \pm {<}10^{-3}$	$1.99 \pm {<}10^{-3}$	$1.86 \pm {<}10^{-3}$	$1.74 \pm 7.1{\cdot}10^{-3}$
3	$2.80 \pm {<}10^{-3}$	$2.50 \pm {<}10^{-3}$	$2.28 \pm {<}10^{-3}$	$2.05 \pm 7.1{\cdot}10^{-3}$	$2.05 \pm {<}10^{-3}$	$1.82 \pm {<}10^{-3}$	$1.77 \pm {<}10^{-3}$	$1.71 \pm {<}10^{-3}$
4	$9.11 \pm 1.4{\cdot}10^{-2}$	$7.44 \pm 3.5{\cdot}10^{-2}$	$5.88 \pm {<}10^{-3}$	$4.55 \pm {<}10^{-3}$	$3.03 \pm {<}10^{-3}$	$2.87 \pm 7.1{\cdot}10^{-3}$	$2.74 \pm {<}10^{-3}$	$2.65 \pm 2.4{\cdot}10^{-2}$
5	$8.20 \pm 9.1{\cdot}10^{-2}$	$7.14 \pm 2.8{\cdot}10^{-2}$	$5.70 \pm 7.1{\cdot}10^{-3}$	$4.82 \pm 7.1{\cdot}10^{-3}$	$3.69 \pm 2.8{\cdot}10^{-3}$	$3.26 \pm {<}10^{-3}$	$3.00 \pm 3.5{\cdot}10^{-2}$	$2.64 \pm 7.1{\cdot}10^{-2}$
6	$5.70 \pm {<}10^{-3}$	$3.58 \pm 2.8{\cdot}10^{-2}$	$2.85 \pm {<}10^{-3}$	$2.05 \pm 1.4{\cdot}10^{-2}$	$2.16 \pm {<}10^{-3}$	$2.03 \pm 7.0{\cdot}10^{-2}$	$1.85 \pm {<}10^{-3}$	$1.30 \pm 3.5{\cdot}10^{-2}$
7	$6.60 \pm {<}10^{-3}$	$4.56 \pm 7.0{\cdot}10^{-2}$	$3.44 \pm 1.4{\cdot}10^{-2}$	$2.80 \pm 3.5{\cdot}10^{-2}$	$2.62 \pm 1.4{\cdot}10^{-2}$	$2.46 \pm {<}10^{-3}$	$2.33 \pm {<}10^{-3}$	$2.27 \pm 3.5{\cdot}10^{-2}$
8	$7.46 \pm {<}10^{-3}$	$4.85 \pm {<}10^{-3}$	$3.90 \pm {<}10^{-3}$	$2.62 \pm {<}10^{-3}$	$5.65 \pm {<}10^{-3}$	$4.38 \pm {<}10^{-3}$	$3.38 \pm {<}10^{-3}$	$2.77 \pm 1.4{\cdot}10^{-2}$
9	$4.12 \pm {<}10^{-3}$	$3.24 \pm 7.1{\cdot}10^{-3}$	$2.70 \pm 8.4{\cdot}10^{-2}$	$2.12 \pm 2.1{\cdot}10^{-2}$	$1.99 \pm {<}10^{-3}$	$1.88 \pm {<}10^{-3}$	$1.82 \pm 7.0{\cdot}10^{-2}$	$1.77 \pm 4.0{\cdot}10^{-3}$
10	$7.03 \pm 1.4{\cdot}10^{-3}$	$5.90 \pm 7.1{\cdot}10^{-3}$	$5.17 \pm 1.4{\cdot}10^{-2}$	$4.08 \pm 7.1{\cdot}10^{-3}$	$4.21 \pm {<}10^{-3}$	$1.88 \pm {<}10^{-3}$	$3.29 \pm {<}10^{-3}$	$3.01 \pm {<}10^{-3}$
11	$4.17 \pm {<}10^{-3}$	$2.96 \pm {<}10^{-3}$	$2.17 \pm {<}10^{-3}$	$2.10 \pm 1.4{\cdot}10^{-2}$	$1.87 \pm 7.1{\cdot}10^{-2}$	$2.06 \pm {<}10^{-3}$	$1.65 \pm {<}10^{-3}$	$1.46 \pm 7.1{\cdot}10^{-3}$
12	$4.60 \pm {<}10^{-3}$	$3.73 \pm 1.4{\cdot}10^{-2}$	$2.71 \pm 2.1{\cdot}10^{-2}$	$2.35 \pm 1.4{\cdot}10^{-2}$	$2.19 \pm {<}10^{-3}$	$2.03 \pm 5.6{\cdot}10^{-2}$	$1.92 \pm {<}10^{-3}$	$1.82 \pm 2.4{\cdot}10^{-2}$
13	$3.54 \pm 7.1{\cdot}10^{-3}$	$3.02 \pm 3.5{\cdot}10^{-2}$	$2.55 \pm 1.4{\cdot}10^{-2}$	$2.23 \pm 7.1{\cdot}10^{-3}$	$2.45 \pm 3.54{\cdot}10^{-2}$	$2.25 \pm {<}10^{-3}$	$2.05 \pm 2.1{\cdot}10^{-2}$	$1.96 \pm {<}10^{-3}$
14	$3.90 \pm {<}10^{-3}$	$3.34 \pm 1.4{\cdot}10^{-2}$	$2.71 \pm 7.1{\cdot}10^{-3}$	$2.36 \pm 7.1{\cdot}10^{-3}$	$2.50 \pm {<}10^{-3}$	$2.29 \pm {<}10^{-3}$	$2.15 \pm {<}10^{-3}$	$2.03 \pm 1.4{\cdot}10^{-3}$
15	$8.50 \pm {<}10^{-3}$	$7.20 \pm 7.1{\cdot}10^{-3}$	$5.71 \pm 6.2{\cdot}10^{-2}$	$4.70 \pm 7.7{\cdot}10^{-2}$	$7.07 \pm 1.4{\cdot}10^{-2}$	$5.83 \pm {<}10^{-3}$	$5.31 \pm {<}10^{-3}$	$4.58 \pm 2.8{\cdot}10^{-3}$
16	$10.35 \pm {<}10^{-3}$	$8.65 \pm 1.4{\cdot}10^{-2}$	$6.51 \pm 1.4{\cdot}10^{-2}$	$5.40 \pm 2.8{\cdot}10^{-2}$	$7.33 \pm {<}10^{-3}$	$6.01 \pm {<}10^{-3}$	$5.40 \pm {<}10^{-3}$	$4.56 \pm {<}10^{-3}$
17	$4.47 \pm {<}10^{-3}$	$3.86 \pm 7.1{\cdot}10^{-3}$	$3.37 \pm 7.1{\cdot}10^{-3}$	$2.78 \pm {<}10^{-3}$	$3.01 \pm {<}10^{-3}$	$2.74 \pm 7.1{\cdot}10^{-3}$	$2.49 \pm {<}10^{-3}$	$2.26 \pm 7.1{\cdot}10^{-3}$
18	$4.42 \pm {<}10^{-3}$	$3.96 \pm {<}10^{-3}$	$3.22 \pm 7.1{\cdot}10^{-3}$	$2.88 \pm {<}10^{-3}$	$3.15 \pm {<}10^{-3}$	$2.84 \pm {<}10^{-3}$	$2.59 \pm {<}10^{-3}$	$2.46 \pm {<}10^{-3}$
19	$16.14 \pm 7.1{\cdot}10^{-3}$	$12.88 \pm 7.1{\cdot}10^{-3}$	$10.52 \pm 1.4{\cdot}10^{-2}$	$7.93 \pm 1.4{\cdot}10^{-2}$	$3.15 \pm {<}10^{-3}$	$9.79 \pm {<}10^{-3}$	$8.75 \pm {<}10^{-3}$	$7.13 \pm {<}10^{-3}$
20	$3.53 \pm {<}10^{-3}$	$2.10 \pm {<}10^{-3}$	$1.75 \pm 7.1{\cdot}10^{-3}$	$1.65 \pm 1.4{\cdot}10^{-2}$	$1.81 \pm {<}10^{-3}$	$1.65 \pm {<}10^{-3}$	$1.56 \pm {<}10^{-3}$	$1.48 \pm {<}10^{-3}$
21	$3.26 \pm {<}10^{-3}$	$2.42 \pm 7.1{\cdot}10^{-3}$	$1.78 \pm 7.1{\cdot}10^{-3}$	$1.59 \pm 7.1{\cdot}10^{-3}$	$1.79 \pm {<}7.1{\cdot}10^{-3}$	$1.70 \pm {<}10^{-3}$	$1.59 \pm 2.8{\cdot}10^{-2}$	$1.53 \pm {<}10^{-3}$
22	$4.23 \pm 1.4{\cdot}10^{-3}$	$3.75 \pm {<}10^{-3}$	$3.28 \pm 2.2{\cdot}10^{-2}$	$2.77 \pm 1.4{\cdot}10^{-2}$	$2.72 \pm 1.4{\cdot}10^{-2}$	$2.43 \pm {<}10^{-3}$	$2.25 \pm 1.4{\cdot}10^{-2}$	$2.12 \pm 7.1{\cdot}10^{-3}$
23	$9.92 \pm 3.5{\cdot}10^{-2}$	$7.97 \pm 5.6{\cdot}10^{-2}$	$6.30 \pm 1.4{\cdot}10^{-2}$	$4.45 \pm 6.36{\cdot}10^{-2}$	$5.65 \pm 3.5{\cdot}10^{-2}$	$4.97 \pm 1.4{\cdot}10^{-2}$	$4.29 \pm 7.1{\cdot}10^{-2}$	$3.80 \pm {<}10^{-3}$
24	$11.88 \pm 2.8{\cdot}10^{-2}$	$8.62 \pm 7.1{\cdot}10^{-2}$	$5.37 \pm 9.9{\cdot}10^{-2}$	$4.63 \pm 2.12{\cdot}10^{-2}$	$4.56 \pm 7.1{\cdot}10^{-3}$	$4.17 \pm 1.1{\cdot}10^{-2}$	$3.74 \pm {<}10^{-3}$	$3.48 \pm 2.8{\cdot}10^{-2}$

TABLE III

COMPARISON OF THE RETENTION CHARACTERIS-
TICS OF POROUS GRAPHITIZED CARBON AND HY-
PERSIL ODS COLUMNS

I = Porous graphitized column; II = ODS column, non-buf-
fered eluent; III = ODS column, buffered eluent. P (%) = 100·
(plate number for compound/plate number for toluene).

Compound	Asymmetry factor			P (%)		
	I	II	III	I	II	III
14	1.12	1.49	1.00	65.8	54.4	47.8
17	1.25	1.50	1.33	61.0	46.2	59.5
18	1.20	1.31	1.08	64.9	23.0	22.1

methods give similar results. The high ratio of var-
iance explained by the first PC may make question-
able the application of PCA for the evaluation of
our data matrix. As the eigenvalue of the second PC
(PCA on the correlation matrix) was > 1, it was
assumed that it also contains important informa-
tion and it is not only the product of the standard
deviation of the original data.

TABLE IV

RESULT OF PRINCIPAL COMPONENT ANALYSIS CAR-
RIED OUT ON THE COVARIANCE MATRIX

No.	Eigenvalue	Variance explained (%)
1	34.657	94.49
2	1.531	98.67
3	0.378	99.70

	PCA loadings		
	1	2	3
1	1.461	−0.146	0.342
2	1.949	−0.171	0.294
3	2.535	−0.379	0.136
4	3.163	−0.605	−0.368
5	1.263	0.286	0.066
6	1.565	0.386	0.033
7	1.778	0.478	−0.067
8	2.253	0.714	−0.098

TABLE V

RESULT OF PRINCIPAL COMPONENT ANALYSIS CAR-
RIED OUT ON THE CORRELATION MATRIX

No.	Eigenvalue	Variance explained (%)
1	7.57	94.71
2	0.31	98.66
3	0.07	99.58

	PCA loadings		
	1	2	3
1	0.968	0.192	−0.150
2	0.978	0.173	−0.076
3	0.975	0.209	0.032
4	0.956	0.215	0.197
5	0.980	−0.156	−0.051
6	0.983	−0.177	−0.012
7	0.977	−0.205	0.034
8	0.966	−0.246	0.043

The parameters of linear correlations between PC
loadings and variables calculated from the covar-
iance and correlation matrices and between the co-
ordinates of the non-linear maps are compiled in
Table VI. According to eqns. 1 and 2, highly signif-
icant correlations were found between the PCA
variables and loadings. This result indicates that in
our case the information content of the PCA
variables and loadings computed from different ma-
trices are similar. The distribution of PCA loadings
(eluent systems) calculated according to the covar-
iance and correlation matrices are illustrated in
Figs. 3 and 4, respectively. In both figures the
eluents containing different organic components
(methanol or acetonitrile) form separate clusters.
This result shows that methanol and acetonitrile
show different selectivities, but this difference is
fairly small (compare the information content of
the first and second principal components in Tables
IV and V).

The two-dimensional non-linear maps of PCA
variables calculated from the covariance and corre-
lation matrices are shown in Figs. 5 and 6. The cen-
tre of the circle represents the mean retention time
and the radius of the circle characterizes the ±2
standard deviation value. It was assumed that the

TABLE VI

LINEAR CORRELATION OF PARAMETERS BETWEEN THE PRINCIPAL COMPONENT VARIABLES AND LOADINGS AND BETWEEN THE NON-LINEAR MAP COORDINATES

$y = a + bx$. y = Calculated from covariance matrix; x = calculated from correlation matrix; n = sample number; a = regression constant; b = regression coefficient; S_b = standard deviation of regression coefficient; r = correlation coefficient; $r_{tabulated}$ = critical value of correlation coefficient.

Dependent and independent variables	Parameters					
	n	a	b	S_b	r	$r_{tabulated}$
(1) PC variables	75	11.10	2.13	0.02	0.9962	0.3799 (99.9%)
(2) PC variables	75	−0.59	−1.50	0.18	0.6789	0.3799 (99.9%)
(3) PC variables	75	0.59	1.81	0.15	0.8077	0.3799 (99.9%)
(1) PCA loadings	8	51.29	−50.66	19.61	0.7257	0.7067 (95%)
(2) PCA loading	8	0.07	−2.07	0.26	0.9547	0.9249 (99.9%)
(3) PCA loading	8	0.02	−1.73	0.43	0.8516	0.8343 (99%)
(1) Coordinates	75	2.84	1.01	0.008	0.9975	0.3799 (99.9%)
(2) Coordinates	75	181.92	−1.05	0.002	0.9747	0.3799 (99.9%)

phenol derivatives can be separated in all eluents with 95% probability when the circles in Figs. 5 and 6 do not overlap each other. The experimental data (see Table II) supported this assumption. It can be concluded that this procedure may represent a new graphical approximation method including the standard deviation in PCA. The phenol derivatives
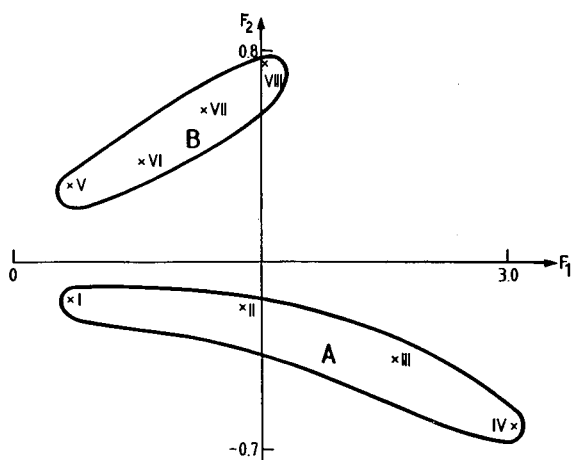
Fig. 3. Distribution of eluent systems according to the covariance matrix. (A) Methanol–water eluents; (B) acetonitrile–water eluents.
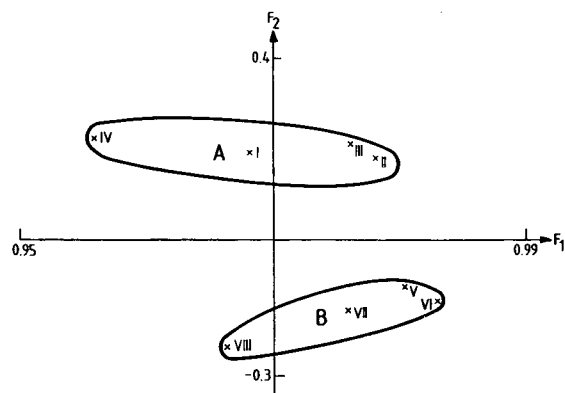
Fig. 4. Distribution of eluent systems according to the correlation matrix. (A) Methanol–water eluents; (B) acetonitrile–water eluents.
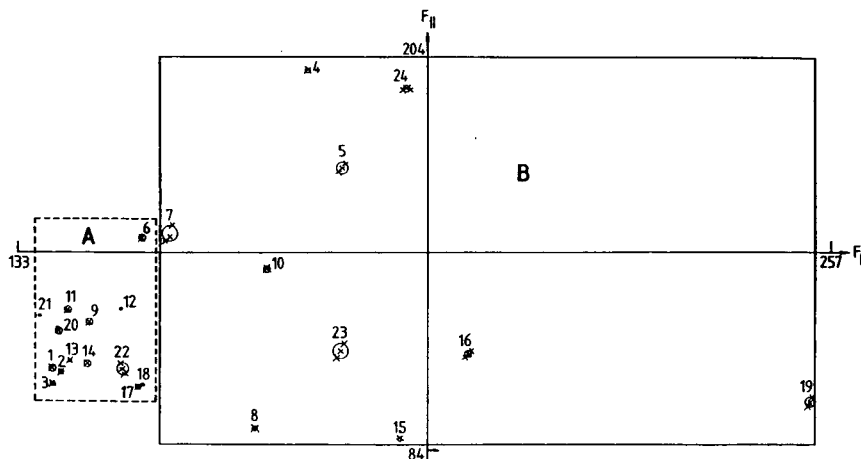
Fig. 5. Two-dimensional non-linear map of PC variables. Covariance matrix; number of iterations, 64; maximum error, $1.00 \cdot 10^{-3}$. Numbers refer to phenol derivatives in Table I.

form two distinct clusters on the basis of the number of substituents; clusters A and B contain the mono- and disubstituted phenol derivatives, respectively.

This finding supports the assumption that the retention behaviour of ring-substituted phenol derivatives on the carbon column is mainly governed by the number of substituents, which is related to the bulkiness of the whole molecule; however, the influ-

ence of lipophilicity on the retention cannot be entirely ruled out. According to our calculations, the mononitro derivatives (compounds **23** and **24** in Table I) show a similar retention behaviour to the other disubstituted compounds. This effect may be due to the bulkiness of the NO_2 substituents.

The parameters of linear correlations between the coordinates of non-linear maps are compiled in Table VI. The data demonstrate again the similar in-
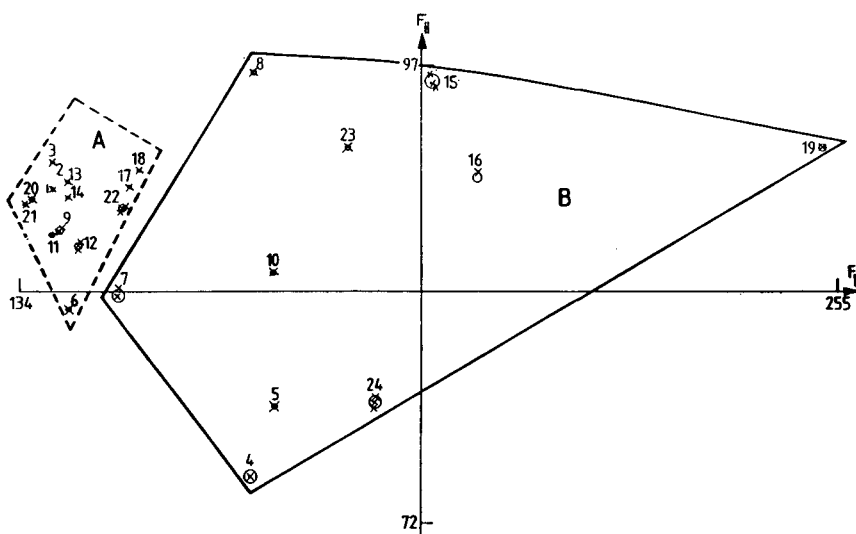
Fig. 6. Two-dimensional non-linear map of PC variables. Correlation matrix; number of iterations, 82; maximum error, $1.03 \cdot 10^{-3}$. Numbers refer to phenol derivatives in Table I.

formation content of the two calculation methods.

It can be concluded from our data that ring-substituted phenol derivatives can be well separated on a graphitized carbon column without buffering the eluent, and monosubstituted phenol derivatives generally show lower retentions than disubstituted derivatives. Calculations indicated that the retention of the ring-substituted phenol derivatives is mainly governed by the bulkiness of the solute molecule.

ACKNOWLEDGEMENT

REFERENCES

1 A. Berthod, *J. Chromatogr.*, 549 (191) 1.
2 A. Nahum and Cs. Horváth, *J. Chromatogr.*, 203 (1981) 53.
3 K. E. Bij, Cs. Horváth, W. R. Melander and A. Nahum, *J. Chromatogr.*, 203 (1981) 65.
4 H. Tayar, H. Waterbeend and B. Testa, *J. Chromatogr.*, 320 (1985) 305.
5 C. J. Laurent, H. A. H. Billiet and L. de Galan, *J. Chromatogr.*, 285 (1984) 161.
6 J. J. Sun and J. S. Fritz, *J. Chromatogr.*, 522 (1990) 95.
7 J. A. Blackwell and P. W. Carr, *J. Chromatogr.*, 549 (1991) 43.
8 J. A. Blackwell and P. W. Carr, *J. Chromatogr.*, 549 (1991) 59.
9 T. Takeuchi, W. Hu and H. Haraguchi, *J. Chromatogr.*, 517 (1990) 257.
10 M. T. Gilbert, J. H. Know and B. Kaur, *Chromatographia*, 16 (1982) 138.
11 J. H. Knox, B. Kaur and G. R. Millward, *J. Chromatogr.*, 352 (1986) 3.
12 B. Kaur, *LC·GC*, 3 (1990) 41.
13 D. Roberts and D. W. Ruane, *J. Pharm. Biomed. Anal.*, 7 (1989) 112.
14 J. C. Berridge, *J. Chromatogr.*, 449 (1989) 56.
15 R. Kaliszan, K. Osmialowski and B. B. Bassler, *J. Chromatogr.*, 499 (1990) 33.
16 N. Tanaka, T. Tanagawa, K. Kimata, K. Hosoya and T. Araki, *J. Chromatogr.*, 549 (1991) 29.
17 T. Cserhati and H. E. Hauck, *J. Chromatogr.*, 514 (1990) 45.
18 L. R. Snyder and J. J. Kirkland, *Introduction to Modern Liquid Chromatography*, Wiley, New York, 2nd ed., 1979, pp. 28 and 222.
19 J. W. Sammon, *IEEE Trans. Comput.*, C18 (1969) 401.
20 T. Cserhati, B. Bordas, L. Ekiert and J. Bojarski, *J. Chromatogr.*, 287 (1984) 386.
21 T. Cserhati and Z. Illes, *Chromatographia*, 31 (1991) 152.
22 C. Hansch and A. Leo, *Substituent Constants for Correlation Analysis in Chemistry and Biology*, Wiley, New York, 1979.

Retention reproducibility of basic drugs in high-performance liquid chromatography on a silica column with a methanol–high-pH buffer eluent

Changes in selectivity with the age of the stationary phase

Roger M. Smith* and James P. Westlake☆

Department of Chemistry, Loughborough University of Technology, Loughborough, Leicestershire LE11 3TU (UK)

Richard Gill and M. David Osselton

Central Research and Support Establishment, Home Office Forensic Science Service, Aldermaston, Reading, Berkshire RG7 4PN (UK)

ABSTRACT

The long-term reproducibility of the separation of basic drugs by high-performance liquid chromatography using a silica column with a methanol–high-pH eluent was examined. The relative capacity factors of specific tertiary amines changed systematically compared with the other drugs on storage of the columns for 1 year. The changes were enhanced on storing the column in mobile phase and were accelerated by prolonged washing with water. A comparison of freshly packed columns suggested that similar changes also occurred with the dry silica on storage. These effects may be a contributor to previously observed batch-to-batch differences in the silica.

INTRODUCTION

The analysis of basic analytes by high-performance liquid chromatography (HPLC) often causes considerable problems because of interactions between the analytes and free silanol groups on the surface of the silica stationary phase [1]. A number of approaches have been used to overcome this problem in reversed-phase chromatography, including the use of deactivating agents such as alkylamines in the mobile phase [1] and highly coated silica stationary phases [2,3]. An alternative technique has been to use silica as an ion-exchange medium [4] with mobile phases containing high proportions of methanol and high-pH buffers. Most of these studies have used eluents consisting of 90:10 methanol–ammonia/ammonium nitrate (pH 9.2) buffers [5].

However, in previous work in these laboratories it was found that although reproducible results could be obtained under closely controlled conditions on a single column over a limited time period within one laboratory [6], considerable variation was found in the relative retentions of a number of the test analytes on different batches and brands of silica [7]. In addition, in collaborative trials large variations in absolute and relative retentions between laboratories were obtained for columns prepared from a single common batch of silica [8,9]. It

---

☆ Present address: Phase Separations Ltd., Deeside Industrial Park, Deeside, Clwyd, UK.

was considered that these differences might be due to variations in the ionic strength of the mobile phase caused by differences in the concentration of the ammonia solutions used to prepare the buffer [9].

In order to develop a more robust method, alternative high-pH buffers were examined. A mixture of 3-(cyclohexylamino)-1-propanesulphonic acid (CAPS) and sodium 3-(cyclohexylamino)-2-hydroxy-1-propanesulphonate (CAPSO-Na), which could be prepared by weight, was selected as this would avoid the problems due to the volatility of the ammonia buffer [10]. This new method showed good robustness and reproducibility but differences were again noted between different batches of the same brand of silica.

This paper extends this work and reports a study of changes in the separation of basic analytes with the age of the silica before packing, changes in the selectivity of columns on storage, the effect of different storage conditions and of accelerated ageing by washing the columns with water. These studies were not possible previously as the limited long-term reproducibility of the ammonia-based mobile phase would have masked any changes. In early work, Wheals [11] found that a silica column was stable towards dissolution for a long period provided that the mobile phase contained a high percentage of methanol and ammonia was used as the source of the high pH. Subsequently, Law [12] noted an overall decrease in retention times with time for the separation of a set of 69 related monofunctional arylalkylamines. Because of widespread scepticism about the stability of the silica when used with these high-pH eluents, Law and Chan [13] carried out an extended study and reported that a single column could be used for over 9 months for a range of antimalarial drugs. However, the selectivity of the column changed with time and this was attributed to irreversible adsorption on the column which might have been prevented by using a guard column.

Few previous studies have examined the long-term stability on silica based column materials. Claessens et al. [14] studied the ageing processes of alkyl-bonded phases and attributed many of the changes to alterations in the underlying silica matrix, in particular the hydrolysis of siloxane groups to silanols. More recently, Hetem et al. [2] used retention and NMR studies to examine the changes in the underlying silica of three bonded-phase materials with different ageing conditions. Although Cox and Stout [15] compared the effects on the retention of bases on silica from different sources and suggested that a slow equilibrium existed between siloxanes and silanols groups, they did not report any changes in properties with time.

EXPERIMENTAL

Chemicals

Sample and eluent components were as reported previously [10]. The eluent buffer was prepared by mixing CAPS (0.8852 g) and CAPSO-Na (1.0372 g) in water and making up to 50 ml.

The columns were all packed using Spherisorb S5W (batch F5493/1 or batch 2752; Phase Separations, Deeside, UK). The former batch had been subdivided into 10-g sub-batches, which were stored separately.

HPLC separations

The equipment and samples were as described previously [10]. The test drugs were injected as mixtures of 2–5 components and were eluted using methanol–buffer (90:10, v/v) at 30°C. Protriptyline was used as an internal standard. The separations were carried out in triplicate and the mean retention times were used to calculate the relative capacity factors compared with protriptyline.

Between separations the columns were stored at room temperature after washing with either methanol or fresh mobile phase. Each column was equilibrated with fresh eluent overnight prior to being tested.

RESULTS AND DISCUSSION

One-year storage trials

Three columns were prepared from a single sub-batch of Spherisorb S5W (batch F5493/1: 10.A, 10.B and 10.C). The columns were tested immediately after packing using a set of 27 test compounds and the CAPS-CAPSO-Na mobile phase and then after ca. 1, 3, 6 and 12 months. In order to determine whether the storage conditions influenced the stability of the silica after each test, columns 10.A and 10.B were washed with methanol prior to storage and column 10.C was washed with fresh eluent.

Results are not given for column 10.B after 6 months because equipment problems caused poor reproducibility. It was also necessary to re-pack the top of this column with fresh silica after 1 year before any meaningful chromatographic results could be recorded. Particular problems were experienced on all three columns with methylamphetamine, the peak shape of which deteriorated in this study compared with earlier work [10]. Reasonable peak shapes could only be obtained using a tenfold diluted test solution. Frequently the methylamphetamine peak was distorted and reliable capacity factors could not be obtained. This problem is the subject of further study.

The capacity factors (k') for the test compounds decreased on all three columns over the period of the study, e.g., for protriptyline on column 10.A, initially $k' = 10.40$, which decreased after 1 year to $k' = 8.04$. This agrees with the study by Law [12], who also found a decrease in retention over a prolonged period of elution. Initially the relative capacity factors of the test compounds compared with protriptyline on each of the three columns were almost identical (Tables I–III). The only differences in elution order were for the closely eluted compounds nortriptyline and prolintane, which were reversed on column 10.A compared with the other two columns, and pholcodine and phenylephrine, which were reversed on column 10.C. However, the variations in the relative capacity factors of these compounds were small and were similar to the variations found earlier for repeated separations on a single column [10].

Over the period of the study, the relative capacity factors for most of the analytes showed only small variations (less than 2 units). However, a number of compounds showed greater changes and their relative capacity factors altered steadily over the year (Table IV and Fig. 1 for column 10.A). For the two columns stored in methanol, the relative capacity factors for morphine, codeine, phenylephrine, pholcodine and methdilazine all increased on average by between 2 and 4 units. In contrast, decreased relative capacity factors were observed for dipipanone (-10 units), prolintane (-6 units) and pipazethate (-4 units). Larger differences were observed for the first group of compounds on column 10.C, which had been stored filled with the high-pH eluent, with many of the compounds changing by 4 to 7 units.

Significant changes were also found on this column for ethoheptazine (3 units) and ephedrine (4 units). The effects on dipipanone (-11 units) and prolintane (-6 units) were similar to the changes on storage in methanol. However, pipazethate showed a small increase in its relative capacity factor on this column rather than a decrease. Propanolol, whose capacity factor changed during the study by Law and Chan [13], was unchanged in this study.

The three compounds which suffered the largest effects, dipipanone, prolintane and pipazethate,

TABLE I

CHANGES IN RELATIVE CAPACITY FACTORS WITH AGE OF SILICA COLUMN 10.A (BATCH F5493/1) STORED IN METHANOL

Relative capacity factors: rel. $k' \times 100$ (relative to protriptylene).

Compound	Rel. $k' \times 100$				
	Time from packing (days)				
	0	34	97	197	370
Nitrazepam	2.0	2.2	2.3	2.4	2.1
Diazepam	2.5	2.8	2.8	2.9	2.6
Papaverine	3.3	3.5	3.9	3.7	3.5
Caffeine	3.9	4.0	4.2	4.3	4.4
Dextropropoxyphene	6.9	6.8	7.0	7.2	6.6
Cocaine	8.2	8.0	8.2	8.5	8.2
Procaine	8.9	8.9	9.2	9.5	9.2
Amitriptyline	16.3	16.4	17.0	17.1	16.9
Chlorpromazine	17.2	17.4	17.8	18.0	18.1
Propranolol	20.2	20.0	20.2	20.6	19.9
Imipramine	25.1	25.0	25.6	25.7	25.4
Morphine	27.8	27.5	28.3	28.7	30.7
Codeine	27.9	27.8	28.3	29.0	30.6
Promazine	29.4	29.5	30.0	30.6	30.7
Phentermine	32.5	31.7	31.9	32.1	31.4
Amphetamine	32.8	31.9	32.5	32.7	32.9
Phenylephrine	38.0	37.4	37.6	38.4	40.7
Pholcodine	38.4	36.8	38.0	38.9	42.2
Dipipanone	40.7	37.5	36.7	36.3	30.9
Ethoheptazine	45.6	45.0	45.7	46.7	47.0
Methdilazine	48.5	48.6	49.7	50.6	51.4
Nortriptyline	53.1	52.8	53.0	53.5	53.1
Prolintane	53.5	50.4	52.0	51.8	47.4
Ephedrine	54.2	53.2	53.6	54.3	55.3
Pipazethate	61.6	58.9	59.0	58.5	57.3
Methylamphetamine	71.4	70.8	N.R.[a]	71.6	N.R.[a]
Protriptyline	100.0	100.0	100.0	100.0	100.0
Strychnine	107.0	104.4	104.4	106.0	107.6

[a] Not reported because of distorted peaks.

TABLE II

CHANGES IN RELATIVE CAPACITY FACTORS WITH AGE OF SILICA COLUMN 10.B (BATCH F5493/1) STORED IN METHANOL

Rel. k' × 100 as in Table I.

Compound	Rel. k' × 100			
	Time from packing (days)			
	0	29	92	365
Nitrazepam	2.2	2.2	2.2	2.1
Diazepam	2.6	2.7	2.7	2.6
Papaverine	3.5	3.5	3.6	3.7
Caffeine	4.1	3.9	4.2	4.4
Dextropropoxyphene	7.0	6.9	6.9	6.5
Cocaine	8.1	7.8	8.1	8.2
Procaine	8.9	8.8	9.1	9.1
Amitriptyline	16.2	16.2	16.6	16.7
Chlorpromazine	17.2	17.4	17.6	18.1
Propranolol	20.0	19.8	20.0	19.7
Imipramine	25.0	24.9	25.2	25.2
Morphine	27.9	27.2	28.0	31.4
Codeine	28.1	27.7	28.4	31.0
Promazine	29.3	29.2	29.8	30.9
Phentermine	31.9	31.7	31.6	31.1
Amphetamine	32.6	32.1	32.2	33.1
Phenylephrine	38.5	37.1	37.7	41.4
Pholcodine	38.6	37.3	37.9	42.2
Dipipanone	39.2	37.6	35.9	28.2
Ethoheptazine	45.1	44.6	45.4	46.7
Methdilazine	48.5	48.7	49.3	51.4
Nortriptyline	52.5	52.8	52.7	53.3
Prolintane	51.9	50.2	51.4	44.9
Ephedrine	53.6	53.2	53.6	55.7
Pipazethate	59.9	58.5	58.8	55.6
Methylamphetamine	68.3	N.R.[a]	67.8	N.R.[a]
Protriptyline	100.0	100.0	100.0	100.0
Strychnine	106.3	105.2	104.1	105.7

[a] Not reported because of distorted peaks.

have been found previously to be particularly sensitive to small changes in the elution conditions [10]. Differences in the relative retentions of these compounds were also a major factor in discriminating different batches of silica, both with this eluent [10] and with the ammonia-buffered eluent [7]. The changes for pipazethate in those studies were smaller than for the other two compounds. Phenylephrine had also been identified as a compound whose retention was sensitive to the separation conditions and, as in this study, its relative retention always changed in the opposite direction to dipipanone but to a lesser extent.

The other compounds, whose relative capacity factors increased, had not been identified in the previous work [6,10] as compounds that were sensitive to separation conditions. In contrast, strychnine, whose relative capacity factor remained virtually constant in this study, had been found to be very sensitive to variations in the ammonia eluent [6,7]. This compound might be particularly sensitive to changes in the ionic strength of the eluent as its relative capacity factor decreased markedly on changing from the ammonia-based eluent to the weaker CAPS–CAPSO-Na eluent [10].

TABLE III

CHANGES IN RELATIVE CAPACITY FACTORS WITH AGE OF SILICA COLUMN 10.C (BATCH F5493/1) STORED IN MOBILE PHASE

Rel. k' × 100 as in Table I.

Compound	Rel. k' × 100				
	Time from packing (days)				
	0	33	96	198	369
Nitrazepam	2.1	2.2	2.3	2.4	2.2
Diazepam	2.8	2.5	2.7	2.8	2.7
Papaverine	3.4	3.5	3.5	3.8	3.5
Caffeine	3.9	4.2	4.3	4.4	4.5
Dextropropoxyphene	6.8	6.8	6.8	6.8	6.2
Cocaine	8.0	8.4	8.5	8.6	8.8
Procaine	8.8	9.1	9.4	9.7	9.6
Amitriptyline	16.1	16.4	16.8	17.1	17.0
Chlorpromazine	17.1	17.6	17.9	18.2	18.3
Propranolol	20.0	20.2	20.2	20.3	20.0
Imipramine	24.1	25.4	25.1	25.4	25.3
Morphine	27.2	29.8	30.3	31.3	33.0
Codeine	27.9	29.7	30.4	31.3	32.7
Promazine	29.1	30.1	30.6	31.1	31.2
Phentermine	32.0	32.0	31.6	31.6	31.3
Amphetamine	32.1	32.6	32.7	32.7	33.6
Phenylephrine	38.3	39.4	39.9	40.7	43.3
Pholcodine	37.7	40.2	40.6	41.6	44.6
Dipipanone	39.1	35.2	33.5	32.0	27.7
Ethoheptazine	44.9	46.7	47.2	47.9	47.9
Methdilazine	47.9	50.0	51.1	52.1	52.7
Nortriptyline	52.5	53.0	53.1	53.1	53.4
Prolintane	52.2	49.6	50.6	49.9	46.4
Ephedrine	53.6	55.5	55.2	55.9	57.3
Pipazethate	59.5	60.0	60.1	59.0	60.9
Methylamphetamine	68.1	N.R.[a]	70.2	70.7	N.R.[a]
Protriptyline	100.0	100.0	100.0	100.0	100.0
Strychnine	107.1	108.7	108.6	109.7	108.7

[a] Not reported because of distorted peaks.

TABLE IV

MAJOR CHANGES IN RELATIVE CAPACITY FACTORS ON STORAGE OF PACKED COLUMNS

Compound	Changes in relative capacity factors over 1 year	
	Storage solvent	
	Methanol[a]	Eluent[b]
Morphine	3.2	5.8
Codeine	2.8	4.8
Phenylephrine	2.8	5.0
Pholcodine	3.7	6.9
Dipipanone	− 10.4	− 11.4
Ethoheptazine	1.5	3.0
Methdilazine	2.9	4.8
Prolintane	− 6.5	− 5.8
Ephedrine	1.6	3.7
Pipazethate	− 4.3	1.4

[a] Mean value from columns 10.A and 10.B
[b] Column 10.C.

Effect of water on the ageing of the columns

It was suspected that the changes in the relative retentions on storage could be due to the effects of water, either from the mobile phase or from the
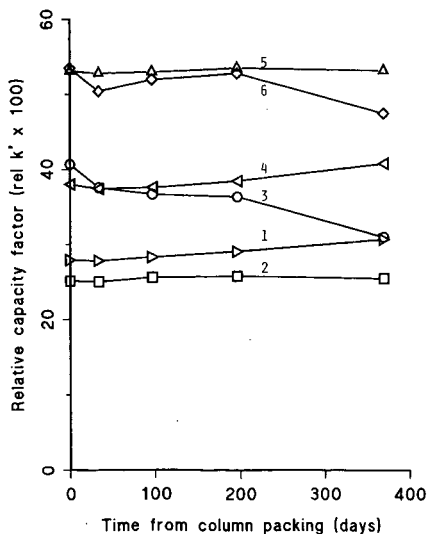
Fig. 1. Changes in relative capacity factors with time for selected analytes on column 10.A batch F5493/1. For conditions, see text. Compounds: 1 = codeine; 2 = imipramine; 3 = dipipanone; 4 = phenylephrine; 5 = nortriptyline; 6 = prolintane.

atmosphere, on the silica surface. After the initial storage trial had been completed, the columns (10.A, 10.B and 10.C) were therefore each washed with 1200–1300 ml of HPLC-grade water without a guard column in an attempt to produce "accelerated ageing" of the silica. This treatment also had the effect of partially restoring the poor peak shapes observed with methylamphetamine. The columns were then re-tested.

The capacity factors of all the analytes decreased as a result of washing, e.g., protriptyline from $k' = 8.04$ to 7.59 on column 10.A. Changes in the relative capacity factors were also observed (for selected examples, see Table V). On all three columns the tertiary amines dipipanone, prolintane and pipazethate showed further reductions in their relative capacity factors compared with the earlier study. The relative capacity factor of pipazethate on column 10.C now matched the value on the other two columns, rather than its much higher relative capacity factor after 1 year in the time trial. In addition, the relative capacity factor of strychnine decreased markedly, which had not been observed previously with these columns. Phenylephrine showed much larger increases in relative capacity factors on each column than in the time study. Ephedrine again showed only small effects. In all instances the increased relative retention for pholcodine over the 1-year study was reversed, the final results being only marginally different from the data recorded on the columns when new (Tables I–III).

Storage changes in dry silica

Because of concern that some changes in the nature of the surface of the silica could be occurring during storage of the stationary phase as a dry powder before packing, the retentions of the drug compounds were compared on four columns, which had been packed over an 18-month period using silica from the same original batch (batch F5493/1). Two of these columns were packed from the same sub-batch (columns 4.A and 4.B) and the others were from different sub-batches. Each column was packed, equilibrated with eluent and then tested within 5 days. In the packed column ageing study, the three columns 10.A, 10.B and 10.C had been packed within a few days so would have had the same age from the manufacture of the silica.

The capacity factors measured on the four col-

TABLE V

EFFECT OF A WATER WASH ON RELATIVE CAPACITY FACTORS OF SELECTED TEST COMPOUNDS

Rel. $k' \times 100$ as in Table I.

Compound	Rel. $k' \times 100$					
	Column 10.A		Column 10.B		Column 10.C	
	Before	After	Before	After	Before	After
Dipipanone	30.9	25.6	28.2	25.3	27.7	24.7
Phentermine	31.4	31.1	31.1	31.3	31.3	30.9
Phenylephrine	40.7	47.8	41.5	49.7	43.3	51.5
Pholcodine	42.2	37.6	42.2	39.5	44.6	37.6
Amphetamine	32.9	34.0	33.1	34.3	33.6	34.1
Prolintane	47.4	38.7	44.9	39.8	46.4	38.1
Ephedrine	55.3	56.3	55.7	57.9	57.3	55.2
Pipazethate	57.3	50.7	55.6	52.3	60.9	49.5
Strychnine	107.6	97.0	105.7	100.2	108.7	96.4

umns decreased with increasing age of the silica before packing (*e.g.*, protriptyline changed from $k' = 10.40$ on column 10.A packed 31 months after manufacture to $k' = 7.84$ on column 9.A packed after 48 months). Differences were also observed in the relative capacity factors of many of the compounds (Table VI). The effects were less than for the columns which had been stored in solvent and were not as systematically related to the age of the silica. The most marked effects in the relative capacity factors were again for prolintane, pipazethate and dipipanone, which all decreased. In contrast to the storage study, the relative capacity factor of strychnine also decreased. Morphine, ephedrine and phenylephrine showed small increases in relative retentions with increasing age of the silica.

Hence silica stored as a dry powder appeared to undergo similar changes in chromatographic properties to silica stored as a packed column in solvent.

Comparison of batches of silica

To determine if these changes in relative capacity factor occurred with other batches of silica, columns were prepared from an older batch of Spherisorb S5W (batch 2752, manufactured about 34 months before batch F5493/1). An initial column (2752.A) was prepared, tested and then stored for 14 months in methanol before being re-tested. At that time a second column (2752.B) was packed from the same batch of silica and was tested to examine the effect of storage on the dry powder (Ta-

ble VII). As expected from previous batch-to-batch comparisons, the retentions on these columns differed from those obtained with batch F5493/1.

The changes in the relative capacity factors with time on column 2752.A were generally smaller than for the F5493/1 batch of silica, but again dipipanone, prolintane and pipazethate showed marked decreases on storage of the column in solvent. In this instance strychnine was also affected. Phenylephrine showed a small increase but the changes for morphine and codeine were negligible.

The differences between the retentions on the two freshly packed columns, which would reflect the effects of the storage of the dry powder, were generally smaller, except for a marked change in strychnine (relative $k' = 95.2$ to 91.7).

It was felt that these changes in the properties of the column material might also have been responsible for some of the differences observed between batches of silica when they were examined using the ammonia buffer [8]. In that case the largest effects were found for the oldest batches and were particularly marked for strychnine.

Examination of the silica surface

To determine whether there had been any changes in the surface characteristics of the silica during the period of study, two silica samples (a dry sample of batch F5493/1 and a sample taken from column 4.A after storage for 18 months) were submitted for surface examination by [29]Si cross-polarization

TABLE VI

COMPARISON OF RELATIVE CAPACITY FACTORS ON NEW COLUMNS PACKED WITH SPHERISORB S5W (BATCH F5493/1) OVER AN 18-MONTH PERIOD

Each column was tested within 5 days of packing. Results for column 10.A from Table I. Rel. $k' \times 100$ as in Table I.

Compound	Rel. $k' \times 100$			
	Column (months from manufacture of silica)			
	4.A (30)	10.A (31)	4.B (46)	9.A (48)
Nitrazepam	2.3	2.0	2.1	2.1
Diazepam	3.1	2.5	2.5	2.6
Papaverine	3.6	3.3	3.3	3.3
Caffeine	4.2	3.9	4.0	4.3
Dextropropoxyphene	7.0	6.9	6.5	6.4
Cocaine	8.0	8.2	7.8	7.9
Procaine	8.8	8.9	8.4	8.5
Amitriptyline	16.2	16.3	16.0	16.3
Chlorpromazine	17.2	17.2	17.1	17.5
Propranolol	19.8	20.2	19.1	19.1
Imipramine	24.7	25.1	24.5	24.7
Morphine	27.8	27.8	28.7	29.6
Codeine	28.1	27.9	28.8	29.2
Promazine	29.0	29.4	29.1	29.7
Phentermine	31.8	32.5	31.5	31.3
Amphetamine	32.8	32.8	33.0	33.1
Phenylephrine	39.4	38.0	40.5	41.2
Pholcodine	38.0	38.4	38.9	38.5
Dipipanone	37.4	40.7	32.1	28.0
Ethoheptazine	43.9	45.6	43.9	44.1
Methdilazine	47.7	48.5	47.6	48.5
Nortriptyline	52.6	53.1	52.8	53.4
Prolintane	50.0	53.5	45.2	40.8
Ephedrine	53.4	54.2	54.4	55.0
Pipazethate	57.3	61.6	52.9	50.2
Methylamphetamine	63.9	71.4	64.1	64.5
Protriptyline	100.0	100.0	100.0	100.0
Strychnine	104.4	107.0	100.3	95.9

magic-angle spinning NMR spectroscopy (^{29}Si-CP-MAS-NMR). The spectra indicated that the ratio of the Q_3:Q_4 peaks (isolated silanols:siloxanes) changed from 2:3 for the dry silica to 3:3 for the sample removed from the column after treatment with eluent. However, the changes were subtle and not easily quantified. It appeared that hydrolysis of siloxanes to silanols had occurred on the silica surface.

These changes would contrast with those obtained by Hetem et al. [2], who found that for octa-decylsilyl-bonded silica, ageing treatment with a methanol–aqueous pH 8 mobile phase caused a decrease in the number of free silanol groups relative to siloxanes. It was proposed that siloxane bridge formation was occurring.

The three compounds, that showed consistent decreases in relative retentions with increasing silica age, dipipanone, pipazethate and prolintane, are all tertiary amines containing an alicyclic tertiary nitrogen atom to which the remainder of the molecule is linked, as an N-substituent on a pyrrolidine or

TABLE VII

COMPARISON OF RELATIVE CAPACITY FACTORS ON COLUMNS PACKED WITH SPHERISORB S5W (BATCH 2752)

Rel. $k' \times 100$ as in Table I.

Compound	Rel. $k' \times 100$		
	Column (days from start of set of experiments)		
	2752.A (0)	2752.A (440)	2752.B (packed 450)
Nitrazepam	2.6	2.2	2.3
Diazepam	3.0	2.7	2.8
Papaverine	3.9	3.4	3.5
Caffeine	4.9	4.7	4.6
Dextropropoxyphene	6.5	5.9	6.2
Cocaine	8.3	8.0	8.0
Procaine	9.3	8.8	8.7
Amitriptyline	17.4	17.2	17.2
Chlorpromazine	18.6	18.5	18.4
Propranolol	19.3	18.8	18.8
Dipipanone	24.0	20.5	22.7
Imipramine	25.7	25.2	25.4
Phentermine	31.2	30.3	30.4
Promazine	31.2	31.2	31.1
Codeine	31.3	31.8	30.5
Morphine	31.6	32.2	31.1
Amphetamine	33.1	33.4	33.0
Prolintane	39.6	36.1	37.2
Pholcodine	39.8	41.1	39.5
Phenylephrine	42.4	44.2	42.9
Ethoheptazine	46.5	46.0	45.2
Pipazethate	48.6	45.8	45.8
Methdilazine	51.8	52.2	51.1
Nortriptyline	53.8	54.0	54.0
Ephedrine	55.9	56.2	54.9
Methylamphetamine	66.3	65.6	64.6
Strychnine	95.2	92.3	91.7
Protriptyline	100.0	100.0	100.0

piperidine ring. The nitrogen atom is therefore sterically hindered compared with the other alicyclic tertiary amines in the test samples, such as cocaine and methdilazine, which contain less hindered N-methyl groups.

CONCLUSIONS

The rapid changes in the relative capacity factors of the basic drugs on treatment with water compared with storage in methanol or eluent and the slower changes on storage as a dry powder suggest that significant changes are occurring in the degree of hydroxylation of the silica surface. These were probably emphasized in this study, which used the silica as an ion-exchange medium, but from the work of Hetem et al. similar changes can also occur in the free silanols on bonded phases. In this study these changes caused differences in the overall retention properties of the silica. The effects on retention were selective and were probably dependent on the specific steric requirements of the interaction between the analyte and the silica surface, although clarification will require considerable further study. However, more than one type of change may be occurring because, although dipipanone and prolintane were always affected in a similar manner, the effect on the retention of strychnine was only observed on dry storage or on washing with water, but its retention was unaffected by storage in mobile phase.

These changes in the retention properties of silica with time or usage suggest that separations based on this mode of interaction might have inherent poor reproducibility over long periods. Irrespective of the consistency of the operating conditions, it will probably be difficult to replicate results in different laboratories unless all the analytes being considered interact with the column material in the same manner. Particular problems will be encountered if a wide range of structural types are being compared as in this study.

The differences in retention with the age of the silica following manufacture suggest that much of the batch-to-batch differences observed in earlier studies might have been due to an ageing process rather than inherent variations in the manufacturing or testing procedures. These changes in the silica surface with time may also be important in reversed-phase chromatography because of the frequently observed effects of interactions with residual silanols on bonded-phase columns, particularly during the separation of bases.

REFERENCES

1 E. Bayer and A. Paulus, J. Chromatogr., 400 (1987) 1.
2 M. J. J. Hetem, J. W. De Haan, H. A. Claessens, C. A. Cramers, A. Deege and G. Schomburg, J. Chromatogr., 540 (1991) 53.
3 Y. Ohtsu, U. Shiojima, T. Okumura, J. Koyama, K. Nakamura, O. Nakata, K. Kimata and N. Tanaka, J. Chromatogr., 481 (1989) 147.
4 B. Law, Trends Anal. Chem., 9 (1990) 31.
5 B. Law, R. Gill and A. C. Moffat, J. Chromatogr., 301 (1984) 165.
6 R. M. Smith, T. G. Hurdley, R. Gill and M. D. Osselton, J. Chromatogr., 398 (1987) 73.
7 R. M. Smith, T. G. Hurdley, J. P. Westlake, R. Gill and M. D. Osselton, J. Chromatogr., 455 (1988) 77.
8 R. Gill, M. D. Osselton, R. M. Smith and T. G. Hurdley, J. Chromatogr., 386 (1987) 65.
9 R. Gill, M. D. Osselton and R. M. Smith, J. Pharm. Biomed. Anal., 7 (1989) 447.
10 R. M. Smith, J. P. Westlake, R. Gill and M. D. Osselton, J. Chromatogr., 514 (1990) 97.
11 B. B. Wheals, J. Chromatogr., 187 (1980) 65.
12 B. Law, J. Chromatogr., 407 (1987) 1.
13 B. Law and P. F. Chan, J. Chromatogr., 467 (1989) 267.
14 H. A. Claessens, C. A. Cramers, J. W. de Haan, F. A. H. den Otter, L. J. M. van de Ven, P. J. Andree, G. J. de Jong, N. Lammers, J. Wijma, and J. Zeeman, Chromatographia, 20 (1985) 582.
15 G. B. Cox and R. W. Stout, J. Chromatogr., 384 (1987) 315.

CHROMSYMP. 2463

New, stable polyamine-bonded polymer gel column

Noriko Hirata*, Yuichi Tamura, Masao Kasai, Yuzo Yanagihara and Kohji Noguchi

Gel Separation Development Department, Asahi Chemical Industry Co., Ltd., 1-3-2, Yakoo Kawasaki-ku, Kawasaki-shi 210 (Japan)

ABSTRACT

The Asahipak NH2P-50 column, packed with polyamine-bonded polymer gel, was investigated in terms of mono- and oligosaccharide separation efficiency, reproducibility and column durability. Elution consistently occurred in the order mono-, di- and trisaccharide, and elution volume increased with increasing acetonitrile concentration. Chromatograms obtained over a period of one week of some 170 saccharide analyses on a single NH2P-50 column were virtually indistinguishable, while under the same conditions the efficiency of an amino-bonded silica gel column steadily decreased. The NH2P-50 column was amenable to both acidic and alkaline eluents, with no decrease in column efficiency after extended alternating passage of acidic and alkaline solutions. It also exhibited high separation efficiency with eluent containing tetrapropylammonium hydroxide and acetic acid solution.

INTRODUCTION

High-performance liquid chromatographic (HPLC) analysis of saccharides is commonly performed on amino-bonded silica gel columns using aqueous acetonitrile as eluent. However, the efficiency of such columns declines rather rapidly with use, apparently because of a loss of their amino groups due to hydrolysis [1].

The Asahipak NH2P-50 column was developed to eliminate this problem, and we investigated its use in saccharides analysis with the following results: (a) it matched aminopropyl silica gels in chromatographic resolution; (b) it fully retained column efficiency in prolonged use; (c) it permitted the use of eluent over a wide pH range; and (d) it underwent little shrinkage or swelling related to eluent polarity.

EXPERIMENTAL

Gel synthesis

NH2P gel was obtained by activating the hydroxyl groups of a vinyl alcohol copolymer gel (average particle diameter, 4.8 μm; pore size, approximately 200 Å; hydroxyl groups, 2.5 mequiv. per g of dry gel) with epichlorohydrin and then reacting the gel

with pentaethylenehexamine of 72.3% purity obtained from Wako (Osaka, Japan). The extent of polyamine bonding was determined by washing the NH2P gel with dilute aqueous sodium hydroxide and then with acetone, dispersing the gel in aqueous 0.5 M potassium chloride, titrating the suspension with 0.1 M hydrochloric acid and calculating the quantity of polyamine groups present from the titration curve.

Equipment and material

The equipment consisted of a degasser (GL Sciences, Tokyo, Japan), an 880-PU pump (Japan Spectroscopic, Tokyo, Japan), an AS-2000 autosampler (Hitachi, Tokyo, Japan) and a Shodex SE-61 refractive index detector (Showa Denko, Tokyo, Japan).

The NH2P-50 column was obtained by packing the above NH2P gel in a steel cylinder of 250 mm inner length × 4.6 mm I.D. The amino-bonded silica gel columns, all 250 mm × 4.6 mm I.D. and having a gel particle size of 5 μm, were the YMC pack PA-03 (pore size, 120 Å), Cosmosil 5NH$_2$ (pore size, 110 Å) and Nucleosil 5NH$_2$ (pore size, 100 Å).

Pure mono- and oligosaccharides were purchased from Wako or Sigma (St. Louis, MO, USA). Sam-

ples were dissolved in acetonitrile–water (50:50) except where otherwise noted. Acetonitrile was HPLC grade.

Solvent regain

The solvent regain (S_R) of the NH2P gel was determined for water and acetonitrile. The dry gel was first dispersed in the solvent and left at room temperature for 16 h or more. The gel dispersion was then centrifuged at 3000 rpm (1318 g) and 0°C for 1 h, or in the case of water at 20°C for 90 min, to remove interstitial solvent. The weight (W_1) of the resulting wet gel was measured. The gel was then dried under vacuum at 60°C for 16 h or more and again weighed to obtain W_2. The solvent regain of the gel was calculated using the equation

$$S_R \text{ (ml/g gel)} = [(W_1 - W_2)/\text{sp.gr.} - 0.036 W_2/d] W_2$$

where sp.gr. and d are the specific gravities of the solvent and the gel, respectively [2].

Equilibration of NH2P-50

The amino bases of the gel in the NH2P-50 column were equilibrated prior to its initial use by passing 100 mM ammonium acetate (pH 9.4) through the column at 0.5 ml/min for 2 h at room temperature. As noted below, the column was also equilibrated following the passage of 0.005 M sodium hydroxide.

Recovery of saccharides

Saccharide recovery was measured as the ratio of the eluted peak area obtained with the column by isocratic elution at 1.0 ml/min at 30°C to that obtained when the same amount (50 μg) of the saccharide was injected into approximately 10 m of.tightly coiled PTFE tubing of 0.5 mm inner diameter and eluted under the same conditions.

Stability in acidic and alkaline eluents

The ability of the NH2P-50 column to resist a reduction in its efficiency by acidic and alkaline eluents was determined by separation of fructose, glucose, sucrose and maltose using water–acetonitrile (25:75) as eluent before and after passage of acidic and alkaline solutions.

The acidic solution 0.005 M sulphuric acid was passed through the NH2P-50 column at room tem-

perature and 0.1 ml/min for 63 h. Before analysis, it was necessary to obtain free amino bases by passing 0.1 M sodium hydroxide through the column at 0.5 ml/min for 2 h at room temperature.

The alkaline solution 0.005 M sodium hydroxide (pH 11.4)–acetonitrile (25:75) was passed through the column at 1.0 ml/min for 160 h at room temperature. Before analysis, it was necessary to equilibrate the amino bases by passing 100 mM ammonium acetate (pH 9.4) through the column at 0.5 ml/min for 2 h at room temperature.

RESULTS AND DISCUSSION

NH2P gel characteristics

The chemical structure of the NH2P gel, having an average particle size of 4.8 μm and a pore size of approximately 200 Å, is X-NH(CH$_2$CH$_2$NH)$_n$-CH$_2$CH$_2$NH$_2$, where X represents the vinyl alcohol copolymer. Titration showed the bonded amino group content of the gel to be 1.38 mequiv. per g of dry gel. Its solvent regain was measured as 0.70 ml/g for water and 0.69 ml/g for acetonitrile. The maximum allowable flow-rate of the packed column was 1.5 ml/min.

Capacity factor, number of theoretical plates and saccharide recovery

Table I shows the capacity factor (k'), number of theoretical plates (N_{TP}) and asymmetry (A_S) as determined for saccharide analysis on the NH2P-50 column and three commercial amino-bonded silica columns with water–acetonitrile (25:75) as eluent. The NH2P-50 exhibited high N_{TP} values for all of the saccharides, including galactose, k' values similar to those of the silica columns, and the same elution order except for a reversal of glucose and galactose and of maltose and lactose. These results suggest that the chromatographic behaviour of saccharides is mainly determined by the amino groups of the gel, although some influence of its base material may be evident in the above reversal of retention order and in the relatively higher N_{TP} for galactose and the generally greater peak symmetry observed with the NH2P-50 column.

The elution curves obtained with the NH2P-50 were generally more symmetrical than those obtained with the silica-based columns, as indicated in Table I by the proximity of its A_s values to 1.0, in

TABLE I

CAPACITY FACTORS, N_{TP} AND A_s VALUES OF SACCHARIDES ON NH2P-50 AND AMINO-BONDED SILICA COLUMNS

Eluent, water–acetonitrile (25:75); flow-rate, 1.0 ml/min; sample concentration, 5 mg/ml; sample volume, 10 μl; detection, refractive index temperature, 30°C. Samples were dissolved in water.

Saccharide	NH2P-50			YMC pack PA-03			Cosmosil 5NH$_2$			Nucleosil 5NH$_2$		
	k'	N_{TP}	A_s	k'	N_{TP}	A_s	k'	N_{TP}	A_s	k'	N_{TP}	A_s
(1) Xylose	1.73	6500	1.2	1.02	5700	0.8	0.93	7700	17.4	1.17	7000	33.0
(2) Rhamnose	1.24	7300	1.4	0.74	4800	11.4	0.64	7700	2.1	0.87	6100	2.1
(3) Fructose	1.90	7900	1.6	1.44	8200	0.7	1.18	9000	2.0	1.65	9900	3.4
(4) Mannose	2.35	8200	2.2	1.69	4700	10.2	1.47	8400	9.7	1.92	6900	13.3
(5) Galactose	2.56	6200	1.8	2.01	2600	25.0	1.70	5100	7.7	2.28	3000	47.6
(6) Glucose	2.70	6200	1.0	1.82	5000	0.5	1.64	6700	1.7	2.05	6200	2.1
(7) Sucrose	4.17	8200	1.2	2.93	9000	0.7	2.62	9300	1.6	3.26	10 800	2.1
(8) Lactose	4.97	6900	1.7	4.45	5900	1.4	3.64	7600	2.4	4.98	7300	5.1
(9) Maltose	5.22	6400	0.9	3.78	5600	0.6	3.46	7400	1.7	4.18	6600	4.3
(10) Raffinose	8.56	8700	1.1	7.42	9100	0.7	6.21	9400	2.7	8.25	10 400	3.3

contrast to the much higher A_s values exhibited by the other columns as a result of peak tailing.

As shown in Fig. 1, the k' value for saccharides increased with increasing acetonitrile concentration on the NH2P-50 column in essentially the same manner as on the silica-based YMC pack PA-03 column. This observation, and the above similar-ities in chromatographic behaviour, indicate that the mechanism of saccharide separation on the NH2P-50 is predominantly that of normal-phase chromatography, and thus essentially the same as that of amino-bonded silica-based columns.

The results show the NH2P-50 column to equal or exceed silica-based columns in terms of peak res-
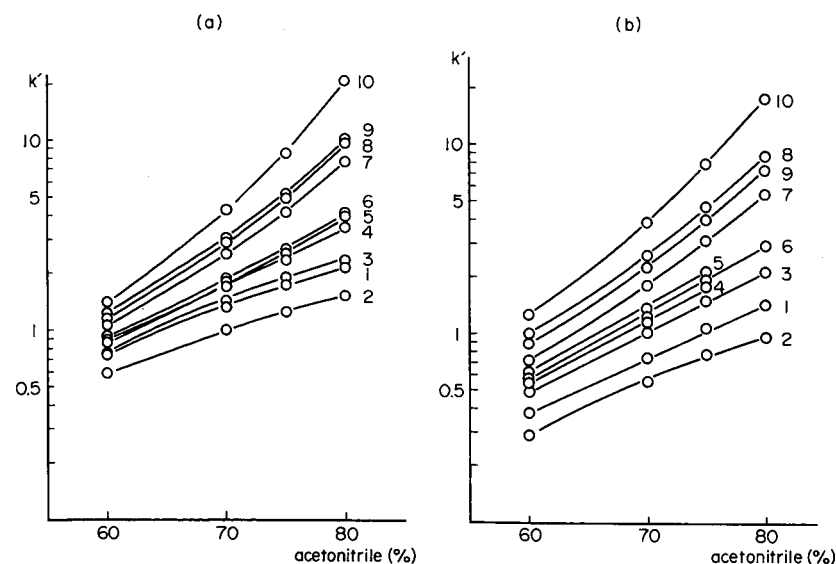
Fig. 1. Capacity factors (k') for mono- and oligosaccharides vs. water–acetonitrile ratio of eluent. Numbers indicate saccharides as listed in Table I. (a) Asahipak NH2P-50; (b) YMC pack PA-03. Conditions as in Table I except eluent.

TABLE II

RECOVERY OF SACCHARIDES

Conditions as in Table I.

Saccharide	Recovery (%)			
	NH2P-50	PA-03	Cosmosil 5NH$_2$	Nucleosil 5NH$_2$
Xylose	40	45	35	64
Rhamnose	58	58	57	64
Fructose	100	97	104	102
Mannose	22	31	12	25
Galactose	22	20	11	44
Glucose	88	74	85	91
Sucrose	107	98	106	106
Lactose	65	53	62	70
Maltose	82	53	70	88
Raffinose	111	113	107	121

olution and symmetry for saccharides, in clear contrast to the common perception of polymer-based columns for reversed-phase HPLC as being inferior to the corresponding silica-based columns in separation efficiency.

As indicated in Table II by the saccharide recoveries observed using water–acetonitrile (25:75) as eluent, the NH2P-50 column was found to be quite similar to amino-bonded silica columns in terms of both the recovery values for individual saccharides and their variation among saccharides.

Stability in aqueous acetonitrile solution

Table III and Figs. 2 and 3 show the N_{TP}, elution times and chromatograms, respectively, for fruc-

tose, glucose, sucrose and maltose on the NH2P-50 column and a silica-based column in a series of 170 or more hourly analyses with water–acetonitrile (25:75) as eluent. On the silica-based column, even with this neutral eluent, the elution times decreased steadily, and a clear difference was observed between initial and final N_{TP} values and chromatograms, all indicative of a relatively short service life for such columns.

On the NH2P-50 column, the elution times, N_{TP} and chromatograms remained unchanged throughout the week-long series of analyses, thus indicating excellent stability in aqueous acetonitrile solution.

Stability in acidic and alkaline eluents

The NH2P gel was found to be stable in eluents ranging in pH from 2 to 11, and apparently up to pH 13.

Table IV shows the elution volumes and N_{TP} obtained with the NH2P-50 column before and after exposure to acidic solution flow (0.005 M sulphuric acid) for 63 h. Table V shows those obtained before and after alkaline solution flow [0.005 M sodium hydroxide (pH 11.4)–acetonitrile (25:75)] for 160 h. No decrease in column efficiency occurred in either instance. The elution volumes and NTP were stable despite the extended exposure to pH 11.4.

As indicated in Table VI, the NH2P-50 column also showed no reduction in column efficiency following exposure to a solution of even higher alkalinity [0.1 M sodium hydroxide (pH 13)–acetonitrile (80:20)] for 6 h.

Chemically bonded silica gels are generally known to lack chemical stability because of the in-

TABLE III

ELUTION VOLUME (V_R) AND N_{TP} ON NH2P-50 AND PA-03 COLUMNS

Eluent, water–acetonitrile (25:75); flow-rate, 1.0 ml/min; sample concentration, 5 mg/ml each; sample volume, 10 μl; detection, refractive index; temperature, 30°C.

Saccharide	NH2P-50				PA-03			
	Initial		At 170 h		Initial		At 170 h	
	V_R (ml)	N_{TP}	V_R (ml)	N_{TP}	V_R (ml)	N_{TP}	V_R (ml)	N_{TP}
Fructose	7.43	11 000	7.43	11 200	9.36	10 000	8.60	8500
Glucose	9.57	6700	9.54	6400	11.00	6200	9.87	5000
Sucrose	13.48	10 500	13.40	10 600	15.58	10 600	13.63	8100
Maltose	16.41	7700	16.29	7100	19.16	7800	16.32	5700
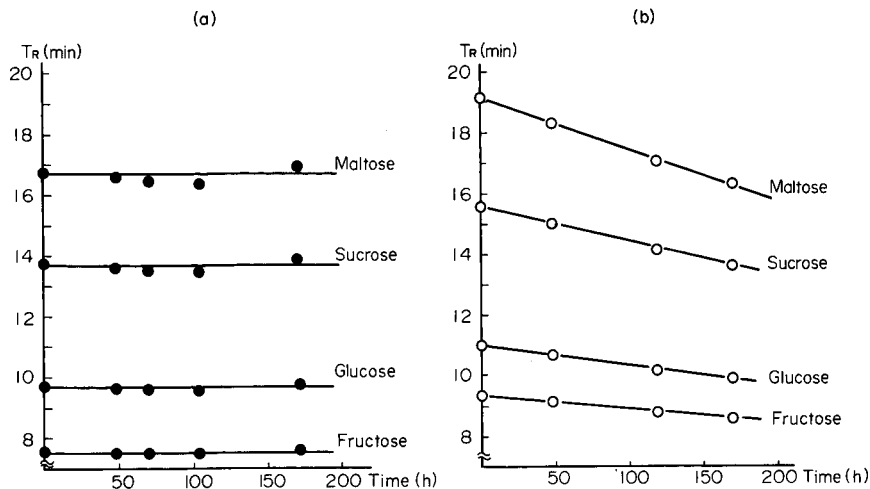
Fig. 2. Elution time (T_R) in repeated usage. (a) Asahipak NH2P-50; (b) YMC pack PA-03. Conditions as in Table III.
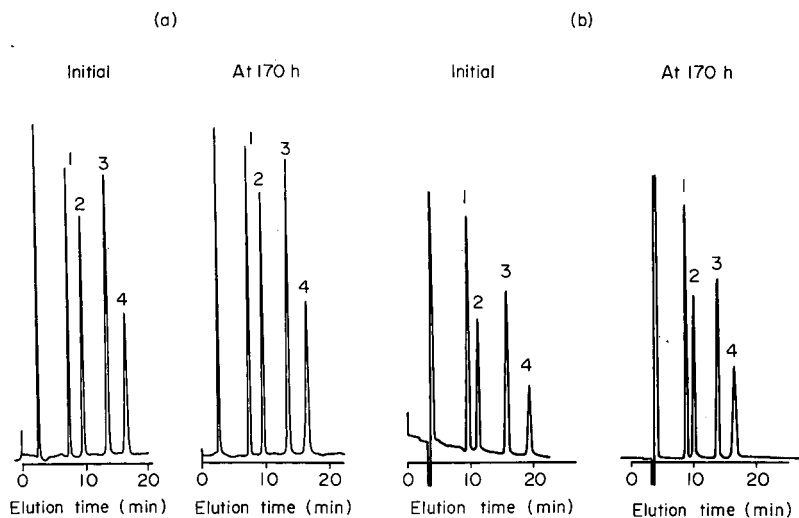
Fig. 3. Chromatograms of saccharides. (a) Asahipak NH2P-50; (b) YMC pack PA-03. Conditions as in Table III.

TABLE IV

COLUMN EFFICIENCY OF NH2P-50 COLUMN BEFORE AND AFTER PASSAGE OF ACIDIC SOLUTION

Conditions as in Table III.

Saccharide	Before		After	
	V_R (ml)	N_{TP}	V_R (ml)	N_{TP}
Fructose	6.73	9600	6.70	8400
Glucose	8.59	7900	8.58	8500
Sucrose	11.88	9600	11.93	9300
Maltose	14.24	8500	13.90	8600

TABLE V

COLUMN EFFICIENCY OF NH2P-50 COLUMN BEFORE AND AFTER PASSAGE OF ALKALINE SOLUTION

Conditions as in Table III.

Saccharide	Before		After	
	V_R (ml)	N_{TP}	V_R (ml)	N_{TP}
Fructose	7.52	7100	7.62	8100
Glucose	9.63	6100	9.68	7700
Sucrose	13.41	8400	13.40	9700
Maltose	16.64	7200	16.08	7400

TABLE VI

COLUMN EFFICIENCY OF NH2P-50 COLUMN BEFORE AND AFTER PASSAGE OF HIGHLY ALKALINE SOLUTION

Conditions as in Table III.

Saccharide	Before		After	
	V_R (ml)	N_{TP}	V_R (ml)	N_{TP}
Fructose	6.80	10 200	6.73	9600
Glucose	8.69	7100	8.59	7900
Sucrose	12.06	9800	11.88	9600
Maltose	14.47	7800	14.24	8500

Fig. 4. Chromatograms obtained with the NH2P-50 column before and after repeated passage of water and acetonitrile alternately. Conditions as in Fig. 3.

stability of the silica base. This limitation does not apply to the NH2P gel, largely because of the excellent chemical stability of its base vinyl alcohol copolymer.

Stability with eluents of differing polarities

The NH2P-50 column was found to retain its efficiency after repeated exposure to eluents of differing polarities, as indicated by the column efficiency and chromatograms of sugar analyses shown in Table VII and Fig. 4. The column was subjected to five cycles of distilled water and then acetonitrile passages each at 1.0 ml/min for 1 h at room temperature, and showed no difference in elution times, N_{TP} or A_s before and after this exposure.

The results thus indicate that the NH2P-50 column undergoes no reduction in efficiency attribut-

able to gel shrinkage and swelling under the influence of eluents of different polarities, as may be expected from the nearly equal solvent regain values (0.70 and 0.69) of the NH2P gel for water and acetonitrile.

Applications

The above results indicate the NH2P-50 column to be superior to other columns for the analysis of saccharides, as it equals or surpasses silica-based columns in terms of separation efficiency and peak symmetry while exhibiting far greater column sta-

TABLE VII

COLUMN EFFICIENCY OF NH2P-50 COLUMN BEFORE AND AFTER ACETONITRILE PASSAGE CYCLE

Water and acetonitrile were passed through the column in five cycles, each consisting of alternating 1-h passages of water and acetonitrile at 1.0 ml/min. Conditions as in Table III.

Saccharide	Before			After		
	V_R (ml)	N_{TP}	A_s	V_R (ml)	N_{TP}	A_s
Fructose	7.31	10 800	1.8	7.29	10 600	1.7
Glucose	9.29	7800	0.9	9.24	7500	0.9
Sucrose	12.91	11 200	1.0	12.84	10 900	1.0
Maltose	15.46	8500	0.9	15.41	8100	0.9
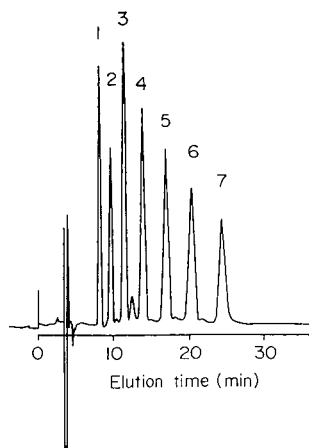
Fig. 5. Separation of maltooligosaccharides. Column, Asahipak NH2P-50; eluent, water–acetonitrile (40:60). Peaks: 1 = glucose; 2 = maltose; 3 = maltotriose; 4 = maltotetraose; 5 = maltopentaose; 6 = maltohexaose; 7 = maltoheptaose; all in water at a concentration of 0.71 mg/ml (1 and 2) or 1.43 mg/ml (3–7). Other conditions as in Table III.
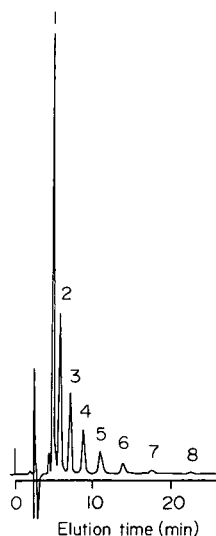
Fig. 6. Effective separation of dextran hydrolysates on Asahipak NH2P-50. Peaks: 1 = glucose; 2 = isomaltose; 3 = isomaltotriose; 4 = isomaltotetraose; 5 = isomaltopentaose; 6 = isomaltohexaose; 7 = isomaltoheptaose; 8 = isomaltooctaose; all in water at a concentration of 10 mg/ml. Other conditions as in Fig. 5.
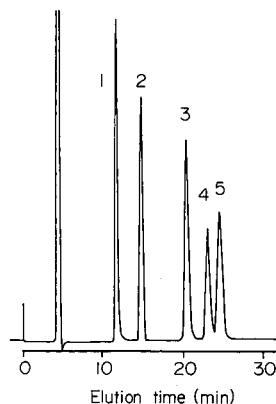
Fig. 7. Separation of saccharides on Asahipak NH2P-50 using an alkaline eluent. Eluent: 10 mM tetrapropyl ammonium hydroxide/acetic acid (pH 10)–acetonitrile (25:75). Peaks: 1 = fructose; 2 = glucose; 3 = sucrose; 4 = lactose; 5 = maltose; all in 10 mM tetrapropyl ammonium hydroxide/acetic acid (pH 10)–acetonitrile (50:50). Other conditions as in Table III.

bility and durability and providing the opportunity for a far wider range of chromatographic conditions. This is supported by the results of the following analyses.

Fig. 5 shows the separation of maltooligosaccharides. Separation was complete, with elution occurring in the order of increasing chain length.

Fig. 6 shows the effective separation of dextran hydrolysates, identified as sugars ranging from glucose to isomaltooctaose.

It is generally preferable to maintain a constant, small proportion of free amino bases in aminobonded columns, and buffers are often added to the eluent for this purpose. Under acidic conditions, however, a small proportion of free amino bases often tends to result in separation of anomers [3]. With the use of a highly alkaline buffer, and thus an alkaline eluent, it is possible in principle to both maintain the proportion of constant free amino base and avoid anomer separation. The NH2P-50 column, because of its high stability in alkaline eluents, is the first amino-bonded gel column to make such applications practical, as shown in Fig. 7.

CONCLUSIONS

Investigation of the Asahipak NH2P-50 column, packed with polyamine-bonded polymer gel, for the

separation of saccharides showed k' values to be similar to those obtained of amino-bonded silica columns, and N_{TP} and A_s values to be equal or superior. The chemical stability of its polymer gel effectively eliminates the problems of declining elution times and short service life commonly associated with silica-based columns. It is also free from the problems of gel shrinkage and swelling associated with conventional polymeric gels exposed to changes in eluent polarity. It is, moreover, stable over a wide pH range. Its stability in alkaline eluents, in particular, may be expected to broaden the range of analysis conditions and applications for saccharide separation by normal-phase HPLC.

REFERENCES

1 K. Koizumi, *J. Jpn. Soc. Starch Sci.*, 34 (1987) 308.
2 N. Hirata, M. Kasai, Y. Yanagihara and K. Noguchi, *J. Chromatogr.*, 396 (1987) 115.
3 V. Kahel and K. Tesarik, *J. Chromatogr.*, 191 (1980) 121.

CHROMSYMP. 2393

Application of a pellicular anion-exchange resin to the separation of inorganic and organic anions by single-column anion exchange

Richard C. Ludwig

Supelco Inc., Supelco Park, Bellefonte, PA 16823-0048 (USA)

ABSTRACT

Applications are shown of a pellicular anion-exchange resin, prepared by hydrophobically coating a quaternized latex on a mono-disperse, non-porous resin. The low capacity material is ideal for single-column ion chromatography with both conductivity and indirect ultraviolet detection. The pellicular nature of the resin allows rapid isocratic and gradient separations. The resin shows excellent efficiency and is stable under high pressures and over a wide pH range. Stability of the coated resin to pressure, solvents and buffers is discussed.

The separation of common inorganic anions, including fluoride, phosphate, chloride, nitrite, bromide, nitrate and sulfate, can be performed at levels below 1 ppm by direct injection. A large number of eluent ions and pH values can be used to optimize the selectivity. Organic acids can be separated rapidly. A rapid separation (11 min) of the common 5'-nucleotide phosphates was performed on the 15-cm column. In addition, a high-efficiency separation of the nucleotides and co-enzymes was performed on a 25-cm column. The elution order of bases was different when performing the separation with acidic and basic eluents.

INTRODUCTION

High-performance ion-exchange chromatography, or ion chromatography, was introduced in 1975 with the advent of suppressed ion chromatography [1]. This was followed by the development of low-capacity ion exchangers, which allowed single-column ion chromatography, in 1979 [2]. The dramatic increase in performance of both techniques has been due to the use of small, rigid particles with easily accessible exchange groups. Porous silicas were used, as functionalization was easily confined to the surface, resulting in rapid diffusion kinetics [3]. Additionally, reversed-phase silicas have been coated with a number of ion-pair reagents or ionic surfactants to create dynamic ion exchangers of variable capacity [4–6]. Pellicular resins have been prepared by agglomerating anion-exchanging microparticles onto the surface of lightly sulfonated supports [7].

In order to increase the speed of analysis for large biomolecules, non-porous supports with very small particle size have been used [8,9]. The small particle size is necessary to obtain sufficient surface area and capacity.

The material described in this report is based on the hydrophobic binding of a submicron anion-exchange latex on mono-disperse, non-porous polystyrene resin as first described by Warth *et al.* [10]. The present material uses a partially cross-linked 5-μm mono-disperse, non-porous resin as the support. The resulting product is a resin-based pellicular anion exchanger of low capacity. As such it is suitable for single-column ion chromatography and provides rapid efficient separations of a number of compound classes.

Initial work on this project concerned characterization and optimization of the coating process. It was found that both salt concentration and the amount of acrylate latex affect the final capacity of the column. In addition it was found that the coated columns were stable to packing and flushing with methanol.

A number of applications have been demon-

strated on this material. While inorganic anions are the most common use of ion chromatography, organic acids, sulfonic acids and nucleotides have also be separated with this material.

EXPERIMENTAL[*]

Column materials

The strong-base anion-exchange latex suspension consisted of a 10% suspension of 0.1 μm functionalised methylmethacrylate. The suspension is commercially available as BPA-1000 (Supelco, Bellefonte, PA, USA). The latex had a surface area of 55 m^2/g, an exchange capacity of 3.1 mequiv./g, and operated from pH 2 to 14.

The support resin was non-porous 5 μm polystyrene containing 3% divinylbenzene.

The materials were slurry packed in stainless-steel columns, 15 and 25 cm × 4.6 mm I.D., and retained with 2 μm stainless steel-frits.

Coating procedure

Loading versus amount of latex. The specified amount of latex suspension was added to 2.25 g of 5 μm resin wetted with methanol. The mixture was diluted to 15 ml with 0.05 M NaCl and sonicated for 25 min to allow equilibration.

Loading versus salt concentration. A 2-ml volume of latex suspension was added to 2.25 g of resin wetted with methanol. The mixture was diluted to 15 ml with the specified concentration of NaCl and sonicated for 25 min to allow equilibration.

Column capacity. The actual column capacity was measured by loading the column with 25 ml of 0.5 M NaNO$_3$. The column was then rinsed with 25 ml of deionised water and the nitrate was displaced using 25 ml of 0.005 M Na$_2$SO$_4$. The nitrate was then quantitated by UV absorption at 230 nm.

Column evaluation

The mobile phases consisted of 0.025 M KH$_2$PO$_4$ (pH 4.5) and the application conditions were as described in the figure legends. The flow-rate was 1 ml/min, unless otherwise stated and the apparatus comprised a Spectra-Physics 8100 pump, a Rheo-

---

* *Patent note:* Preparation of both the coated material and the mono-disperse support are covered by USA Patent Applications.
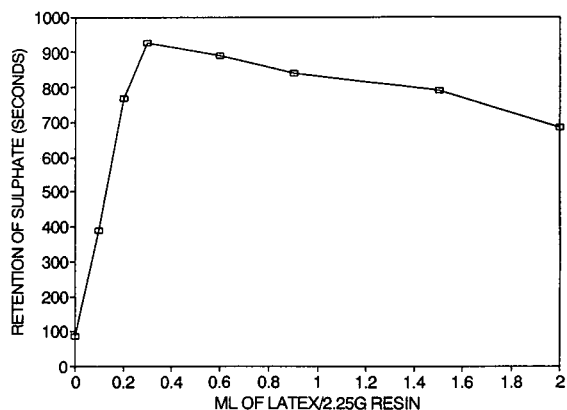
Fig. 1. Retention *versus* amount of latex. The procedure is described in the Experimental section.

dyne 7125, Valco C6U or Wisp 712 injector and a Kratos 757 UV detector at 254 nm.

RESULTS AND DISCUSSION

Coating mechanism

The submicron latex particles are held in place by hydrophobic binding to the polystyrene–divinylbenzene support. Figs. 1 and 2 illustrate the variation in capacity achieved by varying the amount of latex available for coating and the NaCl concentration. Effective capacity was determined by measuring the retention of sulfate ion under constant chromatographic conditions. Fig. 1 shows a rapid increase to the maximum, followed by a much
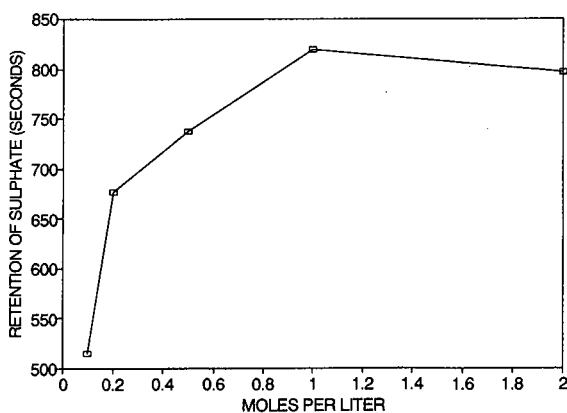
Fig. 2. Retention *versus* sodium chloride concentration. The procedure is described in the Experimental section.

TABLE I

RETENTION OF ANIONS

Conditions: column, 15 cm × 4.6 mm I.D. Sal-PS; buffer, 1 mM phthalate pH 6.5; flow-rate, 1 ml/min; sample, 20 μl of 100 ppm of each anion; detection, indirect UV at 265 nm.

Column	Retention time (s)						
	F^-	$H_2PO_4^-$	Cl^-	NO_2^-	Br^-	NO_3^-	SO_4^{2-}
3336 (preflush)	81	111	150	189	323	397	788
3336 (postflush)	83	111	149	188	316	387	789
3333 (preflush)	80	113	143	178	304	370	710
3333 (postflush)	81	114	137	170	283	348	672
3485 (Initial)	84	105	122	145	217	261	515
3485 (after 500 injections)	86	105	134	148	219	261	511

slower decrease with additional latex. The decrease may be due to dilution of the resin–salt mixture and increasing concentration of the suspending agents. Increasing the NaCl concentration, shown in Fig. 2, increases the capacity up to a maximum at about 1 M NaCl. The binding appears to be mainly governed by hydrophobic interaction of the two resins.

Stability evaluation

Column No. 3336 was flushed with methanol at 30°C. Evaluation after re-equilibration with the phthalate mobile phase indicated that the column exhibited little loss of retention (Table I). The most significant changes were for bromide and nitrate. Tailing, initially present, was significantly reduced and retention was slightly lower. Column No. 3333 was flushed with methanol overnight at 50°C. Chloride, nitrate and sulfate showed 4–5% reduction in retention and the peak shapes of bromide and nitrate were improved.

Column No. 3485 withstood over 500 injections without loss of performance.

Coating reproducibility

Twenty-six columns were prepared using a standardized coating and packing procedure and two lots of the polystyrene support. The capacity of these columns was evaluated using a 0.025 M potassium phosphate mobile phase and guanosine 5'-monophosphate as the test probe. The packing and evaluation were carried out over several days using several lots of mobile phase. No external tempera-

ture control was used. A control chart of the capacity factor is shown in Fig. 3. Control limits calculated using the moving range predict that greater than 95% of the columns should have capacity factors between 5.0 and 6.6. Average efficiency of the 15-cm columns was 6703 plates, with a standard deviation of 1296. The capacity as measured using nitrate adsorption/desorption was 0.3 mequiv. per 15 cm × 4.6 mm I.D. column.

Application

Common inorganic anions. Common inorganic anions, including fluoride, phosphate, chloride, ni-
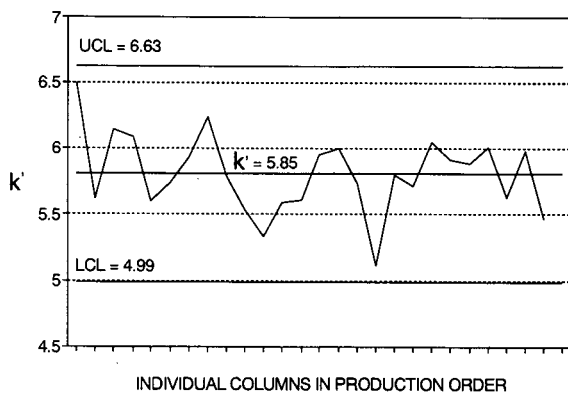
Fig. 3. Control chart of capacity factor (k'). Conditions: column, 15 cm × 4.6 mm I.D. Sal-PS; buffer, 0.025 M KH$_2$PO$_4$; flow-rate, 1 ml/min; sample, 10 μl of uracil (0.7 μg/ml) and adenosine, uridine and guanosine 5'-monophosphates (4 μg/ml each); detection, UV at 254 nm, at ambient temperature. Data shown are for guanosine 5'-monophosphate.
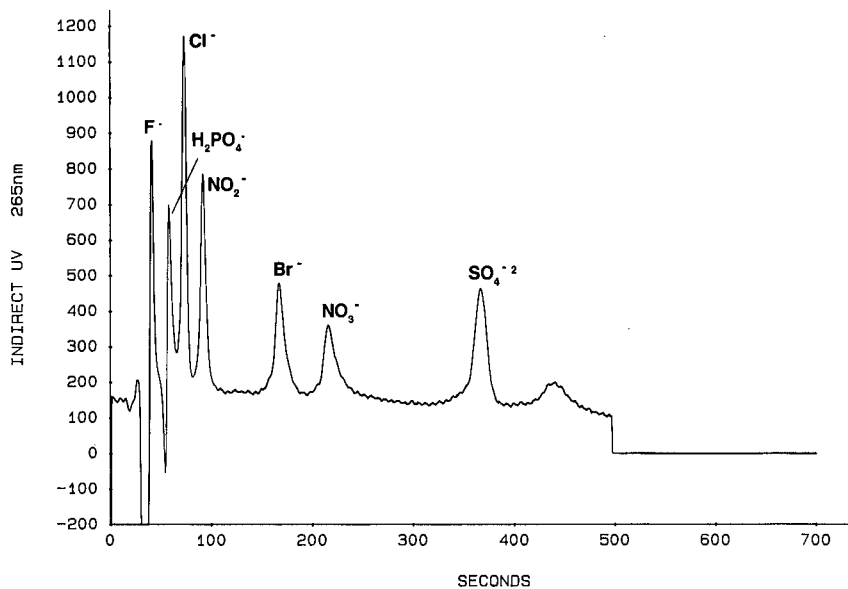
Fig. 4. Chromatogram of common inorganic anions. Conditions: Column, 15 cm × 4.6 mm I.D. Sal-PS; buffer, 1 mM phthalate pH 5.0; flow-rate, 2 ml/min; sample, 100 μl of F$^-$ (0.76 ppm), H$_2$PO$_4^-$ (3.88 ppm), Cl$^-$ (1.4 ppm), NO$_2^-$ (1.84 ppm), Br$^-$ (3.2 ppm), NO$_3^-$ (2.48 ppm) and SO$_4^{2-}$ (3.84 ppm); detection, indirect UV at 265 nm, 0.016 a.u.f.s., at ambient temperature.
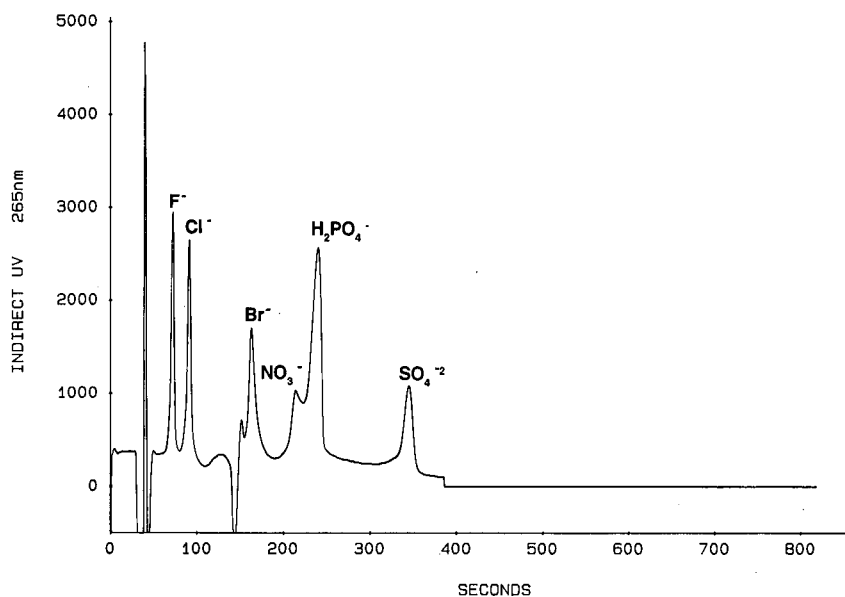
Fig. 5. Chromatogram of common inorganic anions. Conditions: column, 15 cm × 4.6 mm I.D. Sal-PS; buffer, 1 mM p-hydroxybenzoate pH 8.6; flow-rate, 1 ml/min; sample, 20 μl of F$^-$, Cl$^-$, Br$^-$, NO$_3^-$, H$_2$PO$_4^-$ and SO$_4^{2-}$; detection, indirect UV at 265 nm, 0.04 a.u.f.s., at ambient temperature.

trite, bromide, nitrate and sulfate, were determined in a wide variety of samples at widely varying levels. Fig. 4 shows that these anions can be determined quite rapidly at levels approaching 100 μg/l with direct injection in the single-column mode on the pellicular material.

Fig. 5 shows the use of an alternative mobile phase at a pH of 8.5. The higher pH increases the retention of fluoride and carbonate and shifts phosphate towards the end of the chromatogram. Such operation at basic pH is not possible with silica-based materials.

Organic acids. Figs. 6–8 show separations of various organic acids. Formic and acetic acids, important in the power industry, can be separated using various eluents. Concentrated free lactic acid forms intermolecular esterification products which can be separated from the monomeric acid. These impurities were not present in a freshly dissolved sample of the lithium salt. Selectivity on the pellicular material is not as high as on materials specifically designed for organic acid analysis in juices and wines.

Sulfonic acids. Fig. 9 shows the rapid separation of short-chain sulfonic acids, using the conditions similar to those used for inorganic anions. Retention of the sulfonic acids can be varied quite easily by
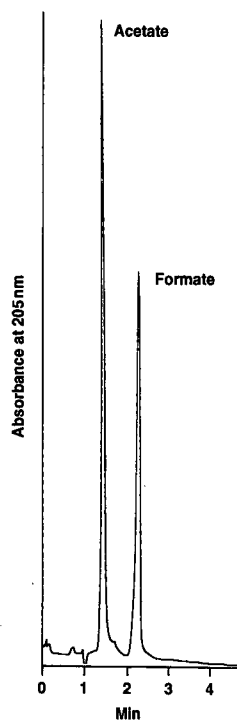
Fig. 6. Chromatogram of organic acids. Conditions: column, 15 cm × 4.6 mm I.D. Sal-PS; buffer, 0.02 M KH$_2$PO$_4$; flow-rate, 1 ml/min; sample, 90 μl of acetate (172 ppm) and formate (133 ppm); detection, UV at 205 nm, 0.016 a.u.f.s., at ambient temperature.
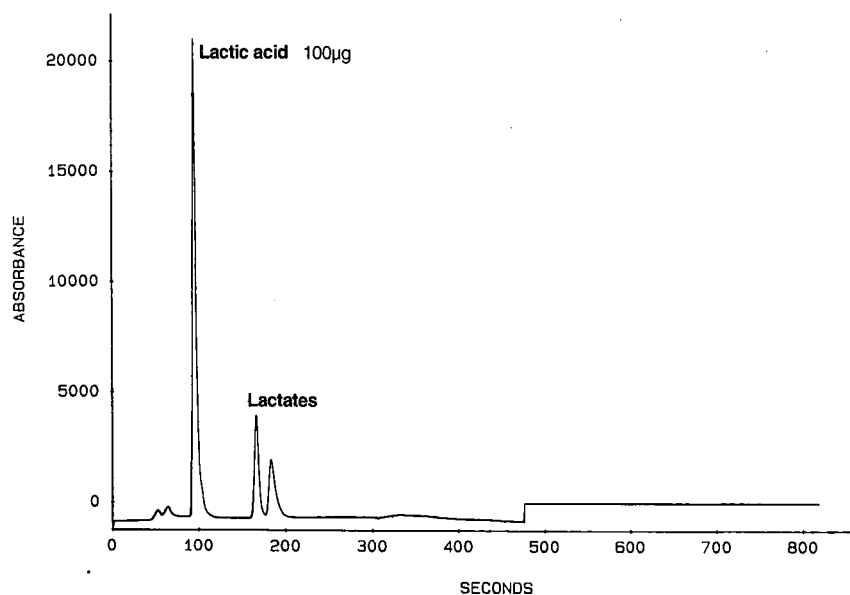
Fig. 7. Chromatogram of lactic acid. Conditions: column, 25 cm × 4.6 mm I.D. Sal-PS; buffer, 0.025 M KH$_2$PO$_4$; flow-rate, 1 ml/min; sample, 10 μl of 10 mg/ml lactic acid; detection, UV at 205 nm, 0.016 a.u.f.s., at ambient temperature.
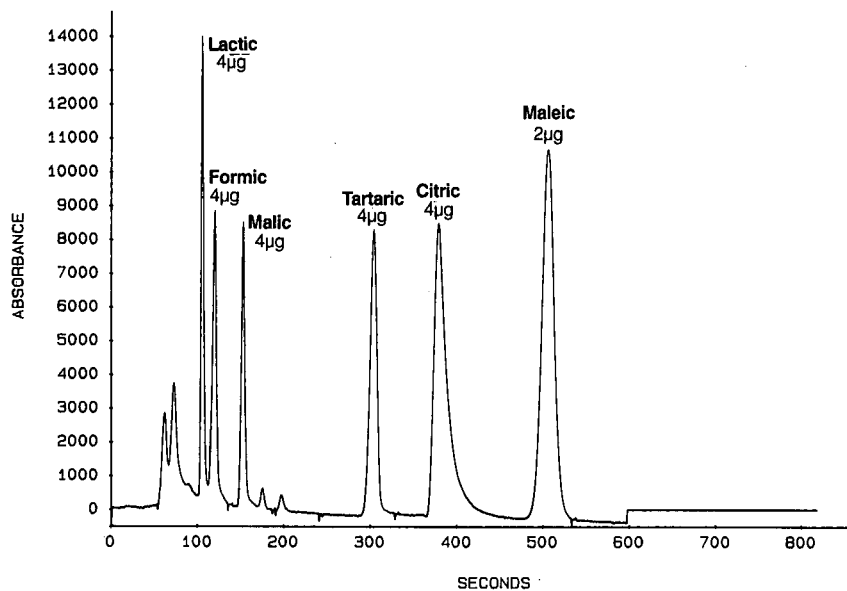
Fig. 8. Chromatogram of organic acids. Conditions: column, 25 cm × 4.6 mm I.D. Sal-PS; buffer, 0.025 M KH$_2$PO$_4$; flow-rate, 1 ml/min; sample, 10 μl of lactic, formic, malic, tartaric and citric acids (0.4 mg/ml each) and maleic acid (0.2 mg/ml); detection, UV at 205 nm, 0.016 a.u.f.s., at ambient temperature.
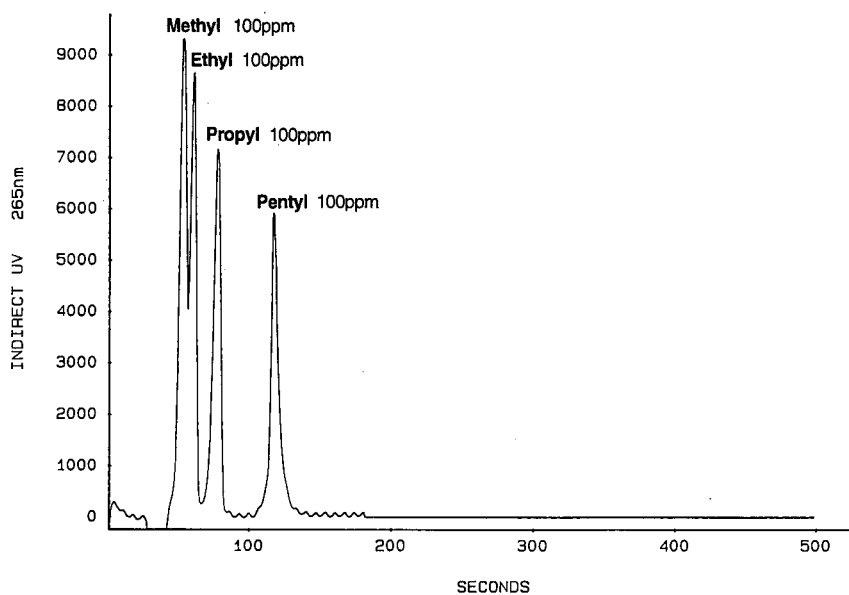
Fig. 9. Chromatogram of sulfonic acids. Conditions: column, 15 cm × 4.6 mm I.D. Sal-PS; buffer, 1 mM phthalate pH 6.0; sample, 20 μl of methyl-, ethyl-, propyl- and pentylsulfonic acids (100 ppm each); detection, indirect UV at 265 nm, 0.04 a.u.f.s., at ambient temperature.
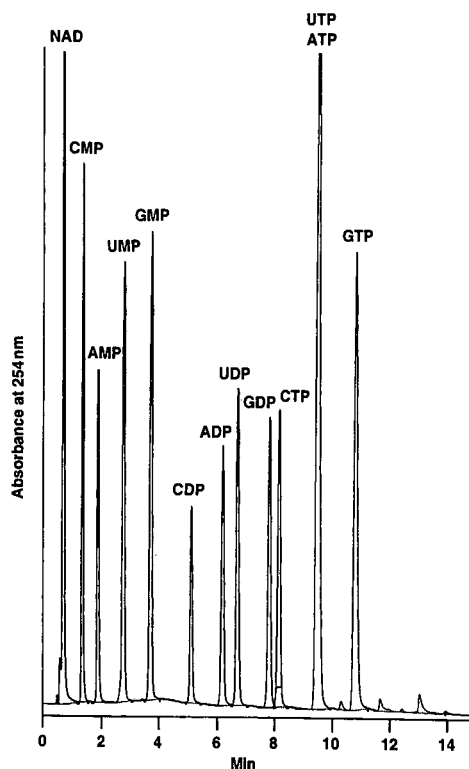
Fig. 10. Chromatogram of nucleotides. Conditions: column, 15 cm × 4.6 mm I.D. Sal-PS; buffer, 0.01 M Tris chloride pH 8.5 with a sodium chloride gradient from 0.05 to 0.3 M in 15 min; flow-rate, 2 ml/min; sample, 100 μl of 30–50 nmol of each nucleotide; detection, UV at 254 nm, 0.04 a.u.f.s., at ambient temperature.

altering the strength of the mobile phase. However, as the aliphatic chain length increases, tailing becomes more evident. Due to the absence of organic modifier, the aliphatic portion may be partitioning into or hydrophobically binding to the resin support.

Nucleotides. Complex nucleotide mixtures are often separated by ion-exchange or ion-pair chromatography. Two mobile phase systems were developed for the separation of nucleotides on the pellicular material. Fig. 10 shows a rapid separation of twelve commonly occurring nucleotides in less than 10 min, using an NaCl gradient in a Tris–acetate buffer of pH 8.5. The Tris buffer eliminates the baseline rise associated with phosphate or citrate buffers. To improve resolution and allow the separation of additional nucleotides and co-enzymes normally found in biological extracts, a 25 cm × 4.6 mm I.D. column was used (Fig. 11).

CONCLUSIONS

The process of coating a quaternized latex on a mono-disperse, non-porous resin can be varied to provide columns with different capacity and retention. The coating process can be standardized to provide reproducible retention.

Hydrophobically coated anion-exchange columns are stable in the presence of methanol and

Fig. 11. Chromatogram of nucleotides. Conditions: column, 25 cm × 4.6 mm I.D. Sal-PS; buffer, 0.005 M KH$_2$PO$_4$ pH 5.6 to 0.5 M KH$_2$PO$_4$ pH 4.5 gradient in 20 min; flow-rate, 2 ml/min; sample, 100 μl of 30–50 nmol of each nucleotide; detection, UV at 254 nm, 0.04 a.u.f.s., at ambient temperature.

buffers.

Inorganic anions can be analyzed at levels as low as 100 $\mu g/l$ by direct injection on this packing material.

Organic acids of various types can be analyzed. Selectivity for the organic acids commonly analyzed in wine is not as great as when specialty ion exclusion-type columns are used.

REFERENCES

1 H. Small, T. Stevens and W. Bauman, *Anal. Chem.*, 47 (1975) 1801.
2 D. Gjerde, J. Fritz and G. Schmuckler, *J. Chromatogr.*, 186 (1979) 509.
3 R. Nieman and R. Clark, *J. Chromatogr.*, 317 (1984) 271.
4 C. Knight, R. Cassidy, B. Recoskie and L. Green, *Anal. Chem.*, 56 (1984) 474.
5 R. Cassidy and S. Elchuck, *J. Chromatogr.*, 262 (1983) 311.
6 D. DuVal and J. Fritz, *J. Chromatogr.*, 295 (1984) 89.
7 H. Small and T. Stevens, *U.S. Pat.*, 4 101 460 (1978).
8 Y. Kato, T. Kitamura, A. Mitsui and T. Hashimoto, *J. Chromatogr.*, 398 (1987) 327.
9 M. Rounds and F. Regnier, *J. Chromatogr.*, 443 (1988) 773.
10 L. Warth, J. Fritz and J. Naples, *J. Chromatogr.*, 462 (1989) 165.

Experimental evaluation of sorbent bed homogeneity in high-performance liquid chromatographic columns

Tibor Macko and Dušan Berek*

Polymer Institute, Slovak Academy of Sciences, Dúbravská cesta 10, 842 36 Bratislava (Czechoslovakia)

ABSTRACT

Base-line perturbations, eigenzones, are generated in a high-performance liquid chromatographic (HPLC) column by sudden pressure variations if particular binary eluents are used. The proposed interpretation of the shape of these eigenzones allows the semi-quantitative evaluation of the packing density distribution along the column. Common HPLC equipment allows the necessary experimental data to be obtained, and their evaluation is simple and straightforward. However, the correction of eigenzones for spreading is necessary in order to draw more reliable, quantitative conclusions.

INTRODUCTION

The regular arrangement of sorbent particles within a high-performance liquid chromatographic (HPLC) column, *i.e.*, homogeneity of the sorbent bed, is one of the necessary conditions for its high efficiency and stability. The average packing density of most real HPLC columns is not very high. The interstitial porosity ε_0, defined as the ratio of the interstitial volume and the total column volume, varies in the range $0.35 < \varepsilon_0 < 0.45$ [1], and is usually higher than 0.4. However, the theoretical value of ε_0 for arrays of spherical particles of equal size with maximum possible density, *i.e.*, for rhombohedral and face-centred cubic arrangements, is only 0.259 [2]. This means that in common HPLC columns the sorbent particles are either loosely packed along the whole column length or the bed of sorbent contains local heterogeneities such as zones with very low packing density or tears, channels, holes, etc. It is widely accepted, however, that the presence of such packing irregularities adversely influences the column quality in a decisive way. It is therefore advantageous both for developing efficient column packing methods and for routine testing of available columns to possess a procedure for determining column packing density variations along the column.

We have recently proposed the use of the pressure dependence of preferential sorption from mixed mobile phases [3] for this purpose [4,5]. The role of pressure in sorption processes has long been overlooked. There have been only a few studies of the influence of pressure on the sorption equilibria in static [6–9] and dynamic (HPLC) [3–5,10–21] systems. In a series of papers [3–5,16–18,21], we studied the effects of pressure on the extent of preferential sorption. The term "preferential sorption" denotes the phenomenon that the composition of a two-component liquid differs in the bulk phase and in the phase sorbed in the domain of a solid sorbent. It was found that sudden changes in pressure cause variations in the sorption equilibrium in many systems consisting of common LC sorbents and two-component mobile phases. Consequently, rapid desorption–extraction processes take place, resulting in the perturbation of the column effluent composition. These perturbances can be easily visualized by a non-specific detector such as a differential refractometer and have the form of fairly well defined "eigenzones" [16].

The height of the eigenzone, h, depends on the particular pressure change, ΔP, and on the difference in the refractive indices of the mobile phase components. Similarly to preferential sorption it-

self, h is also a function of the nature and composition of both the column packing and the mobile phase [3,16,17] and of temperature and the amount of sorbent within the column [5]. On the other hand, h seems not to depend on the mobile phase flow-rate [5]. Under appropriate experimental conditions, h reaches 200 mm at $\Delta P = 10$ MPa. Single liquids under similar experimental conditions produce very small or undetectable baseline perturbations [4].

The width of the eigenzone, with a few exceptions so far observed [18], corresponds roughly to the total volume of liquid within the column [3,4]. The shape of eigenzones depends on the manner in which the pressure change was generated. For example, the pressure strokes produced by a sudden mobile phase flow reversal (column backflushing) yield Z-shaped eigenzones that have been utilized in the qualitative evaluation of both the homogeneity and the stability of the packing bed [4]. On the other hand, the pressure variations induced by inserting a capillary with a large hydrodynamic resistance behind the column give rise to tetragonally shaped eigenzones [5,18].

The advantage of the latter procedure is that the pressure increases almost simultaneously throughout the whole volume of the column to approximately the same, well defined extent, provided that the sorbent bed geometry remains unaffected in the course of the experiments. The shape of such eigenzones gives directly at least qualitative information concerning the column packing geometry [5].

In this paper, we present further experimental results obtained on the generation of eigenzones by the insertion of a hydrodynamic resistor behind the column. We also describe an attempt to evaluate semi-quantitatively the inhomogeneities within LC column packings from the shapes of eigenzones.

EXPERIMENTAL

We used two experimental assemblies, shown in Fig. 1a and b. Liquids were transported either by an FR-30 reciprocating double-piston pumping system (RP) (Knauer KG, Bad Homburg, Germany) (Fig. 1a) or by an HPP 4001 positive displacement (syringe) pumping system (PP) (Laboratory Instruments, Prague, Czechoslovakia) (Fig. 1b). By switching the six-port, three-way valve V (Workshops of Czechoslovak Academy of Sciences,
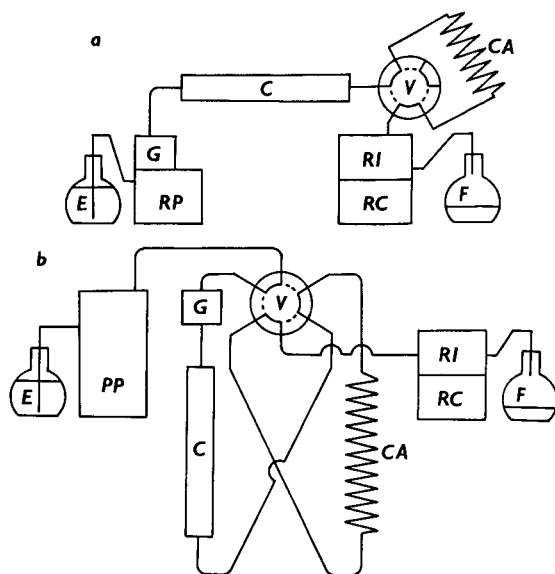
Fig. 1. Schemes of the LC assemblies: E = eluent container; RP = reciprocating pump; PP = piston pump; G = pressure gauge; C = column; V = valve in position a (solid line) and b (dashed line); CA = capillary; RI = detector; RC = recorder; F = waste.

Prague, Czechoslovakia) the resistor capillary CA, 50 or 100 m × 0.25 mm I.D., was inserted behind the column C. The resulting pressure changes were monitored by a flow-through pressure gauge (Institute for Chemical Process Fundamentals, Czechoslovak Academy of Sciences, Prague, Czechoslovakia), G, and recorded by a recorder, RC, simultaneously with the variations of effluent composition that were measured with an RIDK 101 differential refractometer (Laboratory Instruments), RI. The single-piston displacement pump cannot be used in the assembly in Fig. 1a because, owing to the compression of the eluent in the container of the pumping system, the pressure variations within column are slow and not well defined. On the other hand, the system shown in Fig. 1b allows pressure variations to be produced within the column without a change in pressure at the outlet of the pumping system.

All measurements were made at 22 ± 1°C. Stainless-steel columns (100 × 6 mm I.D. or 100 × 8 mm I.D.) (Laboratory Instruments) were packed either with bare silica gel Silpearl (Glassworks Kava-

lier, Votice, Czechoslovakia) or with bare silica gel CH (Lachema, Brno, Czechoslovakia). Some samples of Silpearl were fired at different temperatures in order to decrease their specific surface area. The physical characteristics of the sorbents are given in Table I. The sorbents were packed into the column by the upward slurry method from methanol (Silpearl) or dry tapped (silica gel CH). At the end of experiments, some columns were emptied and the amount of dry sorbent within column was determined by weighing.

The eluent was tetrahydrofuran (THF)–water (80:20, v/v). THF (Laborchemie, Apolda, Germany) was distilled from KOH and stabilized by 0.1 g/l of butylated p-hydroxytoluene. Water was redistilled after oxidation of organic admixtures with an alkaline solution of $KMnO_4$ for 1 week. The use of pure eluent components is necessary because admixtures could participate in sorption processes and complicate the shapes of eigenzones. The amount of the THF stabilizer used, however, was small enough not to produce measurable eigenzones.

The density of the sorbent matrix was determined using a pycnometer and appropriate mixed liquids. The specific pore volume was calculated from GPC data, the density of the sorbent matrix and the mass sorbent within the column.

RESULTS AND DISCUSSION

Extent of pressure effect

Switching the valve V into the position marked with the full line in Fig. 1 and inserting the capillary CA into the eluent path cause an increase in pressure within the column C. Conversely, removal of the capillary CA (valve V in the position marked with a dashed line in Fig. 1) leads to a sudden drop in pressure. Fig. 2a and b show typical eigenzones produced by such pressure changes. Whereas the eigenzone in Fig. 2a is fairly symmetrical, the eigenzone in Fig. 2b does not show a flat top. Such asymmetric eigenzones indicate poor sorbent bed homogeneity. Note the large time delay in the appearance of eigenzone when the capillary CA was inserted behind the column: this corresponds to the volume of capillary CA, which is much larger than the volume of the connecting capillaries between the column and detector. The apparent time delay between

the signal of the pressure gauge and the differential refractometer trace is due to the construction of the two-pen recorder used.

Water molecules are preferentially sorbed on the surface of bare silica gel from THF–water (80:20, v/v) at pressures of 0.1–10 MPa [3]. The amount of preferentially sorbed water, however, decreases with increasing pressure. This means that in an HPLC column flushed with THF–water the pressure increase leads to desorption of water and extraction of THF from the mobile phase. As water has a lower refractive index (RI) than THF, the RI detector response to the corresponding effluent composition perturbation is negative (Fig. 2a and b). The process is fully reversible and a subsequent decrease in pressure to the initial value leads to re-establishment of the initial sorption equilibrium and, consequently, desorption of THF from the column packing and extraction of water from the mobile phase. The eigenzone proper to the latter effluent composition perturbation has a positive sign (Fig. 2). For further evaluation, only columns producing repeatable eigenzones were considered, as a changing eigenzone shape indicates instability of the sorbent bed [4].

Fig. 3 shows the dependence of the areas of the eigenzones on the extent of pressure change ΔP for three different silica gels. The dependences can to a first approximation be represented by straight lines (correlation coefficients 0.997, 0.982, 0.984) and we can consider, at least for small pressure variations, the extent of the column effluent composition change to be directly proportional to ΔP.

In a previous paper [5], we showed that apart from ΔP, the eigenzone size is approximately directly proportional to the amount of sorbent in the column and inversely proportional to the volume of liquid in the column. Sorption processes evidently take place on the sorbent surface and this parameter should be considered in the quantitative evaluation of pressure effects (*cf.*, Fig. 3). In the following series of experiments, the eigenzones were generated in columns containing silica gels with different specific surface areas. These sorbents had different pore sizes and pore volumes. The differences in the physical structures of the sorbent particles together with different average packing densities of particular columns resulted in different volumes of the mobile phase available for compositional
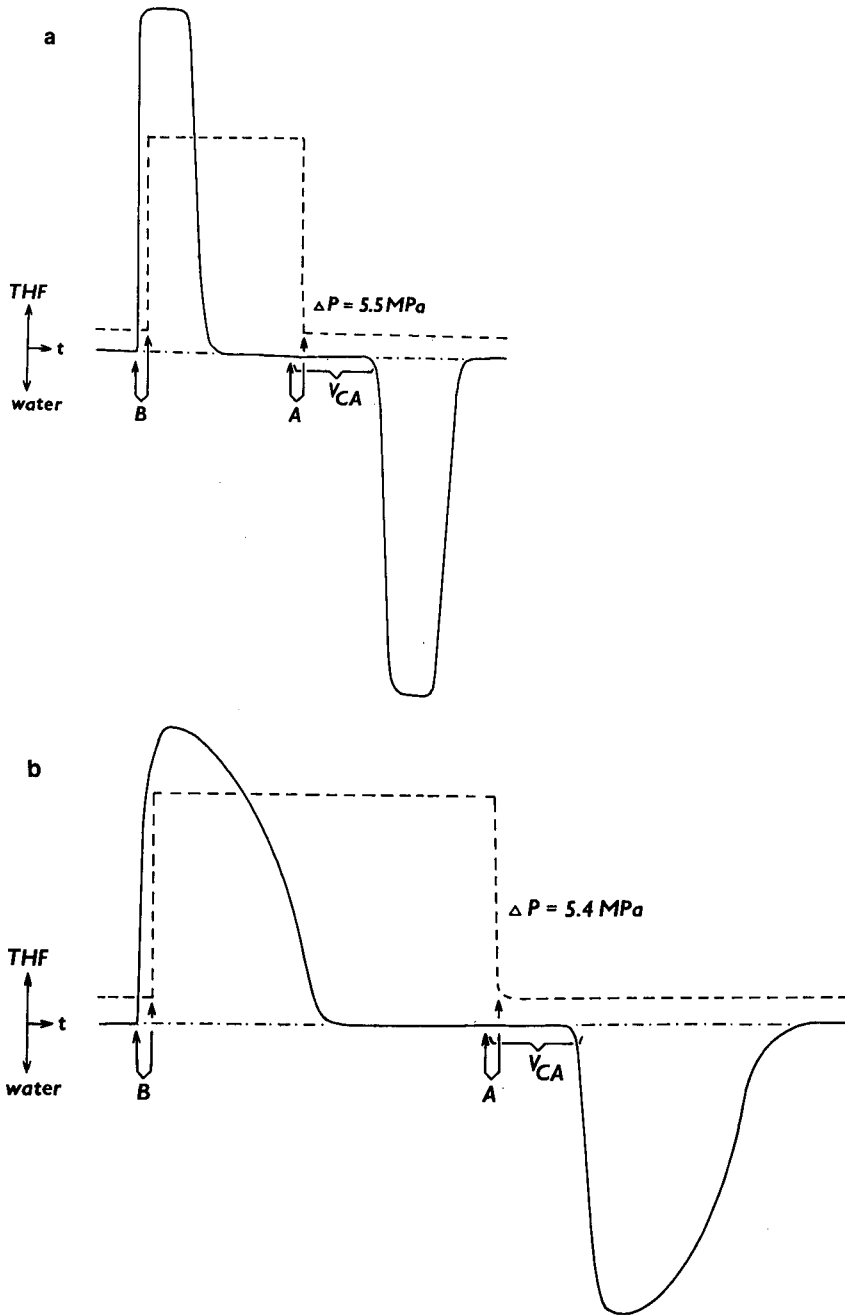
Fig. 2. Examples of eigenzones produced by pressure variations due to inserting (or removing) a capillary with large hydrodynamic resistance in (from) the eluent path. Eluent, THF–water (80:20, v/v); flow-rate, 0.6 ml/min. Column: (a) Silpearl, 13 μm (10 × 0.6 cm I.D.); (b) silica gel CH, 32–70 μm (10 × 0.6 cm I.D.). A, At this time valve V was switched from position b to a (Fig. 1); B, valve V was switched from position a to b; t = elution time; dashed line, response of pressure gauge G; solid line, response of RI detector; V_{CA} = volume of hydrodynamic resistor, capillary CA. The sign of the detector response for the excess of particular eluent components is shown.
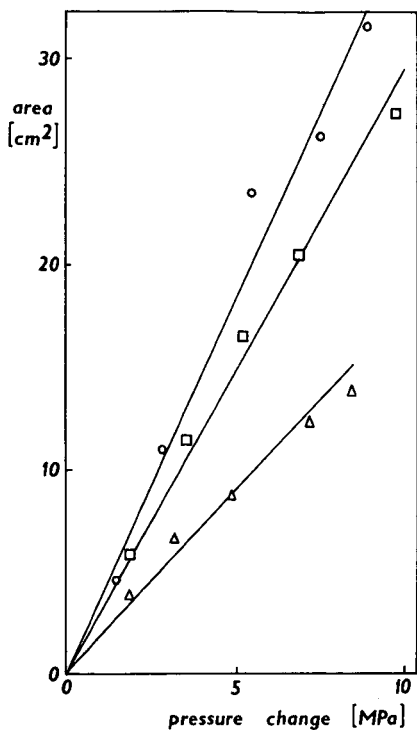
Fig. 3. Dependence of the area of the eigenzone on the pressure change. Eluent, THF–water (80:20, v/v). Column △ = silica gel CH, 70–100 μm; □ = silica gel CH, 100–170 μm; ○ = Silpearl, 13 μm.

contained a substantial amount of micropores not accessible to solvent molecules. Under these circumstances, and neglecting the possible influence of the pore diameter on the sorption processes and the role of temperature variations in the columns packed with particles of different size, we can, at least for low values of X and Y and to a first approximation, consider the dependence in Fig. 4 to be linear (correlation coefficient 0.949). The roughly estimated mean amount of water desorbed from 1 m^2 of the silica gel surface in the mixed eluent THF–water (80:20, v/v) is about $(7 \pm 2) \cdot 10^{-4}$ mg per $\Delta P = 1$ MPa. Generally, we can say that the height of the eigenzone reflects, under otherwise identical conditions, the surface area of the sorbent that is available to the desorption–extraction process when the pressure is varied. This means that the local changes in the packing surface (*i.e.*, in the packing density) along the column will influence the shape of the eigenzone. To prove this idea one would need columns containing defined inhomogeneities. However, it is difficult to prepare such HPLC columns in practice. Still, it is possible to

changes. This is especially pronounced with sample No. 7, which lost most of its porosity in the course of thermal treatment. The results are collected in Fig. 4 and Table I. Fig. 4 shows a plot of $Y = A(\Delta P)^{-1}V^{-1}$ versus $X = SV^{-1}$, where A is the area of the eigenzone, ΔP the pressure variation, V the volume of liquid within the column and S the surface area of the corresponding sorbent. For evaluating the material balance, the detector response was calibrated by means of a set of test mixtures of THF and water of known composition. From the eigenzone area, the amount of water released at $\Delta P = 1$ MPa from 1 m^2 of the sorbent surface was then calculated (Table I). The scatter of the data in Fig. 4 and Table I is pronounced, but one has to bear in mind that the surface concentration of free silanol groups for starting silica gels CH and the thermally treated Silpearl probably differed. On the other hand, the starting Silpearl with a surface area of 615 m^2 g^{-1} at a pore volume of *ca.* 0.5 ml g^{-1} evidently

Fig. 4. Relationship between the area of the eigenzone generated by a 1 MPa pressure change per 1 ml of liquid within the column (Y) and the surface area of sorbent per 1 ml of liquid within the column (X). + = Silica gel CH; △ = thermally modified Silpearl.

TABLE I

PHYSICAL PROPERTIES OF THE SORBENTS AND EXTENT OF THE CHANGE OF AMOUNT OF PREFERENTIALLY ADSORBED WATER WITH PRESSURE

Sorbent No.[a]	Particle diameter (μm)	Specific surface area (m^2/g)	Mass of desorbed water/pressure change/mass of sorbent (mg MPa^{-1} g^{-1})	Mass of desorbed water/pressure change/surface of sorbent (mg MPa^{-1} m^{-2})	Mass of sorbent/ volume of liquid within column (g/ml)
1	7	612	0.32	$5.24 \cdot 10^{-4}$	0.76
2	13	480	0.34	$7.04 \cdot 10^{-4}$	0.81
3	10	440	0.25	$5.66 \cdot 10^{-4}$	0.77
4	10	210	0.15	$7.00 \cdot 10^{-4}$	0.75
5	10	188	0.14	$7.34 \cdot 10^{-4}$	0.79
6	70–100	178	0.16	$9.32 \cdot 10^{-4}$	0.67
7	10	13	0.001	$0.75 \cdot 10^{-4}$	1.79

[a] Sorbents 1–5 and 7, Silpearl; sorbent 6, silica gel CH.

simulate the column inhomogeneity by a set of short columns containing sorbents with different specific surface areas [5]. An example of eigenzones obtained with trains of various columns is shown in Fig. 5. This illustrates that the eigenzone shape reflects the variations in the packing surface. After changing the column sequence, the shape of eigenzones is correspondingly changed [5].

The interpretation of eigenzone shape

For the sake of simplicity, we shall assume that insertion or deletion of the capillary CA produces the same changes in pressure ΔP at any point in the column. This means that the changes in viscosity and density [22] of the eluent with pressure and the variations in temperature within the column due to friction [23] will be neglected. Further, we assume
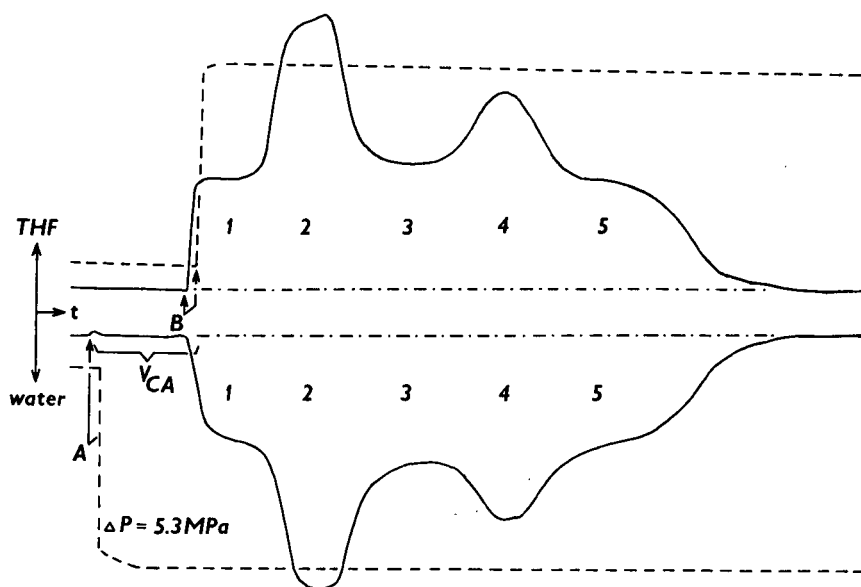
Fig. 5. Eigenzones corresponding to a train of five different columns in series. Eluent, THF–water, 80:20 (v/v); columns, 10 × 0.6 cm I.D. Sorbents: 1 = silica gel CH, 32–70 μm (178 m^2/g); 2 = Silpearl, 13 μm (480 m^2/g); 3 = silica gel CH, 70–100 μm (178 m^2/g); 4 = Silpearl, 7 μm (612 m^2/g); 5 = silica gel CH, 100–170 μm (178 m^2/g).

that the physical and chemical properties of particles of packing along the column, *i.e.*, their pore volume, pore size, specific surface area and concentration of active sites, where the preferential sorption takes place, remain constant. On the basis of the experimental data collected so far [3–5,16,17], we can write for a perfectly homogeneously packed column with one kind of silica gel sorbent:

$$h = \Delta P \rho K \tag{1}$$

where h is the height of eigenzone, ΔP is the pressure change, ρ is the packing density of the column and K is a constant; ρ is expressed as the mass of sorbent per millilitre of liquid situated in both the pores and the interstitial volume of the column. The value of K depends on the nature of both the sorbent and the eluent and on temperature and the detector used. K must be determined by independent experiments for each sorbent–eluent–detector system. For the sake of simplicity, the mass of sorbent is considered in eqn. 1 instead of its specific surface area.

Eqn. 1 allows the distribution of sorbent in the inhomogeneous bed of packing to be estimated by a simple procedure, as follows:

1. Divide the eigenzone into equally small and identical volume elements of eluent, V_i (Fig. 6), so that one can assume that the sorbent bed within each volume element is homogeneous. We chose V_i equal to 0.2 ml to illustrate the calculation procedure.

2. Calculate M_i, *i.e.*, the mass of sorbent corresponding to each volume element of eluent V_i:

$$M_i = V_i \rho_i = V_i \cdot \frac{h_i}{\Delta P K} \tag{2}$$

where V_i is the size of eluent volume element in ml, ρ_i is the mass of sorbent corresponding to 1 ml of eluent, h_i is the mean height of the eigenzone within the volume element V_i, ΔP is the overall pressure change and K the constant in eqn. 1.

3. Calculate the volume of sorbent matrix W_i that corresponds to the mass of sorbent M_i within the eluent volume V_i:

$$W_i = M_i/\rho_s \tag{3}$$

where ρ_s is the density of sorbent matrix (*e.g.*, 2.2 g cm^{-3} for bare silica gel).

4. Calculate the length of column L_i that corresponds to the volume of eluent V_i plus the volume of sorbent matrix W_i:
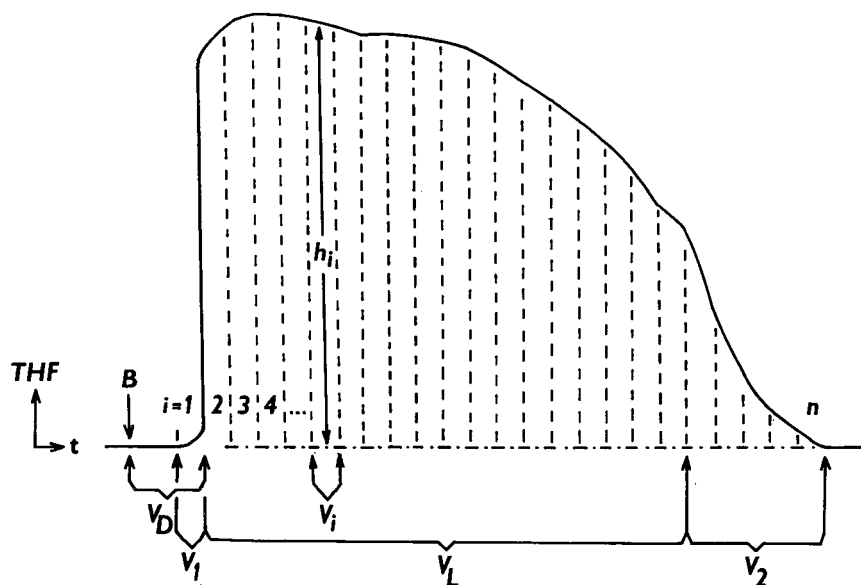
Fig. 6. Example of eigenzone divided into volume elements. V_i = volume element with indices $i = 1 \ldots n$; h_i = height of eigenzone; V_L = volume of effluent equal to the volume of liquid within the column; V_D = volume between the column outlet (column end) and the detector cell; V_1, V_2 = parts of volume of eigenzone due to broadening processes during passage of the eigenzone through the capillaries and the column.

$$L_i = \frac{V_i + W_i}{\pi \cdot \frac{D^2}{4}} \qquad (4)$$

where D is column inside diameter.

5. Construct the plot

$$\frac{\rho_i V_i}{\pi r^2 L_i} = f\left(\sum_{i=1}^{i=n} L_i\right) \qquad (5)$$

which represents the differential distribution of sorbent within the column, *i.e.*, the mass of sorbent per

unit column volume as a function of the length of column L. The dependence

$$\sum_{i=1}^{i=n} (\rho_i V_i) = f\left(\sum_{i=1}^{i=n} L_i\right) \qquad (6)$$

express integral distribution of sorbent mass within the column. Both kinds of distribution calculated for two different columns are shown in Fig. 7a and b.

Theoretically, the sum of L_i should be equal to
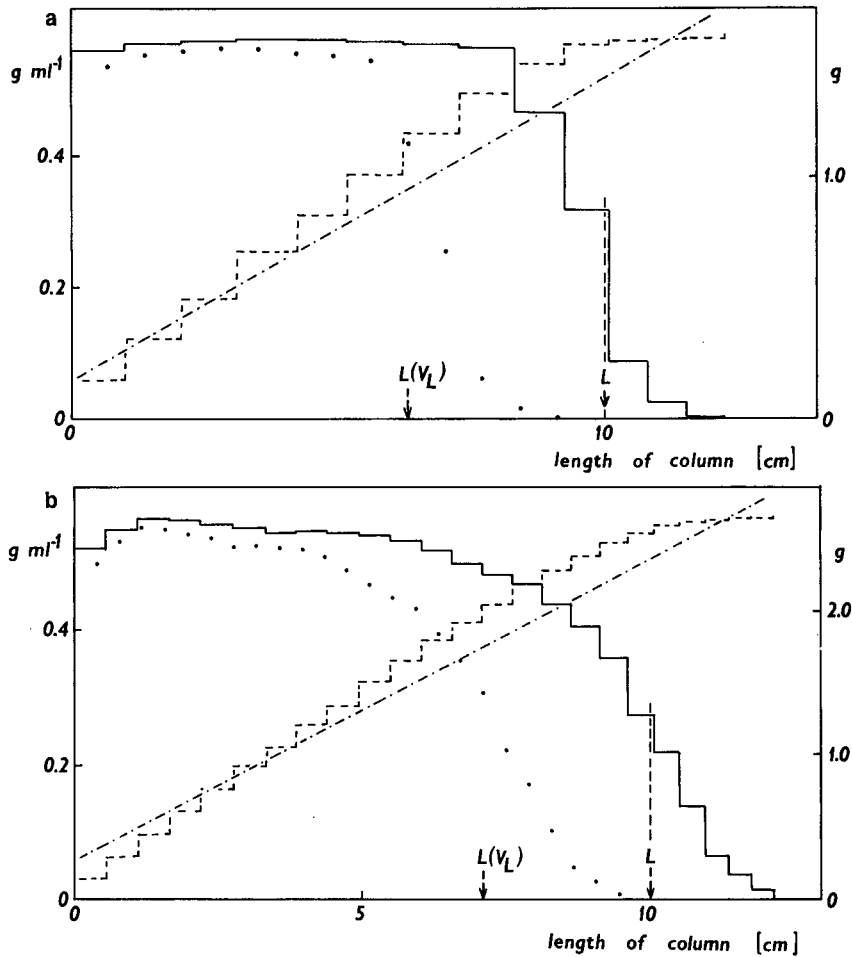
Fig. 7. Example of the calculated sorbent distribution within the column on the base of the whole eigenzone. Left-hand ordinate = grams of sorbent per 1 ml of column volume; right-hand ordinate = grams of sorbent. (a) From the eigenzone in Fig. 2a. Calculated length of column, 12.25 cm; correlation coefficient calculated for integral distribution, 0.9783; calculated average packing density, ρ = 0.601; experimental ρ = 0.797. (b) From the eigenzone in Fig. 2b. Calculated length of column, 12.15 cm; correlation coefficient calculated for integral distribution, 0.9828; calculated average packing density, ρ = 0.550; experimental ρ = 0.709. Dashed line, differential distribution of sorbent; solid line, integral distribution of sorbent; dot-dashed line, calculated by least-squares method; $L(V_L)$ = length corresponding to the volume of liquid within the column; L = actual length of column. Points corresponding to the eigenzone which were used for the calculation are also shown.

the total column length L and the sum of M_i values must correspond to the mass of sorbent within column:

$$L = \sum_{i=1}^{i=n} L_i \qquad (7)$$

$$M = \sum_{i=1}^{i=n} M_i \qquad (8)$$

In practice, however, $L < \Sigma L_i$, as the volume of eigenzone is larger than the total volume of liquid within the column owing to the spreading processes in the packing, column end-pieces, connecting capillaries, valve and detector. For illustration, both the length of the column $L(V_L)$ corresponding to the volume of liquid within the column V_L and corresponding positions of points of eigenzone, which were used for calculation, are shown in Fig. 7a and b.

The spreading effect increases with increasing path length of the eigenzone within the column. The front of the eigenzone presents its least distorted part as it arises in the very end of the sorbent bed and has the shortest path into the detector, whereas the tail of the eigenzone is its most distorted part. The effect of the zone broadening within the capillary resistor CA is especially evident when comparing the shapes of the front parts of eigenzones in Figs. 2 and 5. The uncorrected results are therefore approximate. The comparison of the actual (L) and calculated (ΣL_i) lengths of the column gives semi-quantitative information on band broadening effects within the system studied.

The influence of the spreading effects was tentatively decreased in the following way. Let us assume that the eigenzone is not influenced by the spreading process. In this event the volume of the eigenzone (V_E) equals the volume of liquid within the corresponding column (V_L). It is possible to locate the position of the non-distorted eigenzone on a chromatogram if one knows the volume of the parts of HPLC system between the end of the packing bed and the detector measuring cell (V_D), i.e., the volume of the column end-piece and connecting capillaries and the volume of liquid within the column, V_L (cf., Fig. 6). As a consequence of the broadening process, the height of the eigenzone decreases and its width increases. The parts of the eigenzone produced by the broadening within both

the column and the HPLC hardware are designated in Fig. 6 as V_1 and V_2. The influence of the broadening on the constant K calculated from eqn. 1 is eliminated by applying the relationship

$$K = \frac{h}{\Delta P \cdot \dfrac{M}{V_L}} = \frac{\dfrac{\sum\limits_{i=1}^{i=n} h_i}{(n - x_1 - x_2)}}{\Delta P \cdot \dfrac{M}{V_L}} \qquad (9)$$

where h_i is the average height of the eigenzone in the volume element V_i, n is the number of volume elements V_i in the total volume of the eigenzone V_E, x_1 and x_2 are the number of volume elements V_i in volumes V_1 and V_2 (cf., Fig. 6) and M is the mass of sorbent within the column. For calculation of K from eqn. 9 only that volume of eluent (V_L) is considered which corresponds to the eigenzone at the moment of its generation within the column. In other words, the number of volume elements n is deliberately reduced considering the effect of the zone broadening. On the other hand, the whole area of the eigenzone is used for calculating the constant K because it is assumed that the area of an eigenzone does not depend on its broadening. We used constants K calculated from eqn. 9 in eqn. 1.

Fig. 8a and b show examples of the sorbent distribution curves calculated from that part of the eigenzones which belonged to the volume of liquid within the column. In this instance, the calculated column length approaches the actual length of the column (L) (cf., calculated L in Figs. 7 and 8).

The integral distribution of the sorbent (see Fig. 7a and b) for an ideal, homogeneously packed column would be a straight line. The correlation coefficient of the actual experimental dependence evaluated by the least-squares method can also be a measure of the inhomogeneity of a real column packing.

In our opinion, the effective density of the sorbent matrix, ρ_{eff}, should be used in calculations (eqn. 3) instead of the true density ρ_s; ρ_{eff} is determined in given eluent whereas the ρ_s values are obtained by using liquid media with very small molecules, such as helium. In addition to closed pores, also micropores of the sorbent may be inaccessible to larger molecules of the eluent and ρ_{app} will be lower than ρ_s. Hence the use of ρ_s may lead to errors
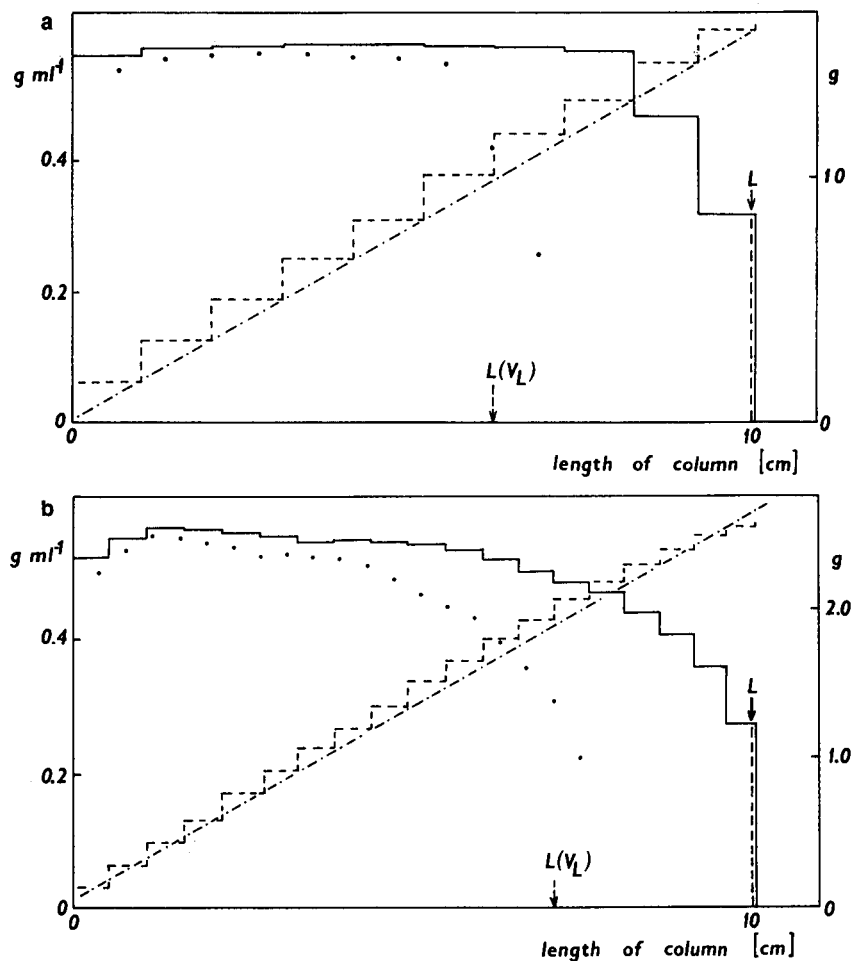
Fig. 8. Distribution of sorbent within the column calculated from that part of the eigenzone which corresponds to the volume of liquid within the column. (a) From the eigenzone in Fig. 2a. Calculated length of column, 10.08 cm; correlation coefficient calculated for integral distribution, 0.9988; calculated average packing density, $\rho = 0.7690$; experimental $\rho = 0.7975$. (b) From the eigenzone in Fig. 2b. Calculated length of column, 10.06 cm; correlation coefficient calculated for integral distribution, 0.9983; calculated average packing density, $\rho = 0.668$; experimental $\rho = 0.709$. Symbols as in Fig. 7. For explanation, see text.

in calculations of the column bed density distribution.

CONCLUSIONS

The eigenzones, *i.e.*, the baseline perturbations due to changes in composition of mixed column effluents, are generated by sudden changes in pressure within HPLC columns. A simple experimental assembly was designed to generate non-destructive and fully repeatable pressure strokes within columns and to create well defined eigenzones.

The shape of the eigenzones was interpreted on the basis of the experimentally found direct proportionality between the height or the area of the eigenzone (*i.e.*, the amount of extracted or desorbed substance) and both the pressure change and the concentration of sorbent within the column. The concentration of sorbent is defined as the mass of sorbent (*i.e.*, its surface area) per unit volume of liquid in the column. A procedure was proposed that permits the calculation of the mass of sorbent at any point along the column.

To obtain more precise data, however, a correla-

tion of the eigenzone shape with respect to the broadening effects will be necessary, especially if the columns contain larger sorbent particles. On the other hand, the closer the volume of the eigenzone approaches the volume of liquid within the column, the more precise data about the packing distribution may be expected. Of course, high sensitivity of the adsorption equilibrium towards pressure changes and good detectability of the resulting effluent composition changes are also required.

The method proposed enables information to be obtained about the inhomogeneity of HPLC column beds. It may help in defining relationships between the sorbent bed structure and its chromatographic efficiency and allow the optimization of column packing procedures.

ACKNOWLEDGEMENT

REFERENCES

1 K. Unger and R. Kern, *J. Chromatogr.*, 122 (1976) 345.
2 J. C. Giddings, *Dynamics of Chromatography*, Marcel Dekker, New York, 1965, p. 200.
3 D. Berek, M. Chalányová and T. Macko, *J. Chromatogr.*, 286 (1984) 185.
4 T. Macko and D. Berek, *J. Chromatogr. Sci.*, 25 (1987) 17.
5 T. Macko, A. Poĩmáková and D. Berek, *Chem. Papers*, 43 (1989) 285.
6 S. Ozawa, K. Kawahara, M. Yamabe, H. Unno and Y. Ogino, *J. Chem. Soc., Faraday Trans 1*, 80 (1984) 1059.
7 M. Zawadski and A. Adamson, *Langmuir*, 2 (1986) 541.
8 V. A. Avramenko, V. Yu. Glushenko, V. L. Zibacevskaja, B. M. Teplyuk and B. P. Stipacev, *Zh. Fiz. Khim.*, 60 (1986) 931.
9 V. L. Bogatyrov, *J. Chromatogr.*, 364 (1986) 125.
10 B. A. Bidlingmeyer, R. P. Hooker, C. H. Lochmüller and L. B. Rogers, *Sep. Sci.*, 4 (1969) 439.
11 B. A. Bidlingmeyer and L. B. Rogers, *Anal. Chem.*, 43 (1971) 1882.
12 B. A. Bidlingmeyer and L. B. Rogers, *Sep. Sci.*, 7 (1972) 131.
13 T. A. Maldacker and L. B. Rogers, *Sep. Sci.*, 8 (1973) 627.
14 T. A. Maldacker and L. B. Rogers, *Sep. Sci.*, 9 (1974) 27.
15 P. P. Nefedov and T. P. Zhmakina, *Vysokomol. Soedin., Ser. A*, 23 (1981) 276.
16 M. Chalányová, T. Macko, J. Kandráč and D. Berek, *Chromatographia*, 18 (1984) 668.
17 T. Macko, D. Berek and M. Chalányová, in B. Sedláček (Editor), *Physical Optics of Dynamic Phenomena and Processes in Macromolecular Systems*, Walter de Gruyter, Berlin, 1985, p. 521.
18 T. Macko, M. Chalányová and D. Berek, *J. Liq. Chromatogr.*, 9 (1986) 1123.
19 D. B. Marshall, J. W. Burns and D. E. Connoly, *J. Chromatogr.*, 360 (1986) 13.
20 N. Tanaka, T. Yoshimura and M. Araki, *J. Chromatogr.*, 406 (1987) 247.
21 D. Berek and T. Macko, *Pure Appl. Chem.*, 61 (1989) 2041.
22 M. Martin, G. Blu and G. Guiochon, *J. Chromatogr. Sci.*, 11 (1973) 641.
23 H. Poppe, J. C. Kraak, J. F. K. Huber and J. H. M. van der Berg, *Chromatographia*, 14 (1981) 515.

Investigation of solid surfaces by high-performance liquid chromatography

A. E. Chalykh, L. N. Kolomiets*, O. G. Larionov and N. I. Vinogradova

Institute of Physical Chemistry, USSR Academy of Sciences, Leninskii Prospect 31, 117915 Moscow (USSR)

ABSTRACT

Strong and weak points of chromatography as a method for physico-chemical research of properties of solid surfaces are discussed. The method was applied for studying the surface properties of γ-iron oxide and their changes during the various treatments.

INTRODUCTION

Chromatography, owing to its high separation efficiency, is firmly established as an important group of techniques for determining and separating substances in complex mixtures. Less attention has been paid to applying chromatography in physico-chemical investigations, however, although there has been research to obtain data on adsorption equilibria in binary [1] and multi-component [2] systems, and to investigate porous structures [3], intermolecular interactions [4] and the comparison and characterization of reversed phases [5] and surfaces [6].

In considering chromatography as a method for physico-chemical studies, we should point out its strong and weak points. The former include the following.

(1) The possibility of identifying and studying very small differences in intermolecular interactions. Unlike stationary research methods employed in studying a one-time distribution or redistribution of substances, chromatographic processes feature multiple redistributions of a substance between the mobile and stationary phases. Each distribution is determined by the difference between the substance interaction energies and that between the mobile and the stationary phases. Therefore, in a study of the distribution under stationary conditions in order to determine differences large enough to be measured,

the distribution coefficients ought to be sufficiently high, *i.e.*, the differences in intermolecular interactions ought to be significant. Owing to multiple repetition of the distribution in a chromatographic process, multiplication of intermolecular interactions occurs in proportion to the number of redistribution acts, *i.e.*, to the number of theoretical plates in a chromatographic column.

The application of a chromatographic method makes it possible to determine extremely small differences in intermolecular interactions, which is accounted for by the high efficiency of the method (which, of course, depends on the efficiency of the chromatographic column used). The adsorption isotherm of a binary solution has the form [1]

$$\frac{x_1^s \gamma_1^s}{x_1 \gamma_1}\left(\frac{x_2 \gamma_2}{x^s \gamma^s}\right)^{m_2/m_1} = \exp\left(\frac{\Phi_2^0 - \Phi_1^0}{m_1 RT}\right) \tag{1}$$

where x_i, x_i^s are mole fractions of component i in the bulk phase and in the surface phase at equilibrium, respectively; γ_i, γ_i^s are activity coefficients of component i in the balk phase and in the surface phase, respectively; m_i is limiting adsorption of pure component i (mmol/g), and in the case of monolayer adsorption $m_i = S/\omega_0 N$, where S is the specific surface area, N is Avogadro's number and ω_0 is the cross-sectional area of the molecule; Φ_i^0 is the change in free energy of wetting of the adsorbent with pure component i; R is the gas constant; and T is absolute temperature.

At low concentrations, when $x_i \to 0$, $x_i^s = n_i^e/m_s$ and eqn. 1 takes the form

$$\frac{n_i^e \gamma_i^s}{x_i \gamma_i m_s} = \exp\left(\frac{\Phi_s^0 - \Phi_i^0}{m_i RT}\right) = K \tag{2}$$

where n_i^e is the excess adsorption of component i, m_s is the limiting adsorption of the solvent and K is the equilibrium constant.

The point with concentration x moves through the column at a rate [7]

$$U_{x_i} = U/V_c + \frac{dn_i^e}{dx_i} \tag{3}$$

where V_c is the free volume of the column, including the volume of the adsorbent pores, and U is the flow-rate of the eluent. From eqn. 3, it follows that

$$\frac{dn_i^e}{dx_i} = \frac{U}{U_{x_i}} - V_c = V_{Ri} - V_c \tag{4}$$

and from eqn. 2 we have

$$\frac{dn_i^e}{dx_i} = K \cdot \frac{m_s \gamma_i}{\gamma_i^s} \tag{5}$$

In the region of symmetrical peaks, $dn_i^e/dx_i =$ constant $= K_H$, where K_H is Henry's constant. From eqns. 5 and 4, it follows that

$$K_H = K \cdot \frac{m_s \gamma_i}{\gamma_i^s} = V_{Ri} - V_c = V'_{Ri} \tag{6}$$

The selectivity coefficient of a column for components 1 and 2 is

$$\alpha = x_1^s x_2 / x_1 x_2^s \tag{7}$$

From eqn. 2, it follows that

$$\alpha = \frac{n_1^e x_2}{n_2^e \cdot x_1} = \frac{\gamma_1 \gamma_2^s}{\gamma_1^s \gamma_2} \cdot \exp\left(\frac{\Phi_s^0 - \Phi_1^0}{m_1 RT} - \frac{\Phi_s^0 - \Phi_2^0}{m_2 RT}\right) \tag{8}$$

If we assume that $\gamma_1 \gamma_2^s/\gamma_1^s \gamma_2 \approx 1$ and $m_1 = m_2$ (this means that the components do not differ much from each other in their physico-chemical properties), then

$$\alpha = K_{H1}/K_{H2} = V'_{R1}/V'_{R2} = k'_1/k'_2 \approx K_1/K_2$$

From eqn. 3, it follows for components i and j that

$$\ln \alpha = (\Phi_j^0 - \Phi_i^0)/mRT \tag{9}$$

Now we can estimate the sensitivity of the method.

Assuming $T = 300$ K and $m = 1$ mmol/g for $\alpha = e$ we obtain (from ref. 9) $\Delta\Phi = \Phi_2^0 - \Phi_1^0 = mRT = 8.314 \times 300 \times 1.10^{-3} = 2.4$ J/g. In other words, even with a high degree of selectivity, the value of $\Delta\Phi$ can be measured, which is normally unattainable through static measurement methods.

(2) The method is not material-intensive and allows small surface areas to be measured.

(3) Measurements can be carried out at various temperatures in the presence of foreign substances.

(4) Studies can be carried out in multi-component solvent systems and for several components simultaneously.

(5) The method can be considered to be rapid and can easily be automated.

The disadvantages of the method refer to the question of mass transfer and achieving an equilibrium. In cases when the equilibrium is achieved slowly, it is doubtful whether the data obtained actually correspond to equilibrium. These difficulties can be overcome by decreasing the flow rate, facilitating the mass transfer by employing small-sized particles for filling the column and increasing the temperature, where possible, for the system under investigation.

One of the limitations of the method in terms of the equipment employed may manifest itself as a difficulty in selecting a suitable detector, especially if the solvent and the substance under investigation have similar physico-chemical properties. On the other hand, the fact that we can not always prepare a column of high efficiency may depend, of course, on the material under investigation.

As new types of materials emerge, they necessitate the development of rapid methods for studying their surface characteristics. In our opinion, chromatography is one of the major methods for this purpose. This paper reports a liquid chromatographic method for studying the properties of γ-iron oxide (γ-Fe_2O_3) and of changes in the surface properties during the course of various treatments.

EXPERIMENTAL

A Milichrom chromatograph (Nauchpribor, USSR) with a UV detector was used. When working with substances that do not absorb in the UV region, an RIDK-101 (Czechoslovakia) refractometer was used as the detector.

Stainless-steel columns (60–120 mm × 2 mm I.D.) diameter were filled with powdered γ-Fe$_2$O$_3$ by the dry method. The size of the powder particles was < 0.5 μm. The agglomerated fraction of the γ-Fe$_2$O$_3$ particles of 0.08–0.25 mm was used. Filling the columns presented certain difficulties as the high density of the column packing causes an increase in its resistance, and when the column packing was highly porous the efficiency of the column was very low and the peaks were very diffuse.

The experiment was designed to measure the retention times of different substances featuring various types of intermolecular interactions, and benzene, toluene, nitrobenzene, benzaldehyde, benzyl alcohol, phenol and aniline were chosen as test substances. In preliminary tests, the retention of a test substance was measured on a new column each time.

n-Heptane and toluene were used as eluents. A certain amount of the test substance was introduced into the column and its retention volume was determined at a flow-rate of 100 μl/min. V_c was measured as V_R of an unretained component (n-octane). When modified samples of γ-Fe$_2$O$_3$ were tested, the original sample was first treated with the respective modifier until it was saturated, then the adsorbent obtained was used to measure the retention time of the test substance.

DISCUSSION AND RESULTS

Table I gives the results for the retention of test substances using the initial sample of γ-Fe$_2$O$_3$. Phenol and aniline, featuring acidic and basic prop-

TABLE I

RETENTIONS OF TEST SUBSTANCES ON ORIGINAL γ-Fe$_2$O$_3$

Substance	V_g (μl/g)	$k' = V_g/V_c$
Benzene	81	0.055
Toluene	90	0.061
Nitrobenzene	694	0.47
Benzaldehyde	1314	0.89
Benzyl alcohol	1889	1.28
Phenol	154 000	> 105
Aniline	70 000	> 85

TABLE II

"CHROMATOGRAPHIC TITRATION" OF γ-Fe$_2$O$_3$ WITH PHENOL

Volume of phenol (1% solution in n-heptane) introduced (μl)	V_g (μl/g)	k'	Peak present
10	> 125 000	–	No
17	158 000	–	No
27	110 000	72.3	Yes
37	25 000	15.7	Yes
57	7200	3.8	Yes
77	6750	3.5	Yes
97	6660	3.4	Yes

erties, respectively, show the strongest retention. Phenol is not eluted even at $k' = 105$, and aniline behaves similarly. It could be suggested that they are adsorbed by the γ-Fe$_2$O$_3$ at basic and acidic centres, respectively. In order to measure the number of such centres, a method arbitrarily referred to as "chromatographic titration" was used. Its essence is as follows: a certain amount of a substance is introduced into the column and is eluted until it reaches a volume equivalent to about $k' = 50$; if the substance is still retained in the column, an additional amount of the substance is introduced and the procedure is repeated. After the substance has been detected at the outlet, the total amount of it introduced into the column is calculated. When a further amount of the substance is subsequently introduced, one can observe the process of the column modification.

Table II gives the results of studies on the phenol modification of γ-Fe$_2$O$_3$. After introducing 27 μl of 1% phenol solution, a phenol peak was obtained. When additional phenol was introduced, the peak increased in height and shifted towards smaller k' and lower retention volume (V_g). After 77 μl of the solution had been introduced, the surface modification of the γ-Fe$_2$O$_3$ was practically completed.

Table III gives corresponding results for aniline modification. When 20 μl of 1% aniline solution had been introduced, an aniline peak was detected. As more aniline solution was introduced, the peak increased in height and shifted to smaller k' and lower retention volume. After introducing 40 μl of 1% aniline solution, the surface modification of the γ-Fe$_2$O$_3$ was practically completed.

TABLE III

"CHROMATOGRAPHIC TITRATION" OF γ-Fe$_2$O$_3$ WITH ANILINE

Volume of aniline (1% solution in n-heptane) introduced (μl)	V_g' ($\mu l/g$)	k'	Peak present
10	>125 000	—	No
20	35 830	22.9	Yes
30	9170	5.11	Yes
40	8417	4.61	Yes
50	8520	4.67	Yes

TABLE V

"CHROMATOGRAPHIC TITRATION" OF γ-Fe$_2$O$_3$ WITH STEARIC ACID (SA)

Volume of SA (0.53% solution in toluene) introduced (μl)	V_g' ($\mu l/g$)	k'	Peak present
50	>48 500	—	No
100	>46 970	—	No
150	29 122	38.8	Yes
200	7128	9.49	Yes
300	4302	4.73	Yes
350	4300	4.73	Yes

In order to establish the mode of filling of the active centres with phenol and aniline, samples of 1% aniline solution were introduced into a phenol-modified column. As with the initial γ-Fe$_2$O$_3$, the initial amounts of the aniline introduced were irreversibly adsorbed on the phenol-modified γ-Fe$_2$O$_3$, with no phenol desorption occurring. In order to investigate the modified surface properties, test substances were used. Results for the retention of the test substances on the initial, phenol-modified and phenol- and aniline-modified surfaces are given in Table IV.

As can be seen, modification of the surface of γ-Fe$_2$O$_3$ resulted in sharp changes in properties. Further studies were made involving substances featuring the same size of molecules but with different functional groups, namely stearic acid (SA)

and octadecylamine (ODA). The initial γ-Fe$_2$O$_3$ sample was "chromatographically titrated" with SA (0.53% solution in toluene) and ODA (0.32% solution in toluene). Toluene was used as the eluent. The results are given in Tables V and VI.

As can be seen, irreversible adsorption of SA and ODA occurs until the surface active centres are blocked, as with phenol and aniline. Subsequently, symmetrical peaks of both SA and ODA are eluted from the modified γ-Fe$_2$O$_3$ surfaces with a constant retention time.

The retention volume of phenol was measured on the ODA-modified γ-Fe$_2$O$_3$. Phenol was eluted as a symmetrical peak without displacement of ODA.

In order to demonstrate that the ODA and SA

TABLE IV

RETENTIONS OF TEST-SUBSTANCES ON ORIGINAL AND MODIFIED γ-Fe$_2$O$_3$

Substance	k'		
	Original	Phenol-modified	Phenol + aniline-modified
Benzene	0.055	—	0
Toluene	0.061	—	0.029
Nitrobenzene	0.47	—	0.34
Benzaldehyde	0.89	1.42	0.42
Benzyl alcohol	1.28	—	0.35
Phenol	>100	3.5	4.14
Aniline	>100	—	5.29

TABLE VI

"CHROMATOGRAPHIC TITRATION" OF γ-Fe$_2$O$_3$ WITH OCTADECYLAMINE (ODA)

Volume of ODA (0.32% solution in toluene) introduced (μl)	V_g' ($\mu l/g$)	k'	Peak present
50	>65 800	—	No
100	>43 900	—	No
150	>21 050	—	No
205	100 526	12.48	Yes
255	10 088	11.92	Yes
355	9210	10.80	Yes
405	7456	8.55	Yes
500	7460	8.55	Yes

TABLE VII

"CHROMATOGRAPHIC TITRATION" OF ODA-MODI-FIED γ-Fe$_2$O$_3$ WITH STEARIC ACID (SA)

Volume of SA (0.53% solution in toluene) introduced (μl)	V_g (μl/g)	k'
50	6140	3.5
100	5260	3.0
150	4780	2.72
200	3640	2.07
250	2130	1.25
300	2130	1.25

TABLE VIII

NUMBER OF ACTIVE CENTRES ON THE SURFACE OF γ-Fe$_2$O$_3$

Substance	Type of centre	No. of centres per m^2 of surface
Phenol	Basic	$1.1 \cdot 10^{17}$
Aniline	Acidic	$3.5 \cdot 10^{17}$
Stearic acid	Basic	$1.3 \cdot 10^{17}$
Octadecylamine	Acidic	$2.2 \cdot 10^{17}$

Fig. 1. Isotherm for irreversible and physical adsorption of stearic acid on original γ-Fe$_2$O$_3$.

adsorptions occur at different centres, the retention of SA was measured on the ODA-modified γ-Fe$_2$O$_3$ and the results are given in Table VII. These results show that, unlike the initial γ-Fe$_2$O$_3$ modification, a peak is observed when 50 μl of SA has been introduced (earlier than on the original γ-Fe$_2$O$_3$) and an additional SA modification of the γ-Fe$_2$O$_3$ surface occurs. As a result, the retention volume and

k' values are decreased, and after introduction of 250 μl of the 0.53% of the SA solution the retention volumes become constant.

The results show that γ-Fe$_2$O$_3$ adsorbs phenol and SA irreversibly as acids and aniline and ODA as bases. Knowing the total amount of irreversibly sorbed substance, as the difference between the amounts introduced and eluted, it is possible to calculate the number of active centres. This corresponds to the number of moles of irreversibly adsorbed substances. The results of the calculations are given in Table VIII.

The close correlation of the base centres determined with respect to phenol and SA confirms the validity of the method. The same can be said about

TABLE IX

PROPORTION OF THE SURFACE-MODIFIED γ-Fe$_2$O$_3$ SCREENED BY IRREVERSIBLY ADSORBED SUBSTANCES

Substance	$n \cdot 10^{-17}$	ω(v) (nm)	ω(h) (nm)	S_s(v)	S_s(h)
Phenol	1.1	0.24	0.45	0.026	0.049
Aniline	3.56	0.24	0.45	0.085	0.160
Stearic acid	1.3	0.2	—	0.026	—
Octadecylamine	2.2	0.2	—	0.044	—
Phenol + aniline				0.111	0.209
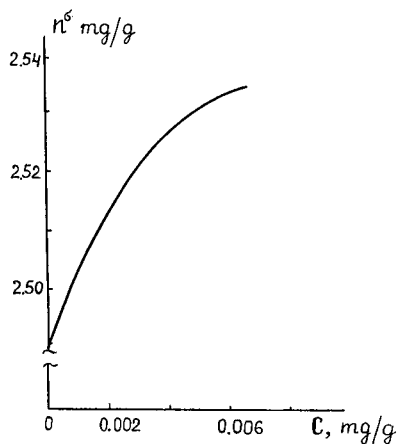
Fig. 2. Isotherm for irreversible and physical adsorption of octadecylamine on original γ-Fe$_2$O$_3$.

Fig. 3. Isotherm for physical adsorption of aniline on γ-Fe$_2$O$_3$ modified by phenol and aniline.

the number of acidic centres, which are about twice as many base centres on the γ-Fe$_2$O$_3$ surface. Knowing the number of active centers and the molecular areas of the test substances, the screening of the surface by modifiers can be calculated as

$$S_s = n\omega$$

where S_s is the screened surface area, n is the number of the active centres per 1 m^2 of the surface of γ-Fe$_2$O$_3$ and ω is the molecular area of the modifier in horizontal (h) or vertical (v) orientations.

Table IX gives the S_s values calculated on the basis of the data obtained. For aniline and phenol the data were calculated for the vertical and horizontal molecule orientations.

The shape of elution curve [1] made it possible to calculate isotherms for the physical adsorption of SA (Fig. 1) and ODA (Fig. 2) from toluene on γ-Fe$_2$O$_3$ modified by these combinations and of aniline on the γ-Fe$_2$O$_3$ surface modified by phenol

and aniline (Fig. 3). As can be seen, the physical adsorpton (n^e) in the concentration range investigated accounts for only a small part of the total adsorbed substance (n^σ).

In conclusion, this research confirms the possibility of using liquid chromatography as a method for the investigation of the surface properties of solids.

REFERENCES

1 S. A. Busev, O. G. Larionov, E. S. Jakubov and S. I. Zverev, *J. Chromatogr.*, 241 (1982) 287.
2 A. A. Zhukhovitskii, A. F. Shlyakhov and A. V. Sokolov, *Zavod. Lab.*, 41 (1975) 25 and 159.
3 A. I. Kalinichev and O. G. Larionov, *Zh. Vses. Khim. Ova.*, 28 (1983) 53.
4 A. V. Kiselev and Ya. Yasin, *Gas- und Flüssigadsorptionschromatographic*, Hüthig, Heidelberg, 1985.
5 H. Engelhardt and M. Jungheim, *Chromatographia*, 29 (1990) 59.
6 H. Engelhardt, *J. Pure Appl. Chem.*, 61 (1989) 2033.
7 D. DeVault, *J. Am. Chem. Soc.*, 62 (1940) 1583.

Effect of temperature and mobile phase on the retention of retinoates in reversed-phase liquid chromatography

Marja Salo*, Heikki Vuorela and Jaakko Halmekoski

Department of Pharmacy, University of Helsinki, Fabianinkatu 35, SF-00170 Helsinki (Finland)

ABSTRACT

The effect of temperature on the retention of seven closely related retinoates in reversed-phase liquid chromatography using three organic mobile phases was studied. Retinoates were chromatographed on an RP-18 column with aqueous organic mobile phases (90% methanol, 87% acetonitrile and 55% tetrahydrofuran). The capacity factors were measured at five temperatures (35–55°C). An increase in temperature decreased the retention. The standard enthalpy changes of the retention process ($-\Delta H^0$) were calculated from the slopes of Van't Hoff plots (ln k' vs. $1/T$). The effect of the molecular structure on the standard enthalpy change was studied. This effect increased significantly as the organic modifier was changed in the order methanol < acetonitrile < tetrahydrofuran.

INTRODUCTION

Reversed-phase chromatography with bonded alkyl stationary phases is widely used in quantitative structure–retention relationship (QSRR) studies. The main objective in these studies is to obtain information about the physico-chemical properties of the solutes that affect both the retention and, for example, the chemical reactivity or biological activity of the compound. The solvophobic theory developed by Horváth et al. [1] can explain the influence of the solvent on the solvophobic interaction between the solute and the stationary phase, but cannot precisely explain the physico-chemical mechanism of the interaction process.

The mechanism behind the separation process can be explored by studying the free-energy relationships of the separation. The equilibrium constant is linearly dependent on the free-energy change of the process. The system is said to express an enthalpy–entropy compensation effect when the free-energy changes are linearly dependent on the corresponding enthalpy change. The retention mechanism in such a system is the same for all participating species [2,3]. A constant retention mechanism is essential for reliable QSRR studies. This

should always be verified before making any postulations from the chromatographic data.

The following equation expresses the enthalpy–entropy compensation [4]:

$$\Delta H^0 = \beta \Delta S^0 + \Delta G_\beta^0 \qquad (1)$$

where ΔG_β^0 denotes the Gibbs free energy of physico-chemical interaction at temperature β, and ΔH^0 and ΔS^0 are the corresponding standard enthalpy and entropy, respectively. At temperatures close to β the changes in ΔH^0 are caused by changes in ΔS^0, and the free-energy changes are virtually independent of temperature. The values of β and G_β^0 are constant when enthalpy–entropy compensation occurs. β is called the compensation temperature.

By combining two equations for the Gibbs free-energy change ΔG^0,

$$\Delta G^0 = \Delta H^0 - T\Delta S^0 \qquad (2)$$

where T temperature, and

$$\Delta G^0 = -RT\ln K = -RT\ln(k'/\varphi) \qquad (3)$$

where R is the gas constant, ln K is the thermodynamic equilibrium constant, k' is the capacity factor and φ is the phase ratio of the column, we

obtain an equation describing the relationship between the capacity factor k' and the temperature T:

$$\ln k' = -\frac{\Delta H^0}{RT} + \frac{\Delta S^0}{R} + \ln \varphi \qquad (4)$$

When the retention mechanism is the same over the temperature range investigated and the enthalpy is constant, the resulting plot of $\ln k'$ against $1/T$ (the Van 't Hoff plot) yields a straight line [2,3].

The $-\Delta H^0$ of the transfer of a solute molecule from the mobile phase to the stationary phase can be calculated from the slope of the Van 't Hoff plots [5]:

$$\text{slope} = \frac{-\Delta H^0}{R} \qquad (5)$$

The enthalpy values are related to the carbon number of the solutes [6]. A more specific method for describing the molecular structure is to use a topological index, the molecular connectivity index [7], which is closely related to many physico-chemical [8–10] and biological [11,12] properties and chromatographic retention [13,14] of the molecules.

The relationship between $-\Delta H^0$, the standard enthalpy of the transfer of a solute molecule from the mobile phase to the stationary phase, and the molecular structure has been examined [6]. The slopes of the regression equations have been considered to be the methylene group increment of $-\Delta H^0$ and found to increase with the retention order of the solute groups. The intercepts were estimated to represent the $-\Delta H^0$ of the transfer of the functional group alone and to indicate the preferences of the mobile phase among the different groups.

The polarity of the mobile phase is the most important factor governing the retention. The polarity of solvents can be expressed quantitatively, e.g. by the polarity parameter P' of Snyder [15]. The retention ($\ln k'$) decreases as the temperature increases, and this reduction is linearly related to the polarity of the mobile phase [16].

The aim of this work was to study the effect of temperature on the retention of seven closely related retinoates in three mobile phases. The second aim was to study the relationships between the enthalpy change of the retention, the molecular structure of the solutes and the nature of the mobile phase.

EXPERIMENTAL

The apparatus consisted of a Hewlett-Packard 1090 liquid chromatograph equipped with a Pye Unicam UV detector and a Hewlett-Packard 3380A integrator. The straight-chain retinoates, methyl to pentyl (Nos. 1–5, Fig. 1), were synthesized from all-*trans* retinoic acid and a corresponding alkyl halide in the presence of potassium carbonate. The branched-chain retinoates, isopropyl and *tert.*-butylcarbinyl esters (Nos. 6 and 7, Fig. 7), were synthesized from a preformed N-retinylimidazolide *p*-toluenesulphonate and a corresponding alcohol (for more details, see ref. 17). Methanol, acetonitrile and tetrahydrofuran were high-performance liquid chromatography (HPLC) grade (Rathburn, Walkerburn, UK), and water was purified with the Alpha-Q system (Millipore, Bedford, MA, USA). Mobile phases were filtered through a 0.22-μm membrane filter (Millipore).

The compounds were chromatographed on a Spherisorb 5-ODS column (5 μm, 100 × 4 mm I.D., LKB Pharmacia, Uppsala, Sweden) equipped with a 10-mm guard column filled with LiChrosorb RP-18 (10 μm, Merck, Darmstadt, Germany). Aqueous organic solvents (90% methanol, 87% acetonitrile and 55% tetrahydrofuran) were used as the mobile phases. The compositions of the mobile phase were selected to give equal retention at a flow-rate of 1.00 ml/min regardless of the solvent used. The compounds were detected at 350 nm. The re-
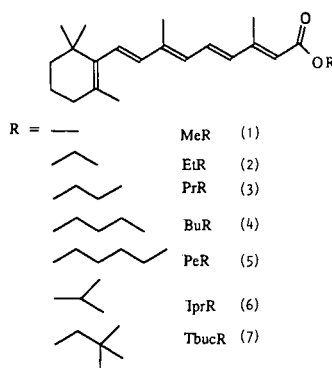
Fig. 1. Structures of the retinoates. MeR, EtR, PrR, BuR, PeR, IprR and TbucR are methyl, ethyl, propyl, butyl, pentyl, isopropyl and *tert.*-butylcarbinyl retinoates, respectively.

tention times were measured at five temperatures (35–55°C), which were controlled by the built-in column oven of the chromatograph. The capacity factors are presented in Table I.

The molecular connectivity indices were calculated using the general equation:

$$^m\chi_t = \sum_{j=1}^{^m n_s} {}^m c_j = \sum_{j=1}^{^m n_s} \left[\prod_{i=1}^{m} (\delta_i)_j^{-1/2} \right] \qquad (6)$$

where $^m c_j$ is the subgraph term for the mth-order subgraph, and $^m m_s$ is the number of subgraphs. The connectivity and valence level path indices of the orders 0–4 were calculated (Table II).

The regression between the capacity factors and temperature (ln k' vs. $1/T$, Van 't Hoff plot) was studied (Table III). The standard enthalpy changes of the retention process $(-\Delta H^0)$ were calculated from the slopes of the regression equations using eqn. 5 (Table III). The values of $-\Delta H^0$ were plotted against indices describing the molecular structure.

RESULTS AND DISCUSSION

The retention times of the solutes were fairly equal in all the mobile phases, but the differences

between the void volumes (methanol 1.01 min, acetonitrile 1.05 min, tetrahydrofuran 1.13 min) caused larger variation between the corresponding capacity factors (Table I).

The Van 't Hoff plots of the retinoates were linear and the slopes positive (Table III, Fig. 2). The enthalpy of association between these compounds and the alkyl stationary phase was calculated using eqn. 5, and is constant and negative. In other words, the mechanism of the retention process was similar over the investigated temperature range, and the strength of the hydrophobic interaction decreased with increasing temperature.

The effect of the molecular structure on the standard enthalpy change was calculated. The carbon number of the solute can be used in the calculations when the investigated compounds are homologous. The series included two branched-chain analogues. The structures were therefore expressed by the connectivity indices, which have selectivity towards the molecular geometry and were found in earlier retention studies to be good descriptors of the molecular structure of retinoates [18]. Nearly all connectivity indices correlated excellently with the enthalpy change ($r^2_{\text{mean}} = 0.907 \pm 0.091$, $n = 30$), the only exception being $^1\chi^v$ ($r^2_{\text{mean}} = 0.685 \pm 0.091$, $n = 3$). The first order connectivity index, $^1\chi$, had the best

TABLE I

CAPACITY FACTORS (k') OF RETINOATES MEASURED AT FIVE TEMPERATURES AND THREE MOBILE PHASES

Temperature (°C)	MeR	EtR	PrR	BuR	PeR	IprR	TbucR
Methanol (90%)							
35	5.31	6.33	7.79	9.82	12.42	7.12	10.68
40	4.77	5.59	6.96	8.66	10.83	6.32	9.40
45	4.33	5.06	6.20	7.75	9.63	5.72	8.40
50	3.90	4.54	5.56	6.87	8.52	5.11	7.43
55	3.52	4.09	4.95	6.07	7.49	4.57	6.60
Acetonitrile (87%)							
35	4.36	5.37	7.79	8.54	10.93	6.41	10.25
40	3.87	4.69	6.96	7.35	9.34	5.56	8.64
45	3.45	4.15	6.20	6.44	8.07	4.97	7.53
50	3.10	3.72	5.56	5.63	7.02	4.36	6.57
55	2.77	3.25	4.93	4.90	6.02	3.81	5.66
Tetrahydrofuran (55%)							
35	4.29	5.18	6.57	8.19	10.00	6.21	9.42
40	3.63	4.43	5.52	6.79	8.17	5.22	7.76
45	3.23	3.89	4.79	5.87	7.01	4.60	6.67
50	2.81	3.35	4.05	4.95	5.82	3.94	5.61
55	2.44	2.89	3.49	4.17	4.86	3.35	4.75

TABLE II

VALUES OF THE CONNECTIVITY INDICES

	MeR	EtR	PrR	BuR	PeR	IprR	TbucR
$^0\chi$	17.46	18.17	18.87	19.58	20.29	19.04	20.67
$^1\chi$	10.76	11.26	11.76	12.26	12.76	11.61	12.40
$^2\chi$	9.56	9.94	10.30	10.65	11.00	10.21	10.75
$^3\chi$	5.41	5.90	6.17	6.42	6.67	6.00	6.51
$^4\chi$	4.32	4.65	4.71	4.90	5.08	4.73	4.84
$^0\chi^v$	15.40	16.11	16.82	17.52	18.23	16.98	18.60
$^1\chi^v$	7.73	8.42	8.92	9.42	9.92	8.01	8.57
$^2\chi^v$	6.18	6.41	6.82	7.18	7.53	6.56	7.33
$^3\chi^v$	4.11	4.21	4.38	4.67	4.92	4.28	4.60
$^4\chi^v$	2.47	2.59	2.67	2.79	2.99	2.68	2.76

correlation with the following equations for the three mobile phases (Fig. 3):

Methanol 90%:
$$-\Delta H^0 = 1.87 \, {}^1\chi - 3.00 \qquad r^2 = 0.99$$
Acetonitrile 87%:
$$-\Delta H^0 = 3.01 \, {}^1\chi - 13.50 \qquad r^2 = 0.96$$
Tetrahydrofuran 55%:
$$-\Delta H^0 = 3.40 \, {}^1\chi - 13.72 \qquad r^2 = 0.99$$

The ΔH^0 of the ester group is expressed by the intercepts, which increase in the order methanol < acetonitrile < tetrahydrofuran. The slopes increased in the same order.

It can be seen from Table III that the regression coefficients and the intercepts of the regression equations $\ln k' = b \cdot (1000/T) + a$ increased with the size of the solute in all three mobile phases. This dependence was studied in two different ways. First,

TABLE III

REGRESSION BETWEEN THE CAPACITY FACTORS AND TEMPERATURE AS THE SLOPE b, THE INTERCEPT a, THE CORRELATION COEFFICIENT r^2 OF THE REGRESSION EQUATIONS $\ln k' = b \cdot (1000/T) + a$ AND THE $-\Delta H^0$ OF THE SEPARATION PROCESS CALCULATED FROM THE SLOPES OF THE REGRESSION EQUATIONS

	MeR	EtR	PrR	BuR	PeR	IprR	TbucR
Methanol							
b	2.07	2.19	2.28	2.41	2.53	2.22	2.42
a	−5.05	−5.27	−5.36	−5.54	−5.69	−5.25	−5.49
r^2	0.999	0.999	1.000	0.999	0.999	0.999	1.000
$-\Delta H^0$	17.23	18.22	18.98	20.04	21.01	18.48	20.12
Acetonitrile							
b	2.27	2.50	2.56	2.78	2.99	2.59	2.95
a	−5.91	−6.43	−6.41	−6.88	−7.30	−6.56	−7.27
r^2	1.000	0.999	0.999	1.000	1.000	0.998	0.999
$-\Delta H^0$	18.91	20.75	21.28	23.11	24.83	21.57	24.55
Tetrahydrofuran							
b	2.81	2.91	3.18	3.37	3.60	3.07	3.43
a	−7.67	−7.81	−8.44	−8.83	−9.39	−8.13	−8.88
r^2	0.998	0.999	0.999	0.999	0.999	0.998	0.999
$-\Delta H^0$	23.35	24.21	26.42	28.00	29,93	25.50	28.48
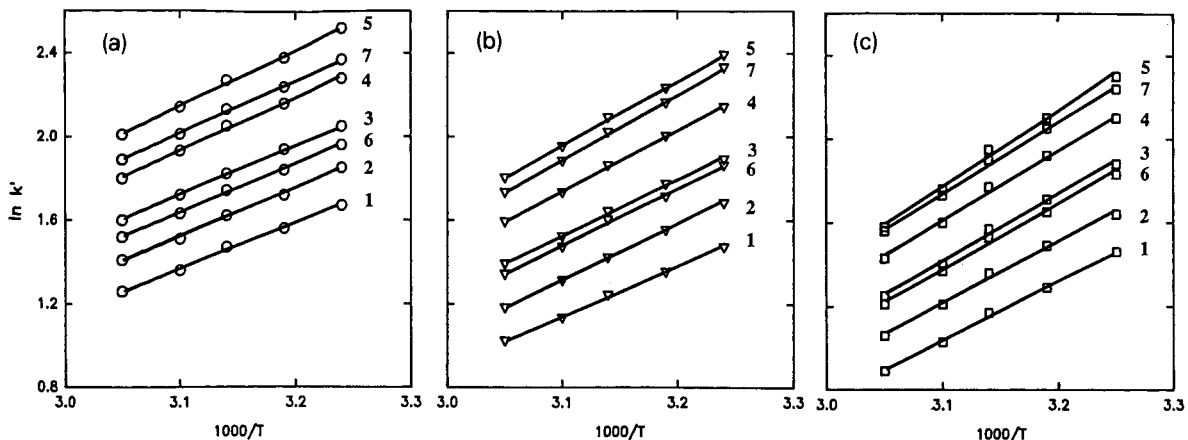
Fig. 2. Capacity factor ln k' vs. the reciprocal temperature $1000/T$: mobile phase (a) 90% methanol; (b) 87% acetonitrile; (c) 55% tetrahydrofuran. Retinoates numbered as in Fig. 1.

the separate equations were fitted to the intercepts and the slopes using the $^1\chi$ index as a descriptor for molecular structure.

The equations for the intercepts were (Fig. 4):

Methanol:
$$a = -0.30\ ^1\chi - 1.89 \qquad r^2 = 0.95$$
Acetonitrile:
$$a = -0.70\ ^1\chi + 1.54 \qquad r^2 = 0.92$$
Tetrahydrofuran:
$$a = -0.88\ ^1\chi - 1.98 \qquad r^2 = 0.97$$

Fig. 3. Dependence of the standard enthalpy change, $-\Delta H^0$, on the molecular structure expressed with the first-order molecular connectivity index$^1\chi$. Mobile phases: $\bigcirc$ = methanol, ∇ = acetonitrile and $\square$ = tetrahydrofuran. Retinoates numbered as in Fig. 1.

and for the slopes (Fig. 5):

Methanol:
$$b = 0.23\ ^1\chi - 0.35 \qquad r^2 = 0.99$$
Acetonitrile:
$$b = 0.36\ ^1\chi + 1.62 \qquad r^2 = 0.96$$
Tetrahydrofuran:
$$b = 0.41\ ^1\chi - 1.65 \qquad r^2 = 0.99$$

The slopes increased and the intercepts decreased in the order methanol < acetonitrile < tetrahydrofuran.

The equations were also calculated using two parameters, the temperature and a connectivity index, using all the indices calculated. Nearly all the correlations were highly significant ($r^2_{mean} = 0.931 \pm 0.065$, $n = 30$), the only exception being again $^1\chi^v$ ($r^2_{mean} = 0.759 \pm 0.030$, $n = 3$). The best correlation was achieved with the $^1\chi$ index:

Methanol:
$$\ln k' = 2.31\frac{1000}{T} + 0.41\,^1\chi - 10.29 \qquad r^2 = 0.992$$

Acetonitrile:
$$\ln k' = 2.63\frac{1000}{T} + 0.45\,^1\chi - 11.86 \qquad r^2 = 0.979$$

Tetrahydrofuran:
$$\ln k' = 3.16\frac{1000}{T} + 0.41\,^1\chi - 13.15 \qquad r^2 = 0.979$$

The regression coefficient for the temperature remained the same irrespective of the index used in

Fig. 4. Relationship between the molecular structure as the first-order molecular connectivity index $^1\chi$ and (a) the slopes and (b) the intercepts of the equations in Table III. Mobile phases: $\bigcirc$ = methanol, ∇ = acetonitrile and $\square$ = tetrahydrofuran. Retinoates numbered as in Fig. 1.

the calculation for a specific mobile phase, but it varied depending on the mobile phase.

The total polarities of the mobile phases were not known. The polarity parameter values, P' [14], of the neat organic modifiers are 3.0 (methanol), 3.1 (acetonitrile) and 4.4 (tetrahydrofuran). The effect of temperature on the retention exhibits a clear trend of being linearly related to the polarity of the organic modifier.

In conclusion, the increase in temperature significantly decreased the capacity factors of the retinoates, resulting in linear Van 't Hoff plots. The decrease in retention in reversed-phase HPLC was linearly correlated with the molecular structure expressed by the molecular connectivity indices, but its magnitude was dependent on the nature of the organic modifier.

REFERENCES

1 C. Horváth, W. Melander and I. Molnar, J. Chromatogr., 125 (1976) 129.
2 W. Melander, D. E. Campbell and C. Horváth, J. Chromatogr., 158 (1978) 215.
3 H. J. Issaq and M. Jaroniec, J. Liq. Chromatogr., 12 (1989) 2067.
4 J. Leffler and E. Grunwald, Rates and Equilibria of Organic Reactions, Wiley, New York, 1963.
5 E. Tomlinson, H. Poppe and J. C. Kraak, Int. J. Pharm., 7 (1981) 225.
6 G. Vigh and Z. Varga-Puchony, J. Chromatogr., 196 (1980) 1.
7 L. B. Kier and L. H. Hall, Molecular Connectivity Indices in Structure Activity Analysis, Research Studies Press Letchworth, 1986, pp. 262.
8 L. H. Hall, L. B. Kier and W. J. Murray, J. Pharm. Sci., 64 (1975) 1974.
9 L. H. Kier, W. J. Murray, M. Randic and L. H. Hall, J. Pharm. Sci., 65 (1976) 1226.
10 L. B. Kier, J. Pharm. Sci., 70 (1981) 1930.
11 L. H. Kier, L. H. Hall, W. J. Murray and M. Randic, J. Pharm. Sci., 64 (1975) 1971.
12 Z. Gabanyi, P. Surjan and G. Naray-Szabo, Eur. J. Med. Chem., 17 (1982) 307.
13 M. J. M. Wells, C. R. Clark and R. M. Patterson, J. Chromatogr. Sci., 19 (1981) 573.
14 H. Vuorela and P. Lehtonen, J. Liq. Chromatogr., 12 (1989) 221.
15 L. R. Snyder, J. Chromatogr. Sci., 16 (1978) 223.
16 D. E. Martire and R. E. Boehm, J. Phys. Chem., 87 (1983) 1045.
17 M. Salo and J. Halmekoski, Acta Pharm. Fenn., 99 (1990) 163.
18 M. Salo, H. Vuorela and J. Halmekoski, in preparation.

CHROMSYMP. 2402

Application of the gradient elution technique

Demonstration with a special test mixture and the DryLab G/plus method development software

R. Däppen

Ciba-Geigy Ltd., Central Analytical Department, CH-4002 Basle (Switzerland)

I. Molnar*

Institut für angewandte Chromatographie, Blücherstrasse 22, D-1000 Berlin 61 (Germany)

ABSTRACT

A mixture of ten compounds with an overlapping peak pair was analysed with a 90-min elution gradient. To improve the separation, two reversed-phase gradients differing by a factor of 3 in their run times, were applied. Contrary to expectation, two peak pairs were less well separated in the gradient run with the lower slope. The relative resolution map provided a rapid solution to the problem: a gradient with 16-min run time gave the best separation of the mixture. The simulated chromatogram was verified experimentally. The differences between the predicted and experimental retention times averaged 0.03 min. Further improvement was obtained using a segmented gradient, which adequately separated all peaks in only 9 min.

INTRODUCTION

The use of gradient elution techniques is increasing in the quality control of pharmaceuticals [1]. The underlying model of the theory of gradient elution [2] has been used in computer simulations for the successful prediction of experimental results [3–6]. Predictions are reliable for small [7] and large molecules [8–10].

There are, however, several experimental problems encountered when the powerful technique of gradient elution is first used routinely. To reduce the difficulties in practical applications, we have developed a course in high-performance liquid chromatography (HPLC) using a special mixture for gradient elution which contains ten compounds of a broad range of polarity from acetone to pyrene. This course uses the method development software DryLab G/plus [11].

EXPERIMENTAL

The chromatograph used was a Hewlett-Packard 1090 M gradient system (Waldbronn, Germany). Water and methanol were degassed with helium prior to use. The detection wavelength was 254 nm. DryLab G/plus software (LC Resources, Orinda, CA, USA; Molnar, Berlin, Germany) was used with an MS-DOS-based computer system.

The chemicals and eluents (HPLC grade) were purchased from Fluka (Buchs, Switzerland). All HPLC parameters are given in Table I. The Nucleosil C_{18} column (125 × 4.6 mm, 5 μm) (Macherey and Nagel, Düren, Germany) was packed by the Central Analytical Department, Ciba Geigy (Basle, Switzerland). Experiments were carried out at 30°C.

TABLE I

INPUT PARAMETERS FOR OPTIMIZATION OF THE MOBILE PHASE USING DRYLAB G/PLUS SOFTWARE

HPLC system		Gradient	
Column length (cm)	12.5	Start (%B)	5
Column I.D. (cm)	0.46	End (%B)	100
Flow-rate (ml/min)	1.0	Gradient time, run 1 (min)	20
Dwell volume[a]	0.35	Gradient time, run 2 (min)	60
Number of peaks	10		

[a] Dwell volume: *ca.* 2 ml for high-pressure mixer; *ca.* 5 ml for low-pressure mixer; *ca.* 0.3 ml for HP-1090.

RESULTS AND DISCUSSION

Sample

The computer-assisted HPLC method development procedure used here has been published previously [12] with several applications to various samples. For teaching the gradient elution technique to beginners, a special sample was mixed. With this test mixture various aspects of gradient elution in reversed-phase chromatography can be illustrated, such as the inversion of peak elution order, early or late eluting peaks and selectivity changes due to steps of different lengths and slopes.

Input data: two gradient runs

Two different gradient runs from 5 to 100% methanol in (a) 20 min (Fig. 1a) and (b) 60 min (Fig. 1b) were carried out using the sample mixture. The system parameters were entered into the DryLab G/plus software (Tables I and II). The measurement of the dwell volume was performed according to the DryLab G/plus instruction manual.

Isocratic conditions

It was not feasible to use isocratic method development for this sample with the DryLab I/plus software. The ratio of the capacity factor (k') values for the last and the first peaks was 1372, much larger than the value of 20 under which isocratic elution is advisable. The DryLab I/plus system recommended the use of gradient elution.

Peak tracking

After the two basic gradient elutions, including the integration reports (Table III), had been per-

formed an attempt was made to correlate the corresponding peaks in the two chromatograms. If the same amount of sample was injected in both runs, it was possible to find the same peak areas or percentage peak areas for well assigned peaks [13].

The same total peak area can be seen in both runs: 30 032 (20-min elution) and 29 498 (60-min elution) peak area units. The difference is only 1.7%. The individual peak areas also have very similar values. A deviation is seen only for naphthalene and xylene. These two peaks overlap in the 60-min run (peak area 5387), but are separated in the 20-min run (peak areas 4326 and 1185). The sum of the areas of both peaks in the 20-min run is very close to the peak area of the overlapping peaks in the 60-min run (5511 *versus* 5387).

In some other instances deviations occur if the integration is not carried out correctly. It is then reasonable to check the position of the baseline and to interpret the integration results. The baseline in both the gradient runs reported here was excellent.

Critical resolution map

The map of critical resolution is shown in Fig. 2. It can immediately be seen where it is possible to separate all the peaks and where this is not possible. It is seen that there are two possible maxima for resolution at about 8 and 16 min. These two runs have the largest critical resolution between the bands for xylene and naphthalene at a gradient time of 13 min, where there is zero resolution between benzene and 4-hydroxybenzoic acid methyl ester. Using such a 13-min gradient (5–100% B), these two peaks completely overlap and appear as a single homogeneous peak.

The 8-min gradient with a slope of 12.5% B per min was considered too steep and was therefore neglected.

Simulation of several runs on the computer

The 16 min gradient run was simulated on the computer. The software generated a chromatogram on the monitor in a few seconds, in which the two cricital band pairs were well separated with nearly baseline resolution. A print-out of this simulated run is given in Fig. 3a.
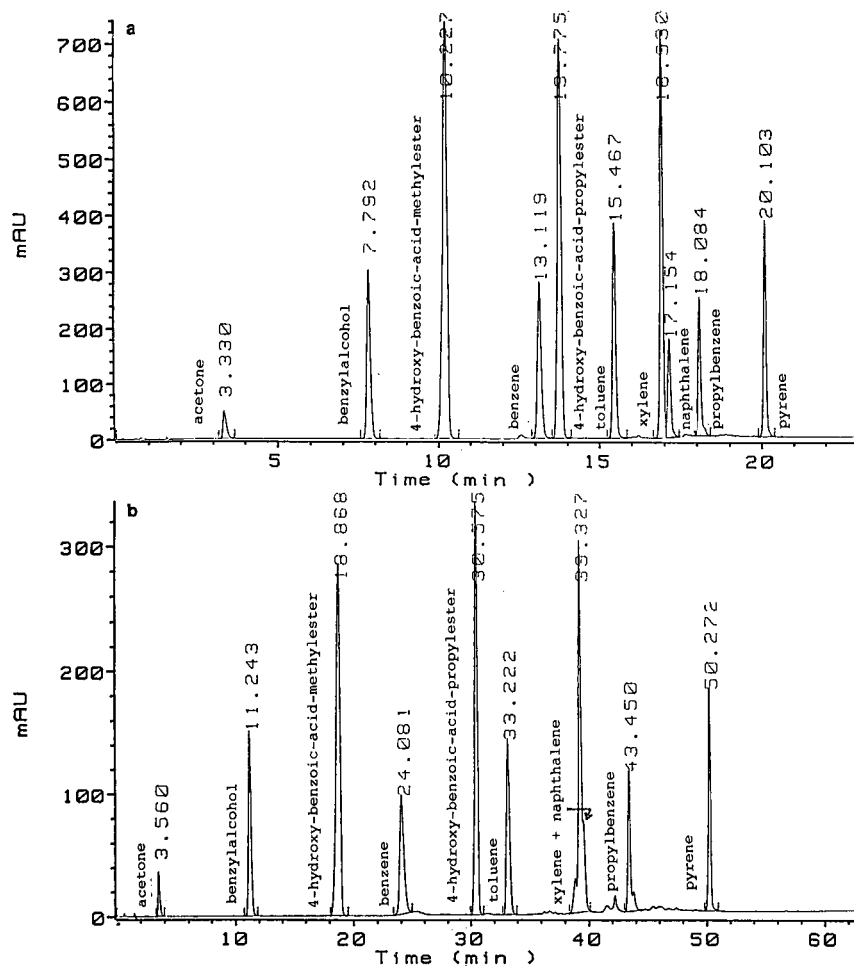
Fig. 1. (a) Basic gradient run No. 1 from 5 to 100% B in **20 min**. Chromatographic conditions as in Tables I and II. Detection wavelength, 254 nm; 1.2 a.u.f.s. (b) Basic gradient run No. 2 from 5 to 100% B in **60 min**.

TABLE II

PEAK PARAMETERS FOR OPTIMIZATION USING DRYLAB G/PLUS SOFTWARE

Peak no.	Compound	Retention time (min)		Peak area[a] (%)
		Run 1	Run 2	
1	Acetone	3.330	3.560	1.21
2	Benzylalcohol	7.792	11.243	7.73
3	4-OH-BA-ME[b]	10.227	18.868	24.93
4	Benzene	13.119	24.081	7.60
5	4-OH-BA-PE[c]	13.775	30.575	19.62
6	Toluene	15.467	33.222	8.61
7	Xylene	16.930	39.327	14.41
8	Naphthalene	17.154	39.600	3.95
9	Propylbenzene	18.084	43.450	4.87
10	Pyrene	20.103	50.272	7.07

[a] Peak area is taken from the reference run (here the 60-min run) and it is only for visualisation of the peaks, not for calculations.
[b] 4-OH-BA-ME = 4-hydroxybenzoic acid methyl ester.
[c] 4-OH-BA-PE = 4-hydroxybenzoic acid propyl ester.

TABLE III

PEAK TRACKING USING PEAK AREAS

60 min		20 min		Area ratio 60/20
Retention time (min)	Area	Retention time (min)	Area	
3.553	356	3.330	1364	0.97
11.241	2315	7.792	2321	0.99
18.868	6773	10.227	7487	0.90
24.080	2412	13.119	2283	1.06
30.575	5602	13.775	5892	0.95
33.222	2702	15.467	2587	1.04
38.920	457	16.930	4326	0.10
39.327	5387	17.154	1185	4.54
43.459	1320	18.084	1462	0.90
50.272	2174	20.103	2125	1.02
Total	29 498		30 032	0.98

Correlation between computer simulation and experimental results

The experimental control of the chromatogram suggested by the software revealed that the correlation between the predicted retention times and those found experimentally, as shown previously [10–14], was fairly good (Fig. 3b).

The average deviation in the retention times was less than 0.03 min (<2 s) (Table IV).

Up to now, participants of the gradient-HPLC-course did not find this simple optimum without the help of DryLab. Their solution was usually a multi-segmented gradient of 20–30 min, with a tendency to longer and longer runs, searching for improved resolution.

A systematic search for an optimum one-step linear gradient is shown in Fig. 4 (Table V). Fixing the content of B at the end of the gradient to 100% and changing the content of B at the start from 10 to 60 in steps of 5%, data were obtained for the critical resolution. It can be seen that gradients starting from 40, 45 and 50% B are not robust. Also gra-
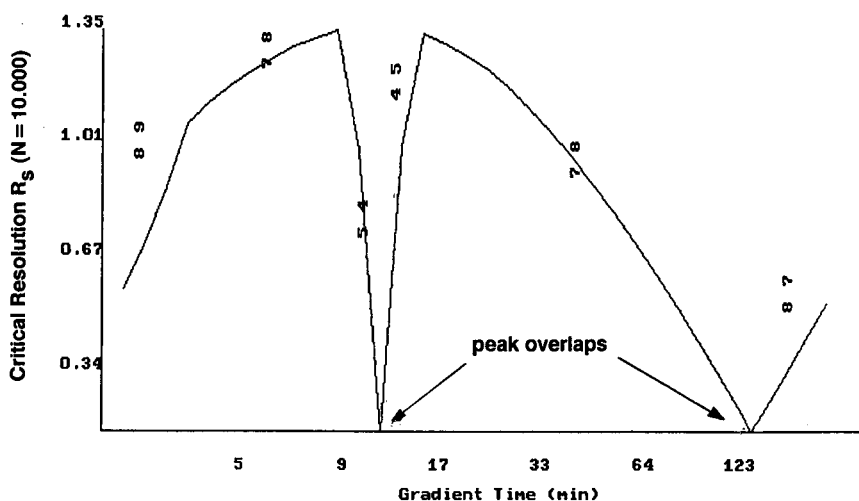
Fig. 2. Critical resolution map showing the lowest (critical) resolution between the two worst separated bands (numbers above the curve) as a function of the gradient time. Highest resolution is observed at 8- and at 16-min gradient run time (5–100% B). All other conditions as in Fig. 1.
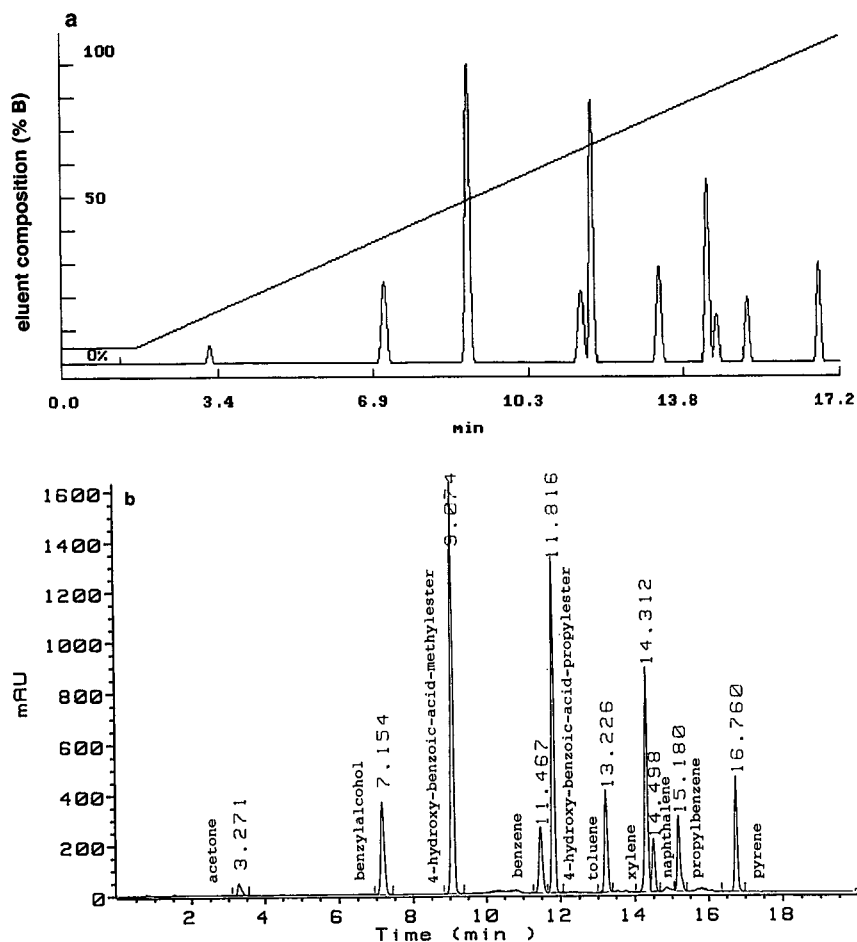
Fig. 3. (a) Predicted 16-min gradient run (5–100% B) by DryLab G/plus software. (b) Experimental 16-min run (5–100% B) (other conditions as in Fig. 1).

TABLE IV

COMPARISON OF RETENTION TIMES PREDICTED BY DRYLAB G/PLUS AND THOSE FOUND EXPERIMENTALLY

Peak no.	Compound	Retention time (min)		Difference in retention time (min)
		Predicted	Experimental	
1	Acetone	3.26	3.27	0.01
2	Benzylalcohol	7.13	7.15	0.02
3	4-OH-BA-ME[a]	8.99	9.07	0.08
4	Benzene	11.51	11.47	0.04
5	4-OH-BA-PE[b]	11.75	11.82	0.07
6	Toluene	13.24	13.23	0.01
7	Xylene	14.32	14.31	0.01
8	Naphthalene	14.52	14.50	0.01
9	Propylbenzene	15.20	15.18	0.02
10	Pyrene	16.78	16.76	0.02

[a] 4-OH-BA-ME = 4-hydroxybenzoic acid methyl ester.
[b] 4-OH-BA-PE = 4-hydroxybenzoic acid propyl ester.
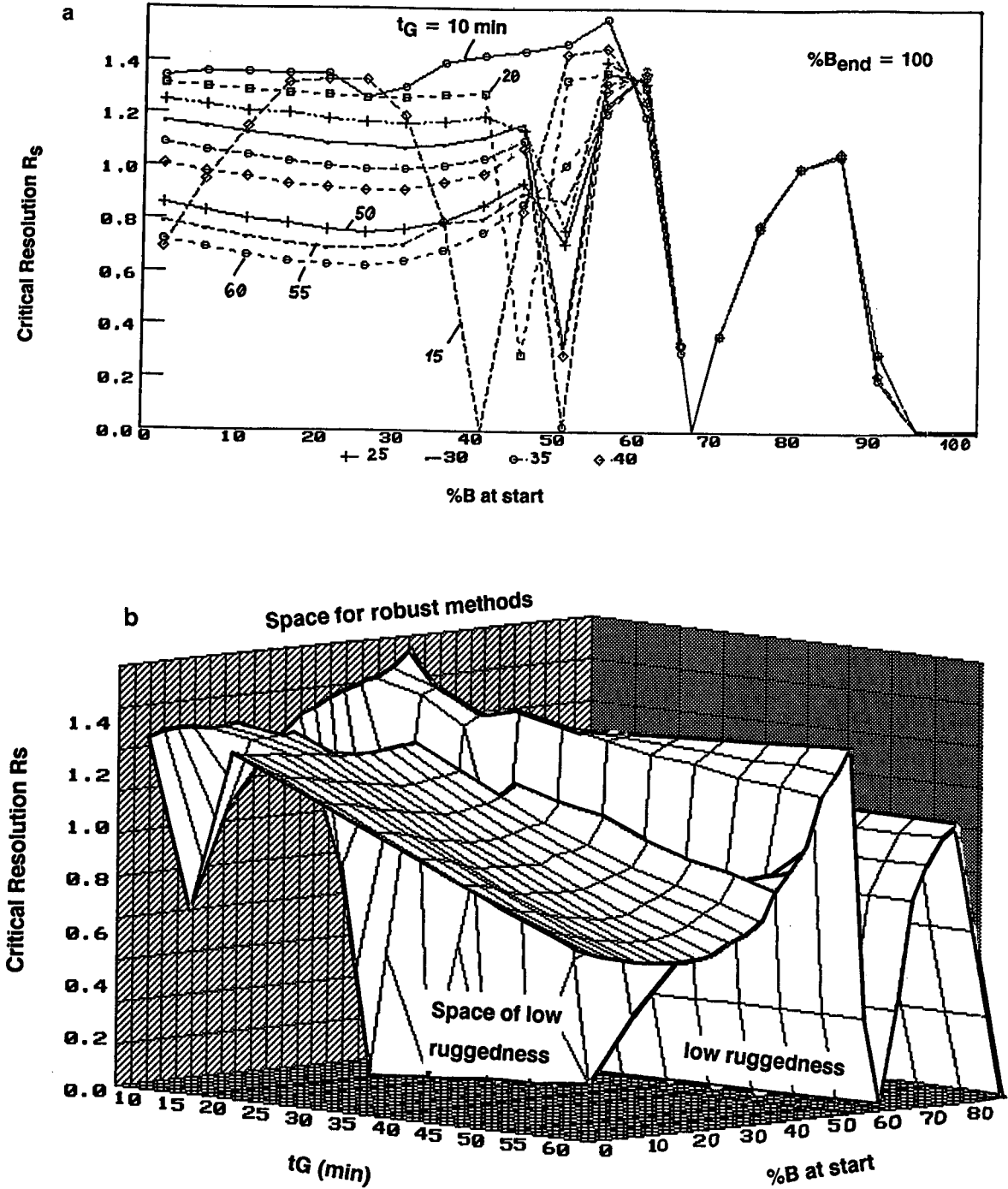
Fig. 4. (a) Multiple relative resolution map for the sample using a one-step linear gradient from a varying percentage of B at the start to a fixed percentage (100%) of B at the end of the run. There are several valleys in this graph, which means that the methods are of low ruggedness. A maximum is seen around a gradient time of 10 min and a percentage of B at the start of 5%. (b) Three-dimensional plot of relative resolution maps as described in (a).

TABLE V

CRITICAL RESOLUTION VALUES USING A FIXED PERCENTAGE OF B AT THE END (100%) AND A VARIABLE PERCENTAGE OF B AT THE START OF THE ELUTION

Elution time varied from 10 to 60 min.

Percentage of B at start	Gradient time (min)										
	10	15	20	25	30	35	40	45	50	55	60
0	1.34	0.69	1.31	1.25	1.17	1.09	1.01	0.93	0.86	0.79	0.72
	1.36	0.95	1.30	1.23	1.15	1.06	0.98	0.90	0.83	0.76	0.69
10	1.36	1.15	1.29	1.21	1.13	1.04	0.96	0.88	0.80	0.73	0.66
	1.35	1.32	1.28	1.20	1.11	1.02	0.93	0.85	0.78	0.71	0.64
20	1.35	1.33	1.27	1.18	1.09	1.00	0.92	0.84	0.76	0.69	0.63
	1.26	1.33	1.26	1.17	1.08	0.99	0.91	0.83	0.75	0.69	0.62
30	1.30	1.19	1.26	1.16	1.07	0.99	0.91	0.83	0.76	0.70	0.64
	1.39	0.79	1.27	1.17	1.08	1.00	0.94	0.86	0.79	0.78	0.68
40	1.42	0.00	1.28	1.19	1.11	1.03	0.97	0.90	0.85	0.80	0.75
	1.44	0.83	0.29	1.14	1.16	1.10	1.07	0.99	0.94	0.90	0.86
50	1.47	1.43	1.33	0.76	0.32	0.02	0.29	0.52	0.71	0.87	1.01
	1.56	1.45	1.36	1.40	1.36	1.32	1.29	1.27	1.24	1.22	1.20
60	1.19	1.25	1.30	1.32	1.33	1.34	1.35	1.36	1.36	1.37	1.37
	0.30	0.32	0.33	0.33	0.33	0.34	0.34	0.34	0.34	0.34	0.34
70	0.36	0.36	0.36	0.36	0.36	0.36	0.36	0.36	0.36	0.36	0.36
	0.78	0.78	0.77	0.77	0.77	0.77	0.77	0.77	0.77	0.77	0.77
80	1.00	1.00	1.00	1.00	1.00	1.00	1.00	1.00	1.00	1.00	1.00
	1.06	1.06	1.05	1.05	1.05	1.05	1.05	1.05	1.05	1.05	1.05
90	0.20	0.22	0.30	0.30	0.30	0.30	0.30	0.30	0.30	0.30	0.30
	0.00	0.00	0.00	0.00	0.00	0.00	0.00	0.00	0.00	0.00	0.00
100	0.00	0.00	0.00	0.00	0.00	0.00	0.00	0.00	0.00	0.00	0.00

dients starting with a content of B higher than 60% are not reasonable, as there is a resolution valley at 68% B. Between 68 and 92% B there is an improvement in resolution up to 1.06, but this is lower than other possible values in this plot.

A relatively robust area is between 55 and 60% B. It was therefore decided to search for a multistep gradient with a higher resolution and faster analysis time in this concentration region.

Multisegmented gradients for faster gradient runs (trial and error)

The software has the advantage of being able to simulate gradients with up to ten steps in any combination. In developing a multisegmented gradient, the goal was to reach a nearly equal band spacing of all bands. This is possible if all the components are at the largest possible distance from each other. This situation is characterized by the highest relative resolution between all bands and by the lowest standard deviation of all resolution (R_s) values for all band pairs.

To begin the optimization procedure, the chromatogram was divided into four parts. A 2-min isocratic step at 50% B was taken to give a large R_s value between bands 2 and 3. As the distance between bands 3 and 4 was large (2.5 min) (Fig. 3b), this distance was shortened by having a sharp step up to 77% B in 0.1 min; the distance between bands 2 and 3 could therefore be reduced to 0.15 min. This step was followed by another isocratic step at 77% B for 2.9 min to resolve bands 4 and 5 ($R_s = 5.08$) and also the critical peak pair 7 and 8 ($R_s = 1.55$). Finally, the content of B was increased from 77 to 100% in 3 min to give a fast elution of the late bands. The total analysis time should be less than 10 min (Fig. 5a).

Using the experimental control, a fairly good correlation was found with the DryLab prediction (Fig. 5b) (Table VI). The deviations are slightly
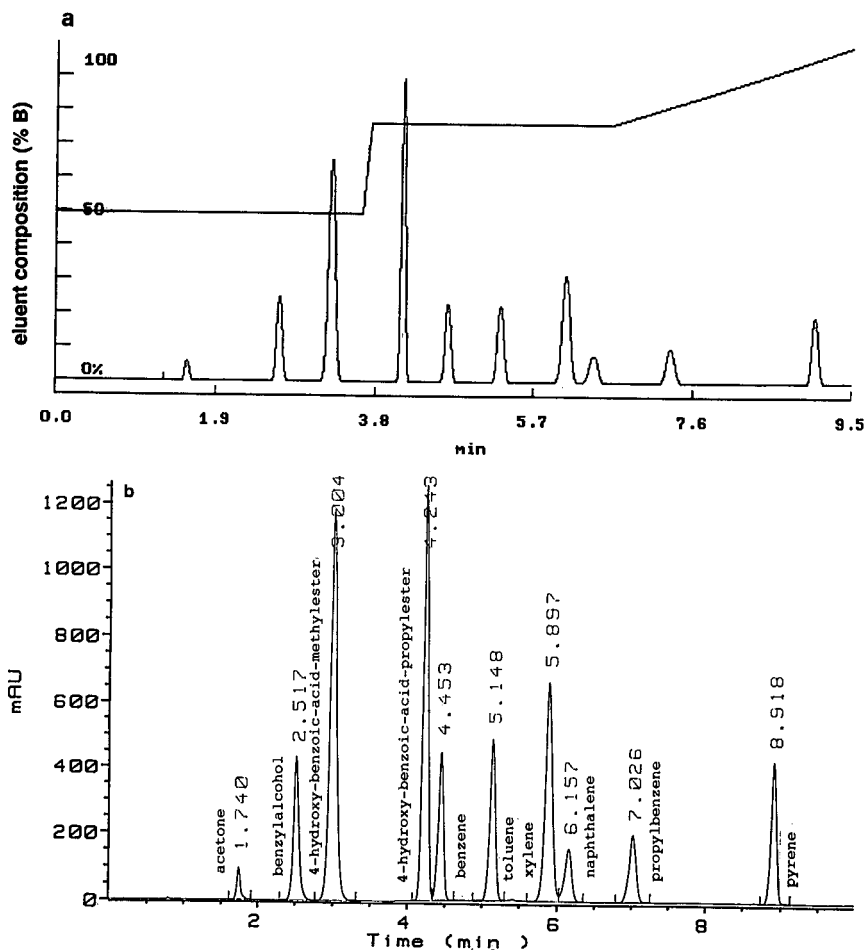
Fig. 5. (a) Predicted multisegmented gradient. Conditions for the steps are given in the text; the %B values were measured in the detector cell. (b) Experimental multisegmented gradient (conditions as in Fig. 1).

TABLE VI

COMPARISON OF RETENTION TIMES PREDICTED BY THE DRYLAB G/PLUS SOFTWARE AND THOSE FOUND EXPERIMENTALLY

Peak no.	Compound	Retention time (min)		Difference in retention time (min)
		Predicted	Experimental	
1	Acetone	1.56	1.74	0.18
2	Benzylalcohol	2.67	2.52	0.15
3	4-OH-BA-ME[a]	3.27	3.00	0.27
4	Benzene	4.65	4.45	−0.20
5	4-OH-BA-PE[b]	4.11	4.24	0.13
6	Toluene	5.30	5.15	−0.15
7	Xylene	6.09	5.90	−0.19
8	Naphthalene	6.43	6.16	−0.27
9	Propylbenzene	7.33	7.03	−0.30
10	Pyrene	9.05	8.92	−0.13

[a] 4-OH-BA-ME = 4-hydroxybenzoic acid methyl ester.
[b] 4-OH-BA-PE = 4-hydroxybenzoic acid propyl ester.

larger than in Table IV, which is probably a result of the large step at the beginning of the run (Fig. 5a) being too harsh for the phase system. The step is actually rounded, which explains the slight deviations.

The predicted inversion of the elution order for benzene and 4-hydroxybenzoic acid propyl ester was also seen in this chromatogram.

Another method of studying the elution order is using the S values, which are the slopes of $\ln k' = f(\%B)$ and which are calculated by the software together with the log k'_w values. Peak cross-overs can often be recovered on the basis of the slopes of the individual compounds.

The DryLab G/plus software can be an efficient tool in teaching gradient elution to those who are not familiar with the technique and who do not have the time to run a large number of trial-and-error experiment. A more robust and less time-consuming method could be developed by shortening the gradient. Pollution is also reduced by the reduction of organic eluent wastes.

REFERENCES

1 F. Erni, *J. Chromatogr.*, 509 (1990) 141.
2 L. R. Snyder, in Cs. G. Horvath (Editor), *High Performance Liquid Chromatography*, Vol. 1, Academic Press, New York, 1980, Chapter 4.
3 R. W. Stout, J. J. DeStefano and L. R. Snyder, *J. Chromatogr.*, 282 (1983) 263.
4 M. A. Quarry, R. L. Grob and L. R. Snyder, *J. Chromatogr.*, 285 (1984) 1.
5 L. R. Snyder and M. A. Quarry, *J. Liq. Chromatogr.*, 10 (1987) 1789.
6 L. R. Snyder, M. A. Quarry and J. L. Glajch, *Chromatographia*, 24 (1988) 33.
7 J. D. Stuart, D. D. Lisi and L. R. Snyder, *J. Chromatogr.*, 485 (1989) 657.
8 L. R. Snyder, in F. E. Regnier and K. M. Gooding (Editors), *HPLC of Biological Macromolecules*, Marcel Dekker, New York, 1990, p. 231.
9 B. F. D. Ghrist, B. S. Cooperman and L. R. Snyder, *J. Chromatogr.*, 459 (1988) 1.
10 I. Molnar, R. I. Boysen and V. A. Erdmann, *Chromatographia*, 28 (1989) 39.
11 J. W. Dolan, D. C. Lommen and L. R. Snyder, *J. Chromatogr.*, 485 (1989) 91.
12 J. L. Glajch and L. R. Snyder (Editors), *J. Chromatogr.*, 485 (1989).
13 I. Molnar, R. I. Boysen and P. Jekow, *J. Chromatogr.*, 485 (1989) 569.
14 I. Molnar, K. H. Gober and B. Christ, *J. Chromatogr.*, 550 (1991) 39.

Gradient elution with shorter equilibration times in reversed-phase ion-pair chromatography

Miklós Patthy

Institute for Drug Research, Berlini út 47–49, 1045 Budapest (Hungary)

ABSTRACT

To reduce the re-equilibration time needed between gradient runs in reversed-phase ion-pair chromatography (RP-IPC), various chromatographic conditions were studied. Five pairing ions of different size (and sorption kinetics), *viz.*, trifluoroacetate, heptafluoro-butyrate, octylsulphonate, dodecyl sulphate and tetrabutylammonium, each at two different concentrations, and three types of gradient (acetonitrile, salt and mixed gradients) were examined. Some common nucleotides, such as adenosine-5'-monophosphate, adeno-sine-5'-diphosphate and adenosine-5'-triphosphate, and some primary amines, such as dopamine, α-methyldopamine and serotonin, were used as analytes. The "efficiency" of the various gradient systems was tested in terms of the "speed" of re-equilibration and the average decrease in retention time achieved. Without solving the general problem of slow equilibration in ion-pair gradient elution, chromatographic conditions are recommended under which 1–3 column volumes of solvent A can be sufficient for re-equilibration between gradient runs, *i.e.*, for obtaining reproducible retention times in gradient RP-IPC.

INTRODUCTION

Isocratic reversed-phase ion-pair chromatography (RP-IPC) has become a popular method for the separation of ionic, ionizable and neutral compounds. Gradient RP-IPC, however, has not gained equal acceptance and has been associated with long run times owing to the need for restoring the initial ionic equilibria on the surface of the reversed-phase packing material. It is generally suggested that of reversed-phase, normal-phase (polar bonded phases), ion-exchange and RP-IPC systems, the last is least suited for gradient elution, requiring more than 15–20 column volumes of solvent A for column regeneration [1], which is not practical for most routine applications.

To understand our approach aimed at reducing re-equilibration volumes in gradient RP-IPC, brief comments on the basis of RP-IPC separations may be appropriate. As discussed recently by Liu and Cantwell [2], retention in RP-IPC is governed both by dynamic ion-exchange (in the diffuse part of the electrical double layer formed on the hydrophobic surface of the stationary phase owing to the selective adsorption of the pairing ion used) and adsorption on the electrically charged surface. In view of the retention of ionic solutes, the surface concentration of the pairing ion is a parameter of major importance as it largely determines both the "ion-exchange capacity" of the system and the electric potential on the surface. Reproducibility of retentions in RP-IPC is, therefore, closely related to the reproducibility of the surface concentration of the pairing ion (on which the reproducibility of the electrical double layer also depends).

In this paper, we are concerned with the "speed" of equilibration in gradient RP-IPC, which is synonymous with the "speed" of restoring the initial surface concentration of the pairing ion after a gradient run. To increase that "speed", the following means can be considered: (i) choosing pairing ions with good kinetic properties; (ii) choosing pairing ion concentrations at which the adsorption isotherm in the RP-IPC system concerned starts to flatten out or which fall on the plateau region of the isotherm; and (iii) keeping the change in pairing ion

surface concentrations to the necessary minimum during a gradient run.

As kinetic properties can vary considerably, depending on the size, and even shape, of the pairing ion used [3], we tested five pairing ions of different size, *viz.*, trifluoroacetate (TFA), heptafluorobutyrate (HFBA), octylsulphonate (SOS), dodecyl sulphate (SDS) and tetrabutylammonium (TBA), at two different eluent concentrations. At pairing ion concentrations that fall on the flattening portion or the plateau region of the adsorption isotherm there is relatively more pairing ion in the mobile phase (than in the stationary phase) to drive the system towards attaining equilibrium in a shorter equilibration time (by a smaller volume of solvent A).

Concerning consideration (iii), it should be mentioned that two main RP-IPC gradient principles can be used [4,5]: partial desorption of the pairing ion by a gradual increase in the percentage of the organic modifier (*e.g.*, acetonitrile) in the eluent; and increasing the counter ion concentration or ionic strength in the eluent by a gradual increase in the (buffer) salt concentration in the mobile phase. The first principle, which has gained a much wider use, is known to affect pairing ion surface concentrations considerably (organic modifiers can change the shape [6] and even modify the type [7] of the adsorption isotherm of a pairing ion). The second principle (salt gradients) reduces the retention of ionic solutes through ion-exchange effects in the diffuse part of the electrical double layer and, as a result, causes relatively smaller changes in pairing ion surface concentrations.

The aim of this work was to test the potential means by which the re-equilibration time between RP-IPC gradient runs can be substantially reduced. Three types of RP-IPC gradient (acetonitrile, salt and acetonitrile–salt mixed type) with each pairing ion were examined and compared in terms of "efficiency", *i.e.*, the "speed" of re-equilibration and the average decrease in retention time achieved. Salt gradients and mixed gradients (at a suitable eluent concentration of HFBA, SOS or TBA as pairing ion) proved to be "efficient", resulting in reproducible gradient retention times after passing only 1–3 column volumes of solvent A through the column between gradient runs.

EXPERIMENTAL

Apparatus and materials

The apparatus used for the RP-IPC experiments was an LKB (Bromma, Sweden) gradient system consisting of two Model 2150 pumps, a Model 2152 controller, a Model 2151 variable-wavelength monitor (at 254 and 275 nm for nucleotides and amines, respectively), a Model 2210 two-channel recorder and a Rheodyne (Cotati, CA, USA) Model 7125 loop injector. The same type of packing material (Nucleosil 100-5 C_{18}, 5 μm, Macherey–Nagel, Düren, Germany) was used throughout the experiments. The BET surface area and the carbon content of the packing material were 310 m^2/g and 14% (w/w), respectively, as specified by the manufacturer. The chromatographic support was packed in stainless-steel columns by Bioseparation Technologies (Budapest, Hungary). The column dimensions were 150 × 4 mm I.D., with a 20 × 4 mm I.D. precolumn. The void volume of the column (V_0) was 1.63 ml (determined by the method of Deelder *et al.* [8]).

Sequanal-grade trifluoroacetic acid and heptafluorobutyric acid were obtained from Pierce (Rockford, IL, USA), sodium octylsulphonate and sodium dodecyl sulphate from Supelco (Bellefonte, PA, USA) and Aldrich (Steinheim, Germany), respectively, tetrabutylammonium bromide and dopamine hydrochloride (DA) from Sigma (St. Louis, MO, USA), adenosine-5'-monophosphoric acid (AMP), adenosine-5'-diphosphate (ADP) and adenosine-5'-triphosphate (ATP) from Calbiochem (La Jolla, CA, USA). Serotonincreatinine sulphate (5-HT) from Reanal (Budapest, Hungary) and α-methyldopamine hydrobromide (MDA) from Merck, Sharp and Dohme (West Point, PA, USA).

For the gas–liquid chromatographic (GLC) determination of TFA and HFBA, a Hewlett-Packard Model 5830 A gas chromatograph equipped with a flame ionization detector (Hewlett-Packard, Palo Alto, CA, USA) was used. The glass chromatographic column (6 ft. × 2 mm I.D.) was packed with Carbopack B (Supelco) coated with 0.3% (w/w) phosphoric acid and 3% (w/w) Carbowax 20M. The carrier gas was nitrogen at a flow-rate of 60 ml/min. The temperatures of the injection port, column and detector were 240, 200 and 240°C, respectively.

For the spectrophotometric determination of

SOS, SDS and TBA, methylene blue and methyl orange (Aldrich) were used. An LKB Ultrospec-II 4050 spectrophotometer was used to determine absorbances.

Acetonitrile, ethanol and chloroform (LiChrosolv) were obtained from Merck (Darmstadt, Germany). All other chemicals were of analytical-reagent grade.

Procedures

The compositions of the gradient systems studied are given in Table I. Solvent A for a given pairing ion (and concentration) was always the same, whereas solvent B was varied, as shown in Table I. [The letters A, S and M represent acetonitrile, salt and mixed gradients, respectively. The notations 1A, 2S, 3M, etc., refer to the respective curves in Figs. 2–11

TABLE I

COMPOSITION OF THE GRADIENT SYSTEMS STUDIED

Notation	Solvent A (with pairing ions)			Solvent B (difference from solvent A): type of gradient		
	pH	Components	Concentration	ACN[a]	Salt	Mixed
1A	2.50	TFA (Na$^+$)	8 mM	—	—	—
1S		Na$^+$ (phosphate)	15 mM	—	100	60
1M		ACN	6% (v/v)	15	—	10
2A	2.50	TFA (Na$^+$)	200 mM	—	—	—
2S		Na$^+$ (phosphate)	15 mM	—	100	60
2M		ACN	6% (v/v)	20	—	14
3A	2.50	HFBA (Na$^+$)	5 mM	—	—	—
3S		Na$^+$ (phosphate)	15 mM	—	100	60
3M		ACN	6% (v/v)	20	—	14
4A	2.50	HFBA (Na$^+$)	50 mM	—	—	—
4S		Na$^+$ (phosphate)	15 mM	—	100	60
4M		ACN	10% (v/v)	30	—	20
5A	2.50	SOS (Na$^+$)	1 mM	—	—	—
5S		Na$^+$ (phosphate)	15 mM	—	100	60
5M		ACN	10% (v/v)	20	—	15
6A	2.50	SOS (Na$^+$)	10 mM	—	—	—
6S		Na$^+$ (phosphate)	15 mM	—	100	60
6M		ACN	15% (v/v)	25	—	20
7A	2.50	SDS (Na$^+$)	0.5 mM	—	—	—
7S		Na$^+$ (phosphate)	15 mM	—	100	—
		ACN	20% (v/v)	35	—	—
8A	2.50	SDS (Na$^+$)	3 mM	—	—	—
8S		Na$^+$ (phosphate)	15 mM	—	100	—
		ACN	25% (v/v)	40	—	—
9A	5.80	TBA (Br$^-$)	5 mM	—	—	—
9S		H$_2$PO$_4^-$ (Na)	15 mM	—	100	60
9M		ACN	12% (v/v)	30	—	18
10A	5.80	TBA (Br$^-$)	60 mM	—	—	—
10S		H$_2$PO$_4^-$ (Na)	15 mM	—	150	100
10M		ACN	12% (v/v)	40	—	18

[a] ACN = Acetonitrile.
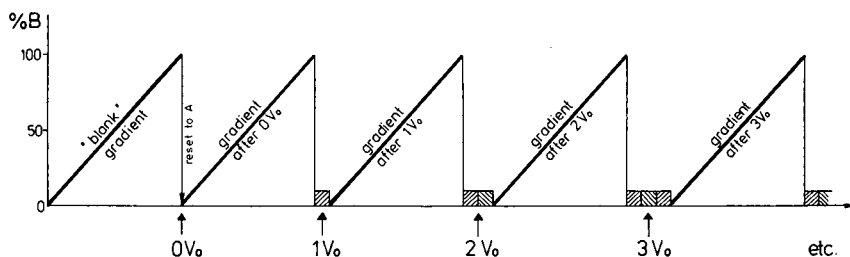
Fig. 1. Scheme for the preparation of graphs of k'_G vs. column volumes between runs. Hatched boxes represent one column volume (V_0) of solvent A between gradient runs.

and for Table III; they are of less relevance for Table I. By mixed gradients are meant gradients in which eluent strength is raised by acetonitrile and salt together, but the concentration of each (in solvent B of an M gradient) is lower than in solvent B of the respective A (acetonitrile only) or S (salt only) gradients.] All gradient experiments were carried out using the same linear gradient (from 100% A to 100% B in 15 min). The flow-rate and the separation temperature were 1 ml/min and 23 ± 1°C, respectively.

The graphs of k'_G vs. column volumes between runs were prepared as follows (for the definition of k'_G, an arbitrary term, see the text below). Following a 60-min equilibration with solvent A, the retention times of the test compounds were determined and the k'_0 values (the k' values in solvent A, determined in the usual way) for each compound were calculated. Then a "blank" gradient was run. After reaching 100% B and immediate resetting to solvent A, samples were injected (and a series of gradients started) at 0.00, 1.63, 3.26, 4.89, 6.52, 8.15, 16.30, 24.45 and 40.75 min after the resetting to solvent A. The time points indicated correspond to the time required to pass 0, 1, 2, 3, 4, 5, 10, 15 and 25 column volumes (V_0), respectively, of solvent A through the column before starting a certain gradient (the working scheme for the series of gradients is shown in Fig. 1). The retention times in each gradient run were measured and the k'_G values [the k' values obtained (by the usual equation) in a gradient performed after a specified number of V_0 of solvent A had been passed through the column] for each analyte calculated. The k'_G values thus obtained were plotted as a function of the V_0 used for re-equilibration before the respective gradient run. The steady-state k'_G values ($k'_{G, \text{"equilibrium"}}$) were read from the horizontal portions of the graphs.

The average retention decrease factors (ARDF values) for each gradient system were obtained as the average of the $k'_0/k'_{G, \text{"equilibrium"}}$ ratios of the compounds tested in the respective gradient system (e.g., as shown in Table III, the ARDF value for gradient system 4A was 1.64, which was obtained as the average of the $k'_0/k'_{G, \text{"equilibrium"}}$ ratio for DA, MDA and 5-HT used as analytes in that system).

The gradient range ($\Delta\varphi$) for acetonitrile gradients is meant as defined in ref. 9 (i.e., the change in the volume fraction of the organic eluent component between the start and end of a gradient run). It varied by a factor of ca. 3 (0.09–0.28) in order to elute the test compounds within the same gradient time (15 min). For salt gradients the gradient range means the change in total counter ion concentrations in the eluent during a gradient run. It was the same (85 mM) in all but one cases.

The surface concentrations of the pairing ions adsorbed by the stationary phase from the respective solvent A after a 60-min equilibration were determined as follows. For the determination of TFA and HFBA eluted after equilibration, the method of Di Corcia and Samperi [10] described for short-chain free acids was adopted, using HFBA as internal standard for TFA measurements, and vica versa. After passing one column volume of distilled water through the column (at a flow-rate of 0.25 ml/min) to remove much of the buffer, desorption of the pairing ion was carried out using acetonitrile as eluent (at a flow-rate of 0.5 ml/min). One 10-ml fraction and ten 2-ml fractions were collected. Aliquots of the collected fractions (containing the internal standard) were acidified with concentrated hydrochloric acid in a volume ratio of 2:1. Volumes of 2 μl were injected into the GLC system. To calculate surface concentrations, the amounts of

TFA (or HFBA) in the various fractions were added.

For the determination of SOS and SDS eluted after equilibration, the methylene blue method of Sharma et al. [11] was used (the volumes in the procedure were reduced by 4:1). After rinsing the column with one column volume of distilled water (0.25 ml/min), desorption of the pairing ion was carried out using 100 ml of absolute ethanol as eluent (0.5 ml/min). Three different aliquots of the eluate (in the volume range 0.02–0.10 ml), with parallels, were pipetted into Pyrex glass centrifuge tubes. After evaporating the solvent under a stream of nitrogen, the pairing ion was redissolved in 1 ml of distilled water and determined as described in ref. 11.

For the determination of TBA eluted (as described above for SOS and SDS) after equilibration, the methyl orange method of Simón et al. [12] was used with minor modifications (the volumes in the procedure were reduced by 2:1 and the Carmody buffer was replaced with 20 mM acetate buffer, pH 4). Three different aliquots of the eluate (in the volume range 0.02–0.20 ml), with paralles, were pipetted into Pyrex glass centrifuge tubes and used in the procedure [12] without evaporating the solvent (the volme of the ethanol to be added in the procedure was accordingly reduced by the volume of the aliquot added).

Precision values [relative standard deviation (R.S.D., %) in Table II] were calculated as follows. The surface concentration of each pairing ion was determined from two independent eluates obtained under identical conditions. Three different aliquots (in parallels of five) resulting in concentrations that fall on the linear portion of the respective calibration graph were selected, and the experimental R.S.D. for each aliquot was calculated. The surface concentration values are the averages of the results obtained for the two eluates, and R.S.D. values are the averages of the R.S.D. data obtained for the 2 × 3 aliquots.

HFBA eluted after equilibration (in 40 ml of absolute ethanol) was also determined by the methylene blue method [11], and both the surface concentration and R.S.D. values were in good agreement with the GLC data presented in Table II.

The data points indicated in Figs. 2–11 are each average k'_G values obtained for two independent series of gradients performed under identical conditions.

RESULTS AND DISCUSSION

Although the recommended eluent volume for column equilibration in RP-IPC is 20–25 V_0, data in the literature on equilibration V_0 vary greatly even for the same pairing ion. For example, Ingebretsen et al. [13] found that over 40 V_0 were necessary for the equilibration of an isocratic RP-IPC system with a concentration of 0.3 mM TBA (as pairing ion) and 1% (v/v) of methanol in the eluent . On the other hand, Werner et al. [14] reported 2.5–3 V_0 for re-equilibration in a gradient RP-IPC system using a 2 mM concentration of the same pairing ion (TBA) and an acetonitrile gradient ($\Delta\varphi = 0.2$). The same group later reported ca. 5.5 V_0 for re-equilibration in an almost identical RP-IPC gradient system [15]. A comparison of the equilibration V_0 values in refs. 13 and 14 underlines the importance of consideration (ii) mentioned earlier.

In order to find guidelines for a judicious selection of "efficient" gradient systems, we examined five pairing ions (of varying alkyl chain length and shape) in two (relatively low and relatively high) concentrations, and gradients with acetonitrile, (buffer) salt and mixtures thereof, as shown in Table I. In this work, gradient system "efficiency" refers to the "speed" of re-equilibration between gradient runs and the ability of the respective gradient to decrease retentions. For the assessment of the latter we used the average retention decrease factor (ARDF), calculated as described under Procedures.

A gradient system was regarded as efficient if the number of V_0 necessary for reproducible retentions did not exceed 3, and (at the same time) the ARDF value was equal to or larger than 1.25 for monovalent ionic analytes (an ARDF of 1.25 usually implies that the retention of the compound eluting last was decreased by a factor of ca. 1.5, which is mostly the minimum goal when using a gradient system).

It should be emphasized that by "reproducible retentions" we do not necessarily mean that the RP-IPC system is in the state of a complete equilibrium. A quasi-equilibrium, which we denote by "equilibrium" or E, can also result in reproducible

TABLE II

SURFACE CONCENTRATIONS OF PAIRING IONS

Adsorbed by the stationary phase [Nucleosil 5 C_{18} (100 Å), 5 μm, 310 m^2/g, 112 m^2/ml] from the solvents A shown in Table I.

Solvent A	Surface concentration		Solvent A	Surface concentration	
	$mol/m^2 \times 10^8$	R.S.D. (%)		$mol/m^2 \times 10^8$	R.S.D. (%)
1: TFA, 8 mM	1.1	20.5	6: SOS, 10 mM	37.5	5.7
2: TFA, 200 mM	6.2	14.6	7: SDS, 0.5 mM	$\sim$19.0	–
3: HFBA, 5 mM	8.4	10.5	8: SDS, 3 mM	54.0	5.2
4: HFBA, 50 mM	41.1	8.1	9: TBA, 5 mM	35.1	4.1
5: SOS, 1 mM	$\sim$12.0	–	10: TBA, 60 mM	68.8	3.6

gradient retention times under circumstances to be specified later.

In this study, we attempted to relate both the mobile phase and stationary phase pairing ion concentrations to the speed of equilibration. The surface concentrations of the pairing ions (obtained after a 60-min equilibration with the respective solvent A) are shown in Table II. The re-equilibration speeds with the gradient systems studied can be obtained from the graphs of k'_G vs. column volumes

between runs presented in Figs. 2–11 (see the V_0 values indicated by E). Table III presents the efficiency of the gradient systems shown in Table I in terms of two (combined) criteria: the ARDF value and the number of V_0 of solvent A needed to reach "equilibrium", E, i.e., reproducible retentions.

Inspection of Figs. 2–11 and Table III shows that the speed of re-equilibration increases in the order acetonitrile gradients < mixed gradients < salt gradients, demonstrating that RP-IPC ionic equilib-
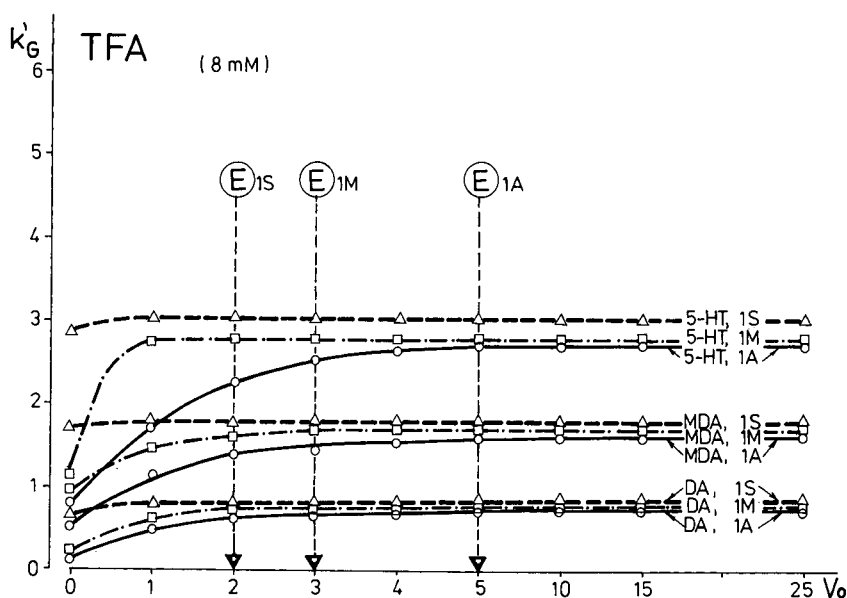
Fig. 2. Plots of k'_G vs. column volumes between runs (V_0 of solvent A) with 8 mM TFA as pairing ion in the eluents, and acetonitrile (A, ○), salt (S, △) and mixed (M, □) gradients. E indicates the number of V_0 which provide satisfactory equilibration between runs for obtaining reproducible retention times in the respective gradient system. Other conditions as in Table I and Experimental.
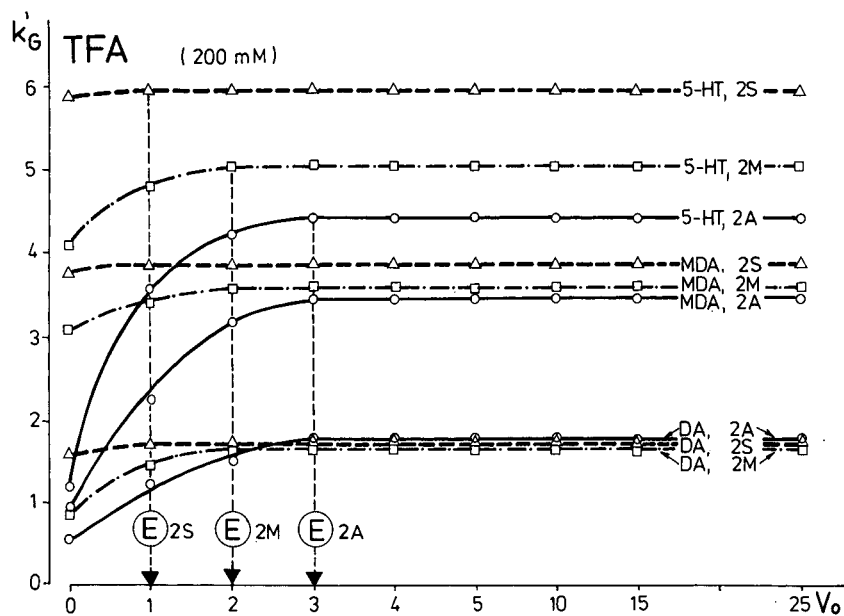
Fig. 3. Plots of k'_G vs. column volumes between runs with 200 mM TFA as pairing ion in the eluents, and A, S and M gradients. For A, S, M and E, see Fig. 2. Other conditions as in Table I and Experimental.
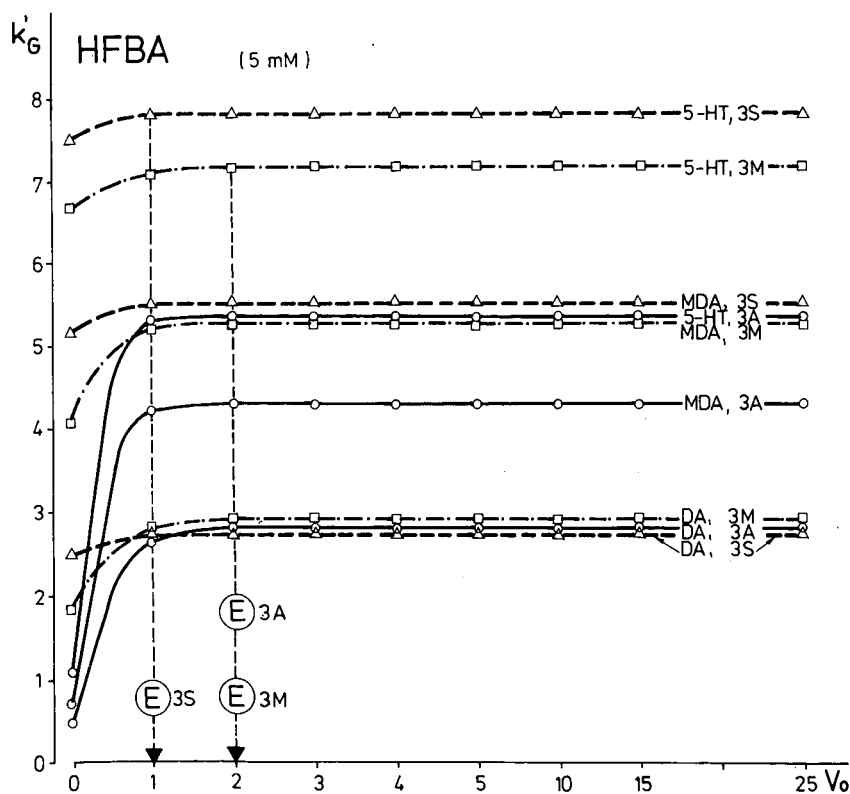
Fig. 4. Plots of k'_G vs. column volumes between runs with 5 mM HFBA as pairing ion in the eluents, and A, S and M gradients. For A, S, M and E, see Fig. 2. Other conditions as in Table I and Experimental.
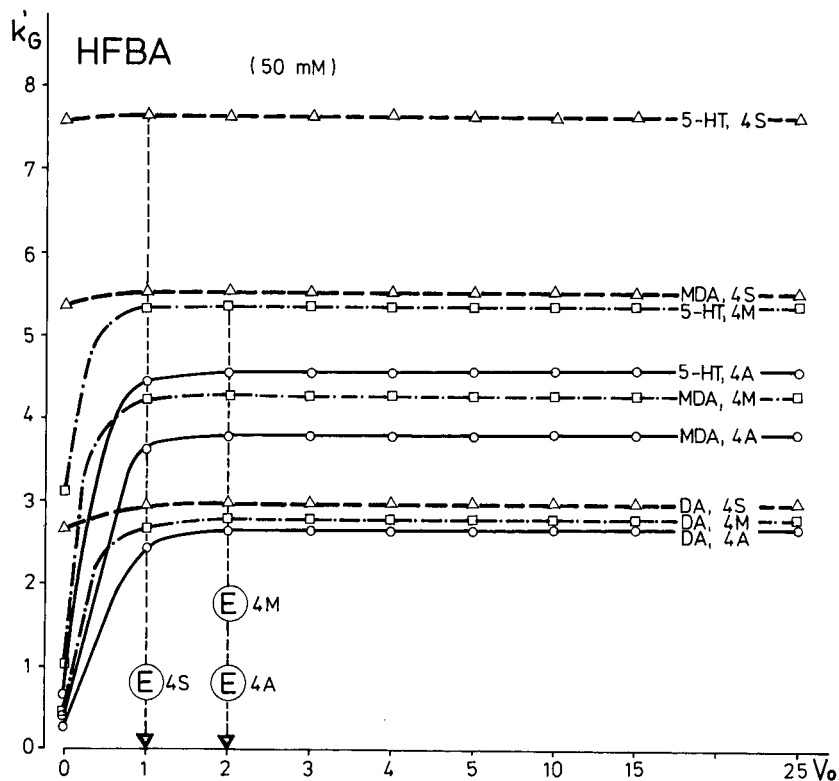
Fig. 5. Plots of k'_G vs. column volumes between runs with 50 mM HFBA as pairing ion in the eluents, and A, S and M gradients. For A, S, M and E, see Fig. 2. Other conditions as in Table I and Experimental.
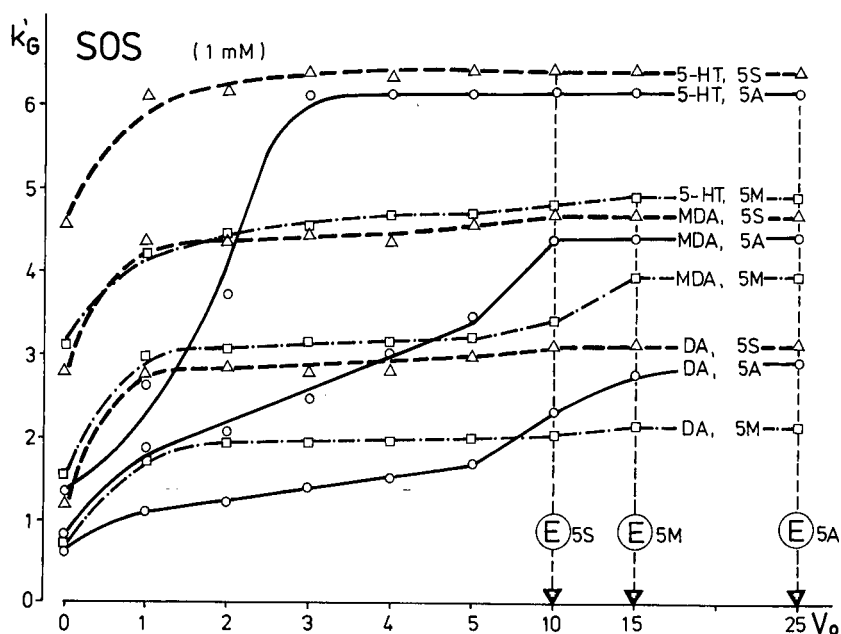
Fig. 6. Plots of k'_G vs. column volumes between runs with 1 mM SOS as pairing ion in the eluents, and A, S and M gradients. For A, S, M and E, see Fig. 2. Other conditions as in Table I and Experimental.
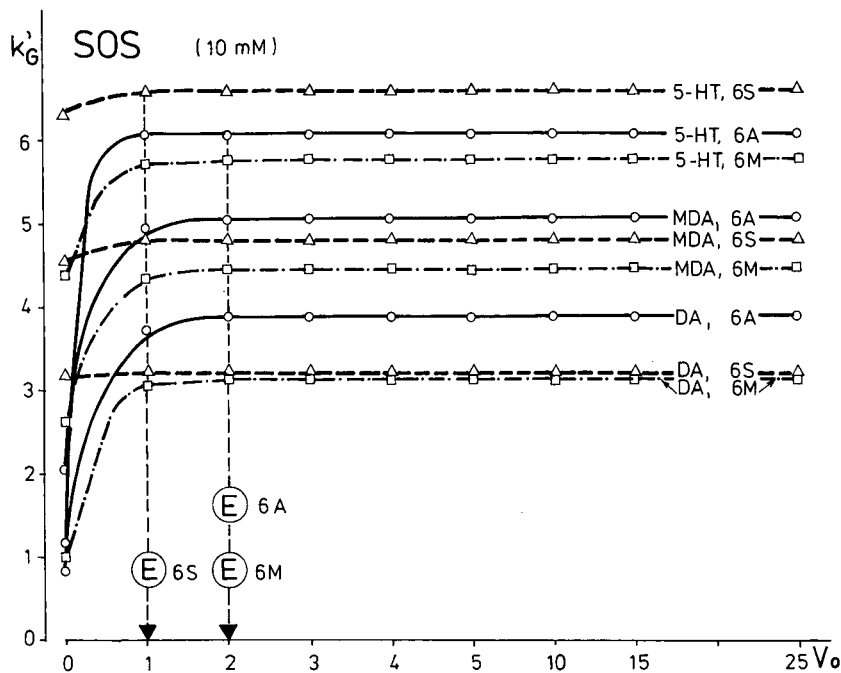
Fig. 7. Plots of k'_G vs. column volumes between runs with 10 mM SOS as pairing ion in the eluents, and A, S and M gradients. For A, S, M and E, see Fig. 2. Other conditions as in Table I and Experimental.
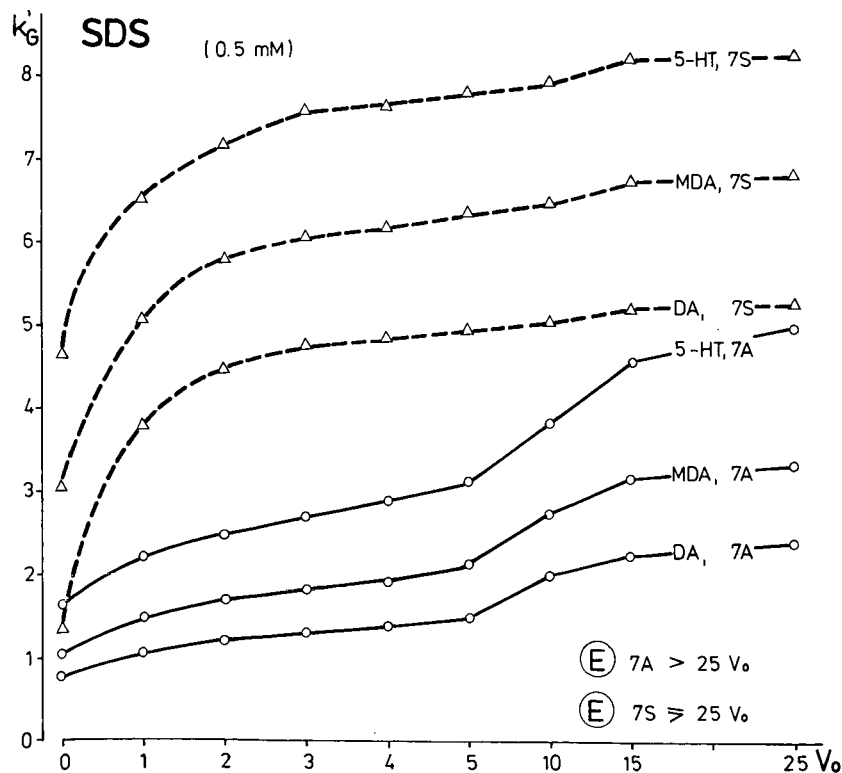
Fig. 8. Plots of k'_G vs. column volumes between runs with 0.5 mM SDS as pairing ion in the eluents, and A and S gradients. For A, S and E, see Fig. 2. Other conditions as in Table I and Experimental.
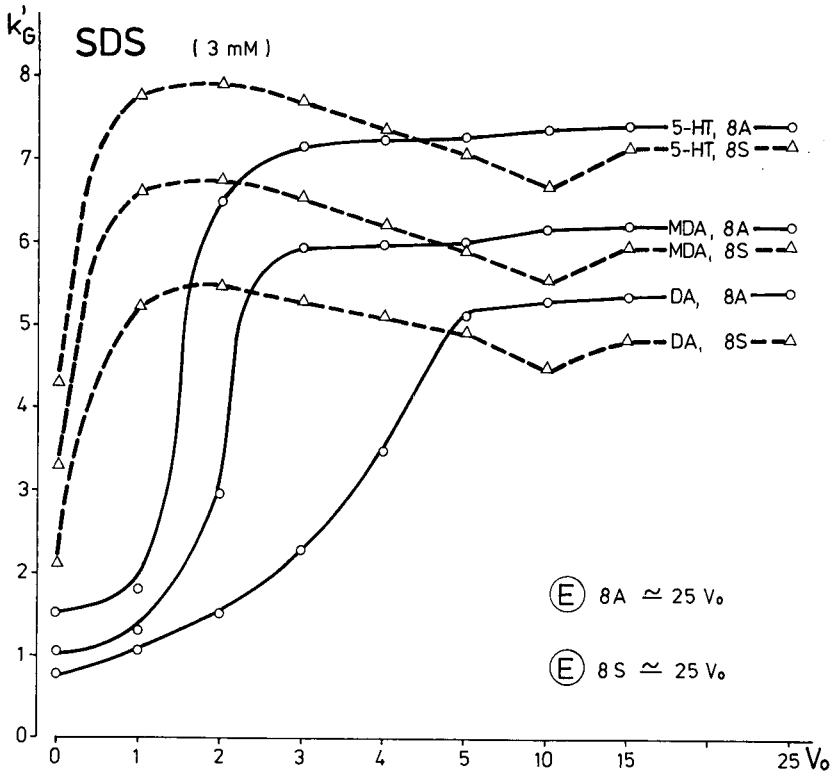
Fig. 9. Plots of k'_G vs. column volumes between runs with 3 mM SDS as pairing ion in the eluents, and A and S gradients. For A, S and E, see Fig. 2. Other conditions as in Table I and Experimental.
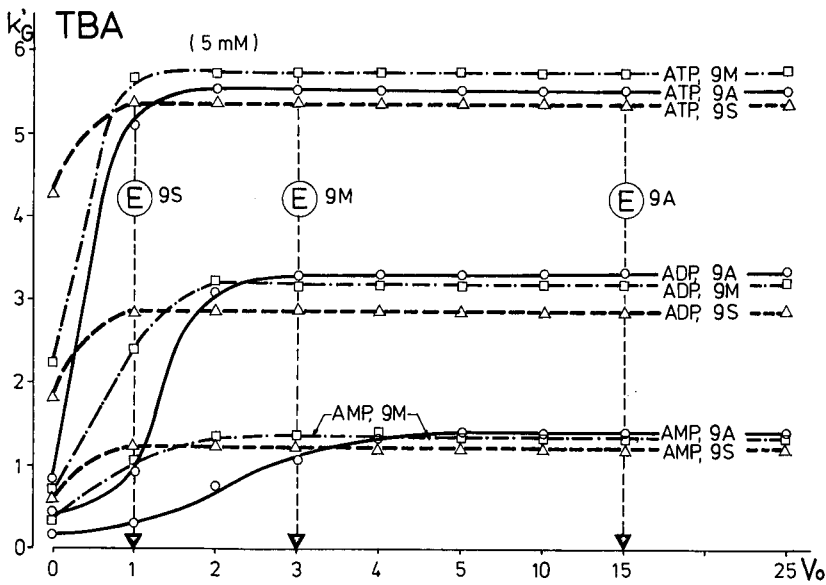
Fig. 10. Plots of k'_G vs. column volumes between runs with 5 mM TBA as pairing ion in the eluents, and A, S and M gradients. For A, S, M and E, see Fig. 2. Other conditions as in Table I and Experimental.
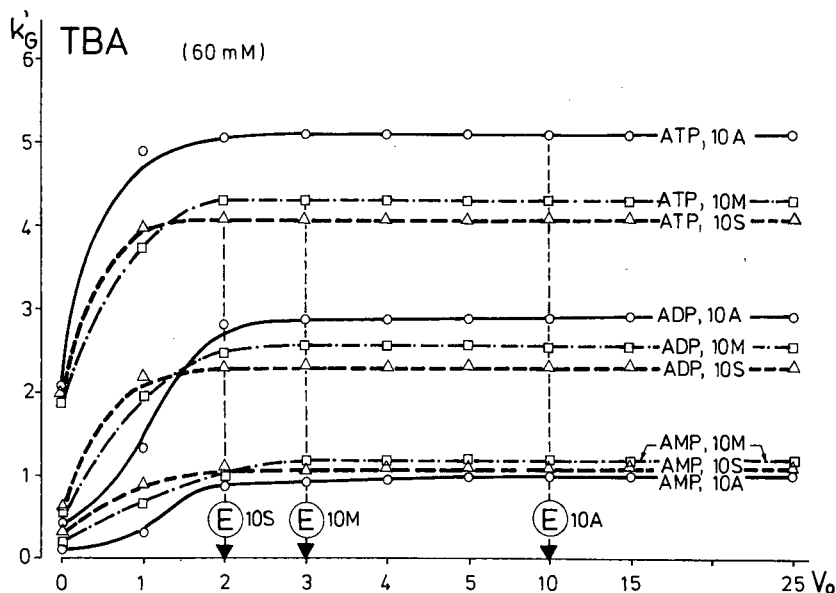
Fig. 11. Plots of k'_G vs. column volumes between runs with 60 mM TBA as pairing ion in the eluents, and A, S and M gradients. For A, S, M and E, see Fig. 2. Other conditions as in Table I and Experimental.

ria are less disturbed by changes in eluent salt concentrations than by changes in the volume ratio of the organic modifier in the eluent.

Based on the two criteria in Table III, the following salt gradient systems were found to be efficient: systems 3S, 6S, 9S (at the same $\Delta\varphi$, i.e.,

TABLE III

"EFFICIENCY" OF THE GRADIENT SYSTEMS

In terms of retention decrease and "speed" of equilibration.

Pairing ion	Gradient notation[c]	ARDF[d]	E[e]	Gradient notation[c]	ARDF[d]	E[e]	Gradient notation[c]	ARDF[d]	E[e]
TFA[a]	1A	1.14	5	1S	1.06	2	1M	1.12	3
	2A	1.21	3	2S	1.03	1	2M	1.15	2
HFBA[a]	3A	1.61	2	3S	1.29	1	3M	1.35	2
	4A	1.64	2	4S	1.13	1	4M	1.45	2
SOS[a]	5A	1.30	25	5S	1.22	10	5M	1.61	15
	6A	1.35	2	6S	1.35	1	6M	1.42	2
SDS[a]	7A	<1.91	>25	7S	<0.98	≥25	7M	—	—
	8A	≃1.51	≃25	8S	≃1.57	≃25	8M	—	—
TBA[b]	9A	1.42	15	9S	1.53	1	9M	1.46	3
	10A	1.58	10	10S	1.42	2	10M	1.65	3

[a] With monovalent sample cations.
[b] With mono-, di- and trivalent sample anions.
[c] A = Acetonitrile gradient; S = salt gradient; M = mixed gradient.
[d] ARDF = Average retention decrease factor.
[e] E = Number of column volumes (V_0) needed to reach "equilibrium".

85 mM) and $10S$ (at $\Delta\varphi = 135$ mM). It is shown in Table II that with systems 3, 6 and 9 the surface concentration of the pairing ion was higher than $8 \cdot 10^{-8}$ mol/m^2, and also that the total counter ion concentration in the starting buffers (the solvent As of these systems, see Table I) did not exceed 25 mM. Hence a satisfactory surface coverage by the pairing ion and, at the same time, a low counter ion concentration in solvent A appear to be two preconditions for an efficient salt gradient system.

Other conclusions drawn from the data in Table III (in combination with Tables I and II and Figs. 2–11) are as follows. The ARDF values in all six gradient systems containing TFA as pairing ion were low. With the salt gradients this is explained by the low surface coverage (system 1S) and/or by the high total counter ion concentration in solvent A (*ca.* 215 mM, system 2S). The ARDF values for the acetonitrile gradients were lower than those of the SOS acetonitrile gradients (actually the lowest among the acetonitrile gradient systems studied), although $\Delta\varphi$ for system 1A was almost the same as for system 5A or 6A (for system 2A it was actually higher). This can be explained by the suggestion put forward by Bidlingmeyer *et al.* [16], *i.e.*, the adsorption of a three-carbon (or shorter) pairing ion (*e.g.*, TFA) from an aqueous buffer on to a hydrophobic surface is less affected by a change in the volume fraction of the organic modifier (methanol or acetonitrile) in the eluent than the adsorption of a pairing ion with a longer alkyl chain. The gradient range in systems 1A and 2A was, therefore, too small for the TFA systems, resulting in the low ARDF values.

For another explanation we must begin by saying that, owing to the very low surface coverage by the pairing ion, TFA systems, in general, are much closer in character to simple reversed-phase high-performance liquid chromatographic systems than to "real" RP-IPC systems in which double-layer sorption effects govern retention [2]. In RP-IPC systems with more hydrophobic pairing ions (and higher surface coverage), organic modifiers are known to decrease the retention of oppositely charged ionic solutes more efficiently than in reversed-phase systems [17] through at least two simultaneous effects: via the decreased hydrophobic adsorption of the solutes and the decreased surface concentration of the pairing ion [18,19]. With TFA systems organic modifiers decrease retentions (almost entirely) by only decreasing the hydrophobic adsorption of the solutes.

The ARDF values with five of the HFBA systems were reasonably good, and the "speed" of equilibration was high in all six gradient systems (see the E values in Table III), demonstrating the excellent kinetic properties of this pairing ion. (With HFBA the surface coverage determined by both the GLC and the methylene blue method was relatively high, but as perfluorinated acids are known to be considerably more hydrophobic than hydrocarbon acids of the same chain length [11], that is easily explained.) The ARDF value of system 4S was low because of the higher than desirable total counter ion concentration (65 mM) in solvent A.

From our point of view, the main gradient "efficiency" problem with RP-IPC systems consisting of eluents (solvent As) with a low concentration of a strongly adsorbed pairing ion (such as SOS, SDS or TBA) and an organic modifier, also in a low concentration, is system stability (see Figs. 6 and 8). TBA and SOS systems can be stable enough when the eluent pairing ion concentration reaches or exceeds 2 mM (see refs. 14 and 15 and Figs. 7 and 10). SDS systems, however, still lack reproducibility of retention at this pairing ion concentration (see Fig. 9).

Although both the surface coverage and the total counter ion concentration in solvent A can be in the right range for salt gradients, the number of re-equilibration V_0s of such RP-IPC systems (with SOS, SDS or TBA concentrations below 2–3 mM in organic modifier-lean solvent As) is unacceptably high (see the E values for systems 5A, 5S, 5M and 7A, 7S, 8A and 8S in Table III). After a 60-min equilibration with solvent A and the determination of the k'_0 values, with such systems the surface coverage continues to increase during the series of salt gradients, resulting in relatively higher k'_G values. This explains the low ARDF value in system 5S and the even lower ARDF value in system 7S in Table III.

Such system stability problems are invariably related to considerations (i) and (ii) in the Introduction, suggesting that for "fast" gradients C_4–C_8-alkyl pairing ions at eluent concentrations larger than 2–3 mM should be preferred, and that pairing ions with slow sorption kinetics, especially those with H-type adsorption isotherms [20] in solvent As

of low organic modifier content, should be avoided.

The pairing ion concentrations in the TBA systems studied were both on the "safe side" of the adsorption isotherm. The 5 mM system was tested with mono-, di- and trivalent sample anions and the 60 mM system was tested with the same anions and higher gradient ranges ($\Delta\varphi$ = 0.28 and 135 mM, respectively).

With system 9, all three ARDF values were acceptable, although lower than expected from ionic solutes of higher charge. The speed of equilibration was excellent with the salt gradient and fairly good with the mixed gradient (systems 9S and 9M, respectively, in Table III). With system 10S, the ARDF value was lower (in spite of the larger $\Delta\varphi$) because the total counter ion concentration in solvent A (75 mM) was higher than desirable. The overall "efficiency" of system 10M was, however, better than that expected based on the results for systems 10A and 10S.

In spite of the "safe" pairing ion concentrations, the speed of equilibration with the acetonitrile gradients of the TBA systems was relatively poor (poorer than those reported in refs. 14 and 15 for similar systems and solutes; see Figs. 10, 11 and the E values for systems 9A and 10A in Table III), indicating either that the kinetic properties of TBA are less than ideal for such gradients or (which is logical and expected) that the retention of ionic solutes of higher charge is more sensitive to changes in pairing ion surface concentrations than the retention of monovalent ions.

To summarize, it appears from the results obtained in this study that the throughput of RP-IPC gradient elution systems can be improved considerably by selecting chromatographic conditions under which the volume of solvent A used for re-equilibration between gradient runs can be reduced to 1–3 column volumes. Chromatographic conditions for such "efficient" RP-IPC gradient systems include: (1) using C_4–C_8-alkyl pairing ions at eluent concentrations of 3–10 mM (depending on the nature of the pairing ion and the organic modifier content of solvent A; solvent A itself should be a stable isocratic system); and (2) keeping the change in pairing ion surface concentrations to the necessary minimum during a gradient run, by using salt gradients (for the separation of ionic compounds) or mixed gradients (for the separation of ionic and neutral compounds), instead of "pure" acetonitrile gradients.

For "efficient" salt gradients and mixed gradients two (additional) preconditions should be met: (a) the adsorbent surface coverage by the pairing ion from solvent A should be larger than (6–8) · 10^{-8} mol/m^2 [with C_4–C_8-alkyl pairing ions this is easily achieved by the eluent concentrations specified above if the acetonitrile or methanol content of solvent A does not exceed 5–15% (v/v)]; and (b) the total counter ion concentration in solvent A should be kept below 20–25 mM, just enough for a satisfactory buffering capacity.

For "efficient" acetonitrile gradients there is special emphasis on the kinetic properties of the pairing ion used. For cationic and neutral analytes HFBA appears to be a very good pairing ion candidate. Theoretically, TFA (used with a relatively larger gradient range) should also exhibit good kinetic properties in such gradients, but we have difficulty in explaining the relatively poor E value with system 1A in Table III (see also Fig. 2).

For satisfactory reproducibility of retention with any of the RP-IPC gradient systems studied, it was essential to reset the system to solvent A always at the same time point at the end of a gradient.

When considering these guidelines for the selection of efficient RP-IPC gradient systems, it should be kept in mind that "efficiency" is meant here only with respect to the "speed" of re-equilibration and for the ability of the respective gradient to reduce retentions. In terms of system selectivity, for example, there may be substantial differences in the chromatographic patterns obtained (for the same group of analytes) by a salt gradient, a mixed gradient or an acetonitrile gradient separation. These gradients may not result in equivalent separations and may not be equally efficient in terms of selectivity.

The steps recommended here for increasing the throughput of RP-IPC gradient separations do not solve the general problem of slow equilibration in ion-pair gradient elution. By adopting the conditions recommended for salt (and mixed) gradients, for instance, one actually strengthens the chances for dynamic ion-exchange in the diffuse part of the electrical double layer (as compared with the chances of surface adsorption) to determine retentions, as can be seen in Fig. 3 in ref. 2. Under the conditions we specified for RP-IPC salt gradients, retention is dominantly determined by ion-exchange processes and concomitant selectivities.

From the foregoing, it is also clear that, because of the very low surface coverage attainable by TFA as pairing ion and, as a result, the very weak presence of ion-exchange features in such RP-IPC systems, this study has little to offer for increasing, *e.g.*, the throughput of peptide separation systems with TFA as pairing ion.

ACKNOWLEDGEMENTS

REFERENCES

1 L. R. Snyder, J. L. Glajch and J. J. Kirkland, *Practical HPLC Method Development*, Wiley-Interscience, New York, 1988, Ch. 6, pp. 156 and 173.
2 H.-J. Liu and F. F. Cantwell, *Anal. Chem.*, 63 (1991) 2032–2037.
3 J. H. Knox and R. A. Hartwick, *J. Chromatogr.*, 204 (1981) 3–21.
4 A. Sokolowski, *J. Chromatogr.*, 384 (1987) 1–12.
5 M. Patthy, T. Balla and P. Arányi, *J. Chromatogr.*, 523 (1990) 201–216.
6 Á. Bartha and Gy. Vigh, *J. Chromatogr.*, 260 (1983) 337–345.
7 C. T. Hung and R. B. Taylor, *J. Chromatogr.*, 209 (1981) 175–190.
8 R. S. Deelder, H. A. J. Linssen, A. P. Konijnendijk and J. L. M. van de Venne, *J. Chromatogr.*, 185 (1979) 241–257.
9 M. A. Stadalius, H. S. Gold and L. R. Snyder, *J. Chromatogr.*, 296 (1984) 31–59.
10 A. Di Corcia and R. Samperi, *Anal. Chem.*, 46 (1974) 140–143.
11 R. Sharma, R. Pyter and P. Mukerjee, *Anal. Lett.*, 22 (1989) 999–1007.
12 M. M. B. Simón, A. D. E. Cózar and L. M. P. Diez, *Analyst (London)*, 115 (1990) 337–339.
13 O. C. Ingebretsen, A. M. Bakken, L. Segadal and M. Farstad, *J. Chromatogr.*, 242 (1982) 119–126.
14 A. Werner, T. Grune, W. Siems, W. Schneider, H. Shimasaki, H. Esterbauer and G. Gerber, *Chromatographia*, 28 (1989) 65–68.
15 T. Grune, W. Siems, A. Werner, G. Gerber, M. Kostič and H. Esterbauer, *J. Chromatogr.*, 520 (1990) 411–417.
16 B. A. Bidlingmeyer, S. N. Deming, W. P. Price, Jr., B. Sachok and M. Petrusek, *J. Chromatogr.*, 186 (1979) 419–434.
17 H. Zou, Y. Zhang and P. Lu, *J. Chromatogr.*, 545 (1991) 59–69.
18 R. B. Taylor, R. Reid and C. T. Hung, *J. Chromatogr.*, 316 (1984) 279–289.
19 Á. Bartha, Gy. Vigh and J. Ståhlberg, *J. Chromatogr.*, 506 (1990) 85–96.
20 C. H. Giles, T. H. MacEwan, S. N. Nakhwa and D. Smith, *J. Chem. Soc.*, (1960) 3973–3993.

Modelling retention in reversed-phase liquid chromatography as a function of pH and solvent composition

Rui M. Lopes Marques⋆ and Peter J. Schoenmakers*

Philips Research Laboratories, P.O. Box 80000, 5600 JA Eindhoven (Netherlands)

ABSTRACT

Models describing the concomitant effects of pH and organic modifier concentration on retention in reversed-phase liquid chromatography are established. Two different octadecyl-modified silica columns were used. The retention behaviour of several acidic, basic and neutral solutes were studied, using methanol as the organic modifier. The suggested models accurately describe retention as a function of pH and composition. A unified formalism for retention modelling that is applicable to all ionogenic solutes is also established. This formalism is tested with the modelling of retention for several weak bases. The resulting (general) model describes retention accurately and is applicable to all solutes studied.

INTRODUCTION

Optimizing chromatographic selectivity (relative retention) in liquid chromatography (LC) is a difficult task. Many procedures have been developed, most of them specifically designed for reversed-phase liquid chromatography (RPLC), owing to the major role of this technique in modern chromatography. It is now generally accepted that the interpretive approach, in which the chromatogram is interpreted as the sum of a number of individual peaks, is the most efficient [1,2].

The problem of optimizing concentration(s) of organic modifier(s) in the mobile phase has been tackled with considerable success [1,3]. The inclusion of pH as one of the optimization parameters presents great potential advantages [4], but also raises several problems. Some of these are specific to the interpretive procedures that we strive to use, others are connected with the chemistry of the problem:

(1) Generally, we cannot use pH as the only parameter in selectivity optimization procedures, because absolute retention also varies with the acidity of the mobile phase. To keep capacity factors in the optimum range, it is necessary to vary another parameter concomitantly (modifier concentration is the logical choice) [4].

(2) If one has a quaternary mobile phase (water plus three organic modifiers), the four apparent variable parameters are interconnected (their percentages add up to 100%). Using the concept of isoeluotropic mixtures, we can reduce the parameter space by including only two optimization parameters [1]. When considering pH as one of the optimization parameters, the parameter space acquires an additional dimension and, most important, a different and more complex structure (in comparison with solvent optimization). To work with the same dimensionality as quaternary solvent optimization, only the concentration of one organic modifier can be considered along with pH. Even then, the structure of the parameter space is different, as is illustrated in Fig. 1. Therefore, the direct application of experimental designs and optimiza-

---

⋆ Present address: Centro de Tecnologia Química e Biológica, Quinta do Marquês, 2780 Oeiras, Portugal.

Neutral solutes   Ionogenic solutes
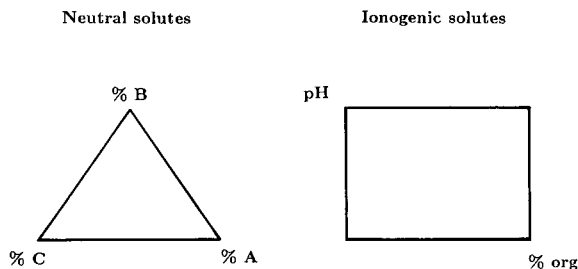
Fig. 1. Compared structure of the parameter space for organic modifier (quaternary mixtures) and for simultaneous pH and organic modifier optimization (binary mixtures).

tion routines already in use for solvent optimization is not possible.

(3) Defining and measuring pH in aqueous–organic mixtures gives rise to some theoretical and practical complications. We shall discuss this later.

(4) In addition to retention and selectivity, there are other characteristics of the peaks of ionogenic solutes that are variable with pH. Peak shape is highly dependent on this factor, as has been shown in a previous paper [4]. This implies that we cannot rely solely on selectivity or retention criteria to assess the quality of a chromatogram.

(5) Peak tracking is essential for interpretive procedures [1]. The peak tracking procedures developed for solvent optimization, based on the spectra of the solutes [5–7], cannot be directly transferred to pH optimization, because the spectra of ionogenic solutes vary with pH.

(6) Owing to the characteristics of interpretive procedures, it is necessary to develop (new) models for the peak characteristics (plate counts, asymmetry factors) as functions of two variables (simultaneously): pH and organic content.

It was the aim of this work to develop and compare models that accurately describe retention as a function of pH and solvent composition throughout a large parameter space. We also aimed to establish an experimental design that allows the coefficients of the above models to be derived from a limited number of experiments. Ultimately, our intention is to use the models and experimental design for the simultaneous interpretive optimization of pH and composition.

THEORY

Our aim is a function to describe the capacity factor k:

$$k = \frac{t_{r,i} - t_0}{t_0} \tag{1}$$

as a function of pH and concentration of organic modifier:

$$k = F([H^+], \varphi) \tag{2}$$

where $t_{r,i}$ is the retention time of the solute i and t_0 the hold-up time of the column (proportional to the retention volume and the void volume, respectively), $[H^+]$ is the concentration of "hydrogen ions" and φ the fraction of organic modifier in the mobile phase.

To obtain a grasp of the kinds of functions that can be used, we first searched the literature for functions that adequately model the variation of k with each of the parameters separately. The variation of retention as a function of the solvent composition (keeping other relevant factors constant) has been extensively studied. Several functions have been proposed. Among others, these include a logarithmic model [8]:

$$\log k = A + B\varphi + C \log (1 + D\varphi) \tag{3}$$

a reciprocal model [9]:

$$\frac{1}{k} = A + B\varphi + C\varphi^2 \tag{4}$$

and quadratic and linear exponential models [10]:

$$\log k = A + B\varphi + C\varphi^2 \tag{5}$$

$$\log k = A + B\varphi \tag{6}$$

Of these, the quadratic exponential model (eqn. 5) works most satisfactorily. Because of its accuracy, simplicity and good numerical behaviour, we judged it to be the best available. The linear exponential model (eqn. 6) fits data very well for most solutes over moderately large ranges, as has been observed by several workers (see, e.g., refs. 10 and 11).

The variation of k with pH (with other factors constant) has also been investigated by several workers (see, e.g., refs. 11–17). Let us consider the case of a weak monoprotic acid HA. If we assume a simple reversible retention mechanism to hold (Fig. 2), several equilibria can be thought to influ-
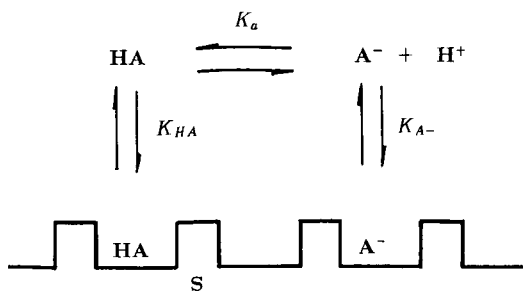
Fig. 2. Model describing the equilibria involved in the retention of a weak monoprotic acid HA.

ence the concentration of the acid in its various forms (S represents the stationary phase):

$$HA + S \overset{K_{HA}}{\rightleftharpoons} HA(S) \tag{7}$$

$$A^- + S \overset{K_{A^-}}{\rightleftharpoons} A(S)^- \tag{8}$$

$$HA \overset{K_a}{\rightleftharpoons} A^- + H^+ \tag{9}$$

The corresponding equilibrium constants are given by

$$K_{HA} = \frac{[HA(S)]}{\{[S]_0 - [HA(S)] - [A(S)^-]\}[HA]} \tag{10}$$

$$K_{A^-} = \frac{[A(S)^-]}{\{[S]_0 - [HA(S)] - [A(S)^-]\}[A^-]} \tag{11}$$

$$K_a = \frac{[H^+][A^-]}{[HA]} \tag{12}$$

where $[S]_0$ is the total "concentration" of substrate (free and occupied sites). This approach is very similar to that recently described by Armstrong *et al.* [16]. One may note that we are implicitly assuming that the number of available sites is the same for all forms of the solute and independent of pH and φ. This may not always be true [4].

If the capacity of the stationary phase is kept significantly above the total concentration of solutes, one may assume that the number of available sites remains constant, simplifying the equilibrium expressions. In fact, if $[S]_0 \gg [HA(S)] + [A(S)^-]$, eqn. 10 reduces to $K_{HA} = [HA(S)]/[HA][S_0]$ and the capacity factor of the protonated species, $k_0 = \beta[HA(S)]/[HA]$, where β is the ratio of stationary

and mobile phase volumes ($\beta = V_s/V_m$), can be written as

$$k_0 = \beta[S_0]K_{HA} \tag{13}$$

and analogously for k_{-1}:

$$k_{-1} = \beta[S_0]K_{A^-} \tag{14}$$

From this, we obtain

$$k = \frac{k_0 + k_{-1}K_a/[H^+]}{1 + K_a/[H^+]} \tag{15}$$

The same result is obtained by assuming from the start that the observed capacity factor is a weighted average of the capacity factors of the individual species [1,4]:

$$k = k_0\left(\frac{[HA]}{[HA] + [A^-]}\right) + k_{-1}\left(\frac{[A^-]}{[HA] + [A^-]}\right) \tag{16}$$

For a weak monoprotic base, a similar equation can be obtained [14]:

$$k = \frac{k_0 + k_1[H^+]/K_a}{1 + [H^+]/K_a} \tag{17}$$

where K_a is defined in terms of the basicity constant K_b and the ionic product of water, K_w ($= [H_3O^+][OH^-]$), as

$$K_a = K_w/K_b \tag{18}$$

and k_0 and k_1 are the capacity factors of B and HB^+, respectively.

For diprotic acids, zwitterions, etc., the principle for the derivation of analogous equations is the same (see, *e.g.*, ref. 14).

It is possible to derive a single equation applicable to all cases by using some ideas taken from complexometric and acid–base studies. To our knowledge, this has not been done before. In the paragraphs that follow, we omit electric charges for the sake of simplicity.

Suppose a completely deprotonated solute A, which establishes the following general equilibria in solution:

$$mH + nA \rightleftharpoons H_mA_n; \quad m, n = 0, 1, 2, ...; \quad n \neq 0 \tag{19}$$
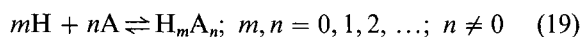
For each of the H_mA_n species we can write a global stoichiometric formation constant

$$\kappa_{m,n} = \frac{[H_mA_n]}{[H]^m[A]^n} \tag{20}$$

Basic species of general formula $A_n(OH)_m$ can be formally accounted for in this set of equations by writing the corresponding equilibrium equations in terms of H^+ instead of OH^- and by redefining the resulting global formation constants. For example, for $A(OH)$, we have

$$A + OH \rightleftharpoons A(OH) \tag{21}$$

or, adding H to both sides,

$$A + H_2O \rightleftharpoons A(OH) + H \tag{22}$$
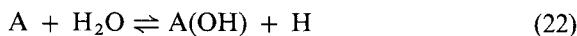
The equilibrium constant for this equation is given by $[A(OH)]/[A][H]^{-1}$, which can be conventionally assigned to a "compound" with the formula AH_{-1} and with a formation constant $\kappa_{-1,1} = K_w/K_a$.

The observed global capacity factor, k, is given by an averaged sum of the capacity factors $k_{m,n}$ of each H_mA_n species:

$$k = \sum_m \sum_n k_{m,n} \frac{[H_mA_n]}{C_A} \tag{23}$$

where m may be zero (completely deprotonated solute), n is at least unity and C_A is the analytical concentration of A (sum of the concentrations of A in all its possible forms).

Developing the above equation leads to

$$k = \frac{\sum\limits_{m,n} k_{m,n}\kappa_{m,n}[H^m][A^{n-1}]}{\sum\limits_{m,n} \kappa_{m,n}[H^m][A^{n-1}]} \tag{24}$$

Note that, in the above equation, $\kappa_{0,1}$ ("formation constant" of the deprotonated solute) is implicitly equal to 1 (eqn. 20).

This systematization, although more complex, unifies all expressions derived from phenomenological approaches to the elution of the various types of ionogenic compounds separable by RPLC (diprotic acids, bases, zwitterions, etc.). It is also potentially useful for developing formalized optimization procedures, because it allows the use of one equation for all kinds of compounds.

There are few reports in the literature in which the capacity factor is studied as a combined function of pH and concentration of organic modifier in the mobile phase. Haddad et al. [18] studied the simultaneous optimization of pH and organic modifier concentration for some aromatic acids, using planar

surfaces to represent $\ln k$ as a function of the two variables. This approach is not sufficiently precise for the purpose of determining modelling functions that are accurate over (moderately) large ranges of the variables. Otto and Wegscheider [19] investigated modelling functions, including the ionic strength of the mobile phase, for the separation of several diprotic acids. The general model derived by these authors included thirteen parameters. Assuming the ionic strength to be constant, this number is reduced to eleven. Grushka et al. [20] studied the combined effects of pH and methanol concentration on the capacity factor and on the selectivity of some deoxyribonucleotides, but only from a descriptional point of view. Modelling functions were not derived.

In the remainder of this section we shall refer to methanol–water mixtures. Most of the discussion should also be applicable to other binary systems. Consider eqn. 15 (valid for weak monoprotic acids). At each methanol concentration, this equation describes a sigmoidal function. The curves are different for different methanol concentrations (φ values), because k_0, k_{-1} and K_a vary with φ, but the general form of the equation is maintained. Establishing functions for the variation of these three parameters with φ and substituting them into eqn. 15, or substituting related functions into eqn. 24, should give us a modelling function for k as a function of both [H] and φ.

The complementary approach is also conceivable. At constant pH, the curves follow eqn. 5. Determining A, B and C functions of [H] and substituting these into eqn. 5 should also produce retention-modelling functions.

The two approaches are not equivalent, because all the functions (eqns. 5 and 15, in addition to equations for the coefficients therein) are approximate.

Considering eqn. 15 first, we observe that k_0 is the capacity factor of the protonated form of the acid, HA. Its variation with φ should logically follow eqn. 5:

$$\ln k_0 = \ln k_0^0 + S_0\varphi + T_0\varphi^2 \tag{25}$$

and analogously for k_{-1},

$$\ln k_{-1} = \ln k_{-1}^0 + S_{-1}\varphi + T_{-1}\varphi^2 \tag{26}$$

It is well known that the acidity constant K_a cannot be assumed to be independent of φ. The

works of Paabo et al. [21] and Rorabacher et al. [22] seem to indicate that a cubical expression is needed to model K_a against φ:

$$\ln K_a = \ln K_a^0 + Q_1\varphi + Q_2\varphi^2 + Q_3\varphi^3 \qquad (27)$$

Substituting eqns. 25–27 (or similar ones) into eqn. 15 and introducing an additional parameter (δ) to account for any constant shift in the observed retention, we obtain a modelling class of functions of the general form

$$k = \delta + \frac{k_0(\varphi) + k_{-1}(\varphi)K_a(\varphi)/[H^+]}{1 + K_a(\varphi)/[H^+]} \qquad (28)$$

Modelling functions belonging to this class will be called "class 1 functions".

The second approach starts with $\ln k = A + B\varphi + C\varphi^2$. We observe that A represents the logarithm of the observed capacity factor for 0% methanol, which should be a sigmoidal function of [H], so that

$$A = \ln \left[\frac{k_0^w + k_{-1}^w K_a^w/[H^+]}{1 + K_a^w/[H^+]} \right] \qquad (29)$$

In this equation, k_0^w represents the capacity factor of HA, k_{-1}^w the capacity factor of A^- and K_a^w the acidity constant of HA (all in pure water). There are no literature reports about the variation of B or C with pH.

We can gain some insight into the expected variation of B with pH if we assume that the linear relation $\ln k = \ln k_0 - S\varphi$ holds. Measuring the capacity factor k at a fixed pH and two different percentages (φ_α and φ_β) of methanol, we can estimate the value of S as the slope of the straight line defined by the two measurements:

$$S \approx \frac{1}{\varphi_\alpha - \varphi_\beta} (\ln k_\beta - \ln k_\alpha) \qquad (30)$$

As the pH varies, the capacity factors at φ_α and φ_β% methanol, k_α and k_β vary according to sigmoidal relationships. This results in the following type of expression for S:

$$S([H]) = \frac{1}{\varphi_\alpha - \varphi_\beta} \left[\ln \left(\frac{k_{0,\beta} - k_{-1,\beta}K_{a,\beta}/[H]}{1 + K_{a,\beta}/[H]} \right) - \ln \left(\frac{k_{0,\alpha} - k_{-1,\alpha}K_{a,\alpha}/[H]}{1 + K_{a,\alpha}/[H]} \right) \right] \qquad (31)$$

It appears that the variation of S with [H] follows a difference of log-sigmoidals. If K_a is constant over the pH range studied, the above equation simplifies to a single log-sigmoidal. After some manipulations we find

$$S([H]) = \frac{1}{\varphi_\alpha - \varphi_\beta} \ln \left(\frac{k_{0,\beta} - k_{-1,\beta}K_a/[H]}{k_{0,\alpha} - k_{-1,\alpha}K_a/[H]} \right) \qquad (32)$$

Modelling functions derived using this approach will be called "class 2 functions" and have the general form

$$k = \delta + k^w([H]) \exp(B([H])\varphi + C([H])\varphi^2) \qquad (33)$$

pH MEASUREMENTS

There is no general consensus on how to measure and report, or even use, the pH values of mixed eluents in the chromatographic literature. The pH is sometimes reported as a pragmatic pH (pH^P), measured before mixing the buffer with the organic modifier, sometimes as an operational pH after mixing, and sometimes as a "true" (thermodynamic) pH. This lack of uniformity is due to two main reasons, one theoretical and the other practical. It is not simple to assess the "true" pH in aqueous–organic media [23] and measurements before mixing can be much more conveniently implemented in a routine method-development procedure [3].

In methanol–water mixtures, the pH^T (thermodynamic pH) is determined by

$$pH^T = pH^O + \zeta \qquad (34)$$

where pH^O (operational pH) is the value measured with a glass electrode calibrated with standard aqueous buffers and ζ is a correction term, which is a function of the methanol content of the solution [22]. Because ζ is tabulated, the difficulties involved in reporting pH^T and pH^O are essentially the same. Using pH^T we may write

$$[H] = 10^{-pH^T} \qquad (35)$$

However, it is much more practical to report and use pH^P. In an automated system, it is technically difficult to measure the pH of the eluent after mixing (pH^O in our nomenclature) and it is experimentally inconvenient to prepare a different eluent for each desired composition in order to measure pH^T before pumping. If one wants a formalized and simple

optimization procedure, one has to simplify this process.

Measuring pH before mixing reduces the required number of measurements, because pH only has to be measured once for each different buffer. We believe that pH^P measurements are adequate, in the sense that they enable us to fit the data accurately with physically meaningful models. We have not studied the relationship between pH^P and pH^T, but our models show no signs of problems that may be attributable to this factor. Of course, physically meaningful parameters, such as K_a, cannot be derived reliably from the model.

EXPERIMENTAL

Retention data for all solutes were taken from a previous paper [4]. The main experimental conditions are given below. The experiments were carried out on an HP 1090 liquid chromatograph (Hewlett-Packard, Palo Alto, CA, USA). The data acquisition was performed using a Waters (Milford, MA, USA) Maxima 820 data station.

Two ODS (octadecyl-modified silica) columns were used: a 5-μm ChromSpher C_{18} glass cartridge (10 cm $\times$ 3 mm I.D.) from Chrompack (Middelburg, Netherlands) and a 10-μm μBondapak-C_{18} stainless-steel column (30 cm $\times$ 3.9 mm I.D.) from Waters. Buffers were 1:2 stoichiometric mixtures of citrate and phosphate, with a total ionic strength of 0.05 M. The organic modifier was high-performance liquid chromatographic-grade methanol.

Samples either were obtained as gifts from Organon (Oss, Netherlands) or were of analytical-reagent grade purchased from Merck (Darmstadt, Germany). All solutes and their structures are listed in ref. 4.

For acidic solutes, methanol concentrations of 30, 40 and 50% were used, and for basic solutes 50, 60 and 70%. For each composition, a number of pH values were studied, ranging from 2.6 to 7.03. The pH values are reported as the pH of the aqueous solution, before mixing with methanol.

Solutes and buffers were filtered before use. Solutes were injected individually to avoid mutual interferences. The flow-rate was 0.5 ml/min for the ChromSpher column and 1.25 ml/min for the μBondapak column. The columns were thermostated at 40°C. For more details, see ref. 4.

Hold-up times for both columns were estimated using replicate injections of saturatad $NaNO_3$, according to ref. 24, as being 2.17 min (75.6% porosity) for the μBondapak column and 0.86 min (60.8% porosity) for the ChromSpher column. These values are slightly different from those given in ref. 4, which were either determined gravimetrically [24] or estimated assuming $\varepsilon = 0.625$.

For one of the data sets described in ref. 4 we noted a significant degradation of the column and subsequently a lack of reproducibility is the observed retention times. In this paper, these data were excluded. For all data considered here the experimental uncertainty is much smaller than the modelling errors.

The evaluation of peak characteristics was performed by feeding the "raw" files created by the Maxima data station into a computer program written by the authors.

All model-fitting calculations were performed on a VAX 11/780 computer (Digital Equipment, Maynard, MA, USA) with a program (written by the authors) based on non-linear least squares. The numerical algorithms were adapted from ref. 25.

RESULTS

Retention modelling

We tried nine different class 1 models, by assigning several functions to k_0, k_{-1}, K_a and δ (eqn. 28). These models are listed in Table I. The results obtained for each acidic and neutral solute that was studied are listed in Tables II–XI.

For class 2, eight different models were tested, using different functions for k_0, B, C and δ (eqn. 33). These are listed in Table XII.

In models 2.A–2.D, we assumed ln k to vary linearly with φ and we tentatively assigned polynomial functions to the slope $S([H])$ (see eqns. 5 and 32), with or without a constant shift parameter (δ) embedded in the models.

In models 2.E and 2.F, ln k was assumed to be a quadratic function of φ. To the quadratic term we assigned a first-degree polynomial and to the linear term a second-degree polynomial for describing the effect of [H].

Models 2.G and 2.H are based on the approximate analysis of the kind of variation expected for S (eqn. 33). We considered ln k to vary linearly with φ, and assigned a sigmoidal function to S.

TABLE I

CLASS 1 MODELS: MODEL k AS A FUNCTION OF pH AND ASSUME THE COEFFICIENTS TO DEPEND ON COMPOSITION

Model No.	Model eqn.	No. of parameters	Comments	Eqn. No.
1.A	$k = \dfrac{k_0^0 \exp(S_0\varphi)[H] + k_{-1}^0 K_a^0 \exp[(Q_1 + S_{-1})\varphi + Q_2\varphi^2]}{[H] + K_a^0 \exp(Q_1\varphi + Q_2\varphi^2)}$	7	Ln k_0 linear with φ, ln k_{-1} linear, ln K_a quadratic, $\delta = 0$	36
1.B	$k = \dfrac{k_0^0 \exp(S_0\varphi)[H] + k_{-1}^0 K_a^0 \exp[(Q_1 + S_{-1})\varphi + Q_2\varphi^2 + Q_3\varphi^3]}{[H] + K_a^0 \exp(Q_1\varphi + Q_2\varphi^2 + Q_3\varphi^3)}$	8	Ln k_0 linear, ln k_{-1} linear, ln K_a cubic, $\delta \neq 0$	37
1.C	$k = \dfrac{k_0^0 \exp(S_0\varphi + T_0\varphi^2)[H] + k_{-1}^0 K_a^0 \exp[(Q_1 + S_{-1})\varphi + (Q_2 + T_{-1})\varphi^2]}{[H] + K_a^0 \exp(Q_1\varphi + Q_2\varphi^2)}$	9	Ln k_0 quadratic, ln k_{-1} quadratic, ln K_a quadratic, $\delta = 0$	38
1.D	$k = \dfrac{k_0^0 \exp(S_0\varphi)[H] + k_{-1}^0 K_a^0 \exp[(Q_1 + S_{-1})\varphi + (Q_2 + T_{-1})\varphi^2]}{[H] + K_a^0 \exp(Q_1\varphi + Q_2\varphi^2)}$	8	Ln k_0 linear, ln k_{-1} quadratic, ln K_a quadratic, $\delta = 0$	39
1.E	$k = \delta + \dfrac{k_0^0 \exp(S_0\varphi)[H] + k_{-1}^0 K_a^0 \exp[(Q_1 + S_{-1})\varphi + Q_2\varphi^2]}{[H] + K_a^0 \exp(Q_1\varphi + Q_2\varphi^2)}$	8	Like model 1.A, except $\delta \neq 0$	40
1.F	$k = \delta + \dfrac{k_0^0 \exp(S_0\varphi)[H] + k_{-1}^0 K_a^0 \exp[(Q_1 + S_{-1})\varphi + (Q_2 + T_{-1})\varphi^2]}{[H] + K_a^0 \exp(Q_1\varphi + Q_2\varphi^2)}$	9	Like model 1.D, except $\delta \neq 0$	41
1.G	$k = \delta + \dfrac{k_0^0 \exp(S_0\varphi + T_0\varphi^2)[H] + k_{-1}^0 K_a^0 \exp[(Q_1 + S_{-1})\varphi]}{[H] + K_a^0 \exp(Q_1\varphi)}$	8	Ln k_0 quadratic, ln k_{-1} linear, ln K_a linear, $\delta \neq 0$	42
1.H	$k = \delta + \dfrac{k_0^0 \exp(S_0\varphi)[H] + k_{-1}^0 K_a^0 \exp[(Q_1 + S_{-1})\varphi]}{[H] + K_a^0 \exp(Q_1\varphi)}$	7	Ln k_0 linear, ln k_{-1} linear, ln K_a linear, $\delta \neq 0$	43
1.I	$k = \delta + \dfrac{k_0^0 \exp(S_0\varphi + T_0\varphi^2)[H] + k_{-1}^0 K_a^0 \exp[(Q_1 + S_{-1})\varphi + Q_2\varphi^2]}{[H] + K_a^0 \exp(Q_1\varphi + Q_2\varphi^2)}$	9	Ln k_0 quadratic, ln k_{-1} linear, ln K_a quadratic, $\delta \neq 0$	44

TABLE II

FITTED PARAMETERS FOR CLASS 1 MODELS

Solute caffeine.

Model	k_0^0	S_0	T_0	k_{-1}^0	S_{-1}	T_{-1}	K_a^0	Q_1	Q_2	Q_3	δ	SSQ^a
ChromSpher												
1.A	6.88	−6.13	—	6.88	−6.2	—	−0.119	−78.7	129	—	—	0.0223
1.B	7.18	−6.26	—	6.55	−6	—	$-0.135 \cdot 10^{-2}$	−51.9	65.9	155	—	0.0208
1.C	23.8	−12.9	8.82	24.2	−13	8.9	$-0.180 \cdot 10^{-2}$	−48.6	73.3	—	—	0.00409
1.D	5.95	−5.49	—	22.9	−13	9	$0.322 \cdot 10^{-16}$	161	−192	—	—	0.00218
1.E	13.4	−8.98	—	13.6	−9	—	$-0.267 \cdot 10^{-4}$	−36.9	81.1	—	0.194	0.00383
1.F	13.4	−8.96	—	13.8	−9.1	0.2	$-0.257 \cdot 10^{-2}$	−50.8	76.6	—	0.191	0.00406
1.G	10.8	−7.65	−2.11	25.2	−10.4	—	$-0.195 \cdot 10^{-10}$	18.0	—	—	0.204	0.00454
1.H	13.0	−8.85	—	20.3	−9.69	—	$-0.215 \cdot 10^{-10}$	17.7	—	—	0.187	0.00455
1.I	10.7	−7.62	−2.18	29.6	−11.2	—	$-0.161 \cdot 10^{-10}$	18.8	−0.807	—	0.205	0.00454
μBondapak												
1.A	12.1	−6.78	—	27.1	−8.35	—	$-0.273 \cdot 10^{-7}$	−0.883	8.55	—	—	0.00982
1.B	12.1	−6.77	—	$-0.164 \cdot 10^9$	−35.1	—	$0.170 \cdot 10^{-14}$	40.5	−10.2	−14.1	—	0.0101
1.C	29.9	−11.8	6.61	42.6	−12.7	6.8	$-0.394 \cdot 10^{-7}$	2.56	2.12	—	—	0.000769
1.D	12.1	−6.78	—	21.6	0.52	−0.68	$-0.342 \cdot 10^{-7}$	−0.893	7.19	—	—	0.00983
1.E	18.4	−8.57	—	84.1	−12.3	—	$-0.207 \cdot 10^{-6}$	−18.5	44.4	—	0.180	0.000738
1.F	18.5	−8.57	—	736	−22.1	11.0	$-0.116 \cdot 10^{-8}$	6.01	15.5	—	0.180	0.000740
1.G	15.6	−7.50	−1.94	87.8	−12.5	—	$-0.115 \cdot 10^{-8}$	12.2	—	—	0.209	0.000762
1.H	18.6	−8.61	—	20.7	−8.83	—	$-0.962 \cdot 10^{-7}$	1.16	—	—	0.184	0.000772
1.I	29.0	−11.6	6.77	64.8	−14.4	—	$-0.301 \cdot 10^{-7}$	3.57	−13.6	—	−0.0372	0.00421

^{a} SSQ = Sum of squares of the residuals (in all tables).

TABLE III

FITTED PARAMETERS FOR CLASS 1 MODELS

Solute benzoic acid.

Model	k_0^0	S_0	T_0	k_{-1}^0	S_{-1}	T_{-1}	K_a^0	Q_1	Q_2	Q_3	δ	SSQ
ChromSpher												
1.A	46.2	−7.07	—	3.92	−2.96	—	$0.869 \cdot 10^{-4}$	−0.936	−2.03	—	—	0.0572
1.B	46.2	−7.07	—	3.92	9.25	—	$0.869 \cdot 10^{-4}$	−0.954	−1.95	−0.0995	—	0.0572
1.C	55.7	−8.08	1.32	2.86	−7.50	−2.55	$0.167 \cdot 10^{-3}$	−4.50	2.65	—	—	0.0544
1.D	46.2	−7.07	—	2.59	−8.77	−3.15	$0.864 \cdot 10^{-4}$	−0.906	−2.07	—	—	0.0572
1.E	46.9	−7.13	—	7.37	−11.8	—	$0.973 \cdot 10^{-4}$	−1.58	−1.17	—	0.0244	0.0567
1.F	47.2	−7.16	—	0.00319	33.6	−65.7	$0.108 \cdot 10^{-3}$	−2.13	−0.434	—	0.0368	0.0558
1.G	54.4	−7.95	1.18	3.35	−8.59	—	$0.116 \cdot 10^{-3}$	−2.51	—	—	−0.00881	0.0547
1.H	47.0	−7.14	—	8.65	−12.3	—	$0.115 \cdot 10^{-3}$	−2.47	—	—	0.0278	0.0566
1.I	55.5	−8.06	1.27	3.16	−7.75	—	$0.178 \cdot 10^{-3}$	−4.85	3.12	—	0.00735	0.0544
μBondapak												
1.A	38.6	−6.78	—	16.4	−18.8	—	$0.352 \cdot 10^{-3}$	−7.52	7.30	—	—	0.104
1.B	38.6	−6.78	—	15.1	−12.8	—	$0.169 \cdot 10^{-3}$	−7.39	−1.76	12.2	—	0.104
1.C	40.2	−7.00	0.300	$0.277 \cdot 10^{-6}$	78.4	−125	$0.263 \cdot 10^{-3}$	−5.98	5.40	—	—	0.103
1.D	38.6	−6.78	—	$0.925 \cdot 10^{-7}$	85.0	−135	$0.255 \cdot 10^{-3}$	−5.81	5.16	—	—	0.103
1.E	36.4	−6.50	—	0.750	−4.37	—	$0.160 \cdot 10^{-3}$	−2.85	0.535	—	−0.131	0.0947
1.F	37.0	−6.57	—	$0.118 \cdot 10^{-4}$	57.1	−85.0	$0.710 \cdot 10^{-4}$	1.61	−5.34	—	−0.0969	0.0878
1.G	51.3	−8.25	5.72	2.47	−0.32	—	$0.156 \cdot 10^{-3}$	−2.57	—	—	−2.18	0.0901
1.H	36.3	−6.49	—	0.738	−4.23	—	$0.149 \cdot 10^{-3}$	−2.45	—	—	−0.137	0.0947
1.I	53.4	−8.49	5.96	1.93	0.77	—	$0.182 \cdot 10^{-3}$	−3.52	1.37	—	−2.09	0.0872

TABLE IV

FITTED PARAMETERS FOR CLASS 1 MODELS

Solute phenol.

Model	k_0^0	S_0	T_0	k_{-1}^0	S_{-1}	T_{-1}	K_a^0	Q_1	Q_2	Q_3	δ	SSQ
ChromSpher												
1.A	12.0	−5.27	—	13.1	−5.43	—	$0.812 \cdot 10^{-4}$	−0.820	41.2	—	—	0.0167
1.B	11.2	−5.05	—	13.1	−5.44	—	$0.581 \cdot 10^{-5}$	−3.71	151	−232	—	0.0162
1.C	9.57	−4.21	−1.06	14.1	−5.84	0.5	$0.162 \cdot 10^{-3}$	3.69	17.9	—	—	0.0163
1.D	10.8	−4.92	—	14.1	−5.85	0.5	$0.676 \cdot 10^{-4}$	4.69	24.0	—	—	0.0163
1.E	11.2	−5.11	—	13.6	−5.63	—	$0.756 \cdot 10^{-4}$	−7.95	40.1	—	0.0530	0.0163
1.F	13.2	−6.10	—	8.21	−2.63	−5.7	$0.218 \cdot 10^{-3}$	1.61	21.2	—	0.341	0.0160
1.G	10.3	−4.67	−0.604	13.6	−5.6	—	$0.190 \cdot 10^{-4}$	16.1	—	—	0.0516	0.0163
1.H	11.2	−5.11	—	13.6	−5.56	—	$0.669 \cdot 10^{-4}$	11.9	—	—	0.0470	0.0163
1.I	7.49	−2.52	−5.25	8.94	−3.153	—	$0.633 \cdot 10^{-3}$	0.993	4.76	—	0.305	0.0161
μBondapak												
1.A	11.3	−5.27	—	7.06	−5.0	—	$0.389 \cdot 10^6$	−129	159	—	—	0.130
1.B	11.3	−5.29	—	7.24	−4.92	—	0.185	8.24	−255	398	—	0.127
1.C	11.3	−5.28	0.0366	0.877	6.5	−14.6	0.163	−50.0	59.5	—	—	0.113
1.D	11.2	−5.25	—	0.878	6.5	−14.6	0.147	−49.5	58.8	—	—	0.113
1.E	10.6	−4.93	—	6.70	−5.0	—	$0.537 \cdot 10^8$	−155	192	—	−0.103	0.127
1.F	11.3	−5.27	—	0.864	6.5	−14.8	0.169	−50.2	59.8	—	0.00456	0.113
1.G	19.3	−1.61	1.26	14.5	−0.44	—	$0.353 \cdot 10^{-4}$	−3.93	—	—	−11.1	0.118
1.H	8.79	−3.63	—	5.65	−2.96	—	$0.421 \cdot 10^{-4}$	−4.61	—	—	−0.647	0.141
1.I	13.4	−5.32	3.28	3.26	0.86	—	$0.892 \cdot 10^{-4}$	−8.32	3.91	—	−1.32	0.115

TABLE V

FITTED PARAMETERS FOR CLASS 1 MODELS

Solute *o*-nitrophenol.

Model	k_0^0	S_0	T_0	k_{-1}^0	S_{-1}	T_{-1}	K_a^0	Q_1	Q_2	Q_3	δ	SSQ
ChromSpher												
1.A	42.0	−6.03	—	10.4	−7.74	—	$0.196 \cdot 10^{-6}$	1.28	−1.31	—	—	0.0949
1.B	42.0	−6.03	—	10.4	−7.74	—	$0.234 \cdot 10^{-6}$	−0.109	2.23	−2.95	—	0.0949
1.C	43.9	−6.27	0.311	17.2	−10.5	3.64	$0.263 \cdot 10^{-6}$	−0.310	0.765	—	—	0.0942
1.D	42.0	−6.03	—	10.6	−7.83	0.12	$0.198 \cdot 10^{-6}$	1.24	−1.26	—	—	0.0949
1.E	42.8	−6.13	—	13.5	−8.80	—	$0.271 \cdot 10^{-6}$	−0.484	0.994	—	0.0601	0.0942
1.F	42.8	−6.12	—	6.96	−5.13	−4.87	$0.227 \cdot 10^{-6}$	0.490	−0.289	—	0.0591	0.0942
1.G	43.4	−6.21	0.178	11.5	−8.13	—	$0.236 \cdot 10^{-6}$	0.274	—	—	0.0242	0.0942
1.H	42.7	−6.11	—	12.4	−8.50	—	$0.234 \cdot 10^{-6}$	0.301	—	—	0.0501	0.0943
1.I	49.7	−5.52	4.20	26.3	−5.39	—	$0.407 \cdot 10^{-6}$	0.888	−5.40	—	−6.93	0.165
μBondapak												
1.A	36.3	−5.95	—	20.9	−8.8	—	$0.421 \cdot 10^{-2}$	−38.4	45.9	—	—	1.06
1.B	36.4	−5.96	—	22.5	−9.06	—	$0.528 \cdot 10^{-4}$	−2.34	−50.5	83.8	—	1.05
1.C	36.8	−6.02	0.0768	0.0350	27.5	−50.0	$0.563 \cdot 10^{-3}$	−27.0	30.5	—	—	1.04
1.D	36.4	−5.96	—	0.0114	33.8	−58.7	$0.293 \cdot 10^{-3}$	−23.5	25.9	—	—	1.04
1.E	35.2	−5.79	—	17.2	−7.9	—	$0.365 \cdot 10^{-2}$	−37.4	44.3	—	−0.104	1.05
1.F	36.4	−5.95	—	0.0277	28.7	−51.4	$0.382 \cdot 10^{-3}$	−25.0	27.9	—	−0.00236	1.04
1.G	40.7	−5.78	3.82	8.66	−1.49	—	$0.875 \cdot 10^{-5}$	−4.05	—	—	−4.04	1.07
1.H	30.3	−5.00	—	8.74	−4.63	—	$0.780 \cdot 10^{-5}$	−3.73	—	—	−0.685	1.11
1.I	41.4	−6.68	2.25	1.69	4.55	—	$0.504 \cdot 10^{-4}$	−13.5	12.3	—	−0.735	1.05

TABLE VI

FITTED PARAMETERS FOR CLASS 1 MODELS

Solute p-nitrophenol.

Model	k_0^0	S_0	T_0	k_{-1}^0	S_{-1}	T_{-1}	K_a^0	Q_1	Q_2	Q_3	δ	SSQ
ChromSpher												
1.A	23.4	−6.18	−	31.7	−16.2	−	$0.356 \cdot 10^{-6}$	−0.862	1.3	−	−	0.0296
1.B	23.4	−6.18	−	31.6	−16.3	−	$0.302 \cdot 10^{-6}$	0.427	−2.01	2.77	−	0.0296
1.C	25.2	−6.59	0.541	0.376	9.32	−35.8	$0.404 \cdot 10^{-6}$	−1.53	2.12	−	−	0.0289
1.D	23.4	−6.18	−	0.0193	25.3	−56.4	$0.274 \cdot 10^{-6}$	0.554	−0.532	−	−	0.0294
1.E	23.6	−6.22	−	66.0	−18.9	−	$0.420 \cdot 10^{-6}$	−1.83	2.68	−	0.0148	0.0295
1.F	23.6	−6.22	−	0.352	10.33	−39.2	$0.369 \cdot 10^{-6}$	−1.11	1.73	−	0.0131	0.0294
1.G	26.3	−6.85	1.11	7.22	−10.5	−	$0.324 \cdot 10^{-6}$	−1.38	−	−	−0.0615	0.0287
1.H	23.5	−6.20	−	22.5	−15.2	−	$0.286 \cdot 10^{-6}$	0.244	−	−	0.00588	0.0296
1.I	26.7	−6.93	1.32	5.48	−9.77	−	$0.259 \cdot 10^{-6}$	1.08	−1.60	−	−0.0903	0.0287
μBondapak												
1.A	25.9	−6.22	−	42.2	−14.0	−	$0.341 \cdot 10^{-2}$	−38.7	46.9	−	−	0.451
1.B	25.9	−6.22	−	49.0	−14.4	−	$0.435 \cdot 10^{-4}$	−3.58	−45.1	78.6	−	0.451
1.C	37.3	−8.20	2.61	$0.527 \cdot 10^{-5}$	77.7	−129	$0.600 \cdot 10^{-2}$	−41.6	50.6	−	−	0.437
1.D	25.9	−6.21	−	$0.646 \cdot 10^{-5}$	75.7	−125	$0.130 \cdot 10^{-2}$	−33.3	39.9	−	−	0.446
1.E	25.6	−6.16	−	31.7	−12.9	−	$0.257 \cdot 10^{-2}$	−37.1	44.8	−	−0.0227	0.451
1.F	25.8	−6.18	−	$0.109 \cdot 10^{-4}$	72.8	−120	$0.135 \cdot 10^{-2}$	−33.5	39.9	−	−0.0123	0.446
1.G	29.5	−4.67	3.78	8.21	−0.62	−	$0.665 \cdot 10^{-5}$	−3.82	−	−	−6.18	0.456
1.H	22.6	−5.53	−	6.03	−6.27	−	$0.544 \cdot 10^{-5}$	−3.26	−	−	−0.285	0.489
1.I	35.6	−7.96	4.42	1.15	3.63	−	$0.250 \cdot 10^{-4}$	−11.0	9.41	−	−0.845	0.445

TABLE VII

FITTED PARAMETERS FOR CLASS 1 MODELS

Solute dinitrophenol (first of two peaks observed for this solute [4]).

Model	k_0^0	S_0	T_0	k_{-1}^0	S_{-1}	T_{-1}	K_a^0	Q_1	Q_2	Q_3	δ	SSQ
ChromSpher												
1.A	14.1	−5.12	−	4.79	−5.86	−	$0.118 \cdot 10^{-4}$	14.8	−12.7	−	−	0.0261
1.B	14.1	−5.13	−	4.79	−5.88	−	$0.689 \cdot 10^{-4}$	1.22	21.5	−28.0	−	0.0260
1.C	7.17	−1.46	−4.70	0.518	6.1	−15.4	$0.133 \cdot 10^{-6}$	39.1	−43.8	−	−	0.0237
1.D	13.9	−5.08	−	1.50	0.4	−8	$0.458 \cdot 10^{-5}$	19.8	−18.8	−	−	0.0253
1.E	11.5	−3.88	−	3.10	−2.6	−	$0.494 \cdot 10^{-6}$	31.9	−34.5	−	−0.583	0.0245
1.F	11.5	−3.87	−	2.40	−1.3	−1.7	$0.298 \cdot 10^{-6}$	34.6	−37.8	−	−0.583	0.0242
1.G	19.0	−6.76	2.03	5.37	−6.40	−	$0.719 \cdot 10^{-4}$	5.03	−	−	0.0363	0.0276
1.H	15.3	−5.52	−	7.96	−8.07	−	$0.800 \cdot 10^{-4}$	4.66	−	−	0.115	0.0281
1.I	18.2	−6.42	2.69	6.91	−7.48	−	$0.359 \cdot 10^{-4}$	8.87	−5.14	−	−0.339	0.0270
μBondapak												
1.A	17.2	−5.39	−	7.11	−6.23	−	$0.395 \cdot 10^{-4}$	8.81	−6.54	−	−	0.241
1.B	17.2	−5.39	−	7.13	−6.24	−	$0.209 \cdot 10^{-4}$	13.8	−19.3	10.6	−	0.241
1.C	22.6	−6.91	2.07	25.7	−13.3	9.6	$0.416 \cdot 10^{-3}$	−4.26	11.0	−	−	0.236
1.D	17.1	−5.36	−	24.1	−13.0	9.03	$0.157 \cdot 10^{-3}$	1.16	3.77	−	−	0.237
1.E	19.3	−5.97	−	14.9	−9.42	−	$0.475 \cdot 10^{-3}$	−4.88	11.7	−	0.219	0.236
1.F	19.9	−6.12	−	6.78	−4.45	−8.41	$0.614 \cdot 10^{-3}$	−6.25	13.5	−	0.264	0.236
1.G	14.7	−4.49	−1.82	12.4	−8.69	−	$0.918 \cdot 10^{-4}$	4.07	−	−	0.186	0.237
1.H	18.3	−5.75	−	11.0	−8.17	−	$0.875 \cdot 10^{-4}$	4.20	−	−	0.158	0.237
1.I	17.1	−5.29	−1.02	7.13	−5.02	−	$0.247 \cdot 10^{-3}$	−1.21	6.74	−	0.242	0.236

TABLE VIII

FITTED PARAMETERS FOR CLASS 1 MODELS

Solute dinitrophenol (second peak).

Model	k_0^0	S_0	T_0	k_{-1}^0	S_{-1}	T_{-1}	K_a^0	Q_1	Q_2	Q_3	δ	SSQ
ChromSpher												
1.A	28.0	−5.94	—	4.01	−6.36	—	$0.531 \cdot 10^{-4}$	6.47	−6.26	—	—	0.0657
1.B	28.1	−5.96	—	4.01	−6.40	—	$0.320 \cdot 10^{-1}$	−43.5	121	−106	—	0.0650
1.C	25.6	−5.47	−6.19	5.72	−8.31	2.57	$0.428 \cdot 10^{-4}$	7.62	−7.74	—	—	0.0652
1.D	27.9	−5.94	—	6.57	−9.06	3.57	$0.650 \cdot 10^{-4}$	5.35	−4.78	—	—	0.0654
1.E	28.4	−6.02	−	4.72	−7.08	—	$0.701 \cdot 10^{-4}$	4.95	−4.27	—	0.0347	0.0655
1.F	27.3	−5.84	—	6.61	−9.17	4.71	$0.505 \cdot 10^{-4}$	6.71	−6.55	—	−0.0469	0.0653
1.G	28.3	−5.78	−0.138	6.11	−8.18	—	$0.126 \cdot 10^{-3}$	1.72	—	—	0.0745	0.0660
1.H	28.9	−6.10	—	5.94	−8.05	—	$0.126 \cdot 10^{-3}$	1.72	—	—	0.0704	0.0660
1.I	27.0	−6.00	−0.717	7.88	−9.75	—	$0.547 \cdot 10^{-4}$	6.27	−5.97	—	−0.0481	0.0654
μBondapak												
1.A	29.7	−5.96	—	6.19	−6.85	—	$0.114 \cdot 10^{-3}$	0.330	1.96	—	—	0.764
1.B	29.7	−5.96	—	6.20	−6.85	—	$0.115 \cdot 10^{-3}$	0.382	1.56	0.544	—	0.764
1.C	25.4	−5.08	−1.21	0.507	7.12	−18.8	$0.207 \cdot 10^{-4}$	9.88	−11.0	—	—	0.753
1.D	30.0	−5.99	—	0.462	7.67	−19.6	$0.299 \cdot 10^{-4}$	7.83	−8.25	—	—	0.754
1.E	25.4	−5.11	—	3.49	−3.3	—	$0.868 \cdot 10^{-5}$	14.7	−17.4	—	−0.510	0.753
1.F	27.0	−5.44	—	2.22	−1.2	−3.9	$0.115 \cdot 10^{-4}$	13.1	−15.3	—	−0.302	0.752
1.G	37.3	−7.23	2.66	3.52	−3.52	—	$0.930 \cdot 10^{-4}$	1.60	—	—	−0.442	0.755
1.H	27.9	−5.64	—	4.31	−4.96	—	$0.929 \cdot 10^{-4}$	1.61	—	—	−0.181	0.759
1.I	37.7	−7.22	3.68	4.34	−3.37	—	$0.707 \cdot 10^{-4}$	2.99	−1.64	—	−1.05	0.755

We also tried other models, using functions for $S([H])$ that were equivalent (or similar) to a difference of log-sigmoidals, but when fitting these models severe numerical problems occurred.

The obtained results for class 2 models are listed in Tables XIII–XXII.

Experimental design

On determining a model to fit experimental retention data with the final objective of using it in a systematic method-development procedure, it is important to consider the number of experimental data points (chromatograms) required in order to

TABLE IX

FITTED PARAMETERS FOR CLASS 1 MODELS

Solute org-9935.

Model	k_0^0	S_0	T_0	k_{-1}^0	S_{-1}	T_{-1}	K_a^0	Q_1	Q_2	Q_3	δ	SSQ
ChromSpher												
1.A	528	−10.6	—	$0.127 \cdot 10^4$	−13.4	—	$0.195 \cdot 10^{-8}$	5.38	132	—	—	2.96
1.B	309	−10.2	—	$0.136 \cdot 10^4$	−13.6	—	$0.187 \cdot 10^{-8}$	5.87	467	−995	—	1.35
1.C	547	−10.6	−0.305	$0.620 \cdot 10^4$	−22.3	13	$0.400 \cdot 10^{-9}$	7.64	140	—	—	1.40
1.D	540	−10.6	—	$0.620 \cdot 10^4$	−22.3	13	$0.400 \cdot 10^{-9}$	7.64	140	—	—	1.40
1.E	522	−10.6	—	$0.183 \cdot 10^4$	−14.7	—	$0.161 \cdot 10^{-8}$	6.03	130	—	0.692	1.41
1.F	625	−11.1	—	$0.513 \cdot 10^4$	−21.2	10	$0.462 \cdot 10^{-9}$	6.96	141	—	0.156	1.40
1.G	951	−10.9	−5.80	$0.170 \cdot 10^6$	−28.4	—	$-0.814 \cdot 10^{-10}$	8.28	—	—	0.882	1.67
1.H	1790	−14.6	—	$0.181 \cdot 10^4$	−14.7	—	$-0.416 \cdot 10^{-9}$	14.6	—	—	0.678	1.65
1.I	966	−10.8	−6.02	$0.123 \cdot 10^4$	−12.6	—	$0.114 \cdot 10^{-7}$	5.70	3.04	—	0.859	1.66

TABLE X

FITTED PARAMETERS FOR CLASS 1 MODELS

Solute 2,3,4-trihydroxybenzophenone.

Model	k_0^0	S_0	T_0	k_{-1}^0	S_{-1}	T_{-1}	K_a^0	Q_1	Q_2	Q_3	δ	SSQ
ChromSpher												
1.A	527	−10.7	−	143	−12.6	−	$0.590 \cdot 10^{-7}$	8.23	−11.2	−	−	2.78
1.B	526	−10.7	−	109	−11.7	−	$0.115 \cdot 10^{-6}$	1.05	12.7	−24.3	−	2.77
1.C	1090	−14.8	5.55	228	−15.6	5.08	$0.315 \cdot 10^{-6}$	−1.28	2.11	−	−	2.22
1.D	526	−10.7	−	4.78	6.2	−24.8	$0.120 \cdot 10^{-7}$	17.0	−22.7	−	−	2.77
1.E	645	−11.5	−	2160	−22.2	−	$0.310 \cdot 10^{-5}$	−14.4	20.3	−	0.593	2.27
1.F	638	−11.4	−	6.03	8.93	−38.6	$0.867 \cdot 10^{-6}$	−7.44	11.3	−	0.568	2.27
1.G	1130	−15.0	5.95	107	−11.5	−	$0.242 \cdot 10^{-6}$	0.223	−	−	−0.0570	2.22
1.H	623	−11.3	−	351	−16.2	−	$0.192 \cdot 10^{-6}$	0.957	−	−	0.503	2.31
1.I	697	−12.0	0.991	218	−12	−	$0.650 \cdot 10^{-6}$	−5.50	8.08	−	0.455	2.26
μBondapak												
1.A	342	−9.62	−	196	−12.3	−	$0.139 \cdot 10^{-7}$	24.8	−30.4	−	−	0.919
1.B	341	−9.61	−	163	−11.8	−	$0.682 \cdot 10^{-7}$	7.08	−24.6	−51.8	−	0.919
1.C	365	−9.92	0.338	597	−17.7	6.54	$0.397 \cdot 10^{-6}$	9.48	−13.1	−	−	0.919
1.D	341	−9.61	−	666	−18.3	7.24	$0.494 \cdot 10^{-6}$	8.46	−11.9	−	−	0.919
1.E	371	−9.86	−	332	−13.8	−	$0.877 \cdot 10^{-6}$	5.92	−9.16	−	0.107	0.919
1.F	352	−9.71	−	504	−16.5	4.46	$0.560 \cdot 10^{-6}$	7.94	−11.4	−	0.0421	0.919
1.G	16800	−11.0	−23.8	−0.101	6.13	−	$0.548 \cdot 10^{-5}$	−2.33	−	−	2.60	0.919
1.H	$0.217 \cdot 10^6$	−26.8	−	−0.0800	6.44	−	$0.434 \cdot 10^{-5}$	−1.79	−	−	2.46	0.920
1.I	68.8	−2.29	−8.38	635	−16.9	−	$0.260 \cdot 10^{-5}$	1.01	−3.69	−	0.0954	0.919

obtain reliable results, *i.e.*, to reproduce to a good approximation the real retention surface.

To assess the behaviour of the models when limited sets of data are available, we selected two prospective experimental designs with 9 and 12 points (3×3 and 4×3, respectively). These are shown in Fig. 3. Next, we refitted all the models using only the set of points defined by each of the

TABLE XI

FITTED PARAMETERS FOR CLASS 1 MODELS

Solute N-vinylpyrrolidone.

Model	k_0^0	S_0	T_0	k_{-1}^0	S_{-1}	T_{-1}	K_a^0	Q_1	Q_2	Q_3	δ	SSQ
ChromSpher												
1.A	9.07	−5.97	−	5.87	−4.8	−	$0.884 \cdot 10^{-17}$	−46.1	316	−	−	0.00398
1.B	8.77	−5.86	−	5.91	−4.8	−	$0.868 \cdot 10^{-17}$	−46.1	573	−660	−	0.00396
1.C	9.06	−5.97	0.00259	25.7	−11.4	7	$0.389 \cdot 10^{-17}$	−42.9	312	−	−	0.00330
1.D	9.06	−5.96	−	25.9	−11.4	8	$0.544 \cdot 10^{-17}$	−43.1	310	−	−	0.00330
1.E	11.9	−7.46	−	13.0	−7.6	−	$0.596 \cdot 10^{-17}$	−44.7	309	−	0.245	0.00335
1.F	9.54	−6.28	−	27.2	−11.6	7	$0.350 \cdot 10^{-17}$	−43.0	312	−	0.0639	0.00330
1.G[a]	−	−	−	−	−	−	−	−	−	−	−	−
1.H[a]	−	−	−	−	−	−	−	−	−	−	−	−
1.I[a]	−	−	−	−	−	−	−	−	−	−	−	−

[a] Values not calculated, owing to numerical problems.

TABLE XII

CLASS 2 MODELS: MODEL k AS A FUNCTION OF COMPOSITION AND ASSUME THE COEFFICIENTS TO DEPEND ON pH

Model No.	Model eqn.	No. of parameters	Comments	Eqn. No.
2.A	$k = \dfrac{k_0^w[H] + k_{-1}^w K_a^w}{[H] + K_a^w} \exp\{\varphi(S_0 + S_1[H] + S_2[H]^2)\}$	6	k^w sigmoidal, B quadratic. $C = 0, \delta = 0$	45
2.B	$k = \delta + \dfrac{k_0^w[H] + k_{-1}^w K_a^w}{[H] + K_a^w} \exp\{\varphi(S_0 + S_1[H] + S_2[H]^2)\}$	7	Like model 2.A, except $\delta \neq 0$	46
2.C	$k = \dfrac{k_0^w[H] + k_{-1}^w K_a^w}{[H] + K_a^w} \exp\{\varphi(S_0 + S_1[H] + S_2[H]^2 + S_3[H]^3)\}$	7	k^w sigmoidal, B cubic, $C = 0, \delta \neq 0$	47
2.D	$k = \delta + \dfrac{k_0^w[H] + k_{-1}^w K_a^w}{[H] + K_a^w} \exp\{\varphi(S_0 + S_1[H] + S_2[H]^2 + S_3[H]^3)\}$	8	Like model 2.C, except $\delta \neq 0$	48
2.E	$k = \dfrac{k_0^w[H] + k_{-1}^w K_a^w}{[H] + K_a^w} \exp\{\varphi(S_0 + S_1[H] + S_2[H]^2) + \varphi^2(T_0 + T_1[H])\}$	8	k^w sigmoidal, B quadratic. C linear, $\delta = 0$	49
2.F	$k = \delta + \dfrac{k_0^w[H] + k_{-1}^w K_a^w}{[H] + K_a^w} \exp\{\varphi(S_0 + S_1[H] + S_2[H]^2) + \varphi^2(T_0 + T_1[H])\}$	9	Like model 2.E, except $\delta \neq 0$	50
2.G	$k = \dfrac{k_0^w[H] + k_{-1}^w K_a^w}{[H] + K_a^w} \exp\left(\dfrac{S_0 + S_1[H]}{S_2 + [H]}\right)$	6	k^w sigmoidal, B sigmoidal, $C = 0, \delta = 0$	51
2.H	$k = \delta + \dfrac{k_0^w[H] + k_{-1}^w K_a^w}{[H] + K_a^w} \exp\left(\dfrac{S_0 + S_1[H]}{S_2 + [H]}\right)$	7	Like model 2.G, except $\delta \neq 0$	52

TABLE XIII

FITTED PARAMETERS FOR CLASS 2 MODELS

Solute caffeine.

Model	k_0^w	k_{-1}^w	K_a^w	S_0	S_1	S_2	S_3	T_0	T_1	δ	SSQ
ChromSpher											
2.A	$-0.920 \cdot 10^6$	6.98	5290	-6.21	226	$-0.515 \cdot 10^5$	—	—	—	—	0.0201
2.B	1.92	13.6	0.136	-9.07	225	$-0.659 \cdot 10^5$	—	—	—	0.194	0.00165
2.C	$-0.920 \cdot 10^6$	6.98	5300	-6.21	269	$-0.114 \cdot 10^6$	$0.187 \cdot 10^8$	—	—	—	0.0209
2.D	11.7	13.6	0.0221	-9.08	289	$-0.161 \cdot 10^6$	$0.284 \cdot 10^8$	—	—	0.194	0.00162
2.E	234	14.2	0.0250	-10.2	-2300	$0.188 \cdot 10^6$	—	5.38	2370	—	0.00431
2.F	79.0	5.41	0.0996	-3.45	-501	$-0.492 \cdot 10^5$	—	-9.09	936	0.239	0.00181
2.G	6.89	35.9	$-0.372 \cdot 10^{-10}$	-4.37	-0.320	0.0519	—	—	—	—	0.0223
2.H	13.6	225	$-0.143 \cdot 10^{-10}$	-6.67	-0.387	0.0427	—	—	—	0.194	0.00269
μBondapak											
2.A	11.8	9.64	$0.110 \cdot 10^{-4}$	-6.57	-259	$0.838 \cdot 10^5$	—	—	—	—	0.0353
2.B	15.9	12.7	$0.765 \cdot 10^{-5}$	-7.89	-210	$0.682 \cdot 10^5$	—	—	—	0.139	0.0290
2.C	12.1	9.44	$0.160 \cdot 10^{-4}$	-6.51	-1290	$0.160 \cdot 10^7$	$-0.450 \cdot 10^9$	—	—	—	0.0319
2.D	16.4	12.7	$0.944 \cdot 10^{-5}$	-7.91	-973	$0.124 \cdot 10^7$	$-0.351 \cdot 10^9$	—	—	0.145	0.0263
2.E	16.5	13.4	$0.148 \cdot 10^{-4}$	-8.41	-245	$0.997 \cdot 10^5$	—	2.51	-186	—	0.0311
2.F	16.6	13.2	$0.931 \cdot 10^{-5}$	-8.08	-186	$0.821 \cdot 10^5$	—	0.121	-195	0.151	0.0281
2.G	11.1	11.0	$-0.337 \cdot 10^{-4}$	-312	22.2	-3.31	—	—	—	—	0.112
2.H	16.3	13.2	$0.817 \cdot 10^{-5}$	$-0.133 \cdot 10^5$	$-0.318 \cdot 10^4$	396	—	—	—	0.149	0.0306

TABLE XIV

FITTED PARAMETERS FOR CLASS 2 MODELS

Solute benzoic acid.

Model	k_0^w	k_{-1}^w	K_a^w	S_0	S_1	S_2	S_3	T_0	T_1	δ	SSQ
ChromSpher											
2.A	43.3	1.76	$0.566 \cdot 10^{-4}$	-6.71	-316	$0.111 \cdot 10^6$	—	—	—	—	0.0844
2.B	43.9	1.59	$0.564 \cdot 10^{-4}$	-6.78	-311	$0.110 \cdot 10^6$	—	—	—	0.0213	0.0832
2.C	44.4	1.70	$0.677 \cdot 10^{-4}$	-6.47	-1450	$0.125 \cdot 10^7$	$-0.301 \cdot 10^9$	—	—	—	0.0615
2.D	44.5	1.67	$0.676 \cdot 10^{-4}$	-6.48	-1440	$0.125 \cdot 10^7$	$-0.299 \cdot 10^9$	—	—	0.00327	0.0615
2.E	52.2	2.14	$0.538 \cdot 10^{-4}$	-8.03	-59.0	$0.924 \cdot 10^5$	—	2.01	-526	—	0.0599
2.F	52.5	2.23	$0.539 \cdot 10^{-4}$	-8.07	-58.2	$0.928 \cdot 10^5$	—	2.09	-533	-0.00690	0.0598
2.G	42.4	1.74	$0.491 \cdot 10^{-4}$	-5.47	-0.395	0.0576	—	—	—	—	0.112
2.H	43.4	1.46	$0.490 \cdot 10^{-4}$	-5.64	-0.350	0.0504	—	—	—	0.0324	0.109
μBondapak											
2.A	34.6	0.129	$0.564 \cdot 10^{-4}$	-6.66	236	$-0.520 \cdot 10^5$	—	—	—	—	0.104
2.B	34.8	0.0309	$0.563 \cdot 10^{-4}$	-6.69	244	$-0.544 \cdot 10^5$	—	—	—	0.00933	0.104
2.C	35.8	0.209	$0.717 \cdot 10^{-4}$	-6.28	-1550	$0.198 \cdot 10^7$	$-0.557 \cdot 10^9$	—	—	—	0.0912
2.D	35.4	0.385	$0.738 \cdot 10^{-4}$	-6.18	-1710	$0.216 \cdot 10^7$	$-0.603 \cdot 10^9$	—	—	-0.0191	0.0905
2.E	31.6	0.0637	$0.531 \cdot 10^{-4}$	-6.54	602	$-0.876 \cdot 10^5$	—	0.190	-701	—	0.0785
2.F	33.0	0.233	$0.532 \cdot 10^{-4}$	-6.80	600	$-0.849 \cdot 10^5$	—	0.611	-724	-0.0161	0.0781
2.G	39.3	-0.0602	$0.115 \cdot 10^{-3}$	-6.78	$-0.166 \cdot 10^{-3}$	$0.380 \cdot 10^{-4}$	—	—	—	—	0.0687
2.H	36.5	6.16	$0.140 \cdot 10^{-3}$	-6.39	$-0.169 \cdot 10^{-3}$	$0.495 \cdot 10^{-4}$	—	—	—	-0.188	0.0469

TABLE XV

FITTED PARAMETERS FOR CLASS 2 MODELS

Solute phenol.

Model	k_0^w	k_{-1}^w	K_a^w	S_0	S_1	S_2	S_3	T_0	T_1	δ	SSQ
ChromSpher											
2.A	13.0	12.7	$0.587 \cdot 10^{-5}$	-5.37	-162	$0.580 \cdot 10^5$	—	—	—	—	0.0103
2.B	13.4	13.1	$0.621 \cdot 10^{-5}$	-5.52	-167	$0.598 \cdot 10^5$	—	—	—	0.0412	0.00994
2.C	13.1	12.7	$0.632 \cdot 10^{-5}$	-5.37	-182	$0.846 \cdot 10^5$	$-0.768 \cdot 10^7$	—	—	—	0.0103
2.D	13.4	13.1	$0.660 \cdot 10^{-5}$	-5.52	-186	$0.853 \cdot 10^5$	$-0.737 \cdot 10^7$	—	—	0.0416	0.00993
2.E	13.3	12.9	$0.102 \cdot 10^{-4}$	-5.43	-253	$0.610 \cdot 10^5$	—	0.0256	213	—	0.00766
2.F	13.1	12.7	$0.584 \cdot 10^{-5}$	-5.33	-244	$0.588 \cdot 10^5$	—	-0.265	208	0.0342	0.00767
2.G	12.9	12.9	$-0.875 \cdot 10^{-4}$	-6.23	-0.559	0.104	—	—	—	—	0.0130
2.H	11.4	13.3	$0.266 \cdot 10^{-2}$	1.96	-0.565	0.103	—	—	—	0.0172	0.0151
μBondapak											
2.A	10.4	7.63	$0.127 \cdot 10^{-4}$	-4.96	-248	$0.933 \cdot 10^5$	—	—	—	—	0.172
2.B	9.52	7.17	$0.145 \cdot 10^{-4}$	-4.43	-261	$0.958 \cdot 10^5$	—	—	—	-0.162	0.168
2.C	10.8	7.37	$0.186 \cdot 10^{-4}$	-4.86	-1730	$0.227 \cdot 10^7$	$-0.643 \cdot 10^9$	—	—	—	0.155
2.D	9.12	6.93	$0.176 \cdot 10^{-4}$	-4.09	-528	$0.477 \cdot 10^6$	$-0.112 \cdot 10^9$	—	—	-0.276	0.161
2.E	7.73	5.72	$0.858 \cdot 10^{-5}$	-3.48	-19.3	$0.587 \cdot 10^5$	—	-1.89	-323	—	0.159
2.F	7.53	5.66	$0.106 \cdot 10^{-4}$	-3.29	-74.8	$0.741 \cdot 10^5$	—	-1.71	-310	-0.0889	0.155
2.G	10.3	7.75	$0.973 \cdot 10^{-5}$	-4.49	-0.217	0.0433	—	—	—	—	0.180
2.H	8.86	6.99	$0.958 \cdot 10^{-5}$	-3.65	-0.197	0.0476	—	—	—	-0.279	0.175

TABLE XVI

FITTED PARAMETERS FOR CLASS 2 MODELS

Solute *o*-nitrophenol.

Model	k_0^w	k_{-1}^w	K_a^w	S_0	S_1	S_2	S_3	T_0	T_1	δ	SSQ
ChromSpher											
2.A	42.5	6.42	$0.274 \cdot 10^{-6}$	-6.04	-88.8	$0.308 \cdot 10^6$	—	—	—	—	0.0912
2.B	40.8	6.88	$0.272 \cdot 10^{-6}$	-5.85	-87.4	$0.301 \cdot 10^6$	—	—	—	-0.118	0.0832
2.C	42.5	6.38	$0.271 \cdot 10^{-6}$	-6.05	-33.8	$-0.454 \cdot 10^6$	$0.225 \cdot 10^8$	—	—	—	0.0904
2.D	40.8	6.81	$0.270 \cdot 10^{-6}$	-5.86	-38.6	$-0.375 \cdot 10^6$	$0.200 \cdot 10^8$	—	—	-0.117	0.0826
2.E	43.3	6.58	$0.275 \cdot 10^{-6}$	-6.10	-151	$0.295 \cdot 10^6$	—	0.0184	176	—	0.0808
2.F	46.7	8.73	$0.275 \cdot 10^{-6}$	-6.59	-131	$0.295 \cdot 10^6$	—	1.13	121	-0.225	0.0651
2.G	42.4	6.19	$0.266 \cdot 10^{-6}$	-6.71	-0.264	0.0437	—	—	—	—	0.105
2.H	40.7	6.71	$0.266 \cdot 10^{-6}$	-6.55	-0.260	0.0443	—	—	—	-0.116	0.0969
μBondapak											
2.A	34.7	7.70	$0.196 \cdot 10^{-5}$	-5.86	26.0	$0.131 \cdot 10^6$	—	—	—	—	1.15
2.B	32.4	8.23	$0.198 \cdot 10^{-5}$	-5.52	16.6	$0.152 \cdot 10^5$	—	—	—	-0.191	1.14
2.C	34.8	7.79	$0.208 \cdot 10^{-5}$	-5.83	-380	$0.663 \cdot 10^6$	$-0.197 \cdot 10^9$	—	—	—	1.14
2.D	32.3	8.34	$0.211 \cdot 10^{-5}$	-5.47	-400	$0.682 \cdot 10^6$	$-0.202 \cdot 10^9$	—	—	-0.207	1.12
2.E	24.7	5.44	$0.195 \cdot 10^{-5}$	-4.05	99.0	$0.115 \cdot 10^5$	—	-2.32	-189	—	1.12
2.F	25.5	6.13	$0.194 \cdot 10^{-5}$	-4.26	114	$0.115 \cdot 10^5$	—	-1.74	-235	-0.125	1.11
2.G	34.6	7.64	$0.193 \cdot 10^{-5}$	11.7	-1.67	0.285	—	—	—	—	1.15
2.H	32.3	8.17	$0.192 \cdot 10^{-5}$	14.3	-1.90	0.342	—	—	—	-0.188	1.14

TABLE XVII

FITTED PARAMETERS FOR CLASS 2 MODELS

Solute *p*-nitrophenol.

Model	k_0^w	k_{-1}^w	K_a^w	S_0	S_1	S_2	S_3	T_0	T_1	δ	SSQ
ChromSpher											
2.A	23.7	1.35	$0.315 \cdot 10^{-6}$	-6.21	-56.6	$0.231 \cdot 10^5$	—	—	—	—	0.0373
2.B	22.5	1.80	$0.313 \cdot 10^{-6}$	-5.97	-56.1	$0.225 \cdot 10^5$	—	—	—	-0.0763	0.0330
2.C	23.7	1.27	$0.309 \cdot 10^{-6}$	-6.22	78.9	$-0.164 \cdot 10^6$	$0.553 \cdot 10^8$	—	—	—	0.0360
2.D	22.5	1.72	$0.308 \cdot 10^{-6}$	-5.99	68.1	$-0.149 \cdot 10^6$	$0.507 \cdot 10^8$	—	—	-0.0745	0.0318
2.E	24.9	1.42	$0.316 \cdot 10^{-6}$	-6.44	-120	$0.218 \cdot 10^5$	—	0.233	179	—	0.0339
2.F	27.1	2.72	$0.316 \cdot 10^{-6}$	-6.98	-95.9	$0.224 \cdot 10^5$	—	1.50	107	-0.135	0.0255
2.G	23.7	1.26	$0.309 \cdot 10^{-6}$	-6.24	-0.266	0.0428	—	—	—	—	0.0395
2.H	22.5	1.76	$0.309 \cdot 10^{-6}$	-6.06	-0.261	0.0436	—	—	—	-0.0754	0.0352
µBondapak											
2.A	25.0	3.26	$0.173 \cdot 10^{-5}$	-6.12	-73.8	$0.475 \cdot 10^5$	—	—	—	—	0.499
2.B	23.1	3.87	$0.173 \cdot 10^{-5}$	-5.76	-75.0	$0.468 \cdot 10^5$	—	—	—	-0.131	0.489
2.C	25.1	3.49	$0.197 \cdot 10^{-5}$	-6.05	-1190	$0.184 \cdot 10^7$	$-0.544 \cdot 10^9$	—	—	—	0.454
2.D	23.0	4.55	$0.198 \cdot 10^{-5}$	-5.63	-1150	$0.178 \cdot 10^7$	$-0.526 \cdot 10^9$	—	—	-0.153	0.442
2.E	22.5	2.93	$0.173 \cdot 10^{-5}$	-5.56	-39.1	$0.473 \cdot 10^5$	—	-0.708	-95.9	—	0.497
2.F	24.4	4.35	$0.172 \cdot 10^{-5}$	-6.12	-5.47	$0.462 \cdot 10^5$	—	0.656	-190	-0.166	0.487
2.G	24.9	3.16	$0.165 \cdot 10^{-5}$	-3.59	-0.289	0.0471	—	—	—	—	0.506
2.H	23.1	3.76	$0.164 \cdot 10^{-5}$	3.65	-1.11	0.192	—	—	—	-0.125	0.497

TABLE XVIII

FITTED PARAMETERS FOR CLASS 2 MODELS

Solute dinitrophenol (first of two peaks observed for this solute [4]).

Model	k_0^w	k_{-1}^w	K_a^w	S_0	S_1	S_2	S_3	T_0	T_1	δ	SSQ
ChromSpher											
2.A	17.6	6.19	$0.168 \cdot 10^{-3}$	-6.82	643	$-0.116 \cdot 10^6$	—	—	—	—	0.0102
2.B	17.5	6.21	$0.169 \cdot 10^{-3}$	-6.77	623	$-0.111 \cdot 10^6$	—	—	—	-0.00658	0.0102
2.C	17.0	6.95	$0.130 \cdot 10^{-3}$	-7.18	1850	$-0.121 \cdot 10^7$	$0.276 \cdot 10^9$	—	—	—	0.00714
2.D	17.9	7.86	$0.964 \cdot 10^{-4}$	-7.87	2830	$-0.198 \cdot 10^7$	$0.458 \cdot 10^9$	—	—	0.0609	0.00565
2.E	22.2	7.41	$0.189 \cdot 10^{-3}$	-7.73	398	$-0.736 \cdot 10^5$	—	1.12	244	—	0.00748
2.F	23.2	7.92	$0.192 \cdot 10^{-3}$	-8.02	387	$-0.592 \cdot 10^5$	—	1.87	118	-0.0368	0.00720
2.G	18.3	5.81	$0.211 \cdot 10^{-3}$	10.2	-0.438	0.0664	—	—	—	—	0.0132
2.H	17.6	5.73	$0.213 \cdot 10^{-3}$	9.81	-0.434	0.0680	—	—	—	-0.0367	0.0124
µBondapak											
2.A	17.0	5.91	$0.153 \cdot 10^{-4}$	-7.33	1960	$-0.499 \cdot 10^6$	—	—	—	—	0.0756
2.B	21.6	2.68	$0.801 \cdot 10^{-5}$	-8.74	2630	$-0.692 \cdot 10^6$	—	—	—	0.192	0.0530
2.C	16.9	5.82	$0.137 \cdot 10^{-4}$	-7.39	2320	$-0.958 \cdot 10^6$	$0.131 \cdot 10^9$	—	—	—	0.0752
2.D	22.5	-5.35	$0.325 \cdot 10^{-5}$	-9.30	4660	$-0.331 \cdot 10^7$	$0.745 \cdot 10^9$	—	—	0.225	0.0512
2.E	327	5.07	0.0122	-4.21	-4760	$0.624 \cdot 10^6$	—	-2.44	4280	—	0.309
2.F	297	5.41	0.0111	-4.44	-4820	$0.698 \cdot 10^6$	—	-0.620	3790	-0.203	0.302
2.G	16.8	5.88	$0.115 \cdot 10^{-4}$	-5.02	-0.00473	$0.629 \cdot 10^{-3}$	—	—	—	—	0.0834
2.H	21.9	2.22	$0.608 \cdot 10^{-5}$	-6.05	-0.00455	$0.499 \cdot 10^{-3}$	—	—	—	0.207	0.0500

TABLE XIX

FITTED PARAMETERS FOR CLASS 2 MODELS

Solute dinitrophenol (second peak).

Model	k_0^w	k_{-1}^w	K_a^w	S_0	S_1	S_2	S_3	T_0	T_1	δ	SSQ
ChromSpher											
2.A	30.0	4.14	$0.173 \cdot 10^{-3}$	-6.53	242	$-0.372 \cdot 10^5$	—	—	—	—	0.0500
2.B	29.9	4.17	$0.174 \cdot 10^{-3}$	-6.50	226	$-0.329 \cdot 10^5$	—	—	—	-0.00526	0.0499
2.C	28.9	4.65	$0.142 \cdot 10^{-3}$	-6.89	1440	$-0.111 \cdot 10^7$	$0.272 \cdot 10^9$	—	—	—	0.0420
2.D	29.4	4.85	$0.117 \cdot 10^{-3}$	-7.35	2250	$-0.177 \cdot 10^7$	$0.428 \cdot 10^9$	—	—	0.0456	0.0383
2.E	34.1	4.49	$0.190 \cdot 10^{-3}$	-6.88	-23.4	6160	—	0.342	294	—	0.0450
2.F	34.0	4.48	$0.189 \cdot 10^{-3}$	-6.86	-21.7	5100	—	0.308	300	0.00199	0.0450
2.G	30.3	4.07	$0.182 \cdot 10^{-3}$	3.47	-0.536	0.0829	—	—	—	—	0.0508
2.H	30.0	4.12	$0.183 \cdot 10^{-3}$	-1.80	-0.242	0.0376	—	—	—	-0.0111	0.0504
μBondapak											
2.A	27.6	5.68	$0.271 \cdot 10^{-4}$	-7.53	2180	$-0.588 \cdot 10^6$	—	—	—	—	0.257
2.B	29.2	5.27	$0.258 \cdot 10^{-4}$	-7.83	2320	$-0.628 \cdot 10^6$	—	—	—	0.0642	0.247
2.C	26.8	6.09	$0.149 \cdot 10^{-4}$	-8.02	4820	$-0.379 \cdot 10^7$	$0.894 \cdot 10^9$	—	—	—	0.224
2.D	29.4	5.24	$0.138 \cdot 10^{-4}$	-8.58	5470	$-0.447 \cdot 10^7$	$0.107 \cdot 10^{10}$	—	—	0.106	0.193
2.E	22.3	4.63	$0.240 \cdot 10^{-4}$	-6.75	2540	$-0.623 \cdot 10^6$	—	-0.643	-664	—	0.233
2.F	21.8	4.18	$0.238 \cdot 10^{-4}$	-6.55	2550	$-0.640 \cdot 10^6$	—	-1.20	-548	0.0362	0.231
2.G	30.4	5.10	$0.767 \cdot 10^{-4}$	12.9	-0.423	0.0631	—	—	—	—	0.452
2.H	29.4	5.28	$0.785 \cdot 10^{-4}$	-104	2.26	-0.345	—	—	—	-0.0465	0.452

experimental designs, for benzoic acid (ChromSpher column only). From the new calculated parameters, we evaluated the difference between the observed and the predicted retention values, both for the design points and for all the data set. This enabled us to obtain a rough idea of the precision of each model (that is, the degree of approximation for predictions

made). The results are given in Tables XXIII and XXIV.

Basic solutes

The general function that we developed (eqn. 24) embodies models for mono-, di- and polyprotic acids and bases and amphoteric compounds. All

TABLE XX

FITTED PARAMETERS FOR CLASS 2 MODELS

Solute org-9935.

Model	k_0^w	k_{-1}^w	K_a^w	S_0	S_1	S_2	S_3	T_0	T_1	δ	SSQ
ChromSpher											
2.A	1270	1230	$0.124 \cdot 10^{-4}$	-13.3	-277	$0.970 \cdot 10^5$	—	—	—	—	2.08
2.B	1840	1770	$0.876 \cdot 10^{-5}$	-14.6	-275	$0.936 \cdot 10^5$	—	—	—	0.701	0.528
2.C	1290	1220	$0.295 \cdot 10^{-4}$	-13.3	-594	$0.461 \cdot 10^6$	$-0.101 \cdot 10^9$	—	—	—	2.03
2.D	1840	1770	$0.893 \cdot 10^{-5}$	-14.6	-434	$0.304 \cdot 10^6$	$-0.615 \cdot 10^8$	—	—	0.700	0.497
2.E	2240	2170	$0.512 \cdot 10^{-5}$	-16.5	-352	$0.879 \cdot 10^5$	—	4.42	324	—	1.15
2.F	1530	1470	$0.224 \cdot 10^{-5}$	-13.6	-206	$0.811 \cdot 10^5$	—	-1.68	-98.7	0.765	0.634
2.G	1160	1300	$0.219 \cdot 10^{-3}$	-13.2	$-0.897 \cdot 10^{-3}$	$0.665 \cdot 10^{-4}$	—	—	—	—	2.41
2.H	1670	1850	$0.273 \cdot 10^{-3}$	-14.5	$-0.103 \cdot 10^{-2}$	$0.698 \cdot 10^{-4}$	—	—	—	0.690	0.902

TABLE XXI

FITTED PARAMETERS FOR CLASS 2 MODELS

Solute N-vinylpyrrolidone.

Model	k_0^w	k_{-1}^w	K_a^w	S_0	S_1	S_2	S_3	T_0	T_1	δ	SSQ
ChromSpher											
2.A	-161	7.40	0.754	-5.29	-1.58	$0.318 \cdot 10^5$	—	—	—	—	0.0124
2.B	-2.45	10.2	0.224	-6.83	-92.1	$0.365 \cdot 10^5$	—	—	—	0.210	0.00239
2.C	4.60	7.41	0.0103	-5.29	-16.3	$0.665 \cdot 10^5$	$-0.121 \cdot 10^8$ —	—	—	—	0.0124
2.D	-2.24	10.2	0.218	-6.83	-127	$0.886 \cdot 10^5$	$-0.157 \cdot 10^8$ —	—	—	0.210	0.00237
2.E	13.2	13.2	$0.547 \cdot 10^{-3}$	-8.46	-97.3	$0.264 \cdot 10^5$	—	4.15	60.2	—	0.00246
2.F	10.7	10.7	$0.433 \cdot 10^{-3}$	-7.14	-140	$0.399 \cdot 10^5$	—	0.671	55.2	0.190	0.00238
2.G	6.44	7.42	$0.200 \cdot 10^{-2}$	2.92	-0.574	0.108	—	—	—	—	0.0125
2.H	9.71	10.2	$0.709 \cdot 10^{-3}$	-4.84	-0.649	0.0951	—	—	—	0.207	0.00253

that is required is the substitution of the appropriate functions in eqn. 24. The model was tested by applying a derived model (described below) to the solutes from the database that showed basic behaviour (see ref. 4). The model was designed taking into account the results obtained for the class 1 model. There, we showed that the best model was obtained by assigning parabolic functions of the organic modifier concentration to the logarithms of the

capacity factors of the individual species and to the pK_a of the solute (*cf.*, eqns. 25–27 and 38).

When we write eqn. 24 applied to a weak base HB^+, we obtain

$$k = \frac{k_{0,1} + k_{1,1}\kappa_{1,1}[H]}{1 + \kappa_{1,1}[H]} \tag{53}$$

where $k_{0,1}$ and $k_{1,1}$ are the capacity factors of B and HB^+, respectively, and $\kappa_{1,1}$ is the global stoichio-

TABLE XXII

FITTED PARAMETERS FOR CLASS 2 MODELS

Solute 2,3,4-trihydroxybenzophenone.

| Model	k_0^w	k_{-1}^w	K_a^w	S_0	S_1	S_2	S_3	T_0	T_1	δ	SSQ
ChromSpher											
2.A	530	94.8	$0.305 \cdot 10^{-6}$	-10.6	-291	$0.983 \cdot 10^6$	—	—	—	—	1.07
2.B	592	100	$0.310 \cdot 10^{-6}$	-11.0	-299	$0.102 \cdot 10^6$	—	—	—	0.302	0.845
2.C	530	95.8	$0.307 \cdot 10^{-6}$	-10.6	-354	$0.187 \cdot 10^6$	$-0.262 \cdot 10^8$ —	—	—	—	1.07
2.D	593	99.0	$0.309 \cdot 10^{-6}$	-11.0	-357	$0.184 \cdot 10^6$	$-0.243 \cdot 10^8$ —	—	—	0.311	0.838
2.E	986	173	$0.301 \cdot 10^{-6}$	-14.1	-367	$0.988 \cdot 10^5$	—	4.60	238	—	0.501
2.F	977	177	$0.302 \cdot 10^{-6}$	-14.1	-362	$0.981 \cdot 10^5$	—	4.83	229	-0.110	0.486
2.G	526	87.6	$0.281 \cdot 10^{-6}$	-13.1	-0.446	0.0419	—	—	—	—	1.96
2.H	584	88.7	$0.280 \cdot 10^{-6}$	-13.4	-0.453	0.0410	—	—	—	0.292	1.74
μBondapak											
2.A	366	102	$0.296 \cdot 10^{-5}$	-9.75	-142	$0.643 \cdot 10^5$	—	—	—	—	1.06
2.B	290	87.8	$0.279 \cdot 10^{-5}$	-9.09	-120	$0.565 \cdot 10^5$	—	—	—	-0.284	1.04
2.C	366	101	$0.337 \cdot 10^{-5}$	-9.68	-972	$0.138 \cdot 10^7$	$-0.397 \cdot 10^9$ —	—	—	—	0.969
2.D	287	86.4	$0.317 \cdot 10^{-5}$	-8.99	-864	$0.124 \cdot 10^7$	$-0.356 \cdot 10^9$ —	—	—	-0.301	0.944
2.E	878	216	$0.247 \cdot 10^{-5}$	-13.8	-140	$0.484 \cdot 10^5$	—	4.55	115	—	0.942
2.F	784	211	$0.230 \cdot 10^{-5}$	-13.8	-56.8	$0.427 \cdot 10^5$	—	5.42	-49.9	-0.330	0.911
2.G	366	102	$0.271 \cdot 10^{-5}$	-8.59	-0.374	0.0382	—	—	—	—	1.11
2.H	291	88.3	$0.265 \cdot 10^{-5}$	-7.95	-0.362	0.0396	—	—	—	-0.275	1.09
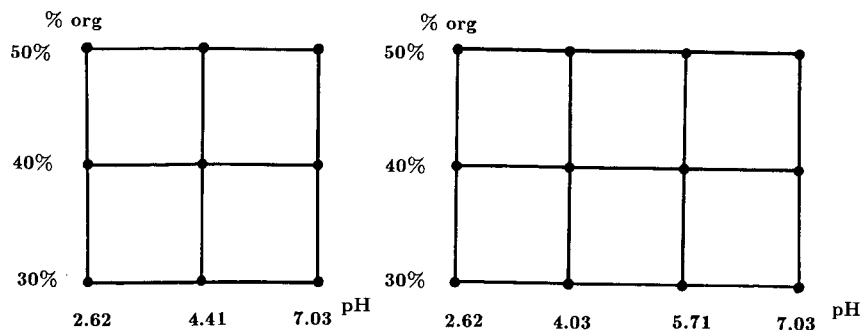
Fig. 3. 3 × 3 and 4 × 3 experimental designs used in the study of the behaviour of the models over limited sets of data.

metric formation constant of HB^+.

Assigning a parabolic function of the organic-modifier concentration to each of these three parameters results in a nine-parameter model that is essentially equivalent to model 1.C, but this time applied to basic compounds:

$$k = \frac{\left\{ \begin{array}{l} k_{0,1}^0 \exp(S_0 \varphi + T_0 \varphi^2) + k_{1,1}^0 \kappa_{1,1}^0 \exp[(Q_1 + \\ S_1)\varphi + (Q_2 + T_1)\varphi^2][H] \end{array} \right\}}{1 + \kappa_{1,1}^0 \exp(Q_1 \varphi + Q_2 \varphi^2)[H]}$$

(54)

The results are shown in Table XXV.

TABLE XXIII

RESULTS OBTAINED BY FITTING CLASS 1 MODELS TO LIMITED FRACTIONS OF THE DATA SET (3 × 3 AND 3 × 4 EXPERIMENTAL DESIGNS)

Solute, benzoic acid; column, ChromSpher ODS.

Model	NP^a	$SSQ_M{}^b$	$SSQ_T{}^c$	MD^d
1.A	9	$0.110 \cdot 10^{-3}$	0.105	0.136
	12	$0.509 \cdot 10^{-2}$	0.101	0.141
1.B	9	$0.110 \cdot 10^{-3}$	0.105	0.136
	12	$0.509 \cdot 10^{-2}$	0.101	0.141
1.C	9	$0.853 \cdot 10^{-10}$	0.106	0.138
	12	$0.508 \cdot 10^{-2}$	0.101	0.141
1.D	9	$0.677 \cdot 10^{-5}$	0.105	0.136
	12	$0.508 \cdot 10^{-2}$	0.101	0.141
1.E	9	$0.510 \cdot 10^{-4}$	0.104	0.134
	12	$0.508 \cdot 10^{-2}$	0.101	0.141
1.F	9	$0.751 \cdot 10^{-2}$	0.094	0.106
	12	$0.508 \cdot 10^{-2}$	0.101	0.141
1.G	9	$0.121 \cdot 10^{-3}$	0.105	0.136
	12	$0.508 \cdot 10^{-2}$	0.102	0.142
1.H	9	$0.138 \cdot 10^{-3}$	0.104	0.133
	12	$0.509 \cdot 10^{-2}$	0.101	0.141
1.I	9	$0.158 \cdot 10^{-5}$	0.115	0.146
	12	$0.508 \cdot 10^{-2}$	0.101	0.141

[a] NP = Number of points in the experimental design.
[b] SSQ_M = Sum of squares of the residuals, model points.
[c] SSQ_T = Sum of squares of the residuals, all points.
[d] MD = Maximum deviation between predicted and observed capacity factors.

TABLE XXIV

RESULTS OBTAINED BY FITTING CLASS 2 MODELS TO LIMITED FRACTIONS OF THE DATA SET (3 × 3 AND 3 × 4 EXPERIMENTAL DESIGNS)

Solute, benzoic acid; column, ChromSpher ODS.

Model	NP^a	$SSQ_M{}^b$	$SSQ_T{}^c$	MD^d
2.A	9	$0.317 \cdot 10^{-3}$	$-^e$	$-^f$
	12	$0.129 \cdot 10^{-1}$	34.2	4.01
2.B	9	$0.169 \cdot 10^{-3}$	$-^e$	$-^f$
	12	$0.445 \cdot 10^{-2}$	61.2	5.08
2.C	9	$0.317 \cdot 10^{-3}$	$-^e$	$-^f$
	12	$0.104 \cdot 10^{-2}$	$-^e$	$-^f$
2.D	9	$0.169 \cdot 10^{-3}$	$-^e$	$-^f$
	12	$0.441 \cdot 10^{-2}$	63.7	5.19
2.E	9	$0.932 \cdot 10^{-4}$	$-^e$	$-^f$
	12	$0.208 \cdot 10^{-2}$	$-^e$	$-^f$
2.F	9	$0.279 \cdot 10^{-3}$	0.638	0.389
	12	$0.215 \cdot 10^{-2}$	0.879	0.559
2.G	9	$0.139 \cdot 10^{-2}$	5.58	1.27
	12	$0.145 \cdot 10^{-1}$	1.01	0.535
2.H	9	$0.746 \cdot 10^{-3}$	6.49	1.36
	12	$0.104 \cdot 10^{-1}$	1.40	0.627

[a–d] See Table XXIII.
[e] Higher than 10^2.
[f] Higher than 6.

TABLE XXV

RESULTS OBTAINED BY FITTING THE RETENTION DATA FOR BASIC SOLUTES WITH A MODEL DERIVED BY THE APPLICATION OF A GENERAL EQUATION TO THE PARTICULAR CASE OF A WEAK BASE HB^+ (cf., EQNS. 24 AND 54)

Solute	$k_{0,1}^0$	S_0	T_0	$k_{1,1}^0$	S_1	T_1	$\kappa_{1,1}^0$	Q_1	Q_2	SSQ	MD^a	RMD^b
Org-20494	$0.502 \cdot 10^7$	-3.98	-22.7	0.341	12.2	-88.0	$0.534 \cdot 10^{10}$	9.96	-33.2	0.0563	0.141	3.4%
Org-3770	$0.602 \cdot 10^9$	-46.2	26.8	36.4	-7.7	-0.7	$0.393 \cdot 10^{11}$	-27.1	11.4	0.0678	0.154	6.2%
Org-5222	$0.151 \cdot 10^{14}$	-49.9	14.0	53.8	-2.1	-7.6	$0.126 \cdot 10^{14}$	-16.8	-12.5	1.073	0.635	31%
Org-5730	$0.118 \cdot 10^{11}$	-41.8	33.8	$0.302 \cdot 10^6$	-23.3	8.6	$0.844 \cdot 10^{10}$	-15.0	18.3	0.101	0.222	4.5%
Org-gb94	$0.101 \cdot 10^6$	-12.4	-2.06	13.5	0	-8.3	$0.281 \cdot 10^5$	21.7	-28.9	0.473	0.451	8.5%

[a] MD = Maximum deviation between observed and calculated capacity factors.
[b] RMD = Relative MD for observed capacity factors higher than 1.

DISCUSSION

Neutral solutes

Solutes with predominantly neutral behaviour in the pH zone of interest (phenol, caffeine, org-9935, N-vinylpyrrolidone) were included in the fitting calculations for acidic compounds. There were two reasons to do so: first, to assess the behaviour of the models for these compounds; second, if the models fit the data for neutral solutes without problems, it will not be necessary to establish a rigorous threshold to distinguish between "almost acidic" and "almost neutral" solutes.

We conclude that the models do fit the data with good accuracy, as can be seen from Tables I, III, VIII and IX (class 1 models) and Tables XIII, XV, XX and XXI (class 2 models).

The fitted parameters show a peculiar but understandable behaviour. As the capacity factors of neutral solutes are almost constant (the variations are mainly due to experimental error), some of the calculated parameters have no physical meaning and are just circumstantial. Other parameters will compensate the retention behaviour within the model. For example, the calculated k_0 and k_{-1} values may be very different (Table I, model 1.D) if the acidity constant has a very high or low value, so that only one of the species is predicted to be present. In some instances, such as phenol in Table XV (model 2.G, ChromSpher data), the calculated K_a is negative. In this instance, k_0 and k_{-1} have the same value, so that retention will be essentially independent of the value assigned to K_a.

Stationary phases

From the results obtained for class 2 models (Tables XIII–XXII), it seems that the observed acidity constant of the solutes, equal to the [H] at which both forms of the acidic solute are present in equal concentrations, is higher on the μBondapak than on the ChromSpher column for some solutes, and lower for others. This is most apparent for phenol. This solute shows a decrease in retention for pH > 5 on the μBondapak column, like a typical acidic solute, whereas on the ChromSpher column it appears to be neutral in the pH range considered. The calculated K_a for several models illustrates this behaviour. 2,3,4-Trihydroxybenzophenone (Table XXII), *o*-nitrophenol (Table XVI) and *p*-nitro-

phenol (Table XVII) appear to be more acidic on the μBondapak column, whereas peaks 1 and 2 of dinitrophenol, a solute that turned out to be impure [4], (Tables XVIII and XIX) are apparently more basic on that column.

Similar comparisons could be made for class 1 models, but as the acidity constant K_a^0 evaluated using these models corresponds to an extrapolation for 0% methanol, it would be more hazardous to make such comparisons.

Class 1 models

The nine models tested give, in general, similar results. Apart from some exceptions, the quality of fit is comparable. This is mainly due to the fact that class 1 models are not very flexible, *i.e.*, they cannot adapt to irregularities in the retention surfaces. The addition of new parameters to a base model undoubtedly improves this flexibility, but within a restricted range of values.

When determining the "best" model, one must take into account the practicality in addition to the accuracy. Too many parameters are undesirable, because many chromatograms are required to determine their values. A small number of parameters requires a small number of chromatograms, but usually implies a less accurate description of the retention surface. We fixed a maximum number of nine parameters for all models tested.

Comparing models 1.E and 1.F with their analogues 1.A and 1.D, we see that, in the models in which a constant shift parameter δ is added (1.E and 1.F), the resulting sum of squares of the residuals (*SSQ*) is for all solutes at least equal and in two cases significantly lower (2,3,4-trihydroxybenzophenone, caffeine). However, the results for benzoic acid are, in our opinion, a warning. Although showing a good fit, models 1.G and 1.I (μBondapak) give δ values of about -2, which (in absolute terms) is very high in comparison with the values of about 0.1 for the other models. The introduction of this type of parameter increases the probability of the model converging to a false minimum, because as k_0^0 and k_{-1}^0 are asymptotic values, variations in both may be compensated by changing the δ value accordingly. In this way, the particular model obtained for a given solute, with a constant shift parameter added, may somehow be circumstantial.

The cubic factor in the ln K_a expression (*cf.*,

eqn. 27; parameter Q_3 in Tables I–X) is not important in the range of methanol percentages used in this work. The improvement from model 1.A to model 1.B is very small, except for the neutral solute org-9935 on the ChromSpher column.

Comparing model 1.A with models 1.C and 1.D, we can conclude that the inclusion of quadratic terms in the capacity factor expressions for the individual species (cf., eqns. 25–26; coefficients T_0 and T_{-1} in Tables I–X) is beneficial, especially for the k_0 factor; see, for example, Tables II, VI and X (ChromSpher data) and Table V (μBondapak data). It is possible to compare the beneficial effects of both parameters separately, by comparing the SSQ of models 1.G and 1.H, for T_0, and models 1.E and 1.F, for T_{-1}. The improvements found by including T_0 in the models are, understandably, more important, because for acidic solutes the neutral species has a greater capacity factor than the negative species so that k_0 accounts for a greater part of the observed capacity factor than k_{-1}.

From the discussion above about each of the parameters, it seems that models 1.C, 1.F, 1.G and 1.I are the most useful. The smaller SSQ values are in most instances obtained for models 1.C and 1.I. Choosing one between them is mostly a matter of common sense. If we are to use the model in relatively large parameter species, it seems logical to use parabolical expressions for ln k_0, ln k_{-1} and ln K_a (model 1.C, with nine parameters). A constant shift parameter may be excluded, for two reasons. First, as was explained above, this reduces the danger of having a model converging to a false minimum. Second, model 1.C is as good as any other model tested with the inclusion of a δ parameter. A model "1.C + δ" would require ten parameters. The difficulty in fitting the model increases noticeably with increase in the number of parameters, and so does the need for good initial estimates. Model 1.C is, in our opinion, the best compromise between precision and practicality.

Class 2 models

In this class of models, the inclusion of a δ term gives much greater improvements than for class 1 models (cf., results for N-vinylpyrrolidone and 2,3,4-trihydroxybenzophenone, Tables XX and XXII). Comparing models 2.B and 2.D, which differ by the cubic factor S_3, shows model 2.D to be

significantly better for some solutes. Going from model 2.D to 2.F, that is, removing the cubic term and assuming ln k to be a quadratic function of φ, gives mixed results: nine lower and nine higher values for SSQ. Some of the variations are fairly large. This indicates that a blending of both models, that is,

$$k = \delta + \frac{k_0[H] + k_{-1}K_a}{[H] + K_a} \exp\{\varphi(S_0 + S_1[H] + S_2[H]^2 + S_3[H]^3) + \varphi^2(T_0 + T_1[H])\} \quad (55)$$

might perform better. However, this model contains ten parameters, which we believe is too many.

Models 2.G and 2.H did not live up to our expectations, giving results that were worse than most of the other models. Their advantage is that they have a small number of parameters (six and seven, respectively).

Comparison of class 1 and class 2 models

We show in Fig. 4 representative retention surfaces for one model from each class. They are almost identical within the parameter space covered by the experiments.

In general, models from class 2 give marginally better SSQ values. However, any slight extrapolation for the class 2 models (Fig. 5) results in the prediction of very high retention values towards lower pH. This indicates why class 2 models fit the data better. They are more "curvable", in other words, they have a potentially higher number of inflections, which enables them to adjust better to deviations in the data.

If we use a relatively large number of data points (at least twenty), we can describe the data with high precision by using any model from 1.C, 2.D or 2.F (nine parameters at most). Models with ten parameters, which would probably do better, are model 1.C with a constant shift term added, or eqn. 53. However, nine parameters are adequate for practical purposes.

Experimental design

The results were surprising. Although models from class 2 perform "better" (lower SSQ values) when using the whole data set for calculating the model parameters, reducing the number of design points led them to "explode", oscillating violently

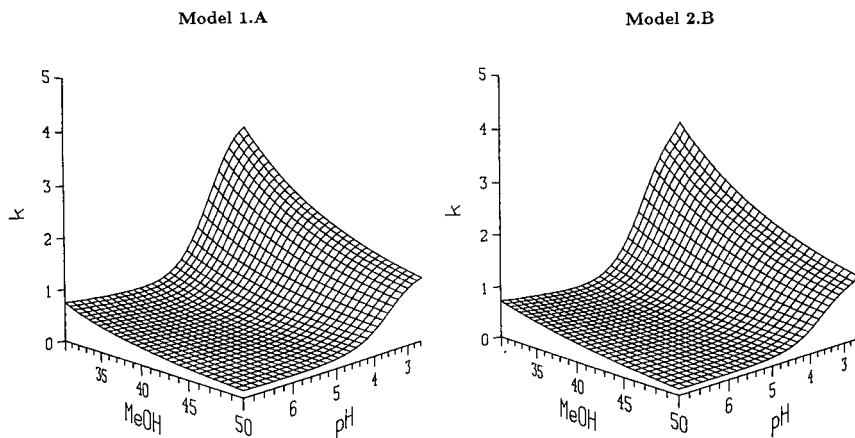Model 1.A   Model 2.B

Fig. 4. Calculated retention surfaces for a class 1 and a class 2 model (1.A and 2.B, respectively) over the parameter space covered by the experimental data available. Solute, dinitrophenol (peak 2); column, ChromSpher ODS. MeOH = Methanol.

between points of the experimental design and therefore resulting in grossly inaccurate predictions for intermediate control points.

In contrast, all class 1 models give very good (and similar) results. Their precision is good. In absolute terms, the greatest deviation between the predicted and observed capacity factors is about 0.15. The relative deviations at certain combinations of pH and organic modifier concentration, where the capacity factors are small, can be high. For capacity factors higher than 1.0, the maximum relative

deviation was about 6% and for capacity factors between 0.5 and 1.0 it was 12%.

Judging from the results (Tables XXIII and XXIV), nine points may suffice but twelve are preferable. The latter reduces the probability of having one bad experimental run ruining the optimization.

Basic solutes

The results in Table XXV show that eqn. 54 provides a good representation of the retention

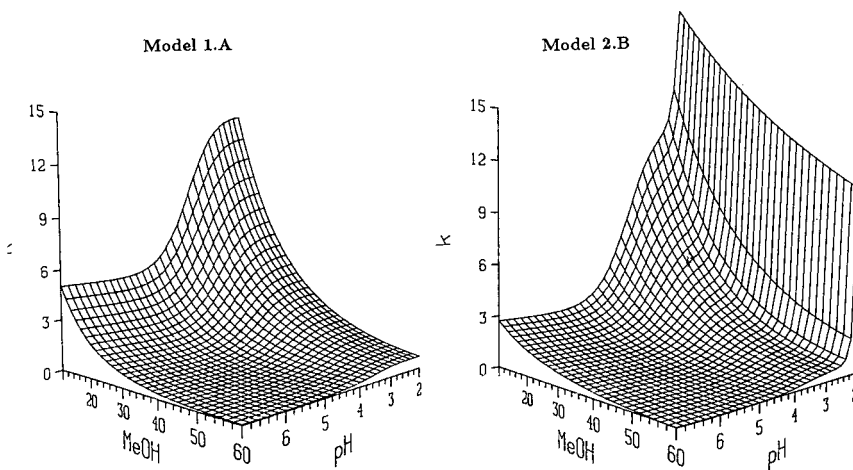Model 1.A   Model 2.B

Fig. 5. Extrapolation of the calculated retention surfaces for a class 1 and a class 2 model (1.A and 2.B, respectively). Note expansion of the scale in comparison with Fig. 4. Solute, dinitrophenol (peak 2); column, ChromSpher ODS.

surface of the basic solutes studied. The major discrepancies that are apparent in Table XXV concern the relative deviations between the observed and calculated capacity factors, which for capacity factors around 1 can be as high as 30%, and for smaller capacity factors (not shown) they can be much higher (we observed a deviation of 60% for org-20494). There is a major reason why these values should be considered "normal". It is convenient to employ an absolute minimization criterion (sum of squares of deviations) to perform the model calculations, because if we were to use a relative criterion (e.g., sum of squares of relative deviations) then we would have disproportionated contributions for that sum around zero. In this way, relative deviations are not minimized and it is natural that high (and seemingly unacceptable) values are obtained for small capacity factors. Another factor that may be included in the data and contributing in some extent to the deviations between observed and calculated values is column degradation between successive experiments. The effect of column degradation has been discussed elsewhere [4].

CONCLUSIONS

We can describe capacity factors for monoprotic acids with good accuracy using models derived from two distinct approaches. When a limited number of data points is available, models derived by first describing the capacity factor as a function of pH and then assuming the coefficients in this equation to be a function of composition are to be preferred over models derived the other way around. In the latter instance the numerical curve-fitting approach may give rise to anomalous results. Using an experimental design of twelve points, it is possible to predict capacity factors accurately using several of the models derived from eqn. 15. From these results, taking into account the modelling work done with larger data sets, we conclude that of the models studied the best one is

$$
k = \frac{\left\{ \begin{aligned} & k_0^0 \exp(S_0\varphi + T_0\varphi^2)[\mathrm{H}] + k_{-1}^0 K_\mathrm{a}^0 \exp[(Q_1 \\ & + S_{-1})\varphi + (Q_2 + T_{-1})\varphi^2] \end{aligned} \right\}}{[\mathrm{H}] + K_\mathrm{a}^0 \exp(Q_1\varphi + Q_2\varphi^2)}
$$

(56)

(referred to in the text as model 1.C).

Assigning a parabolic function of the organic modifier concentration to the logarithm of each parameter figuring in

$$
k = \frac{\sum\limits_{m,n} k_{m,n}\kappa_{m,n}[\mathrm{H}^m][\mathrm{A}^{n-1}]}{\sum\limits_{m,n} \kappa_{m,n}[\mathrm{H}^m][\mathrm{A}^{n-1}]}
$$

results in a general model that is applicable with good results to the modelling of retention as a simultaneous function of pH and organic modifier concentration for weak acids and bases, as well as for neutral compounds.

The extension of this model to polyprotic compounds is not straightforward, because each new parameter in the equation above means three more parameters in the model. Two solutions seem apparent: either an experimental design with more points is developed, or linear instead of parabolic functions may be used for describing the logarithm of the capacity factor. This will be the object of future work.

Our ultimate aim is not to describe retention functions, but to optimize separations. We have incorporated model 1.C into selectivity optimization procedures and are currently studying their applicability in this context.

SYMBOLS

β	ratio between stationary and mobile phase volumes
C_A	sum of the concentrations of a solute A in all its possible forms
δ	constant shift parameter included in some retention models
k	observed capacity factor
k_0	capacity factor of neutral species
k_0^w	capacity factor of neutral species in pure water
k_{-1}	capacity factor of negatively charged species
k_{-1}^w	capacity factor of negatively charged species in pure water
k_1	capacity factor of positively charged species
k_α	observed capacity factor of a solute at $\alpha\%$ of organic modifier
$k_{i,\alpha}$	capacity factor of a solute with charge i at $\alpha\%$ of organic modifier

k_i^0 $\ln k_i^0$ is the first coefficient of a polynomial model for $\ln k_i$ as a function of the fraction of organic modifier (constant pH)

$k_{m,n}$ capacity factor of H_mA_n

k^w observed capacity factor of a solute in water

K_a acidity constant of a monoprotic acid HA

K_a^0 $\ln K_a^0$ is the first coefficient of a polynomial model for $\ln K_a$ as a function of the fraction of organic modifier (constant pH)

K_a^w acidity constant of a monoprotic acid HA in pure water

K_A equilibrium constant for the partition of A^- between mobile and stationary phases

K_{HA} equilibrium constant for the partition of HA between mobile and stationary phases

$\kappa_{m,n}$ stoichiometric formation constant of H_mA_n

pH^O pH of a mixed eluent as measured with a glass electrode calibrated with aqueous buffers (operational pH)

pH^P pH of a mixed eluent as measured before mixing the buffer with the organic modifier (pragmatic pH)

pH^T thermodynamic pH

φ fraction of organic modifier in the mobile phase

Q_1, Q_2, Q_3 second, third and fourth coefficients, respectively, of a polynomial model for $\ln K_a$ as a function of the fraction of organic modifier (constant pH)

S slope of a linear model for $\ln k$ as a function of the fraction of organic modifier (constant pH)

$S([H])$ variation of the slope S with the acidity of the mobile phase

S_n second coefficient of a polynomial model for $\ln k_n$ as a function of the fraction of organic modifier (constant pH), or the n-degree coefficient of a polynomial model for minus S as a function of pH (constant φ)

SSQ sum of squares of the differences between calculated and observed values

t_0 hold-up time

T_n third coefficient of a polynomial model for $\ln k_n$ as a function of the fraction of organic modifier (constant pH), or the n-degree coefficient of a polynomial model for the variation of T in the model describing $\ln k$ as a function of the organic modifier concentration: $\ln k = \ln k_0 - S\varphi + T\varphi^2$

$t_{r,i}$ retention time of solute i

ACKNOWLEDGEMENTS

REFERENCES

1 P. J. Schoenmakers, *Optimization of Chromatographic Selectivity, A Guide to Method Development*, Elsevier, Amsterdam, 1986.
2 J. C. Berridge, *Chemometr. Intell. Lab. Syst.*, 3 (1988) 175.
3 L. R. Snyder, J. L. Glajch and J. J. Kirkland, *Practical HPLC Method Development*, Wiley, New York, 1988.
4 P. J. Schoenmakers, S. v. Molle, C. M. G. Hayes and L. G. M. Uunk, *Anal. Chim. Acta*, 250 (1991) 1.
5 E. P. Lankmayr, W. Wegscheider, J. Daniel-Ivad, I. Kolossvary, G. Csonka and M. Otto, *J. Chromatogr.*, 485 (1989) 557.
6 I. Molnar, R. Boysen and P. Jekow, *J. Chromatogr.*, 485 (1989) 569.
7 B. Vandeginste, R. Essers, Th. Bosman, J. Reijnen and G. Kateman, *Anal. Chem.*, 57 (1985) 1971.
8 P. Xu and X. Lu, *J. Chromatogr.*, 292 (1984) 169.
9 M. McCann, J. H. Purnell and C. A. Wellington, *Faraday Soc. Symp. Ser.*, 15 (1980) 82.
10 P. J. Schoenmakers, H. A. H. Billiet and L. de Galan, *J. Chromatogr.*, 218 (1981) 261.
11 G. Vigh, Z. Varga-Puchony, A. Bartha and S. Balogh, *J. Chromatogr.*, 241 (1982) 169.
12 E. P. Kroeff and D. J. Pietrzyk, *Anal. Chem.*, 50 (1978) 502.
13 M. D. Grieser and D. J. Pietrzyk, *Anal. Chem.*, 45 (1973) 1348.
14 C. Horváth, W. Melander and I. Molnar, *Anal. Chem.*, 49 (1977) 142.
15 D. J. Pietrzyk, E. P. Kroeff and T. D. Rotsch, *Anal. Chem.*, 50 (1978) 497.
16 D. W. Armstrong, G. L. Bertrand, K. D. Ward, T. J. Ward, H. V. Secor and J. I. Seeman, *Anal. Chem.*, 62 (1990) 332.
17 S. Deming and M. L. H. Turoff, *Anal. Chem.*, 50 (1978) 546.
18 P. R. Haddad, A. C. J. H. Drouen, H. A. H. Billiet and L. de Galan, *J. Chromatogr.*, 282 (1983) 71.
19 M. Otto and W. Wegscheider, *J. Chromatogr.*, 258 (1983) 11.
20 E. Grushka, P. R. Brown and N.-I. Yang, *Anal. Chem.*, 60 (1988) 2104.
21 M. Paabo, R. A. Robinson and R. G. Bates, *J. Am. Chem. Soc.*, 87 (1965) 415.
22 D. B. Rorabacher, W. J. MacKellar, F. R. Shu and S. M. Bonavita, *Anal. Chem.*, 43 (1971) 561.

23 R. G. Bates, *Determination of pH, Theory and Practice*, Wiley-Interscience, New York, 1973.
24 G. E. Berendsen, P. J. Schoenmakers, L. de Galan, G. Vigh, Z. Varga-Puchony and J. Inczedy, *J. Liq. Chromatogr.*, 3 (1980) 1669.
25 W. H. Press, B. P. Flannery, S. A. Teukolsky and W. T. Vetterling, *Numerical Recipes, The Art of Scientific Computing*, Cambridge University Press, Cambridge, 1986.

Computer simulation for the prediction of separation as a function of pH for reversed-phase high-performance liquid chromatography

I. Accuracy of a theory-based model

J. A. Lewis, D. C. Lommen, W. D. Raddatz, J. W. Dolan and L. R. Snyder*

LC Resources Inc., 2930 Camino Diablo, Walnut Creek, CA 94596 (USA)

I. Molnar

Institut für angewandte Chromatographie, Berlin (Germany)

ABSTRACT

Computer simulation software (DryLab I/mp) is described for predicting high-performance liquid chromatographic separation as a function of changes in mobile phase pH. Three experimental runs with pH (only) varied are used to derive values of pK_a plus capacity factors (k') for the ionized and non-ionized form of each ionizable solute. Various tests of the experimental data then allow classification of each solute as acidic, basic, neutral (including strong or weak acids or bases) and amphoteric. Experimental data are reported for the separation of several substituted anilines as a function of pH and solvent composition (%B). Experimental requirements for the accurate prediction of separation (*ca.* ± 2–4% in α) as a function of pH are discussed. The reliability of the software is demonstrated for three different samples: mixtures of (a) substituted benzoic acids, (b) substituted anilines and (c) catecholamine-related compounds.

INTRODUCTION

A considerable literature exists for resolution mapping in high-performance liquid chromatography (HPLC) method development [1,2]. In most instances, empirical fitting functions are used with a small number of experimental measurements in order to predict separation as a function of some mobile phase variable or variables. A well known example of this approach is the work of Glajch *et al.* [3] for mapping resolution as a function of mixtures of methanol, acetonitrile and tetrahydrofuran, based on only seven experimental runs. Sachok *et al.* [4] first decribed a similar approach for predicting separation as a function of pH and ion-pair reagent concentration.

The usual goal of resolution-mapping procedures is to achieve accurate predictions of separation for a reasonably broad range of conditions, with a minimum number of initial experimental runs. When only one variable is to be mapped, the number of required experiments may be reasonably small. However, the simultaneous variation of two or more variables leads to a rapid increase in the number of experiments that are necessary. This problem is exacerbated by a need for peak tracking [1,2], *i.e.*, the matching of bands for a given sample component among the various experimental runs.

We have recently developed a software package (DryLab I/mp) which allows the chromatographer to use computer simulation for the mapping of any mobile phase parameter, including temperature. In

this paper we examine the use of this software for predicting sample retention and separation as a function of mobile phase pH. In Part II [5] this discussion is extended to separation as a function of simultaneous change in pH and solvent strength (%B).

THEORY

General considerations

Resolution vs. retention: allowable errors in predicted values of α. Most comparisons of experimental data with predictions from resolution mapping emphasize the accuracy of predicted retention times for individual solutes. However, the chromatographer is usually more interested in accurate predictions of resolution, R_s, or *differences* in retention time. The effect on predicted values of resolution of a $\pm 3\%$ error in α is illustrated in Fig. 1 for two different (average) values of k': $k' = 1$ and 20. Gen-

erally, we aim for a resolution of $R_s = 1.5$ or greater, as in the example in Fig. 1. If the experimental separation is within ± 0.5 resolution units of the predicted value ($R_s = 1.5$), then computer simulation can be useful in method development. For $k' = 20$, a $\pm 3\%$ error in α results in an error in R_s of ± 0.4 units, *i.e.*, an acceptable prediction. For $k' = 1$, the error in R_s that results from a $\pm 3\%$ error in α is even smaller (only ± 0.2 units), and the allowable error in α for $k' = 1$ is about $\pm 7\%$. The fundamental resolution equation[2]

$$R_s = \tfrac{1}{4}(\alpha - 1) \, N^{1/2} \, [k'/(1 + k')] \qquad (1)$$

allows us to generalize the example in Fig. 1 as follows. For an acceptable error in R_s of ± 0.5 units, the allowable fractional error in α ($\delta\alpha$) is

$$\delta\alpha \approx 2 \, N^{-1/2} \, [(k' + 1)/k'] \qquad (2)$$

that is, the accuracy in predicted values of α become more important as (a) k' increases and (b) N be-
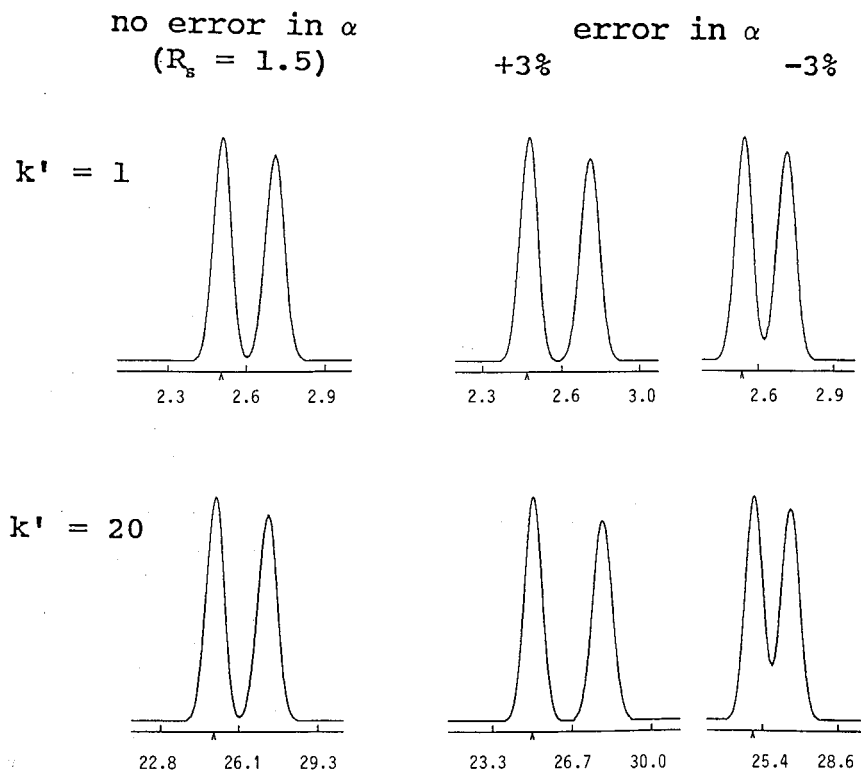

Fig. 1. Effect of error in the prediction of α on a resulting computer-simulated separation. A plate number of $N = 5000$ is assumed; the value of α ("no error") is 1.18 for $k' = 1$ and 1.09 for $k' = 20$.

comes larger (N = 5000 in the example in Fig. 1). Sample resolution is usually more critical for small values of k'; for representative values of k' = 2 and N = 10 000, eqn. 2 suggests that errors as large as ±4% in predicted values of α should be acceptable in the use of computer simulation for HPLC method development. However, when the column plate number is large, e.g., N = 20 000, the required accuracy of predicted values of α may increase significantly (e.g., allowable errors no larger than ±2%). The preceding analysis assumes that $\alpha \approx 1.0$, which will be the case for the critical (most overlapped) pair of bands in the chromatogram of a "difficult" separation.

Predicting retention as a function of pH

A general theory for the reversed-phase retention of monoprotic acidic or basic solutes as a function of pH is available [6–10]. It can be assumed that a given solute exists in ionized (±) and non-ionized (^{0}) forms, in which case the solute capacity factor value k' is given by

$$k' = k^0 (1 - F^{\pm}) + k^+ F^{\pm} \qquad (3)$$

where k^0 and k^+ refer to k' values for the non-ionized and ionic forms and $F^{\pm}$ is the fraction of solute molecules that are ionized. The fraction $F^{\pm}$ of ionized molecules is

$$F^+ = 1/\{1 + (K_a/[H^+])\} \qquad (4)$$

for the case of a basic solute and

$$F^- = 1/\{1 + ([H^+]/K_a)\} \qquad (5)$$

for an acidic compound.

Several studies [7,8,11] have compared experimental data for acidic solutes with eqns. 3 and 5 (corresponding comparisons for basic solutes with eqns. 3 and 4 are less common); data for a reasonably wide pH range were fitted to eqns. 3–5 with good agreement. However, significant deviations from theory sometimes occur, especially for pH values that are either $\gg pK_a$ or $\ll pK_a$. Resolution mapping has also been applied as a means of optimizing mobile phase pH in reversed-phase HPLC. Eqns. 3–5 [4,8,9,12], polynomial equations [13] or hybrid relationships [14] have been used as fitting functions. The use of eqns. 3–5 allows predictions of separation as a function of pH, based on three initial experiments [three unknowns exist for each solute: k^0, k^+ (or k^-) and K_a].

Potential errors in the use of eqns. 3–5. The use of eqns. 3–5 for mapping retention vs. pH is based on certain approximations. Error in predicted separations can be expected as a result of various effects:

(i) retention of solutes (especially protonated bases) by processes other than solvophobic interaction; e.g., interactions with exposed silanols or metal contaminants [15], whose pK_a or complexing constants can also vary with pH;

(ii) change in K_a values as a function of ionic strength; i.e., buffer concentration is usually maintained constant, but the fraction of the buffer that is ionized then varies with pH;

(iii) solvophobic effect of ionic strength on solute retention (hydrophobic interaction);

(iv) ion-pair interaction of sample ions with ionized buffer species;

(v) change in the microscopic nature (and sorption properties) of the stationary phase (C_8 or C_{18}) as a result of changing ionization of silanols;

(vi) a change in buffer type, when more than one buffer is needed to cover a given pH range.

Additional complications in pH mapping are presented by the presence of neutral, polybasic and/or amphoteric sample components [9,16]. A retention-mapping scheme must be able to recognize these various solute types and treat them differently. Finally, the retention of neutral species is in some instances dependent on sample pH, although this dependence is much less pronounced than for ionizable species. The questions then are the extent to which eqns. 3–5 are useful for mapping resolution vs. pH, assuming only three experimental runs as a starting point, and the means that can be used to avoid major errors as a result of this approach.

Software development

Identifying solute type. Prior to the use of eqns. 3–5 for mapping retention vs. pH, it is necessary to distinguish among four possible situations, as summarized in Fig. 2. From the experimental retention times of a solute at three different pH values, it is possible to recognize each solute type: acid, base, amphoteric or neutral. The use of retention data for this purpose is complicated, however, by various effects, including experimental error in these retention time measurements. As seen in the idealized plot of retention vs. pH for the basic solute in Fig. 3, the major change in solute retention (and resulting
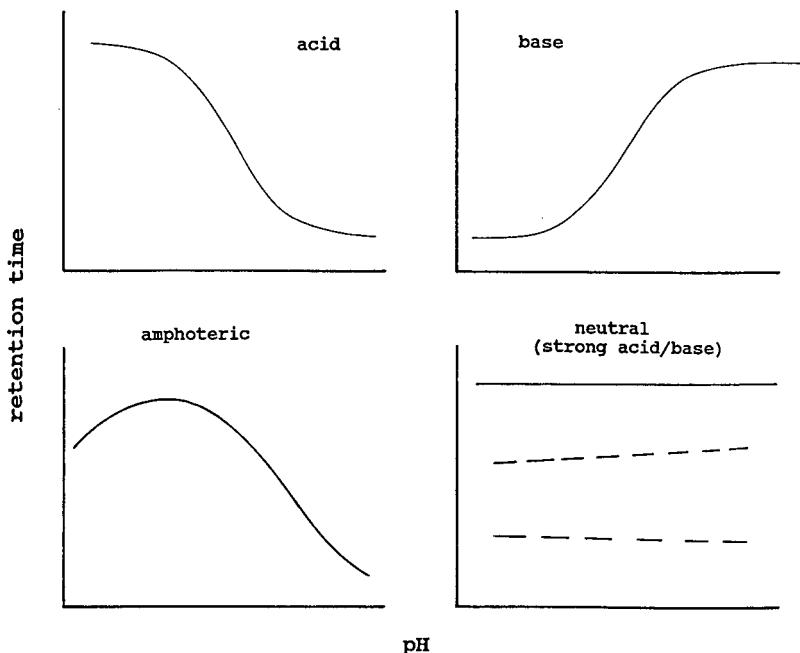
Fig. 2. Illustration of the dependence of retention time on pH for different solute types.

values of α) occurs for pH values that are close to the pK_a value of the solute. For this reason, pH values that bracket the pK_a range of the sample offer the greatest opportunity for varying selectivity and optimizing separation. The open circles in Fig. 3 represent possible experimental data to be used as input for computer simulation. Derived values of K_a, k^+ and k^0 will be most accurate when the experimental input data bracket the pK_a value of the solute, *e.g.*, pH range B in Fig. 3 or pH = 3, 4 and 5 in this example (pK_a = 4).

Retention data collected in pH ranges A or C in Fig. 3 may not be accurate enough to use for deriving values of K_a, k^+ and k^0, as small errors in retention can result in large errors in the derived solute parameters and in related predictions outside this pH range. Further, it may not be possible to distinguish acidic or basic solutes from neutral compounds when there is little change in retention as the pH is varied. For this reason, it is necessary to set up test conditions that arbitrarily assign different solutes to different groups (acid, base, neutral, etc.) on the basis of changes in retention with pH. This is discussed further in the Appendix.

EXPERIMENTAL

Equipment and software

An LC Analyst Expert Method Development System (Perkin-Elmer, Norwalk, CT, USA) was used to carry out the HPLC experiments. Computer simulations were performed with DryLab I/mp
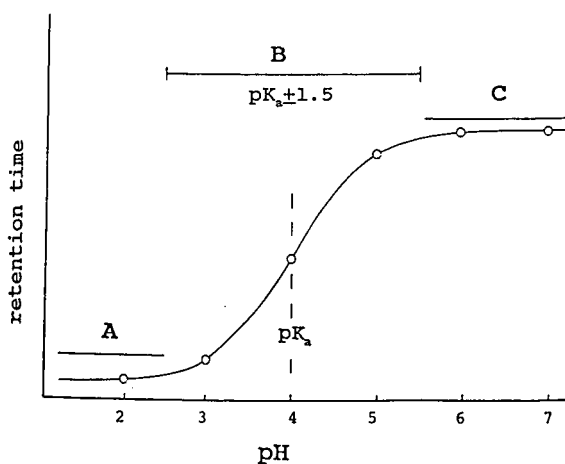

Fig. 3. Retention time *vs.* pH for a basic solute: effect of experimental pH values on accuracy of predicted separation.

TABLE I

RETENTION TIMES FOR SUBSTITUTED ANILINES AS A FUNCTION OF pH AND METHANOL CONCENTRATION

Conditions: 25 × 0.46 cm I.D. StableBond CN column; methanol–buffer mobile phases, 25 mM sodium citrate (pH ⩾ 4.0) or potassium phosphate buffer (pH < 4.0); flow-rate, 1 ml/min; temperature, 35°C.

Methanol concentration (%)	pH	Retention time (min)[a]									
		A	B	C	D	E	F	G	H	I	J
25	2.00	2.84	3.01	5.84	7.19	3.58	4.27	3.60	3.01	13.84	29.03
	2.25	2.93	3.13	6.80	8.54	3.94	5.09	3.92	3.15	18.09	33.8
	2.50	3.13	3.43	8.22	10.43	5.00	6.95	4.30	3.40	24.85	39.1
	2.75	3.13	3.52	8.71	11.09	5.80	8.21	4.46	3.51	28.19	40.7
	3.00	3.28	3.80	9.13	11.57	6.86	9.52	4.85	3.71	30.25	41.30
	3.25	3.31	4.04	9.35	11.88	8.11	10.68	5.35	3.90	32.68	42.94
	3.50	3.53	4.58	9.42	12.12	9.54	11.79	6.23	4.39	33.41	42.67
	4.00	3.85	5.53	9.75	12.39	11.54	12.87	8.26	5.56	34.63	43.32
	4.50	4.75	7.33	9.64	12.49	12.52	13.44	10.88	8.74	34.35	42.25
	5.00	5.67	8.36	9.80	12.59	13.11	13.77	13.10	11.77	35.15	43.13
	5.50	6.59	8.98	9.87	12.73	13.37	13.94	14.39	14.2	35.50	43.52
	6.00	7.07	9.31	10.05	12.97	13.65	14.19	15.15	15.5	36.38	44.57
	6.50	7.28	9.47	10.16	13.14	13.82	14.36	15.54	15.9	36.98	45.30
35	2.0	2.59	2.77	5.19	6.29	3.308	4.02	3.08	2.77	10.84	18.92
	2.5	2.90	3.16	6.41	8.02	4.753	6.33	3.65	3.09	16.41	22.56
	3.0	3.05	3.55	6.66	8.36	6.228	7.80	4.21	3.41	17.85	22.66
	3.5	3.19	4.38	6.78	8.58	7.903	8.86	5.63	4.24	19.12	23.58
	4.0	3.68	5.14	6.86	8.69	8.719	9.27	6.56	5.41	19.08	23.25
	4.5	4.20	5.91	6.67	8.50	8.665	9.07	7.90	7.27	18.25	22.14
	5.0	4.73	6.40	6.79	8.70	8.929	9.40	9.00	8.80	18.84	22.86
	5.5	5.11	6.70	6.83	8.73	9.081	9.40	9.40	9.83	19.03	23.09
	6.0	5.30	6.82	6.93	8.89	9.252	9.59	9.73	10.32	19.51	23.70
	6.5	5.36	6.92	6.97	8.96	9.321	9.71	9.88	10.51	19.72	23.95

[a] Solutes: A, 4-methoxyaniline; B, 3-methylaniline; C, 3-cyanoaniline; D, 2-chloroaniline; E, 4-chloroaniline; F, 3-chloroaniline; G, 3,5-dimethylaniline; H, N-ethylaniline; I, 3,4-dichloroaniline; J, 3,5-dichloroaniline.

software (LC Resources, Lafayette, CA, USA). This program allows the user to begin with a single isocratic experiment and then map separation as a function of different experimental conditions with one or two additional runs for each parameter (e.g., percent organic component, ternary solvent mixtures, temperature, pH, ion-pair reagent or buffer concentrations).

Materials and procedures

All solvents were of HPLC grade (Burdick & Jackson, Muskegon, MI, USA). The substituted-aniline sample (Table I) was formulated from compounds supplied by Aldrich (Milwaukee, WI, USA). StableBond CN and C_8 columns (25 × 0.46 cm I.D.) MacMod Analytical, Chadds Ford, PA,

USA) were used. These new stationary phases are synthesized by the reaction with silica of a sterically protected, monofunctional silane: ClSi(i-$C_3H_7)_2(CH_2)_3CN$ or ClSi(i-$C_3H_7)_2(CH_2)_3C_8$. The silica contains undetectable amounts (<1 ppm) of heavy metals such as iron or aluminium and is processed so as to avoid the presence of "acidic" silanols [17,18].

All separations were carried out at 35°C with a flow-rate of 1.0 ml/min. UV detection at 255 nm was used. The mobile phase was formulated from methanol (B) plus aqueous buffer. The buffer was variously 25 mM sodium citrate (pH 4–6.5) or 25 mM sodium phosphate (pH 2–4). When a change in mobile phase pH was made, equilibration with the new mobile phase was carried out for at least 20 min

(eight column volumes) before injecting the next sample. An equilibration time of 10 min was found to achieve 95% equilibration (as measured by retention time values) for a change in pH from 3 to 6 for the substituted-aniline sample; smaller changes in pH from run to run were the rule.

The precision of reported values of retention time and α was determined from replicate separations during the time the data in Table I were collected. Retention times were repeatable within ± 0.8% (1 S.D.) and values of α had a precision of ± 1.5% (1 S.D.).

RESULTS AND DISCUSSION

Accuracy of computer simulation for a change in mobile phase pH

Assume that three mobile phases of different pH ($pH_1 < pH_2 < pH_3$) are selected for the initial experimental runs with a given sample; we need to know the likely error in predicted values of α for other pH values. In this way, computer simulations can be restricted to a range in pH that allows sufficiently accurate predictions. Presumably the error in the predicted values of α will depend on the values of pH_1, pH_2 and pH_3.

Returning to Fig. 3, assume that the pH values for the initial experimental runs are 3, 4 and 5. There will then be some error in the predicted values of α for other pH values. In general, predictions should be more reliable for the case of interpolation ($3 < pH < 5$) than for extrapolation (pH < 3 or > 5). Similarly, as the difference between pH_3 and pH_1 becomes smaller, interpolation should become more accurate and extrapolation less accurate. The most useful predictions will generally be possible when $pH_2 \approx pK_a$ for a given solute, as in this pH region α and resolution usually change the most as pH is varied.

Substituted aniline sample. A mixture of ten substituted anilines was used as sample for these studies. The mobile phase pH was varied from 2 to 6.5 in 0.25- or 0.50-unit increments for mobile phases that contained either 25 or 35% methanol. Table I summarizes the retention data for each of these sample components, using a StableBond CN column. A 25 m*M* phosphate buffer was used to control pH for pH < 4.0, and citrate buffer was used for higher pH values. Retention times (t_R) for pH =

4.00 (25% and 35% methanol) were similar for either citrate or phosphate buffer. Thus, we observed that at pH 4.0

$$t_R \text{ (phosphate)} = 1.02 \, t_R \text{ (citrate)} \qquad (6)$$

within ±2% (1 S.D.). At pH 3.0, there was a greater deviation between retention times for the two buffers:

$$t_R \text{ (phosphate)} = 1.11 \, t_R \text{ (citrate)} \qquad (7)$$

within ±6% (1 S.D.). The greater difference in retention at lower pH for citrate *vs.* phosphate buffers is expected, as the sample becomes significantly ionized at pH < 4.

Our present software was used with these data to predict separation (resolution, retention times, etc.) and values of α. Input data were selected for three pH values, and values of α for other pH values were subsequently obtained by computer simulation. Predicted and experimental results were then com-

TABLE II

PREDICTED *vs.* EXPERIMENTAL SEPARATION OF SUBSTITUTED ANILINE SAMPLES

Conditions as in Table I, except pH = 3.5 and 25% B. Computer simulation based on input data for pH of 3, 4 and 5.

Solute[a]	Retention time (min)		α		pK_a
	Expt.	Calc.	Expt.	Calc.	
4-Methoxy	3.54	3.47	1.88	1.95	4.54
N-Ethyl	4.40	4.33	1.10	1.07	4.15
3-Methyl	4.58	4.46	1.82	1.91	Neutral[b]
3,5-Dimethyl	6.24	6.19	1.86	1.91	Neutral[b]
3-Cyano	9.42	9.46	1.02	1.03	3.26
4-Chloro	9.54	9.65	1.32	1.31	2.96
3-Chloro	11.8	11.8	1.03	1.02	4.08
2-Chloro	12.1	12.0	3.21	3.25	4.55
3,4-Dichloro	33.2	33.3	1.31	1.30	Acid[c]
3,5-Dichloro	42.6	42.4			Neutral[b]
Av. error		±1%		±2%	

[a] Substituent on aniline listed, *e.g.*, 4-methoxyaniline.
[b] DryLab I/mp classifies solute as a neutral species as described in the Appendix.
[c] Data cannot be fitted to eqns. 3–5; linear-segment fit to data.

pared in order to assess the accuracy of computer simulation. This procedure is illustrated in Table II.

The data of Table II show good agreement between experimental and predicted retention times (±1%) and values of α (±2%). Fig. 4 compares the predicted and actual separations for pH 3.5 and 25% B. In this example, the accuracy of predicted values of α is excellent. [Note also that three solutes are classified as "neutral", because retention did not change much with pH. Also, one solute (3,4-dichloroaniline) required adjustment of the experimental retention times (by the computer) in order to obtain a fit of the data to eqns. 3–5; see the discussion in the Appendix]. The procedure in Table II was re-
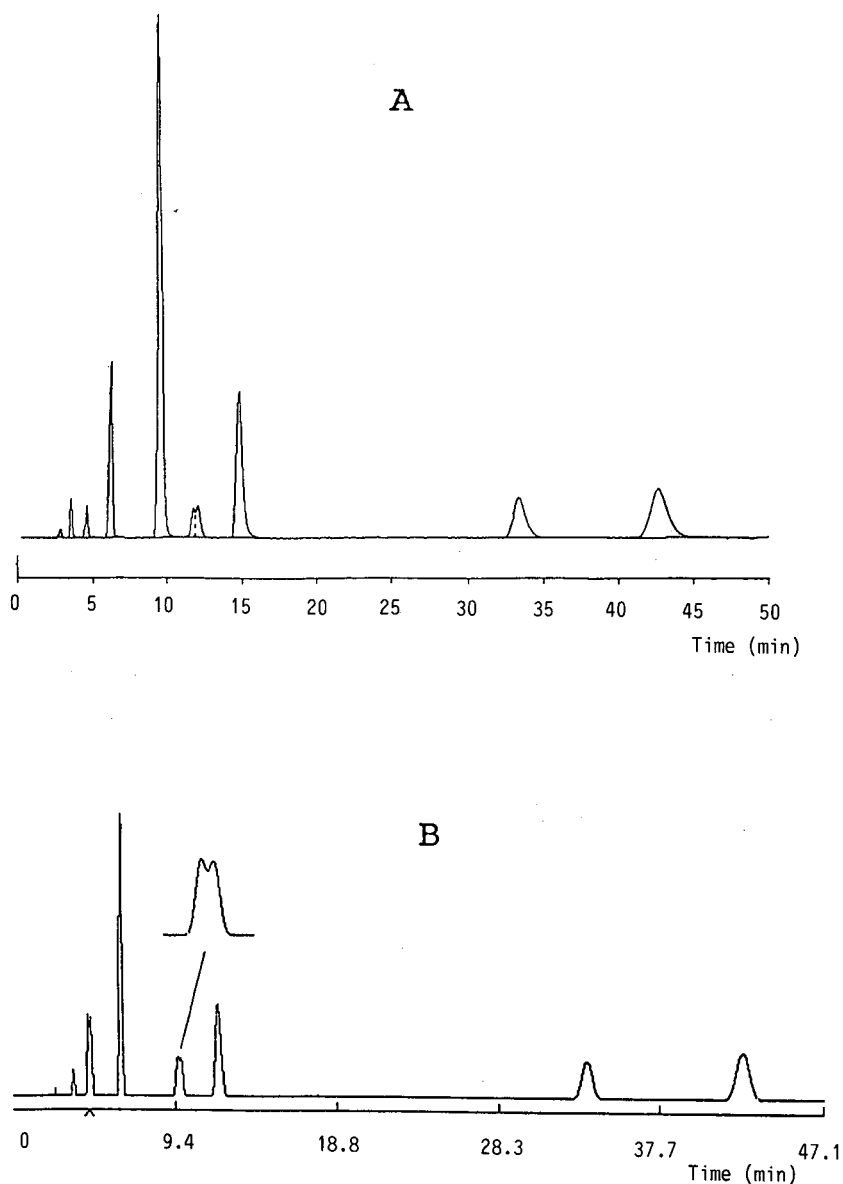
Fig. 4. Experimental and predicted chromatograms for separation of a substituted aniline sample. Conditions as in Table II (pH 3.5, 25% B).

TABLE III

SUMMARY OF EXPERIMENTAL *vs.* SIMULATED RETENTION DATA FOR SUBSTITUTED ANILINES (AS IN TABLE II)

Based on experimental data in Table I (25% and 35% B data averaged together).

ΔpH	Error in retention time (%)					Error in α (%)				
	Int.	Extrapolated[a]				Int.	Extrapolated[a]			
		−1.0	−0.5	0.5	1.0		−1.0	−0.5	0.5	1.0
0.5	—		25	7				13	10	
1.0	1	21	4	3	8	2	15	8	8	21
2.0	2	23	8	2	4	2	15	8	3	6
3.0	2		23	2	4	3	15	2	2	
4.0	7					5				

[a] Numbers (−1.0, −0.5, etc.) refer to extrapolation range; *e.g.*, if pH_1 is 3.0, −0.5 refers to a pH of 2.5.

peated for various combinations of input runs and for different pH values for the predicted separation, *e.g.*, pH 2, 3 and 4 for input runs with prediction of separation for pH = 2.25, 2.5, 2.75, 3.25, etc. Table III summarizes the results of these computer simulations as a function of (a) the range of pH values used as input ($ΔpH = pH_3 − pH_1$) and (b) whether interpolation or extrapolation was used to obtain the predicted separation.

The data in Table III for the substituted anilines show that interpolated values of α are accurate to better than ±3% (values of α were generally less reliable when $k' < 1$ for one or both bands; data for $k' < 1$ are not included in the summaries in Tables III and IV, because $k' > 1$ for all solutes is a general goal of method development [19]), when ΔpH is no greater than 3.0. For ΔpH = 4 the accuracy of interpolated predictions is ±5%, which is marginal for the use of computer simulation as an aid in HPLC method development. This is intuitively reasonable. For extrapolation to higher values of pH, small values of ΔpH give unacceptable accuracy in α (±8–10%) for an extrapolation of 0.5 units, while an extrapolation of 1 unit gives even larger errors (6–21%). Extrapolation to lower pH values is in every instance unreliable, yielding errors of 8% or larger in α for extrapolation by −0.5 units or more. The reason for the poorer predictions when extrapolating to lower pH values (and lower retention times) is the result of several factors: generally

smaller values of k', larger changes in k' and α for this sample and a failure of eqns. 3–5 to apply exactly. The accuracy of simulated separations was generally better at pH values which correspond to decreased ionization of the sample.

To conclude, the data in Table III for this aniline sample suggest that ΔpH should be no larger than 3 pH units for this sample, interpolated predictions of

TABLE IV

SUMMARY OF EXPERIMENTAL *vs.* SIMULATED RETENTION DATA FOR SUBSTITUTED BENZOIC ACIDS (AS IN TABLE III)

Based on experimental data in ref. 6.

ΔpH	Error in retention time (%)		Error in α (%)	
	Int.	Extrapolated[a]	Int.	Extrapolated[a]
Without phthalic acid				
1.6	—	7	—	3
1.2	1	4	0	2
1.8	1	—	1	—
With phthalic acid[b]				
0.6	—	11	—	6
1.2	2	7	1	7
1.8	2	—	3	—

[a] Extrapolated 0.3–0.6 pH units.
[b] Retention time data for all solutes averaged together under "with phthalic acid" category.

α will then be reliable to ±2% and extrapolation is only recommended for pH values that are higher (by no more than 1.0 pH unit) than the pH values used as input for computer simulation.

Substituted benzoic acid sample. We have previously reported retention *vs.* pH data [6] for several substituted benzoic acids, similar to the data of Table I for the substituted anilines. The pH range covered in that study [6] was 2.6–4.4, in increments of 0.3 pH units. Table IV summarizes the application of computer simulation to these data, as in Table III for the anilines. Errors in predicted retention times range from 1 to 7% for all monoprotic solutes, including both interpolated retention times and values extrapolated by as much as 0.6 pH units. Predicted values of α are of greater interest: if phthalic acid is excluded, interpolated values of α are predicted with an average accuracy of ±1%, *i.e.*, quite good. Values of α obtained by extrapolation by as much as ±0.6 pH units are also reliable (±2–3%), in contrast to the case with the aniline sample.

Phthalic acid is a diprotic solute (pK_a values of 2.9 and 5.4) and as such its retention should not be described exactly by eqns. 3–5 (for pH values outside the range 2.9–5.4, the fit of retention data for phthalic acid to eqns. 3–5 should be better). The errors in predicted values of α (based on eqns. 3–5) for band pairs that include phthalic acid are generally about three times greater than for the remaining substituted benzoic acids in Table IV. This means that interpolated α-values are predicted with an accuracy of ±1–3%, depending on the value of ΔpH, which is acceptable for purposes of method development. Computer simulation based on extrapolation appears to be unreliable in the case of phthalic acid. By analogy we assume that this will also be true for other polyprotic acidic solutes.

Catecholamine metabolites. Data for the retention of seven catecholamine solutes as a function of pH are reported in ref. 20. Over the pH range 2.5–5.5, three of these compounds behave as acids (retention decreasing with pH) and the remaining four compounds are neutral. These data could be used to assess the accuracy of computer simulation, as in the prior examples summarized in Tables III and IV. An example is provided in Table V, and a summary as in Tables III and IV is given for the catecholamines in Table VI.

The nature of the solute (acidic or neutral) was

TABLE V

PREDICTED *vs.* EXPERIMENTAL SEPARATION OF CATECHOLAMINE METABOLITES

Conditions as in ref. 20, except pH = 3.0. Simulation based on input data for pH of 2.5, 3.5 and 4.5.

Solute[a]	Retention time (min)		α		pK_a
	Expt.	Calc.	Expt.	Calc.	
NA	1.56	1.55	3.20	3.21	Neutral
DA	2.94	2.91	2.23	2.29	Neutral
α-MDA	5.42	5.48	1.20	1.18	Neutral
DOPAC	6.32	6.31	1.24	1.25	Acid
5-HT	7.59	7.68	1.76	1.71	Neutral
5-HIAA	12.66	12.45	1.42	1.45	Acid
HVA	17.62	17.59			Acid

[a] NA = Noradrenaline; DA = Dopamine; α-MDA = α-methyldopamine; DOPAC = 3,4-dihydroxyphenylacetic acid; 5-HT = 5-hydroxytryptamine; 5-HIAA = 5-hydroxyindoleacetic acid; HVA = homovanillic acid.

correctly identified in every case (see Table V). The data in Table VI show that acceptable accuracy is obtained for interpolated values of α, when ΔpH < 3, but extrapolated values of α are at best marginally reliable. These results are probably representative of what can be expected by the average chromatographer.

Other errors. The components of the substituted aniline and benzoic acid samples are known to consist of either acids or bases. When the mobile phase

TABLE VI

SUMMARY OF EXPERIMENTAL *vs.* SIMULATED RETENTION DATA FOR CATECHOLAMINES (AS IN TABLE III)

Based on experimental data in ref. 20.

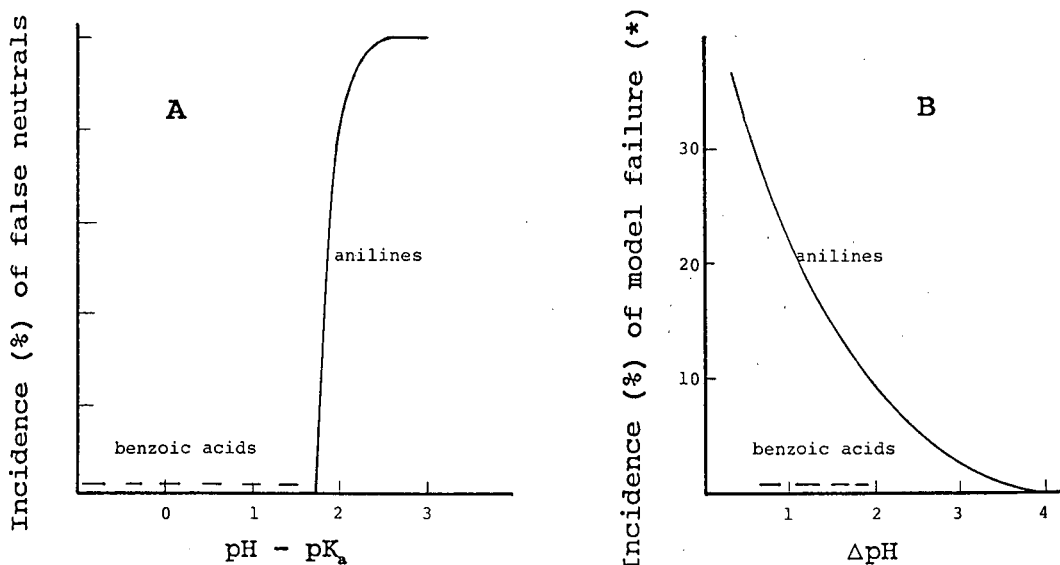| ΔpH	Error in α (%)	
	Int.	Extrapolated[a]
1.0	–	6
2.0	1	6
3.0	3	–

[a] Extrapolation by ±0.5 pH units.

Fig. 5. Error rate in the application of computer simulation to the substituted aniline and benzoic acid samples. (A) Incidence of "false neutrals" as a function of pH; (B) incidence of error flags (*) as a function of ΔpH.

pH is far removed from the pk_a of a solute, the present software will classify that compound as neutral. We determined the incidence of "false neutrals" in these two samples as a function of pH − pK_a, as summarized in Fig. 5A. The pH range over which the benzoic acids were studied was not sufficiently different from the pK_a values of these compounds to result in any "false neutrals". With the aniline sample, where pH was varied over wider limits, a sharp rise in the incidence of "false neutrals" is seen when pH − pK_a exceeds 1.8. This is expected from the discussion of Fig. 3.

When a compound has been classified as either an acid or a base, but the experimental retention data cannot be fitted to eqns. 3–5 without adjustment (Appendix), DryLab I/mp flags these data with an asterisk. The incidence of error flags (asterisk) as a function of ΔpH is indicated in Fig. 5B for both the benzoic acid and aniline samples. It is seen that these errors are much more frequent for the aniline sample than for the benzoic acids. This observation together with the lower accuracy of predicted separations for the anilines suggests that computer simulation may be generally less reliable with basic samples (if the model of eqns. 3–5 is used). We also see in Fig. 5B that error flags become less frequent as ΔpH increases. The data in Tables III–V in conjunction with Fig. 5B suggest that ΔpH

values between 1 and 3 are preferred for the most reliable predictions based on computer simulation (and eqns. 3–5). Smaller values of ΔpH make peak tracking easier, whereas larger ΔpH values allow computer simulation to be used over a wider range of pH values.

DryLab I/mp informs the user when a predicted separation for a requested pH value is likely to be unreliable, because of excessive extrapolation or the use of initial data with too large a value of ΔpH. Without these or similar computer advisories, the use of computer simulation (*i.e.*, based on eqns. 3–5 with three input runs) for the optimization of mobile phase pH is likely to be a frustrating experience for the user.

Derived values of pK_a: selection of the optimum pH range

A knowledge of the pK_a values of the components of a sample can be useful for a number of reasons, especially as an aid in selecting experimental conditions during method development [19]. If the initial three runs required for predictions of separation as a function of pH are found not to bracket the pK_a values of the sample, the predicted values of pK_a (from the first simulation) can be used to guide further experimentation: one or more additional runs with pH varied can be used to expand the pH

range accessible to accurate computer simulation. The question then arises of how accurate these predicted values of pK_a are. We can examine this question in two different ways: (a) by testing the consistency of pK_a values predicted from different sets of input data (different values of pH_1, pH_2 and pH_3) and (b) by comparison of derived values of pK_a with literature values.

Consistency of predicted values of pK_a. Table VII summarizes values of pK_a derived via computer simulation for the various benzoic acid samples. The pH values selected for the input data vary as shown. It is seen that the pK_a values predicted on the basis of runs with different pH (values of pK_1, pK_2, pK_3) are in reasonable agreement (± 0.1–0.2 units), except for 2-nitrobenzoic and phthalic acids. The larger variation in the pK_a values for phthalic acid is expected, as the model of eqns. 3–5 is not applicable to this diprotic acid. The greater imprecision of predicted pK_a values for the case of 2-nitrobenzoic acid is also expected; the pH range used for the initial experimental runs does not overlap the (low) pK_a value of this compound, and k' values for this compound are generally small ($0.5 < k' < 2$).

Values of pK_a for the anilines in Table VI show greater variability than for the benzoic acids. There are also more cases where the model of eqns. 3–5 does not fit the input data (shown as footnote c in Table VII). This reflects the lower accuracy of predicted retention data for the substituted anilines *vs.* benzoic acids, as seen earlier in Tables III and IV.

Accuracy of predicted values of pK_a

Table VII lists approximate values of pK_a for the various substituted anilines ("Lit."), as estimated from data in refs. 21 and 22. The overal agreement between pK_a values predicted by computer simulation (eqns. 3–5) and these literature estimates is fairly good (± 0.4 units). This is probably no worse than the uncertainty of these literature estimates, which are based on (1) the Hammett σ–ρ relationship and (2) approximations of the effect or %B on pK_a.

CONCLUSIONS

Computer simulation based on a theoretical model (eqns. 3–5) is able to predict accurately retention and resolution for acidic and basic solutes as a

TABLE VII

VALUES OF pK_a FOR SUBSTITUTED ANILINES AND BENZOIC ACIDS AS DETERMINED FROM EQNS. 3–5

Compound[a]	pK_a[b] for indicated value of pH_2				
	3.2	3.5	3.8	S.D.	Lit.[e]
2-Nitrobenzoic acid	2.3	2.8	3.1	± 0.4	2.2
Phthalic acid	2.9	3.2	3.6	± 0.4	2.9
Impurity	3.3	3.5	3.5	± 0.1	
2-Fluorobenzoic acid	3.5	3.6	3.7	± 0.1	
3-Cyanobenzoic acid	3.4	3.5	3.6	± 0.1	
2-Chlorobenzoic acid	3.0	3.2	3.3	± 0.2	2.9
3-Nitrobenzoic acid	3.3	3.4	3.5	± 0.1	3.5
3-Fluorobenzoic acid	3.8	$-$[c]	3.9	± 0.1	
2,6-Dimethylbenzoic acid	3.4	3.6	3.6	± 0.1	

	pK_a[b] for indicated value of pH_2			
	3.0	4.0	5.0	Lit.[d]
4-Methoxyaniline	3.3	4.5	4.7	3.9
3-Methylaniline	3.6	4.1	4.4	4.3
3-Cyanoaniline	2.1	$-$[c]	$-$[c]	2.3
2-Chloroaniline	2.1	$-$[c]	$-$[c]	$-$
4-Chloroaniline	3.3	3.3	$-$[c]	3.6
3-Chloroaniline	2.9	3.0	$-$[c]	3.1
3,5-Dimethylaniline	3.7	4.1	4.3	3.8
N-Ethylaniline	3.7	4.5	4.6	$-$
3,4-Dichloroaniline	2.3	$-$[c]	$-$[c]	2.5
3,5-Dichloroaniline	2.0	$-$[c]	$-$[c]	2.1
Average difference (Lit. $-$ calc.) ± 0.4				

[a] Conditions: benzoic acids, see Table IV; anilines, cyano column, 25% B.
[b] Benzoic acids: $\Delta pH = 1.2$; *e.g.*, for $pH_2 = 3.2$, $pH_1 = 2.6$, $pH_3 = 3.8$. Anilines, $\Delta pH = 2.0$.
[c] DryLab I/mp did not accept a fit to eqns. 1–3.
[d] Literature values; data from ref. 21 (water as solvent) corrected for 25% methanol–water (ref. 22).
[e] Uncorrected literature values (in water, 25°C) [23].

function of pH. Three experimental runs with only pH varying are required as input for computer simulation. The most reliable predictions of retention are obtained for interpolations of the initial three experimental runs, and it is recommended that these runs span a range of no more than 2–3 pH units. Predicted retention time and α values were significantly more accurate for the case of acidic solutes (benzoic acids) than basic solutes (anilines). This

may be due to silanol effects, which play a more important role with basic solutes. The effective use of computer simulation for the prediction of separation as a function of pH requires that the computer flags predictions of marginal accuracy and recommends additional experimental data for more reliable predictions.

SYMBOLS

Symbols used in this paper and Part II [5] are summarized here.

A, B, C	constants in eqn. 1 in Part II
B	organic solvent used in the mobile phase (%B refers to solvent strength)
DMA	3,5-dimethylaniline
F^+, F^-	fraction of solute molecules that carry a positive or negative charge
$[H^+]$	hydrogen ion concentration
I/mp	isocratic, multi-parameter program for computer simulation
k'	solute capacity factor
$k°, k^+, k^-$	values of k' for non-ionized, positively charged, and negatively charged solute molecules, respectively
k_w	value of k' for water as mobile phase; see eqn. 2 in Part II
K_a	ionization constant for an acidic or basic solute
N	column plate number
pH_1, pH_2, pH_3	values of pH for mobile phases in initial experimental runs for pH mapping; $pH_1 < pH_2 < pH_3$
R_s	resolution of two adjacent bands
S	parameter that measures the change in solute retention as a result of change in %B (eqn. 2 in Part II)
$S°$	value of S for the non-ionized solute
t_R	solute retention time (min)
X, Y	hypothetical solutes in Fig. 8 in Part II
α	separation factor for two adjacent bands
$\delta\alpha$	error in a predicted value of α from computer simulation (eqn. 2)
ΔpH	pH range covered by initial experimental data used for pH mapping; equal to $pH_3 - pH_1$
φ	volume fraction of organic solvent in the mobile phase; equal to $0.01 \cdot$ %B

APPENDIX

DryLab I/mp Software

The DryLab I/mp software assigns different solutes to the various categories (acid, base, neutral, amphoteric) on the basis of retention times for a given solute at each of three pH values. Strong acids or bases, which exhibit little change in retention over the pH range 2–7, are classified as neutrals for the purpose of computer simulation. For solutes that are not classified as acidic or basic, DryLab I/mp uses a parabolic fit to the data for retention *vs.* pH. Solutes that are classified as acids or bases are fitted by eqns. 3–5.

The use of eqns. 3–5 for computer simulation is sensitive to errors in retention time or pH[a] for the input experimental data, resulting in some instances in negative values of k^+ or imaginary values of K_a. The present software assumes that small errors in retention time or mobile phase pH are likely. When unacceptable values of K_a, k^+ or $k°$ are encountered, the pH value of the intermediate mobile phase is adjusted by ± 0.01 increments, until acceptable values of the solute parameters are obtained for all components of the sample. If no pH

---

[a] It should be noted that the measurement of mobile phase pH values with an accuracy of better than ± 0.05–0.1 unit is not always achieved in routine practice. This problem is considerably more serious if the pH of the final mobile phase (including organic solvent) is measured, compared with the recommended practice of measuring the pH of the aqueous buffer followed by addition of organic solvent. By taking special precautions, an accuracy of ± 0.02 pH units was achieved in this study. See also the discussion in ref. 14.

gives acceptable solute parameter values for all components, or if the required adjustment in pH is > -0.1 unit, problem solutes are flagged and a parabolic fit is used as with neutral of amphoteric solutes.

REFERENCES

1 P. J. Schoenmakers, *Optimization of Chromatographic Selectivity*, Elsevier, Amsterdam, 1986.
2 J. L. Glajch and L. R. Snyder (Editors), *Computer-Assisted Method Development for High-Performance Liquid Chromatography*, Elsevier, Amsterdam, 1990.
3 J. L. Glajch, J. J. Kirkland, K. M. Squire and J. M. Minor, *J. Chromatogr.*, 199 (1980) 57.
4 B. Sachok, R. C. Kong and S. N. Deming, *J. Chromatogr.*, 199 (1980) 317.
5 J. A. Lewis, L. R. Snyder and J. W. Dolan, *J. Chromatogr.*, 592 (1992) 197.
6 J. W. Dolan, D. C. Lommen and L. R. Snyder, *J. Chromatogr.*, 535 (1990) 55.
7 Cs. Horváth, W. Melander and I. Molnar, *Anal. Chem.*, 49 (1977) 142.
8 S. N. Deming and M. L. H. Turoff, *Anal. Chem.*, 50 (1978) 546.
9 F. Szokoli, Zs. Nemeth and J. Inczedy, *Chromatographia*, 29 (1990) 265.
10 B. Rittich and M. Pirochtova, *J. Chromatogr.*, 523 (1990) 227.
11 L. R. Snyder, J. W. Dolan and D. C. Lommen, *J. Chromatogr.*, 535 (1990) 75.
12 C. Herrenknecht, D. Ivanovic, E. G.-Nivaud and M. Guernet, *J. Pharm. Biomed. Anal.*, 8 (1990) 1071.
13 W. Lindberg, E. Johansson and K. Johansson, *J. Chromatogr.*, 211 (1981) 201.
14 R. M. L. Marques and P. J. Schoenmakers, *J. Chromatogr.*, 592 (1992) 157.
15 M. A. Stadalius, J. S. Berus and L. R. Snyder, *LC · GC*, 6 (1988) 494.
16 M. Patthy, T. Balla and P. Aranyi, *J. Chromatogr.*, 523 (1990) 201.
17 J. Kohler and J. J. Kirkland, *J. Chromatogr.*, 385 (1986) 125.
18 J. Kohler, D. B. Chase, R. D. Farlee, A. J. Vega and J. J. Kirkland, *J. Chromatogr.*, 352 (1986) 275.
19 L. R. Snyder, J. L. Glajch and J. J. Kirkland, *Practical HPLC Method Development*, Wiley-Interscience, New York, 1988.
20 M. Patthy and R. Gyenge, *J. Chromatogr.*, 449 (1988) 191.
21 L. P. Hammett, *Physical Organic Chemistry*, McGraw-Hill, New York, 1940, pp. 188–189.
22 B. L. Karger, J. N. LePage and N. Tanaka, in Cs. Horváth (Editor), *High-Performance Liquid Chromatography —Advances and Perspectives*, Vol. 1, 1980, p. 113.
23 *Handbook of Chemistry and Physics*, Chemical Rubber Co., Cleveland, OH, 52nd ed., 1972, D-117, D-120.

CHROMSYMP. 2441

Computer simulation for the prediction of separation as a function of pH for reversed-phase high-performance liquid chromatography

II. Resolution as a function of simultaneous change in pH and solvent strength

J. A. Lewis, J. W. Dolan and L. R. Snyder*

LC Resources Inc., 2930 Camino Diablo, Walnut Creek, CA 94596 (USA)

I. Molnar

Institut für angewandte Chromatographie, Berlin (Germany)

ABSTRACT

The optimization of reversed-phase high-performance liquid chromatographic separation by the simultaneous variation of pH and solvent strength (%B) was studied for acidic (substituted benzoic acids) and basic samples (substituted anilines). The combination of these two variables was expected to be more useful than either variable alone. This proved to be the case for the benzoic acid sample, but not for the aniline sample. Column plate numbers were also studied for each sample and as a function of pH. With the exception of one compound (3,5-dimethylaniline) in one particular pH range (3.0–4.5), plate numbers of 12 000–20 000 were observed for each sample.

INTRODUCTION

In Part I [1] we discussed the use of computer simulation (based on a theoretical model) for the prediction of high-performance liquid chromatography (HPLC) separation as a function of pH. It was shown that this approach to HPLC method development is reliable if (a) appropriate experimental data are selected as input to computer simulation and (b) predictions are restricted to a suitable range of mobile phase pH. HPLC method development based on selecting an optimum mobile phase pH is only effective for samples that contain acidic or basic solutes whose ionization and retention change as a function of pH. As retention (k') can decrease by

a factor of ten or more for an ionized *vs.* a non-ionized compound, it is often necessary to combine pH optimization with variation in solvent strength (%B) in order to maintain a reasonable k' range for the resulting separation. Ideally, the retention of sample components in the final (optimized) separation should fall in the range $1 < k' < 20$ [2].

A few recent papers [3–5] have dealt with the combined variation of mobile phase pH and solvent strength; empirical functions for retention as a function of both pH and %B were used in conventional factorial-design procedures. Marques and Schoenmakers [6] provide a detailed study of several models for use in mapping the combined effects of pH and %B on sample retention.

When solvent strength is varied apart from a change in mobile phase pH, significant changes in band spacing (values of α) can occur [7]. This may lead in turn to useful changes in sample resolution as a function of %B. We have shown previously that computer simulation of separation as a function of %B can be a valuable aid in HPLC method development [7,8]. Simultaneous changes in both pH and %B therefore seem likely to result in further improvements in separation for acidic and/or basic samples, compared with the case of changes in either %B or pH alone. This was in fact demonstrated by a preceding study of a sample of substituted benzoic acids [9,10].

In this paper we shall examine several experimental systems that involve simultaneous changes in mobile phase pH and %B. Changes in both retention and column efficiency as a function of these variables were studied. As a result, it was possible to draw some general conclusions on how sample resolution varies as a function of mobile phase pH and %B.

THEORY

A quantitative model for sample retention in reversed-phase HPLC as a function of pH was described in Part I [1]. Reversed-phase retention as a function of %B is much more complicated and difficult to model in terms of basic theory. The use of solubility-parameter theory leads to an expression of the form [11]

$$\log k' = A\varphi^2 + B\varphi + C \tag{1}$$

where A, B and C are constants for a given solute and mobile phase organic solvent and φ is the volume-fraction of organic solvent B in the mobile phase; $\varphi = 0.01$ (%B). The model on which eqn. 1 is based is overly simplistic, but actual experimental data are described by eqn. 1 fairly well [12]. For many HPLC systems, eqn. 1 can be simplified (with little error) to

$$\log k' = \log k_w - S\varphi \tag{2}$$

Here $\log k_w$ is equal to C in eqn. 1, S is equal to $-B$ and the term $A\varphi^2$ is ignored. We have previously used eqn. 2 as a basis for computer simulations as a function of %B [8–10]. Our latest computer simulation software (DryLab I/mp) allows the use of

either eqn. 1 or 2 as a basis for predicting separation as a function of %B. Eqn. 1 requires three initial HPLC runs where only %B is varied, whereas eqn. 2 requires only two runs.

Simultaneous variation of mobile phase %B and pH

In this study we used DryLab I/mp for the simultaneous optimization of both %B and pH, in order to maximize sample resolution. Although the present version of this software provides for variation of only one separation variable at a time, two-variable optimization can be achieved as follows. Three experimental runs at different pH values (*e.g.*, pH = 3, 4 and 5) are carried out for two different values of %B (*e.g.*, 25 and 35% methanol). Computer simulation can be used to predict retention as a function of pH for each %B value. Now the predicted retention times for any pH value can be used to predict separation as a function of %B. The end result is that six initial experimental runs allow the prediction of separation as a function of both pH and %B (based on eqn. 2). If three different %B values are selected instead (nine runs), more accurate predictions of separation as a function of %B and pH can be carried out (in the same way) based on eqn. 1. Later versions of DryLab I/mp will allow the more convenient, simultaneous variation of pH and %B (without re-entry of data for variation of %B).

EXPERIMENTAL

The equipment, materials and procedures used in this study were described in Part I [1]. Plate numbers are calculated by $N = 5.54 \, (t_R/W_{1/2})^2$, where $W_{1/2}$ refers to the band width at half-height.

RESULTS AND DISCUSSION

Solute band widths

The primary goal of computer simulation is the estimation of resolution as a function of experimental conditions. This in turn requires predictions of both retention time and band width for each sample component as one or more conditions are varied during method development. In Part I [1] we discussed the prediction of resolution (values of α) as a function of mobile phase pH, while earlier papers addressed retention as a function of %B [9,12].

Band width can be used interchangably with column plate number, and a vast literature exists concerning plate number as a function of experimental conditions [13–15]. In many instances it is possible to predict plate number and band width as a function of solute structure and experimental conditions with reasonable accuracy [16]. Computer simulation based on DryLab software makes use of this prior theory. However, these predictions of plate number assume "ideal" chromatography, which is not always observed experimentally. Acidic and basic solutes are often found to deviate from "ideal" behavior [17,18], generally exhibiting wider (often tailing) bands than are predicted by theory. In this study we examined solute plate number as a function of experimental conditions for the acidic and basic solutes described in Part I [1].

Experimental band widths vs. values predicted by theory. Several dozen runs were carried out for the benzoic acid and aniline samples discussed in Part I [1] as a function of pH, %B and other variables. The resulting chromatograms were generally comparable in terms of band width and average plate

number; calculated values of N for the various sample components in most cases fell within a range of $N = 10\,000$–$20\,000$, with average values of about $16\,000$. Fig. 1 shows a typical example: the separation of the substituted aniline sample with a mobile phase of pH = 3.00 and 25% B. Table I summarizes plate number measurements for all of the aniline bands as a function of pH.

DryLab I/mp can provide estimates of solute plate number as a function of solute molecular weight and experimental conditions; these values correspond to plate numbers expected for "ideal" chromatography. Fig. 2 shows two typical comparisons of experimental *vs.* predicted values of N as a function of solute retention time, t_R. The solid curve represents values predicted by theory (DryLab I/mp) and the open circles are experimental values. Data in Fig. 2A are taken from a separation of the substituted benzoic acid sample [10] and Fig. 2B is from a separation of the present aniline sample. There is reasonable agreement between experimental and predicted values of N in each instance[a], *i.e.*, the average deviation of predicted *vs.* experimental values is ±13% for the benzoic acid sample and ±23% for the substituted anilines. These deviations correspond to errors in resolution (and band width) of ±6 and ±11%, respectively. Other sep-
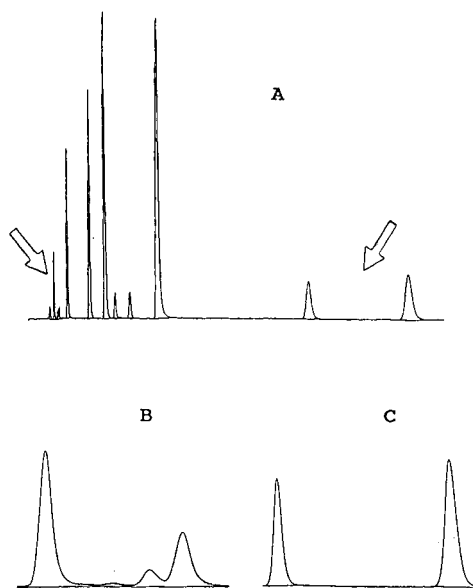

Fig. 1. Separation of substituted anilines sample. Conditions: 25 × 0.46 cm I.D. StableBond CN column; 25% methanol–buffer (25 mM, pH 3.00); 35°C; 1 ml/min. (A) Whole chromatogram; (B) enlargement of front of A (arrow); (C) enlargement of end of A (arrow).

TABLE I

AVERAGE PLATE NUMBERS FOR THE SUBSTITUTED ANILINE SAMPLE AS A FUNCTION OF MOBILE PHASE pH

Conditions: 25 × 0.46 cm I.D. StableBond CN column; 25% methanol–buffer (25 mM); 35°C; 1 ml/min.

pH	N^a
2.00	15 800 ± 1300
3.00	16 200 ± 3300
4.00	16 100 ± 1600
6.00	16 300 ± 800
Average	16 100 ± 1800

[a] Average value for all solutes; excludes dimethylaniline (DMA) for 3 < pH < 4.5.

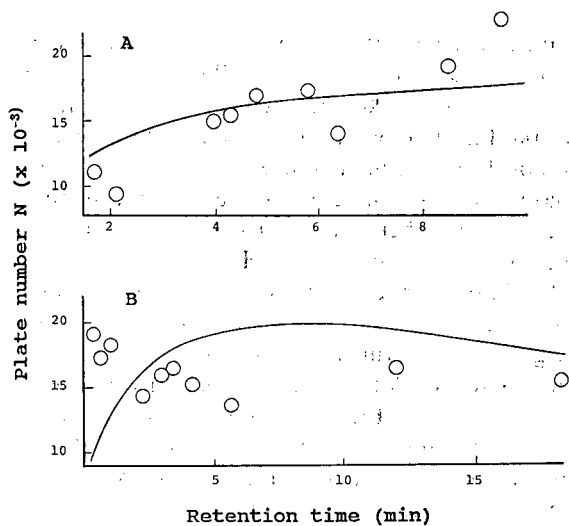[a] Note the expanded *y*-axis in Fig. 2.

Fig. 2. Plate number as a function of retention time. (A) Benzoic acid sample, 25 × 0.46 cm I.D. Zorbax C_8 column, 35% methanol–buffer (25 mM, pH 2.9), 30°C, 1 ml/min; (B) aniline sample, conditions as in Table I except pH = 3.00. Solid curves are predicted by DryLab I/mp.

arations from the present study showed similar agreement of experimental and calculated values of N. The absence of "non-ideal" effects leading to excessive band broadening for the aniline sample is noteworthy, particularly as no amine modifiers were added to the mobile phase. The StableBond CN column used for these separations seems to be relatively free of these "non-ideal" effects.

Band width anomalies. The above discussion of values of N for the benzoic acid and aniline samples has one exception. The compound 3,5-dimethylaniline (DMA) also gave reasonable plate numbers in most separations, but this was not the case for mobile phases with pH values in the range 3.0–4.5. Fig. 3 summarizes the band shape of DMA as a function of pH values that overlap the range 3.5–4.5. For a pH of 3.00, the DMA band tails, but its plate number is normal ($N = 14\,200$). For pH values of 3.5–4.0, the band fronts markedly and the plate number is less than 3000. For pH values of 4.5 or higher, the band shape is normal and the plate number is again

pH = 3.0   pH = 3.5   pH = 3.75

pH = 4.0   pH = 4.5

pH = 6.5
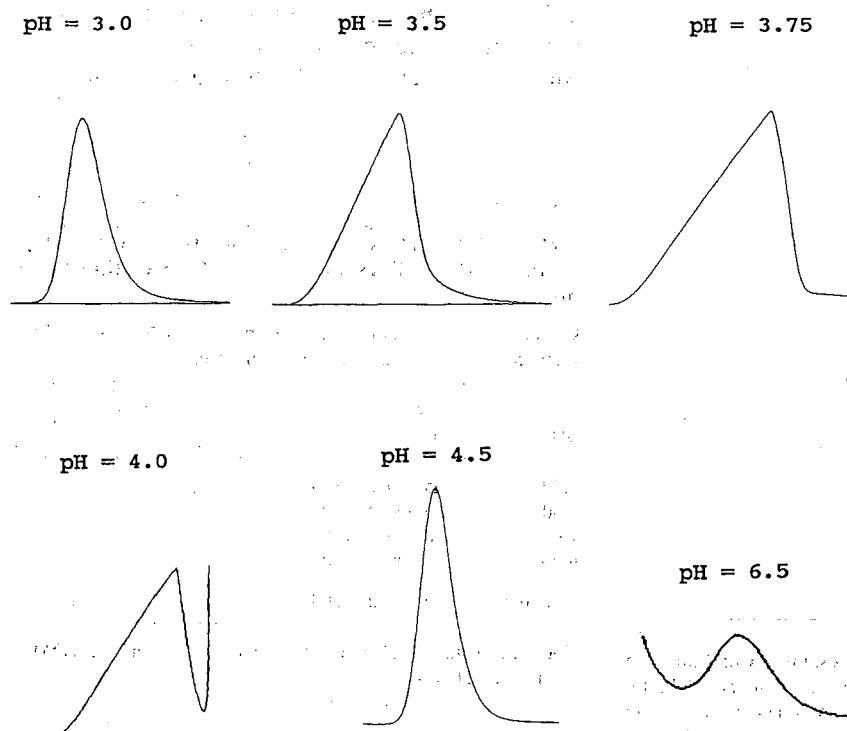
Fig. 3. Anomalous behavior of 3,5-dimethylaniline band. Conditions as in Table I except for indicated pH.

normal (N = 11 400–13 000). The pK_a value of DMA is believed to be about 3.8–4.0 (see Table VII in ref. 1), which approximates the pH of maximum band distortion in Fig. 3. Why this should be so, however, is unclear. A similar example of peak deterioration at intermediate pH values has been reported for the reversed-phase separation of 1-naphthoic acid [19].

The present StableBond CN column is manufactured from a silica that is relatively free from heavy-metal contamination. The excellent band shapes and high plate numbers observed for the remaining substituted anilines (Table I) suggest that this column packing is relatively free of the adverse silanol effects that often result in wider, tailing bands for basic amine solutes. However, the results shown in Fig. 3 emphasize the possibility of unexpected band broadening for some compounds (and some experimental conditions), suggesting a need to take this possibility into account during method development and optimization. Computer simulation (DryLab I/mp or other software) in its present form is unable to predict the behavior shown in Fig. 3. In the example in Fig. 3, this could lead to erroneous predictions of resolution (values that are too high) when the mobile phase pH is between 3.5 and 4.0.

Resolution as a function of pH and %B

Substituted benzoic acid sample. Retention data were reported previously [10] for the separation of the benzoic acid sample as a function of %B and a pH range of 2.6–3.2. These data do not allow a complete optimization of this separation as a function of pH (because of errors in pH extrapolation noted in ref. 1), but a partial optimization is possible. Fig. 4 summarizes our results in the form of resolution maps[a] as a function of pH for different %B values. Fig. 4A–C show resolution maps as a function of pH for values of %B of (A) 35%, (B) 40% and (C) 45%. The resolution (R_s) varies with both pH and %B, and a maximum value of R_s requires optimization of both pH and %B; R_s = 2.0 for pH = 3.08 and 35% B. Fig. 4D shows a similar map for R_s vs. %B and pH 2.9; for reasonable val-

ues of k', the methanol concentration must be >30%, and the maximum possible resolution is seen to be R_s = 1.6.

Substituted aniline sample. The separation of the aniline sample was carried out for a wide range of pH values (2–6.5) and mobile phases with 25 or 35% B (Table I in ref. 1). This allowed a more complete optimization of pH and %B than was possible for the benzoic acid sample (above). Fig. 5 shows a resolution map vs. pH for 25% B over the pH range 2.5–5.0; the resolution at lower and higher pH values is <0.5. The maximum resolution is R_s = 1.4 for pH = 4.1.

We next obtained similar resolution maps (anilines sample) for other values of %B, as in Fig. 4 for the benzoic acid sample. To summarize these data (not shown), no other combination of pH and %B yielded a higher R_s value than could be obtained for 25% B and a pH of 4.1. While unexpected, this result was initially rationalized as being due to the fortuitous initial selection of an optimum %B value (25%). Further study of resolution as a function of %B and pH, however, disclosed a curious finding: there existed a number of pH–%B combinations that gave similar resolution (R_s = 1.0–1.4) as for our optimum pH and 25% B.

We next examined resolution maps of R_s vs. %B for different pH values. These revealed an even more surprising finding: maps of R_s vs. %B were surprisingly similar to corresponding maps of R_s vs. pH, especially when the comparison involves similar values of pH and %B between the two maps. This is illustrated in Fig. 6. Fig. 6A reproduces the resolution map of Fig. 5 for pH = 2.9–3.6. Fig. 6B is an R_s vs. %B map for a pH of 3.0, *i.e.*, bracketed by the pH range in Fig. 6A. The two maps are virtually superimposable; not only is the resolution trace the same, but also the critical band pairs (indicated by numbers within the figure, *e.g.*, 10/2 refers to bands 10 and 2) are the same for corresponding regions of each resolution map.

A similar comparison is made in Fig. 6C and D, where the map for R_s vs. pH covers the pH range 4.3–4.9, and the R_s vs. %B map is for a pH of 4.5. Again, the two maps are remarkably similar. What is the significance of the comparisons shown in Fig. 6? If values of pH and %B are defined for a given separation, *e.g.*, pH = 3.0 and 25% B for the example in Fig. 6A and B, a change in either pH or %B

---

[a] An average plate number is assumed in these resolution maps, as determined from data for the input runs.
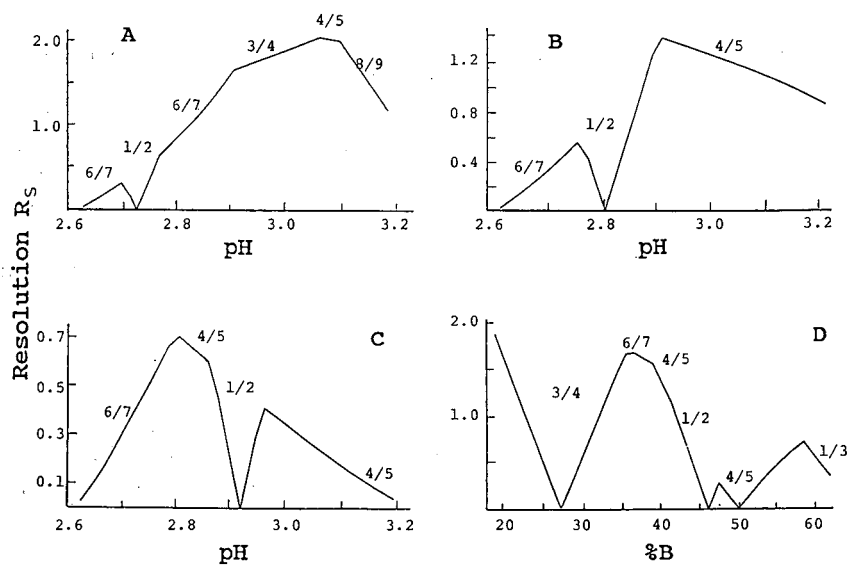
Fig. 4. Resolution maps for the separation of the benzoic acid sample. Conditions as in Fig. 2A except for pH and %B: (A) 35% B; (B) 40% B; (C) 45% B; (D) pH 2.9. Numbers in the figure (*e.g.*, 4/5) refer to "critical" band pairs for which resolution is least.

around these values will produce similar changes in band spacing and resolution. That is, the effects of %B or pH on the separation are not independent but instead highly correlated.

Selectivity as a function of pH and %B. Changes in band spacing or selectivity as a function of pH result from changes in the ionization of acidic or basic sample components. Changes in selectivity as a function of %B reflect differences in the values of
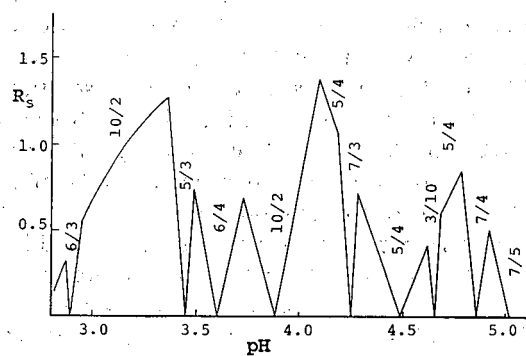
Fig. 5. Resolution map for the separation of the aniline acid sample. Conditions as in Table I, except 25% B and pH varies. Numbers in the figure (*e.g.*, 4/5) refer to "critical" band pairs for which resolution is least.
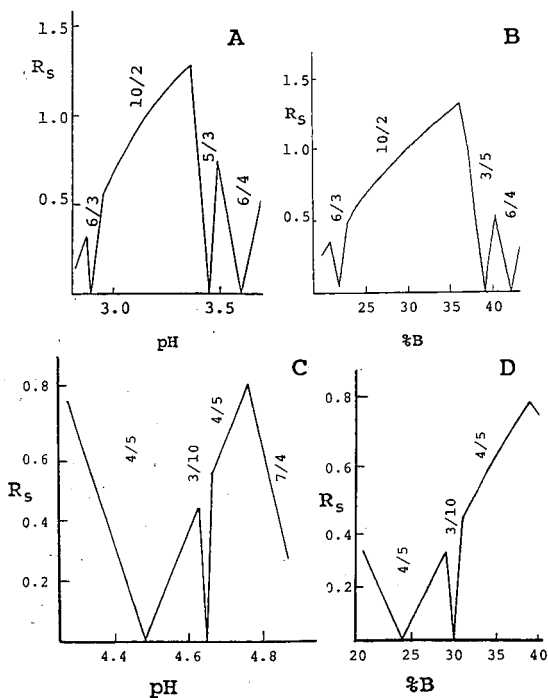
Fig. 6. Resolution maps for the separation of the aniline sample: similarity of changes in selectivity as either pH or %B is varied. Conditions as in Table I, except as noted. (A) 25 %B; (B) pH = 3.0; (C) 25% B; (D) pH = 4.5. Numbers in the figure (*e.g.*, 4/5) refer to "critical" band pair for which resolution is least.

TABLE II

VALUES OF S FOR THE SUBSTITUTED ANILINES AS A FUNCTION OF pH; STABLEBOND CN COLUMN

Derived from the retention data in Table I in Part I [1] by means of eqn. 2. Conditions as in Table I except for pH and %B.

Aniline solute	Parameter	pH									
		2.0	2.5	3.0	3.5	4.0	4.5	5.0	5.5	6.0	6.5
4-Methoxy-	S	$-^a$	–	–	–	0.9	1.2	1.6	2.0	2.2	2.3
	F^+	0.95	0.86	0.66	0.38	0.16	0.06	0.02	0.01	0.00	0.00
3-Methyl-	S	–	–	–	0.4	0.9	1.5	1.8	1.9	2.0	2.0
	F^+	0.97	0.92	0.79	0.55	0.28	0.11	0.04	0.01	0.00	0.00
3-Cyano-	S	0.9	1.7	2.0	2.1	2.3	2.4	2.3	2.3	2.2	2.2
	F^+	0.57	0.30	0.12	0.04	0.01	0.00	0.00	0.00	0.00	0.00
2-Chloro-	S	0.9	1.6	1.9	2.0	2.1	2.2	2.1	2.2	2.2	2.2
	F^+	0.55	0.28	0.11	0.04	0.01	0.00	0.00	0.00	0.00	0.00
4-Chloro-	S	–	0.5	0.7	1.2	1.7	2.1	2.2	2.2	2.2	2.2
	F^+	0.95	0.85	0.65	0.37	0.16	0.06	0.02	0.01	0.00	0.00
3-Chloro-	S	0.7	0.7	1.2	1.7	2.0	2.2	2.1	2.2	2.2	2.2
	F^+	0.88	0.70	0.42	0.19	0.07	0.02	0.01	0.00	0.00	0.00
3,5-Dimethyl-	S	–	–	–	0.8	1.8	1.9	2.1	2.4	2.4	2.5
	F^+	0.98	0.94	0.83	0.61	0.33	0.14	0.05	0.02	0.00	0.00
N-Ethyl-	S	–	–	–	0.4	0.7	1.2	1.7	2.1	2.2	2.2
	F^+	0.98	0.94	0.83	0.62	0.34	0.14	0.05	0.02	0.00	0.00
3,4-Dichloro-	S	1.3	2.1	2.6	2.7	2.9	3.1	3.0	3.0	3.0	3.0
	F^+	0.69	0.41	0.18	0.07	0.02	0.01	0.00	0.00	0.00	0.00
3,5-Dichloro	S	2.1	2.6	2.9	2.8	3.0	3.1	3.0	3.0	3.0	3.0
	F^+	0.49	0.24	0.09	0.03	0.01	0.00	0.00	0.00	0.00	0.00

^{a} Dashes indicate inaccurate value of S due to small values of k' used in eqn. 2.

S for two adjacent bands in the chromatogram (see eqn. 2 and the discussion in refs. 7 and 9). The results in Fig. 6, which show a marked correlation between changes in selectivity due to variation of either pH or %B thus imply a strong correlation between values of S and the fractional ionization F^+ of these substituted anilines. We therefore examined values of S for these compounds as a function of pH. Table II summarizes these values of S and includes corresponding values of F^+ calculated via eqns. 3–5 in Part I [1], using values of K_a from Table II in Part I [1] for $pH_2 = 3.0$.

For pH > 5.0, the various components of the aniline sample are almost completely non-ionized: $F^+ < 0.05$ (Table II). Over this range of pH it is seen in Table II that values of S are independent of pH, as is normally the case for neutral solutes. For

lower pH values, however, where $F^+ > 0.05$, the values of S are seen to decrease sharply. This is further shown in Fig. 7, where the ratio of S to its value at high pH ($S°$) is plotted vs. fractional ionization F^+; values of $S/S°$ (open circles) are seen to decrease regularly as F^+ increases[a]. We shall show in a following section that the dependence of S on F^+ in Fig. 7 is consistent with the similarity of band spacing changes that results from changes in either pH or %B (Fig. 6).

Also shown in Fig. 7 (dashed line) is the dependence of S on solute ionization (F^-) for the benzoic acid sample. While there is a tendency toward lower

[a] The closed circles in Fig. 7 are derived from k' values that are < 1 and therefore less accurate; we can ignore these data points for the purpose of discussion.
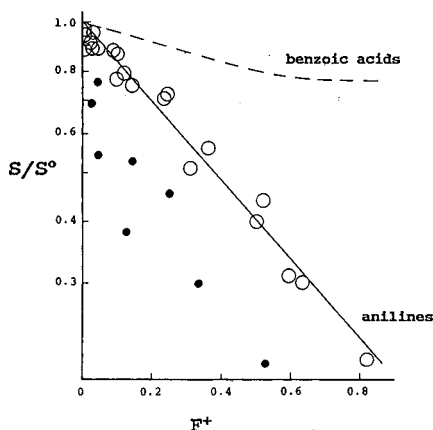
Fig. 7. Dependence of values of S (eqn. 2) on fractional ionization, F^+, of solute. Data in Table II for anilines (solid line); dashed line, data for benzoic acids (conditions as in Fig. 1; see ref. 9 for raw data). ● = Data which are considered to be of low accuracy owing to small values of k' (see text); ○ = other data.
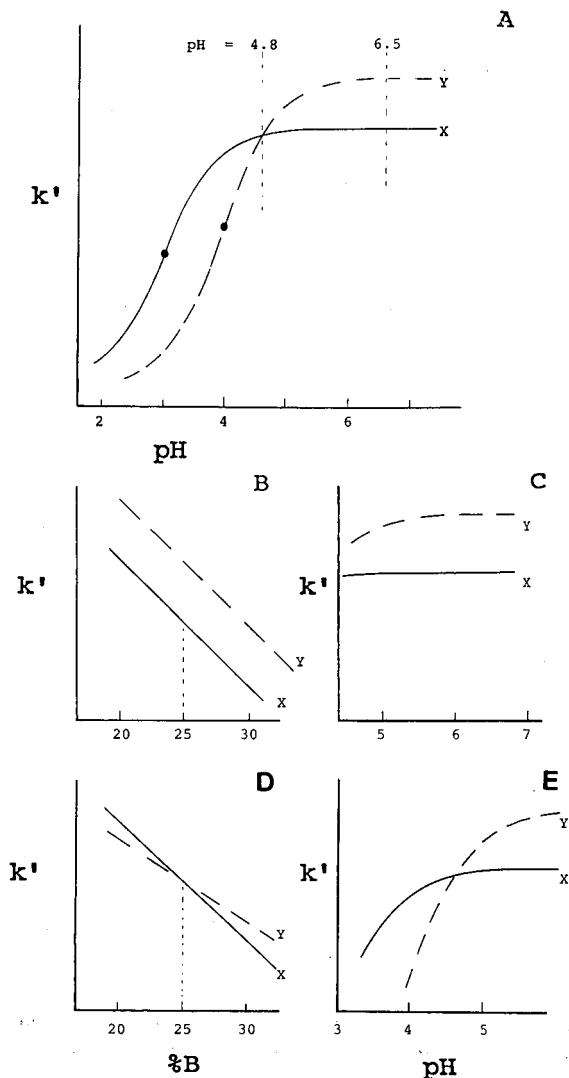

Fig. 8. Hypothetical example that further illustrates the basis of similar changes in band spacing as a function of either pH or %B for the aniline sample, assuming 25% B; see text for further details. (A) Plots of k' *vs.* pH for solutes X and Y; $pK_a = 3$ for X and 4 for Y (●); (B) plot of k' *vs.* %B for pH = 6.5 (see A); (C) plot of k' *vs.* pH for 25% B; (D) plot of k' *vs.* %B for pH = 4.8 (see A); (E) plot of k' *vs.* pH for 25% B.

values of S for more highly ionized solutes in this sample, the dependence of S on F^+ is *much* less pronounced. This smaller change in S with solute ionization is also consistent with our finding that band spacing changes that result from a change in pH or %B are *not* the same for the benzoic acid sample. That is, the simultaneous variation in pH and %B as a means of maximizing sample resolution is much more effective for the benzoic acid sample than for the aniline sample.

Simple description of the basis of the similar dependence of selectivity on pH and %B for the aniline sample. The chromatograms in Fig. 1 show that eight of the ten components of the aniline sample elute early, with the last two bands (3,4- and 3,5-dichloroaniline) eluting much later (see also Table I in Part I [1]). Sample resolution is determined mainly by overlapping bands within the first group of eight compounds (excluding the dichloroanilines). It can be seen in Table II that the $S°$ values of these early-eluting anilines are relatively constant; *i.e.*, the value of S for pH > 5.0 ranges from 2.0 to 2.5. Assume for the moment that the $S°$ values for this group of compounds are about the same.

Next assume that two of these bands overlap completely for some value of pH. This situation is illustrated in the hypothetical example in Fig. 8A, where k' is plotted *vs.* pH for two bands X (solid

curve) and Y (dashed curve); we assume also that %B = 25%. Band X has a pK_a value of 3.0 and the pK_a value for band Y is 4.0 (solid circles in Fig. 8A). The two bands overlap completely for pH = 4.8. Now consider the separation of the two bands as experimental conditions (pH and %B) are varied

TABLE III

RETENTION TIMES (min) FOR SUBSTITUTED ANILINE SAMPLE AS A FUNCTION OF pH AND %B

Conditions: 25 × 0.46 cm I.D. StableBond C_8 column, other conditions as in Table I.

Methanol concentration (%)	Compound	pH					
		2.5	3	3.5	4	4.5	5
30	p-Anisidine	3.18	3.46	3.59	4.62	5.44	6.63
	3-Aminobenzonitrile	9.04	9.83	10.29	10.48	10.48	10.56
	m-Toluidine	4.18	4.88	6.23	9.77	12.18	13.88
	4-Chloroaniline	6.87	10.09	14.09	18.45	19.32	19.91
	3-Chloroaniline	10.72	14.90	18.27	20.60	20.88	21.13
	2-Chloroaniline	17.71	19.54	20.39	20.86	20.84	20.74
	N-Ethylaniline	3.84	4.54	6.32	11.80	18.69	25.74
	Nitrobenzene	24.83	24.79	24.77	24.86	24.69	24.84
	3,5-Dimethylaniline	6.79	7.91	10.69	19.32	23.74	28.32
	3,4-Dichloroaniline	41.84	49.42	54.75	55.29	54.65	55.29
	3,5-Dichloroaniline	75.91	80.70	83.58	82.69	80.75	81.44
40	p-Anisidine	3.01	3.21	3.35	4.06	4.40	5.13
	3-Aminobenzonitrile	6.45	6.64	6.7	6.69	6.65	6.68
	m-Toluidine	3.73	4.51	5.52	7.46	8.31	9.02
	4-Chloroaniline	6.61	8.72	10.27	11.25	11.52	11.64
	3-Chloroaniline	8.99	10.82	11.79	12.13	12.31	12.19
	2-Chloroaniline	11.74	12.09	12.41	12.47	12.43	12.32
	N-Ethylaniline	3.50	4.35	5.7	9.82	12.90	15.89
	Nitrobenzene	14.57	14.35	14.58	14.37	14.43	14.37
	3,5-Dimethylaniline	5.08	6.28	8.32	12.28	14.06	15.64
	3,4-Dichloroaniline	23.27	24.42	25.94	25.55	26.16	25.50
	3,5-Dichloroaniline	36.55	36.65	38.10	37.00	37.98	36.85

for an initial separation with a mobile phase of 25% B and pH = 6.5. Fig. 8B and C show the variation of k' as a function of %B (pH = 6.5) and pH (25% B). Because the two compounds are essentially non-ionized in this pH range, the values of $S = S°$ and are therefore the same (we assumed equal $S°$ values). Fig. 8B shows that band spacing does not change as %B is varied[a], because the S values for each band are the same. Similarly, band spacing does not change as pH is varied (Fig. 8C), because the ionization of the two compounds remains unchanged for small changes in pH.

Now consider how separation changes with pH and %B in the region of pH = 4.8, where the two bands overlap (Fig. 8A). Because band B is significantly ionized for pH = 4.8, its value of S will

decrease significantly (Fig. 7). Band X is not significantly ionized at pH = 4.8, so its value of S remains about the same as at pH 6.5. Fig. 8D reflects this situation, where the slope of the k' vs. %B plot for band X is seen to be greater than that for band Y. As a result, an increase in %B leads to the later elution of band Y vs. band X, and the separation of the two bands for %B values either greater or less than the original values of 25%.

Fig. 8E shows a similar situation as pH is varied; band Y is more retained for higher pH values than band X, and the two bands can be separated by either an increase or decrease in pH. Thus for these two bands, our preceding discussion suggests that an increase in %B will give a comparable change in band spacing and resolution as for some increase in pH.

The examples in Fig. 8 can be repeated for every pair of bands in the sample. The result will then be similar resolution maps for the sample as a function

---

[a] Straight-line plots as in Fig. 8B and D are expected when log k' is plotted vs. %B (eqn. 2). Here we have ignored the actual curvature of plots of k' vs. %B.

TABLE IV

VALUES OF *S* FOR THE SUBSTITUTED ANILINES AS A FUNCTION OF pH; STABLEBOND C_8 COLUMN

Derived from the retention data in Table III by means of eqn. 2. Conditions as in Table III.

Aniline solute	Parameter[a]	pH					
		2.5	3.0	3.5	4.0	4.5	5.0
4-Methoxy-	*S*	$-$[b]	$-$	1.2	1.4	1.9	2.0
	F^+		0.86	0.66	0.38	0.16	0.06	0.02
3-Methyl-	*S*	$-$	0.8	0.97	1.7	2.2	2.4
	F^+		0.92	0.79	0.55	0.28	0.11	0.04
3-Cyano-	*S*	2.2	2.5	2.7	2.8	2.9	2.9
	F^+	0.30	0.12	0.04	0.01	0.00	0.00
2-Chloro-	*S*	2.2	2.5	2.6	2.7	2.7	2.7
	F^+	0.28	0.11	0.04	0.01	0.00	0.00
4-Chloro-	*S*	0.3	0.9	1.8	2.6	2.7	2.8
	F^+	0.85	0.65	0.37	0.16	0.06	0.02
3-Chloro-	*S*	1.0	1.7	2.3	2.7	2.7	2.8
	F^+	0.70	0.42	0.19	0.07	0.02	0.01
3,5-Dimethyl-	*S*	$-$	$-$	1.5	2.4	2.7	2.9
	F^+	0.94	0.83	0.61	0.33	0.14	0.05
N-Ethyl-	*S*	$-$	0.4	0.7	1.1	1.9	2.4
	F^+	0.94	0.83	0.62	0.34	0.14	0.05
3,4-Dichloro-	*S*	2.8	3.3	3.5	3.6	3.4	3.6
	F^+	0.41	0.18	0.07	0.02	0.01	0.00
3,5-Dichloro	*S*	3.3	3.6	3.6	3.7	3.4	3.6
	F^+	0.24	0.09	0.03	0.01	0.00	0.00

[a] Values of F^+ are the same as for Table II (not corrected for difference in %B).
[b] See footnote in Table II.

of either %B or pH, as seen in the experimental examples in Fig. 6. A more fundamental question, however, is *why* the values of *S* for the anilines correlate with the fractional ionization of these solutes. Also, why do the benzoic acids not show a similar behavior? We shall not address these questions here, but they are surely worthy of further investigation.

C_8 vs. cyano columns. One experimental difference between the separations reported here of the anilines and benzoic acids is the use of a cyano column for the aniline separations and a C_8 column for the benzoic acids. It might be argued that silanol effects preferentially affect the retention of anilines *vs.* benzoic acids, and a cyano column is likely to have a greater number of accessible silanols. For these reasons we repeated our study of aniline re-

tention as a function of pH, but substituted a C_8 column for the original cyano column.

Table III summarizes retention times as a function of pH for a C_8 column and two different %B values, 30% and 40%. Table IV provides derived values of *S* for each solute as a function of pH (Table III and eqn. 2). A similar pattern of decrease in *S* with increase in solute ionization (value of F^+) is observed as in Table II for the cyano column. We have not yet attempted a more detailed comparison of the data in Tables II and IV.

Optimizing separation as a function of %B and pH

When changes in resolution as a function of mobile phase pH and %B are not equivalent, as in the case of the benzoic acid sample, it is obviously useful to be able to map separation as a function of all

SUMMARY OF MAXIMUM RESOLUTION AND RELATED k'-RANGE AS A FUNCTION OF BOTH pH AND %B FOR THE SUBSTITUTED ANILINES SAMPLE

25% B, pH varied

pH	R_s	k' range
3.35	1.3[a]	0.4–16
4.10	1.4[b]	0.6–16

pH 3–4.5, %B varied

pH	%B	R_s	k' range
2.5	42	1.0[a]	0.1–5.8
3.0	36	1.3[a]	0.2–7
3.5	21	1.3[a]	0.5–20
	36	1.1[b]	0.2–8
4.0	28	1.0[a]	0.5–13
	38	0.6[b]	0.4–7
4.5	39	0.8[b]	0.6–5.8

[a] Bands 10/2 critical.
[b] Bands 5/4 critical.

possible values of pH and %B. In this way the best compromise can be obtained in terms of resolution, run time and k' range. When the effects of pH and %B on band spacing are similar, as for the case of the anilines, the usefulness of this same approach is more limited. Table V summarizes the results of combined %B vs. pH mapping for the anilines.

Two primary resolution maxima exist in the map of Fig. 5 for 25% B, at pH 3.4 and 4.1. These resolution maxima are defined by two different overlapping bands: 10/2 and 5/4[a]. Table V shows that as pH is increased, the 10/2 maximum[a] shifts to lower values of %B, but the maximum resolution when this band pair is limiting remains relatively constant ($1.0 < R_s < 1.3$). The 5/4 maximum[a] occurs at about the same value of %B as pH is varied, and the maximum resolution for this band pair occurs for about pH 3.5.

A more interesting observation in Table V is that for roughly the same maximum resolution, the mobile phase composition (%B and pH) can be varied

[a] In Fig. 2 bands 2 and 10 are 3-methyl- and N-ethylanilines; bands 4 and 5 are 2- and 4-chloroanilines.

to adjust the k' range of the sample. For $R_s > 1.0$, the k' range can be varied from 0.1–5.8 to 0.6–16. As $k' < 0.5$ should be avoided, this favors the choice of 25% B and a pH = 4.1 in this example.

CONCLUSIONS

Column efficiency was studied for the separation of the present samples composed of substituted anilines and benzoic acids as a function of mobile phase pH. Comparisons of experimental band widths with values predicted by computer simulation showed reasonable agreement: ±6% for the benzoic acids and ±11% for the substituted anilines. With the exception of 3,5-dimethylaniline (DMA), plate numbers for the aniline sample did not vary with pH over the range 2–6.5. DMA showed anomalous band-broadening behavior in the pH range 3.5–4.0; strong fronting and excessive band broadening were seen. For pH < 3.5 and > 4.0, band broadening for DMA was similar to that for the other anilines in this sample.

The use of the simultaneous variation of mobile phase pH and %B values was studied for both the benzoic acid and aniline samples. With the benzoic acids, it was useful to vary each of these two variables for maximum sample resolution. The aniline sample behaved differently in this respect. It was found that changes in selectivity as a function of either pH or %B were similar, and either variable could be used to achieve a similar maximum resolution for the aniline sample.

Further study showed that the slope of the retention vs. %B plot (value of S) for each aniline was strongly dependent on sample ionization; values of S decrease markedly when the extent of ionization of an aniline increases. This observation explains the similar band spacing changes that result when either pH or %B is varied for the aniline sample. A similar decrease in values of S as the sample ionization increases was noted for the benzoic acid sample, but the magnitude of this effect was much smaller. No explanation for the fundamental cause of these observations has been found.

REFERENCES

1 J. A. Lewis, D. C. Lommen, W. D. Raddatz, J. W. Dolan, L. R. Snyder and I. Molnar, J. Chromatogr., 592 (1992) 183.

2 L. R. Snyder, J. L. Glajch and J. J. Kirkland, *Practical HPLC Method Development*, Wiley-Interscience, New York, 1988.

3 J. S. Kiel, S. L. Morgan and R. K. Abramson, *J. Chromatogr.*, 485 (1989) 585.

4 E. Grushka, N.-I. Jang and P. R. Brown, *J. Chromatogr.*, 485 (1989) 617.

5 M. Lema, J. Otero and J. Marco, *J. Chromatogr.*, 547 (1991) 113.

6 R. M. L. Marques and P. J. Schoenmakers, *J. Chromatogr.*, 592 (1992) 157.

7 L. R. Snyder, M. A. Quarry and J. W. Dolan, *Chromatographia*, 24 (1987) 33.

8 L. R. Snyder, *J. Chromatogr.*, 485 (1989) 65 and 91.

9 J. W. Dolan, D. C. Lommen and L. R. Snyder, *J. Chromatogr.*, 535 (1990) 55.

10 L. R. Snyder, J. W. Dolan and D. C. Lommen, *J. Chromatogr.*, 535 (1990) 75.

11 P. J. Schoenmakers, H. A. H. Billiet, R. Tijssen and L. de Galan, *J. Chromatogr.*, 149 (1978) 519.

12 P. J. Schoenmakers, H. A. H. Billiet and L. de Galan, *J. Chromatogr.*, 185 (1979) 179.

13 J. C. Giddings, *Dynamics of Chromatography*, Marcel Dekker, New York, 1965.

14 J. H. Knox and H. P. Scott, *J. Chromatogr.*, 282 (1983) 297.

15 S. G. Wever and P. W. Carr, in P. R. Brown and R. A. Hartwick (Editors), *High Performance Liquid Chromatography*, Wiley-Interscience, New York, 1989, p. 1.

16 R. W. Stout, J. J. DeStefano and L. R. Snyder, *J. Chromatogr.*, 282 (1983) 263.

17 J. W. Dolan and L. R. Snyder, *Troubleshooting LC Systems*, Humana Press, Clifton, NJ, 1989, pp. 404–411.

18 M. A. Stadalius, J. Berus and L. R. Snyder, *LC · GC*, 6 (1988) 494.

19 P. C. Sadek, C. J. Koester and L. D. Bowers, *J. Chromatogr. Sci.*, 25 (1987) 489.

CHROMSYMP. 2384

Nitrogen-specific liquid chromatography detector based on chemiluminescence

Application to the analysis of ammonium nitrogen in waste water

Eugene M. Fujinari*

Antek Instruments Inc., 300 Bammel Westfield Road, Houston, TX 77090 (USA)

Laurent O. Courthaudon

Antek Instruments GmbH, Wacholderstrasse 7, W-4000 Düsseldorf 31 (Germany)

ABSTRACT

A novel high-performance liquid chromatography–chemiluminescent nitrogen detection (HPLC–CLND) system is described. The analysis of ammonium nitrogen in metropolitan waste water by a new ion chromatographic method is presented. The significance of this novel nitrogen-specific detector is the capability for a routine and continuous operation. HPLC–CLND applications for anion and particularly reversed-phase techniques are also amenable. A nitrogen-specific detector for liquid chromatography opens a new dimension of analytical chemistry.

INTRODUCTION

Increasing environmental regulations and concerns have made it vital to analyze ammonia nitrogen in waste water systems in order to monitor and prevent unnecessary discharges. Ammonia is a product of microbiological activity and consequently present in many surface and ground waters. We describe a novel nitrogen-specific detection and analytical method by high-performance liquid chromatography–chemiluminescent nitrogen detection (HPLC–CLND) for the analysis of ammonium ions in waste water samples.

Ion chromatography (IC) has become the pre-ferred analytical tool for the determination of ammonium ions in water [1–5]. Conductivity detectors are generally used for IC applications. How-ever, difficulties may be encountered when analyzing complex sample matrices due to the non-selective nature of this detector. Alternatively, HPLC–CLND is highly specific for analyzing nitrogen-containing compounds. In 1970, Fontijn *et al.* [6] studied the analytical gas-phase reaction of nitric oxide and ozone which produced chemiluminescence.

A "nitrogen-specific" gas chromatography–pyro-chemiluminescent nitrogen detection (GC–CLND) system was developed several years later [7]. GC–CLND has demonstrated high nitrogen specificity for nitrogen-containing pesticides [8] and a wide range of applications were previously studied including nitrosamines, pesticide residue, food-flavor, pharmaceutical and petroleum light cycle oil samples [9]. The detection mechanism for CLND is as

follows: as each sample component elutes from the end of the chromatographic column, it undergoes high-temperature (1000°C) oxidation. All nitrogen-containing compounds are converted into nitric oxide (NO). The resulting gases are dried and mixed with ozone (O_3) in the reaction chamber. This results in the formation of nitrogen dioxide (NO_2^*) in the excited state. Light (*hv*) is emitted by this chemical reaction and is detected by a photomultiplier tube (PMT).

$$\begin{array}{c} R \\ | \qquad 1000°C \\ R{-}N + O_2 \quad \rightarrow \quad CO_2 + H_2O + NO \\ | \\ R \end{array}$$

$$NO + O_3 \rightarrow NO_2^* \rightarrow NO_2 + hv$$
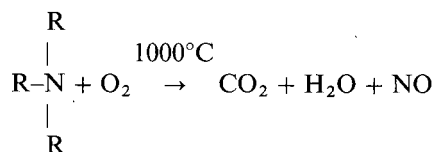
The chemiluminescence of chemically bound nitrogen is therefore detected and the resulting signal is processed by a computer. Although the above CLND mechanism is the same for HPLC and GC methods, a novel HPLC–CLND instrumentation was necessary as the analytical tool to be useful for HPLC. To date, several HPLC–chemiluminiscence detection methods based on the gas-phase nitric oxide–ozone reaction have been reported, but these have not been widely used [10]. The major limitation of previous instrumentation is the inefficient removal of water prior to the reaction chamber where the chemiluminescence is detected. Typical operation time is 2–3 h with frequent instrument downtime for drying the reaction chamber and transfer lines. One of the new design innovations incorporated in this novel HPLC–CLND instrumentation (Fig. 1) is the unique capability for continuous water removal for routine and uninterrupted operation [11]. This detector is shown in Fig. 1 and is described in the following manner. A liquid sample is injected from a sample valve (*i.e.* equipped with a sample loop) onto an HPLC column using a suitable mobile phase which is stored in a solvent reservoir. An HPLC pump is used to control the mobile phase flow-rate. A sample is chromatographed on a column and eluting compounds are introduced into the furnace of the novel HPLC–CLND system. At the furnace inlet, the inert gas carrier (helium or argon) is utilized along with the oxygen carrier for the oxidation of sample components. The resulting

nitric oxide and gases pass through the membrane drying/dewatering chamber. The key feature is the continuous removal of water (generated from both the mobile phase and sample) after oxidation. The nitric oxide is then reacted with ozone in the reaction chamber. The resulting chemiluminescence is detected by the PMT. The signal(s) from the HPLC–CLND system is processed by a computer and reports are printed from a printer. Gases exit the reaction chamber and pass through the scrubber. The flow-rates of inert gas and oxygen carriers from the gas cylinders are controlled by the gas flow meters. Oxygen passing through the ozone generator is the source for the ozone supply for this detector. The description (Fig. 1) and the explanation of this HPLC–CLND system are thus provided here for the first time in a journal publication and patent is pending for this detector.

The quantitative analysis of ammonium nitrogen in metropolitan waste water by the novel HPLC–CLND nitrogen-specific detection in the IC mode is discussed. The method, data, linearity of detector response and sensitivity are presented. Also demonstrated are the HPLC–CLND methods for anion and reversed-phase techniques.

EXPERIMENTAL

Apparatus

HPLC analysis was performed on a Micromeritics Model 760 HPLC pump with a micro flow pump head purchased from Alcott Chromatography (Norcross, GA, USA), Antek HPLC–CLND nitrogen-specific detector from Antek Instruments (Houston, TX, USA) and Delta chromatography software (Digital Solutions, Margate, Australia) run on an IBM 286 compatible computer. Sample injection was performed on a Rheodyne (Cotati, CA, USA) Model 8126 injection valve (5-μl sample loop). The HPLC columns used in this study were obtained from Keystone Scientific (Bellefonte, PA, USA). All HPLC mobile phases were filtered through a Millipore (Bedford, MA, USA) HV filter with a pore size of 0.45 μm.

Reagents and standards

Ammonium sulfate standard and methanol were obtained from Fisher Scientific (Fair Lawn, NJ, USA). L-Tartaric acid was purchased from Aldrich
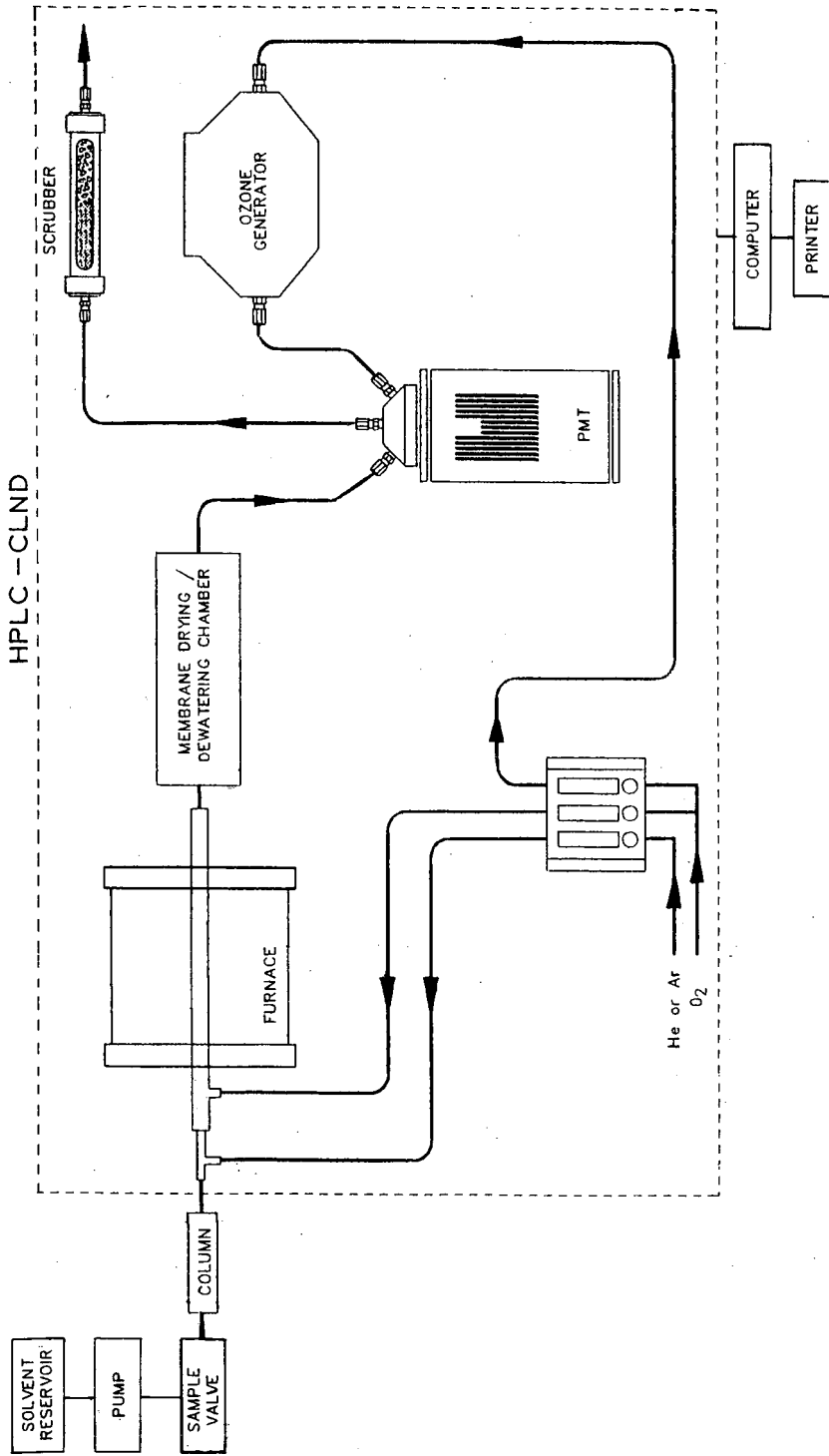
Fig. 1. Schematic diagram of the HPLC–CLND system. © Antek Instruments Inc.

(Milwaukee, WI, USA). Sodium nitrate, sodium nitrite and urea standards were obtained from J. T. Baker (Phillipsburg, NJ, USA). All reagents and standards were greater than 99% pure and were used without further purifications. Distilled water used for making standard solutions and mobile phases was obtained from Ozarka Drinking Water Company (Houston, TX, USA).

Standard preparation and analytical method

Analytical ammonium ion standards (10, 15, 20 and 80 ppm nitrogen) were prepared from a 1000-ppm nitrogen aqueous ammonium sulfate stock standard solution and used for the quantitative determination of ammonium nitrogen in waste water samples by HPLC–CLND in the IC mode. The waste water samples were analyzed without preliminary sample clean-up, by a 2-μl partial filled injection into a 5-μl sample loop. Ammonium ions were analyzed using an HPLC (150 mm × 1 mm I.D., 10 μm particle size) Hamilton PRP-X200 column. The mobile phase, 0.1 M L-tartaric acid–water (20:80, v/v), was utilized at a flow-rate of 30 μl/min. The CLND pyrolysis temperature was 1037°C.

A mixed nitrate–nitrite standard solution containing 40 ppm nitrogen from sodium nitrate and 80 ppm nitrogen from sodium nitrite was prepared from the 1000-ppm nitrogen stock standard (aqueous) solutions. The anion standards were analyzed by HPLC–CLND in the IC mode. The IC trace was achieved by the same injection technique using the HPLC (150 mm × 1 mm I.D., 10 μm particle size) Hamilton PRP-X100 column. The mobile phase, 4 mM potassium hydrogenphthalate (pH 4.5), was utilized at a flow-rate of 40 μl/min.

The urea standard (76 ppm nitrogen in methanol) was prepared and analyzed by reversed-phase HPLC–CLND. The HPLC analysis was performed by the same 2-μl injection on a Partisil ODS 3 (250 mm × 1 mm I.D., 5 μm particle size) column. The mobile phase, methanol–water (95:5, v/v), was used at a flow-rate of 40 μl/min.

RESULTS AND DISCUSSION

HPLC detection with high nitrogen specificity may be obtained by using the capabilities of the novel HPLC–CLND system. The chromatographic separations of ammonia and a mixture of several
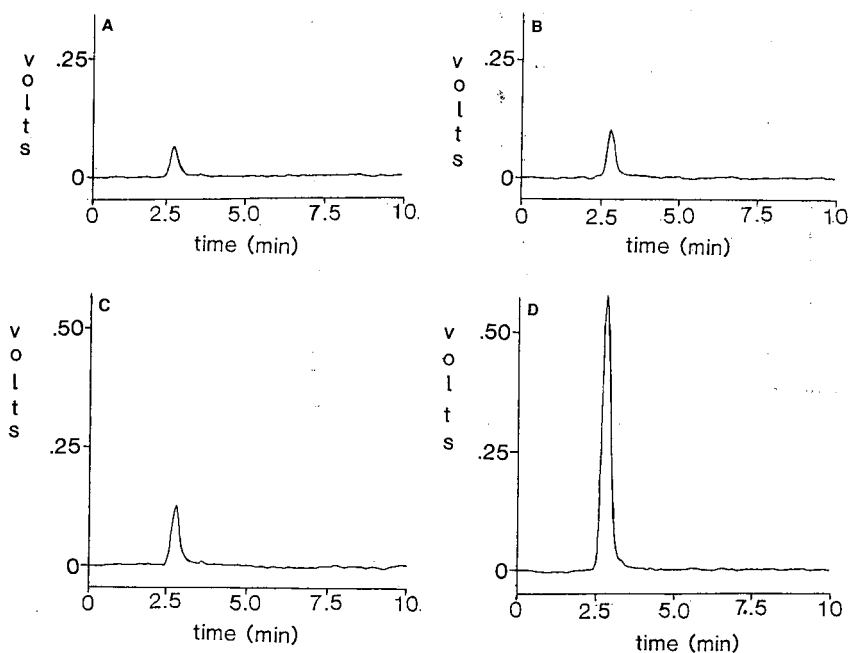
Fig. 2. HPLC–CLND tracings of the four ammonium ion standard solutions: (A) 20 ng, (B) 30 ng, (C) 40 ng and (D) 160 ng nitrogen.

volatile organic amines have been achieved by GC–chemiluminescence detection and reported in the literature [12,13]. However, by using nitrogen-specific detection (HPLC–CLND) in the IC mode, it is also possible to utilize an additional mode of selectivity (for molecular ions). This is accomplished by using the optimized IC mobile phase. In this way, two modes of selectivity (detector and mobile phase) are available resulting in greater specificity than obtained with GC–CLND. To demonstrate the utility of this powerful tool, ammonium nitrogen in metropolitan waste water samples were quantitatively analyzed by HPLC–CLND in the IC mode. A sensitivity down to 5 ng nitrogen was observed in this experiment. Lower ammonium nitrogen levels (picograms) would be achievable by sample concentration techniques such as solid-phase extraction (SPE). The linear detector response with the ammonium nitrogen calibration was obtained and the results from the linear regression analysis are presented in Table I (where r = correlation coefficient, m = slope and b = y-intercept). The four-point standard curve was obtained by the HPLC–CLND ammonium ion method using the L-tartaric acid mobile phase and the Hamilton PRP-X200 HPLC column. The standard chromatograms representing the ammonium ion standards (20, 30, 40 and 160 ng nitrogen) are given in Fig. 2. The HPLC–CLND trace of the metropolitan waste water samples A and B are provided in Fig. 3. The chromatograms showed only a single peak, at a retention time (t_R) of 2.8 min, and the samples were quantitated from the ammonium ion standard calibration curve. Ammo-

nium nitrogen levels of 16.8 and 18.0 ppm nitrogen, respectively, were found in these samples. Calculations were performed by linear regression analysis with a correlation coefficient of 0.99952.

Nitrogen-specific detection of anions by HPLC–CLND in the IC mode is amenable. An HPLC–CLND profile (nitrite t_R = 6.1 min; nitrate t_R = 7.2 min) of a mixed nitrate–nitrite standard (80 and 160 ng, respectively) is shown in Fig. 4. Studies of using inorganic salts as mobile phase modifiers for prolonged usage still need to be determined and is currently under investigation.

A reversed-phase HPLC–CLND trace of urea standard in methanol was obtained, with t_R = 4.7 min (Fig. 5). The scope for methods and applications using this detector at this time is primarily in the reversed-phase mode. The amount of water in the mobile phase is unlimited (100% water may be used if desired). The organic portion of the mobile phase is limited to non-nitrogen-containing solvent mixtures. The use of nitrogen-containing compounds well below the detection limit as mobile phase modifiers is yet to be investigated. Alternative solutions would be directed to stationary phase specialists to develop HPLC columns for the separations of various classes of nitrogen-containing molecules which are compatible for nitrogen-specific detection. The preferred flow-rates for optimum detector response are 1 to 5 μl/min for micro HPLC and up to 60 μl/min for microbore HPLC. Microbore HPLC columns with 1–2 mm I.D. are preferred. Other HPLC–CLND applications are currently underway and will be reported elsewhere.

TABLE I

HPLC–CLND ANALYSIS OF AMMONIUM NITROGEN IN METROPOLITAN WASTE WATER

$(NH_4^+)_2SO_4$ standard was prepared in distilled water and the ammonium nitrogen in waste water samples were calculated as parts per million nitrogen (ppm N) by linear regression analysis: r = 0.99952; m_r = 0.00001; b = −0.00687.

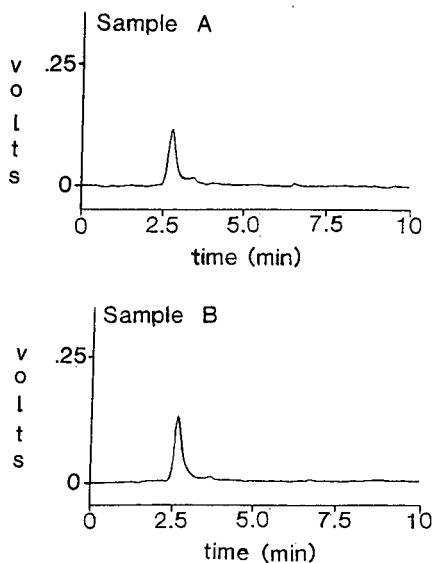| Sample	Standard $(NH_4^+)_2SO_4$ (ppm N)	Sample size (μl)	Integration of peak area	NH_4^+ (ng N)	NH_4^+ (ppm N)
	10	2	2279.18	20	
	15	2	2875.11	30	
	20	2	3452.41	40	
	80	2	13039.02	160	
A		2	3150.92	34	16.8
B		2	3351.79	36	18.0

Fig. 3. HPLC–CLND tracings of the metropolitan waste water samples A and B.

HPLC method development can be facilitated using nitrogen-specific detection in many areas of agricultural chemistry and environment studies. The technique may also be used to generate confirmatory methods for pharmaceutical and environmental studies. Other potential use of this detector may extend into the area of biotechnology research in the
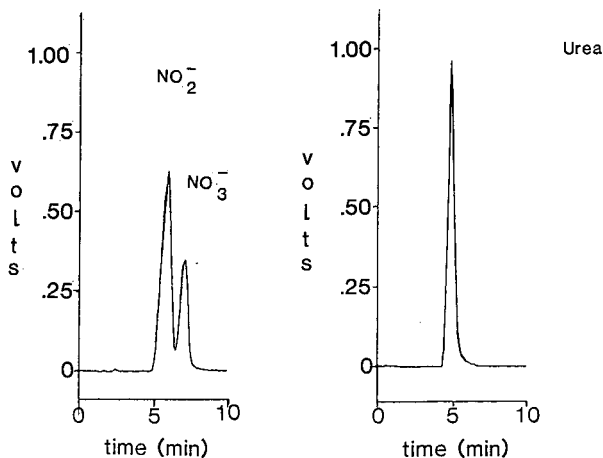
analysis of proteins as well as into biochemistry method development where amino acids may be analyzed without derivatization.

CONCLUSIONS

A novel HPLC–CLND system is presented and described for the first time. The quantitation of ammonium nitrogen in metropolitan waste water in the IC mode is demonstrated.

HPLC–CLND has many advantages. A nitrogen-specific detector can simplify the analysis of complex samples and often shorten the analysis time by resolving only the nitrogen-containing components. This novel HPLC detector provides a sensitive method with excellent linear detector calibration and is a tool for routine and continuous operation. There is a wide range of analytical applications for which the detector can be used. HPLC–CLND applications for reversed-phase techniques are particularly amenable. Investigation of prolonged usage of inorganic salts as mobile phase modifiers is still underway. The instrumental method with nitrogen specificity for HPLC provides a new dimension of analytical chemistry and is just the beginning of a new trend in HPLC.

REFERENCES

1 L. R. Snyder and J. J. Kirkland, *Introduction to Modern Liquid Chromatography*, Wiley, New York, 2nd ed., 1979, p. 438.
2 James M. Miller, *Chromatography: Concepts and Contrasts*, Wiley, New York, 1988, p. 182.
3 P. Kolla, J. Kohler and G. Schomburg, *Chromatographia*, 23 (1987) 465.
4 S. A. Bouyoucos, *Anal. Chem.*, 49 (1977) 401.
5 H. Small, T. S. Stevens and W. C. Bauman, *Anal. Chem.*, 47 (1975) 1801.
6 A. Fontijn, J. Sabadell and R. J. Ronco, *Anal. Chem.*, 42 (1970) 575.
7 R. E. Parks and R. L. Marietta, *U.S. Pat.*, 4 018 562 (1975).
8 A. J. Britten, *Res. Dev.*, 31 (1989) 76.
9 L. O. Courthaudon and E. M. Fujinari, *LC · GC*, 9 (1991) 732.
10 A. Robbat, Jr., N. P. Corso and T.-Y. Liu, *Anal. Chem.*, 60 (1988) 173.
11 E. M. Fujinari and A. J. Britten, Patent pending.
12 N. Kashihira, K. Makino, K. Kirita and Y. Watanabe, *J. Chromatogr.*, 239 (1982) 617.
13 D. P. Rounbehler, S. J. Bradley, B. C. Challis, D. H. Fine and E. A. Walker, *Chromatographia*, 16 (1982) 354.

Fig. 4. HPLC–CLND tracing of nitrite and nitrate ions.

Fig. 5. Reversed-phase HPLC–CLND tracing of urea in methanol.

Practical on-line determination of biopolymer molecular weights by high-performance liquid chromatography with classical light-scattering detection

Gavin Dollinger*, Bob Cunico☆, Michael Kunitani, Deborah Johnson and Robert Jones

Department of Analytical Chemistry, Cetus Corporation, 1400 Fifty-Third Street, Emeryville, CA 94608 (USA)

ABSTRACT

Most biopolymer molecules are much smaller than the wavelength of light used in classical light-scattering experiments (*ca.* 500 nm), and thus the simple Rayleigh equation and a 90° light-scattering photometer are sufficient to determine their molecular weight. In combination with high-performance liquid chromatography (HPLC), it is demonstrated that a simple HPLC fluorimeter can be used as a 90° light-scattering detector for biopolymer molecular weight determinations. To simplify data handling, only relative molecular weights are measured. Three mathematical assumptions are adopted, and their validity for proteins is shown. To place the work in perspective, the relative advantages and limitations of this 90° light-scattering detector are compared with the more commonly used low-angle laser light-scattering detector. Two examples of protein molecular weight determinations are given to illustrate the broad utility of 90° classical light scattering to the study of biopolymer structures and interactions.

INTRODUCTION

The determination of the molecular weight of a biopolymer such as a protein or oligonucleotide is crucial to its identification. Mass spectrometry is the method of choice, but its usefulness is limited to a restricted range of molecular weights [1]. Another drawback of mass spectrometry is that it yields only the primary structure of proteins and cannot be used to study their behavior in solution, such as their non-covalent quaternary structure, and associations with other proteins.

The three most common physical methods for determining the molecular weight of biopolymers in solution are osmometry, analytical ultracentrifugation and classical light scattering. Osmometry and analytical ultracentrifugation are time consuming. In contrast, classical light scattering can be per-

formed rapidly, although it requires careful and sometimes difficult clarification of the solutions. Techniques such as size-exclusion chromatography (SEC) and dynamic light scattering (DLS) measure the size of a biopolymer (*i.e.*, its hydrodynamic radius) and that result is often used to infer molecular weight. The approach has great utility but it can be unreliable owing to the lack of a unique relationship between molecular size and molecular weight, even under strongly denaturing conditions [2,3]. Denaturing polyacrylamide gel electrophoresis is the most commonly used method to estimate the apparent molecular weights of biopolymers. This technique may be inaccurate owing to the poorly defined relationship between both the charge and the residual biopolymer structure on the one hand and molecular weight on the other.

In this context, the link between classical light scattering and high-performance liquid chromatography (HPLC), particularly SEC for biopolymers, is natural [4–14]. Chromatography clarifies the

---

☆ Present address: Bay Bioanalytical Laboratory, Inc., 4197 Lakeside Dr., Suite 210, Richmond, CA 94806, USA.

biopolymer solution and separates its components to allow a more detailed analysis. A classical light-scattering photometer connected to the chromatographic column allows the molecular weight of the biopolymer to be determined on-line. Depending on the type of chromatography, this analytical system can simultaneously provide additional information such as size, charge and hydrophobicity of the biopolymer.

Most classical light-scattering biopolymer molecular weight determinations have been performed with low-angle laser light-scattering (LALLS) detectors in combination with refractive index and/or UV detectors. Takagi and co-workers applied this combination of detectors coupled to SEC to determine the molecular weight of biopolymers and have published extensively on molecular weight measurements of membrane proteins [8,12–14]. Krull and co-workers have demonstrated that these detectors can be used to determine biopolymer molecular weights when coupled with reversed-phase [7] and hydrophobic-interaction [10] chromatography as well as SEC [6].

Although both groups used LALLS detectors, they developed different basic approaches to the performance of the classical light scattering experiment. Takagi and co-workers make a relative determination of molecular weight by measuring the detector response to biopolymers of known molecular weight and to the sample of unknown molecular weight. Krull and co-workers calibrated the equipment in an absolute manner, a process which yields absolute molecular weight. Both approaches have their advantages. Takagi and co-workers' method is simple and straightforward but requires that the known samples or standards be well characterized and appropriately chosen. Krull and co-workers' method yields results which do not rely on external standards but the calibration procedure is exacting. Both groups have published excellent reviews of the LALLS HPLC field [15,16].

This paper presents an alternative detection method for classical light-scattering experiments. In 1935, Putzeys and Brosteaux [17] demonstrated that a 90° light-scattering photometer could be used to measure the (relative) molecular weight of proteins in solution. In the Theory section, we briefly describe the background, advantages and inherent limitations of using 90° detection, the principle

limitation being that the biopolymer must be small relative to the wavelength of light used in the scattering experiment. The theoretical framework is then used in an experimental demonstration that a simple 90° HPLC fluorimeter can be used as a 90° classical light-scattering detector for the on-line molecular weight determination of biopolymers [18]. This detector is shown to be sensitive, relatively immune to dust and column particulates and easy to use. Further, as this is a variable-wavelength device, the scattering wavelength can be optimized for the experiment at hand. It is also ubiquitous in modern analytical laboratories. To simplify the data analysis and the discussion, we shall adopt the relative molecular weight determination methodology of Takagi and co-workers. To illustrate the general utility of this approach, we describe the quaternary structure of RNase, lysozyme and bovine serum albumin using trifluoroacetic acid–acetonitrile reversed-phase elution and 90° classical light scattering. Finally, we show how the method can be used, in combination with SEC and DLS, to study the conformational changes induced in human Glu-plasminogen by the presence of a lysine analogue.

THEORY

The starting point for this brief discussion of classical light-scattering theory is the Rayleigh–Gans–Debye approximation [19]:

$$\frac{KC}{\bar{R}_\theta} \approx \frac{1}{\bar{M}_w P_{(\theta)}} + 2A_2C + O(C^2) + \dots \tag{1}$$

where K is the optical constant, C is the weight concentration of the solute, $\bar{R}_\theta$ is the excess Rayleigh ratio, $P_{(\theta)}$ is a size/shape scattering factor and the expansion is in powers of C with virial coefficients. The term $O(C^2)$ is shorthand notation for a term of second order of concentration. The quantity one usually wishes to determine is the molecular weight, which for polydisperse samples is given as the weight-average molecular weight, $\bar{M}_w$.

The quantity measured in classical light-scattering experiments is $\bar{R}_\theta$, the excess Rayleigh ratio. $\bar{R}_\theta$ is the differential light scattering intensity of the solution, $i_{solution}$, minus that of the pure solvent, $i_{solvent}$, divided by the incident light intensity, I_0, and multiplied by a constant, whose value is determined

by the photometer geometry and the solvent refractive index, g:

$$\bar{R}_{\theta} = \frac{i_{\text{solution}} - i_{\text{solvent}}}{I_0} \cdot g \qquad (2)$$

If one zeroes the output of the detector with the pure solvent in the scattering cell, then the output of the scatterometer, I_s, during the experiment will be proportional to $\bar{R}_{\theta}$.

In eqn. 1, the fundamental constant which relates the scattered light intensity $\bar{R}_{\theta}$ to $\bar{M}_w$ is the optical constant K, given by

$$K = \frac{2\pi^2 n^2 (\mathrm{d}n/\mathrm{d}c)^2}{\lambda^4 N} \qquad (3)$$

where n is the refractive index of the solvent, $\mathrm{d}n/\mathrm{d}c$ is the specific refractive index increment of the solute (*i.e.*, the biopolymer in that solvent), λ is the wavelength of the incident light and N is Avogadro's number.

The concentration of the solute, C, must be measured in an independent experiment in order to implement eqn. 1. The coefficients of the concentration terms on the right-hand side of eqn. 1 are functions of the virial coefficients, which are related to the non-ideal nature of the solvent. In more practical terms, they are measurements of the solute's propensity in that solvent to self-associate. The second virial coefficient, A_2, is proportional to the excluded volume of the solute.

The final variable in eqn. 1 that needs to be described is $P_{(\theta)}$, which alone is explicitly dependent on molecular size. This variable is a dimensionless size/shape scattering factor, a function of the size of the scatterer relative to the wavelength of incident light and of the scattering angle:

$$P_{(\theta)} = 1 - \frac{16\pi^2 n^2 <r_g^2>_z \sin^2(\theta/2)}{3\lambda^2} +$$
$$O^2 \left[\frac{n^2 x^2 \sin^2(\theta/2)}{\lambda^2} \right] \dots \qquad (4)$$

where $<r_g^2>_z$ is the z-averaged radius of gyration of the scatterer (biopolymer), θ is the scattering angle measured from the forward direction and x is a function of a size parameter characteristic of the shape of the scatterer (*e.g.*, for a sphere x is simply the radius). Thus, in general, $\bar{R}_{\theta}$ will have an angular dependence due to the size dependence of $P_{(\theta)}$.

In the most general application of eqn. 1, $\bar{R}_{\theta}$ is measured as a function of C and θ with a variable-angle or fixed multi-angle detector. These data are reduced using the methodology of Zimm and yield the excluded volume, which is proportional to A_2, the size, $<r_g^2>_z$, and the weight-average molecular weight, $\bar{M}_w$ of the scatterer [20]. Specifically, it is the angular component of the scattering data that is used to determine $<r_g^2>_z$. Alternatively, one can measure $\bar{R}_{\theta}$ at angles as low as 5–7°, where $\sin^2\theta/2$ is approximately zero and consequently $P_{(\theta)} = 1$. This method eliminates the size dependence of $\bar{R}_{\theta}$ at low-angles and $\bar{R}_{\theta}$ needs to be measured only as a function of C yielding A_2 and $\bar{M}_w$ [21]. The size information is lost but the low-angle experiment is considerably simpler, and usually only $\bar{M}_w$ is of interest. This is the principle of the LALLS detector.

However, most biopolymers of common interest are very small relative to the wavelength of light used in a scattering experiment, *i.e.*,

$$\frac{<r_g^2>_z}{\lambda^2} \ll 1 \qquad (5)$$

Substituting relationship 5 in eqn. 4 reveals that the cumbersome terms with angular dependence will be much less than 1 and therefore, even at large scattering angles such as 90°, $P_{(\theta)}$ will be very close to 1. For example, an immunoglobulin M (IgM) of 10^6 dalton molecular weight with a typical partial specific volume of 0.73 ml/g and a roughly globular structure has a radius of *ca.* 7 nm. Its radius of gyration will therefore be *ca.* 5 nm (the relationship between the radius, r, and the radius of gyration, $<r_g^2>$, is $<r_g^2> = (3/5)r^2$ [19]). Thus, for IgM, in aqueous solution ($n = 1.33$) when 500-nm light is scattered at 90°,

$$P_{(90°)} \approx 1 - 0.005 \qquad (6)$$

Even for this large protein, $P_{(90°)}$ differs from 1 by less than 1%. For smaller proteins $P_{(90°)}$ will be even closer to 1, and for all scattering angles $P_{(\theta)}$ will also be close to 1. Therefore, for most compact proteins, $P_{(\theta)}$ will be *ca.* 1 throughout the range of experimentally accessible scattering angles, *i.e.*, from 5 to 150°. Measuring $P_{(\theta)}$ at multiple angles and then plotting $P_{(\theta)}$ against $\sin^2(\theta/2)$ would yield an essentially flat curve, giving little information about molecular size, $<r_g^2>_z$. $\bar{R}_{\theta}$ will then be sensitive to scattering angle only by virtue of its dependence on the geometry of

the light-scattering photometer (g in eqn. 2) and not by its relation to size through $P_{(\theta)}$. In other words, for compact biopolymers of molecular weight less than *ca.* 1×10^6 dalton, $<r_g^2>_z$ cannot be determined by measuring $\bar{R}_\theta$ as a function of angle, and the choice of scattering angle can be based on simplicity of experimental design, equipment availability and sensitivity. In deference to these experimental considerations, we have chosen to use a 90° light-scattering photometer and the approximation that $P_{(90°)} = 1$ throughout this work.

As the molecular weight of a biopolymer increases past 1×10^6 dalton for compact structures, the size dependence at 90° in the size/shape factor $P_{(\theta)}$ and hence in eqn. 1 is no longer negligible. For a highly denatured protein, which assumes a random coil configuration [22], a 1% deviation from $P_{(\theta)} = 1$ will be evident at a molecular weight of *ca.* 2.5×10^5 dalton [this value was estimated using polyglutamic acid as a model compound for a denatured protein and eqns. 5 and 7; the value for σ (eqn. 7) was taken from ref. 23]. For double-stranded DNA, which can be described as a worm-like coil, a 1% deviation will occur at *ca.* $5 \cdot 10^4$ dalton (*ca.* 80 base pairs) (the relationship between molecular weight and $<r_g^2>$ for DNA was taken from ref. 24). Under these conditions, the radius of gyration must be either measured in an independent experiment or expressed as a function of $\bar{M}_w$. In the latter case, the size/shape factor $P_{(\theta)}$ and in turn the Rayleigh–Gans–Debye approximation become a function of $\bar{M}_w$ without any explicit size dependence. For example, the relationship between $\bar{M}_w$ and $<r_g^2>$ for a random coil is

$$\bar{M}_w = \sigma <r_g^2> \tag{7}$$

where σ is a constant whose value can be found or determined from the literature [23,24], or approximated. Using eqn. 7, the Rayleigh–Gans–Debye approximation for a random coil becomes a simple quadratic in $\bar{M}_w$. Using this mathematical technique, one can (at least in theory) extend the range of a 90° light-scattering photometer to several million daltons for compact biopolymers, *ca.* 10^6 dalton for the denatured proteins (random coils) and *ca.* $2.5 \cdot 10^5$ dalton DNA (worm-like coils).

Although 90° detection is limited to a lower molecular weight range than low-angle scattering, it has important advantages. One is that a 90° light-

scattering photometer is not as sensitive as a LALLS detector to dust and other large particles. This relative insensitivity to particulates can considerably simplify the experimental design. Biopolymer solutions invariably contain particulate matter (*e.g.*, dust and other insoluble components) and bubbles which are relatively large and "massive" compared with most biopolymer molecules of common interest. Even following chromatography, the eluent contains column-derived particulates which are limited in size to *ca.* 0.5 μm by frits and other in-line filters. Air bubbles may also be present. These particulates scatter light strongly in the forward, low-angle, direction and only relatively weakly at 90° [19]. Thus they contribute much more to the noise in a LALLS experiment than they do in a 90° light-scattering experiment. This is an especially important consideration for experiments with small biopolymers at low concentrations, where scattering from these large particulates can obscure that from the biopolymers. In general, when using an HPLC LALLS detector, great care must be taken to filter particulates eluting from the column. No such special precautions are necessary using a 90° HPLC light-scattering photometer, making for much greater ease of system and sample preparation.

Another advantage of 90° light-scattering methodology is the availability of suitable detectors. As will be demonstrated below, the output of a simple fluorimeter (in this instance an HPLC detector), under specific conditions, obeys basic light-scattering relationships and can therefore be used to determine molecular weight. Further, if a variable- or multi-wavelength fluorimeter is used, the scattering wavelength can be optimized to minimize the undesirable effects of scatterer or solvent absorption, if any, or to match the scattering wavelength to that used in the available refractive index detector. Wavelength matching may be an important consideration for precision work [6]. In general, these HPLC detectors are robust, easy to use and sensitive.

Detector sensitivity is an especially important parameter in light scattering, as it sets the lower limit of detectable molecular weight. Additionally, under certain conditions, with a highly sensitive detector, experiments can be performed on solutions of low enough concentration that the virial expansion (eqns. 1 and 4) can be neglected. The Rayleigh–

Gans–Debye approximation [with $P_{(\theta)} = 1$] is then reduced to the simple Rayleigh relationship

$$\bar{R}_\theta = KC\bar{M}_w \qquad (8)$$

The Rayleigh equation can be used to determine absolute molecular weight if the light-scattering and UV and/or refractive index detectors are calibrated in an absolute manner [6,21]. Alternatively, the light-scattering photometer can be calibrated relative to a solvent of known scattering power such as toluene [25]. However, for the purposes of this paper, the methodology of Takagi [15] will be used, in which the light-scattering photometer and concentration detector responses are referenced to or calibrated against well defined protein or DNA standards. According to Takagi's methodology, eqn. 8 is rewritten in the following form:

$$I_s = K'(\mathrm{d}n/\mathrm{d}c)^2\, C\bar{M}_w \qquad (9)$$

where K' is a system constant which is determined empirically. If the concentration is measured using a UV detector and solving for $\bar{M}_w$, eqn. 9 becomes

$$\bar{M}_w = \frac{I_s A}{K''(\mathrm{d}n/\mathrm{d}c)^2\, UV} \qquad (10)$$

where K'' is another empirical system constant, UV is the output of the UV detector and A is the absorptivity of the biopolymer. If a refractometer is used to measure concentration, eqn. 9 becomes

$$\bar{M}_w = \frac{I_s}{K'''(\mathrm{d}n/\mathrm{d}c)\, RI} \qquad (11)$$

where K''' is a third constant and RI is the output of the refractometer.

If one is dealing with a class of compounds which all have, or are assumed to have, equivalent specific refractive index increments, i.e., $\mathrm{d}n/\mathrm{d}c$ values, then eqns. 10 and 11 can be simplified to

$$\bar{M}_w = \frac{I_s A}{\kappa'' \, UV} \qquad (12)$$

and

$$\bar{M}_w = \frac{I_s}{\kappa''' \, RI} \qquad (13)$$

respectively, where κ'' and κ''' are two other empirical system constants. In the simplest mode, a well defined protein of known molecular weight,

$\bar{M}_w^k$, is used as a standard to determine the molecular weight of an unknown protein, $\bar{M}_w^u$. If a ratio is made of the UV and light-scattering responses of two chromatographic runs, the system constant cancels out, to yield the equation

$$\bar{M}_w^u = \bar{M}_w^k \cdot \frac{I_s^u\, UV^k\, A^u}{I_s^k\, UV^u\, A^k} \qquad (14)$$

where I_s^u and I_s^k are the light-scattering photometer response to the unknown and known protein, respectively, and A^u and A^k are the respective absorptivities of these proteins. When the HPLC peaks of interest have the same absorptivities (i.e., when they are conformers of the same protein) or if a refractometer is used, eqn. 14 is similar to that for the RI detector, namely,

$$\bar{M}_w^u = \bar{M}_w^k \cdot \frac{I_s^u\, C^k}{I_s^k\, C^u} \qquad (15)$$

where C^u and C^k are the respective concentration detector responses to these proteins. If the chromatogram containing the unknown peak also contains a peak of known weight-average molecular weight, the two peaks can be used in the calculations of eqns. 14 and 15 to yield directly a value for $\bar{M}_w^u$. Examples using both of these methods will be shown in the Results and Discussion section.

EXPERIMENTAL

Apparatus

Chromatographic system A, used to demonstrate light-scattering photometer linearity and sensitivity as functions of molecular weight and weight concentration, consisted of a Model 250 Bio-Series pump (Perkin-Elmer, Mountain View, CA, USA), a Rheodyne Model 7125 injector (Alltech, Deerfield, IL, USA) fitted with a 100-μl sample loop and a Model 650-15 fluorescence detector (Perkin-Elmer). The fluorescence detector contained a 12-μl flow cell and was modified for use as a 90° light-scattering photometer by placing a Schott GG435 yellow second-order filter (Melles Griot, Irvine, CA, USA) in front of the excitation window with monochromators matched at the xenon arc source emission maximum of 467 nm. The time constant was set to 3 s. An alternative configuration used a Fluorolog II double–double monochromator fluorimeter (Spex

Industries, Edison, NJ, USA) with the same filter and monochromator settings as described above and a 25-μl flow cell (Hellma Cells, Jamaica, NY, USA). A Model 235 diode-array detector (Perkin-Elmer), monitored at 280 nm, served as the concentration detector. The detectors were arranged in series, with the UV preceding the light-scattering photometer. Care was taken to minimize the delay volume resulting in band spreading between the detectors. The Omega data system (PE-Nelson Analytical, Cupertino, CA, USA) was used for real-time monitoring and data storage. When the Spex fluorimeter was used, the Omega system monitored and stored the UV data channel while the Spex DM3000 acquisition and analysis system acquired the light-scattering photometer output. Data processing and presentation were done using Lab Calc (Galactic Industries, Salem, NH, USA). The column used for SEC was a 25 cm × 9.4 mm I.D. Zorbax GF-250 (Mac-Mod Analytical, Chadds Ford, PA, USA), fitted with a Rheodyne Model 7315 column inlet filter (Alltech) and operated at ambient temperature. The isocratic aqueous mobile phase was 50 mM sodium phosphate–100 mM KCl (pH 7.1) at a flow-rate of 0.7 ml/min. Spectroscopic measurements of protein concentrations were made using an Aviv Model 14DS (Aviv Assoc., Lakewood, NJ, USA) spectrophotometer.

Chromatographic system B consisted of all the hardware described for system A less the UV detector. Concentration measurements were obtained from a Model 5902 interference refractometer (RI) modified for use at 488 nm, incorporating a Model 5911 1-mm path length measuring cell (Tecator, Hoganas, Sweden). The SEC column was placed inside a column water-jacket (Rainin Instrument, Emeryville, CA, USA). The column and refractometer were thermostated at 30.3 ± 0.1°C using a Model F4-K dual-compensation circulating water-bath (Haake Buchler Instruments, Saddle Brook, NJ, USA). Detectors were arranged in series with the refractometer ahead of the light-scattering photometer. The mobile phase was 20 mM sodium phosphate–100 mM Na$_2$SO$_4$ (pH 7.0) at a flow-rate of 0.7 ml/min.

Experiments were designed to simulate the earlier work of Stuting et al. [16] with the 90° HPLC light-scattering detector in place of the LALLS detector. System A hardware, consisting of pump,

diode-array detector monitored at 220 nm and fluorimeter, were used for these experiments. In place of the C$_8$ column employed by Stuting et al., we used a 214TP54 25 cm × 4.5 mm I.D. C$_4$ column from Vydac. The mobile phases, flow-rate and gradient were as described in ref. 16.

Plasminogen chromatographic experiments were carried out using system A. Two sets of data were obtained under two different mobile phase conditions. The first set used the mobile phase described for system A. The second set used the system A mobile phase containing 10 mM of the lysine analogue 6-aminohexanoic acid (6-AHA), which has been shown to affect the conformation of Glu-plasminogen [26]. Sample preparation for dynamic light-scattering (DLS) measurements required the use of a Model HSC10K high-speed centrifuge with a Model HSR-16 rotor (Savant Instruments, Farmingdale, NY, USA). DLS measurements were performed on plasminogen samples buffered under both mobile phase conditions, using a Nicomp 370 submicron particle size analyzer (Pacific Scientific Instrument Division, Silver Spring, MD, USA). The light source for DLS was an Innova 90 argon ion laser (Coherent Laser Products Division, Palo Alto, CA, USA) operating at a wavelength of 488 nm.

Materials

The criteria used for selecting proteins as reference materials were that they be of the highest available purity, have established molecular weights and absorptivities and yield a single peak, or at least resolvable peaks on SEC. Proteins meeting these criteria and used in these studies were immunoglobulin M (IgM) (1 · 10^6 dalton, $A_{280}^{0.1\%} = 1.2$ cm^2/mg)[a], immunoglobulin G (IgG) (150 000 dalton, $A_{280}^{0.1\%} = 1.4$ cm^2/mg)[a], tumor necrosis factor (TNF, non-covalent trimer of 51 000 dalton, $A_{280}^{0.1\%} = 1.3$ cm^2/mg)[a] and macrophage colony stimulating factor (M-CSF, covalent dimer of 49 700 dalton, $A_{280}^{0.1\%} = 0.72$ cm^2/mg)[a] obtained from Cetus; human Glu-plasminogen (Pg, 94 000 dalton, $A_{280}^{0.1\%} = 1.69$ cm^2/mg)[b] obtained from American Diagnostica (Greenwich, CT, USA); thyroglobulin (Tyr, 669 000 dalton, $A_{280}^{0.1\%} = 1.08$ cm^2/mg) [27], bovine serum

---

[a] In-house determination.
[b] Data supplied by American Diagnostica.

albumin (BSA, 66 000 dalton, $A_{278}^{0.1\%} = 0.66$ cm^2/mg) [28], ovalbumin (Oval, 44 000 dalton, $A_{280}^{0.1\%} = 0.74$ cm^2/mg) [29], carbonic anhydrase (CA, 29 000 dalton, $A_{280}^{0.1\%} = 1.68$ cm^2/mg) [29], soybean trypsin inhibitor (STI, 20 100 dalton, $A_{280}^{0.1\%} = 1.02$ cm^2/mg) [29], lysozyme (Lys, 14 700 dalton, $A_{280}^{0.1\%} = 2.59$ cm^2/mg) [28] and ribonuclease (RNase, 13 500 dalton, $A_{278}^{0.1\%} = 0.73$ cm^2/mg) [28] from Sigma (St. Louis, MO, USA). Size-exclusion standards were obtained from Bio-Rad Labs. (Richmond, CA, USA). Potassium chloride and 6-amino-hexanoic acid were obtained from Sigma, sodium sulfate from Fluka (Buchs, Switzerland), Acrodisc 13 0.2-μm low-protein-binding syringe filters from Gelman Sciences (Ann Arbor, MI, USA), aceto-nitrile from J. T. Baker (Philipsburg, NJ, USA); trifluoroacetic acid (TFA) from Pierce (Rockford, IL, USA), Centricon 10 microconcentrators from Amicon (Danvers, MA, USA) and disposable boro-silicate glass culture tubes (50 × 6 mm I.D.) from Fisher Scientific (Pittsburgh, PA, USA). Water used for the preparation of all samples and solutions was Type 1, produced with a Lab 5 reagent-grade water purification system (Zyztech, Seattle, WA, USA).

Evaluation of light-scattering photometer response

(A) Experiments for evaluating the light-scatter-ing photometer response as a function of molecular weight, using a UV detector as the concentration detector (system A), were conducted by injecting 15–50 μg of each standard protein. Three replicate injections were made for each protein standard. The volumes injected never exceeded 100 μl. Peak areas obtained from the UV and light-scattering chroma-tograms were used to generate detector response values (see eqn. 12). The three values obtained for each protein standard were averaged and plotted against their literature molecular weights using linear regression analysis. The plot obtained re-presents a weight-average molecular weight calibra-tion graph, the inverse of the slope of which is the system constant κ''. This curve was used to establish the weight-average molecular weight for plasmin-ogen in a subsequent experiment. All calculations were based on integrated areas.

(B) Light-scattering photometer response as a function of injected mass was evaluated using IgG and STI. IgG in the range 1.1–10.8 μg and STI in the range 7.7–77 μg were injected on to system A.

The light-scattering photometer response, as quanti-fied by integrated areas, was then plotted against the injected mass. Light-scattering photometer sensi-tivity, defined as the minimum amount injected necessary to achieve a signal-to-noise ratio of *ca.* 4, was *ca.* 1.1 μg for IgG and *ca.* 7.7 μg for STI. To unambiguously discriminate protein peaks from detector noise, larger amounts of protein were injected.

(C) Experiments evaluating the light-scattering photometer response as a function of molecular weight using an RI detector as the concentration detector (system B) were performed by injecting 10–75 μg of each standard protein. Experiments were conducted as described in (A). The ratio of light-scattering to RI peak areas constituted the detector response values (see eqn. 13), which were plotted against the literature molecular weights. The inverse of the slope in the linear regression analysis of these data correspond to the system constant κ'''.

Human Glu-plasminogen

Chromatography. Glu-plasminogen was sup-plied in sealed ampules containing 1 mg of protein plus excipients. One ampule was reconstituted with 1 ml of water and the concentration was measured spectroscopically. Replicate 25-μg injec-tions of plasminogen were made on to System A. The detector response values obtained from the chromatographic data were averaged. Using the calibration graph generated as described in (A), weight-average molecular weights for the peaks observed in the chromatograms were determined by interpolation, using their detector response values. For comparison purposes, the molecular weight of Glu-plasminogen was estimated from a log–linear plot of molecular weight *versus* retention volume, using standard SEC methodology. The chroma-tograms used to construct the molecular weight-based calibration graph as described in (A) were also used to produce the retention-based calibration graph.

To assess the effects of conformational changes of Glu-plasminogen, calibration graphs of log (molec-ular weight) *versus* retention volume and molecular weight *versus* mass detector response were recon-structed, using the system A mobile phase contain-ing 10 mM 6-AHA. Each reference protein used to construct the calibration graphs was spiked to

contain 10 mM 6-AHA. One ampule of plasminogen was reconstituted and spiked to contain 10 mM 6-AHA; triplicate 25-μg injections were then chromatographed on system A and the results averaged. Mass detector response values and retention volumes were recorded for both the native and the extended forms of plasminogen. These values were used to calculate the molecular weight of these species using both the log (molecular weight) *versus* retention volume and the molecular weight *versus* mass detector response curves.

Dynamic light scattering. Dimer was observed to be present in Glu-plasminogen at the level of 5%. To assess accurately the changes in monomer hydrodynamic radius accompanying the transition from native to extended forms, dimer was removed. Monomer and dimer were baseline resolvable under system A chromatography conditions. Therefore, in a series of injections, one ampule of 1 mg/ml plasminogen was chromatographed and the monomer fraction collected. Centricon 10 ultrafiltration at 4°C was used to concentrate the sample to 1 mg/ml. The concentrated plasminogen was then rechromatographed and shown to be exclusively monomer with a retention volume characteristic of the native form. For DLS measurements, a 300-μl aliquot of this monomeric plasminogen was transferred to a clean, dust-free culture tube, sealed and centrifuged at room temperature for 4 min at 13 000 g. A second 300-μl aliquot spiked to contain 10 mM 6-AHA was similarly prepared. These centrifuged samples were measured by DLS at 25.0 $\pm$ 0.1°C using 700 mW of single-mode power. The resulting hydrodynamic radius obtained by DLS was then used to estimate molecular weight using the equation

$$\bar{M}_{\text{w}}^{\text{est}} = 1.6 \, R_{\text{h}}^{3} \tag{16}$$

where $\bar{M}_{\text{w}}^{\text{est}}$ is the estimated molecular weight, R_{h} is the hydrodynamic radius in ångstroms and the proportionality constant, 1.6, was empirically derived using the molecular weight and radii of hydration of the proteins listed in Table II in ref. 30. The uncertainty in this constant based on those data is $\pm 50\%$.

Reversed-phase HPLC of ribonuclease, bovine serum albumin and lysozyme

A solution consisting of BSA at 3.2 mg/ml,

RNAse at 9.8 mg/ml and Lys at 10.1 mg/ml [16] was prepared by adding powdered lyophilized Lys and BSA to a dilute RNAse solution. The mixture was passed through a 0.2-μm Acrodisc 13 filter and immediately chromatographed. Detector response values were calculated as before using integrated peak-area ratios combined with the appropriate absorptivities (see eqn. 12). To establish the identity of the resulting peaks, each protein was also chromatographed separately. These single protein solutions were allowed to equilibrate in solution for at least 1 h prior to injection.

RESULTS AND DISCUSSION

Experimental validation of theory and methodology

The use of a simple HPLC fluorimeter as a 90° light-scattering photometer appears to be both novel and somewhat controversial [31]. The purpose of this section is to show that the output of such a device obeys the Rayleigh relationship (eqn. 8) and can therefore be used to determine, on-line, the molecular weights of biopolymers. Further, the applicability of three working assumptions is demonstrated in the context of our methodology. These assumptions are (1) that $P_{(\theta)} \approx 1$ for compact biopolymers of $\bar{M}_{\text{w}} < 1 \cdot 10^{6}$ dalton; (2) that under normal HPLC conditions the virial expansion is negligible; and (3) that dn/dc for all proteins under similar chromatographic conditions is the same. Although none of these assumptions is crucial to our methodology, together they allow the use of the simplified data handling techniques outlined in ref. 15 and incorporated here as eqns. 9–15. The validity of the three assumptions is not rigorously individually proved, but their plausibility and applicability are demonstrated below.

First, eqn. 9 predicts that the output of the 90° light-scattering photometer should be a linear function of concentration, with a slope proportional to the $\bar{M}_{\text{w}}$ of the injected species. Hence there should be a linear relationship between the integrated light-scattering photometer output and the total injected protein mass. Fig. 1 shows that the integrated output of the light-scattering photometer for two proteins, soybean trypsin inhibitor (20 100 dalton) and an IgG (*ca.* 150 000 dalton) has a linear relationship with total injected mass ($r > 0.999$). The virial expansion in the Rayleigh–Gans–Debye approxi-
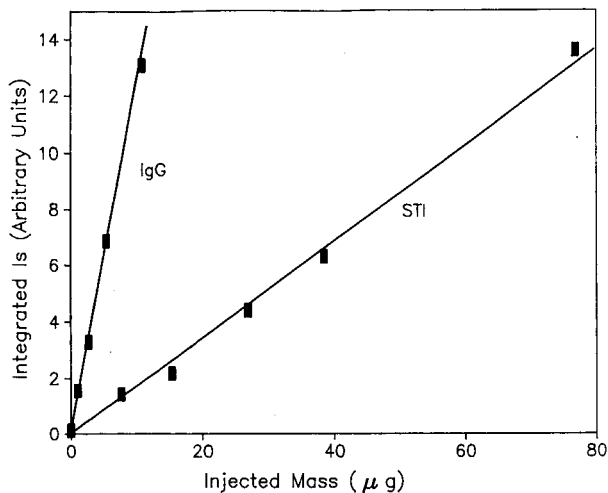
Fig. 1. Plot of the integrated output of the 90° light-scattering detector, I_s, *versus* the total injected mass for an IgG (molecular weight *ca.* 150 000 dalton) and for soybean trypsin inhibitor (STI, molecular weight 20 100 dalton).

mation (eqn. 1) gives rise to a higher than first-order (*i.e.*, non-linear) relationship between the scattered light intensity, I_s, and the concentration. The absence of any non-linearity in these data supports the assumption that the virial expansion is negligible over these concentrations. The ratio of the slopes for these two proteins, *ca.* 0.13, is equal to the ratio of their molecular weights (eqn. 15). Hence Fig. 1 shows that, over practical HPLC concentrations, I_s is proportional to injected mass and the virial expansion is negligible.

Second, eqn. 9 also predicts that the output from a 90° light-scattering photometer should be a linear function of biopolymer molecular weight. Fig. 2 demonstrates that the light-scattering photometer displays exceptional linearity ($r > 0.999$) with molecular weight, as predicted by eqn. 9, when the weight concentrations were measured using an on-line UV detector. The proteins ranged in molecular
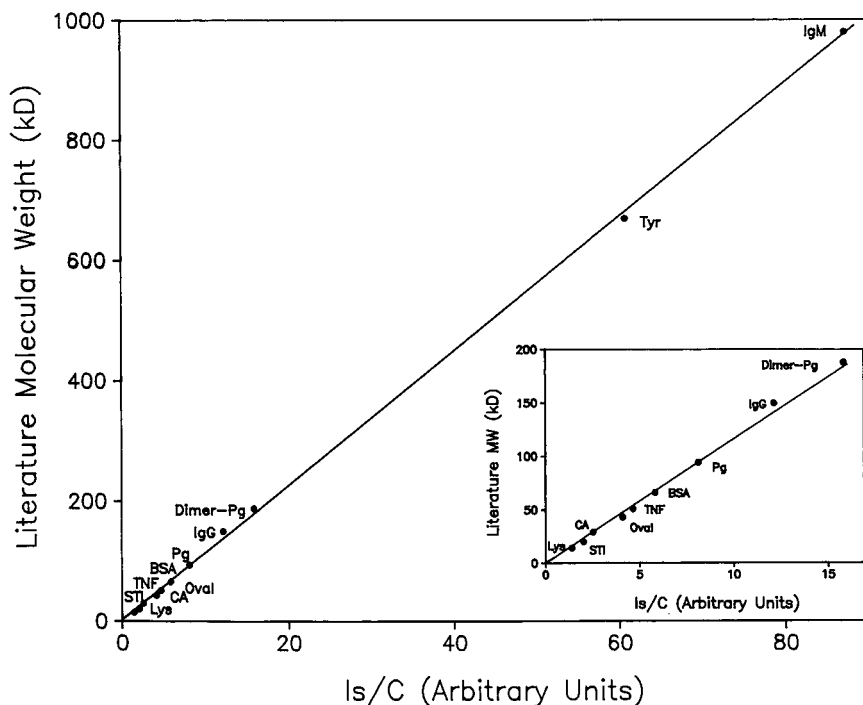
Fig. 2. Plot of literature molecular weight *versus* I_s/C for IgM (*ca.* 1 · 10⁶ dalton), IgG (150 000 dalton), plasminogen (Pg, 94 000 dalton) and its dimer, bovine serum albumin (BSA, 66 000 dalton), tumor necrosis factor (TNF, non-covalent trimer of molecular weight 51 000 dalton), ovalbumin (Oval, 44 000 dalton), carbonic anhydrase (CH, 29 000 dalton), soybean trypsin inhibitor (STI, 20 100 dalton) and lysozyme (Lys, 14 500 dalton). The inset shows the lower molecular weight region expanded for clarity. The concentrations were measured using UV adsorption detection (eqn. 12). kD = kilodalton.
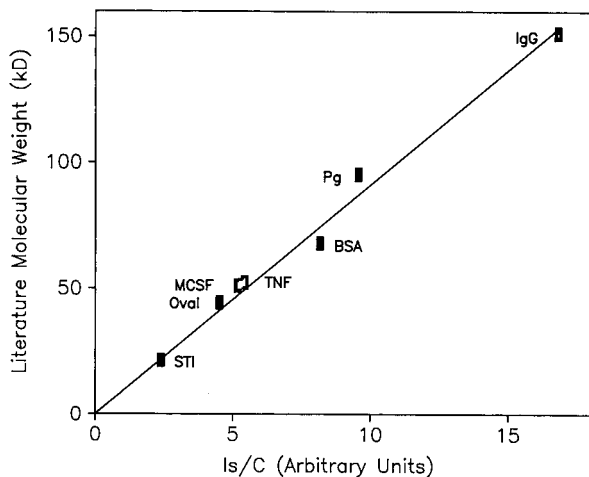
Fig. 3. Plot of literature molecular weight *versus* I/C for IgG (*ca.* 150 000 dalton), plasminogen (Pg, 94 000 dalton), bovine serum albumin (BSA, 66 000 dalton), tumor necrosis factor (TNF, non-covalent trimer of molecular weight 51 000 dalton), macrophage colony stimulating factor (M-CSF, covalent dimer of molecular weight 49 700 dalton), ovalbumin (Oval, 44 000 dalton) and soybean trypsin inhibitor (STI, 20 100 dalton). Concentrations were measured using a refractometer (eqn. 13).

weight from 14 500 to $1 \cdot 10^6$ dalton. Although smaller proteins yielded signal-to-noise ratios large enough to be detected, they were not quantifiable owing to the lack of chromatographic resolution between the protein and the inclusion volume of the column. Fig. 3 shows the same linear relationship between I_s and $\bar{M}_w$ when a refractometer is used to measure concentration (eqn. 11). Eqns. 1 and 4 taken together imply that a biopolymer large enough to cause $P_{(\theta)}$ to deviate from 1 would scatter less, on a weight basis, than a smaller biopolymer. This phenomenon would give rise to an upward curvature in the plot of molecular weight *versus* light-scattering photometer response. The linearity in Figs. 2 and 3 demonstrates that, in fact, for these proteins, $P_{(\theta)} \approx 1$.

Third, if the dn/dc values for various proteins were dissimilar, the value of $I_s/C\bar{M}_w$ would vary from protein to protein (eqn. 9). The goodness of fit of the data to the line in both Figs. 2 and 3 justify using the assumption that they are similar. Individual proteins vary slightly in dn/dc but, as a whole, this approach to data handling has broad applicabil-

ity. From a theoretical viewpoint, assuming that proteins have similar dn/dc values is equivalent to assuming that, on a weight basis, they have similar amino acid compositions [32]. In fact, this is true for most proteins. To the extent that different length polymers of each type of nucleic acid (*e.g.*, double-stranded DNA) have the same average composition, any length polymer of that type will have the same dn/dc as any other length polymer of the same type under similar conditions. The dn/dc value is measured on a per weight basis and is, therefore, not a function of polymer length or number of basis pairs.

The assumption that the dn/dc values of the species of interest are similar simplifies not only the mathematics, but also the experimental design in that only two detectors are needed, a light-scattering photometer and concentration detector. However, this assumption should be used with caution. For example, a heavily glycosylated protein may have a dn/dc that is significantly different from that of a non-glycosylated protein. Whenever the composition of the biopolymer of interest is unusual (*e.g.*, a protein with an unusually high number of aromatic residues) or unknown (glycosylated?), the dn/dc should be measured. This can be done on-line in either an absolute or relative manner, using a UV detector for concentration and a refractometer for solution refractive index. The combined outputs are used to calculate the dn/dc which, when combined with the output of the light-scattering photometer, yields molecular weight (eqn. 9). These three detection methods (light-scattering photometer, UV detector and refractometer) are described in detail for relative measurements in ref. 12 and for absolute measurements in ref. 6. A 90° light-scattering detector such as that described here can be substituted for the LALLS detector in ref. 12 and, if it can be absolutely calibrated, for that in ref. 6.

The choice of concentration detector to be used in light-scattering experiments is mostly a matter of convenience. An HPLC fluorimeter, a UV detector or a refractometer (when using the assumption of similar dn/dc values) could be employed. The UV detector is useful for proteins and nucleic acids and is robust, easy to set up and applicable to gradient HPLC methods. However, the absorptivity of the biopolymer needs to be known (eqns. 10, 12 and 14). Also, the error in the dn/dc (arising, for example, from the failure of the assumption of similar dn/dc

values) produces an error in the calculated $\bar{M}_w$ that is proportional to the square of the error in dn/dc. In this context, a fluorimeter is very similar to a UV detector except that the fluorescence quantum yield of the biopolymer now needs to be known, in addition to its absorptivity. The product of the quantum yield multiplied by the absorptivity needs to be substituted for the absorptivity in eqns. 10, 12 and 14. If a refractometer is used, the absorptivity of the biopolymer need not be known and the error in dn/dc contributes only in a linear fashion to that of the $\bar{M}_w$ (eqn. 11). Unfortunately, refractometers are not as easy to use as UV detectors, owing to their temperature and pulse sensitivity, and they cannot be readily applied to gradient methods. The signal-to-noise ratio of the concentration detector is not of prime importance in light scattering, as the sensitivity of the light-scattering photometer is typically limiting.

In order to be practical, a light-scattering photometer must be able to detect reliably biopolymers at the injected masses commonly used in modern HPLC. Fig. 4 shows that the light-scattering photometer that we used, an HPLC fluorimeter, can reliably detect *ca.* 8 μg of soybean trypsin inhibitor (20 000 dalton) and 1 μg of IgG (150 000 dalton). Eqn. 9 establishes that the output of the light-scattering photometer, I_s, is proportional to the product of C and $\bar{M}_w$, explaining the differential sensitivities of the detector to these two proteins. The Spex Fluorolog II, which was used to cross-validate many of the above results (data not shown), had a sensitivity roughly equivalent to that of the PE 650-15.

Applicability of 90° HPLC light scattering in biochemistry

The theoretical and experimental results above confirm that a simple 90° fluorimeter can be used as a light-scattering photometer in a fairly straightforward manner to obtain the molecular weights of biopolymers eluted from HPLC columns. Therefore, these simple devices can be used to address many of the same problems investigated with LALLS photometers. To emphasize this point, two examples are given.

First, reversed-phase chromatography is widely used to purify and characterize proteins, and is capable of resolving conformers as well as monomers from aggregates. However, it is usually not possible, on the basis of retention volume or percentage of organic modifier alone, to distinguish between peaks that differ only in conformation and those which differ in their state of aggregation. Light scattering can accomplish this task.

Fig. 4. Chromatograms of I_s (PE 650-15) *versus* retention time for (A) soybean trypsin inhibitor (20 100 dalton, total injected mass = 7.7 μg) and (B) IgG (150 000 dalton, total injected mass = 1.1 μg). Both chromatograms show early-eluting material marked with an asterisk.
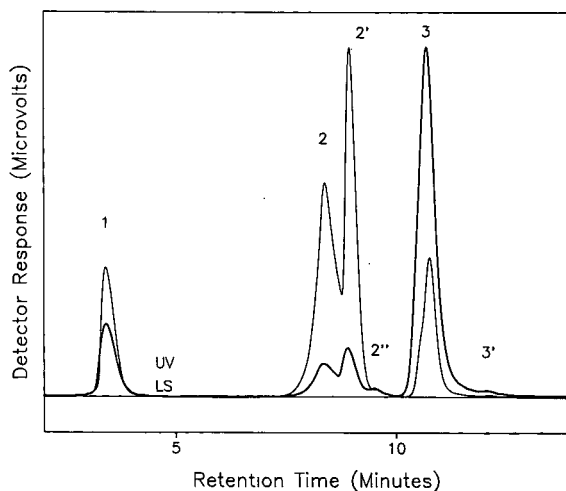

Fig. 5. Linear gradient reversed-phase HPLC of RNase (13 500 dalton), lysozyme (14 500 dalton) and BSA (66 000 dalton).

Fig. 5 shows the reversed-phase chromatography of a mixture of RNase, Lys and BSA [16]. Individual injections of each protein showed that whereas RNase appears to be eluted as a single monomeric species, Lys has three peaks and BSA two. The I_s/UV ratios of Lys peaks 2 and 2′ are equal and therefore the $\bar{M}_w$ of 2 and 2′ are equal, suggesting that they are separable as conformers of equivalent mass (eqn. 14). Further, the experimentally derived ratio (eqn. 15) of the molecular weights of Lys peaks 2 and 2′ to that of RNase is 0.97, while the theoretical ratio of the molecular weights of Lys (14 500 dalton) to RNase (13 500 dalton) is 1.05. The close agreement between the ratios establishes that peaks 2 and 2′ are forms of Lys monomer. The error between the theoretical value of 1.05 and the experimentally derived value of 0.97 may arise from the uncertainty in absorptivity and dn/dc values of these two proteins under the reversed-phase chromatographic conditions at which they are eluted. Again, using the simple ratio method embodied in eqn. 14, the material eluted under Lys peak 2″ is calculated to be approximately nine times as massive as that of peaks 2 and 2′. It is therefore aggregated material. BSA peaks 3 and 3′ are equally massive and are both approximately 4.5 times the molecular weight of RNase, indicating that they are conformers of monomeric BSA (66 000 dalton).

The identification of Lys peaks 2 and 2′ as resulting from conformational change rather than primary structural differences is supported by an experiment in which the dissolution time was increased prior to reversed-phase (RP) HPLC injection. The protein mixture chromatographed in Fig. 5 was prepared by adding lyophilized Lys and BSA to a dilute RNase solution and immediately injecting the mixture. When Lys was allowed to equilibrate in solution for *ca.* 1 h before being injected on-column, peak 2 almost disappeared and nearly all the mass was found in peak 2′ (Fig. 6). As 2 and 2′ are capable of interconversion, their separation is probably due to differences or changes in conformation. This inference is supported by previous work by Benedek *et al.* [33] and Lu *et al.* [34], who have shown that Lys can be eluted in RP-HPLC as two peaks, one of which has undergone a reversible conformational change while on the column. The absence of peak 2″ in Fig. 6 suggests that the additional time in solution prior to injection allowed the Lys aggregates to dissociate.
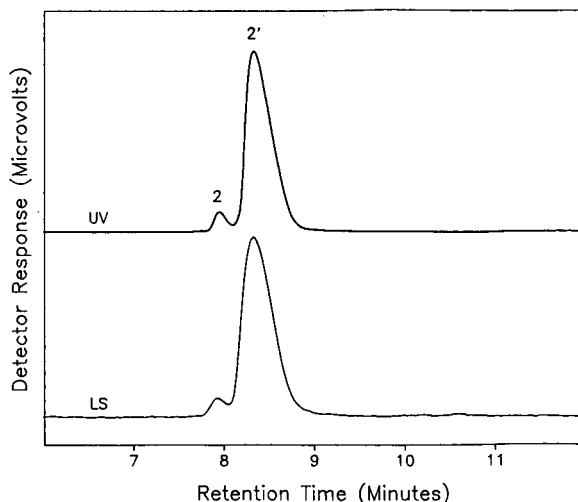

Fig. 6. Linear gradient reversed-phase HPLC of lysozyme (gradient and chromatographic system identical to Fig. 5). Peaks 2 and 2′ correspond to the similarly labeled peaks in Fig. 5.

The second example is used to illustrate the utility of combining classical light-scattering with SEC and DLS to investigate protein conformational changes and protein–matrix interactions. Specifically, we studied the effects of the presence of the lysine analogue 6-AHA on the conformation and chromatography of human Glu-plasminogen (Pg). In the
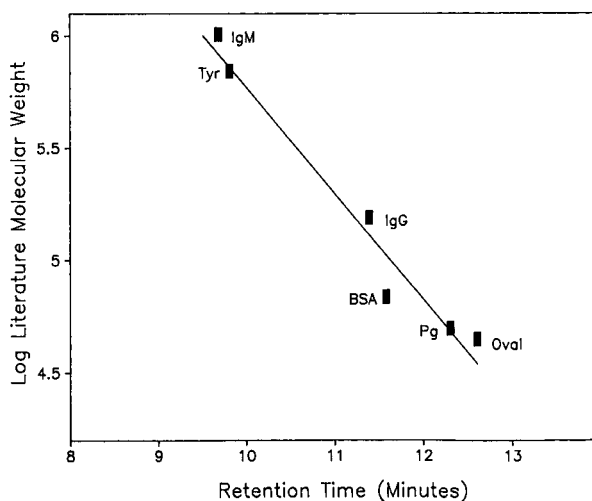

Fig. 7. Log(molecular weight) *versus* retention time for GF-250 SEC column used to estimate the molecular weight of plasminogen in the absence of the lysine analogue 6-AHA. Abbreviations of protein names as in Fig. 2.
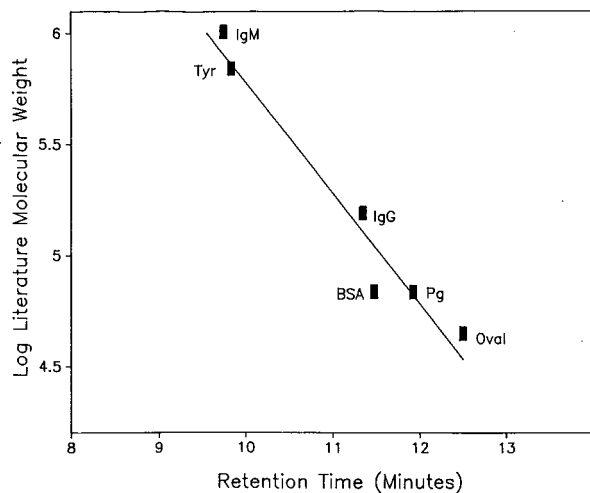
Fig. 8. Log (molecular weight) *versus* retention time for GF-250 SEC column used to estimate the molecular weight of plasminogen in the presence of 6-AHA. Abbreviations of protein names as in Fig. 2. The buffer used contained 10 mM 6-AHA.
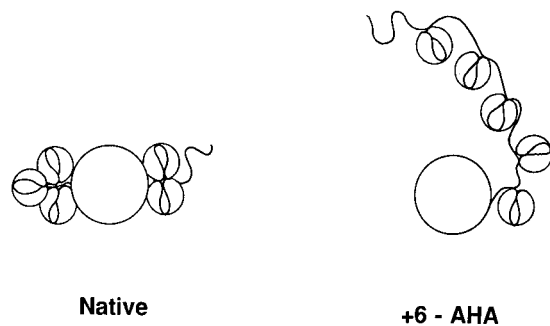

Native   **+6 - AHA**

Fig. 10. Plasminogen (94 000 dalton) undergoes a transition from a compact native state to an extended structure in the presence of the lysine analogue 6-AHA [26].

absence of 6-AHA, the log (molecular weight) *versus* retention time curve for Pg on the GF-250 SEC column yields an estimated molecular weight of *ca* 50 000 dalton (Fig. 7). When Pg was chromatographed with 10 mM 6-AHA added to the eluent, the apparent molecular weight increased to *ca.* 61 000 dalton (Fig. 8). Both calibration graphs were derived using standard SEC methodology and the

Fig. 9. SEC of plasminogen in (A) the absence and (B) the presence of 10 mM 6-AHA.

chromatography of the protein standards and Pg appeared normal (Fig. 9). Taken in isolation, these data are difficult to understand as the molecular weight of Pg is known to be 94 000 dalton [35].

DLS measurements determined a hydrodynamic radius of 3.8 nm for Pg in the absence of 6-AHA and of 4.7 nm when 6-AHA was added to the Pg solution. These data are consistent with either a dimerization of Pg (170 000 dalton, eqn. 16) or an unusually .large conformational change of Pg monomer.

Using the 90° light-scattering photometer and the calibration graph shown in Fig. 2, the molecular weight of Pg in both the presence and absence of 6-AHA was determined to be 91 000 dalton (Pg was not included in the data used to generate the calibration graph). In the light of these results, the appropriate interpretation of the DLS data is that they show that Pg monomer undergoes a large unfolding on addition of the lysine analogue (Fig. 10). This is in fact the case, as has been reported previously [26]. The anomalous SEC data presumably are caused by shape and/or other secondary interactions between the protein and the column matrix which result in increased retention.

CONCLUSIONS

Starting from the Rayleigh–Gans–Debye theory of light scattering, we have shown that there is no appreciable size dependence of the scattering function at 90° for compact biopolymers of up to $1 \cdot 10^6$ dalton. For less compact structures, such as highly denatured proteins, the same principles should hold

true up to a molecular weight of $2 \cdot 10^5$ dalton and for double-stranded DNA up to molecular weight of $5 \cdot 10^4$ dalton. Therefore, a 90° light-scattering photometer can be used to determine the molecular weight of these biopolymers without having to measure their size. We have demonstrated this experimentally for native proteins using a simple 90° HPLC fluorimeter with matched excitation and emission monochromators as a 90° HPLC light-scattering photometer. The light-scattering photometer showed excellent linearity and goodness of fit with molecular weight and weight concentration.

REFERENCES

1 R. D. Smith, J. A. Loo, C. G. Edmonds, C. J. Barinaga and H. R. Udseth, *Anal. Chem.*, 62 (1990) 882.
2 K. M. Gooding and F. E. Regnier, in K. M. Gooding and F. E. Regnier (Editors), *HPLC of Biological Macromolecules*, Marcel Dekker, New York, 1990, Ch. 3, p. 47.
3 M. E. McDonnell and A. M. Jamieson, *Biopolymers*, 15 (1976) 1283.
4 Y. Sato, N. Ishikawa and T. Takagi, *J. Chromatogr.*, 507 (1990) 25.
5 T. Kumo, K. Shimogawara, H. Fukuzawa, S. Muto and S. Miyachi, *Eur. J. Biochem.*, 192 (1990) 557.
6 H. M. Stuting and I. S. Krull, *Anal. Chem.*, 62 (1990) 2107.
7 R. Mhatre, I. S. Krull and H. H. Stuting, *J. Chromatogr.*, 502 (1990) 21.
8 Y. Hayashi, H. Matsui and T. Takagi, *Methods Enzymol.*, 172 (1989) 514.
9 C. Jackson, L. M. Nilsson and P. J. Wyatt, *J. Appl. Polym. Sci. Appl. Polym. Symp.*, 43 (1989) 99.
10 I. Krull, H. H. Stuting and S. C. Krzysko, *J. Chromatogr.*, 442 (1988) 29.
11 T. Nicolai, L. Van Dijk, J. A. P. P. Van Dijk and J. A. M. Smit, *J. Chromatogr.*, 389 (1987) 286.
12 S. Maezawa and T. Takagi, *J. Chromatogr.*, 280 (1983) 124.
13 S. Maezawa, Y. Hayashi, T. Nakae, J. Ishii, K. Kameyama and T. Takagi, *Biochim. Biophys. Acta*, 747 (1983) 291.
14 K. Kameyama, T. Nakae and T. Takagi, *Biochim. Biophys. Acta*, 706 (1982) 19.
15 T. Takagi, *J. Chromatogr.*, 506 (1990) 409.
16 H. H. Stuting, I. S. Krull, R. Mhatre, S. C. Kerzysko and H. G. Barth, *LC · GC*, 7 (1989) 402.
17 P. Putzeys and J. Brosteaux, *Trans. Faraday Soc.*, 31 (1935) 1314.
18 G. Dollinger, B. Cunico and M. Kunitani, *Anabiotec '90 Meeting, San Francisco, CA, 1990*, Abstract L85.
19 P. Kratochvil, *Classical Light Scattering from Polymer Solutions*, Elsevier, Amsterdam, 1987, Ch. 1, p. 7.
20 P. Kratochvil, *Classical Light Scattering from Polymer Solutions*, Elsevier, Amsterdam, 1987, Ch. 3, p. 113.
21 R. C. Jordan, *J. Liq. Chromatogr.*, 3 (1980) 439.
22 C. Tanford, K. Kawahara and S. Lapange, *J. Am. Chem. Soc.*, 89 (1967) 729.
23 M. Kurata and Y. Tsunashima, in J. Brandrup and E. H. Immergut (Editors), *Polymer Handbook*, Wiley, New York, 3rd ed., 1989, Section VII, Table C, p. 43.
24 D. Jolly and H. Eisenberg, *Biopolymers*, 15 (1976) 61.
25 P. Kratochvil, *Classical Light Scattering from Polymer Solutions*, Elsevier, Amsterdam, 1987, Ch. 2, p. 61.
26 W. F. Mangel, B. Lin and V. Ramakrishnan, *Science (Washington, DC)*, 248 (1990) 69.
27 G. Salvatore, G. Vecchio, M. Salvatore, H. Cahnmann and J. Robbins, *J. Biol. Chem.*, 240 (1965) 2935.
28 T. A. Bewley, *Anal. Biochem.*, 123 (1982) 55.
29 G. D. Fasman (Editor), *Handbook of Biochemistry and Molecular Biology, Vol. II, Proteins,* CRC Press, Cleveland, OH, 3rd ed., 1976, p. 383.
30 M. Potschka, *Anal. Chem.*, 162 (1987) 47.
31 K. P. M. Heirwegh, J. A. T. P. Meuwissen and R. Lantie, *J. Biochem. Biophys. Methods*, 14 (1987) 303.
32 P. Kratochvil, *Classical Light Scattering from Polymer Solutions*, Elsevier, Amsterdam, 1987, Ch. 7, p. 295.
33 K. Benedek, S. Dong and B. L. Karger, *J. Chromatogr.*, 317 (1984) 227.
34 X.-M. Lu, A. Figueroa and B. L. Karger, *J. Am. Chem. Soc.*, 110 (1988) 1978.
35 P. Wallen and B. Wiman, *Biochim. Biophys. Acta*, 257 (1972) 122.

CHROMSYMP. 2462

Constant-potential amperometric detection of carbohydrates at metal electrodes in high-performance anion-exchange chromatography

Teruhisa Ueda*,☆, Rosalind Mitchell and Fumito Kitamura☆

Shimadzu–Kansas Research Laboratory in the Center for Bioanalytical Research, University of Kansas, 2095 Constant Avenue, Lawrence, KS 66047 (USA)

Akira Nakamoto

R & D Engineering Department, Analytical Instruments Division, Shimadzu Corporation, 1 Nishinokyo-Kuwabaracho, Nakagyo-ku, Kyoto 604 (Japan)

ABSTRACT

Preliminary experiments were performed to detect carbohydrates at various metal electrodes in anion-exchange chromatography (AEC). The metallic wire forms of copper, rhodium, cobalt, silver, iridium, palladium, iron, tantalum, zirconium, niobium, nickel and copper–nickel alloy were investigated as working electrodes. Some of these materials exhibited an electrocatalytic response for the oxidation of glucose with sodium hydroxide solution as a mobile phase in AEC. Copper electrodes produced the lowest detection limit for glucose among the materials examined. For the development of a highly sensitive detection method for carbohydrates, copper wire electrodes have been extensively investigated in AEC. A linear response for glucose was obtained ranging from 1 pmol to 1 nmol for the 10-μl sample volume employed. The detection limit was 110 fmol for glucose at a signal-to-noise ratio of 3. The experimental parameters which affected the response of carbohydrates were also examined.

INTRODUCTION

Recent advances in protein chemistry have been generating a substantial need for methods for trace determinations of glycoproteins and glycopeptides. The resulting demand for carbohydrate detection with high sensitivity has necessitated a new detection scheme, as conventional detection methods for these compounds were not sensitive enough to detect small amounts of carbohydrates owing to the absence of a chromophore or a fluorophore in the structure of the molecule.

In the last decade, several electrochemical approaches have been explored to detect carbohy-

drates in connection with high-performance liquid chromatography (HPLC) [1–8]. The main difficulty with the electrochemical detection of these compounds is primarily due to a high overpotential for the oxidation of carbohydrates, which results in poor selectivity and high detection limits. Hence metal electrodes [1–3], chemically modified electrodes [4–6] and conventional carbon electrodes with electrochemically active reagents [7,8] have been employed to overcome this problem. When carbohydrate detection is investigated at various electrodes without a postcolumn reaction system, the electrode material may require an appropriate detection mode, *e.g.*, pulsed amperometric [1,2,9] or constant-potential amperometric [3,4], to maintain a reproducible response.

Pulsed amperometric detection (PAD), which employs platinum or gold electrodes for the oxida-

---

☆ Present address: R & D Engineering Department, Analytical Instruments Division, Shimadzu Corporation, 1 Nishinokyo-Kuwabaracho, Nakagyo-ku, Kyoto 604, Japan.

tion of carbohydrates, has become popular in conjunction with AEC because of the improved sensitivity. For example, a detection limit of 3 pmol was reported for xylitol in blood serum [10]. In this detection mode, double or triple pulsed potential waveforms are required to restore the electrochemical response for carbohydrates because of the necessity for cleaning and reactivation processes for the gold electrode. However, careful selection of the applied potentials for detection, cleaning and reactivation is necessary to ensure reproducible responses for carbohydrates [11]. As carbohydrates undergo an oxidation reaction on the oxide-free surface of a gold electrode, the presence of a gold oxide film inhibits the oxidation of carbohydrates [12]. The optimum potentials for PAD are related to the potentials at which the oxide film is formed and reduced on the gold electrode. Because this voltammetric behavior of the gold electrode is dependent on pH and solvent composition, mobile phase conditions in AEC will determine the optimum potentials for PAD. This aspect of the detection mode requires guidelines for the reasonable selection of pulse potentials for each mobile phase composition. Further, PAD seems inherently less sensitive than constant-potential amperometric detection because of the high charging current [5], even though the concept of the electrochemical reactivation of the electrode is reasonable.

Other electrochemical approaches have been made by employing an oxide-covered metal electrode such as nickel [3], chemically modified copper electrodes [5] and carbon paste electrodes containing ruthenium dioxide [6] in constant-potential amperometric detection. While the actual detection mechanism of carbohydrates on these electrodes is complicated [13], the oxide films on these electrodes seem to catalyze the oxidation reaction of carbohydrates in alkaline solution. Among these electrodes, the copper-based chemically modified electrode displayed the lowest detection limit of 1.2 pmol for glucose at a signal-to-noise ratio of 3 in AEC. Although the kinetics of glucose electrooxidation on some metal electrodes have been examined in a batch system [14], the electrochemical detection of carbohydrates in a flowing system is still of great interest.

In this study, various metal electrodes were evaluated in terms of the response for glucose in the constant-potential amperometric detection mode. The limits of detection for glucose at these electrodes were determined by AEC utilizing 150 mM sodium hydroxide solution as a mobile phase. Copper electrodes, which exhibited the lowest detection limits for glucose, were extensively investigated to optimize the response characteristics for carbohydrates in AEC. The detection mechanism of carbohydrates at metal electrodes is also discussed.

EXPERIMENTAL

Apparatus

All chromatographic experiments were performed with a chromatograph consisting of a Model LC-6A pump, a Model SIL-6B autoinjector, a Model CTO-6A column oven, a Model L-ECD-6A electrochemical detector and a Model CR601 data processor (all from Shimadzu Scientific Instruments, Columbia, MD, USA). The thin-layer electrochemical cell with an Ag/AgCl reference electrode was purchased from Bioanalytical Systems (West Lafayette, IN, USA). All metallic wires were obtained from Johnson Matthey (Ward Hill, MA, USA) at highest purity, except a Cu–Ni (55:45) alloy wire. Working electrodes were prepared by inserting a metal wire into a Kel-F block. Each electrode was polished with 0.05-μm alumina particles (Baikowski International, Charlotte, NC, USA) before use. The electrochemical cell was also installed in the column oven. A Wescan Anion/R column (25 cm × 4.1 mm I.D.) was obtained from Alltech (Deerfield, IL, USA) and used to evaluate the metal electrodes. A CarboPac PA1 column (25 cm × 4 mm I.D.) was purchased from Dionex (Sunnyvale, CA, USA) and used to investigate further the response characteristics of metallic copper electrodes for carbohydrates. After each electrode had been placed in the thin-layer cell, 150 mM sodium hydroxide solution was passed over the electrode surface for at least 24 h to form an oxide-covered surface.
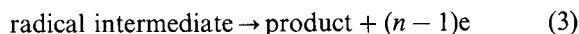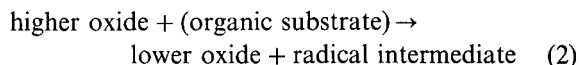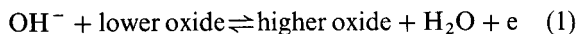
Reagents

Sodium hydroxide of semiconductor grade was purchased from Aldrich (Milwaukee, WI, USA). Carbohydrates obtained from Sigma (St. Louis, MO, USA) were dissolved in NANOpure water (Sybron Barnstead, Boston, MA, USA). Sodium hydroxide solutions were prepared in NANOpure water.

RESULTS AND DISCUSSION

Signal-to-noise ratio at various metal electrodes

The anodic oxidation of organic compounds such as amines, alcohols and carbohydrates at metal electrodes has been studied by a number of workers [15,16]. When a metal is placed in contact with an alkaline solution, its surface becomes covered with a layer of metal hydroxide, which eventually leads to the metal oxide. This process is strongly dependent on the applied potential, pH and temperature. The electrocatalytic oxidation of the compounds takes place on the oxide-covered surface of the metal electrode. The kinetics of these processes, including the catalytic oxidation of the organic compound, have been studied by Fleischman *et al.* [15]. Based on observations of the surface transition, such as Ni(II) to Ni(III), a mechanism involving a rate-determining reaction between the higher oxide and the organic compound has been established:

$$OH^- + lower\ oxide \rightleftharpoons higher\ oxide + H_2O + e \quad (1)$$

higher oxide + (organic substrate) →
$$lower\ oxide + radical\ intermediate \quad (2)$$

$$radical\ intermediate \rightarrow product + (n-1)e \quad (3)$$

The higher oxide layer on the electrode surface behaves as a strong oxidizing agent and reacts with the organic compound to yield a radical intermediate, which was confirmed by the differences in the rate constants for CH_3OH and C^2H_3OH at a nickel electrode. The radical intermediate evolves several electrons to result in a product. The electrochemical measurement of the electrons allows quantification of the organic compound.

Fig. 1 shows the chromatograms of 100 pmol of glucose detected at 1-mm-diameter wires of several metal electrodes with a 0.002-in.-thick gasket in AEC. As an alkaline medium is required for the formation of a metal oxide surface, an AEC mode utilizing a basic solution is suitable for evaluating these materials in terms of the electrochemical responses for carbohydrates. As can be seen in Fig. 1, the copper electrode exhibited the highest re-
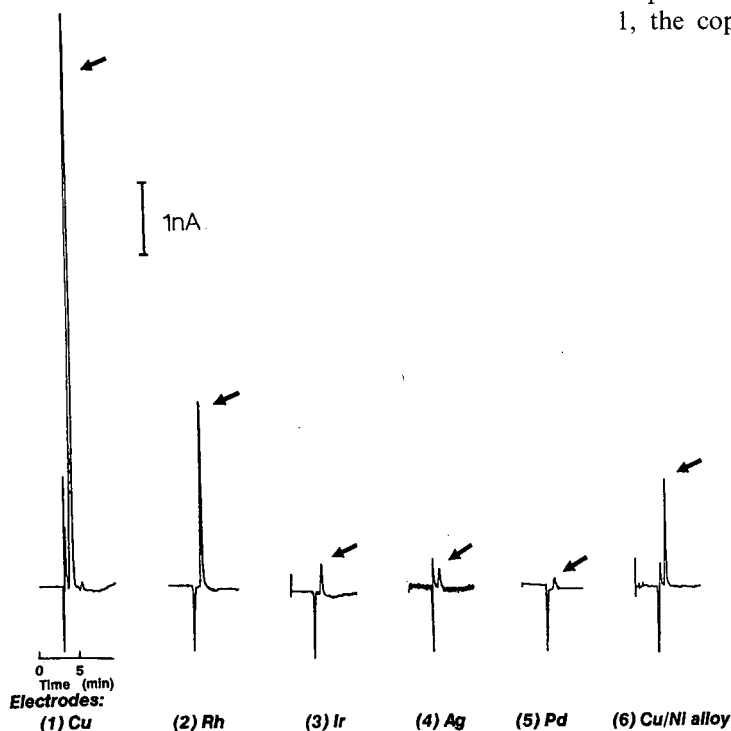

Fig. 1. Chromatograms of 100 pmol of glucose obtained at metal electrodes. Column, Wescan Anion/R; mobile phase, 150 mM sodium hydroxide; flow-rate, 0.7 ml/min; oven temperature, 35°C. Applied potentials: (1 and 3) +450 mV; (2) +480 mV; (4) +100 mV; (5 and 6) +500 mV. Background currents: (1) 51; (2) 28; (3) 32; (4) 22; (5) 33; (6) 34 nA. Arrows indicate glucose peaks. Glucose was dissolved in water at a concentration of 10 μM and the injection volume was 10 μl.

TABLE I

COMPARISON OF THE LIMITS OF DETECTION OF GLUCOSE AT VARIOUS 1-mm-DIAMETER METAL ELECTRODES

Analytical conditions as in Fig. 1.

Parameter	Cu	Rh	Cu–Ni	Ni	Co	Ag	Ir	Pd	Fe
LOD (pmol) (S/N = 3)[a]	0.22	1.6	4.5	5.7	8.8	13.0	13.6	30.0	60.0
Applied potential (mV)	450	480	480	500	450	100	450	500	500
Background current (nA)	51	28	32	50	15	22	32	33	8
Noise current (pA)	30	20	22	33	22	71	59	15	30
Signal (pA)[b]	40 200	3700	1450	1740	750	1600	1300	150	148
S/N ratio	1340	185	66	53	34	23	22	10	5

[a] LOD values were calculated from signal-to-noise (S/N) ratios for 100 pmol of glucose.
[b] Signal intensities were measured for 100 pmol of glucose.

sponse for glucose of any electrode examined. Rhodium, silver, iridium, palladium and copper–nickel alloy electrodes gave a response for glucose while no response was observed with tantalum, zirconium or niobium electrodes even at high applied potentials, *e.g.*, +800 mV.

Table I lists the detection limits for glucose at the optimum applied potential for each electrode. These metal electrodes allowed the detection of glucose at the picomole level in conjunction with AEC. Even though an increased applied potential produced an enhanced signal current for glucose at each electrode, a concomitant increase in background current caused an increased noise current, which resulted in a high detection limit. Therefore, the detection limit of glucose for each electrode was determined at the potential which produced the highest signal-to-noise ratio.

For example, oxide formation on a silver electrode in alkaline solution exhibited a high background current even at low applied potentials, which led to increased noise current. Hence, a limit of detection (LOD) at this electrode was measured at an applied potential of +100 mV with an acceptable background current. Although the signal current at the silver electrode was higher than those obtained at the cobalt and copper–nickel alloy electrodes, a higher noise current at the silver electrode led to an increased detection limit for glucose compared with those obtained at the cobalt and copper–nickel alloy electrodes. The increased noise current at this electrode seemed to be related to the surface roughness, which was primarily caused by anodic corrosion of the electrode material itself.
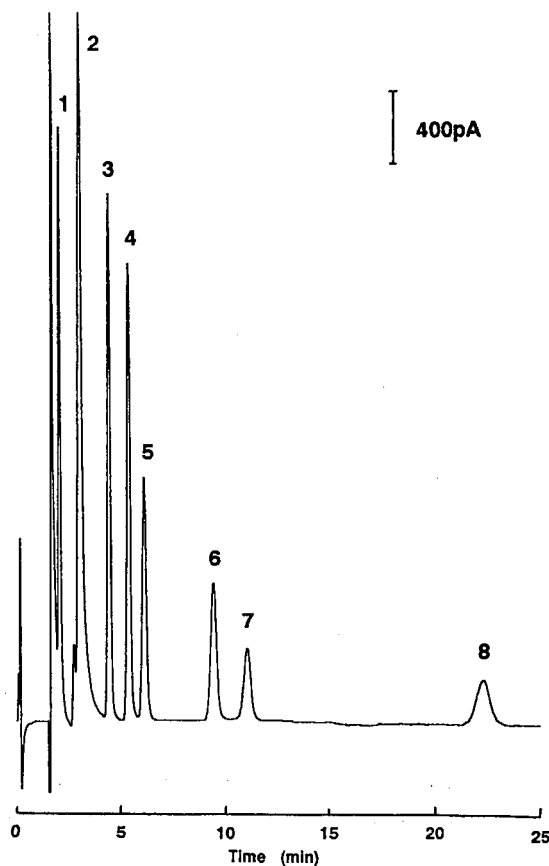

Fig. 2. Chromatogram of a mixture of carbohydrates obtained at a copper electrode. Column, CarboPac PA1; mobile phase, 150 m*M* sodium hydroxide; flow-rate, 0.7 ml/min; oven temperature, 25°C; applied potential, +450 mV. Each carbohydrate was dissolved in water at a concentration of 1 μM and the injection volume was 10 μl. Peaks: 1 = inositol; 2 = sorbitol; 3 = arabinose; 4 = glucose; 5 = fructose; 6 = lactose; 7 = sucrose; 8 = maltose.

The lowest LOD of 220 fmol for glucose was obtained at a copper electrode because of a high signal current. This may arise from a strong interaction between copper and carbohydrates, as is demonstrated by the separation of sugars on copper-modified packing materials in HPLC [17]. The response characteristics of carbohydrates at the copper electrode in AEC are discussed later.

The LOD obtained at a nickel wire electrode was 5.7 pmol, which compares favorably with that obtained at a tubular nickel electrode in AEC [3]. The LOD at this electrode may be improved by the addition of copper to the electrode material, as indicated by the LOD value at the copper–nickel alloy electrode. Even though the current study was focused mainly on the pure metal electrodes, it would be of great interest to evaluate various alloy electrodes in future work.

A rhodium electrode exhibited a lower LOD for glucose than nickel or other materials except copper. It should be noted, however, that a slight increase in applied potential incurred a dramatic increase in background current, which required precise control of the analytical conditions to ensure a stable baseline in AEC.

Response characteristics of metallic copper electrodes for carbohydrates

On the basis of the preliminary results described above, metallic copper electrodes were extensively investigated to understand the response characteristics for carbohydrates and to explore the improved sensitivity of carbohydrate detection. Amperometric detection of carbohydrates at a metallic copper electrode of 1 mm diameter with the 0.002-in.-thick gasket following AEC is demonstrated in Fig. 2. For both carbohydrate separation and detection, 150 mM sodium hydroxide is used as the mobile phase. The sample solution contains 10 pmol of each carbohydrate. As the pK_a values of neutral carbohydrates are usully between 12 and 13, these solutes are converted into anions at high pH and can be separated by AEC [2]. Further, the mobile phase condition produces a copper oxide layer on the surface of a copper electrode. Therefore, electrocatalytic oxidation of carbohydrates at the oxide-covered surface allows the constant-potential amperometric detection of the solutes with high sensitivity. As shown in Fig. 2, carbohydrates can be easily
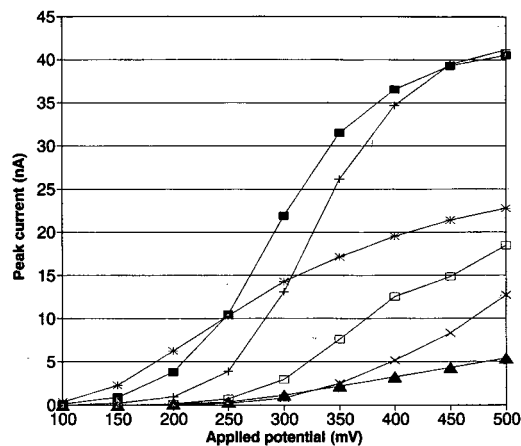

Fig. 3. Hydrodynamic voltammograms for several carbohydrates obtained at a copper electrode. Analytical conditions as in Fig. 2, except 10 μM of each sample concentration. ■ = Arabinose ($k' = 1.7$); + = glucose ($k' = 2.3$); ✱ = fructose ($k' = 2.7$); □ = lactose ($k' = 4.9$); × = sucrose ($k' = 6.1$); ▲ = maltose ($k' = 13.2$).

detected at the low picomole level with this methodology. This system has not been reported previously although the amperometric detection of carbohydrates at a copper-coated glassy carbon electrode has been investigated by Baldwin and co-workers [4,18].

The hydrodynamic voltammograms (HDVs) for several carbohydrates obtained at the copper electrode are shown in Fig. 3. The peak height for each carbohydrate was determined following separation in AEC. An increase in the applied potential led to an increased response for each carbohydrate. High background currents at applied potentials higher than +500 mV incurred an unstable baseline which interfered with the precise measurement of the peak heights for carbohydrates. Fig. 4 illustrates the potential dependence of the LODs of several carbohydrates at the copper electrode. The LOD values for the compounds decreased with increasing applied potential owing to the enhanced responses for carbohydrates. However, an increased applied potentil caused a high noise current because of an increased background current. Therefore, the LOD values almost reached a plateau at potentials higher than +450 mV. Taking into account the possible anodic corrosion of the copper material itself in alkaline solution, optimum potentials for carbo-
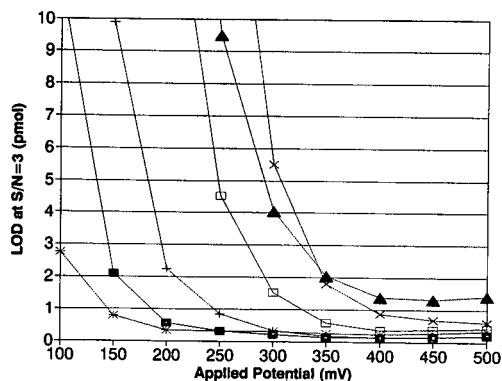
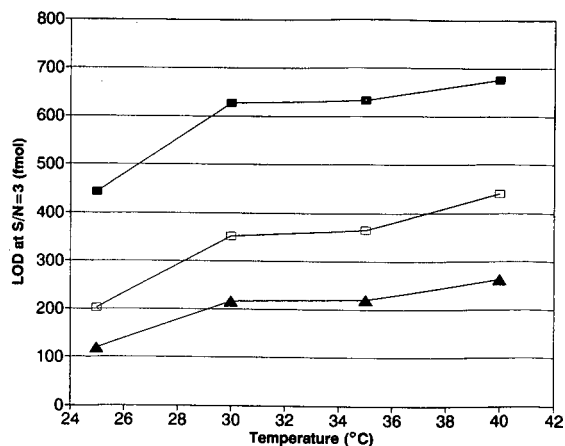Fig. 4. Plots of LOD *vs.* applied potential at the copper electrode. Analytical conditions and symbols as in Fig. 3.

Fig. 5. Plots of LOD *vs.* temperature at the copper electrode. Applied potential, +500 mV. Other conditions as in Fig. 3. ▲ = Sorbitol; □ = glucose; ◧ = lactose.

hydrate oxidation may lie between +450 and +500 mV at the copper electrode.

Temperature is one of the important factors which may affect the response for a solute in addition to the background current in electrochemical detection. Usually, a high temperature leads to an increased electrochemical response. Therefore, the effect of temperature on the LOD for a solute should be observed in order to optimize the detection conditions. The temperature dependence of the LOD values for carbohydrates at the copper electrode is shown in Fig. 5. Although an elevated temperature produced increased responses for the solutes, concomitant increases in both noise and

background current gave rise to increased LOD values for these solutes. Judging from Fig. 5, temperature control at sub-ambient levels may be required to improve further the signal-to-noise ratios for carbohydrates at the copper electrode. For practical applications of this electrode to real samples, the electrochemical cell equipped with a copper electrode needs to be operated at a constant temperature to ensure reproducible responses for carbohydrates.

A large linear dynamic range is characteristic of

TABLE II

COMPARISON OF THE LIMITS OF DETECTION OF GLUCOSE AT COPPER ELECTRODES WITH DIFFERENT DIAMETERS

Conditions as in Fig. 2, except for the electrode diameters.

Parameter	Diameter (mm)		
	0.5	1.0	2.0
LOD (pmol) (S/N = 3)[a]	0.14	0.17	0.15
Applied potential (mV)	450	450	450
Background current (pA)	7000	30 000	120 000
Noise current (pA)	4	15	59
Signal current (pA)[b]	8500	26 000	118 000
S/N ratio	2130	1730	2000
Surface area (cm^2)	$2.0 \cdot 10^{-3}$	$7.9 \cdot 10^{-3}$	$3.1 \cdot 10^{-2}$
Signal density (μA/cm^2)	4.3	3.3	3.8

[a,b] See Table I.

modern electrochemical detectors combined with HPLC. The linearity of response for glucose at the copper electrode was examined with injections of the solute at different concentrations in AEC. The linear dynamic range extended from 0.1 to 100 μM for the 10-μl sample volume injected and the correlation coefficient was greater than 0.99 (data not shown).

Optimization of detector elements

In the thin-layer cell design used in this study, the column effluent flows parallel to the working electrode surface which faces an auxiliary electrode block. The size of the layer is determined by the thickness of the gasket held between these electrodes. A rectangular channel framed by the thin gasket can be regarded as an electrochemical flow cell. Therefore, the actual cell volume in this study may be dependent on the size of the working electrode and the thickness of the gasket.

The surface area of the working electrode in contact with the column effluent contributes to the background current, noise and signal current represented by the analyte peak current. The dependence of the electrochemical response for glucose oxidation on the surface area of the copper electrode was investigated at metallic copper electrodes with different diameters using AEC. As summarized in Table II, the background current and noise increased proportionally to the surface area of the copper electrode. As the signal current for glucose oxidation increased almost proportionally to the surface area of the electrode, the LOD values calculated from signal-to-noise ratios for 100 pmol of glucose were nearly the same, within experimental error. Although the decreased surface area of the electrode may produce improved signal-to-noise ratios for carbohydrates, successful results can be obtained with precise measurement of small signal currents in the picoampère range. This aspect of miniaturization of the electrode also requires careful shielding of the flow cell from both electrical and thermal viewpoints.

The thickness of a gasket is also an important factor in determining the volume of a flow cell. In an HPLC system, the thickness of the gasket affects the linear velocity of the column effluent in the flow cell. At a constant flow-rate, the linear velocity of the column effluent increases with decreasing thickness of the gasket. The thickness of the diffusion layer in

the flow cell depends on the linear velocity of the effluent. Therefore, the gasket thickness can be expected to affect the thickness of the diffusion layer, which is related to the signal current for carbohydrate oxidation.

Table III lists the LOD values for glucose with different PTFE gaskets using the experimental results at the same copper electrode of 1 mm diameter in AEC. As the gasket became thinner, the background current increased with a concomitant increase in the signal current for glucose. However, the noise current decreased with the 0.002-in.-thick gasket. Hence the signal-to-noise ratios for glucose increased with decreasing thickness of the gasket. With the 0.002-in-thick gasket, the LOD was 110 fmol for glucose at a signal-to-noise ratio of 3. This value is significantly lower than those obtained with pulsed amperometric detection at a gold electrode [2] or a cobalt phthalocyanine-containing chemically modified electrode [4,19] and ten times lower than that obtained with constant-potential amperometric detection at a copper-based chemically modified electrode [5]. As demonstrated in Table III, however, careful maintenance of the thin-layer cell will be necessary to ensure reproducible responses for carbohydrates at the copper electrode in AEC.

The LODs of several carbohydrates at the 1-mm-diameter copper electrode with a 0.002-in.-thick gasket are summarized in Table IV. Under the typical analytical conditions shown in Fig. 2, the LOD values were in the femtomole range.

TABLE III

EFFECT OF THE GASKET THICKNESS ON THE LIMITS OF DETECTION FOR GLUCOSE AT THE COPPER ELECTRODE

Conditions as in Fig. 2, except for the gasket thicknesses.

Parameter	Thickness (in.)		
	0.002	0.005	0.015
LOD (pmol) (S/N = 3)[a]	0.11	0.25	0.44
Applied potential (mV)	450	450	450
Background current (pA)	50 000	34 000	22 000
Noise height (pA)	15	22	22
Signal current (pA)[b]	41 900	26 600	15 000
S/N ratio	2800	1200	680

[a] See Table I.

TABLE IV

LIMITS OF DETECTION OF SEVERAL CARBOHY-DRATES AT THE COPPER ELECTRODE

Conditions as in Fig. 2.

Sample	LOD (fmol) (S/N = 3)	k'
Inositol	60	0.2
Sorbitol	70	0.7
Arabinose	110	1.6
Glucose	110	2.1
Fructose	200	2.5
Lactose	270	4.4
Sucrose	410	5.3
Maltose	920	11.7

a See Table I.

Stability of response for glucose at the copper electrode in AEC

Amperometric responses for the anodic oxidation of carbohydrates at the copper electrode were generated on the oxide-covered surface in contact with alkaline solution. The stability of the response for carbohydrates at the copper electrode in AEC may be related to the stability of the oxide layer on the electrode surface at a positive potential in sodium hydroxide solution.

The run-to-run stability of response in AEC was examined by measuring the chromatographic peak current for glucose over a 15-h period. The catalytic activity for anodic oxidation of glucose was maintained over long periods of time (data not shown). The relative standard deviation of the peak area for glucose was 1.3% during this set of experiments. As far as the run-to-run stability of response is concerned, the metallic copper electrode exhibits reproducible response characteristics for carbohydrates in AEC. However, the posssible anodic corrosion of the copper material itself in alkaline media may restrict the long-term stability of the response for carbohydrates in AEC.

The day-to-day stability of the response at the copper electrode is being investigated to explore further the utility of this system in practical trace analyses of carbohydrates. As mentioned above, careful maintenance of the flow cell and control of the analytical conditions, such as temperature and applied potential, will be necessary to ensure a stable response for carbohydrates on a day-to-day basis.

Detection mechanism

In this study, it was assumed that the anodic oxidation of a carbohydrate takes place on the oxide-covered surface at a metal electrode in alkaline solution as described above. For example, Reim and Van Effen [3] utilized an active nickel(III) oxide formed in alkaline medium as a strong oxidant for carbohydrates. However, the actual mechanism of the carbohydrate oxidation at various electrodes may be difficult to specify with certainty because the formation of a surface oxide at a metal electrode is strongly dependent on both applied potential and mobile phase pH. Recently, Luo *et al.* [13] examined the mechanism of the electrocatalytic oxidation of glucose at copper-based electrodes in 0.5 M sodium hydroxide solution using cyclic voltammetry. Although higher oxide species such as copper(III) are considered to play an important role in carbohydrate oxidation, the active surface state may contain other species, such as copper(II), as suggested by Luo *et al.* [13].

On the other hand, the presence of the surface oxide inhibits the oxidation of carbohydrates at some metal electrodes, such as gold and platinum, as carbohydrates are oxidized on oxide-free surfaces. Hence these electrodes necessitate a pulsed amperometric detection scheme in which double or triple pulsed potential waveforms are required for surface cleaning and regeneration of the oxide-free metal electrodes.

From this viewpoint, the electrochemical detection scheme should be optimized at each electrode to produce the maximum signal-to-noise ratios for carbohydrates. Therefore, future research includes both understanding the detailed detection mechanism and optimization of the electrochemical detection scheme at various electrodes to improve further the LODs for carbohydrates.

CONCLUSION

Carbohydrates can be detected without any derivatization at several metal electrodes with a constant-potential amperometric detection method. In connection with AEC, it is possible to determine these compounds at picomole levels. Among the electrodes investigated in this study, copper is the best material as a metal electrode in terms of signal-to-noise ratio. The LODs for carbohydrates

at a copper electrode in AEC are at the femtomole level.

ACKNOWLEDGEMENTS

REFERENCES

1 S. Hughes, P. L. Meschi and D. C. Johnson, *Anal. Chim. Acta*, 132 (1981) 1.
2 R. D. Rocklin and C. A. Pohl, *J. Liq. Chromatogr.*, 6 (1983) 1557.
3 R. E. Reim and R. M. Van Effen, *Anal. Chem.*, 58 (1986) 3203.
4 L. M. Santos and R. P. Baldwin, *Anal. Chem.*, 59 (1987) 1766.
5 S. V. Prabhu and R. P. Baldwin, *Anal. Chem.*, 61 (1989) 852.
6 J. Wang and Z. Taha, *Anal. Chem.*, 62 (1990) 1413.
7 N. Watanabe and M. Inoue, *Anal. Chem.*, 55 (1983) 1016.
8 S. Honda, T. Konishi and S. Suzuki, *J. Chromatogr.*, 299 (1984) 245.
9 D. C. Johnson and W. R. LaCourse, *Anal. Chem.*, 62 (1990) 589A.
10 K. Osawa, *Anal. Sci.*, 2 (1986) 165.
11 R. W. Andrews and R. M. King, *Anal. Chem.*, 62 (1990) 2130.
12 G. G. Neuberger and D. C. Johnson, *Anal. Chem.*, 59 (1987) 203.
13 P. Luo, S. V. Prabhu and R. P. Baldwin, *Anal. Chem.*, 62 (1990) 752.
14 Y. B. Vassilyev, O. A. Khazova and N. N. Nikoleva, *J. Electroanal. Chem.*, 196 (1984) 127.
15 M. Fleischman, K. Korinek and D. Pletchner, *J. Chem. Soc., Perkin Trans. 2*, (1972) 1396.
16 G. Vertes and G. Horanyi, *J. Electroanal. Chem.*, 52 (1974) 47.
17 J. L. Leonard, F. Guyon and P. Fabiani, *Chromatographia*, 18 (1984) 600.
18 S. V. Prabhu and R. P. Baldwin, *J. Chromatogr.*, 503 (1990) 227.
19 A. M. Tolbert and R. P. Baldwin, *Electroanalysis*, 1 (1989) 389.

High-temperature open-tubular capillary column liquid chromatography

G. Liu☆, N. M. Djordjevic and F. Erni*

Sandoz Pharma AG, Analytical Research and Development, CH-4002 Basle (Switzerland)

ABSTRACT

In open-tubular liquid chromatography (OTLC), elevation of the column temperature has the same effect as reduction of the column diameter in obtaining high column efficiencies, with the additional benefits of easier column handling and fewer problems with detection. On an experimental set-up with commercially available 50 and 100 μm I.D. reversed-phase columns working in the 100–200°C range, all the advantages predicted by OTLC theory for elevated column temperatures were confirmed: smaller slope of the plate height *vs.* linear velocity (*H* vs. *u*) curve, higher optimum linear velocity (*u*$_{opt}$) value and less pronounced influence of the retention on efficiency. High-temperature operation makes high-efficiency and high-speed OTLC analysis feasible. On a 19.6 m × 50 μm I.D. SB-Methyl-100 column operated at 200°C with acetophenone as the test sample, 1 143 000 theoretical plates were obtained within 50 min.

INTRODUCTION

In open-tubular capillary column liquid chromatography (OTLC) there is a large discrepancy between the theoretical and fundamental research and the practical application of the technique. Almost 40 years ago, Taylor [1,2] first described the band broadening of a solute in a liquid flow passing through tubular columns. A few years later, Golay [3] published his classical paper on capillary column chromatography. These works, together with Sternberg's detailed analysis of the band dispersions caused by various extra-column factors [4], built up the theoretical framework of capillary chromatography. The correctness of Golay's theory was proved by a large number of experiments [5–8]. In the meantime, Golay [9] and Tijssen [10] carried out important complementary studies on the secondary flow effect. Many groups have been involved in recent years [11–14] in the development of high-efficiency OTLC systems by using small bore (I.D. < 10

μm) columns. In all instances the established theory proved to be reliable.

In contrast, reports on the practical application of OTLC are rarely found in the literature. One explanation for this situation is in the fact that OTLC, when operated at room temperature, is of relatively low efficiency as compared with other separation techniques, such as capillary GC, capillary zone electrophoresis and capillary supercritical fluid chromatography. When very small-bore columns are used to obtain reasonable efficiency, the existing detection problem of OTLC becomes even more serious [15].

The height equivalent to a theoretical plate (HETP or *H*) of an open-tubular column is given by the Golay equation:

$$H = \frac{2D_\mathrm{m}}{u} + \frac{1 + 6k' + 11k'^2}{96(1 + k')^2} \cdot \frac{d_\mathrm{c}^2}{D_\mathrm{m}} \cdot u$$
$$+ \frac{2k'}{3(1 + k')^2} \cdot \frac{d_\mathrm{f}^2}{D_\mathrm{s}} \cdot u \qquad (1)$$

where D_m is the diffusivity of the solute in the mobile phase (cm²/s), D_s is the diffusivity of the solute in the stationary phase (cm²/s), d_c is the column inner

---

☆ On leave from the Southwest Research Institute of Chemical Industry, Chengdu 610047, China.

diameter (cm), d_f is the film thickness (cm), u is the velocity of the mobile phase (cm/s) and k' is the capacity factor of the solute. For larger bore (I.D. $\geqslant 50$ μm) and thin-film (thickness $\leqslant 0.25$ μm) columns, the Golay equation can be simplified to the following forms:

$$H = \frac{2D_m}{u} + \frac{1 + 6k' + 11k'^2}{96(1 + k')^2} \cdot \frac{d_c^2}{D_m} \cdot u \qquad (2)$$

or, for $k' = 0$,

$$H = \frac{2D_m}{u} + \frac{1}{96} \cdot \frac{d_c^2}{D_m} \cdot u \qquad (3)$$

The optimum velocity (u_{opt}), at which the plate height reaches the minimum, is given by

$$u_{opt} = (1 + k') \cdot \frac{D_m}{d_c} \left(\frac{192}{1 + 6k' + 11k'^2} \right)^{1/2}$$

or, for $k' = 0$,

$$u_{opt} = 13.86 \cdot \frac{D_m}{d_c} \qquad (4)$$

The analysis time for a practical separation problem is given by

$$t_R = N \cdot \frac{H}{u} \cdot (1 + k') = N \cdot \frac{1 + 6k' + 11k'^2}{96(1 + k')} \cdot \frac{d_c^2}{D_m} \qquad (5)$$

where N is the plate number needed for the separation. From eqns. 4 and 5, it is seen that both a decrease in column diameter and an increase in D_m improve the efficiency. For aqueous systems, an increase in column temperature from 20 to 200°C has the same effect in reducing the analysis time as a decrease in column diameter from 50 to 12 μm, because D_m increases with increasing column temperature [$D_{m200} = D_{m20}(\eta_{20}/\eta_{200})$ (473/293) = 17.47 D_{m20}, where D_{m200} and D_{m20} are the diffusivities of the solute and η_{200} and η_{20} are the viscosities of water at 200 and 20°C, respectively].

The effect of column temperature on efficiency has been studied by many workers on conventional RP-LC columns [16–19]. Antia and Horváth [20] performed an in-depth theoretical analysis of the effect of elevated column temperature on column performance for both porous and pellicular packings. Erni [21] recently pointed out not only that elevated column temperature is beneficial for packed-column chromatography, but also HPLC in open-column chromatography, but also HPLC in open

tubes is more feasible at higher temperatures even when the inner diameters are in the range 50–100 μm. He also showed that the strong dependence of the column efficiency on the k' values is much less noticeable at higher temperatures.

Even though the beneficial effect of higher column temperatures in OTLC is reasonable in theory, this has not so far been proved experimentally. The aim of this work was to verify the benefits predicted by OTLC theory for elevated column temperatures, study the influences of various instrumental and operating parameters, realize high-efficiency OTLC separations with commercially available columns and instruments and finally develop a prototype of high-temperature (HT) OTLC equipment that can be transferred to other users. This paper reports the experimental set-up and our preliminary results.

EXPERIMENTAL

The layout of the experimental unit is shown in Fig. 1. It consisted of two Kontron Model 420 HPLC pumps, a Rheodyne Model 7125 sample valve, a split tee-piece (Valco 1/16-in. tee, 0.01-in. bore), a capillary column, a Kratos Model 783 UV detector and a 0.5-1 stainless-steel cylinder (Model DOT3E1800, Swagelok) which was used for generating a back-pressure. A 20-μl loop was used for the 20-m column and a 5-μl loop was used for other
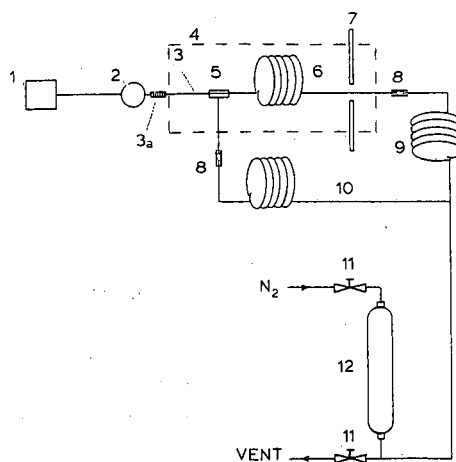

Fig. 1. Experimental set-up. 1 = HPLC pump; 2 = sample valve; 3 = preheating tube; 3a = heater; 4 = oven; 5 = split tee-piece; 6 = capillary column; 7 = optical fibre; 8 = zero dead-volume connector; 9 = restriction tube; 10 = split tube; 11 = needle valve; 12 = back-pressure vessel.

columns. A 3-mm segment of the polyimide coating of the capillary column (about 12 cm from the column end) was burned off to make a window for UV detection. The Kratos UV detector was modified in order to work with optical fibres (Superguide SFS 200/240 T; Luxmatic, Baar, Switzerland) to carry out on-column detection. A Valco 0.01-in. bore cross was used as detector cell where the capillary column passed through one channel, and the source and the collecting optical fibres were positioned on opposite sides of the window.

The split tee-piece, the capillary column and the detector cell were placed in an oven of our construction which was controlled by a temperature regulator (Digitemp mC 5100; Schuntermann & Benninghoven, Hilden, Switzerland). A 40 cm × 0.2 mm I.D. serpentine tube (Scientific Systems, State college, PA, USA) was used as the preheating tube between the injection valve and the split tee-piece. This was heated separately. The preheating temperature was always 4–6°C higher than the column temperature used. The coil diameter was 8.5 cm for all columns.

Fused-silica tubes of 2.0 m × 100 μm I.D. and 2.4 m × 18.5 μm I.D. were used as the split tube and the restriction tube (components 10 and 9 in Fig. 1), respectively, to give a splitting ratio of about 1000.

SB Series columns of 50 and 100 μm I.D. and of different lengths were obtained from Lee Scientific (Salt Lake City, UT, USA) and fused-silica capillaries of different sizes from Polymicro Technologies (Phoenix, AZ, USA). Acetonitrile and methanol were HPLC-grade solvents from Rathburn (Walkerburn, UK). All other chemicals were of analytical-reagent grade from Fluka (Buchs, Switzerland) and were used as received.

Data collection and processing were carried out on a Perkin-Elmer CLAS system. Sodium nitrite in water or in methanol was used to determine column dead volumes. Other water-soluble substances, such as thiourea, can also be used; they all gave the same dead volume value.

RESULTS AND DISCUSSION

HT-OTLC system

In order to check the working performance of the high-temperature split system, the reproducibility of column flow-rate was determined at different split-

ting ratios and at different temperatures up to 200°C. In most instances the relative standard deviation of the column flow-rate was between 0.3 and 0.6%. This precision indicates that the stability of the flow-rate and the temperature control system is acceptable for most practical applications.

When very long columns (16–20 m) were used, especially new columns, partial blockage of the restriction tube by column bleeding may bring larger variations in column flow-rate (sometimes up to 5–10%). Even under these unfavourable conditions the relative standard deviations of the capacity factors were still in the range 0.4–0.6%, except for the early eluting solutes (Table I). These results show that the working performance of the HT-OTLC system is satisfactory.

Extra-column band broadening in HT-OTLC system

In the development of a high efficiency OTLC system, the study of extra-column band broadening is of great importance. The total peak variance, σ^2, is the sum of the column variance and all other independent extra-column variances:

$$\sigma^2 = \sigma_c^2 + \sigma_d^2 + \sigma_t^2 + \sigma_{inj}^2 + \sigma_s^2 \qquad (6)$$

where σ_c^2 is the column variance, σ_d^2 is the variance caused by detector cell volume, σ_t^2 is the variance caused by the preheating tube, σ_{inj}^2 is the variance caused by injection volume and σ_s^2 is the contribution of all other factors, such as dead volumes between connections, electrical response delay, insufficient preheating and column diameter inhomogeneity.

In our system with on-column detection, the detector dead volume is in the range 0.16–0.4 nl, depending on the column diameter. Its contribution to the observed peak dispersion is negligible.

For a rectangular sample plug of volume V_{inj}, using the manual peak half-width method, $\sigma_{inj}^2 = 0.25V_{inj}^2$ [22]. This relationship is also valid in HT-OTLC (Fig. 2). If a 20% efficiency loss is the acceptable limit, it can be calculated that an 8-nl injection volume is allowed for a 1.2 m × 50 μm I.D. column in fast analysis and a 30-nl volume can be used for a 16-m column.

It has also been proved in HT-OTLC [23] that σ_t^2 can be calculated by the equation

$$\sigma_t^2 = \sigma_{tube}^2/(SR)^2 \qquad (7)$$

TABLE I

PRECISION OF THE CAPACITY FACTORS (k')

Column, SB-Methyl-100 (20 m $\times$ 50 μm I.D.); temperature, 180°C; mobile phase, acetonitrile–water (50:50); flow-rate, 0.66 μl/min.

Injection No.	k'					
	Benzene	Chloro-benzene	1,4-Dichloro-benzene	1,3,5-Trichloro-benzene	1,2,4,5-Tetrachloro-benzene	Petachloro-benzene
1	0.0278	0.0329	0.0426	0.0759	0.0835	0.1077
2	0.0282	0.0331	0.0428	0.0761	0.0834	0.1074
3	0.0279	0.0331	0.0427	0.0766	0.0842	0.1089
4	0.0271	0.0322	0.0424	0.0762	0.0840	0.1086
5	0.0277	0.0326	0.0425	0.0760	0.0835	0.1082
6	0.0279	0.0330	0.0429	0.0766	0.0843	0.1090
7	0.0276	0.0326	0.0426	0.0762	0.0836	0.1080
Mean	0.0277	0.0328	0.0426	0.0762	0.0838	0.1083
S.D.[a]	$\pm$0.00034	$\pm$0.00033	$\pm$0.00017	$\pm$0.00028	$\pm$0.00037	$\pm$0.00061
R.S.D.[a] (%)	1.2	1.0	0.4	0.4	0.4	0.6

[a] S.D. = Standard deviation; R.S.D. = relative standard deviation.

where σ^2_{tube} is the band broadening in the preheating tube calculated by the Taylor equation [1,2] and SR is the splitting ratio. For efficient preheating, a 40 cm $\times$ 0.2 mm I.D. tube was used in our work. This size is much larger than that for a normal connection tube. Calculation shows that even for the 1.2-m column, the efficiency loss caused by this tube is less than 4%, provided that a splitting ratio of about 1000 is used.

The term σ^2_s is hard to predict and can only be evaluated experimentally. In Fig. 2, the difference between the theoretical column variance σ^2_c, and the intercept of the σ^2 vs. V^2_{inj} plot with the ordinate is about 25.2 nl^2. Although this value contains the contribution of the preheating tube, it is a good estimation of σ^2_s, as σ^2_t is insignificant. The small σ^2_s value indicates that other extra-column factors and factors which effect the column efficiency itself do not contribute much to the overall band broadening. Therefore, the HT-OTLC system can be used in high-efficiency separations.

Influence of mobile phase preheating on column efficiency

Many workers [24,25] have noticed that the effect of temperature on column efficiency is strongly influenced by the mobile phase preheating. Only when the mobile phase entering the column is at the same temperature as the column can the beneficial effect of temperature be fully exploited. Any "cold point" in the column inlet must be removed. For a
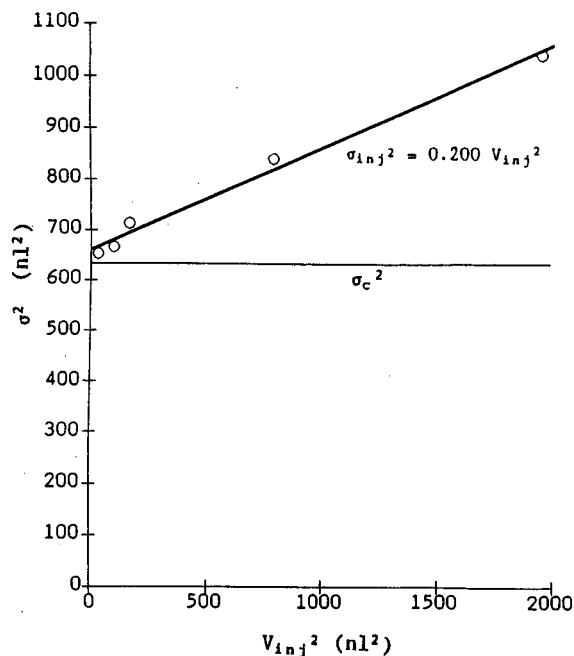

Fig. 2. σ^2 vs. V^2_{inj} plot. Column, 8.4 m $\times$ 51 μm I.D. SB-Octyl-50; temperature, 100°C; mobile phase, methanol; $u = 0.27$ cm/s; sample, 0.2% acetophenone in methanol.

better understanding of this influence, a quantitative study of the effectiveness of different heating methods was carried out.

In Fig. 3, the *H vs. u* curves obtained for different heating methods are presented, together with the theoretical curve. The vertical distance between the experimental and theoretical curves is an indication of efficiency loss:

$$\text{loss}\,(\%) = [(H_{\text{obs}} - H_{\text{c}})/H_{\text{obs}}] \cdot 100 \tag{8}$$

where H_{c} is the theoretical and H_{obs} the experimental plate height. The most effective heating method should give the least loss. If the efficiency loss is calculated at a relatively high linear velocity (*e.g.*, at $u = 1.5$ cm/s), the contribution of other extra-column factors becomes less important. The calculated values thus reflect the effectiveness of different heating methods. Table II gives the results; the effectiveness of different heating methods is tabulated without separating the contributions of the preheating tube and the additional heating tube before the injection valve.

According to Table II, the simultaneous mobile phase heating before and after the sample valve is the most effective way to diminish the "cold point" effect. However, this is not feasible for higher operating temperatures (150–200°C) owing to the need for a high-temperature sample valve. The serpentine tube performs very well in view of mobile phase heating, although its variance contribution is
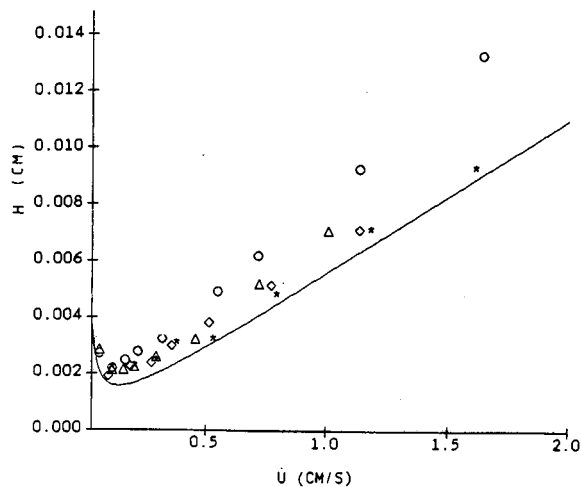
Fig. 3. Influence of heating methods on column efficiency. Column, 124 cm × 54 μm I.D. SB-Octyl-50; temperature, 100°C; mobile phase, methanol; sample, acetophenone in methanol. Solid line: theoretical *H vs. u* curve. Experimental points: ○ = method A; △ = method B; ◇ = method C; ✳ = method D in Table II.

still significant (0.05 μl²/cm). This, however, does not cause appreciable problems even for the 1.2-m column, provided that the splitting ratio is about 1000 or higher.

Validity of OT theory in HT-OTLC

A fused-silica colmn (85 cm × 75 μm I.D.) was

TABLE II

EFFECTIVENESS OF DIFFERENT HEATING METHODS

Column, 124 cm × 54 μm I.D.; temperature, 100°C; mobile phase, methanol; $u = 1.5$ cm/s.

Method	Additional heating tube before sample valve	Preheating tube	Column oven heating medium	Loss (%)
A	None	12 cm × 0.52 mm I.D. stainless steel, in oven	Air	31.9
B	60 cm × 0.5 mm I.D. stainless steel, in oven	100 cm × 75 μm I.D. fused silica, in oven	Metal powder	18.9
C	None	40 cm × 0.2 mm I.D. serpentine tube, separate heating, 105°C[a]	Metal powder	9.2
D	40 cm × 0.2 mm I.D. serpentine tube, separate heating, 105°C	20 cm × 0.12 mm I.D. stainless steel, separate heating, 105°C[a]	Metal powder	5.1

[a] Measured at the tube wall surface.

used to show the influence of the column temperature on column efficiency. Methanol was used as the mobile phase to eliminate possible retentions caused by column wall adsorption. As $k' = 0$, the H vs. u curves obtained at different column temperatures (20, 100 and 150°C, respectively; Fig. 4) simply indicate the influence of temperature. As can be seen from Fig. 4, the H vs. u curve became much flatter in the high-velocity region when the column temperature increased from 20 to 150°C.

The diffusivity of the solute (acetophenone) at the three temperatures is $1.64 \cdot 10^{-5}$, $5.55 \cdot 10^{-5}$ and $10.16 \cdot 10^{-5}$ cm²/s, respectively (calculated from the Wilke–Chang eqation). Eqn. 4 gives u_{opt} values of 0.030 (20°C), 0.103 (100°C) and 0.188 cm/s (150°C). From the curves in Fig. 4, the corresponding $_{opt}$ values were found to be ca. 0.03, 0.09 and 0.19 cm/s. The experimental results confirmed the theoretical predictions.

At room temperature, the observed plate height becomes noticeably smaller than the theoretical value at velocities above 0.3 cm/s. Knox nd Gilbert [7] reported similar results and attributed this effect to the additional mixing due to the secondary flow. At higher column temperatures this has not been observed. Perhaps the "cold point" effect caused by insufficient heating predominated over the secondary flow effect.

To verify the correctness of the retention correction expression, the H vs. u dependence of naphthalene and tropolone on an SB-Octyl-50 colmn was studied. They have identical D_m vales but different retentions. The H vs. u curves were measured at 22 and at 100°C, respectively (Fig. 5). As the D_m value is the same, the ratio of the slopes of their respective H vs. u curves equals the retention correction factor according to eqns. 2 and 3.

Tropolone had no retention under the chromatographic conditions used and the capacity factor of naphthalene was 0.354 (22°C) and 0.303 (100°C). The calculated slope ratio of retained and unretained solutes was 2.46 (22°C) and 2.25 (100°C), while the experimentally obtained slope ratio was 2.40 (22°C) and 2.18 (100°C). The agreement was fairly good and confirms the validity of the retention correction factor. If the peak shape of naphthalene and tropolone obtained at room temperature is compared with that at 100°C (Fig. 6), it is clear that the influence of retention on efficiency is much less at higher temperatures.
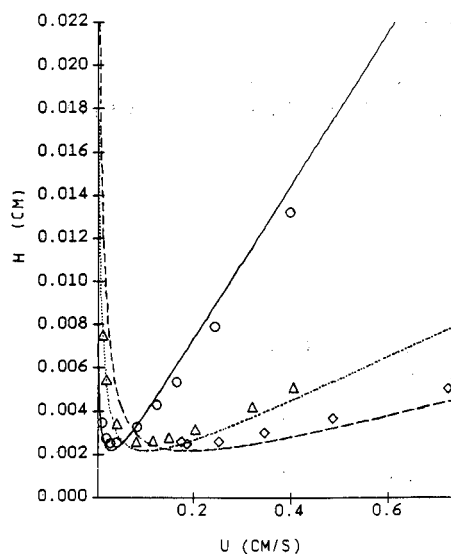

Fig. 4. Influence of temperature on column efficiency. Column, 0.85 m × 75 μm I.D. fused silica; mobile phase, methanol; sample, acetophenone in methanol. Solid line, theoretical curve at 22°C; ○ = experimental data at 22°C. Dotted line, theoretical curve at 100°C; △ = experimental data at 100°C. Dashed line, theoretical curve at 150°C; ◇ = experimental data at 150°C.
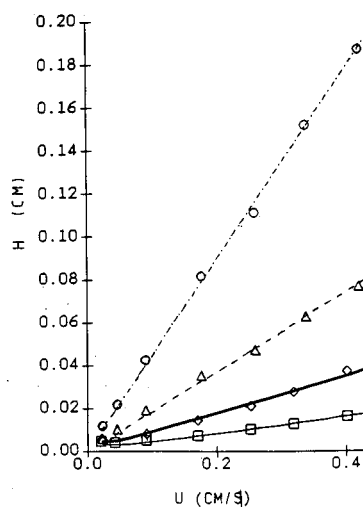
Fig. 5. Influence of retention on column efficiency. Column, 121 cm × 100 μm I.D. SB-Octyl-50. Mobile phase: broken lines, methanol–water (50:50), 22°C, ○ = naphthalene ($k' = 0.354$) and △ = tropolone ($k' = 0$); solid lines, methanol–water (30:70), 100°C, ◇ = naphthalene ($k' = 0.303$) and □ = tropolone ($k' = 0$).
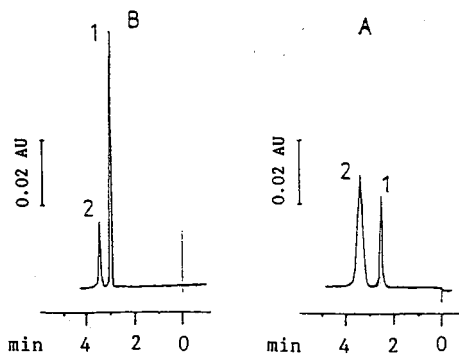
Fig. 6. Influence of temperature on peak shape. Column, 121 cm × 100 μm I.D. SB-Octyl-50. Mobile phase: (A) methanol–water (50:50), 22°C; (B) methanol–water (30:70), 100°C. Peaks: 1 = tropolone; 2 = naphthalene.

The performance $P = N/t$, as expressed by the plate numbers generated in unit time for an unretained peak with retention time t_0, is given by

$$\frac{N}{t_0} = \frac{48D_m}{d_c^2} \qquad (9)$$

for $u = u_{opt}$, or

$$\frac{N}{t_0} = \frac{96D_m}{d_c^2} \qquad (10)$$

for $u \geqslant 3u_{opt}$. To obtain the highest plate number for a certain column, one must work at $u = u_{opt}$. In order to obtain the highest analysis speed, one must work at a higher velocity. Eqn. 10 indicates that the analysis speed reaches a maximum and becomes independent of the velocity after $u \geqslant 3\ u_{opt}$. To

prove this conclusion, the experimental N/t_0 values obtained on a 54 μm I.D. column at 100°C and on a 51 μm I.D. column at 150°C are listed in Table III. The theoretical N/t values are also given. According to the results, compared with the speed at $u = u_{opt}$, a doubled analysis speed was obtained experimentally at $u = 3u_{opt}$, as predicted by eqns. 9 and 10.

High-efficiency separations

The minimum plate height, H_{min}, can be calculated by the equation

$$H_{min} = \frac{1}{1 + k'}\left(\frac{1 + 6k' + 11k'^2}{12}\right)^{1/2} d_c$$

or, for $k' = 0$,

$$H_{min} = 0.2887d_c \qquad (11)$$

If 50 μm I.D. columns are used, 10^6 plates could be obtained on a 14.5-m column. If a 10–20% efficiency loss is taken into consideration, a 16–17-m column will be long enough to generate this order of plate number. On a 19.6 m × 51.2 μm I.D. SB-Methyl-100 colmn operated at 200°C with methanol as the mobile phase and with acetophenone as the test sample, the following results were obtained as averages of six injections: retention time $t_R = 49.32 \pm 0.34$ min, $N = 1\ 143\ 000 \pm 39\ 000$ plates and $N/t = 386 \pm 11$ plates/s. The efficiency obtained shows a 14% loss relative to the theoretical value.

One million plates have also been realized in the separation of chlorobenzenes (Fig. 7). All peaks are highly symmetrical, indicating the excellent performance of the system.

TABLE III

PERFORMANCE N/t AS A FUNCTION OF LINEAR VELOCITY u

System[a]	Parameter	Values							
A	u (cm/s)	1.61	1.18	0.785	0.521	0.372	0.289	0.200	0.106
	t_0 (min)	1.28	1.75	2.63	3.96	5.54	7.15	10.30	19.40
	N	13 400	17 600	26 100	39 200	40 800	51 900	56 600	57 700
	N/t_0 (s^{-1})	175	167	165	165	123	121	92	50
B	u (cm/s)	1.53	1.05	0.710	0.505	0.391	0.273	0.256	
	t_0 (min)	9.15	13.3	19.8	27.8	35.9	51.4	54.6	
	N	160 000	243 000	334 000	406 000	442 000	494 000	470 000	
	N/t_0 (s^{-1})	291	305	282	244	205	160	143	

[a] (A) Column, 123.7 cm × 54.07 μm I.D. SB-Octyl-50; temperature, 100°C; $D_m = 5.55 \cdot 10^{-5}$ cm^2/s; $u_{opt} = 0.142$ cm/s; $N/t = 91$ ($u = u_{opt}$), 182 ($u = 3u_{opt}$). (B) Column, 842 cm × 51.43 μm I.D. SB-Octyl-50; temperature, 150°C; $D_m = 10.16 \cdot 10^{-5}$ cm^2/s; $u_{opt} = 0.274$ cm/s; $N/t = 185$ ($u = u_{opt}$), 369 ($u = 3u_{opt}$).
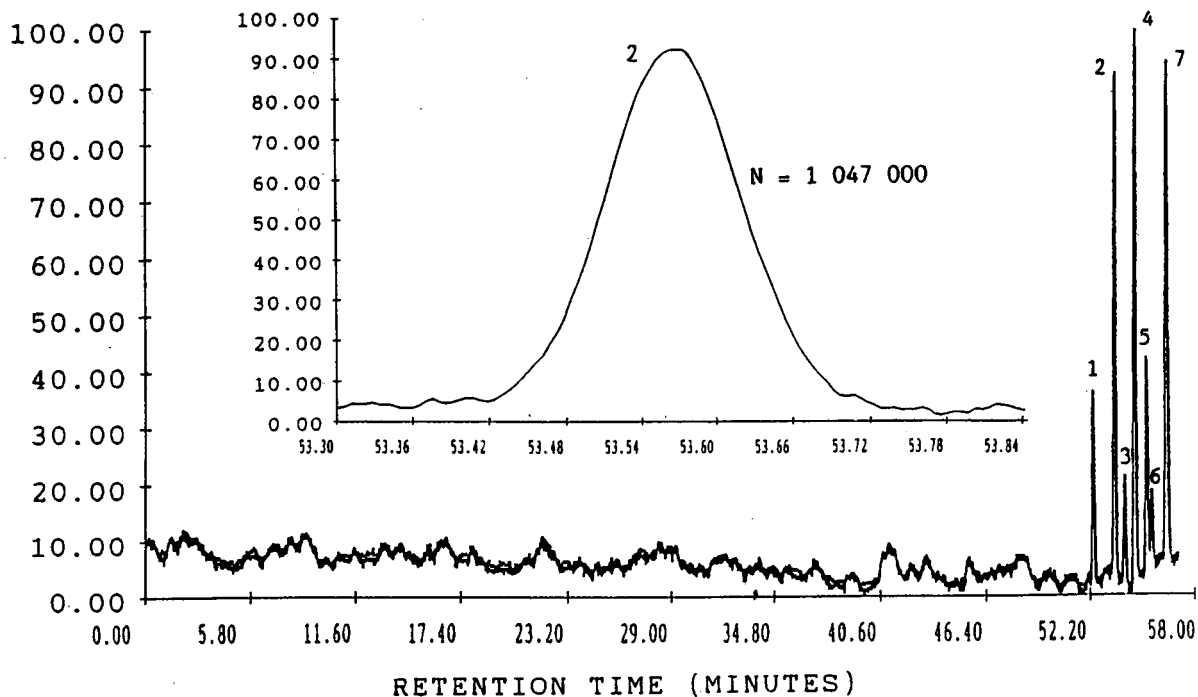
Fig. 7. Separation of chlorobenzenes. Column, 20 m × 51 μm I.D. SB-Methyl-100; temperature, 200°C; mobile phase, acetonitrile–water (50:50); flow-rate 0.65 μl/min. Peaks: 1 = tropolone; 2 = benzene (N = 1 047 000); 3 = 1,4-dichlorobenzene (N = 922 000); 4 = 1,2,4-trichlorobenzene; 5 = 1,3,5-trichloro-benzene (N = 800 000); 6 = 1,2,4,5-tetrachlorobenzene; 7 = pentachlorobenzene (N = 692 000).
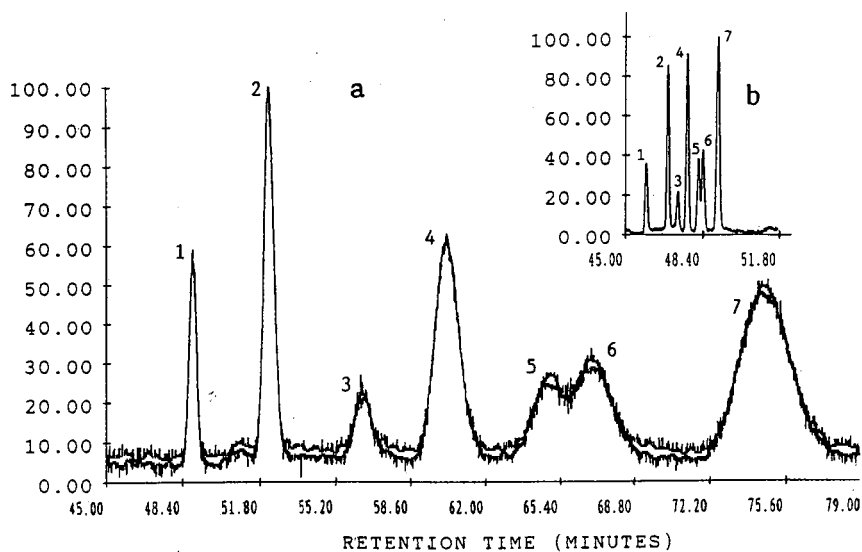

Fig. 8. Comparison of separations at different column temperatures: (a) 22°C; (b) 200°C. Chromatographic conditions (except temperature and flow-rate 0.75 μl/min) and peak identities as in Fig. 7.

Fig. 8 shows two chromatograms obtained under the same chromatographic conditions except for the column temperature: (a) room temperature and (b) 200°C. Although the k' value of the last peak at 200°C is about one seventh of the value at room temperature, the separation does not suffer, owing to the high efficiency obtained at elevated temperature.

CONCLUSIONS

Our preliminary results have shown that the existing OTLC theory is applicable in HT-OTLC. All practical benefits predicted by the theory for a higher column temperature are experimentally verified. At higher temperature the serious limitation on analysis speed due to a linear flow-rate is eased, and high-efficiency separations can now be performed in a realistic analysis time. At present, the highest analysis speed obtained on our system is 395 plates/s, or 10^6 plates in *ca.* 42 min (51 μm I.D. column operated at 200°C).

Another advantage of a higher column temperature is a higher total efficiency. The reduced mobile phase viscosity at higher temperature allows the use of very long columns. On a 19.6 m × 51 μm I.D. column, the highest efficiency obtained was 1 180 000 plates; this represents only an 11% loss relative to the theoretical value (1 326 000 plates).

In the separation of chlorobenzenes, 10^6 plates were obtained on a 20-m column in less than 60 min. It is therefore possible to obtain 40 000–50 000 plates in 3 min on a 1.2-m column. This efficiency could meet the demands of most routine work.

Studies on the stabilities and selectivities of different column types and studies of rapid separations on short columns are in progress.

REFERENCES

1 G. Taylor, *Proc. R. Soc. London, Ser. A*, 219 (1953) 186.
2 G. Taylor, *Proc. R. Soc. London, Ser. A*, 225 (1954) 473.
3 M. J. E. Golay, in D. H. Desty (Editor), *Gas Chromatography 1958*, Academic Press, New York, 1959, p. 36.
4 J. C. Sternberg, *Adv. Chromatogr.*, 2 (1966) 205.
5 J. H. Knox and J. F. Parcher, *Anal. Chem.*, 41 (1969) 1599.
6 T. Tsuda and M. Novotny, *Anal. Chem.*, 50 (1978) 632.
7 J. H. Knox and M. T. Gilbert, *J. Chromatogr.*, 186 (1979) 405.
8 T. Tsuda, K. Hibi, T. Nakanishi, T. Takeuchi and D. Ishii, *J. Chromatogr.*, 158 (1978) 227.
9 M. J. E. Golay, *J. Chromatogr.*, 186 (1979) 341.
10 R. Tijssen, *Sep. Sci. Technol.*, 13 (1978) 681.
11 S. Egchi, J. G. Kloosterboer, C. P. G. Zegers, P. J. Schoenmakers, P. P. H. Tock, J. C. Kraak and H. Poppe, *J. Chromatogr.*, 516 (1990) 301.
12 W. D. Pfeffer and E. S. Yeung, *Anal. Chem.*, 62 (1990) 2178.
13 O. van Berker, H. Poppe and J. C. Kraak, *Chromatographia*, 24 (1978) 739.
14 S. R. Meller, W. Simon, H. M. Widmer, K. Grolimnd, G. Schomberg and P. Kolla, *Anal. Chem.*, 61 (1989) 2747.
15 M. Novotny, *Anal. Chem.*, 60 (1988) 500A.
16 K. Tsuji and J. F. Goetz, *J. Chromatogr.*, 157 (1978) 185.
17 G. Herbut and J. S. Kowalczyk, *J. High Resolut. Chromatogr. Chromatogr. Commun.*, 4 (1981) 27.
18 J. A. Schmidt, R. A. Henry, R. C. Williams and J. F. Dieckman, *J. Chromatogr. Sci.*, 9 (1971) 645.
19 F. V. Warren and B. A. Bidlingmeyer, *Anal. Chem.*, 60 (1988) 2824.
20 F. D. Antia and Cs. Horváth, *J. Chromatogr.*, 435 (1988) 1.
21 F. Erni, *J. Chromatogr.*, 507 (1990) 141.
22 H. H. Lauer and G. P. Rozing, *Chromatographia*, 24 (1987) 617.
23 G. Liu, N. Djordjevic and F. Erni, to be published.
24 G. P. Rozing and H. Goetz, *J. Chromatogr.*, 476 (1989) 3.
25 J. Bowermaster, *Dissertation*, Virginia Polytechnic Institute and State University, University Microfilms International, Ann Arbor, MI, 1984, p. 136.

CHROMSYMP. 2388

Automated high-performance liquid chromatographic and size-exclusion chromatographic sample preparation by means of a robotic workstation

Andreas Bruns*, Heinrich Waldhoff, Anneliese Wilsch-Irrgang and Walter Winkle

Henkel KGaA, P.O.B. 1100, 4000 Düsseldorf (Germany)

ABSTRACT

A robotic workstation was used for the automation of standard and sample preparation for three applications: the size-exclusion chromatographic analysis of residual toluene 2,4-diisocyanate and 4,4′-diphenylmethane diisocyanate in polyurethane adhesives; the high-performance liquid chromatographic analysis of the formaldehyde, glutaraldehyde and glyoxal content of aqueous surfactant formulations; and the high-performance liquid chromatographic analysis of the tetradecanedioic acid and methylmyristate content of a reaction matrix. Sample weighing, solvent addition, mixing, standard dilutions, filtrations and solid-phase extractions were performed automatically by the workstation. The standard and sample solutions were injected on-line via the built-in injection valves into the high-performance liquid chromatographic or size-exclusion chromatographic systems.

INTRODUCTION

Today's instrumentation for high-performance liquid chromatography (HPLC) and size-exclusion chromatography (SEC) is fully automated and computer-controlled. This allows for time-efficient, unattended operation. In contrast to this, the preparation of standards and samples is very often the most tedious and time-consuming part of an analytical procedure and usually has to be done manually. In addition to time efficiency considerations, being able to avoid the manual handling of potentially toxic compounds can be a critical requirement. The use of robots for the automation of such manual procedures is common practice in today's technical environments [1,2]. The approach taken here was to use an easy-to-handle and compact robotic workstation [3] instead of a complex robot to automate simple routine procedures in liquid chromatography (LC) such as sample weighing, standard dilution, filtration or solid-phase extraction, including on-line sample injection into the chromatographic systems. A built-in balance allows for the weight tracking of all precision-relevant steps of a procedure. The workstation is designed for dedicated use as a sample preparation and injection device for liquid chromatography. Compact dimensions allow for an installation side by side with a chromatographic system on a laboratory bench or in a conventional fume hood.

EXPERIMENTAL

A Zymark "BenchMate" workstation was used, equipped with a solid-phase extraction and filtration unit and two built-in Rheodyne LC injectors with 20-μl injector loops. For filtration, disposable 30-mm PTFE filters (0.45-μm) were used. For solid-phase extraction Waters Sep-Pak Vak C_{18} cartridges were used. The 5-ml "airpush" syringe of the BenchMate was replaced by a 2-ml syringe for applications where methylene chloride had to be used to handle the high vapour pressure of this solvent. In this configuration, one of the six reagent lines had to be used for an additional airpush step at certain positions of the program to empty the sol-

vent lines completely.

Waters 510 pumps, a Waters 680 controller, a Waters 490 four-wavelength UV detector and Waters 510 and 401 refractive index detectors were used in combination with a Nelson 6900 chromatography data system. All organic solvents were HPLC grade; water was purified with a Millipore Milli-Q system. The chromatography conditions were developed in-house. Detailed conditions are given in the figure captions.

The BenchMate procedures were written by selecting certain "preprogrammed" routines ("steps") from the BenchMate software and adding the numbers for volumes, weights, densities, etc, according to the specific application.

BenchMate procedure: 1:4 standard dilution for the SEC analysis of residual monomeric isocyanates in polyurethane adhesives

Step 1:   add 2 ml of toluene 2,4-diisocyanate (TDI)–4,4'-diphenylmethane diisocyante (MDI) stock
Step 2:   dilute (density: 1.3255 g/ml) 1:4 with methylene chloride making a total of 3 ml
Step 3:   vortex mix for 10 s at speed 1
Step 4:   wash syringe with 2 ml of air
Step 5:   pre-wet filter with 0.3 ml of sample; filter 3.2 ml into next tube
Step 6:   rinse filter holder with 2 ml of methylene chloride
Step 7:   wash syringe with 2 ml of methylene chloride
Step 8:   wash syringe with 2 ml of air
Step 9:   wash LC injector with 0.7 ml of sample
Step 10: inject sample on LC 1; elute for 20 min
Step 11: end

Only the dilution ratio had to be changed to obtain the other standard concentrations. The procedures for the standard dilution for the other applications were written according to the same principle.

BenchMate procedure: sample preparation for the SEC analysis of residual monomeric isocyanates in polyurethane adhesives

Step 1:   add 5 ml of methylene chloride
Step 2:   wash syringe with 2 ml of air
Step 3:   vortex mix for 600 s at speed 3
Step 4:   pre-wet with 0.5 ml of sample and filter 4.5 ml into next tube
Step 5:   rinse filter holder with 2 ml of methylene chloride
Step 6:   wash syringe with 2 ml of methylene chloride
Step 7:   wash syringe with 2 ml of air

Step 8:   wash LC injector with 0.7 ml of sample
Step 9:   inject sample on LC 1 with run time of 20 min
Step 10: end

The sample weighing is performed automatically before the BenchMate starts with step 1 of the program.

BenchMate procedure: sample preparation for the HPLC analysis of aldehydes in an aqueous surfactant formulation

Step 1:   add 5 ml of 0.0167 *M* orthophosphoric acid
Step 2:   vortex mix for 60 s at speed 2
Step 3:   pre-wet filter with 0.5 ml of sample; filter 4 ml into next tube
Step 4:   rinse filter holder with 2 ml of 0.0167 *M* orthophosphoric acid
Step 5:   wash LC injector with 0.5 ml of sample
Step 6:   inject sample on LC 2 with run time of 20 min
Step 7:   end

The sample weighing is performed automatically before the BenchMate starts with step 1 of the program.

BenchMate procedure: sample preparation for the HPLC analysis of dicarboxylic acids in a reaction matrix

Step 1:   add 1 ml of 0.2 *M* sodium hydroxide
Step 2:   condition column with 2 ml of methanol
Step 3:   condition column with 5 ml of water
Step 4:   vortex mix for 10 s at speed 3
Step 5:   load 0.6 ml of sample onto column
Step 6:   rinse column with 2 ml of 1 *M* hydrochloric acid
Step 7:   rinse column with 6 ml of water
Step 8:   collect 7.5-ml fraction into next tube using isopropanol–acetonitrile–water–acetic acid (40:40:20:0.1, v/v)
Step 9:   vortex mix for 10 s at speed 2
Step 10: pre-wet with 0.3 ml of sample; filter 3 ml into next tube
Step 11: rinse filter holder with 2 ml isopropanol–acetonitrile–water–acetic acid
Step 12: inject sample on LC 1 with run time of 15 min
Step 13: inject sample on LC 2 with run time of 15 min
Step 14: end

The sample weighing is performed automatically before the BenchMate starts with step 1 of the program.

RESULTS AND DISCUSSION

Automated standard and sample preparation for the SEC analysis of residual monomeric isocyanates in polyurethane adhesives

Residual TDI and MDI in polyurethanes can be analyzed by using a SEC technique. The standard and sample preparation for this method consisted of the following two general steps which had to be automated: (i) perform a standard dilution series, filter and inject standards to create an external standard calibration graph; (ii) weigh adhesive samples, add methylene chloride, mix to dissolve, filter and inject for analysis.

A manually prepared standard stock solution is used for the dilution series. Note the airpush steps that were performed with the reagent syringe ("Wash syringe with 2 ml of air", see Experimental section). All the standards were run in triplicate using the BenchMate to perform the dilutions and LC injections. The reproducibility (relative standard deviations for the peak areas of each triplicate were 1.2–3.5%) and linearity of the calibration graph (correlation factor 0.9998) were excellent. The weight-tracking results for these dilutions showed that the experimental weight ratios for the different dilutions were within ± 0.5% of the programmed (theoretical) values.
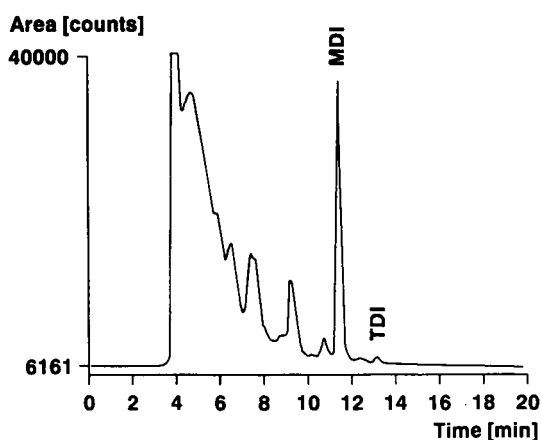
Fig. 1 shows a typical chromatogram for a polyurethane adhesive sample. Reproducibility studies, where all samples were prepared and analyzed in triplicate using the BenchMate, showed relative standard deviations (R.S.D.s) ranging from 1% to 17% for residual MDI and TDI, depending on the level of residual isocyanate (0.01–5%, w/w) in the polyurethane sample.

Automated standard and sample preparation for the HPLC analysis of aldehydes in an aqueous surfactant formulation

An HPLC technique was used to analyze glyoxal, formaldehyde and glutaraldehyde in aqueous surfactant formulations. The manual procedure consisted of the following two steps which again had to be automated: (i) perform a standard dilution series using a standard stock solution, filter and inject standards to create the external standard calibration graph; (ii) weigh samples, add 0.0167 M orthophosphoric acid, mix to dissolve, filter and inject for analysis.

Because an aqueous system was used for the sample preparation and chromatography, no vapour pressure problems were experienced, and the standard 5-ml airpush syringe was used without problems. It was expected that during the sample preparation the solutions might foam because of the
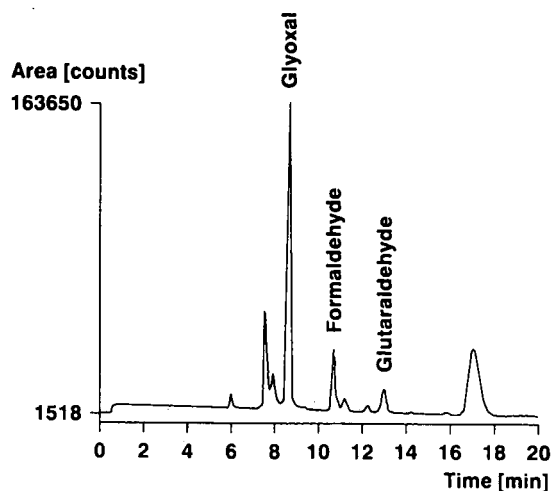

Fig. 1. Typical chromatogram of the residual MDI and TDI analysis in a polyurethane adhesive sample. Chromatographic conditions: 3 × PLGel 50 A column (5 μm particle size, 300 × 7.6 mm I.D.); methylene chloride at 1.5 ml/min; 20 μl injection volume; UV detection at 240 nm for TDI and at 280 nm for MDI.

Fig. 2. Typical chromatogram of the aldehydes in an aqueous surfactant formulation. Chromatographic conditions: Shodex KC-811 column (5 μm particle size, 300 × 8 mm I.D.) with C-811 P guard column; 0.12% (v/v) orthophosphoric acid at 1 ml/min; 20 μl injection volume; refractive index detection.

TABLE I

COMPARISON OF THE ALDEHYDE ANALYSIS RESULTS FOR THE AUTOMATED *VERSUS* THE MANUAL PROCE-
DURE

Sample No.	Glyoxal		Formaldehyde		Glutaraldehyde	
	Automated	Manual	Automated	Manual	Automated	Manual
1	8.8	8.8	–	–	4.1	4.5
2	11.8	12.0	10.8	11.1	3.6	3.8
3	8.8	8.8	–	–	4.2	4.5
4	4.3	3.8	1.4	1.4	0.7	0.8

presence of surfactants in the aqueous formulation. No such problems were experienced.

The standard dilution programs were very similar to the adhesive application. Again, triplicate standard dilutions and calibration runs resulted in excellent linearity (correlation factor 0.9999) and reproducibility with R.S.D.s ranging from 0.3 to 2.9% for the peak-area counts of each triplicate. The weight-tracking results for these dilutions showed that the experimental weight ratios for the different dilutions were within ± 0.3% of the programmed (theoretical) values.

Fig. 2 shows an example of a typical chromato-

gram of the aldehydes in an aqueous surfactant formulation. A comparison of manually generated aldehyde analysis results with the results from the BenchMate shows excellent agreement (Table I). Reproducibility studies, where all samples were prepared and analyzed in triplicate, showed that the R.S.D.s ranged from 0.2 to 16.3% depending on the aldehyde level.

Automated standard and sample preparation for the HPLC analysis of dicarboxylic acids in a reaction matrix

α, ω-Dicarboxylic acids, in this case tetradecanedioic acid, can be analyzed by reversed-phase HPLC [4]. The manual procedure consisted of the following two steps which had to be automated: (i) a standard dilution series, filtration of the standard solutions and injection into the HPLC system; (ii) sample weighing, addition of 0.2 M sodium hydroxide, solid-phase extraction, filtration and injection into the HPLC system for analysis.

Via the BenchMate's two built-in injection valves, the sample was injected into two independent isocratic HPLC systems. Elution times of 10 min allowed for a fast analysis of the two components of interest, the reaction product tetradecanedioic acid and methylmyristate, which is the starting material for this reaction. Fig. 3 shows a typical chromatogram of the tetradecanedioic acid portion in a sample. Good analytical precision was found with a correlation factor of 0.9972 for the linearity of the calibration graphs, R.S.D.s of ± 0.5% for the standard dilution series, and R.S.D.s of 1.7–4.0% for the dicarboxylic acid content of the samples.
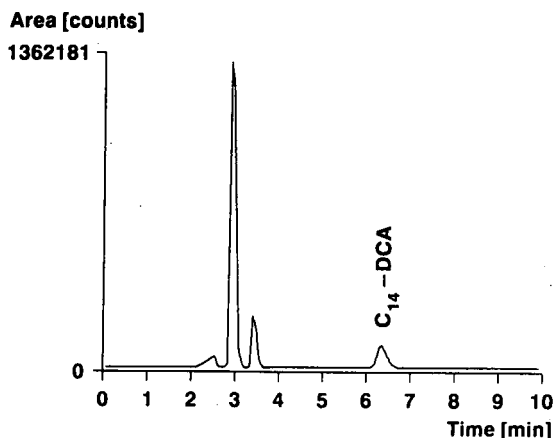

Fig. 3. Typical chromatogram of tetradecanedioic acid (C_{14}-DCA) from a reaction matrix. Chromatographic conditions: LiChrosorb C_{18} column (10 μm particle size, 250 × 4.6 mm I.D.; Phenomenex); isopropanol–acetonitrile–water–acetic acid, 40:40:20:0.1 (v/v), for tetradecanedioic acid; 45:45:10:0.1 (v/v) for methylmeristate (chromatogram not shown) at 1 ml/min; 20 μl injection, volume: refractive index detection.

CONCLUSIONS

The results of the three applications discussed here demonstrate that a robotic workstation can provide nearly complete automation of many of the most tedious and time-consuming sample preparation procedures for liquid chromatography. Utilizing the BenchMate robotic workstation proved to be straightforward. The system's weight-tracking feature provided excellent reliability and precision. In principle, this workstation could be used for routine gas chromatography sample preparation and even simple derivatization procedures. The only drawback is its current inability to handle autosampler vials. This feature would be the most desirable option for such a robotic workstation in a chromatography laboratory.

REFERENCES

1 A. R. Newmann, *Anal. Chem.*, 62 (1990) 29.
2 T. L. Isenhour, S. E. Eckert and J. C. Marshall, *Anal. Chem.*, 61 (1989) 805.
3 L. A. Simonson and B. Lightbody, *Lab. Robot Autom.*, 2 (1990) 221.
4 A. Bruns, H. Waldhoff and W. Winkle,. *Chromatographia*, 27 (1989) 340.

CHROMSYMP. 2446

Rapid and sensitive determination of urinary 2,5-hexanedione by reversed-phase high-performance liquid chromatography

M. Perla Colombini

Dipartimento di Chimica e Chimica Industriale, Via Risorgimento 35, 56100 Pisa (Italy)

Patrizio Carrai

Dipartimento di Tossicologia, Ospedale Campo di Marte, U.S.L. 6, Lucca (Italy)
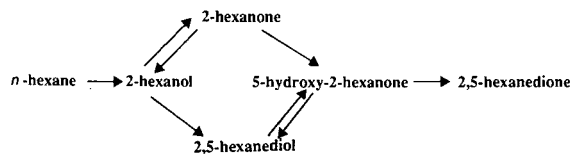
Roger Fuoco* and Carlo Abete

Istituto di Chimica Analitica Strumentale del CNR, Via Risorgimento 35, 56100 Pisa (Italy)

ABSTRACT

A rapid and sensitive method for the determination of 2,5-hexanedione (HD) (the principal metabolite of *n*-hexane) in urine samples by reversed-phase high-performance liquid chromatography (HPLC) is described. The sample preparation procedure was based on solid–liquid extraction after acid hydrolysis; it was optimized to enable accurate HD determination in less than 30 min. Analysis of spiked real samples showed a recovery of more than 85% at the 0.1-ppm level, with a relative standard deviation of 5% and a detection limit as low as 0.01 ppm. Intra-assay and inter-assay coefficients of variation at the 0.5-ppm level were 4 and 5%, respectively. The chromatographic peak assigned to HD was identified by collecting the HPLC eluate at the retention time of HD and analysing it using Fourier transform infrared spectrometry coupled with high-resolution gas chromatography. Urine samples of unexposed and exposed subjects were analysed following the proposed analytical procedure. HPLC and high-resolution gas chromatographic analyses were also compared on these samples. A correlation factor of 0.992 was obtained, which showed a good agreement between the two sets of data.

INTRODUCTION

n-Hexane is a widely used solvent contained in paints, varnished and glues, as well as in petroleum ether and gasoline. Occupational exposure to it causes polyneuritis and pheripheral neuropathies which manifest themselves as leg weakness leading to paralysis [1,2]. Absorption of *n*-hexane in exposed workers occurs almost entirely through the respiratory system [3,4] and follows this biotransformation cycle:

n-hexane ⟶ 2-hexanol ⟶ 2-hexanone ⟶ 5-hydroxy-2-hexanone ⟶ 2,5-hexanedione
2-hexanol ⟶ 2,5-hexanediol ⟶ 2,5-hexanedione

Its neurotoxic effect has been attributed to the metabolite 2,5-hexanedione (HD), which may be bonded to DNA, RNA and essential proteins [4,5]. Studies [6–8] on the urinary excretion of the *n*-hexane metabolite HD, determined in exposed factory workers, have shown a correlation between the metabolite and *n*-hexane concentrations in the work-

room air. Owing to the neurotoxic effects of HD, which are closely related to the concentration of *n*-hexane in air, it is advantageous to have a rapid and sensitive method which can determine this compound in urine samples for biological monitoring of occupational exposures, even at very low levels.

High-resolution gas chromatography (HRGC) [8–11] has been proposed for the determination of urinary HD levels. Acid hydrolysis [9–12] has significantly lowered the time of sample preparation compared with the enzymatic method [8]; and solid–liquid extraction, with octadecylsilane microcolumns [9–11], has made quantitative analysis by HRGC much less time-consuming than extraction with solvents [9,12].

In the analytical procedure for reversed-phase high-performance liquid chromatography (HPLC) reported in the literature [12] the sample is subjected to liquid–liquid extraction, and the extract is evaporated to dryness and reconstituted with water before chromatographic analysis is performed. This is quite time-consuming and, moreover, the drying step may cause some irreproducible loss of HD at low concentration levels. Reliability at these levels is important, for example to evaluate low urinary HD levels in subjects exposed to small amounts of solvent who may suffer long-term effects as a result of chronic poisoning.

This paper describes a rapid and sensitive procedure for the determination of HD in urine samples by reversed-phase HPLC. The extraction of HD from the sample and the clean-up of the extract are based on solid–liquid extraction. Commercial microcolumns were used. Elution solvent sequences along with elution volumes and times were optimized for better results and shorter analysis times. The optimized procedure reduces sample preparation to less than 15 min, leading to a very low detection limit (0.01 ppm) with a typical recovery of about 85% and a relative standard deviation (R.S.D.) of 5% at the 0.1 ppm level. Results obtained on real samples collected from exposed and unexposed subjects, and the correlation between HRGC and HPLC measurements, are also discussed. Fourier transform infrared (FTIR) spectrometry, coupled with HRGC by a cooled moving-plate interface developed in our laboratory [13–15], was employed for confirming the identity of the chromatographic peak assigned to HD.

EXPERIMENTAL

Reagents

HPLC-grade organic solvents were supplied by either Carlo Erba (Italy) or Riedel-deHaen, (Germany). Sodium hydroxide and hydrochloric acid were Suprapur reagent grade (Merck, Germany); sodium carbonate, cyclohexanone and *trans*-2-butenal were analytical reagent grade (Carlo Erba). 2,5-Hexanedione was supplied by Aldrich Chimica (Italy). Standard solutions of 2 g/l were prepared weekly in dichloromethane, methanol or water and stored at 4°C. Anydrous sodium sulphate (Carlo Erba) was kept at 450°C for 6 h, stored in a dessicator and washed with dichloromethane before use. Double-distilled water (Carlo Erba) was treated in an ELGASTAT UHQ system to produce ultrahigh-quality pure water (18 MΩ/cm resistivity at 25°C) and was used throughout.

Octadecyl spe (C_{18}, J. T. Baker, USA) and Supelclean LC-Si spe (LC-Si, Supelco, USA) 3-ml cartridges were used for HD extraction and extract clean-up, respectively. Millex HV_{13} filter units (0.45 μm, Millipore, USA) were used for filtering urine samples.

Apparatus

An LC-410 series HPLC system (Perkin Elmer, USA) equipped with a Reodyne Model 7125 injector (20 μl injection loop), an LC-95 UV–VIS spectrophotometric detector and a C-R3A chromatopac integrator (Shimadzu) was used for LC analysis. Chromatographic separation was performed on an S5ODS1 C_{18} reversed-phase spherisorb column (Phase Separation, USA), 250 × 4.6 mm I.D., 5 μm particle size. Isocratic elution was carried out by 15% acetonitrile in water at a flow-rate of 1 ml/min (overall time for one run: 12 min). The spectrophotometric detector was set at a wavelength (λ) of 230 nm, where HD exhibits the maximum absorbance.

An HRGC-5160 Mega series chromatograph (Carlo Erba) equipped with an automatic cold on-column injection port, a flame ionization detector heated at 250°C and a Hewlett-Packard Model 3396A integrator was used for GC analysis. Chromatographic separation was performed on a fused-silica Series 007 capillary column (Quadrex, USA), methyl phenyl 5% silicone, 25 m × 0.32 mm I.D., 0.25 μm film thickness. The chromatographic con-

ditions were: initial temperature, 40°C; 1°C/min increase up to 50°C and 25°C/min increase up to 250°C; and hold for 4 min. Helium was used as the carrier gas.

A Model 740 FTIR spectrometer (Nicolet, USA) equipped with a narrow-range 1-mm square element mercury–cadmium–telluride (MCT) detector and a Model Spectra-Scope microscope unit (Spectra-Tech, USA), with a variable aperture from 20 μm to 15 mm, was coupled to the HRGC system by a moving-plate interface [13–15] and was used for collecting 8 cm^{-1} resolution IR spectra.

Procedure

The overall analytical procedure proposed was as follows: load the C_{18} column with 5 ml of urine (pH 2); wash with 3 ml of water, 3 ml of 0.1 M sodium carbonate and 6 ml of water; elute with 1.5 ml of dichloromethane; dry on sodium sulphate; load the LC-Si column with dichloromethane eluate; wash with 1 ml of dichloromethane and 1 ml of diethyl ether, 25% in dichloromethane; elute with 1 ml of methanol.

Urine pretreatment. Following a slightly modified version of a procedure proposed by Perbellini *et al.* [11], urine (20 ml) was acidified with concentrated hydrochloric acid (1 ml) and kept in a closed vessel at 100°C in an oven for 1 h. After cooling, the pH was adjusted to 2 by adding concentrated sodium hydroxide solution, and urine was filtered by using a Millex filter unit and immediately processed. A series of experiments carried out on spiked urine in which the pH was varied from 0 to 7 showed that HD losses were more than 80%, except for pH ranging between 1.5 and 3.5.

Cartridge preparation. Octadecyl spe cartridges were preconditioned immediately before use by washing them under vacuum with methanol (6 ml), water (3 ml) and hydrochloric acid at pH 2 (3 ml).

LC-Si spe cartridges were preconditioned by washing them only with dichloromethane (6 ml). A 2-g sample of anydrous sodium sulphate was put on the top of the LC-Si column to eliminate water traces which may have been present in the dichloromethane eluate.

HD extraction and extract clean-up. A 5-ml sample of pretreated urine was loaded on an octadecyl spe cartridge and washed with 3 ml of water, followed by 3 ml of 0.1 M sodium carbonate solution

and 6 ml of water. This washing procedure was needed in order to eliminate most of the organic substances which may cause severe interferences in the chromatographic determination. HD was eluted with 1.5 ml of dichloromethane by pumping with a gas–tight glass syringe. Before eluting, the cartridge containing HD was dried under mild vacuum. The results showed low recoveries and high standard deviations, and very strict experimental conditions had to be respected. This was explained by considering the quite high volatility of HD and the stripping out process from the cartridge. Therefore, the solvent was dried on anydrous sodium sulphate.

HPLC analysis of dichloromethane extract, after evaporating to dryness under argon flow and reconstituting with methanol highlighted the fact that some interfering substances were still present. In order to remove them, a final clean-up was done by loading dichloromethane extract on an anydrous sodium sulphate LC-Si spe cartridge, washing with 1 ml of dichloromethane, followed by 1 ml of diethyl ether, 25% in dichloromethane, and eluting HD with 1 ml of methanol by pumping with a gas–tight glass syringe. A total of 0.5 ml of eluate was collected, 20 μl of which were injected into the HPLC system for HD determination. For low HD content, the extract was concentrated to 0.1 ml in a micro-Kuderna-Danish evaporator under argon flow at room temperature before being injected.

HRGC analysis procedure. For the sake of comparison, HRGC analysis was performed on the dried dichloromethane extract of some urine samples processed following the proposed procedure. Quantitation was done by using calibration plots obtained with spiked real samples.

Internal standard. *trans*-2-Butenal and cyclohexanone were used as internal standards (I.S.) for HPLC and HRGC, respectively. In both cases, these compounds elute before HD, having been sufficiently resolved from the HD and from other peaks present in real samples. Cyclohexanone and *trans*-2-butenal were added directly to dichloromethane or methanol extract, respectively.

RESULTS AND DISCUSSION

Quantitation and detection limits

In biological samples, metabolic products may interfere with the determination of the compound

under investigation. In order to take into account any possible interferences, quantitative HPLC determinations of HD were performed using calibration curves obtained by means of a calibration solution prepared from urine samples collected from unexposed subjects which were tested in advance and showed a non-detectable HD level. Spiked samples, with a concentration range of 0.1—50 ppm, were processed following the proposed procedure. Linear regression analysis for the 95% confidence limit of all data collected gave the formula $y = 0.70 + 37.05 x$ ($r = 0.9998$), where y is the peak area in arbitrary units and x is the concentration in ppm. The following remarks can be made from these results: (i) the calibration curve is linear in the observed concentration range and shows a fairly high correlation coefficient (r); (ii) the intercept value expressed in ppm and the relative error on the slope are typically 0.02 and 1%, respectively.

To calculate the detection limit (c_L), the following definition, recommended by IUPAC [16], was used:

$$c_L = k \, s_B/S \tag{1}$$

where k is a numerical constant for which IUPAC strongly suggests a value of 3, s_B is the standard deviation of the field blank and S is the sensitivity of the method. Since, in the present case, true field blanks were not available, s_B was considered to be equivalent to the standard deviation (σ_0) obtained by extrapolating at zero concentration the standard deviations on seven replicate analyses of five spiked samples at low concentration levels (0.1–0.5 ppm). From the calculated σ_0 values, a detection limit of 0.05 ppm using eqn. 1 was obtained. Moreover, since organic extracts can be reduced to a volume of 0.1 ml under argon flow at room temperature, the detection limit can be lowered to 0.01 ppm. Replicate analysis on the same sample containing 0.01 ppm showed a relative standard deviation of 31%.

To calculate the concentration of the sample, the measured peak area was first corrected for the I.S. response and then converted into ppm by means of the slope of the corresponding calibration plot. The urinary concentrations of HD were finally corrected to a specific gravity of 1024.

Recovery and precision

The reliability of the present method was tested by using spiked urine samples prepared as outlined earlier. Triplicate samples of urine were spiked with various amounts of HD in the range 0.1–50 ppm and analysed using the proposed method. The results for HPLC analysis are reported in Table I. These data show recoveries of more than 85% for concentrations as low as 0.1 ppm.

In order to improve the validation of the analytical procedure proposed, three more calibration solutions containing 0.5, 1.0 and 1.5 ppm HD were prepared. These calibration solutions were analysed ten times per day, on three non-consecutive days, interspersing them with urine samples collected from exposed and unexposed subjects. Thus it was possible to obtain intra-assay and inter-assay statistical figures on ten and thirty pieces of data, respectively. The results are reported in Table II and show that at the 0.5-ppm level the coefficient of variation

TABLE I

RECOVERY OF HD FROM SPIKED URINE SAMPLES

Concentration (ppm)	Recovery[a] (%)	
	Mean	R.S.D.
0.1	85	5
0.2	86	4
0.4	85	4
1.0	89	3
5.0	88	3
10.0	92	2
50.0	94	2

[a] Three replicate measurements.

TABLE II

INTRA-ASSAY AND INTER-ASSAY COEFFICIENT OF VARIATIONS FOR HD DETERMINATIONS

Concentration (ppm)	Coefficient of variation (%)	
	Intra-assay[a]	Inter-assay[b]
0.5	4	5
1.0	3	4
1.5	3	4

[a] Ten replicate measurements.
[b] Thirty replicate measurements.

is always more than 5%, even for inter-assay analysis.

One of the urine samples analysed, collected from a subject not known to have been exposed to *n*-hexane, showed a signal at the HD retention time whose concentration was estimated to be 0.15 ppm. To confirm its identity the following procedure was used: recovery of the HPLC fraction eluted at HD retention time, liquid–liquid extraction with dichloromethane, reduction to 0.02 ml in a microKuderna-Danish evaporator under argon flow at room temperature and analysis by HRGC–FTIR. The cooled moving-plate interface described elsewhere [13–15] was kept at −40°C during the trapping of HD on its surface. IR transmission spectra collected after a 1-μl injection of a standard solution containing 50 ng/μl HD and after a 1-μl injection of concentrated dichloromethane solution showed the same features, so the assignment to HD of the peak obtained at 9.15 min retention time is correct.

Real samples

Urine samples were collected from shoe factory

employees working in different environmental conditions following the procedure proposed in ref. 6. All samples were divided into two groups: weakly exposed and exposed to vapours of *n*-hexane, depending on the exposure level. Control samples were collected from unexposed voluntary subjects. For each group, four samples were collected from four different subjects and analysed in triplicate. For the first two groups the maximum concentration of *n*-hexane in the workroom air was estimated to be about 20 and 200 mg/m^3, respectively. The only purpose of the sample analysis was to verify the ability of the proposed analytical procedure to determine also low levels of HD which occur after occupational exposure to *n*-hexane, and to compare HPLC and HRGC data.

HPLC chromatograms of samples from an unexposed and an exposed subject are shown in Fig. 1. Curve a reveals undetectable HD concentrations in one sample of an unexposed subject. This chromatogram also shows that in the time intervals where the signal under consideration falls, the baseline is quite flat and unaffected by the presence of possible interferences. For one sample of a weakly exposed subject (curve b) the HD concentration was estimated to be 0.10 ppm. Curve c refers to another aliquot of the sample b after an addition of 0.3 ppm HD.

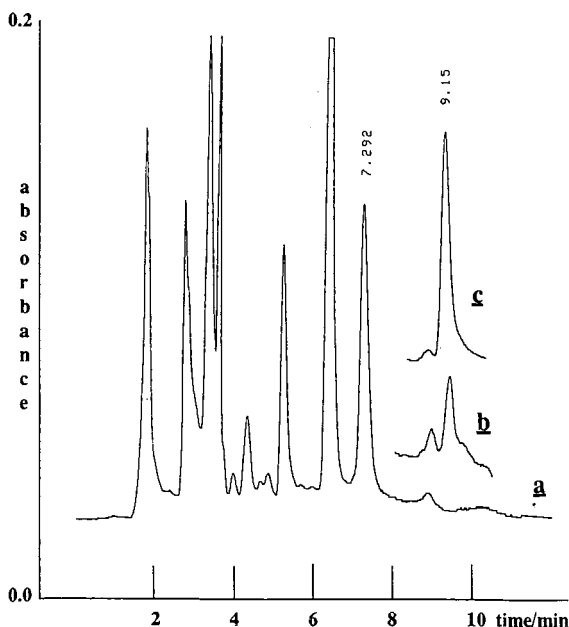The results for all the real samples analysed by

Fig. 1. HPLC chromatograms for samples of unexposed (a) and weakly exposed (b) workers. Curve c refers to sample b with a 0.3-ppm standard addition of HD. Signals at 7.29 and 9.15 min relate to I.S. and HD, respectively.

TABLE III

HD CONCENTRATION IN REAL SAMPLES

Subject group	Concentration (ppm)	
	HRGC	HPLC
Exposed	3.80	3.50
	1.10	1.30
	1.80	2.00
	2.80	2.40
Weakly exposed	0.15	0.16
	0.45	0.40
	0.12	0.10
	0.22	0.28
Unexposed	n.d.	n.d.
	0.13	0.15
	0.08	0.05
	0.03	0.04

both HPLC and HRGC are summarized in Table III. Linear regression analysis between two sets of data was performed, and a correlation factor of 0.992 was obtained, which shows that there is good agreement between the HPLC and HRGC results. The data in Table III also demonstrate a fairly high variability of the HD urinary level within the first and second groups. This expected variability may be explained by considering the differences in exposure time and level of exposure to *n*-hexane between subjects from whom samples were collected. Finally, small amounts of HD were found in some urine samples of unexposed subjects (third group) for whom a non-detectable level should be expected. The occurrence of these low HD levels may be the result of an occasional exposure to *n*-hexane or of other unknown metabolic reactions which may induce urinary HD [12,17].

CONCLUSIONS

An overall analytical procedure is described for a sensitive and accurate determination of HD urinary level. Sample preparation was optimized to enable HPLC analysis in a short time. After acid hydrolysis, the overall analysis time was less than 30 min. The proposed procedure is reliable and can be used for a routine analysis with an intra-assay coefficient of variation of 4% and inter-assay coefficient of variation of 5% even at the 0.5-ppm level. HPLC and HRGC procedures were performed on several urine samples and compared, and gave a correlation factor of 0.992. The detection limit is about 0.01 ppm, so the presence of HD in urine samples can also be estimated for workers exposed to very low quantities of *n*-hexane.

REFERENCES

1 M. Iwata, Y. Takeuchi, N. Hisanaga and Y. Ono, *Int. Arch. Occup. Environ. Health*, 51 (1983) 253.
2 H. H. Schawmburg and P. S. Spencer, *Brain*, 99 (1976) 183.
3 D. Couri and M. Milks, *Am. Rev. Pharmacol. Toxicol.*, 32 (1982) 145.
4 R. Toftgard and J. Gustafsson, *Scand. J. Work Environ. Health.*, 6 (1980) 1.
5 A. P. De Caprio and E. A. O'Neil, *Toxicol. Appl. Pharmacol.*, 78 (1985) 235.
6 I. Ahonen and K. W. Schimberg, *Br. J. Ind. Med.*, 45 (1988) 133.
7 H. Mat and H. Kenneth Dillon, *Biological Monitoring of Exposure to Chemicals*, Wiley, London, 1987.
8 L. Perbellini, F. Brugnone and G. Faggionato, *Br. J. Ind. Med.*, 38 (1981) 20.
9 L. Perbellini, F. Tagliaro, S. Maschio, A. Zedde and F. Brugnone, *Med. Lav.*, 77 (1986) 628.
10 N. Fedtke and H. M. Bolt, *Int. Arch. Occup. Environ. Health*, 57 (1986) 149.
11 L. Perbellini, D. Marhuenda Amoros, A. Cardona Llorens, C. Giuliari and F. Brugnone, *Br. J. Ind. Med.*, 47 (1990) 421.
12 I. Marchiseppe, M. Valentino, M. Governa and V. Stocchi, *J. Chromatogr.*, 492 (1989) 288.
13 K. H. Shafer, P. R. Griffiths and R. Fuoco, *J. High Resolut. Chromatogr. Chromatogr. Commun.*, 9 (1986) 124.
14 R. Fuoco, K. H. Shafer and P. R. Griffiths, *Anal. Chem.*, 58 (1986) 3249.
15 R. Fuoco, in S. Caroli, G. Rossi, E. Sabbioni and K. Zimmer (Editors), *Biomedical Research and Spectrochemistry*, C.E.C. No. EUR 11702 EN, Brussels, 1989, p. 203.
16 Analytical Methods Committee, *Analyst*, 112 (1987) 199.
17 H. Altenkirch, G. Stoltenburg and H. M. Wagner, *J. Neurol.*, 219 (1978) 159.

CHROMSYMP. 2383

Trace analysis of phthalocyanine pigments by high-performance liquid chromatography

Christian-Herbert Fischer

Hahn-Meitner-Institut Berlin, Bereich S2, Glienicker Strasse 100, W-1000 Berlin 39 (Germany)

ABSTRACT

A new sensitive and specific method for the analysis of insoluble phthalocyanine pigments is described. In a special microchemical procedure phthalocyanine pigments were converted to the corresponding phthalimides by oxidation, and these were identified by high-performance liquid chromatography and diode-array detection by their retention times and ultraviolet spectra. Detection limits were found to be 2.5 ng for copper phthalocyanine and 27 ng for copper perchlorophthalocyanine. The method was also used for commercial artistic dyes containing copper phthalocyanine.

INTRODUCTION

Phthalocyanine (PC), discovered in 1907, has the typical complex ring system (**1**, Fig. 1). The two hydrogen atoms in the center of the molecule can be replaced by various metals. The metal PCs were widely studied and synthesized in the 1920s, commercially introduced for use as pigments in the late 1930s and since that time widely used in dyes and lacquers for artistic and industrial purposes. The most important compounds of this group are phthalocyanine blue (PC blue) (= copper phthalo-

cyanine, CuPC, **2**, Fig. 2)) and phthalocyanine green (PC green) (= copper perchlorophthalocyanine, CuCl$_{16}$PC, **3**, Fig. 2). Both have ideal pigment properties, as they have deep colors, are absolutely insoluble in any solvent except concentrated sulphuric acid and have a very high thermal stability. Sensitive and specific analyses of PCs may be
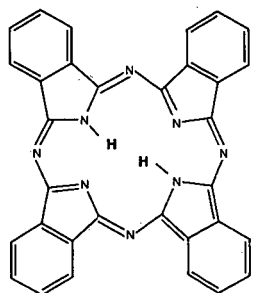
1 phthalocyanine

Fig. 1. Structure of phthalocyanine (**1**).
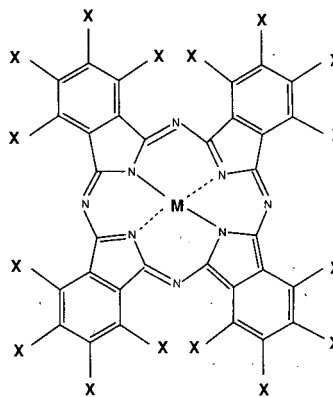
2 M = Cu , X = H   copper phthalocyanine (CuPC)

3 M = Cu , X = Cl   copper perchlorophthalocyanine (CuCl$_{16}$PC)

Fig. 2. Structures of copper phthalocyanine (**2**) and copper perchlorophthalocyanine (**3**).

required in forensic science for the identification of traces of lacquer (*e.g.* of cars) and in archaeometry, where positive PC result in a painting of the twentieth century enables either a dating (introduction of PC-containing artistic dyes = *terminus post quem*) or a decision about authenticity, if the supposed painter had died before the introduction of PCs or if the signature carries an earlier date.

The analytical methods for these important pigments are still mainly restricted to the observation of colors after treatment with concentrated sulphuric or nitric [1] or trichloroacetic acid [2] or N-methyl-pyrrolidone–alkaline hydrogensulphite solution [3]. There are, however, doubts bout the non-ambiguity of these techniques, especially in dye mixtures [1]. Moreover, the decisions are often very subjective (*e.g.* if the solution should turn "slightly greenish yellow") and the results cannot be easily documented. A combined thin-layer chromatographic (TLC) method which measures the optical reflection spectra directly from the thin-layer plate has been described [4]. Because of their general insolubility, PCs do not migrate during TLC. Therefore no chromatographic result is obtained and a superposition of spectra might often be measured, because quite often several substances remain at the starting position on the TLC plate. There is only one modern method [5], in which the derived phthalic esters are determined by gas chromatography. Unfortunately this three-step reaction cannot be adapted for trace analyses. So the objective of our work was the development of a modern unambiguous trace method, the results of which can be easily documented.

EXPERIMENTAL

Chemicals

CuPC was purchased from Aldrich, $CuCl_{16}PC$ from BASF, potassium dichromate and concentrated sulphuric acid (analytical grade) from Merck and acetonitrile (HPLC grade) from Promochem. The phthalo blue and titan white artistic dyes were manufactured by Schmincke.

Oxidation procedure

The sample was weighed in a special, small, conical glass tube, which was closed at one end (Chrompack Cat. No. 10381, 3 cm long, outer diameter 5 mm reducing to 2 mm). A 20-μl aliquot of

concentrated sulfuric acid was added, and the mixture was heated to 80°C for 30 s and put into an ultrasound bath for 2 min. After the addition of 10 μl of a saturated aqueous potassium dichromate solution, the tube was heated to 90°C for 10 min and placed in a brass block with holes of the correct size to hold the tubes and a thermometer. Removal of excess dichromate and dilution of sulphuric acid was carried out by addition of 20 μl of 0.05 M sodium hydroxide in methanol–water (1:1, v/v). For commercial dyes, which also contain other materials, centrifugation was carried out while the tube was standing in a septum screw-cap vial (Chrompack Cat. No. 10271); in order to keep it centered in the centrifuge. The supernatant was injected into the HPLC system.

Chromatography

The chromatographic system consisted of an L 6000 Merck–Hitachi pump, a 20-μl sample loop and either an L 4200 Merck–Hitachi UV–VIS detector operating at 219 nm or a Waters 990 diode-array detector. The separation was carried out on a LiChrospher 100 RP-8 (5 μm) column, 120 mm × 4 mm I.D., using acetonitrile–diluted aqueous phosphoric acid at pH 2.8 (20:80) as eluent at a flow-rate of 1.5 ml/min. For the calibration a stock solution of CuPC or $CuCl_{16}PC$ was diluted in concentrated sulphuric acid.

RESULTS AND DISCUSSION

The ideal pigment properties of PC blue and green, insolubility and complete non-volatility, prevent any direct chromatographic analysis, either by HPLC or by gas chromatography. Thus the PC must be converted via a specific reaction to a soluble and easily detectable product. The PC skeleton cleaves to form phthalimide by a well defined oxidation [5,6] (Fig. 3). During this process halogen substituents at the aromatic ring remain unchanged, and $CCl_{16}PC$ yields tetrachlorophthalimide. Dichromate is used as the reagent. The oxidation has been designed for microchemical purposes as a one-vessel procedure. Dissolution of the pigment, reaction at elevated temperature, removal of excess reagent and removal of insoluble sample material were carried out in the same vessel. A special type of small glass tube, conical and closed at one end, was used to keep
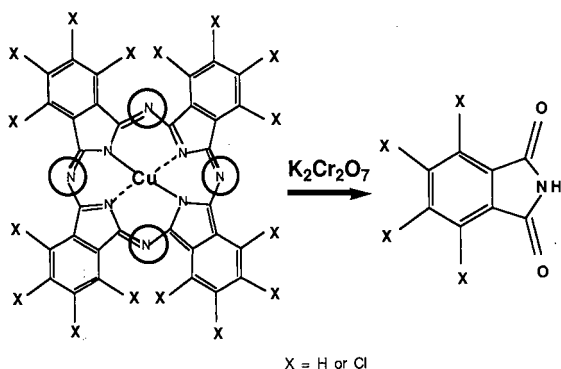
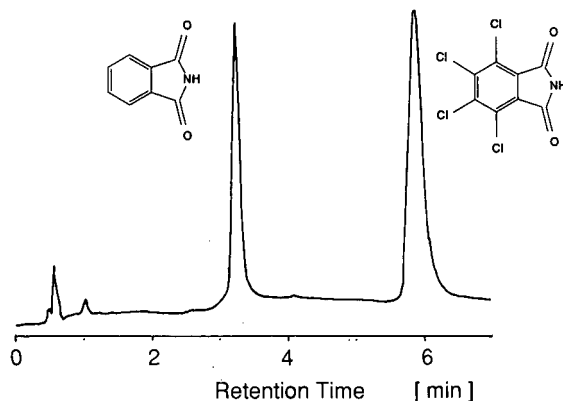Fig. 3. Oxidation of copper phthalocyanine.

X = H or Cl

Fig. 4. Separation of phthalimide and tetrachlorophthalimide. Column: LiChrospher RP-8. Mobile phase: acetonitrile–80% diluted aqueous phosphoric acid at pH 2.8 (20:80). Flow-rate: 1.5 ml/min. Detector: photometer operating at 219 nm. For further details see Experimental section.

volumes as small as possible and to allow centrifugation of insoluble components of the sample before HPLC analysis. The phthalimides have poor solubilities in organic solvents. However, for an extraction of the unsubstituted PC dichloromethane could be used, and nitrobenzene could be used for the tetrachloro derivative, if the amount of PC was not too large, as indicated by a turbid organic phase. Because mixtures of PC blue and PC green were also possible, no extraction of the oxidation products from the reaction mixture was carried out in the standard procedure. In order to avoid injection of concentrated sulphuric acid, still containing dichromate, onto the column, the dichromate was removed and the acid diluted. This was accomplished by adding 15 μl of a 0.05 M solution of sodium hydroxide in methanol–water (1:1, v/v).

The separation and determination of the chlorinated and non-chlorinated phthalimide were performed by isocratic HPLC on an RP-8 phase with optical detection in 7 min (Fig. 4). It should be noted that both compounds adsorb very strongly to any kind of surface, and because of their poor solubility syringes and injection port have to be cleaned very carefully. For this reason a blank check was carried out before each analysis, to rule out contamination from previous samples. Fig. 5 shows the chromatograms of five analyses starting with different amounts of PC blue between 2.5 and 41.8 ng. Only about one third of the resulting reaction mixture was injected into the HPLC system. Even in the presence of the huge amount of sulphuric acid, the phthalimide peak of the smallest sample was still detectable. From the calibration lines based on the weight of the

PC sample (Fig. 6) it was shown that the sensitivity for CuCl$_{16}$PC was lower than for the non-chlorinated one. The reasons are, firstly, that in a plot like Fig. 4 the difference in the molecular weights (1120 as compared with 576) is not taken into account, whereas the measured extinction is a molar value. Secondly, the longer retention time (poorer signal-to-noise ratio) and, thirdly, the even higher adsorption contribute to this effect. The first factor results
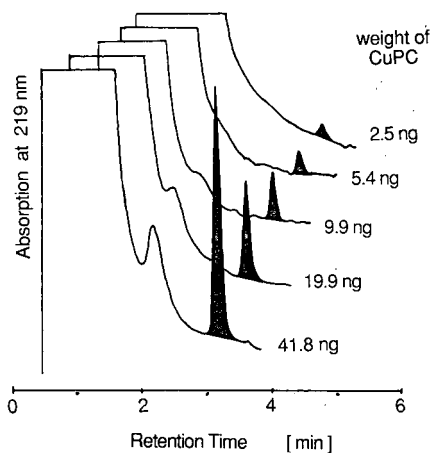

Fig. 5. Chromatograms obtained from the reaction mixtures of copper phthalocyanine and potassium dichromate according to the described procedure (details in the Experimental section). The actual weight of the sample is given to the right of the chromatograms.
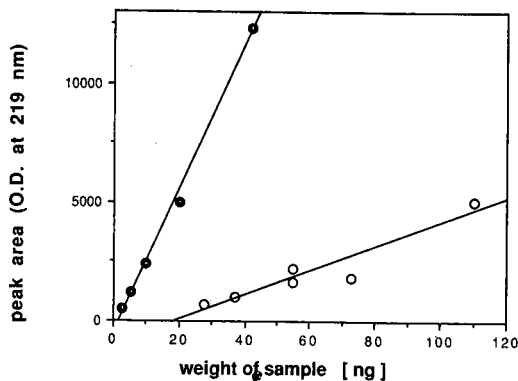
Fig. 6. Calibration at copper phthalocyanine (●) and copper perchlorophthalocyanine (○), determined as the corresponding phthalimide according to the described procedure: phthalimide peak area as a function of the weight of the PC sample.

Fig. 7. Optical absorption spectra of phthalimide and tetra-chlorophthalimide as measured by a diode-array detector.

in a lower slope of the calibration line, the second leads to a large intercept on the concentration axis and the third factor contributes to both effects.

An even more definite identification of the PCs can be achieved by using a diode-array detector. The spectra of both phthalimides, given in Fig. 7, are quite typical; they have a strong band at about 220 nm and the non-chlorinated a weak supplementary peak at 300 nm. It was found that sufficient chromatographic and spectral results were still obtained from a 0.5-mg sample of dried, light-blue artist dye, prepared from commercial phthalo blue and white dye in a 1:10 weight ratio. The results were not masked by other components, such as binding agents or loading material, which were present in high concentration.
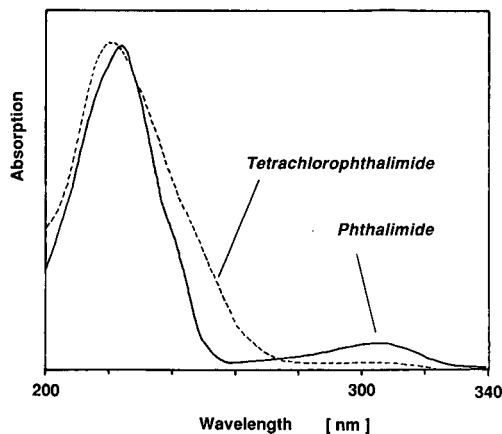
REFERENCES

1 M. de Keijzer, *ICOM, Triennial Meet.*, 8 (1987) 33.
2 F. H. Moser and A. L. Thomas, *The Phthalocyanines*, CRC Press, Boca Raton, FL, 1983, p. 115.
3 H. Schweppe, *6th Fatipec Congress, May 21–25, 1962, Wiesbaden*, Verlag Chemie, Weinheim, 1962, p. 162.
4 N. A. Fuller, *Forensic Sci. Int.*, 27 (1985) 189.
5 J. Kranz, BASF, Ludwigshafen, personal communication.
6 A. M. Islam, A. M. Naser, A. A. El-Mariah and A. A. Salman, *J. Oil Col. Chem. Assoc.*, 57 (1974) 134.

Automated determination of aflatoxin B₁ in cattle feed by two-column solid-phase extraction with on-line high-performance liquid chromatography

J. A. van Rhijn

State Institute for Quality Control of Agricultural Products (RIKILT), Bornsesteeg 45, 6708 PD Wageningen (Netherlands)

J. Viveen

Sopar Biochem, Wattbaan 6, 3439 ML Nieuwegein (Netherlands)

L. G. M. Th. Tuinstra*

State Institute for Quality Control of Agricultural Products (RIKILT), Bornsesteeg 45, 6708 PD Wageningen (Netherlands)

ABSTRACT

A method has been developed for the determination of aflatoxin B₁ in cattle feed which is an automated version of the method which was ring-tested by the European Community. The method uses a two-column clean-up with intermediate solvent evaporation and is coupled on-line to a high-performance liquid chromatographic system. The automated and manual methods are compared with regard to repeatability, accuracy and recovery of the analyte. Both methods have comparable repeatability at a concentration of 5 μg/kg of aflatoxin B₁; however, due to the lower recovery of the automated method, it differs significantly from the manual method with respect to accuracy. Nevertheless, the method may be used for screening purposes due to its good reproducibility.

INTRODUCTION

The presence of aflatoxin B_1 in feed stuffs for dairy cows may give rise to the occurrence of its metabolite, aflatoxin M_1, in their milk. As about 2% of the ingested aflatoxin B_1 is excreted in the milk as the suspected carcinogen aflatoxin M_1, high levels of aflatoxin B_1 in cattle feed pose a threat to human health. For this reason there is an official tolerance level for aflatoxin B_1 in cattle feed in the European Community (EC) of 10 μg/kg. However, this tolerance level does not result in a low enough concentration of aflatoxin M_1 in the milk produced. Therefore, in The Netherlands, manufacturers of cattle feed have agreed to attempt to have less than 5 μg/kg in their products.

For the control of this level a method, which was recently ring-tested by the EC [1], will become the official method. This method uses a two-column solid-phase extraction (SPE) with Florisil and RP-C_{18} cartridges [2,3]. Initially the extract is applied to a Florisil cartridge. Following elution, the solvent is evaporated and the residue is redissolved. This extract is applied to the RP-C_{18} cartridge. The resulting extracts can be analysed by high-performance liquid chromatography (HPLC) with post-column derivatisation [2–4]. However, this method is laborious and time-consuming and therefore does not have a very high sample turnover.

In this paper an automated method of analysis is described for aflatoxin B_1 in cattle feed based on the same principles as the EC ring-tested method.

EXPERIMENTAL

The automated clean-up was performed using an ASPEC system (Gilson, Villiers le Bel, France) with a 100-mg disposable extraction column (DEC), which was equipped with a module for on-line evaporation (Meyvis, Bergen op Zoom, Netherlands). The evaporation module consisted of a thermostated container for the collection vessels and a three-way valve to supply nitrogen via the ASPEC needle. The standard software of the ASPEC system is suitable for the application of a straightforward clean-up using one SPE column. The software necessary to perform a more complicated two-column clean up was developed at the RIKILT and is available from the authors or Meyvis & Co. The ASPEC system was equipped with an extra solvent rack to contain the washing and eluting solvents.

Florisil (100 mg) and RP-C_{18} (50 mg) DECs were obtained from Analytichem (Harbor City, CA, USA).

The ASPEC system was coupled on-line to an HPLC system consisting of a Waters 590 pump (Waters, Milford, MA, USA), a 200 × 3.0 mm Chromsphere RP-C_{18} column (Chrompack, Middelburg, Netherlands), a KOBRA device (Lamers & Pleuger, Den Bosch, Netherlands) for generating bromine for the post-column derivatisation and a Perkin-Elmer LS4 fluorescence detector (Perkin Elmer, Norwalk, CT, USA). The excitation wavelength was 369 nm and emission was measured at 422 nm.

An aflatoxin B_1 standard solution in chloroform (25 μg/ml) was obtained from the National Institute of Public Health and Environmental Protection (RIVM, Bilthoven, Netherlands). Calibration standards were prepared by dilution of this standard solution to obtain solutions containing 0.4, 0.8, 1.6 and 2.4 mg/ml, corresponding to 100, 200, 400 and 600 pg of aflatoxin B_1 in the injected volume, respectively. Aflatoxicol was used as an internal standard to determine the relative retention time; it was not used for quantification.

All reagents were purchased from Merck (Darmstadt, Germany) and were of analytical-reagent grade. Water was obtained from a Milli-Q system (Millipore, Bedford, MA, USA).

The HPLC eluent was a mixture of 1300 ml of water, 700 ml of methanol and 400 ml of aceto-

nitrile to which were added 286 mg of potassium bromide and 152 μl of 85% nitric acid.

Samples were prepared as described elsewhere [2] to obtain sample extracts in chloroform, corresponding to 0.2 g of product per ml of extract. Blank samples were spiked with aflatoxin B_1, resulting in sample extracts corresponding to 5 and 10 μg/kg. Development and testing of the method was mainly carried out using a standard solution of aflatoxin B_1 containing 1 ng/ml, which corresponds to 5 μg/kg for a true sample extract when 100% recovery of the analyte is attained.

RESULTS AND DISCUSSION

To achieve automation of the analysis of aflatoxin B_1 using an ASPEC system, the manual method [2] had to be scaled down by approximately a factor of 10. To achieve this, a 100-mg Florisil-containing DEC and a DEC containing 50 mg RP-C_{18} were used. All volumes were decreased by a factor of 10. Scaling down is necessary because the elution volume is limited to 3.5 ml when using an ASPEC instrument. Scaling down almost always makes the procedure more critical and is not always a linear process. Therefore the elution profiles of aflatoxin B_1 had to be determined and possible breakthrough and other recovery losses had to be investigated for the redesigned procedure.

Figs. 1 and 2 show the elution profile of aflatoxin B_1 as a function of eluent composition on the Florisil and RP-C_{18} DEC respectively, obtained by fractionating the effluent of the DECs into nine 350-μl portions. It can be seen that the elution of aflatoxin B_1 from the Florisil DEC shows severe tailing. This cannot be significantly decreased by increasing the eluent strength (Fig. 1). Therefore a mixture of 5% water in acetone was used as the eluent in all experiments. However, this choice is more or less arbitrary as there is no significant effect from the eluent composition. Elution profiles on the RP-C_{18} DEC show a significant influence of the eluent composition. To achieve the maximum recovery within the allowable elution volume of 3.5 ml, the acetone content had to be increased, compared with the manual method, from 15 to 20%.

Unfortunately, the overall recovery was poor. Further investigation indicated that the Florisil clean-up gave rise to an approximate 50% loss of
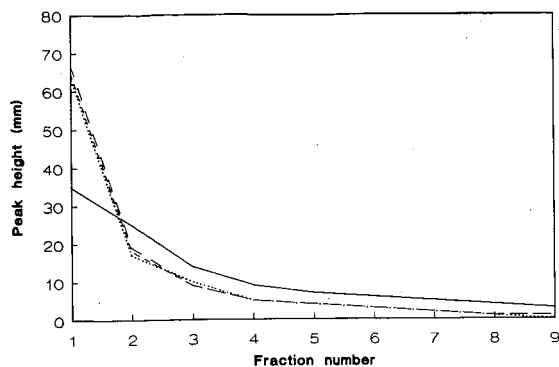
Fig. 1. Fraction number and peak height of aflatoxin B$_1$ chromatographed on the Florisil column with eluents of various water–acetone compositions: (—) 2:98; (- - -) 3:97; (– – –) 4:96); (. . . . .) 5:95. The effluent from the Florisil column was collected in 350-μl portions.

the analyte. The subsequent RP-C$_{18}$ clean-up adds another 20% loss of the remaining analyte, resulting in an overall recovery of approximately 40% (Table I). It is obvious that the recovery needs improvement as recovery values of 80–90% can easily be achieved using the manual method. The loss of aflatoxin B$_1$ from the Florisil clean-up was studied more closely.

No breakthrough of the analyte is observed during the application of the sample, nor during the washing of the Florisil DEC. Repeated elution of the Florisil DEC did not show any additional afla-
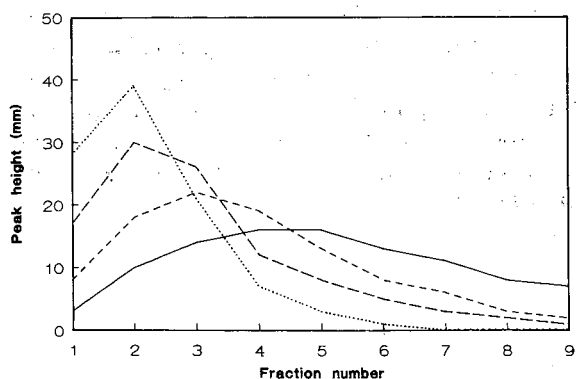

Fig. 2. Fraction number and peak height of aflatoxin B$_1$ chromatographed on the RP-C$_{18}$ column with eluents of various water–acetone compositions: (—) 85:15; (- - -) 82.5:17.5; (– – –) 80:20; (. . . . .) 77.5:22.5. The effluent from the RP-C$_{18}$ column was collected in 350-μl portions.

TABLE I

MEAN RECOVERIES AND CORRESPONDING COEFFICIENTS OF VARIATION FOR THE AFLATOXIN B$_1$ STANDARD ON THE SEPARATE FLORISIL AND RP-C$_{18}$ COLUMNS AND FOR THE OVERALL PROCEDURE USING BOTH COLUMNS

Column	Mean recovery (%)	C.V. (%)	n
Florisil	50	9.2	10
RP-C$_{18}$	81	1.4	10
Overall procedure	44	12	20

toxin B$_1$ in the effluent. Therefore the low recovery on the Florisil clean-up is probably due to irreversible adsorption of the aflatoxin B$_1$ onto the Florisil, onto the wall of the DEC, or onto the frits of the DEC. It has not so far been possible to increase the recovery of the analyte from the Florisil clean-up.

The automated solvent evaporation may be another cause of the low recovery. Manual solvent evaporation and the subsequent redissolution of the residue did not cause losses of aflatoxin B$_1$. The automated solvent evaporation, however, is a time-based process which can easily be influenced by environmental conditions. Therefore it is a critical step in the analytical procedure.

Low recovery obviously results in low results of the analysis and affects the limit of determination (LOD). Nevertheless, because the recovery percentage is constant, the losses can be taken into account and the method can still be used for screening purposes, although a higher recovery is preferable.

The repeatability is comparable with that of the manual method, with a coefficient of variation (C.V.) of 12% for the overall procedure ($n=20$). Again, the Florisil clean-up shows the largest fluctuations (Table I), whereas the RP-C$_{18}$ clean-up is very reproducible. The replicate analysis of a spiked sample (5 μg/kg aflatoxin B$_1$) showed a C.V. which was remarkably low compared with that obtained with standard aflatoxin solutions (C.V. = 3.0%; n = 5). Fig. 3 shows two chromatograms of samples to which aflatoxin B$_1$ had been added, corresponding to 5 and 10 μg/kg, respectively, prepared and analysed using the ASPEC–HPLC combination. The sample clean-up is good. The chromatograms are very similar to those obtained with the manual
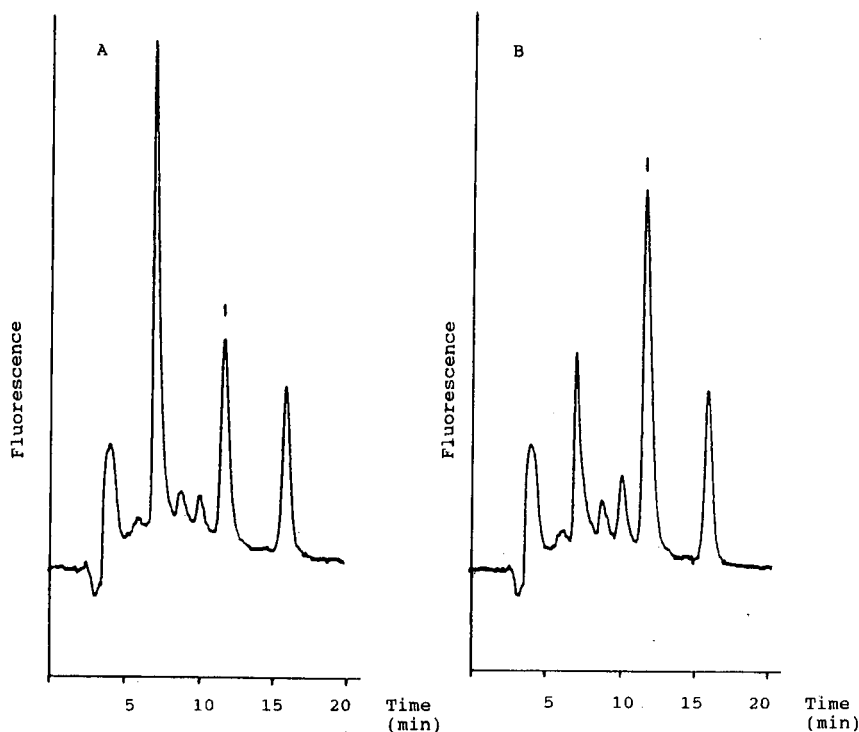
Fig. 3. Chromatograms of samples to which (A) 5 and (B) 10 μg/kg aflatoxin B₁ had been added. The last eluted peak is the internal standard aflatoxicol.

method. The LOD in spiked samples is approximately 2 μg/kg even when the recovery is as low as 40%.

The developed system is capable of calibrating the HPLC system with up to six calibrants. Up to 36 samples can be prepared and analysed in 24 h in unattended operation. Recalibration after ten samples is included in the automated protocol.

CONCLUSIONS

Automation of the method of analysis for aflatoxin B₁ which has been ring tested by the EC has been achieved. The recovery of the analyte is low but reproducible. This low recovery is probably due to losses during the Florisil clean-up procedure. With regard to repeatability and efficiency, the automated method is comparable with the manual method. Until there is an improvement in the percentage recovery, the developed method may only be used for screening purposes, with a LOD of approximately 2 μg/kg, taking the low but reproducible recovery into account. Its high sample turnover makes it useful in spite of the important drawback of incomplete recovery compared with the manual method.

The ASPEC software developed works well in the two-column clean-up with unattended intermediate solvent evaporation. With only minor adjustments this software can be used for other two-column clean-up procedures with or without solvent evaporation.

REFERENCES

1 H. P. van Egmond, S. H. Heisterkamp and W. E. Paulsch, *Food Addit. Contam.*, 8 (1991) 17–29.

2 W. E. Paulsch, E. A. Sizoo and H. P. van Egmond, *J. Assoc. Off. Anal. Chem.*, 71 (1988) 957–961.

3 W. A. Traag, J. M. P. van Trijp, L. G. M. Th. Tuinstra and W. Th. Kok, *J. Chromatogr.*, 396 (1987) 389–394.

4 W. Th. Kok, Th. C. H. van Neer, W. A. Traag and L. G. M. Th. Tuinstra, *J. Chromatogr.*, 367 (1986) 231–236.

CHROMSYMP. 2436

Quantitation of mutagenic/carcinogenic heterocyclic aromatic amines in food products[*]

G. A. Gross* and A. Grüter

NESTEC Ltd., Research Centre, Vers-chez-les-Blanc, Post Office Box 44, CH-1000 Lausanne 26 (Switzerland)

ABSTRACT

A method for screening genotoxic heterocyclic aromatic amines in cooked foods using solid-phase extraction and high-performance liquid chromatography with ultraviolet and fluorescence detection is described. Solid-phase extraction includes basic extraction on diatomaceous earth (Extrelut) and subsequent purification on propylsulphonic acid silica gel. This convenient procedure separates the analytes into a polar group and an apolar group. We have identified the following components in the two groups. The polar group contains aminoimidazoazaarenes *i.e.* 2-amino-3,8-dimethylimidazo[4,5-*f*]quinoxaline, 2-amino-3,4,8-trimethylimidazo[4,5-*f*]quinoxaline, 2-amino-3-methylimidazo[4,5-*f*]quinoline, 2-amino-3,4-dimethylimidazo[4,5-*f*]quinoline, 2-amino-1-methyl-6-phenylimidazo-[4,5-*b*]pyridine, and glutamic acid pyrolysates, *i.e.* 2-amino-6-methyldipyrido[1,2-a:3',2'-*d*]imidazole and 2-aminodipyrido[1,2-a:3',2'-*d*]-imidazole. The apolar group consists of five carbolines: 3-amino-1,4-dimethyl-5H-pyrido[4,3-*b*]indole, 3-amino-1-methyl-5H-pyrido-[4,3-*b*]indole, 2-amino-9H-pyrido[2,3-*b*]indole, 9H-pyrido[3,4-*b*]indole and 1-methyl-9H-pyrido[3,4-*b*]indole. The extraction efficiencies range from 45 to 90%, and the detection limits are in the low nanogram per gram range. The method was applied to the analysis of heterocyclic aromatic amines in pan-fried, oven-cooked and barbecued salmon.

INTRODUCTION

Frying or broiling of meat and other protein-rich foods may generate several heterocyclic aromatic amines (HAAs; for structures, see Fig. 1), *i.e.* amino acid pyrolysates or aminoimidazoazaarenes (AIAs) [1]. All the HAAs tested so far induce tumors at multiple sites in rodents and may be potential human carcinogens [2,3]. Therefore, accurate quantification of heterocyclic amines in cooked foods is essential for human risk assessment.

Most HAAs have shown potent mutagenic activity in the Ames test using *Salmonella typhimurium* frame shift trains TA98 or TA1538 and metabolic activation [4,5]. This assay successfully operates even with fairly crude or partially purified materials which are too dirty for liquid or gas chromatographic analysis. Many HAAs were isolated by bioassay-directed purification using the Ames test as a detection method.

Older methods for isolation or quantitative determination of HAAs included extensive fractionations in multiple steps (reviewed in ref. 1). These methods, therefore, were not suitable for routine screening. Specific monoclonal antibodies (MAbs) allowed the purification of MeIQx, IQ or PhIP (for abbreviations, see Table I) to be simplified [6–8], but these MAbs were not made commercially available. For food quality control the need for a more universal but also sensitive and convenient clean-up method still exists.

We previously reported two solid-phase extraction methods for the analysis of many HAAs [9]. Both methods relied on combined extraction and adsorption on coupled columns (tandems) of diatomaceous earth and a cation-exchange resin, *i.e.* propylsulphonic acid silica (PRS) or copper phthalocyanine-bound Sephasorb HP. However, neither of these procedures allowed the analysis of all HAAs.

---

[*] This paper has been dedicated to the memory of Hans-Ulrich Aeschbacher.

Polar Amines

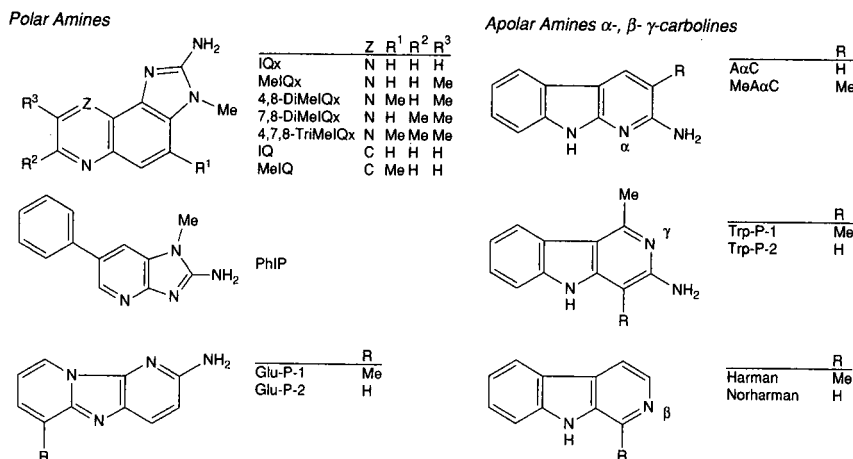Apolar Amines α-, β- γ-carbolines

Fig. 1. Chemical structures of heterocyclic aromatic amines. Me = Methyl.

We now report an improved fractionation method for purifying the entire range of HAAs on PRS resin.

EXPERIMENTAL

Chemicals and solvents were high-performance liquid chromatography (HPLC) or analytical grade. Water was from a Milli-Q water purification system (Millipore, Bedford, MA, USA). MeIQx, 2-amino-3,4,7,8-tetramethylimidazo[4,5-*f*]quinoxaline(4,7,8-TriMeIQx), IQ, MeIQ, PhIP and 2-amino-9H-pyrido[2,3-*b*]indole [amino-α-carboline (AαC)] were from Toronto Research Chemicals (Toronto, Canada). 3-Amino-1,4-dimethyl-5H-pyrido[4,3-*b*]-indole (Trp-P-1), 3-amino-1-methyl-5H-pyrido[4,3-*b*]indole (Trp-P-2), Glu-P-1 and Glu-P-2 were from Wako (Neuss, Germany). 1-Methyl-9H-pyrido[3,4-*b*]indole (harman) and norharman were from Aldrich (Steinheim, Germany). 4,8-DiMeIQx and 7,8-DiMeIQx were synthesized in house [10]. 2-Amino-3-methylimidazo[4,5-*f*]quinoxaline (IQx) was a gift from Professor J. Felton, Lawrence Livermore National Laboratory, University of California. Reference standards were used without further purification. Their purity was checked by HPLC and, where available, by comparison of extinction coefficients with values from the literature [11]. Stock mixtures of 5 ng/μl MeIQx, 4,8-DiMeIQx, IQ, MeIQ, PhIP, Glu-P-1, Glu-P-2, Trp-P-1, Trp-P-2, amino-α-carboline, norharman and harman in methanol (mix-

ture A) and 5 ng/μl TriMeIQx in methanol (mixture B) served as internal standard solutions. Extrelut extraction cartridges (20 ml) and refill material were from Merck (Darmstadt, Germany). Bond-Elut PRS (500 mg) and C_{18} (100 mg and 500 mg) cartridges and stopcocks were from Analytichem International (ICT, Basle, Switzerland). Cartridge-coupling adapters were from Supelco (Gland, Switzerland). Connections between cartridges and the peristaltic pump were made with Luer-lock male connectors (Econo column system, Bio-Rad, Glattbrugg, Switzerland). Fine Luer-lock injection needles (25G × 5/8 in.) served to reduce flow-rates during extraction with dichloromethane (DCM). Purified extracts were stored in 1.1-ml Chromacol gold microvials (Infochroma, Zug, Switzerland).

Instrumentation

A Minipuls-2 peristaltic pump (Gilson, Viller-le-Bel, France) and a Supelco Visiprep SPE vacuum manifold were used for manipulations with solid-phase extraction cartridges. Fried fish samples were mixed with a Bamix ESGE M122 household blender (Menotec, Lausanne, Switzerland) and homogenized with an Ultra-Turrax Typ TP 18/10 high-speed blender (Jahnke & Kunkel, Staufen, Germany). HPLC was performed using a Merck L-6200 pump, a Gilson 231-401 automated sample processor and injector and Hewlett Packard Model 1040A diode array UV and Model 1046A programmable fluor-

escence detectors, both driven by an HP9000 Series 300 workstation (Chemstation). The column was a TSK gel ODS80 (Toyo Soda), 25 cm × 4.6 mm I.D. (5 μm particle size), protected by a Supelguard LC-8-DB (Supelco) precolumn which was attached via a "direct-connect" column coupler (Alltech, Lausanne, Switzerland). The mobile phase was as follows: solvent A, 0.01 M triethylamine adjusted with phosphoric acid to pH 3.2; solvent B, same as A but adjusted to pH 3.6; solvent C, acetonitrile. The linear gradient program was: 0–10 min, 5–15% C in A; 10–10.1 min, exchange of A with B; 10.1–20 min, 15–25% C in B; 20–30 min, 25–55% C in B; 30–55 min, column rinse and re-equilibration. Separations were carried out at ambient temperature. Peak identification was achieved by comparison of retention time and on-line recorded UV spectra with library entries.

Sample preparation

A commercial meat extract and fresh salmon steaks of 150 g per slice served as samples. Salmon steaks were pan-fried over a gas flame, cooked in a hot-air oven or barbecued while measuring the frying temperature with a Newport 267B-T2 thermocouple (Seyffer, Zürich, Switzerland). After frying, the bone was removed and the salmon was mixed with a household blender.

Solid-phase extraction

To prepare the meat extract, 3-g samples were solubilized in 12 ml of 1 M sodium hydroxide and loaded individually onto Extrelut columns. In the case of fried fish, 10 g per determination of fried fish mix were homogenized in 20 ml of 1 M sodium hydroxide using a high-speed blender. Aliquots were thoroughly mixed with Extrelut refill material with the aid of a spatula and used to fill empty Extrelut columns.

Bond-Elut PRS cartridges were fitted with coupling adapters, and with fine needles for flow reduction. The cartridges were quickly rinsed with 2 ml of DCM under positive pressure, and another 2 ml were pipetted into each cartridge. The Extrelut columns were then filled with DCM. The PRS cartridges were coupled as soon as the liquid levels reached the bottom of the Extrelut. The extraction was stopped at 30 ml of DCM by separating the Extrelut and PRS cartridges. Extrelut cartridges

were discarded and the PRS cartridges placed on a Visiprep and dried for at least 4 min under maximum vacuum. The PRS cartridges were then connected to a peristaltic pump and successively rinsed at about 1–2 ml/min with 6 ml of 0.1 M hydrochloric acid, 15 ml of methanol–hydrochloric acid 0.1 M in various proportions as specified in the Results section and 2 ml of water. The 0.1 M hydrochloric acid wash was discarded and the methanol–hydrochloric acid and water eluates (apolar amines) were collected into empty Extrelut column reservoirs fitted with stopcocks. PRS cartridges were then coupled to Bond-Elut C_{18} cartridges (100 mg), previously conditioned with 1 ml of methanol and 10 ml of water. These tandems were rinsed with 20 ml of 0.5 M ammonium acetate adjusted to pH 8 with ammonia solution. The PRS cartridges were then discarded. The C_{18} cartridges were rinsed with 2 ml of water and dried by applying strong positive nitrogen pressure. The adsorbed polar amines were carefully eluted into microvials using 0.8 ml of methanol–concentrated ammonia solution (9:1, v/v). The eluates containing apolar amines were neutralized by adding 500 μl of ammonia solution and diluted with water to less than 20% methanol. These mixtures were passed at 4–5 ml/min through Bond-Elut C_{18} cartridges (500 mg) conditioned with 2 ml of methanol and 10 ml of water. The C_{18} cartridges were rinsed with 2 ml of water, dried by applying strong positive nitrogen pressure, and adsorbed *apolar amines* carefully eluted into microvials using 1.2 ml of methanol–ammonia solution (9:1, v/v). Apolar and polar extracts were concentrated under nitrogen and redissolved in 40 μl (unspiked samples) or 100 μl (spiked samples) of internal standard solution B. For HPLC, 20-μl aliquots were injected into a 50-μl loop.

Measure of extraction efficiencies, quantitative determinations of HAAs

The standard addition method was used to measure HAA extraction efficiencies (quadruplicate determinations with two unspiked samples and two samples spiked with 50 μl of HAA standard mixture A) as well as to quantitatively determine HAAs (triplicate extractions with two unspiked samples and one spiked with 50 μl of standard mixture A). The extraction efficiencies were thus calculated for each analyte as the slope of the linear regression line
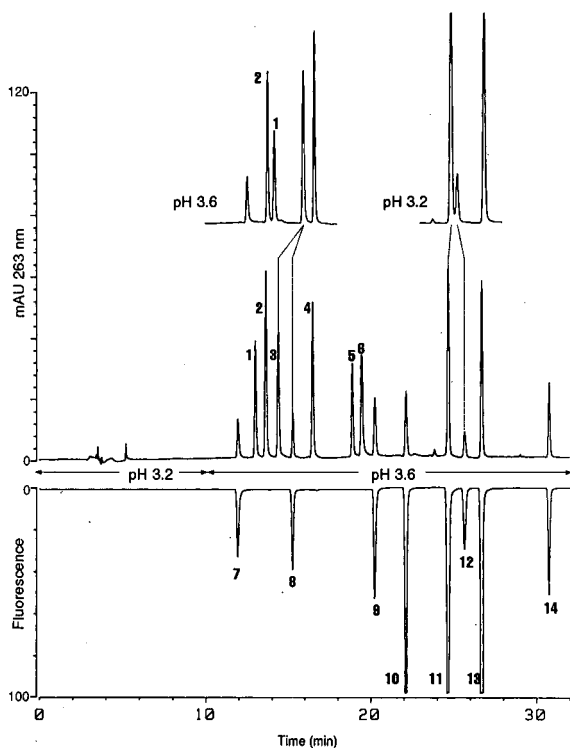
Fig. 2. HPLC separation of HAA standards. Complete chromatograms (UV and fluorescence, scaled to about equal peak heights) were obtained with a ternary gradient as specified in Experimental section. The two offset chromatogram extracts above show peak distribution with binary gradients at the indicated pH values. Peaks (excitation wavelength/emission wavelength): 1 = IQ; 2 = IQx; 3 = MeIQ; 4 = MeIQx; 5 = 7,8-DiMeIQx; 6 = 4,8-DiMeIQx; 7 = Glu-P-2 (360/450); 8 = Glu-P-1 (360/450); 9 = norharman (300/440); 10 = harman (300/440); 11 = Trp-P-2 (265/410); 12 = PhIP (315/390); 13 = Trp-P-1 (265/410); 14 = AαC (335/410).

"added analyte concentration (x) *versus* measured analyte concentration (y)".

Quantitative HAA measures were corrected for incomplete analyte recovery. Uncorrected results were calculated as the y-axis intercept of the regression line "added analyte concentration" *versus* "measured analyte concentration". The corrected result was obtained by dividing the intercept by the slope. The standard error of the corrected result therefore included contributions from both the intercept and the slope errors:

$$a = \bar{y} - b\bar{x}$$

$$\frac{a}{b} = \frac{\bar{y}}{b} - \bar{x}$$

$$\mathrm{Var}\left(\frac{a}{b}\right) = \mathrm{Var}\left(\frac{\bar{y}}{b}\right)$$

$$\mathrm{S.E.} = \sqrt{\mathrm{Var}\left(\frac{\bar{y}}{b}\right)} = \sqrt{\frac{1}{b^2}\,\mathrm{Var}\,(\bar{y}) + \frac{\bar{y}^2}{b^4}\,\mathrm{Var}\,(b)}$$

where x is the added concentration, y is the measured concentration, b is the slope, a is the intercept and S.E. is the standard error.

RESULTS

HPLC separation of HAAs

Baseline separation of all HAAs was a prerequisite for our study. Many reversed-phase silica columns were screened, but the TSK gel column showed the best peak symmetry and separation efficiency. Binary mobile phase gradients with acidic buffer between pH 3 and 4 and acetonitrile gave

TABLE I

EXTRACTION EFFICIENCY OF POLAR AMINES[a]

Substance	Abbreviation	Fish (%)	S.E. (%)	Meat extract (%)	S.E. (%)
2-Amino-3,8-dimethylimidazo[4,5-f]quinoxaline	MeIQx	77	11	69	8
2-Amino-3,4,8-trimethylimidazo[4,5-f]quinoxaline	4,8-DiMeIQx	85	9	84	6
2-Amino-3-methylimidazo[4,5-f]quinoline	IQ	73	10	68	4
2-Amino-3,4-dimethylimidazo[4,5-f]quinoline	MeIQ	60	5	72	6
2-Amino-6-methyldipyrido[1,2-a:3′,2′-d]imidazole	Glu-P-1	63	8	83	5
2-Aminodipyrido[1,2-a:3′,2′-d]imidazole	Glu-P-2	63	9	85	5
2-Amino-1-methyl-6-phenylimidazo[4,5-b]pyridine	PhIP	44	6	33	6

[a] Average from nine determinations with ratios of methanol to 0.1 M hydrochloric acid varied from 10 to 90% (see text).

good peak shapes, but above pH 3.2 Glu-P-1 and MeIQ co-eluted, and below pH 3.5 Trp-P-2 and PhIP were not baseline separated. A ternary gradient including pH switching from pH 3.2 to pH 3.6 during the run solved this problem (Fig. 2).

Solid-phase extraction method development

For the development of the extraction method a meat extract and fried salmon were used as samples. This allowed the simultaneous assessment of possible matrix effects on the extraction efficiency and selectivity. Purified extracts were analyzed by HPLC
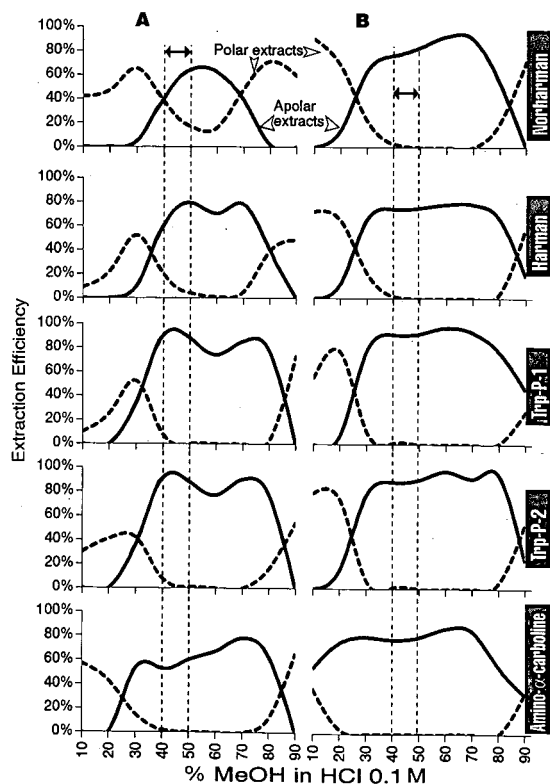

Fig. 3. Extraction efficiency of apolar amines. The apolar amines were partitioned in the apolar or the polar extract depending on the amount of methanol in the rinse phase. Extraction efficiencies from pan-fried fish (A) and meat extract (B) are shown. Smooth curves were plotted through each set of data points to illustrate solvent-dependent partition of carbolines in the polar (broken lines) or apolar extract (continuous lines) with maximal extraction efficiency in the apolar extract near 1:1 0.1 M methanol-hydrochloric acid (best range marked for each sample by a pair of vertical dashed lines).

with UV and fluorescence detection. Briefly, alkaline sample preparations were loaded onto Extrelut columns. HAAs and other basic organosoluble materials were extracted with DCM and immediately retained on coupled PRS cation-exchange cartridges. The dried PRS cartridges containing adsorbed amines were re-equilibrated with 0.1 M hydrochloric acid. Retention of AIAs, especially of PhIP, was better when using 0.1 M than 0.01 M hydrochloric acid, as reported [9]. Subsequent rinsing of PRS with methanol–hydrochloric acid selectively desorbed carbolines (apolar extract). This acid extract was neutralized and diluted to 20% methanol for on-line concentration on C_{18} cartridges. The PRS cartridge was then coupled to a C_{18} cartridge and flushed with aqueous ammonium acetate buffer to release the polar amines as previously described [9].

The methanol–hydrochloric acid rinse step was studied in detail to optimize extraction efficiency and selectivity of apolar amines. Several determinations were carried out, varying the proportion of methanol to hydrochloric acid from 10 to 90% in steps of 10%. The volume was kept at a constant value in order to limit the number of determinations. Polar amines, including all AIAs, were so strongly bound to PRS that their extraction efficiencies remained remarkably constant at any proportions from 10 to 90% methanol in 0.1 M hydrochloric acid (see Table I). Matrix effects were minimal, as similar results from fish and meat extracts were observed.

The extraction efficiency of apolar amines showed a clear optimum with intermediate mixing ratios of methanol to hydrochloric acid (see Fig. 3). Theoretically, rinsing PRS with less than 20% or more than 80% methanol containing hydrochloric acid would allow the preparation of one unique, polar extract containing all amines. However, under such conditions the extraction efficiency was matrix-dependent (see Fig. 3) and co-eluting impurities interfered with low-level quantifications of AIAs, especially MeIQx. Therefore, the preparation of an apolar extract was advantageous. Elution with 40–70% methanol–hydrochloric acid gave an apolar extract with maximal extraction efficiency for most carbolines. However, below 50% methanol the apolar extracts were cleaner, therefore the best compromise between selectivity and recovery was 40–50% methanol–hydrochloric acid.

INTRODUCTION

Application

We examined HAA formation during cooking of fish. Salmon slices were fried and extracted using the optimized extraction conditions as explained above (for the results, see Table II). Less than 6 min of pan broiling or oven cooking at about 200°C or barbecuing at 270°C produced no or low amounts of MeIQx, PhIP, AαC, norharman and harman. MeIQx and PhIP even showed an apparent decrease with time during pan broiling. We believe that unequal heating of the gas flame-heated pan was responsible for this effect.

Barbecuing samples for more than 6 min resulted in a ten-fold increase in levels of PhIP, AαC, norharman and harman. Surprisingly, MeIQx formation did not follow this trend, and less than 1 ng/g MeIQx was found in such samples. Fig. 4a and b shows typical chromatograms.

DISCUSSION

HPLC with UV and fluorescence detection proved to be a convenient method of analyzing

HAAs. All the amines of interest could be baseline-separated by a ternary mobile phase gradient including pH switching on a suitable C_{18} reversed-phase silica column. A detection limit of about 1 ng/g in purified extracts was obtained, and for fluorescent HAAs this limit was slightly lower. Identification of HAAs was feasible using their typical UV spectra even at low nanogram per gram levels.

The improved PRS tandem extraction method allowed the screening of nanogram per gram levels of ten genotoxic HAAs and two co-mutagenic β-carbolines. Compared with our previous method, we introduced as the major modification the separation of analytes into two groups, *i.e.* a polar group including AIAs and glutamic acid pyrolysates, and an apolar group including α-, β- and γ-carbolines.

Tandem extraction combines the selectivities of basic organic solvent extraction on Extrelut and cation-exchange chromatography on PRS. The focus in this work was to optimize PRS clean-up by selectively releasing analytes while letting co-extracted impurities bound to the sorbent. Extraction efficiencies were more than 60%, except for PhIP. However doubling the DCM extraction volume on Extrelut to 60 ml improved its recovery to more than

TABLE II

FORMATION OF HETEROCYCLIC AROMATIC AMINES IN FRIED FISH

Sample	MeIQx[a]	S.E.[b]	PhIP	S.E.	AαC	S.E.	Norharman	S.E.	Harman[c]	S.E.
Pan-broiled at 200°C[c]										
2 × 3 min	1.4	0.01	1.7	0.7	n.d.[d]		8	0.1	2	0.1
2 × 6 min	5	0.01	23	7	4.6	0.1	26	1.4	20	1.4
2 × 9 min	4.7	0.3	14	2.8	8	0.3	24	4.4	34	3.5
2 × 12 min	3.7	0.2	17	0.6	9	0.04	28	1.8	16	0.1
Oven-cooked at 200°C										
20 min	<1		n.d.		n.d.		2	0.9	<1	
30 min	4.6	0.3	18	0.1	n.d.		11	0.7	3	0.2
40 min	3.1	0.02	5.9	1.4	n.d.		15	0.9	3	0.1
Barbecued at 270°C										
2 × 4 min	<1		2	0.3	2.8	0.2	8	0.1	3	0.1
2 × 6 min	<1		6.2	0.6	6.9	0.5	44	0.2	13	0.1
2 × 9 min	<1		69	23	73	2	160	46	108	3
2 × 12 min	<1		73	0.45	109	22	184	95	130	34

[a] Values (ng/g fried fish) are corrected for incomplete recovery as specified in Experimental section.
[b] Standard error of corrected result.
[c] Initial temperature displayed on thermocouple.
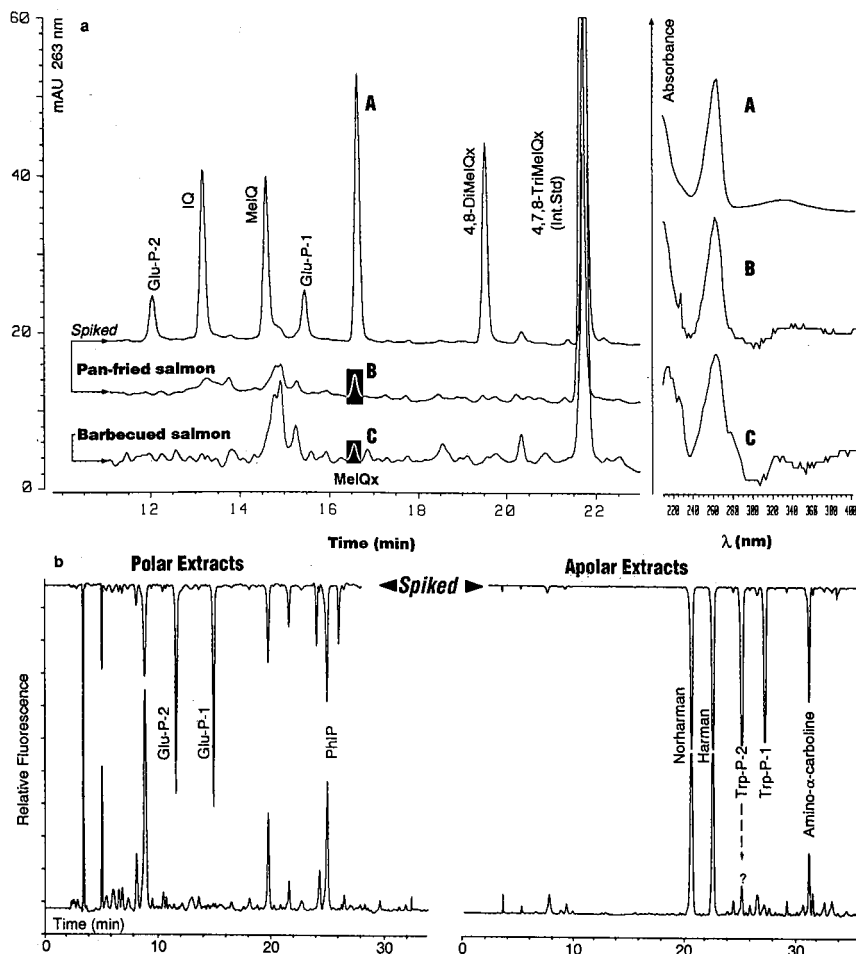[d] n.d. = not detected.

Fig. 4. (a) Polar extracts of fish pan-fried and barbecued for 9 min. Pan frying at 200°C produced more MeIQx (peak B) than barbecuing for the same time at 270°C (peak C). MeIQx peak C (< 1 ng/g) illustrates the detection limit of the method. On-line recorded UV spectra from MeIQx peaks are shown at the right. (b) Polar and apolar extracts of fish barbecued for 9 min per side at 270°C. These samples contained easily detectable PhIP in the polar extract (left), and AαC, norharman and harman in the apolar extract (right). A trace (< 0.1 ng/g) of Trp-P-2 might be present, but the peak (marked by "?") was too small to allow substance identification by a UV spectrum.

80% (data not shown). The absence of off-line transfer steps was beneficial for good analyte recovery and was also time-saving. Purifying a series of samples, typically four at a time, took only about 2 h of bench-work. The method may therefore be considered suitable for routine work.

In the kinetic study with fried fish we found MeIQx, PhIP, AαC and β-carbolines (norharman and harman) at levels which were in reasonable agreement with expectations from previous analysis and literature values (ref. 9 and references cited

therein). The formation of PhIP, AαC and the β-carbolines was markedly influenced by cooking temperature and was clearly non-linear. However, more data are required to define accurately the relation between time and temperature and mutagen formation. Surprisingly, MeIQx formation did not follow the same trend but rather was triggered by the cooking method. These results require further investigation. Nevertheless, our data suggest that pan frying and oven cooking generate low levels of HAAs whereas prolonged barbecuing at high tem-

perature mainly facilitates formation of PhIP and carbolines.

In conclusion, the improved "PRS tandem extraction" is a simple, efficient and selective purification method for mutagenic/carcinogenic HAAs. The basic approach of extraction and purification on coupled cartridges should prove applicable to the determination of other related compounds.

REFERENCES

1 J. S. Felton and M. G. Knize, in C. S. Cooper and P. L. Grover (Editors), *Chemical Carcinogenesis and Mutagenesis I*, Springer, Berlin, Heidelberg, New York, 1990, p. 471.

2 T. Sugimura, in P. A. Finot, H. U. Aeschbacher, R. F. Hurrell and R. Liardon (Editors), *The Maillard Reaction in Food Processing, Human Nutrition and Physiology*, Birkhäuser, Basel, Boston, Berlin, 1990, p. 323.

3 R. J. Turesky, in M. W. Pariza, J. S. Felton, H. U. Aeschbacher and S. Sato (Editors), *Mutagens and Carcinogens in the Diet*, Wiley, New York, 1990, p. 39.

4 D. M. Maron and B. N. Ames, *Mutat. Res.*, 113 (1983) 173.

5 M. G. Knize, N. H. Shen, S. K. Healy, F. T. Hatch and J. S. Felton, *Dev. Ind. Microbiol.*, 28 (1987) 171.

6 M. Vanderlaan, B. E. Watkins, M. Hwang, M. G. Knize and J. S. Felton, *Carcinogenesis*, 9 (1988) 153.

7 R. J. Turesky, C. M. Forster, H. U. Aeschbacher, H. P. Würzner, P. L. Skipper, L. J. Trudel and S. R. Tannenbaum, *Carcinogenesis*, 10 (1988) 151.

8 M. Vanderlaan, B. E. Watkins, M. Hwang, M. G. Knize and J. S. Felton, *Carcinogenesis*, 10 (1989) 2215.

9 G. A. Gross, *Carcinogenesis*, 11 (1990) 1597.

10 R. J. Turesky, H. Bur, T. Huynh-Ba, H. U. Aeschbacher and H. Milon, *Food Chem. Toxicol.*, 26 (1988) 501.

11 F. T. Hatch, J. S. Felton, D. H. Stuermer and L. F. Bjeldanes, in F. J. de Serres (Editor), *Chemical Mutagens: Principles and Methods for their Detection*, Vol. 9, Plenum Press, New York, 1984, p. 111.

Rapid high-performance liquid chromatographic determination of urinary N-(1-methylethyl)-N'-phenyl-1,4-benzenediamine in workers exposed to aromatic amines

Sergio Pellegrino* and Michele Petrarulo

Central Analysis Laboratory, Ospedale Mauriziano, Turin (Italy)

Elio Testa and Andrea Nicolotti

Department of Toxicology, Laboratorio C. Battisti, Chieri (Italy)

ABSTRACT

A procedure has been developed for determining N-(1-methylethyl)-N'-phenyl-1,4-benzenediamine in urine by using high-performance liquid chromatography. The method uses chloroform extraction for partial clean-up of the urine sample. The separation is carried out on a reversed-phase column using 65 mmol/l aqueous ammonium acetate in acetonitrile (30:70, v/v) as the mobile phase. The column effluent is monitored at 290 nm with an ultraviolet detector. The analyte is separated from other normal urine constituents in less than 4 min. Peak height and concentration are linearly related. Coefficients of variation assessed for within-day reproducibility were 5.9 and 3.7% at concentrations of 22.3 and 92.1 µg/l, respectively. The mean analytical recovery from urine samples spiked with known amounts of amine was 89.7 ± 6.8%. The request of only a small volume of urine and the simple pre-treatment procedure makes it suitable for the routine monitoring of the exposure of rubber vulcanization workers to aromatic amines.

INTRODUCTION

Aromatic amines derived from *p*-phenylenediamine are widely used as anti-oxidants in rubber vulcanization. N-(1-Methylethyl)-N'-phenyl-1,4-benzenediamine (IPPD) is the most commonly used rubber anti-oxidant in Italy. Control of the working environment and biological monitoring for rubber anti-oxidants is mandatory because IPPD is a suspected carcinogen [1] and a potent skin sensitizer [2]. The concentration of IPPD in the urine of workers is an index of exposure to this compound in their workplace [2]. A method has been described for the determination of IPPD in urine based on the solid-phase extraction of the amine from the urine matrix and subsequent analysis by high-performance liquid chromatography (HPLC) of the redissolved extract. As a result of the need for large sample volumes and the complex manipulation required, this procedure is not applied in large-scale routine analyses [3]. This paper describes a simple and rapid HPLC technique for the accurate determination of IPPD in human urine samples. The method is based on a liquid–liquid extraction, followed by back-extraction and HPLC assay.

EXPERIMENTAL

Materials

The IPPD standard was supplied by Bayer (Germany). Chromatography-grade acetonitrile and other reagents were purchased from Merck (Germany). A 2000 mg/l solution of IPPD in acetonitrile was prepared monthly and stored frozen in the dark. The concentrated standard was diluted daily with water to produce 2.0 and 20.0 mg/l standard

solutions. Non-exposed urine samples supplemented with 20 and 200 $\mu g/l$ IPPD were used as working standards.

Urine samples

Urine samples were collected at the workplace after the last shift from 62 rubber vulcanization workers on Fridays for one work-month and from 15 non-exposed control subjects. Dark-glass containers were used and the urine samples, stored at 4°C, were analysed within 24 h.

Extraction procedure

A 5.0-ml aliquot of urine was added to 200 mg of sodium chloride and 1.5 ml of chloroform in a PTFE-stoppered glass tube; the mixture was extracted by shaking vigorously for 15 min with an automatic stirrer. The tube was centrifuged for 5 min at 1000 *g* and, after the separation of the two phases, the organic layer was transferred into a glass test vial. The chloroform was evaporated to dryness in a water-bath at 40°C under a weak oxygen-free stream of helium. The residue was dissolved in 0.5 ml of acetonitrile and 20 μl of the resultant solution were injected into the chromatograph. Samples and standards must be handled with extreme care to avoid serious contamination from the IPPD present. The use of very clean glass vials and disposable materials for sampling and processing the urine samples is necessary.

Apparatus and chromatographic conditions

A Perkin-Elmer 620 quaternary pump liquid chromatograph equipped with an octadecylsilyl Li-Chrospher 100 RP-18 (10 μm) column (250 × 4 mm I.D.) (Merck), connected to a Perisorb RP-18 (30–40 μm) (Merck) guard column (30 × 4 mm I.D.) and a Perkin-Elmer 235 diode-array UV–visible detector set at 290 nm were used for the chromatographic analysis. The detector was operated at 0.02 absorbance units full scale. A Perkin-Elmer ISS-100 auto-sampling injector was used. The chromatographic procedure and data management were controlled by a PC AX2 computer (Epson, Japan) equipped with expert system software (Analyst, Perkin-Elmer, UK); the chromatograms were printed out with an Epson FX-850 printer.

Isocratic elution was performed at a flow-rate of 2.0 ml/min, with a acetonitrile–65 mmol/l ammonium acetate aqueous solution (70:30, v/v), adjusted to pH 6.5 with ammonium hydroxide solution, as the mobile phase.

RESULTS

Separation of IPPD in urine

The extraction of urine with chloroform in the presence of sodium chloride, followed by centrifugation, allowed the optimum separation between the two phases to be obtained. Fig. 1. shows typical chromatograms obtained with samples prepared from urine from a non-exposed control subject, the same urine spiked with 100 $\mu g/l$ IPPD and a urine sample taken from an exposed subject at the end of a shift. IPPD eluted as a well resolved peak in a blank zone of the chromatogram which usually contains the peaks of highly lypophylic compounds.

Accuracy and precision

The analytical recovery of IPPD, determined by analysing urine samples spiked with known amount of amine, ranged between 83.5 and 102.0% (Table I). The first extraction step with chloroform was able to separate most of the amine from the urine; further extraction did not improve the recovery yield. Recoveries were not affected by variations of the pH of the urine sample within the range 2–12.

IPPD shows a typical UV absorption spectrum with a maximum at 290 nm. To investigate the specificity of the method, the IPPD peaks in urine samples from 20 workers were examined on-line by UV spectroscopy and compared with those of the synthetic compound. The spectra were the same, which indicates that IPPD was well separated from other components in urine. The reproducibility has been tested with replicated intra-assay determinations to give coefficients of variation (C.V.) of 5.9 and 3.7% at IPPD concentrations of 22.3 and 92.1 $\mu g/l$, respectively.

The detector response at 290 nm was linearly related to the concentration of IPPD in urine over the range 0–300 $\mu g/l$. By using a calibration graph, the concentration of IPPD in urine samples was easily determined after measurement of its peak height. The sensitivity was 5 $\mu g/l$ at a signal-to-noise ratio of 3:1.
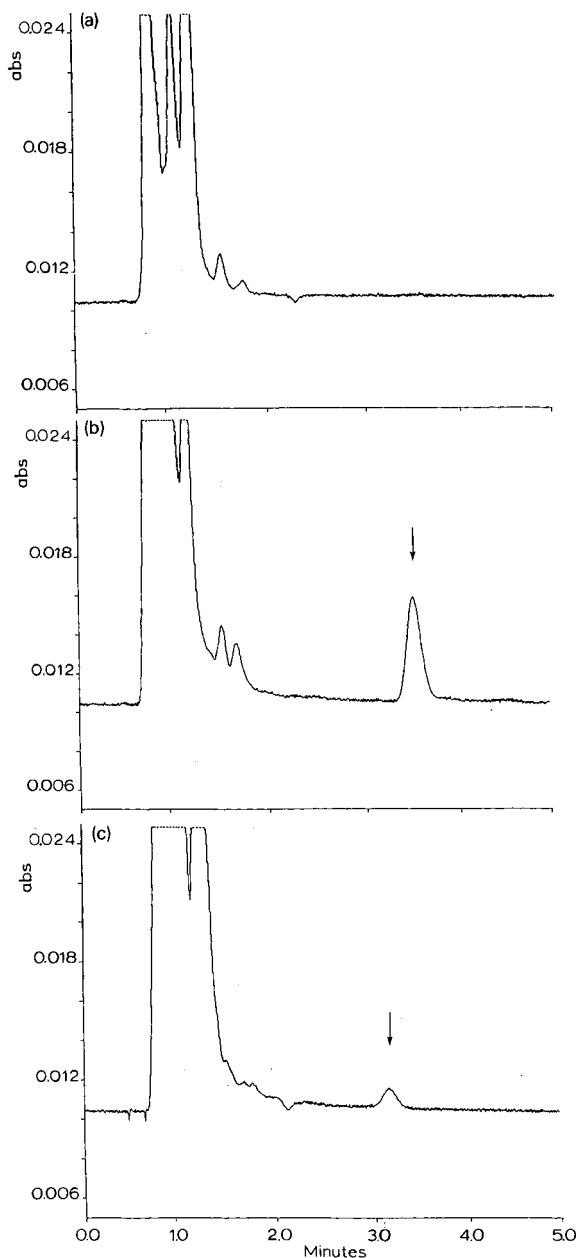
Fig. 1. Chromatographic traces of (a) urine from a non-exposed control subject, (b) the same urine supplemented with 200 $\mu g/l$ IPPD and (c) a urine sample collected from an exposed subject at the end of a shift (35 $\mu g/l$).

Biological results

Concentrations of IPPD in urine samples from 15 non-exposed control subjects were less than 5 $\mu g/l$. The concentrations measured in urine samples col-

TABLE I

ANALYTICAL RECOVERY OF IPPD ADDED TO A POOLED URINE SAMPLE FROM A NON-EXPOSED SUBJECT

Means ($\pm$ S.D.) from ten assays are shown. The data fit the line $IPPD_{found} = (0.86 \pm 0.02) IPPD_{added} + (2.12 \pm 2.05)$, with a standard error of the estimate, $s_{y \cdot x} = 1.4$, and a correlation coefficient $r = 0.995$.

Added ($\mu g/l$)	Found ($\mu g/l$)	Recovery (%)	C.V. (%)
–	<5.0	–	–
20.0	18.8 ± 1.5	94.1 ± 7.6	8.1
100.0	88.5 ± 5.9	88.5 ± 5.9	6.7
200.0	173.0 ± 9.4	86.5 ± 4.7	5.4

lected from 62 rubber vulcanization subjects after the end of a shift ranged from 4.3 to 174 $\mu g/l$ (29.3 $\pm$ 32.5 $\mu g/l$, mean $\pm$ 1 S.D.). These results confirm the significant absorption of IPPD during the working week.

CONCLUSIONS

A liquid–liquid extraction procedure, followed by HPLC separation, has been developed for the determination of IPPD in urine samples. The isocratic chromatographic step requires 4 min to be completed and a simple mobile phase composition. The extraction is easy to perform and relatively fast; twenty batched samples can be processed within 1 h. No improvement of the recovery yields was obtained either by increasing the volume ratio of chloroform to urine or further extracting or varying the pH of the urine samples.

The method described requires small amounts of urine, is sensitive, accurate and suitable for large-scale routine analyses, and its application could be extended to other similar aromatic amines.

REFERENCES

1 *Monographs on the evaluation of the carcinogenic risk of chemicals to humans, The Rubber Industry, Vol. 28*, IARC, Lyon, 1982, p. 252.
2 Toxicity and safe handling of rubber chemicals, in British Rubber Manufacturers' Association Ltd. (Editors) *Code of Practice*, White and Farrell, Birmingham, 1985.
3 I. Pavan, F. Belliardo, E. Buglione and M. M. Massiccio, *Chromatographia*, 24 (1987) 651.

CHROMSYMP. 2483

Determination of National Survey of Pesticides analytes in groundwater by liquid chromatography with postcolumn reaction detection

Carl J. Miles☆

Environmental Biochemistry Department, University of Hawaii, 1800 East–West Road, Honolulu, HI 96822 (USA)

ABSTRACT

   Multi-residue methods for pesticides in water were developed using liquid chromatography (LC) with postcolumn reaction detection. Over 100 analytes from the US Environmental Protection Agency's National Survey of Pesticides in Drinking Water Wells were screened for response using postcolumn photolysis followed by fluorescence (PFD), electrochemical (PED) or conductivity (PCD) detection. LC–PED and LC–PFD are suitable for multi-residue pesticide determinations in groundwater. These two detection methods are complementary as PED responds to several sulfur-containing pesticides whereas PFD responds to many nitrogenous pesticides. Approximately half of these analytes could be determined in low nanograms amounts using these two detection systems and multi-residue separations with gradient reversed-phase LC are demonstrated. The LC–PCD system tested was not suitable for sensitive, multi-residue determinations and further examination of this technique is recommended using the commercial PCD instrument.

INTRODUCTION

   The US Environmental Protection Agency (EPA) has identified 126 pesticides and degradation products that are potential groundwater contaminants. These compounds have been designated for study because of health effect concerns, high volumes of sales nationally, prior occurrence in groundwater or propensity to leach into groundwater and contaminate drinking water under normal use conditions [1]. The EPA has conducted a National Survey of Pesticides (NPS) in Drinking Water Wells for these analytes to provide nationwide estimates for pesticides and nitrates in drinking water. Results of the survey showed that about 10% of community water system wells have detectable levels of one or more pesticides, although less than 1% have concentrations over the maximum contaminant level (MCL) [1]. A need exists for continued monitoring.

   Central to this monitoring effort are the multi-residue methods (MRMs) for groundwater analysis. Although gas chromatography (GC) is the traditional method for pesticides, liquid chromatography (LC) is becoming more widely used. In fact, the polar nature of most of these analytes, which makes them potential groundwater contaminants, also makes LC separation a more viable technique. Of the four MRMs used for the EPA survey, two use LC separation. One employs UV detection at 254 nm (method 4) and the other (method 5) uses postcolumn reaction detection consisting of alkaline hydrolysis followed by fluorogenic labeling with *o*-phthalaldehyde–2-mercaptoethanol (OPA–MERC) [1].

   Recently, photolysis has been used as a LC postcolumn reaction for the sensitive determination of pesticides with a variety of detectors. Photolysis–fluorescence detection has been used both with [2–4] and without [3,4] OPA–MERC additions. Photoly-

_____
   ☆ Present address: Toxikon Environmental Sciences, 106 Coastal Way, Jupiter, FL 33477, USA.

sis–electrochemical detection showed sensitive and selective detection of organophosphate insecticides [5] and a wide variety of pharmaceuticals and environmental pollutants [6]. Photolysis–conductivity detection of pesticides has been demonstrated with a commercial unit [7,8] and a laboratory-constructed system [9]. This investigation examined LC separations using postcolumn photolysis with fluorescence (PFD), electrochemical (PED) and conductivity (PCD) detection of 101 of the EPA NPS analytes. Method detection limits were determined for several analytes and mult-residue separations are demonstrated.

EXPERIMENTAL

Reagents and standards

Analytical standards were obtained from the EPA chemical repository (Research Triangle Park, NC, USA) with the following exceptions; tetrachlorvinphos, etridizole, tricyclazole and DCPA diacid (Chem Service, West Chester, PA, USA), deisopropyl atrazine, fenarimol, MGK 264, 4-nitrophenol, methyl paraoxon, terbufos and triadimefon (Crescent Chemical, Hauppauge, NY, USA), aldicarb, aldicarb sulfoxide and aldicarb sulfone (Rhone-Poulenc, Research Trangle Park, NC, USA), disulfoton sulfoxide, disulfoton sulfone, fenamiphos, fenamiphos sulfoxide, fenamiphos sulfone, metribuzin DA, metribuzin DADK and metribuzin DK (Mobay Chemical, Kansas City, MO, USA), 5-hydroxy-dicamba (Sandoz Crop Protection, Des Plaines, IL, USA), carboxin sulfoxide (UniRoyal Chemical, Middlebury, CT, USA), 3,5-dichlorobenzoic acid (Aldrich, Milwaukee, WI, USA), 2,4,5-TP (Dow Chemical,Midland, MI, USA) and pronamide and pronamide metabolite (Rohm and Haas, Spring House, PA, USA). All standards were of $\geqslant 97\%$ purity, except for atraton (88.3%), disulfoton sulfoxide (96.5%), disulfoton sulfone (88.3%), merphos (88.2%), metribuzin DADK (84.8%), methyl paraoxon (96%), swep (95%) and tricyclazole (96%). Stock standard solutions (1 mg/ml) were prepared in acetonitrile except for simazine [0.5 mg/ml in acetonitrile–methanol (1:1)].

Solvents were Fisher (Fairlawn, NJ, USA) OPTIMA grade. All other reagents were of analytical-reagent grade or better. Reagent water was obtained from a Milli-Q water purification system (Millipore, Milford, MA, USA). The *o*-OPA–MERC reagent was prepared as described previously [3]. Borate solution was prepared identically to the OPA–MERC reagent but without *o*-phthalaldehyde or 2-mercaptoethanol added.

Apparatus and procedure

Photolysis conductivity detector. Liquid chromatography and flow-injection analysis (FIA) were performed with a Dionex (Sunnyvale, CA, USA) gradient pump module, a Dionex eluent degas module, a Dionex Model II conductivity detector and a Dionex Model II automated chromatography interface. The interface was connected to an IBM (Southbury, CT, USA) PS2/386 computer. Postcolumn photolysis was achieved in a commercial photoreactor (Beam Boost, ASTEC, Whippany, NJ, USA with a 10 m × 0.4 mm I.D. PTFE woven reactor coil. Injections (20 μl for LC; 1 μl for FIA) were made with a Perkin-Elmer (Norwalk, CT, USA) Model ISS 100 autoinjector. Reversed-phase columns (Perkin-Elmer, 3 cm × 0.46 I.D., 3-μm C_{18} with reduced activity) were used.

All analytes were screened by FIA (acetonitrile–water, 1:1) to avoid time-consuming LC separations. Also, FIA eliminates the possibility of a lack of response caused by compounds not eluted from the LC column. The FIA response was calculated as the difference between the average of duplicate peak areas with the lamp on and duplicate measurements with the lamp off divided by the nanomoles of analyte injected. A response ratio was calculated relative to an equimolar amount of bromobenzene (see refs. 3 and 9 for calculations of response ratios). Compounds with a response ratio $\geqslant 0.5$ (50% of bromobenzene) were analyzed by reversed-phase LC with acetonitrile–water gradients (5 to 90% in 60 min). Two gradients with different slopes were required for input into the DryLab G (LC Resources, Lafayette, CA, USA) computer program designed to optimize multi-component separations by gradient LC [10]. After the optimum gradient had been found, method detection limits (MDLs) were determined on fortified groundwater using the procedure recommended by the EPA [11] and described elsewhere [3]. The recovery of analytes from fortified groundwater was not determined as no sample preparation steps were used except fortifica-

tion of groundwater with analytes. Groundwater was obtained from the Palolo section of the Pearl Harbor–Honolulu basin aquifer.

Photolysis fluorescence detector. LC and FIA were performed with the system described above except using a Gilson (Middleton, WI, USA) Model 121 fluorimeter (λ_{ex} 356 nm; λ_{em} 450 nm), a Hewlett-Packard (Waldbronn, Germany) Model 1046A fluorimeter (λ_{ex} 335 nm; λ_{em} 450 nm) or an Applied Biosystems (Ramsey, NJ, USA) Model 980 fluorimeter (λ_{ex} 235 nm; λ_{em} >418 nm) and a Dionex minipump (Model RP-1). All analytes were screened by FIA (acetonitrile–water, 1:1) with (1) addition of the OPA–MERC reagent (0.2 ml/min), (2) addition of 0.05 M borate solution only (0.2 ml/min) and (3) no reagent addition. A response ratio was determined relative to an equimolar amount of methylamine (OPA–MERC addition) or 1-naphthol (borate or no addition). Analytes with a response ratio ⩾0.01 (1% of methylamine) or 0.09 (9% of 1-naphthol) were analyzed by reversed-phase LC with two acetonitrile–water gradients for DryLab G as described above. MDLs were determined as described above.

Photolysis electrochemical detector. LC was performed with the system described above except using a Dionex inert injection valve (20 μl), a Dionex Model II pulsed electrochemical detector (glassy carbon electrode at +1.0 V *vs.* Ag/AgCl) and a laboratory-constructed photoreactor [3] with a 10 m × 0.6 mm I.D. PTFE reactor coil woven with KOT3 [12]. Because of highly electroactive impurities in many of the pesticide standards, FIA was not reliable. Analytes were screened using a gradient (30 to 90% methanol in 20 min). Acetonitrile could not be used a solvent because photolysis produces compounds that polymerize on the carbon electrode [6]. Analytes with a response ratio ⩾ 0.2 (20% of malathion) were analyzed by a second gradient for DryLab G as described above. MDLs were determined as described above.

RESULTS AND DISCUSSION

Photolysis conductivity detector

Fifty eight of the 103 analytes tested (55%) yielded a response ⩾50% of the response for an equimolar amount of bromobenzene (Table I). Compound types that usually gave a favorable response were

phosphorothioates, phosphorodithioates, halogenated aromatics, triazines and uracils and aliphatics, aromatics and triazines with a methylthio group. Photolytic release of halide and sulfate ions acounts for the conductimetric response [9]. MDLs were determined for 33 of these analytes. MDLs were not determined for those compounds which were not retained by the reversed-phase column (*i.e.*, chloramben, dicamba-5OH, etc.) or those compounds which eluted after the gradient was completed (90% acetonitrile; *i.e.*, ametryn, terbutryn). Acidic compounds can be retained by ion suppression but the addition of acid to the mobile phase increases the conductivity background and increases detection limits [9]. Strongly retained compounds can be eluted with >90% acetonitrile, but use of this solvent shortens the lifetime of the Teflon photoreactor coils [3,9].

This photoreaction coil has been tested with an in-line UV detector and shown to add only a minor amount of band spreading to the chromatographic system [13]. Multi-residue separations are possible but changes in the background conductivity during the gradient cause sloping baselines which make peak detection difficult (Fig. 1). However, isocratic analysis using PCD as described here with a small range of analytes is possible [9]. Injection of groundwater caused increased, but consistent, baseline shifts. These problems can be solved in part by a differential cell used on a commercial photoconductivity detector [7], although problems using gradient elution with this detector have been reported [8]. Further study with the commercial PCD instrument is warranted.

Photolysis fluorescence detector

Photolysis of the analytes produced a response with this detector by formation of an aliphatic primary amine which reacts with OPA–MERC, formation of a fluorescent product or a combination of these two responses. To determine the response source, the analytes were screened by FIA with the complete OPA–MERC reagent, with borate only and with no postcolumn reagent addition. With the OPA–MERC reagent, 39 of the 103 analytes tested (38%) yielded a response ⩾1% of the response for an equimolar amount of methylamine (Table I). With borate only added postcolumn, 25 gave a response ⩾9% of 1-naphthol. Most of these re-

TABLE I

METHOD DETECTION LIMIT[a] AND FLOW-INJECTION RESPONSE[b] OF SELECTED PESTICIDES ON THE USEPA NATIONAL PESTICIDES IN GROUNDWATER SURVEY LIST USING LC WITH POSTCOLUMN REACTION DETECTION

Common name	CAS No.	PFD[c]	PFD[d]	PED[e]	PCD[f]
Acifluorfen	62476-59-9	—	—	—	—
Alachlor	15972-60-8	—	—	15	4.3
Aldicarb	116-06-3	0.5	—	0.6	9.6
Aldicarb sulfoxide	1646-87-3	1.3	—	+	+
Aldicarb sulfone	1646-88-4	35	—	—	—
Ametryn	834-12-8	—	—	6.1	+
Atraton	1610-17-9	—	—	ND[j]	—
Atrazine	1912-24-9	—	—	ND	6.5
Atrazine, de-isopropyl	1007-28-9	—	—	—	1.7
Barban	101-27-9	+	+	2.8	5.4
Bentazon	25057-89-0	+	+	+	—
Bromacil	314-40-9	—	—	ND	2.0
Butachlor	23184-66-9	19	—	ND	3.6
Butylate	2008-41-5	5.3	—	+	—
Carbaryl	63-25-2	36	+	+	—
Carbofuran	1563-66-2	5.1	—	9.4	—
Carbofuran-OH	1563-38-8	—	—	0.9	—
Carbofuran-OH,-3KET	11781-16-7	—	—	0.5	—
Carbofuran-3OH	16655-82-6	5.7	—	2.5	—
Carboxin	5234-68-4	—	+	0.9	21
Carboxin sulfoxide[g]	17757-70-9	—	+	0.7	3.1
Chloramben	133-90-4	—	+	+	+
Chloroneb	2675-77-6	—	—	—	—
Chlorobenzilate	510-15-6	—	+	1.6	6.8
Chlorothalonil	1897-45-6	—	—	—	+
Chlorpropham	101-21-3	+	+	1.3	+
Cyanazine	21725-46-2	—	—	ND	16
Cycloate	1134-23-2	11	—	—	—
D-2,4 acid	94-75-7	—	—	10	+
DB-2,4 acid	94-82-6	—	—	+	—
Dalapon	75-99-0	—	—	ND	—
DCPA	1861-32-1	—	—	+	2.1
DCPA diacid metabolite	2136-79-0	—	—	—	—
Diazinon	333-41-5	—	—	+	5.5
Dicamba	1918-00-9	—	—	+	—
Dicamba-5OH	7600-50-2	+	+	+	+
3,5-Dichlorobenzoic acid	51-36-5	—	—	11	—
Dichlorprop	120-36-5	—	—	13	—
Dichlorvos	62-73-7	—	—	ND	—
Dinoseb	88-85-7	—	—	+	—
Diphenamid	957-51-7	0.4	—	0.3	—
Disulfoton	298-04-4	—	—	3.1	2.0
Disulfoton sulfoxide	2497-07-6	—	—	3.0	+
Disulfoton sulfone	2497-06-5	—	—	5.2	+
Diuron	330-54-1	2.0	+	+	6.7
EPTC	759-94-4	6.8	—	—	—
Ethoprop	13194-48-4	—	—	+	+
Etridiazole	2593-15-9	—	—	+	+
Ethylenethiourea	96-45-7	—	—	+	—
Fenamiphos	22224-92-6	+	—	3.1	3.9
Fenamiphos sulfoxide	31972-43-7	—	—	12	6.5
Fenamiphos sulfone	31972-44-8	—	—	—	6.0
Fenarimol	60168-88-9	9.5	1.5	1.6	7.4
Fluometuron	2164-17-2	32	+	4.0	11

TABLE I *(continued)*

Common name	CAS No.	PFD[c]	PFD[d]	PED[e]	PCD[f]
Fluridone	59756-60-4	–	+	–	–
Hexazinone	51235-04-2	–	–	ND	–
Linuron	330-55-2	9.0	+	28	7.9
Merphos	150-50-5	–	–	ND	40
Methiocarb	2032-65-7	5.0	–	+	15
Methomyl	16752-77-5	2.8	–	1.9	+
Metolachlor	51218-45-2	–	–	3.0	2.5
Metribuzin	21087-64-9	–	–	0.9	–
Metribuzin DA	34045-02-4	–	–	2.0	2.4
Metribuzin DADK	52236-30-3	–	–	5.4	–
Metribuzin DK	56507-37-0	–	–	2.1	–
Mevinphos	7786-34-7	–	–	+	–
MGK 264[h]	70322-82-6	–	–	ND	–
Molinate	2212-67-1	17	–	–	–
1-Naphthol[g]	90-15-3	6.1	0.9	0.7	+
Napropamide	15299-99-7	3.4	0.6	0.7	+
Neburon	555-37-3	11	+	+	1.7
4-Nitrophenol	100-2-7	–	–	+	–
Norflurazon	27314-13-2	+	–	6.8	–
Oxamyl	23135-22-0	2.6	–	24	+
Paraoxon-methyl	950-35-6	–	–	–	–
Pentachlorophenol	87-86-5	–	–	+	+
Pebulate	1114-71-2	4.9	–	–	–
cis-Permethrin	54774-45-7	+	+	ND	+
trans-Permethin	51877-74-8	+	+	ND	+
Picloram	1918-02-1	+	–	+	+
Prometon	1610-18-0	–	–	ND	–
Prometryn	7287-19-6	–	–	6.2	+
Pronamide	23950-58-5	–	–	–	–
Pronamide metabolite[i]	29918-41-0	–	–	10	+
Propachlor	1918-16-7	+	+	1.5	16
Propanil	709-98-8	5.4	0.5	2.9	12
Propazine	139-40-2	–	–	ND	12
Propham	122-42-9	+	+	–	–
Propoxur	114-26-1	1.8	+	6.0	–
Simazine	122-34-9	–	–	ND	–
Simetryn	1014-70-6	–	–	3.6	+
Swep	1918-18-9	+	0.9	3.0	10
T-2,4,5 acid	93-76-5	–	–	11	+
TP-2,4,5 acid	93-72-1	–	–	11	3.8
Tebuthiuron	34014-18-1	57	–	6.7	–
Terbacil	5902-51-2	–	–	–	–
Terbufos	13071-79-9	–	–	ND	19
Terbutryn	886-50-0	–	–	2.8	+
Tetrachlorvinphos	961-11-5	–	–	+	+
Triadimefon	43121-43-3	–	+	1.6	6.9
Tricyclazole	41814-78-2	–	–	ND	–
Trifluralin	1582-09-8	–	–	ND	–
Vernolate	1929-77-7	6.5	–	–	–

[a] MDL in nanograms.

[b] Where + denotes a detector response ⩾ the selected response ratio and − denotes a detector response ⩽ the selected response ratio.

[c] Photolysis–fluorescence detection (with OPA–MERC).

[d] Photolysis–fluorescence detection (with borate only).

[e] Photolysis–electrochemical detection.

[f] Photolysis–conductivity detection.

[g] Not on the USEPA list.

[h] Trade name for N-octylbicyloheptanedicarboximide.

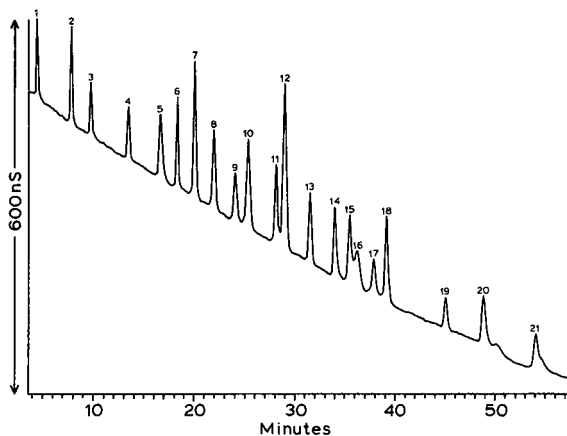[i] N-(1,1-Dimethylacetonyl)-3,5-dichlorobenzamide.

[j] ND = Not detected.

Fig. LC–PCD with gradient elution from 30 to 60% acetonitrile in 60 min. Peaks are 50 ng each of: 1 = desisopropyl atrazine; 2 = carboxin sulfoxide; 3 = metribuzin DA; 4 = bromacil; 5 = fenamiphos sulfoxide; 6 = atrazine; 7 = fenamiphos sulfone; 8 = diuron; 9 = propachlor; 10 = propazine; 11 = methiocarb; 12 = swep; 13 = fenarimol; 14 = fenamiphos; 15 = metolachlor; 16 = alachlor; 17 = barban; 18 = neburon; 19 = DCPA; 20 = disulfoton; 21 = butachlor.

sponses observed with the OPA–MERC reagent flowing were the result of fluorescent products formed during photolysis. The major exceptions were the N-methylcarbamates and carbamoyloximes, carbamothioic acids and some phenylureas
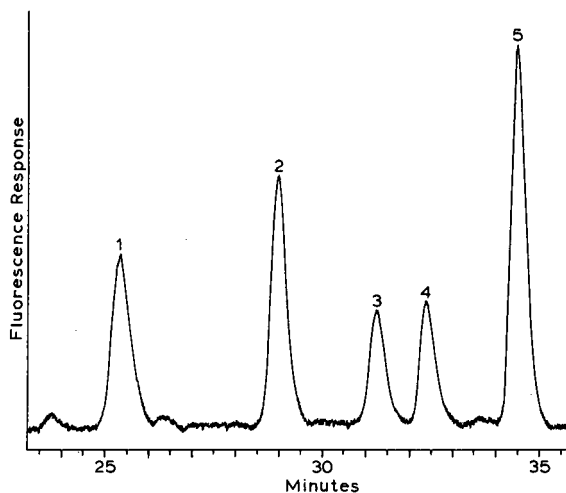

Fig. 2. LC–PFD (borate only) with gradient elution from 5 to 80% acetonitrile in 60 min. Peaks are 10 ng each of: 1 = 1-naphthol; 2 = propanil; 3 = swep; 4 = fenarimol; 5 = napropamide.

which formed primary amines after photolysis [3]. The response from the phenylureas was a mixture of primary amine and fluorescent products as described previously [3].

All compounds that yielded a photolysis–fluorescence response without OPA–MERC gave an enhanced response when borate was added, with the exception of chloramben and carbofuran phenol-3KET. The response for the latter compound was $\leqslant 9\%$ 1-naphthol with the borate reagent. Apparently, most of the fluorescent photodegradation products have higher fluorescence intensity under alkaline conditions. Many of these analytes also responded well with the PED system, suggesting that phenolic moieties are formed during photolysis. Ionization of phenolic groups often results in more conjugation and light absorption at longer wavelengths. The response of many of these analytes was better when no OPA–MERC was present, suggesting that this reagent can interfere with the fluorescent species. Thus, optimum response for some compounds is achieved with the borate reagent addition (Fig. 2).

The MDLs varied significantly with the fluorimeter used. The Gilson and Hewlett-Packard detectors were coupled together and the MDLs were comparable, except for compounds that fluoresced without OPA–MERC addition. Apparently these photodegradtion products fluoresce in the range used by the broad bandpass filter fluorimeter (Gilson) as opposed to the narrow bandpass (excitation and emission grating monochromaters) fluorimeter (Hewlett-Packard). Comparison of the MDLs in this study and similar studies [3,4] indicated that significant improvements could be realized using a different fluorimeters. Using a fluorimeter (ABI) with a deuterium source, excitation grating monochrometer (235 nm) and emission filter (>418 nm), the signal-to-noise ratio improved significantly. Use of the Hewlett-Packard fluorimeter with an excitation wavelength of 235 nm yielded no significant improvement in signal-to-noise ratio. Table I lists data collected with the filter fluorimeter (Gilson) only.

With the exceptions of aldicarb sulfone and carbaryl, the MDLs using the PFD compare favorably with the standard base hydrolysis–OPA–MERC postcolumn reaction detector [1,3,4]. However, the PFD instrument described here also detects several

other analytes on the NPS list, indicating that it is complementary to EPA method 5. Representative chromatograms of multi-residue separations using this detector have been shown [3,4].

Photolysis electrochemical detector

Sixty eight of the 103 analytes (66%) gave a response ≥ 20% of malathion (Table I). Phenylamides, phenylcarbamates, aliphatic carbamates and carbamoyloximes, methylthiotriazines, phosphorothioates and phosphorodithioates were among the compounds with high sensitivity. Many of the analytes with high sensitivity contained sulfur, although the carbamothioic acids responded poorly as a group. Several analytes, especially phenolic metabolites, gave a good response with the lamp off and the response with the lamp on usually deminished slightly. The species responsible for the electrochemical response are unknown, but photohydrolyses of sulfur-containing compounds to thiols or other oxidizable species and aromatic derivatives to phenols are likely candidates. Other mechanisms for the production of the photolysis–

electrochemical response have been discussed [14].

MDLs were determined for 46 analytes using this detector and the sensitivity and selectivity for groundwater analysis was excellent. Several analytes were not detected, probably because of elution after gradient completion. Some acidic analytes were retained on the reversed-phase column at neutral pH, suggesting ion exchange on residual silanol groups. Multi-residue separations are difficult because of the large number of analytes and broad peaks (Figs. 3 and 4). The decreased separation efficiency observed when using methanol compared with acetonitrile is consistent with the higher viscosity of methanol. The broad peaks observed with the methanol–water mobile phase were not significantly affected by the laboratory-constructed photoreactor and the photolysis efficiency was comparable to that of the commercial photolysis unit using a variety of analytes. Band spreading from the laboratory-constructed photoreactor was slightly greater than that from the commercial unit using acetonitrile–water [13]. Negative peaks occurred at the tails of some peaks, suggesting adsorption at the electrode
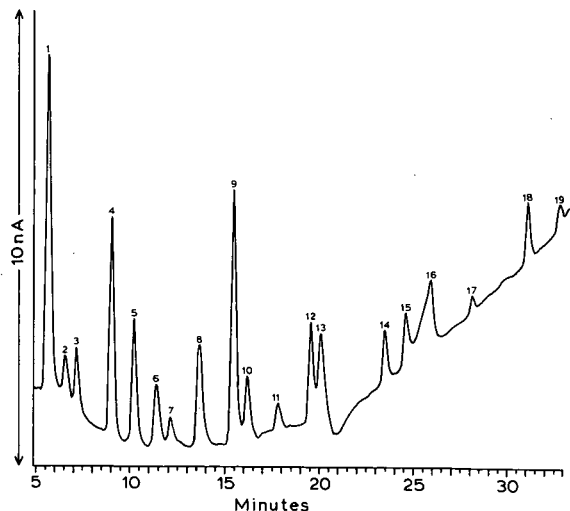

Fig. 3. LC–PED with gradient elution from 30:70 to 77:23 methanol–10 mM NaCl in 35.3 min. Peaks are approximately five times the MDL each of: 1 = metribuzin DK and 3,5-DCBA; 2 = carbofuran phenol-3KET; 3 = metribuzin DADK; 4 = metribuzin and 2,4,5-T; 5 = propoxur; 6 = carbofuran phenol; 7 = carboxin; 8 = fenamiphos sulfoxide; 9 = disulfoton sulfoxide; 10 = disulfoton sulfone; 11 = norflurazon; 12 = propanil; 13 = pronamide metabolite; 14 = barban; 15 = prometryn; 16 = alachlor and metolachlor; 17 = fenamiphos; 18 = disulfoton; 19 = chlorobenzilate.
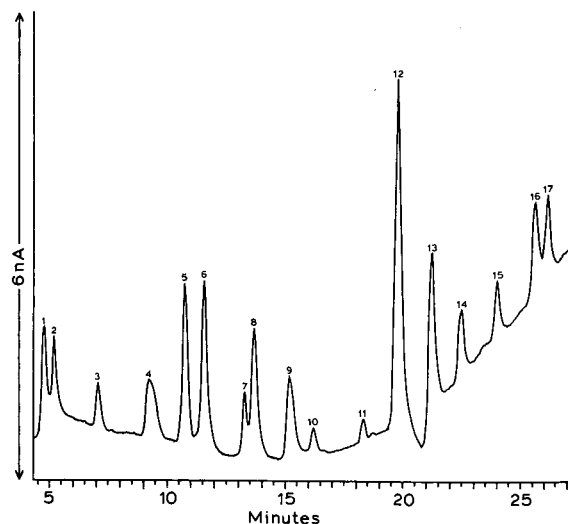

Fig. 4. LC–PED under conditions identical with those in Fig. 3. Peaks are five times the MDL each of: 1 = carbofuran-3OH; 2 = carboxin sulfoxide; 3 = aldicarb; 4 = metribuzin DA; 5 = carbofuran; 6 = tebuthiuron; 7 = fluometuron; 8 = 1-naphthol; 9 = simetryn; 10 = propachlor; 11 = unknown; 12 = diphenamid and linuron; 13 = swep; 14 = chlorpropham; 15 = triadimefon; 16 = fenarimol; 17 = napropamide.

surface. The large negative peak at about 21 min occurred under all conditions and the cause is unknown.

Because of the large number of suitable analytes for each LC system, a gradient that separated all components was not possible. Nevertheless, the DryLab G program was valuable for testing various gradient conditions without additional experiments and eliminated unnecessary time at the front and end of the chromatogram. The DryLab G program also allowed an examination of the effect of column conditions such as length and particle size on these multi-component separations and even allowed the testing of columns types that were not available in our laboratory.

LC–PED and LC–PFD are suitable for multi-residue pesticide determinations in water. These two systems are complementary and approximately half of the analytes tested have MDLs $\leqslant$ 10 ng with these detection methods combined. Low-μg/l detection limits in water samples can be realized by injecting large volumes (*ca.* 500 μl). Although this has been demonstrated with the PFD instrument, similar efforts with the PED instrument have been unsatisfactory. Nevertheless, analyte concentration by solvent extraction, as described in the original NPS methods [1], or by solid-phase extraction [15] can improve detection limits. Coupling these detectors in series (PFD instrument downstream) would decrease the analytical time, but it has not been demonstrated. The LC–PCD system tested was not suitable for sensitive, multi-residue determinations in groundwater, but isocratic analysis of a limited range of analytes is possible.

REFERENCES

1 US Environmental Protection Agency, Office of Water and Office of Pesticides Programs, *National Survey of Pesticides in Drinking Water Wells; Phase I Report: 1990*, US Government Printing Office, Washington, DC, 1990, EPA-570/9-90-015.
2 R. G. Luchtefeld, *J. Chromatogr. Sci.*, 23 (1985) 516–520.
3 C. J. Miles and H. A. Moye, *Anal. Chem.*, 60 (1988) 220–226.
4 C. J. Miles and H. A. Moye, *Chromatographia*, 24 (1987) 628–632.
5 X. D. Ding and I. S. Krull, *J. Agric. Food Chem.*, 32 (1984) 622–628.
6 I. S. Krull, C. M. Selavka, M. Lookabaugh and W. R. Childress, *LC · GC*, 7 (1989) 758–769.
7 D. J. Popovich, J. B. Dixon and B. J. Ehrlich, *J. Chromatogr. Sci.*, 17 (1979) 643–650.
8 S. M. Walters, *J. Chromatogr.*, 259 (1983) 227–242.
9 C. J. Miles and M. Zhou, *J. Agric. Food Chem.*, 38 (1990) 986–989.
10 J. W. Dolan and L. R. Snyder, *LC · GC*, 5 (1987) 970–976.
11 *Fed. Reg.*, 49 (1984) 43430–43431.
12 C. M. Selavka, K. S. J. Jiao and I. S. Krull, *Anal Chem.*, 59 (1987) 2221–2224.
13 M. Zhou and C. J. Miles, *J. Assoc. Off. Anal. Chem.*, 74 (1991) 546–550.
14 I. S. Krull and W. R. LaCourse, in I. S. Krull (Editor), *Reaction Detection in Liquid Chromatography*, Marcel Dekker, New York, 1986, Ch. 7.
15 A. Di Corcia and M. Marchetti, *Anal. Chem.*, 63 (1991) 580–585.

CHROMSYMP. 2386

Direct separation of enantiomers by high-performance liquid chromatography on a new chiral ligand-exchange phase

Naobumi Ôi*, Hajimu Kitahara and Reiko Kira

Sumika Chemical Analysis Service, Ltd., 3-1-135, Kasugade-naka, Konohana-ku, Osaka 554 (Japan)

ABSTRACT

Two novel chiral ligand-exchange phases for high-performance liquid chromatography, N,S-dioctyl-(D)-penicillamine (I) and N,S-dioctyl-N-methyl-(D)-penicillamine (II) were prepared. The direct separation of more than twenty amino acid enantiomers was achieved using octadecylsilanized silica coated with these phases and water or hydro-organic eluents containing copper(II) ion as a mobile phase. Various enantiomers including amino acid derivatives, hydroxy acids and amino alcohols were also well resolved directly. Generally, phase I showed higher enantioselectivity than phase II, which, however, was very efficient for the separation of some long-retained racemic compounds such as tryptophan and mandelic acid. These phases are very promising for the direct separation of a variety of enantiomers by ligand-exchange high-performance liquid chromatography.

INTRODUCTION

Since the pioneering work of Davankov and co-workers [1] a great number of publications have appeared dealing with the separation of amino acid enantiomers by means of ligand-exchange high-performance liquid chromatography (HPLC) using either sorbents with covalently bonded chiral complex-forming ligands [1–6] or soluble chiral reagents in the mobile phase [7–9].

Davankov *et al.* [10] have presented a novel chiral-phase system which is composed of a reversed-phase packing coated with an appropriate resolving agent and a hydro-organic eluent containing the complexing metal ion. This system combines important advantages of the two approaches to resolving racemates by means of ligand-exchange chromatography: the use of chiral stationary phases and the use of chiral eluents. Many chiral coating agents,

such as N-alkylhydroxyproline [10] (where alkyl is n-C_7H_{15}, n-$C_{10}H_{21}$ and n-$C_{16}H_{33}$), N-decylhistidine [11] and N,N-dioctylalanine [12], produced good enantioselectivity, but the separation of some amino acids was still not good enough.

In this study two novel chiral ligand-exchange phases, N,S-dioctyl-(D)-penicillamine (I) and N,S-dioctyl-N-methyl-(D)-penicillamine (II) (Fig. 1), were prepared and their chromatographic properties were examined in order to investigate the effect of structure in the chiral ligand phase on the enantiomeric separation by ligand-exchange HPLC.

EXPERIMENTAL

Preparation of chiral stationary phases

N,S-dioctyl-(D)-penicillamine (phase I). This phase was prepared from (D)-penicillamine by the action of 1-bromooctane and triethylamine in a chloroform–methanol mixture at 70–80°C; m.p. 123–124°C. Analysis. Calculated for for $C_{21}H_{43}NO_2S$: C, 67.51; H, 11.60; N, 3.74%. Found: C, 67.12; H, 11.33; N, 3.68%. ^{1}H NMR (C^2HCl_3) δ 0.87 (t, 3H), 0.88 (t, 3H), 1.12–1.38 (m,
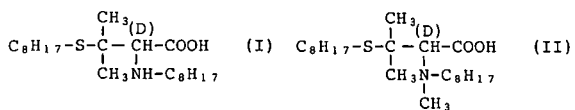

Fig. 1. Structures of phases I and II.

20H), 1.41, 1.63 (s, 6H), 1.49–1.59 (m, 2H), 1.75–1.92 (m, 2H), 2.38-2.62 (m, 2H), 2.89–3.40 (m, 2H), 3.55 (s, 1H), 6.50 (m, 1H), 10.20 (s, 1H).

N,S-dioctyl-N-methyl-(D)-penicillamine (phase II). This phase wass prepared by the reductive N-methylation of N,S-dioctyl-(D)-penicillamine (I). Analysis. Calculated for $C_{22}H_{45}NO_2S$: C, 68.15; H, 11.72; N, 3.61%. Found: C, 68.05; H, 11.61; N, 3.68%. ^{1}H NMR (C^2HCl_3) δ 0.83 (t, 6H), 1.08–1.39 (m, 20H), 1.40–1.65 (m, 4H), 1.46, 1.47 (s, 6H), 2.40-2.61 (m, 2H), 2.71 (s, 3H), 2.82–3.29 (m, 2H), 3.51 (s, 1H), 10.20 (s, 1H).

General

Commercially available SUMIPAX ODS col-

umns (150, 50 or 10 mm × 4 mm I.D.) packed with octadecylsilanized silica (5 μm) were used. The coating of phase I and II on the reversed-phase support was accomplished by passing a 0.1% methanol–water (50:50, v/v) solution of I and II through the column followed by a 1 mM aqueous solution of copper(II) sulfate. These columns are available from Sumika Chemical Analysis Service (Osaka, Japan), as Sumichiral OA-5000 and OA-5100. All chemicals and solvents of reagent grade were purchased from Wako (Osaka, Japan). The experiments were carried out using a Waters 510 high-performance liquid chromatograph equipped with a variable-wavelength UV detector (operated at 254 nm and 280 nm) or a fluorescence detector. In the fluoro-

TABLE 1

ENANTIOMER SEPARATION OF AMINO ACIDS

Mobile phase: (A) 1 mM copper(II) sulfate in water; (B) 2 mM copper(II) sulfate in water–methanol (85:15); (C) 2 mM copper(II) sulfate in water–methanol (70:30). A flow-rate of 1 ml/min was typically used for the 150 mm × 4.6 mm I.D. column at room temperature. An injection volume of 5 μl (2 mg/ml) was typically used. k'_L, k'_D = capacity factors of L- and D-isomer; α = separation factor (k'_D/k'_L)

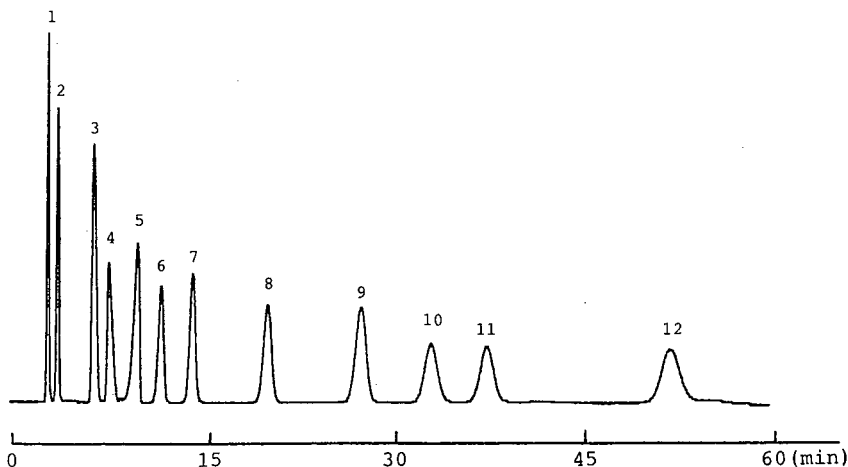| Amino acid	Phase I				Phase II			
	k'_L	k'_D	α	Mobile phase	k'_L	k'_D	α	Mobile phase
Ornithine	0.86	1.04	1.21	A	0.52	0.34	0.65	A
Lysine	1.06	1.61	1.52	A	1.06	1.06	1.00	A
Arginine	1.72	3.26	1.90	A	2.08	2.59	1.25	A
Serine	3.28	3.75	1.14	A	1.83	1.56	0.85	A
Alanine	3.49	5.52	1.58	A	2.95	3.66	1.24	A
Threonine	3.86	4.57	1.18	A	2.41	2.41	1.00	A
Glutamine	3.99	6.66	1.67	A	3.53	4.20	1.20	A
Asparagine	4.03	4.03	1.00	A	2.00	1.18	0.59	A
2-Amino-n-butyric acid	6.75	11.70	1.73	A	7.61	8.96	1.18	A
Proline	8.76	21.33	2.43	A	11.42	10.29	0.90	A
Valine	12.57	23.68	1.88	A	17.81	16.26	0.91	A
Norvaline	18.31	35.16	1.92	A	18.14	26.02	1.43	A
Histidine	23.11	17.55	0.76	A	7.42	5.20	0.70	A
tert.-Leucine	7.49	13.58	1.81	B	6.37	7.73	1.21	B
Alloisoleucine	8.18	13.29	1.62	B	5.08	4.66	0.92	B
Methionine	8.36	10.68	1.28	B	5.00	5.00	1.00	B
Isoleucine	9.98	16.38	1.64	B	5.08	6.71	1.32	B
Aspartic acid	10.87	15.27	1.40	B	1.02	0.87	0.85	B
Leucine	11.51	17.68	1.54	B	6.27	9.52	1.52	B
Glutamic acid	20.74	22.80	1.10	B	1.69	2.27	1.34	B
Phenylglycine	4.74	7.52	1.59	C	2.48	7.99	3.22	C
Tyrosine	5.20	6.79	1.31	C	3.21	2.85	0.89	C
DOPA[a]	5.69	7.25	1.27	C	3.69	3.69	1.00	C
Phenylalanine	11.51	16.19	1.41	C	10.16	8.66	0.85	C
Tryptophan	34.49	37.60	1.09	C	24.23	19.21	0.79	C

[a] 3,4-Dihydroxy-phenylalanine.

Fig. 2. Enantiomeric separation of six racemic amino acids on phase I. Chromatographic conditions as in Table I. Peaks: 1 = L-lysine; 2 = D-lysine; 3 = L-alanine; 4 = L-glutamine; 5 = D-alanine; 6 = D-glutamine; 7 = L-proline; 8 = L-valine; 9 = L-norvaline; 10 = D-proline; 11 = D-valine; 12 = D-norvaline.

metry, the post-column reaction using *o*-phthalal-dehyde was employed [13].

RESULTS AND DISCUSSION

The direct separation of more than twenty race-mic amino acids was accomplished by ligand-ex-change HPLC using octadecylsilanized silica coated with phase I and II and aqueous or hydro-organic solutions containing copper(II) ion as a mobile phase. The capacity factors and separation factors are summarized in Table I. Excellent enantioselec-tivities were obtained with the two phases at room temperature. These results show that the structures

Fig. 3. Enantiomeric separation of racemic tryptophan on phase II. Chromatographic conditions as in Table I.

of two phases are effective for the chiral recognition of a wide range of amino acids.

Generally, higher retention and enantioselectivity were obtained with the phase I system than with the pase II system. Fig. 2 shows a typical chromato-gram of six amino acids on phase I. Larger sep-aration factors and more moderate capacity factors were obtained for some amino acids, such as glu-tamic acid and tryptophan, on phase II than on phase I (Fig. 3). There was a very noticeable differ-ence in the elution order of enantiomers between the phase I system and the phase II system. The D-isomer was always more strongly retained than the L-isomer on phase I, with the exception of histi-dine. The inverse elution order of the enantiomers of histidine may depend upon the nature of the imi-dazole group of histidine, as indicated by Davan-kov *et al.* [10]. On the other hand, the L-isomer was strongly retained in many amino acids on phase II. As both phases contain the same alkyl chain, these chromatographic results suggest that the hydrogen bonding effect of the NH group in phase I and the steric effect of the N-CH$_3$ group in phase II may produce a difference in the three-dimensional inter-action for chiral recognition. We consider that the explanation of the recognition mechanism needs further examination.
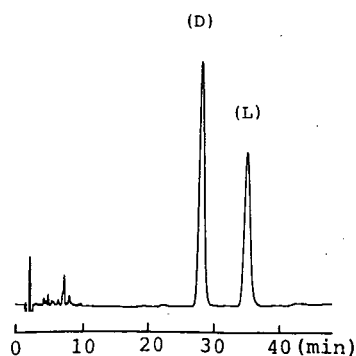
Table II summarizes the results of the separation of racemic N-acetylamino acids, glycylpeptides and

TABLE II

ENANTIOMER SEPARATION OF N-ACETYLAMINO ACIDS, GLYCYL DIPEPTIDES AND HYDROXY ACIDS

Mobile phase: (A) 1 mM copper(II) sulfate in water; (B) 2 mM copper(II) sulfate in water–methanol (85:15); (C) 2 mM copper(II) sulfate in water–methanol (70:30). A flow-rate of 1 ml/min was used for the 150 mm × 4.6 mm I.D. column at room temperature. An injection volume of 5 μl (2 mg/ml) was typically used. k'_1, k'_2 = capacity factors of first- and second-eluted isomer; α = separation factor (k'_2/k'_1)

Compound	Phase I				Phase II			
	k'_1	k'_2	α	Mobile phase	k'_1	k'_2	α	Mobile phase
N-Acetylalanine	6.34	7.24	1.14	B	2.29	2.92	1.28	B
N-Acetylvaline	20.33	29.43	1.45	C	6.95	8.05	1.16	C
N-Acetylmethionine	21.10	25.97	1.23	C	8.66	10.00	1.15	C
N-Acetylleucine[a]	37.45	50.59	1.35	C	24.00	33.52	1.40	C
Glycylalanine	1.52	2.71	1.78	A	0.55	0.74	1.35	A
Alanylglycine	0.66	1.49	2.26	A	0.56	0.66	1.18	A
Glycylvaline	5.54	9.39	1.69	C	0.62	1.27	2.05	C
Alanylglycyl-glycine	2.56	4.15	1.62	A	1.21	1.52	1.26	A
Leucylglycyl-glucine	4.92	6.67	1.36	C	1.28	1.44	1.13	C
Lactic acid	14.66	19.32	1.32	A	8.77	9.94	1.13	A
Glyceric acid	10.73	14.41	1.34	B	2.29	2.85	1.24	B
2-Hydroxy-n-butyric acid	15.30	24.61	1.61	B	7.69	9.75	1.27	B
Leucic acid[a]	44.94	62.96	1.40	C	35.18	49.21	1.40	C
Mandelic acid[a]	42.64	54.73	1.28	C	24.59	61.31	2.49	C
Malic acid[b]	24.10	268.95	11.16	C	1.20	4.90	4.08	C
Tartaric acid[b]					9.85	15.95	1.62	C

[a] Column: 50 mm × 4.6 mm I.D.
[b] Column: 10 mm × 4.6 mm I.D.

hydroxy acids. These enantiomers could be well resolved in the same way as amino acids. Racemic hydroxy acids are generally more retained on phase I. Faster elution was achieved by the addition of methanol or acetonitrile, or by the use of shorter
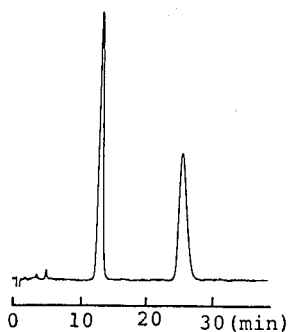

Fig. 4. Enantiomeric separation of racemic mandelic acid on phase II. Chromatographic conditions as in Table II.

columns with both phases. An example of the efficient chromatogram is shown in Fig. 4.

Amino alcohol enantiomers of pharmaceutical interest were well resolved with these novel phases, as shown in Table III. The effect on these separations of the pH and the concentration of copper(II) ion in the eluent was large as reported by Yamazaki et al. [13], and good results were obtained with the eluent containing 5 mM copper(II) acetate at pH 6.0. Fig. 5 shows a typical chromatogram. The post-column derivatization with o-phthalaldehyde and subsequent fluorimetric detection was available for some amino alcohols, as shown in Fig. 6. Some other racemic compounds, for example 3-amino-ε-caprolactam, can be also resolved with these phases, as shown in Fig. 7.

As far as column durability is concerned, it can be stated that 600 analyses of some amino acids on the column coated with phase I did not cause any change in their retention parameters, enantioselec-

TABLE III

ENANTIOMER SEPARATION OF AMINO ALCOHOLS AND OTHERS

Mobile phase: (A) 5 mM copper(II) acetate in water (pH 6.0); (B) 0.05 M ammonium acetate buffer (pH 6.0) containing 5 mM copper-(II) acetate; (C) 1 mM copper(II) sulfate in water. A flow-rate of 1 ml/min was typically used for the 150 × 4.6 mm I.D. column at room temperature. An injection volume of 5 μl (2 mg/ml) was typically used. k'_1, k'_2 = capacity factors of first- and second-eluted isomer; α = separation factor (k'_2/k'_1)

Compound	Phase I				Phase II			
	k'_1	k'_2	α	Mobile phase	k'_1	k'_2	α	Mobile phase
Octopamine	1.98	2.53	1.28	A	1.09	1.61	1.48	A
Norphenylephrine	6.61	8.41	1.27	A	3.06	4.58	1.50	A
Normethanephrine	5.47	6.73	1.23	A	2.57	3.94	1.53	A
p-Hydroxynorephedrine	2.07	2.95	1.43	A	1.71	2.18	1.27	A
Norephedrine[a]	15.28	28.14	1.84	B	16.60	21.11	1.27	B
2-Amino-1-phenylethanol[a]	14.14	19.57	1.38	B	10.42	12.95	1.24	B
3-Amino-ε-caprolactam	2.01	2.61	1.30	C	1.80	2.83	1.57	C
Homocystein thiolactone	1.46	1.66	1.14	C	1.18	1.18	1.00	C

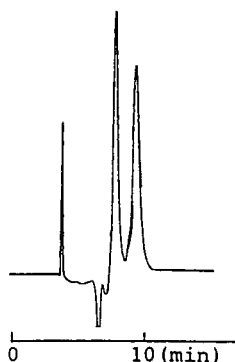[a] Detected with a fluorescence detector.

Fig. 5. Enantiomeric separation of racemic norphenylephrine on phase I. Chromatographic conditions as in Table III.

tivity or efficiency when water or methanol–water (30:70, v/v) was used as the eluent. Unfortunately however, the stability of the column coated with phase II was not as good as that of the phase I column, therefore the phase II system should be utilized carefully.

CONCLUSION

Two novel chiral phases, I and II, are very promising as coating agents on reversed-phase materials
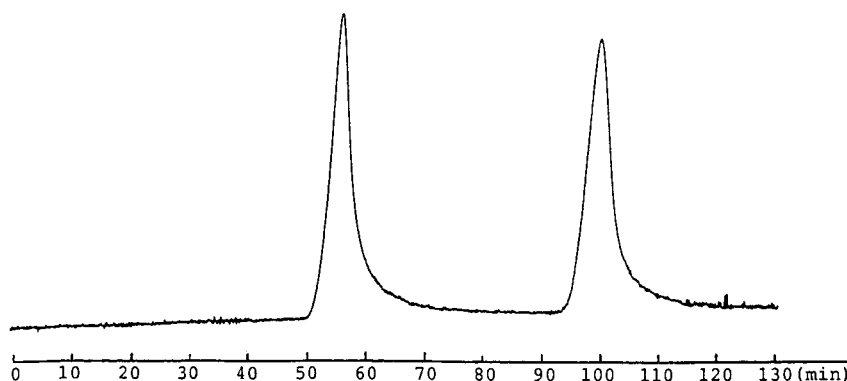

Fig. 6. Enantiomeric separation of racemic norephedrine on phase I. Chromatographic conditions as in Table III.
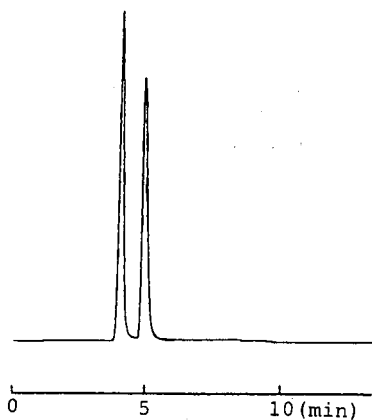
Fig. 7. Enantiomeric separation of racemic 3-amino-ε-caprolac-
tam on phase I. Chromatographic conditions as in Table III.

for the direct separation of a variety of enantiomers
including amino acids, hydroxy acids and amino al-
cohols by ligand-exchange HPLC.

REFERENCE

1 S. V. Rogozhin and V. A. Davankov, *Chem. Commun.*,
(1971) 490.
2 V. A. Davankov, Yu. A. Zolotarev and A. A. Kurganov, *J.
Liq. Chromatogr.*, 2 (1979) 1191.
3 V. A. Davankov and Yu. A. Zolotarev, *J. Chromatogr.*, 155
(1978) 285, 295, 303.
4 B. Lefebre, R. Audebert and C. Quivoron, *J. Liq. Chroma-
togr.*, 1 (1978) 761.
5 G. Gübitz, W. Jellenz, G. Löfler and W. Santi, *J. High Reso-
lut. Chromatogr. Chromatogr. Commun.*, 2 (1979) 145.
6 A. Foucault, M. Caude and L. Oliveros, *J. Chromatogr.*, 185
(1979) 345.
7 J. N. LePage, W. Lindner, G. Davies, D. E. Seitz and B. L.
Karger, *Anal. Chem.*, 51 (1979) 433.
8 W. Lindner, J. N. LePage, G. Davies, D. E. Seitz and B. L.
Karger, *J. Chromatogr.*, 185 (1979) 323.
9 P. E. Hare and E. Gil-Av, *Science*, 204 (1979) 1226.
10 V. A. Davankov, A. S. Bochkov and A. A. Kurganov, *Chro-
matographia*, 13 (1980) 677.
11 V. A. Davankov, A. S. Bochkov and Yu. P. Belov, *J. Chro-
matogr.*, 218 (1981) 547.
12 H. Kiniwa, Y. Baba, T. Ishida and H. Katoh, *J. Chroma-
togr.*, 461 (1989) 397.
13 S. Yamazaki, T. Takeuchi and T. Tanimura, *J. Liq. Chroma-
togr.*, 12 (1989) 2239.

Chiral high-performance liquid chromatographic separations on an α_1-acid glycoprotein column

II*. Separation of the diastereomeric and enantiomeric analogues of vinpocetine (Cavinton)

Bulcsu Herényi and Sándor Görög*

Chemical Works, Gedeon Richter Ltd., P.O. Box 27, H-1475 Budapest (Hungary)

ABSTRACT

A chiral α_1-acid glycoprotein column (Chiral-AGP) was used for the separation of vinpocetine and its three diastereomeric and enantiomeric analogues. As a consequence of the extremely large differences between the affinities of the isomers to the chiral stationary phase, gradient elution [up to 35% (v/v) 2-propanol] and a relatively high pH (7.73) were necessary to achieve a good separation within a reasonable time. The elution order of the isomers was *cis*-(+)- (vinpocetine), *trans*-(−)-, *cis*-(−)-, *trans*-(+)-. Because of the unfavourable elution order the method does not seem to be suitable for the determination of the optical purity of vinpocetine.

INTRODUCTION

One of the most succesful chiral high-performance liquid chromatographic columns for the enantioseparation of drugs and related materials is the Chiral-AGP column introduced by Hermansson [2]. This contains the second generation of the chiral stationary phase consisting of α_1-acid glycoprotein chemically bonded to silica. The enantioseparation of a large variety of acidic, basic and non-protolytic drugs and related materials using the Chiral-AGP column was described by Hermansson (2). In our laboratory the enantioseparation of various α-ethylbenzhydrols, amino acid derivatives and heterocycles has been achieved [1].

The aim of this study was to check the possibility of using the Chiral-AGP column for the solution of a more complicated problem, namely the separation of the four enantiomers of the two diastereomers of a synthetic vincamine analogue, vinpocetine (Cavinton).

EXPERIMENTAL

A Hewlett-Packard Model 1090A high-performance liquid chromatograph equipped with a Model 1040 diode-array UV detector was used. The column (100 × 4.6 mm I.D.) containing Chiral-AGP was purchased from ChromTech (Norsborg, Sweden). The eluent components were (A) 0.1 *M* phosphate buffer (pH 4.5–7.73) and (B) 2-propanol.

The over-all concentration of the isomers of vinpocetine in the test solution was about 0.1%, the solvent being water–2-propanol (1:1). Aliquots of 20 μl of this solution were injected into the chromatograph. The following gradient programme was used: 0–10 min, 18% (v/v) B, isocratic; 10–25 min, from 18 to 25% (v/v) B; 25–30 min, 25% B, isocratic; 30–40 min, from 25 to 35% (v/v) B; 40 min, 35%
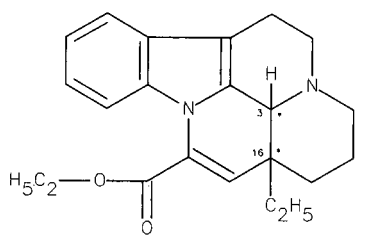
---

* For Part I, see réf. I.

B, isocratic (see Fig. 3). The flow rate was 0.8 ml/min. The separations were performed at ambient temperature. The chromatograms were monitored at the maximum of the UV spectrum of vinpocetine at 315 nm.

RESULTS AND DISCUSSION

Vinpocetine (Cavinton) is a cerebral oxygenation enhancer made by Chemical Works Gedeon Richter (Budapest, Hungary). The structures of this synthetic eburnane derivative together with its three isomers (enantiomers of the two diastereomeric forms) are shown in Fig. 1.

The chiral chromatography of pharmacologically active eburnane derivatives has been described by Szepesi et al. [3]. Using cyanopropylsilica as the stationary phase and camphorsulphonic acid as a chiral mobile phase additive, they separated the eight enantiomers of the four diastereomers of vincamine. Making use of the advantageous feature of dinamic chiral chromatography, namely that the elution order can be regulated by the polarity of the chiral additive, they solved the problem of the determination of the optical purity of vinpocetine. Using (+)-camphorsulphonic acid, the peak of the cis-(−)-enantiomeric impurity is eluted first, allowing its determination down to the 0.2% level.

In the course of investigations using a Chiral-AGP column for the separation of the four enantiomers, the main problems were the separation of the trans-(−)-isomer from vinpocetine, which is the cis-(+)-isomer, and the elution of the other two isomers [especially the trans-(+)-isomer] from the column, as they are extremely strongly bound to the α_1-acid glycoprotein.

The main factors influencing the retention of the analytes on the Chiral-AGP column are the nature and proportion of the organic modifier, the pH of the buffer and temperature. In most instances described by Hermansson [2], 2-propanol was used as the organic modifier at concentrations below 20% (v/v). By using the above concentration of 2-propanol at pH 6.5, poor resolution of the cis-(+)- and trans-(−)-isomers was found and the other two isomers were not eluted at all within a reasonable time. For the elution of the cis-(−)- and trans-(+)-isomers, high 2-propanol concentrations [up to 35% (v/v)] were necessary and the resolution of the four isomers could be achieved by gradient elution only, which is unusual in chiral chromatography. The replacement of 2-propanol with other organic solvents such as methanol and acetonitrile did not afford better results. The pH profile of the separation of the four isomers is illustrated in Fig. 2. Acceptable resoltuion of the first two peaks can only be

	3-H	16-C$_2$H$_5$
cis(+)	α	α
cis(-)	β	β
trans(+)	α	β
trans(-)	β	α

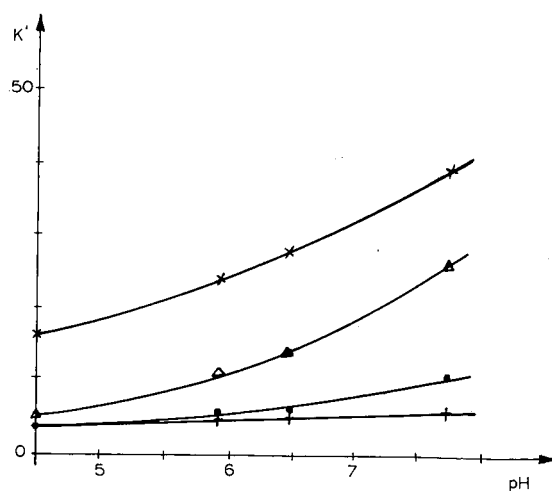Fig. 1. Structures of vinpocetine [cis-(+)-; 3 (S), 16 (S)] and its diastereomeric and enantiomeric analogues.

Fig. 2. pH profile of the separation of vinpocetine [cis-(+)-] and its diastereomeric and enantiomeric analogues. + = cis-(+).; ○ = trans-(−)-; △ = cis-(−)-; × = trans-(+)-. k' = capacity factor.
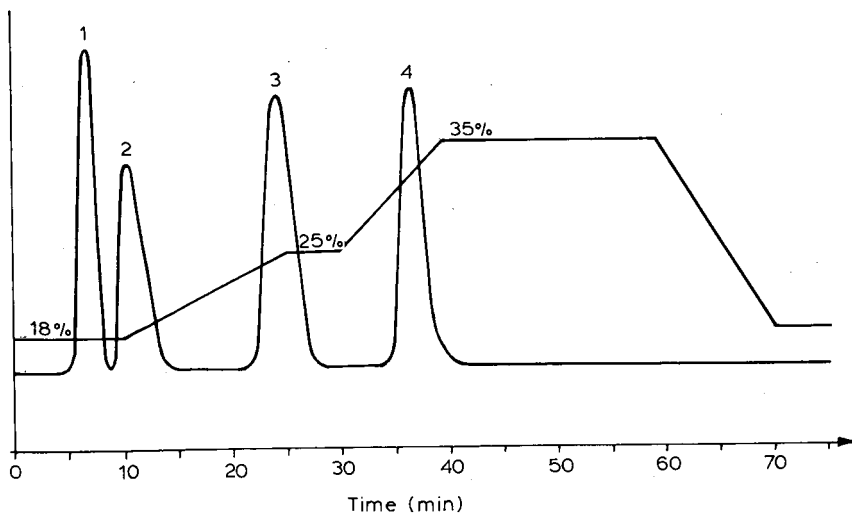
Fig. 3. Separation of vinpocetine [*cis*-(+)-] and its diastereomeric and enantiomeric analogues on the Chiral-AGP column. Peaks: 1 = *cis*-(+)-; 2 = *trans*-(−)-; 3 = *cis*-(−)-; 4 = *trans*-(+).

achieved at a pH value close to the highest value of the recommended range: a pH of 7.73 for the buffer component of the eluent was selected for the separation, which was carried out at ambient temperature. The chromatogram is shown in Fig. 3.

Unlike the above-mentioned method of Szepesi *et al.* [3], this method does not seem to be suitable for the determination of the optical purity of vinpocetine (first peak): the enantiomeric *cis*-(−)-isomer impurity (third peak) is eluted far after the peak of the drug substance.

It is interesting to compare the elution order of the diastereomers and enantiomers found in this study and the equilibrium constants (K) found by Fitos *et al.* [4] in a non-chromatographic equilibrium binding study between α_1-acid glycoprotein and various vinca alkaloid analogues. Of the four isomers in this study two were investigated in the equilibrium study: a ratio of $K_{trans-(+)-}/K_{cis-(+)-} = 30$

was found, which is in good agreement with the chromatographic results. As a consequence of the complexity of binding mechanism in which both nitrogens and the aromatic ring system are involved [4], the elution order of the enantiomers of the individual diastereomers is not easily predictable: it is + , − for the *cis* and − , + for the *trans* derivatives. Similar observations were made among the derivatives investigated by Fitos *et al.* [4].

REFERENCES

1 S. Görög and B. Herényi, *J. Pharm. Biomed. Anal.*, 8 (1990) 837.
2 J. Hermansson, *Trends Anal. Chem.*, 8 (1989) 251; and references cited therein.
3 G. Szepesi, M. Gazdag and R. Iváncsics, *J. Chromatogr.*, 244 (1982) 33.
4 I. Fitos, J. Visy and M. Simonyi, *Biochem. Pharmacol.*, 41 (1991) 377.

CHROMSYMP. 2413

Retention and enantioselectivity of racemic solutes on a modified ovomucoid-bonded column

I. Cross-linking with glutaraldehyde

Jun Haginaka*, Chikako Seyama and Hiroyuki Yasuda

Faculty of Pharmaceutical Sciences, Mukogawa Women's University, 11–68, Koshien Kyuban-cho, Nishinomiya 663 (Japan)

Hiroya Fujima and Hiroo Wada

Shinwa Chemical Industries Ltd., 50 Kagekatsu-cho, Fushimi-ku, Kyoto 612 (Japan)

ABSTRACT

Ovomucoid (OVM)- and cross-linked OVM-bonded materials were prepared for the chiral resolution of racemic solutes. OVM was immobilized to aminopropylsilica via an N,N-disuccinimidyl carbonate coupling reaction. The OVM materials were cross-linked with glutaraldehyde (OVM-GA) and further reduced with sodium borohydride (OVM-GA-R). The retentive and enantioselective properties of acidic, basic and uncharged solutes on OVM, OVM-GA and OVM-GA-R materials were investigated with respect to eluent pH and organic modifier. The retention properties of all solutes tested on these three materials were similar except that they were less retained on the OVM-GA and OVM-GA-R than the OVM material. The enantioselectivity of various solutes decreased in the order OVM, OVM-GA and OVM-GA-R. However, the OVM materials whose primary amino groups were cross-linked with glutaraldehyde retained a chiral recognition ability.

INTRODUCTION

Recently, several protein-bonded stationary phases have been developed for the chiral resolution of racemic solutes by high-performance liquid chromatography (HPLC) [1]. Protein-bonded stationary phases include albumins such as bovine serum albumin [2] and human serum albumin [3], glycoproteins such as α_1-acid glycoprotein (AGP) [4] and ovomucoid (OVM) [5] and enzymes such as α-chymotrypsin [6], trypsin [7] and fungal cellulase (an acid glycoprotein) [8]. Above all, glycoprotein-bonded phases are more stable and have wider chiral recognition properties owing to the presence of proteins and carbohydrates, which are chiral molecules. It is suggested that carbohydrates are essential for the chiral recognition of racemic solutes on

glycoprotein-bonded columns [9,10]. OVM, which is an acid glycoprotein from egg white, was bonded to aminopropylsilica via N,N-disuccinimidyl carbonate activation reaction by Miwa *et al.* [5], and an OVM-bonded column is now commercially available. The OVM-bonded column has been utilized for the chiral resolution of acidic, basic and uncharged solutes [11–14], and has been applied to the chiral resolution of basic drugs in biological fluids [15–17].

Recently, Kirkland *et al.* [18] compared commercially available glycoprotein-bonded columns based on OVM and AGP. They reported that the former column showed generally higher enantioselectivity and column efficiency and better long-term stability than the latter. However, our preliminary results suggest that the OVM column is unstable against

repetitive injections of solutes and/or changes in eluent composition (eluent pH, type and content of organic modifier) (see Results and Discussion) [19]. In order to improve the stability of the OVM column, and to expand the applicability of the OVM column, we tried to cross-link the OVM-bonded column. Cross-linking of the OVM protein might result in improvement of column stability owing to its greater conformational rigidity. In this study, we prepared OVM and cross-linked OVM columns: OVM was immobilized to aminopropylsilica via an N,N-disuccinimidyl carbonate coupling reaction [5]. The OVM materials were cross-linked with glutaraldehyde (OVM-GA) and further reduced with sodium borohydride (OVM-GA-R). This paper deals with the comparison of the retentive and enantioselective properties of acidic, basic and uncharged solutes on OVM, OVM-GA and OVM-GA-R columns with respect to eluent pH and organic modifier. Also, the stabilities of OVM and OVM-GA columns were preliminarily compared.

EXPERIMENTAL

Reagents and materials

Ibuprofen, ketoprofen, flurbiprofen, chlorpheniramine maleate, oxprenolol hydrochloride, tolperisone hydrochloride and hexobarbital were kindly donated by Kaken Pharmaceutical (Tokyo, Japan), Chugai Pharmaceutical (Tokyo, Japan), Essex Nippon (Osaka, Japan), Nippon Ciba-Geigy (Takarazuka, Japan), Nippon Kayaku (Tokyo, Japan) and Teikoku Chemicals (Osaka, Japan). The structures of racemic solutes used in this study are shown in Fig. 1. Methanol, ethanol and acetonitrile of HPLC grade and 20% glutaraldehyde solution were obtained from Wako (Osaka, Japan). OVM from egg white was kindly donated by Dr. T. Miwa (Eisai, Kawashima, Gifu, Japan). Other reagents were of analytical-reagent grade and were used as received.

Water purified with a Nanopure II unit (Barnstead, Boston, MA, USA) was used for the preparation of the eluent and the sample solution.
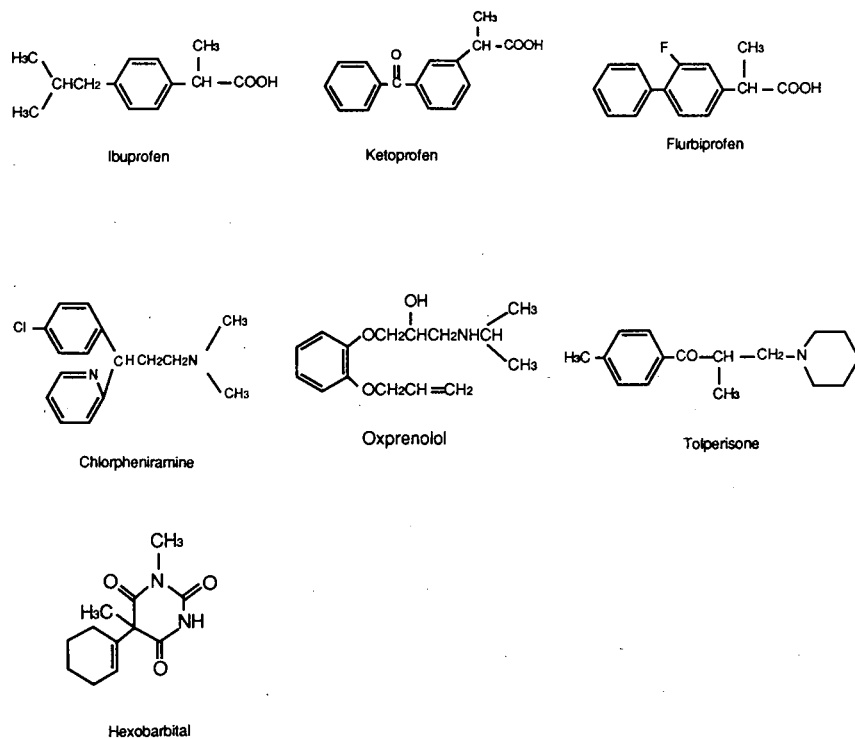

Fig. 1. Structures of racemic solutes used.

Preparation of OVM, OVM-GA and OVM-GA-R materials

OVM was bonded to an aminopropyl-silica gel (Ultron NH_2, 5 μm, 120 Å; Shinwa Chemical Industries, Kyoto, Japan) via the N,N-disuccinimidyl carbonate reaction as reported previously [5].

Five grams of the OVM materials were added to 50 ml of 100 mM ammonium dihydrogenphosphate buffer solution (pH 4.4) and sonicated for 5 min, then 500 μl of 5% glutaraldehyde solution were slowly added. The mixture was slowly rotated at 30°C for 15 h, filtered and washed with 100 mM ammonium dihydrogenphosphate buffer solution (pH 4.4), 50 mM sodium phosphate buffer (pH 7.0), water and methanol. The isolated materials (OVM-GA) were dried in vacuo over P_2O_5 at 40°C for 6 h.

Five grams of the OVM-GA materials were added to 50 ml of sodium phosphate buffer (pH 7.0) and sonicated for 5 min, then 60 ml of 10% sodium borohydride solution were added. The mixture was slowly rotated for 4 h at 10°C, filtered and washed with 50 mM sodium phosphate buffer (pH 7.0), water and methanol. The isolated materials (OVM-GA-R) were dried in vacuo over P_2O_5 at 40°C for 6 h.

These packing materials were packed into a 150 × 4.6 mm I.D. stainless-steel column by the slurry packing method.

Chromatography

The HPLC system was composed of a Model 880-PU pump (Japan Spectroscopic, Tokyo, Japan), a Rheodyne (Cotati, CA, USA) Model 7125 injector equipped with 100-μl loop and an SPD-6A spectrophotometer (Shimadzu, Kyoto, Japan). The flow-rate was maintained at 1.0 ml/min. Chromatograms were recorded and integrated with a Chromatpac C-R6A integrator (Shimadzu).

Capacity factors were calculated from the equation of $k' = (t_R - t_0)/t_0$, where t_R and t_0 are elution times of retarded and unretarded solutes, respectively; k'_1 and k'_2 correspond to the capacity factors of the first- and second-eluted peaks, respectively. The retention time of an unretarded solute, t_0, was measured by injecting a solution whose organic modifier content was slightly different from that of the eluent used. The enantioseparation factor is calculated from the equation $\alpha = k'_2/k'_1$. All separations were performed at 25°C using a CO-1093C column oven (Uniflows, Tokyo, Japan).

The eluents, which were prepared by using phosphoric acid–sodium dihydrogenphosphate or sodium dihydrogenphosphate–disodium hydrogenphosphate and organic modifier, are specified in the figure and table legends.

Sample preparation

A known amount of racemic solute was dissolved in methanol or water and the solution was diluted with the eluent to desired concentration. A 20-μl aliquot of the sample solution was loaded onto the column. The on-column weight was 0.2 μg, except when measuring retention times above 60 min, for which it was 0.5 μg.

RESULTS AND DISCUSSION

Effect of eluent pH on retention and enantioselectivity of charged and uncharged solutes

Tables I–III show the effects of eluent pH on the retention and enantioselectivity of acidic, basic and uncharged solutes on OVM, OVM-GA and OVM-GA-R materials, with 20 mM phosphate buffer containing 10% ethanol as the eluent. The trends of the capacity factors (k'_1) and enantioseparation factors (α) oserved with these three columns were similar except that they decreased in the order OVM, OVM-GA and OVM-GA-R materials. The capacity factors of acidic solutes (ibuprofen, ketoprofen and flurbiprofen) gave maximum values at an eluent pH of ca. 4. This could be elucidated by taking account into the pK_a values of 2-arylpropionic acid derivatives (4.0–4.5) and the isoelectric point of ovomucoid (pI = 3.8–4.3) [20]. The decrease in the capacity factors of 2-arylpropionic acid derivatives is ascribable to ion exclusion in addition to ionic repulsion between the carboxyl groups of 2-aryl-propionic acid derivatives and negatively charged OVM with increase in eluent pH. As at eluent pH values below the pI of OVM the OVM became positively charged, the capacity factors of undissociated 2-arylpropionic acid derivatives could be decreased by decreasing the eluent pH.

Taking into account the same trends in the capacity factors of 2-arylpropionic acid derivatives on the OVM-GA and OVM-GA-R as on the OVM material, the changes in the pI values of these materials due to cross-linking should be small. On the other

TABLE I

EFFECT OF pH ON RETENTION AND ENANTIOSELECTIVITY OF ACIDIC DRUGS ON OVM, OVM-GA AND OVM-GA-R COLUMNS[a]

Column	Compound	pH 3.2[b]		pH 3.9		pH 5.1		pH 6.0		pH 6.9	
		k'_1	α	k'_1	α	k'_1	α	k'_1	α	k'_1	α
OVM	Ibuprofen	7.17	1.42	10.3	1.44	5.14	1.28	1.38	1.16	0.39	1.00
	Ketoprofen	24.6	1.36	35.6	1.27	11.5	1.15	2.50	1.07	0.67	1.00
	Flurbiprofen	32.7	1.39	46.5	1.39	16.1	1.21	3.67	1.10	1.10	1.00
OVM-GA	Ibuprofen	6.45	1.26	10.3	1.29	5.34	1.15	1.66	1.07	0.48	1.00
	Ketoprofen	18.2	1.23	29.9	1.17	9.86	1.05	2.73	1.00	0.76	1.00
	Flurbiprofen	30.4	1.29	44.2	1.26	15.9	1.09	4.57	1.00	1.41	1.00
OVM-GA-R	Ibuprofen	5.25	1.19	8.30	1.17	6.13	1.09	2.14	1.00	0.68	1.00
	Ketoprofen	13.2	1.20	20.1	1.13	10.1	1.02	3.13	1.00	1.05	1.00
	Flurbiprofen	21.2	1.19	33.5	1.19	17.1	1.09	5.26	1.00	1.74	1.00

[a] 20 mM phosphate buffer–ethanol (90:10, v/v) was used as the eluent.
[b] Buffer pH.

hand, the capacity factors of basic solutes (chlorpheniramine, oxprenolol and tolperisone) increased with increase in eluent pH. Because of the pK_a values of these solutes (9.0–9.5), the retention of basic solutes should be due to electrostatic interactions with the positively charged solutes and the negatively charged protein, in addition to hydrophobic interactions. At eluent pH value below the pI of OVM, these solutes were eluted rapidly because of electrostatic repulsion between positively charged solutes and the protein. Hence, the capacity factors of these solutes at low eluent pH were not measured. Although the capacity factor of an uncharged solute (hexobarbital) showed almost no influence of eluent pH, a slight increase was observed with increasing eluent pH. This increase might be

TABLE II

EFFECT OF pH ON RETENTION AND ENANTIOSELECTIVITY OF BASIC DRUGS ON OVM, OVM-GA AND OVM-GA-R COLUMNS[a]

Column	Compound	pH 3.9[b]		pH 5.1		pH 6.0		pH 6.9	
		k'_1	α	k'_1	α	k'_1	α	k'_1	α
OVM	Chlorpheniramine	0.23	1.46	2.65	1.75	12.9	1.95		
	Oxprenolol	0.20	1.00	3.04	1.18	15.1	1.30		
	Tolperisone			0.90	1.77	4.04	1.42	16.7	1.21
OVM-GA	Chlorpheniramine	0.42	1.00	1.50	1.58	7.14	1.81	28.6	1.92
	Oxprenolol	0.25	1.00	1.03	1.29	7.16	1.25	29.4	1.32
	Tolperisone			0.49	1.72	2.29	1.39	8.67	1.28
OVM-GA-R	Chlorpheniramine			0.95	1.49	4.63	1.73	20.7	1.87
	Oxprenolol			0.71	1.15	4.44	1.20	18.4	1.31
	Tolperisone			0.29	1.70	1.57	1.34	6.32	1.25

[a] 20 mM phosphate buffer–ethanol (90:10, v/v) was used as the eluent.
[b] Buffer pH.

TABLE III

EFFECT OF pH ON RETENTION AND ENANTIOSELECTIVITY OF HEXOBARBITAL ON OVM, OVM-GA AND OVM-GA-R COLUMNS[a]

Column	pH 3.2[b]		pH 3.9		pH 5.1		pH 6.0		pH 6.9	
	k'_1	α	k'_1	α	k'_1	α	k'_1	α	k'_1	α
OVM	1.10	1.40	1.46	1.51	1.79	1.51	2.13	1.56	2.59	1.78
OVM-GA	0.85	1.25	1.04	1.40	1.14	1.40	1.19	1.48	1.54	1.71
OVM-GA-R	0.81	1.24	0.84	1.31	0.90	1.33	1.09	1.41	1.14	1.56

[a] 20 mM phosphate buffer–ethanol (95:5, v/v) was used as the eluent.
[b] Buffer pH.

due to changes in the binding properties of the protein resulting from changes in the eluent pH. The above results suggest that hydrophobic and electrostatic interactions should play an important role in the retention and enantioselectivity of racemic solutes on OVM, OVM-GA and OVM-GA-R columns.

The maximum enantioseparation factors of 2-arylpropionic acid derivatives were obtained with the use of an eluent pH of 3.2–3.9. The enantioseparation factors of chlorpheniramine and oxprenolol increased with increase in eluent pH, whereas that of tolperisone decreased with increase in eluent pH. However, when acetonitrile was used as an organic modifier, the enantioseparation factor of tolperisone increased with increasing eluent pH. These results might be correlated with the enantiomeric elution order of tolperisone, as reported previously [21]. Generally, acidic solutes gave higher enantioselectivities with decrease in eluent pH, whereas basic solutes were well resolved with increase in eluent pH. The enantioseparation factor of hexobarbital increased with increasing eluent pH.

Almost the same retention of these solutes as obtained with the use of eluents containing 10% ethanol were observed with the use of eluents containing 15% methanol or 8% acetonitrile on OVM, OVM-GA and OVM-GA-R materials. This indicates that the solvent strength decreases in the order acetonitrile, ethanol and methanol on OVM, OVM-GA and OVM-GA-R columns. However, the enantioselectivity of these solutes was dependent on the organic modifier used, as described below.

Effect of organic modifier on enantioselectivity of charged and uncharged solutes

Table IV shows effects of organic modifier on the enantioseparation factors of acidic, basic and uncharged drugs on OVM, OVM-GA and OVM-GA-R materials. For acidic drugs, the eluents used were 20 mM phosphate buffer (pH 3.9) containing 10% ethanol, 15% methanol and 8% acetonitrile. The results show that the use of methanol as an organic modifier gives the highest enantioselectivity of ibuprofen and ketoprofen, and that for the chiral resolution of flurbiprofen a higher enantioselectivity is obtained with the use of acetonitrile. For basic and unchanged drugs, 20 mM phosphate buffer (pH 6.0) containing ethanol, methanol and acetonitrile was used. It was found that almost the same enantioseparation factors of chlorpheniramine and tolperisone were obtained with the use of ethanol and methanol, and that of oxprenolol was independent of the organic modifier used. Racemic hexobarbital gave the highest enantioselectivity with the use of methanol. Fig. 2 shows typical chromatograms of 2-arylproprionic acid derivatives on OVM-GA and OVM-GA-R materials.

These results indicate that for chiral resolution of solutes it is necessary to select the most suitable eluent pH and organic modifier to give the maximum enantioselectivity on OVM, OVM-GA and OVM-GA-R materials. Also, methanol might be a suitable organic modifier for the chiral resolution of solutes. The enantioselectivity of the solutes on the materials prepared decreased in the order OVM, OVM-GA and OVM-GA-R. OVM-GA and OVM-

TABLE IV

EFFECT OF ETHANOL, METHANOL AND ACETONITRILE (ACN) ORGANIC MODIFIERS ON ENANTIOSELECTIV-
ITY OF ACIDIC, BASIC AND UNCHARGED DRUGS ON OVM, OVM-GA AND OVM-GA-R COLUMNS

Type of drug	Compound	OVM column			OVM-GA column			OVM-GA-R column		
		Ethanol	Methanol	ACN	Ethanol	Methanol	ACN	Ethanol	Methanol	ACN
Acidic[a]	Ibuprofen	1.44	1.54	1.19	1.29	1.43	1.13	1.17	1.22	1.09
	Ketoprofen	1.27	1.39	1.27	1.17	1.29	1.17	1.13	1.20	1.13
	Flurbiprofen	1.39	1.44	1.49	1.26	1.34	1.35	1.19	1.33	1.26
Basic[b]	Chlorpheniramine	1.95	1.97	1.82	1.81	1.84	1.64	1.73	1.68	1.52
	Oxprenolol	1.30	1.27	1.32	1.25	1.25	1.28	1.20	1.25	1.25
	Tolperisone	1.42	1.41	1.11	1.39	1.33	1.00	1.34	1.25	1.00
Uncharged[c]	Hexobarbital	1.56	1.70	1.38	1.48	1.63	1.40	1.41	1.50	1.30

[a] Eluents used were a mixture of 20 mM phosphate buffer (pH 6.0) and 10% ethanol, 15% methanol or 8% acetonitrile.
[b] Eluents used were a mixture of 20 mM phosphate buffer (pH 3.9) and 10% ethanol, 15% methanol or 8% acetonitrile.
[c] Eluents used were a mixture of 20 mM phosphate buffer (pH 6.0) and 5% ethanol, 7.5% methanol or 4% acetonitrile.

GA-R materials were slightly positive against the ninhydrin reaction, indicating that the OVM materials whose primary amino groups were cross-linked with glutaraldehyde retained their chiral recognition ability.

One of the disadvantage of protein-bonded phases is low long-term stability. In preliminary studies,
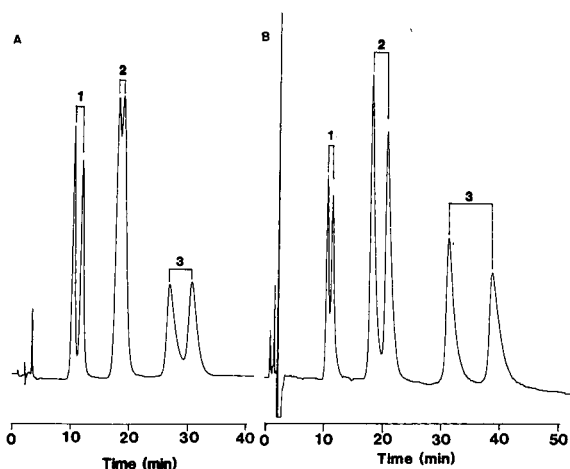

Fig. 2. Typical chromatograms of racemic 2-arylpropionic acid derivatives on (A) OVM-GA and (B) OVM-GA-R materials. Peaks: 1 = ibuprofen; 2 = ketoprofen; 3 = flurbiprofen. Eluents: (A) 20 mM phosphate buffer (pH 5.1) containing 10% ethanol; (B) 20 mM phosphate buffer (pH 3.2) containing 8% acetonitrile. Injection volume: 20 μl (each solute concentration, 10 μg/ml). Sensitivity, 0.016 a.u.f.s.

we compared the long-term stability of OVM and OVM-GA columns: 20 mM phosphate buffer (pH 3.9)–acetonitrile (90:10, v/v) was pumped at 1.0 ml/min for 60 min and then 20 mM phosphate buffer (pH 6.9)–ethanol (90:10, v/v) was passed through for 60 min. Hexobarbital was loaded under the latter eluent conditions. This cycle was repeated for about 200 times. For the OVM column the decreases in the capacity factor and enantioseparation factor were of the order of 17 and 5.7%, respectively, after 204 injections, whereas for the OVM-GA column the decreases were 7.7 and 1.6%, respectively, after 217 injections. These results suggest that the OVM-GA materials are more stable towards repetitive injections and/or changes in eluent composition (eluent pH, type of organic modifier) than the OVM materials. Hence the OVM-GA materials might be a promising candidate for the chiral resolution of racemic solutes. This aspect is now being investigated.

REFERENCES

1 G. Gubitz, Chromatographia, 30 (1990) 555, and references cited therein.
2 S. Allenmark, B. Bomgren and H. Boren, J. Chromatogr., 237 (1982) 473.
3 E. Domenici, C. Bertucci, P. Salvadori, G. Felix, I. Cahagne, S. Motellier and I. W. Wainer, Chromatographia, 29 (1990) 170.

4 J. Hermansson, *J. Chromatogr.*, 269 (1983) 71.
5 T. Miwa, M. Ichikawa, M. Tsuno, T. Hattori, T. Miyakawa, M. Kayano, Y. Miyake, *Chem. Pharm. Bull.*, 35 (1987) 682.
6 I. W. Wainer, P. Jadaud, G. R. Schnbaum, S. V. Kadodkar and M. P. Henry, *Chromatographia*, 25 (1988) 903.
7 S. Thelohan, Ph. Jadaud and I. W. Wainer, *Chromatographia*, 28 (1989) 551.
8 P. Erlandsson, I. Marle, L. Hansson, R. Isaksson, C. Pettersson and G. Pettersson, *J. Am. Chem. Soc.*, 112 (1990) 4573.
9 J. Hermansson, *J. Chromatogr.*, 298 (1984) 67.
10 T. Miwa, H. Kuroda, S. Sakashita, N. Asakawa and Y. Miyake, *J. Chromatogr.*, 511 (1990) 89.
11 T. Miwa, T. Miyakawa, M. Kayano and Y. Miyake, *J. Chromatogr.*, 408 (1987) 316.
12 M. Okamoto and H. Nakazawa, *J. Chromatogr.*, 504 (1990) 445.
13 M. Okamoto and H. Nakazawa, *J. Chromatogr.*, 508 (1990) 217.

14 J. Haginaka, J. Wakai, K. Takahashi, H. Yasuda and T. Katagi, *Chromatographia*, 29 (1990) 587.
15 G. Tamai, M. Edani and H. Imai, *Biomed. Chromatogr.*, 4 (1990) 157.
16 T. Takahashi, J. Haginaka, S. Tamagawa, T. Nishihata, H. Yasuda and T. Katagi, *J. Pharm. Pharmacol.*, 42 (1990) 356.
17 Y. Oda, N. Asakawa, T. Kajima, Y.Yoshida and T. Sato, *J. Chromatogr.*, 541 (1991) 411.
18 K. K. Kirkland, K. L. Nelson and D. A. McCombs, *J. Chromatogr.*, 545 (1991) 43.
19 H. Wada, H. Fujima and J. Haginaka, unpublished results.
20 M. D. Melamed, in A. Gottschalk (Editor), *Glycoproteins*, Elsevier, New York, 1966, p. 317.
21 J. Haginaka, C. Seyama, H. Yasuda and K. Takahashi, *J. Chromatogr.*, submitted for publication.

CHROMSYMP. 2420

Investigations of the influence of silanol groups on the separation of enantiomers by liquid and supercritical fluid chromatography

René Brügger and Hans Arm*

Institute of Organic Chemistry, University of Berne, Freiestrasse 3, CH-3012 Berne (Switzerland)

ABSTRACT

Chiral stationary phases based on (R)-N-(1-phenylethyl)-N'-(propylsilyl)urea covalently bonded to silica at different coverage densities with or without end-capped silanol groups were tested by liquid and supercritical fluid chromatography. Greater enantioselectivities and in most instances unexpectedly greater retentions were observed with the end-capped phases. This indicates that silanol groups may influence the interactions between the analyte and a chiral stationary phase.

INTRODUCTION

The direct chromatographic separation of enantiomers by liquid chromatography has become an important tool for the separation of optical isomers [1]. Chiral stationary phases based on small molecules covalently bonded to silica are often used because they combine good enantioselectivity with high efficiency. Different phases consist of molecules with π-donor or π-acceptor groups as chiral selectors. The chiral recognition mechanism for such donor–acceptor phases has been reviewed [2]. A complex between the chiral selector and the more retained enantiomer caused by different interactions was proposed in order to discuss the enantioselectivity of such donor–acceptor phases.

Only a few retention mechanisms lead to enantioselectivity. The retention on the chiral stationary phase (CSP) can be described as a sum of non-chiral and chiral interactions [3]. Silanol groups may influence the separation of enantiomers by non-chiral retention [4,5]. The influence of silanol groups on the chiral retention has also been investigated recently by Pirkle and Readnour [6].

To investigate the influence of silanol groups, we synthesized seven CSPs with different coverage densities. Three CSPs were end-capped by reaction of

the residual silanol groups with hexamethyldisilazane. As a chiral selector we used (R)-N-(1-phenylethyl)-N'-(propylsilyl)urea covalently bonded to silica. This CSP is extremely easy to prepare by the reaction of isocyanate with aminopropylsilane and is also commercially available as Supelcosil LC)-(R)-phenyl urea (Supelco, Gland, Switzerland). Such urea-linked CSPs were introduced by Ôi et al. [7]. The separation mechanisms of related CSPs were investigated by Pirkle and co-workers [8–10].

EXPERIMENTAL

General

LiChrospher Si 100 (Merck, Darmstadt, Germany) with a particle size of 5 μm was used. All other chemicals were purchased from Fluka (Buchs, Switzerland).

Chiral stationary phases were slurry-packed into 250 × 3.2 mm I.D. stainless-steel columns as a dibromomethane–hexane slurry.

(R)-N-(1-Phenylethyl)-N'-(diethoxymethylsilylpropyl)urea

A 7.48-g (36-mmol) amount of 3-aminopropylmethyldiethoxysilane was dissolved in 40 ml of dry

diethyl ether. To the stirred solution 5 ml (36 mmol) of (R)-(+)-1-phenylethyl isocyanate were added dropwise. After stirring the reaction mixture under a nitrogen atmosphere for 12 h at room temperature, the solvent was removed and the urea was purified by flash column chromatography and identified by ^{1}H NMR spectrometry.

Chiral stationary phases

Different amounts of (R)-N-(1-phenylethyl)-N'-(diethoxymethylsilylpropyl)urea in 15 ml of dry toluene were added to 2.20 g of LiChrospher Si 100 (dried at 180°C and 0.1 mbar for 4 h). The mixture was heated at reflux for about 4 h. After cooling, the gel was washed with toluene, methanol and hexane.

End-capping

Three chiral stationary phases with different coverage densities were heated at reflux with an excess of hexamethyldisilazane in 20 ml of dry toluene under a nitrogen atmosphere. After cooling, they were washed with toluene, methanol and hexane.

Liquid chromatography

Chromatography was performed using a Kontron (Zürich, Switzerland) LC 410 pump, a Rheodyne (Berkeley, CA, USA) Model 7125 injection valve with a 20-μl loop, a Uvikon LCD 725 variable-wavelength UV detector (Kontron) at 254 nm and a HP 3396A integrator (Hewlett-Packard, Widen, Switzerland).

Packed column supercritical fluid chromatography

The laboratory-constructed apparatus for supercritical fluid chromatography (SFC) consisted of a System Gold 116 high-performance liquid chromatographic (HPLC) pump (Beckman Instruments, Basle, Switzerland) controlled by a NEC PC-8201A computer. The pump head was cooled by an ethanol cooling bath at −10°C. The cooling jacket was laboratory-built. The sample was introduced by a Rheodyne Model 7125 HPLC injection valve with a 5-μl loop. Temperature control for the column was provided by a Sigma 2 oven (Perkin-Elmer, Küsnacht, Switzerland). The outlet pressure was regulated by a Tescom restrictor (Matkemi, Therwil, Switzerland) at 40°C. The inlet and outlet pressures were controlled by a laboratory-built

pressure controller. A Uvikon 720 LC UV detector (Kontron) was used at 254 nm. The results were recorded with a HP 3396A integrator (Hewlett-Packard).

Carbon dioxide (48-grade) and carbon dioxide (40-grade) containing 5% methanol were obtained from Carbagas (Berne, Switzerland).

RESULTS AND DISCUSSION

CSPs were prepared according to the scheme in Fig. 1. Isocyanate treated with 3-aminopropylsilane yielded a silylurea. Different amounts of the silylurea were bonded to silica to give CSPs with different coverage densities. Three CSPs with different coverage densities were additionally treated with hexamethyldisilazane to eliminate silanol groups (Fig. 2). The coverage densities were calculated from the nitrogen content obtained by elemental analysis (Table I).

In the following chromatographic experiments the capacity factors, k', and separation factors, α, are given as means of three measurements. The standard deviation was less than 5% for the capacity factors and less than 0.5% for the separation factors.

The phases were first tested with 3,5-dinitrobenzoyl (DNB) derivatives of several amines and amino acid esters (Tables II and III). Figs. 3 and 4 show the relationship between the separation factor and the coverage density of the chiral urea. For the non-end-capped CSPs the separation factor decreases with lower coverage densities. This is not the case if end-capped CSPs are used; the separation factor does not decrease with lower coverage densities and
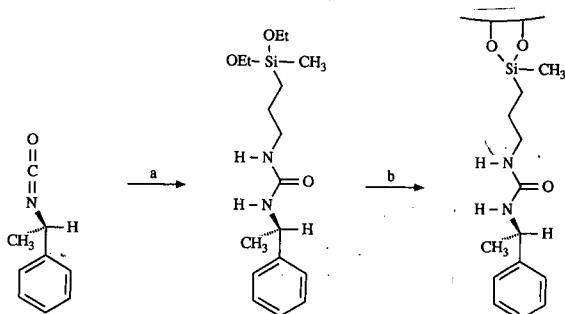

Fig. 1. Preparation of the chiral stationary phases. Conditions: (a) 3-aminopropylmethyldiethoxysilane, diethyl ether, room temperature; (b) 5-μm silica gel, toluene, reflux.
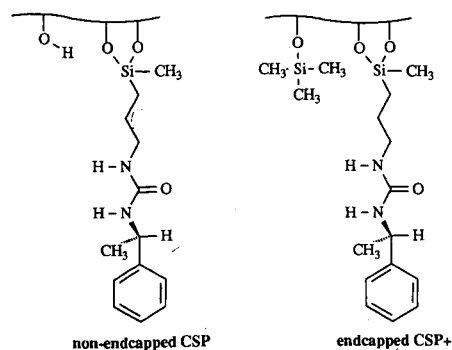
Fig. 2. Structure of the non-end-capped and the end-capped chiral stationary phases.

is even slightly greater at lower coverage densities. On the end-capped CSPs a lower coverage density leads to reduced chiral and non-chiral interactions. Hence the retention decreases but not the separation factor because the ratio of chiral and non-chiral interactions remains more or less constant. In contrast, on the non-end-capped CSPs additional non-chiral interactions with silanol groups become possible so that the ratio of chiral and non-chiral interactions changes with lower coverage densities, which leads to lower separation factors.

To show the reduction of accessible silanol groups by the end-capping, the phases were tested

TABLE I

CHARACTERISTICS OF THE NON-END-CAPPED (CSP) AND THE END-CAPPED (CSP+) CHIRAL STATIONARY PHASES

CSP	Carbon content (%)	Nitrogen content (%)	Concentration of chemically bonded groups (mmol/g)	Groups/nm² [a]
CSP1	3.40	0.57	0.20	0.33
CSP2	4.79	0.76	0.27	0.45
CSP3	6.92	1.06	0.38	0.65
CSP4	7.79	1.29	0.46	0.81
CSP5	9.67	1.64	0.58	1.07
CSP6	10.83	1.75	0.62	1.16
CSP7	11.63	2.05	0.73	1.40
CSP1 +	6.69	0.45		0.33
CSP3 +	9.03	1.00		0.65
CSP6 +	12.46	1.78		1.16

[a] Concentration of chemically bonded chiral groups calculated with a specific surface area of 392 m²/g.

TABLE II

RESOLUTION OF N-(3,5-DINITROBENZOYL)-1-PHENYLETHYLAMINE (DNB-PEA) AND N-(3,5-DINITROBENZOYL)-1-NAPHTHYLETHYLAMINE (DNB-NEA)

LC conditions: mobile phase, n-hexane–2-propanol (80:20); flow-rate, 1 ml/min; detection, UV at 254 nm. k'_1 = Capacity factor of the first-eluted enantiomer; k'_2 = capacity factor of the second-eluted enantiomer; α = separation factor; absolute configuration of the second-eluted enantiomer is R.

Stationary phase	DNB-PEA			DNB-NEA		
	k'_1	k'_2	α	k'_1	k'_2	α
Silica	0.2	0.2	1.00	0.1	0.1	1.00
CSP1	0.5	0.6	1.15	0.5	0.8	1.47
CSP2	0.9	1.1	1.18	0.9	1.4	1.56
CSP3	1.2	1.4	1.21	1.2	1.9	1.67
CSP4	1.4	1.7	1.23	1.4	2.4	1.70
CSP5	1.7	2.1	1.25	1.7	3.0	1.76
CSP6	1.8	2.3	1.26	1.9	3.4	1.78
CSP7	2.2	2.7	1.27	2.3	4.1	1.79
CSP1 +	0.6	0.9	1.57	0.5	1.2	2.41
CSP3 +	1.8	2.8	1.58	1.6	3.9	2.47
CSP6 +	2.2	3.4	1.53	2.1	4.9	2.36

with acetophenone using carbon dioxide as a supercritical mobile phase.

Fig. 5 shows that the retention of acetophenone on the CSPs is mainly affected by silanol interactions. The retention increases with lower coverage densities where more silanol groups are accessible.

TABLE III

RESOLUTION OF SOME DNB AMIDES OF AMINO ACID METHYL ESTERS

LC conditions: mobile phase, n-hexane–2-propanol (80:20); flow-rate, 1 ml/min; detection, UV at 254 nm. k'_1 = Capacity factor of the first-eluted enantiomer; α = separation factor; absolute configuration of the second eluted enantiomer is R.

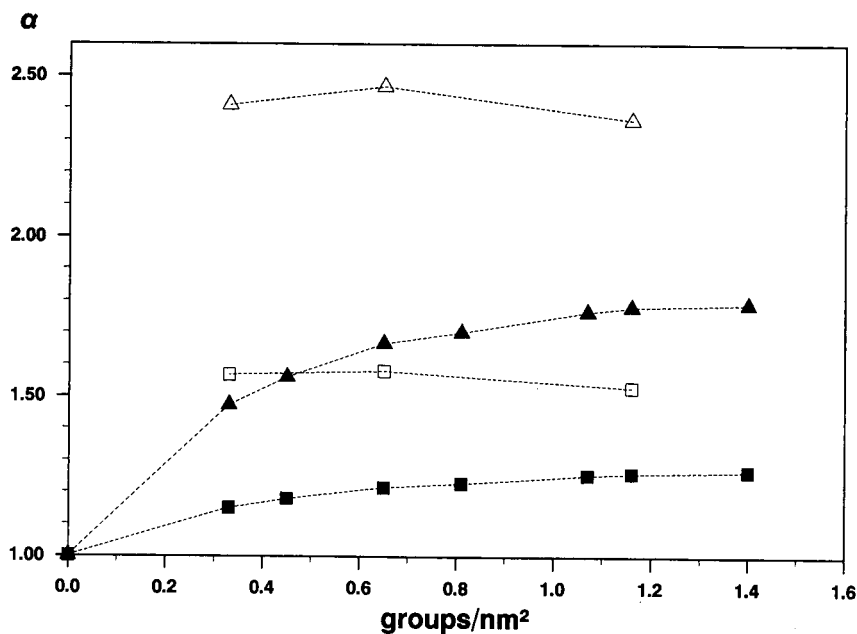| CSP	Alanine		Leucine		Phenylalanine	
	k'_1	α	k'_1	α	k'_1	α
CSP1	0.9	1.13	0.4	1.19	0.6	1.18
CSP3	1.3	1.25	0.7	1.29	1.1	1.28
CSP6	1.7	1.33	1.1	1.31	1.7	1.29
CSP1 +	0.5	1.59	0.3	1.50	0.4	1.40
CSP3 +	1.3	1.63	1.0	1.54	1.2	1.45
CSP6 +	1.7	1.58	1.2	1.48	1.7	1.44

Fig. 3. Separation factor, α, of (■) N-(3,5-dinitrobenzoyl)-1-phenylethylamine and (▲) N-(3,5-dinitrobenzoyl)-1-naphthylethylamine on the (□, △) end-capped and (■, ▲) non-end-capped CSPs as a function of the coverage density. The chromatographic conditions are described in Table II.
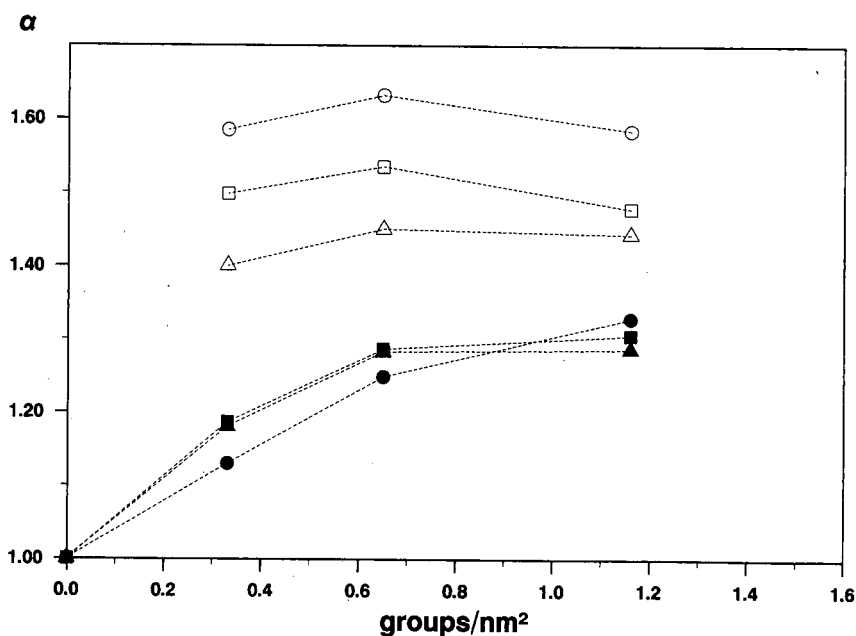

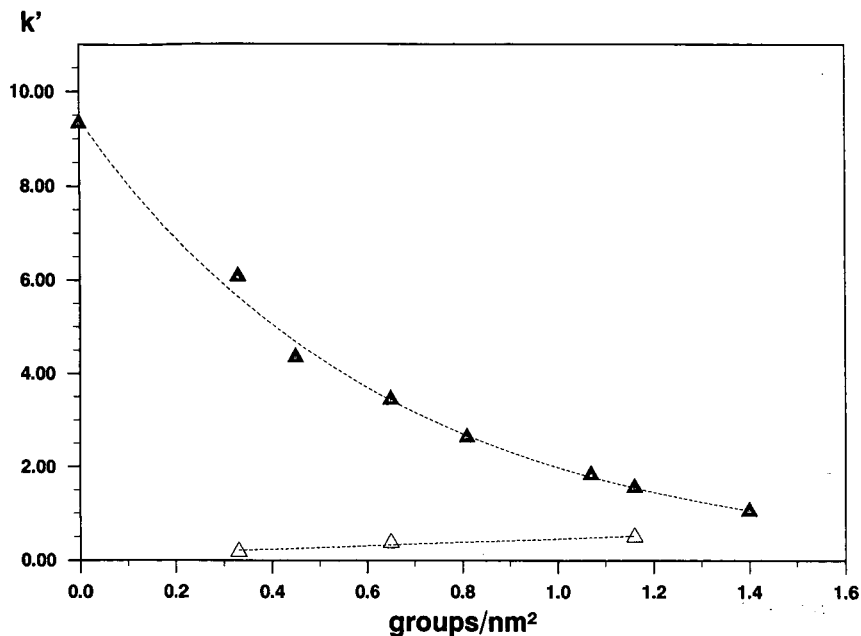Fig. 4. Separation factor, α, of (■) N-(3,5-dinitrobenzoyl)leucine methyl ester, (▲) N-(3,5-dinitrobenzoyl)phenylalanine methyl ester and (●) N-(3,5-dinitrobenzoyl)alanine methyl ester on the (□, △, ○) end-capped and (■, ▲, ●) non-end-capped CSPs as a function of the coverage density. The chromatographic conditions are described in Table III.

k'

Fig. 5. Capacity factor, k', of acetophenone on ($\triangle$) end-capped and ($\blacktriangle$) non-end-capped CSPs as a function of the coverage density. SFC conditions: mobile phase, carbon dioxide; flow-rate, 3 ml/min; temperature, 50°C; column inlet pressure, 220 bar; column outlet pressure, 180 bar.

A totally different effect can be seen with the end-capped CSPs. In this instance, the retention decreases with lower coverage densities. This indicates that most of the accessible silanol groups are converted into inactive species.

For the separation of enantiomers with n-hexane–2-propanol (80:20) as mobile phase, the retention should also be smaller on the end-capped CSPs if a reduction of interactions with silanol groups

Dipole-Stacking Mechanism
(R)-Enantiomer selectively retained

Hydrogen-Bonding Mechanism
(S)-Enantiomer selectively retained

Fig. 6. Competing chiral recognition mechanisms.

were the only reason for the greater separation factors. However, surprisingly, the separation factors and the retentions are greater on the end-capped CSPs (Figs. 3 and 4), so an additional effect must cause the greater enantioselectivity.

Previously, Pirkle et al. [8] proposed the occurrence of two competing chiral recognition processes which have opposite senses of enantioselectivity for the resolution of 3,5-dinitrobenzoylamide enantiomers on amide or urea chiral stationary phases. The degree of chiral recognition is determined by the extent of each competing chiral recognition process. The two mechanisms are shown in Fig. 6. According to the results of Pirkle et al., who investigated series of α-arylalkylamines as their 3,5-dinitrobenzoyl derivatives, the dipole-stacking mechanism dominates for the sepration of analytes with short alkyl tails, such as 3,5 dinitrobenzoyl-1-phenylethylamine. Hence the R-enantiomer is retained more when (R)-N-(1-phenylethyl)-N'-(propylsilyl)urea is used as a chiral stationary phase. The hydrogen-bonding mechanism would dominate for analytes with longer alkyl tails, where the S-enantiomer is retained more. In contrast, the
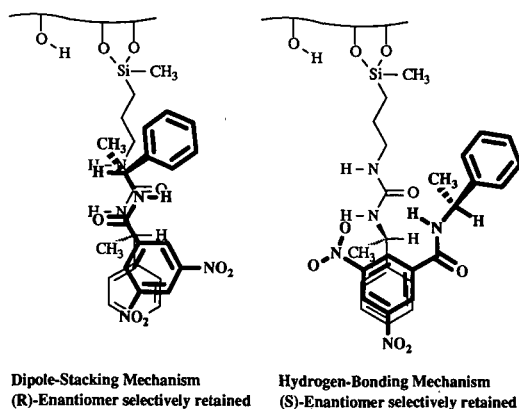
TABLE IV

RESOLUTION OF SOME DNB AMIDES OF 1-PHENYL-ALKYLAMINES

LC conditions: mobile phase, n-hexane–2-propanol (80:20); flow-rate, 1 ml/min; detection, UV at 254 nm. k'_1 = Capacity factor of the first-eluted enantiomer; k'_2 = capacity factor of the second-eluted enantiomer; α = separation factor; n = carbon number of the alkyl group. In case of resolution the last eluted enantiomer is R for $n < 7$ and S for $n > 7$.

CSP	n	CSP			CSP+		
		k'_1	k'_2	α	k'_1	k'_2	α
CSP1	1	0.5	0.6	1.15	0.6	0.9	1.57
	2	0.5	0.6	1.16	0.6	0.9	1.51
	3	0.5	0.5	1.00	0.5	0.7	1.36
	4				0.5	0.6	1.23
	5				0.4	0.5	1.14
	7				0.4	0.4	1.00
	8				0.4	0.4	1.00
	9				0.4	0.4	1.00
	10				0.4	0.4	1.00
	13				0.3	0.3	1.00
	17	0.2	0.2	1.00	0.3	0.3	1.00
CSP3	1	1.3	1.6	1.22	1.7	2.7	1.57
	2	1.3	1.6	1.21	1.7	2.6	1.50
	3	1.2	1.4	1.16	1.6	2.2	1.34
	4	1.1	1.2	1.09	1.6	1.9	1.21
	5	1.1	1.1	1.00	1.4	1.6	1.13
	7	0.9	0.9	1.00	1.4	1.4	1.00
	8	0.9	0.9	1.00	1.2	1.2	1.00
	9	0.8	0.8	1.00	1.2	1.2	1.00
	10	0.7	0.7	1.00	1.1	1.1	1.00
	13	0.6	0.6	1.00	0.9	0.9	1.00
	17	0.5	0.5	1.00	0.9	0.9	1.00
CSP6	1	1.8	2.3	1.26	2.2	3.4	1.53
	2	1.8	2.3	1.22	2.3	3.3	1.44
	3	1.7	1.9	1.15	2.1	2.7	1.29
	4	1.6	1.7	1.07	1.9	2.2	1.15
	5	1.5	1.5	1.00	1.9	2.0	1.06
	7	1.3	1.3	1.00	1.7	1.7	1.00
	8	1.2	1.2	1.00	1.5	1.5	1.00
	9	1.1	1.2	1.07	1.4	1.5	1.08
	10	1.0	1.1	1.08	1.3	1.4	1.09
	13	0.8	0.9	1.10	1.3	1.4	1.09
	17	0.8	0.9	1.12	1.0	1.2	1.14

3,5-dinitrobenzoyl derivatives of amino acid esters show a preference for the hydrogen-bonding mechanism because of the additional hydrogen bonding site (*i.e.*, the ester carbonyl oxygen) [8]. In this instance the R-enantiomer is retained more (inversion of substituent priority).

To investigate if the separation factor is greater on the end-capped CSPs because the distribution of the two competing chiral recognition processes is different for end-capped and non-end-capped CSPs, we tested CSPs with a homologous series of 3,5-dinitrobenzoyl derivatives of 1-phenylalkylamines (Table IV). For the analytes with alkyl tails longer than five carbons, inversion of the elution order was observed with the end-capped and non-end-capped CSP6 (Fig. 7). According to Pirkle *et al.* [8], this result can be explained by an increasing contribution of the hydrogen-bonding mechanism with increasing length of the alkyl tail, which results in the opposite sense of enantioselectivity. As a result, the S-enantiomer is retained more. For CSP1 and CSP3 the enantioselectivity is too low to cause a separation of analytes with longer alkyl tails if the retention is so short. In any case, the end-capped CSPs afford greater retention and greater enantioselectivity for both mechanisms. Hence a different distribution of the two competing chiral recognition processes is not the reason for the greater separation factors on the end-capped CSPs.

The results indicate that the mechanisms which afford retention and enantioselectivity are suppressed on CSPs with non-end-capped silanol groups. Probably the chiral selector is blocked by interactions with silanol groups. A reduction of non-chiral retention caused by silanol groups may yield a greater enantioselectivity but would also yield shorter retentions. As we found greater retention on the end-capped CSPs, we consider that the

TABLE V

RESOLUTION OF N-(3,5-DINITROBENZOYL)-1-PHENYLETHYLAMINE BY SFC

SFC conditions: mobile phase, carbon dioxide–methanol (95:5); flow-rate, 3 ml/min; temperature, 40°C; column inlet pressure, 220 bar; column outlet pressure, 180 bar; detection, UV at 254 nm. k'_1 = Capacity factor of the first-eluted enantiomer; k'_2 = capacity factor of the second-eluted enantiomer; α = separation factor.

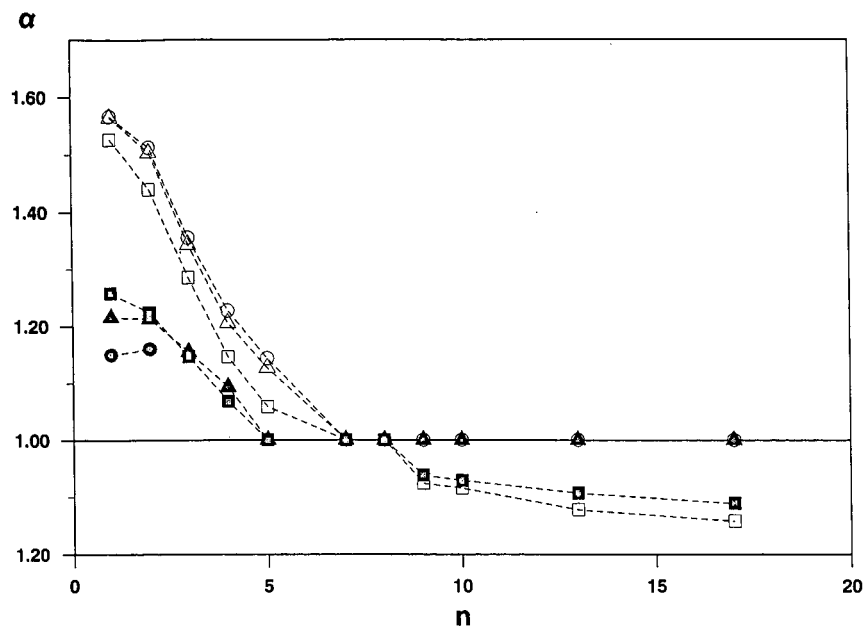| CSP	CSP			CSP+		
	k'_1	k'_2	α	k'_1	k'_2	α
CSP1	2.1	2.2	1.06	1.4	1.9	1.30
CSP3	4.3	4.8	1.11	4.3	5.7	1.33
CSP6	7.4	8.6	1.16	6.4	8.4	1.30

Fig. 7. Separation factor, α, of N-(3,5-dinitrobenzoyl)-1-phenylalkylamines on the end-capped (○) CSP1+, (△) CSP3+ and (□) CSP6+ and non-end-capped (●) CSP1, (▲) CSP3 and (■) CSP6 as a function of the carbon number, n, of the alkyl group. The chromatographic conditions are described in Table IV.

reason for the greater separation factors is probably a better accessibility of the chiral selector when the silanol groups are end-capped.

Pirkle and Hyun [10] also found greater enantioselectivities for the separation of 3,5-dinitrobenzoyl-1-phenylethylamine on an amide CSP filled with alkyl groups. Because the retention was shorter on this CSP, they ascribed this phenomenon to the end-capping of residual silanol groups which afford retention without enantioselectivity. In contrast to their results, we observed in most instances greater retention on the end-capped CSPs (Table III and IV).

Table V shows the separation of N-(3,5-dinitrobenzoyl)-1-phenylethylamine by SFC with carbon dioxide–methanol (95:5) as the mobile phase on different CSPs. The enantioselectivity is still greater with the end-capped CSPs, but the retention is smaller in some instances. The solvation interactions of the polar urea group with the methanol modifier are stronger than with 2-propanol. As a result, the urea group is less accessible and so chiral interactions are reduced. Therefore, the enantiose-

lectivity is lower when carbon dioxide–methanol (95:5) is used as the mobile phase, but there is still a difference between end-capped and non-end-capped phases.

CONCLUSIONS

Silanol groups may influence the separation of enantiomers by non-chiral retention. In addition, they may also interfere with the interactions between the analyte and the chiral selector. The enantioselectivity may be substantially greater when the silanol groups are end-capped. This is the case for analytes which are separated on (R)-N-(1-phenylethyl)-N'-(propylsilyl)urea. Moreover, the retention is in most instances greater on the end-capped CSPs when hexane–2-propanol is used as the mobile phase. We assume that analyte–chiral selector interactions are suppressed by interactions between the chiral selector and the silanol groups and that the end-capping prevents this suppression. Similar effects were recently observed by Pirkle and Readnour [6].

REFERENCES

1 S. G. Allenmark, *Chromatographic Enantioseparation*, Ellis Horwood, Chichester, 1988.
2 W. H. Pirkle and T. C. Pochapsky, *Chem. Rev.*, 89 (1989) 347.
3 R. Däppen, V. R. Meyer and H. Arm., *J. Chromatogr.*, 464 (1989) 39.
4 H. Engelhardt, H. Löw, W. Eberhardt and M. Mauss, *Chromatographia*, 27 (1989) 535.
5 Y. Dobashi and S. Hara, *J. Org. Chem.*, 52 (1987) 2490.
6 W. H. Pirkle and R. S. Readnour, *Chromatographia*, 31 (1991) 129.
7 N. Ôi, H. Kitahara, T. Doi and S. Yamamoto, *Bunseki Kagaku*, 32 (1983)345.
8 W. H. Pirkle, M. H. Hyun and B. Bank, *J. Chromatogr.*, 316 (1984) 585.
9 W. H. Pirkle and M. H. Hyun, *J. Chromatogr.*, 322 (1985) 295.
10 W. H. Pirkle and M. H. Hyun, *J. Chromatogr.*, 328 (1985) 1.

CHROMSYMP. 2461

Determination of the enantiomers of fenoldopam in human plasma by reversed-phase high-performance liquid chromatography after chiral derivatization

Venkata K. Boppana*, Lauren Geschwindt, Matthew J. Cyronak and Gerald Rhodes

Department of Drug Metabolism and Pharmacokinetics, SmithKline Beecham Pharmaceuticals, P.O. Box 1539, Mail Code L-712, King of Prussia, PA 19406 (USA)

ABSTRACT

Fenoldopam, a selective agonist at peripheral dopaminergic (DA-1) receptors, is administered as a racemic mixture and, consequently, an indirect stereospecific high-performance liquid chromatographic assay was developed to study the disposition of the individual enantiomers in human subjects. Fenoldopam enantiomers were extracted from alkalinized plasma into ethyl acetate prior to precolumn derivatization with the chiral reagent 2,3,4,6-tetra-O-acetyl-β-D-glucopyranosyl isothiocyanate (GITC). The resulting diastereomers were separated on a reveresed-phase butylsilica column and determined using triple-electrode coulometric detection. The limits of determination and detection for the S- and R-enantiomers of fenoldopam were 0.5 and 0.25 ng/ml, respectively. A linear response was observed for (S)- and (R)-fenoldopam concentrations ranging from 0.5 to 50 ng/ml in plasma. The intra-day relative standard deviations (R.S.D.s) for the plasma assay at nominal concentrations of 0.5, 5 and 50 ng/ml were 17.4, 5.2 and 6.9%, respectively, for (S)-fenoldopam and 9.9, 6.2 and 7.4%, respectively, for (R)-fenoldopam. The inter-day R.S.D.s of the method at these concentrations were 9.3, 7.7 and 7.4%, respectively, for (S)-fenoldopam and 9.5, 1.9 and 7.3%, respectively, for (R)-fenoldopam. The mean accuracy of the method at concentrations of 0.5, 5 and 50 ng/ml in plasma was found to be 106.4, 111.8 and 108.9%, respectively, for (S)-fenoldopam and 116.2, 104.2 and 111.2%, respectively, for (R)-fenoldopam. The assay developed was sufficiently sensitive, accurate and precise to support pharmacokinetic studies in human subjects.

INTRODUCTION

Fenoldopam (SK&F 82526, **I**, Fig. 1) [6-chloro-2,3,4,5-tetrahydro-1-(4-hydroxyphenyl)-1*H*-3-benz-azepine-7,8-diol], a potent agonist at peripheral dopamine-1 (DA-1) receptors, has been shown to produce beneficial effects including an improvement in
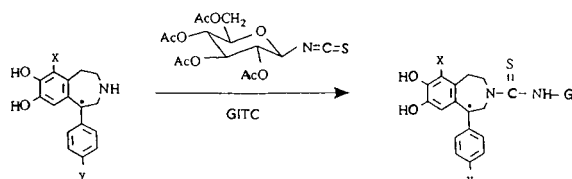

Fig. 1. Derivatization of fenoldopam (X = Cl; Y = OH) and internal standard (SK&F 38393, X = Y = H) with GITC to form the corresponding diastereomeric thiourea products. Ac = Acetyl.

renal blood flow and a reduction in blood pressure following intravenous and oral administration [1,2]. Fenoldopam contains a chiral center and exists in two enantiomeric forms (S and R), of which only the R-enantiomer exhibits the desired pharmacological activity [3]. As fenoldopam is administered as the racemate, a stereospecific assay method was required in order to study the disposition of the individual enantiomers in human subjects.

Previously described methods based on high-performance liquid chromatography (HPLC) with electrochemical detection (ED) for the measurement of racemic fenoldopam and its metabolites [4–7] in various biological fluids were not readily modifiable for the direct measurement of (S)- and (R)-fenoldopam in plasma. Consequently, this paper describes an indirect stereospecific HPLC–ED method for the simultaneous determination of the,

individual enantiomers of fenoldopam in human plasma.

EXPERIMENTAL

Chemicals and supplies

Fenoldopam mesylate (racemic mixture), internal standard (racemic SK&F 38393-A, I.S., Fig. 1) and the mesylate salts of (*R*)- and (*S*)-fenoldopam were obtained from Drug Substances and Products, SmithKline Beecham Pharmaceuticals (Swedeland, PA, USA). Dibasic sodium phosphate and HPLC-grade methanol, acetonitrile and ethyl acetate were obtained from J.T. Baker (Phillipsburg, NJ, USA). The chiral reagent 2,3,4,6-tetra-O-acetyl-β-D-glucopyranosyl isothiocyanate (GITC) was purchased from Polysciences (Warrington, PA, USA). Glacial acetic acid was obtained from Mallinckrodt (Paris, KY, USA). HPLC-grade water (Milli-Q water purification system; Millipore, Bedford, MA, USA) was used in the preparation of buffer and reagent solutions. All other chemicals were of analytical-reagent grade. Microfilterfuge centrifugal filter tubes, with 0.45-μm pore size nylon 66 membrane, were obtained from Rainin Instruments (Woburn, MA, USA).

Standard solutions and reagents

Stock standard solutions of fenoldopam and internal standard were prepared separately by dissolving 13.14 mg of fenoldopam mesylate and 11.4 mg of SK&F 38393 (hydrochloride salt) in 0.05 *M* acetic acid in a 10-ml volumetric flask to give a final concentration of 1 mg/ml. Appropriate dilutions of the stock solutions of fenoldopam were made with 0.05 *M* acetic acid to generate a series of working standard solutions (100, 10, 1, 0.1 and 0.01 μg/ml). All stock and working standard solutions were stable for 4 weeks when stored at 4°C. Freshly prepared ascorbic acid solution in water was added to plasma to give a final concentration of 0.5% (w/v). Samples were protected from light.

GITC reagent solution (200 μg/ml). A 2 mg/ml solution of GITC in ethyl acetate was prepared by dissolving a weighed amount of GITC in an appropriate volume of ethyl acetate. This was further diluted with ethyl acetate to give a final concentration of 200 μg/ml. This solution was prepared fresh daily just before use.

Citrate–acetate buffer (pH 5.6). A 22.0-g amount of sodium acetate trihydrate, 21 g of citric acid monohydrate, 9.8 g of sodium hydroxide and 0.63 g of disodium EDTA were dissolved in 2 l of water. The ionic strength and pH of the solution were 260 m*M* and 5.6, respectively.

Mobile phase. A 75-ml volume of methanol, 85 ml of acetonitrile, 140 ml of citrate–acetate buffer (pH 5.6) and 210 ml of water were mixed and filtered through a Millipore 0.45-μm type HA membrane filter. The mobile phase was recycled for a period of 7 days.

Calibration. A set of 1-ml plasma calibration standards [concentrations of (*S*)- and (*R*)-fenoldopam of 0.25, 0.5, 1, 2, 5, 10, 20 and 50 ng/ml] was prepared from working standard solutions of fenoldopam and analyzed with each determination of fenoldopam enantiomer plasma concentrations. The peak-height ratios of (*S*)- and (*R*)-fenoldopam to the internal standard were weighted by $1/y$ (based on analysis of residual plots) and plotted against analyte concentration for both (*S*)- and (*R*)-fenoldopam. Linear regression analysis gave calibration lines that were used to calculate the concentrations of (*S*)- and (*R*)-fenoldopam in spiked control or unknown plasma samples.

Collection of clinical samples

Ten healthy male volunteers received an intravenous infusion of fenoldopam at a rate of 1 μg/kg for 2 h. Blood samples were collected at 0, 5, 15, 30, 45, 60, 90, 120, 122.5, 125, 130, 135, 140, 150, 165, 180, 210, 240, 270, 300, 330 and 360 min in heparinized Vacutainers and centrifuged at 3000 *g*. Samples of 4.75 ml of plasma were transferred into 100 × 17 mm I.D. polypropylene tubes containing 0.25 ml of 10% ascorbic acid (freshly prepared), mixed and stored immediately at −20°C. Addition of ascorbic acid is essential to ensure stability of fenoldopam in plasma during the storage in the freezer.

Extraction procedure

An aliquot of plasma (1 ml), containing fenoldopam as standard or as an unknown, was mixed with 50 μl of working internal standard (I.S.) solution (500 ng/ml) in a 100 × 13 mm I.D. screw-capped Pyrex glass tube. Ethyl acetate (5 ml) was added to the tube, followed by 0.5 m*M* of dibasic sodium phosphate solution (0.5 ml). After mixing the con-

tents by inverting the tube, the latter was placed on a reciprocal shaker and the contents were mixed at low speed (60 cycles/min) for 10 min. Following centrifugation of the sample tube at 2000 g for 10 min, the ethyl acetate fraction (4.5 ml) was transferred into a 100 × 13 mm I.D. borosilicate tube and the solvent was evaporated under nitrogen at 40°C. The dried samples was then subjected to derivatization with GITC.

Derivatization procedure

To the dried extract, 100 μl of GITC solution (200 μg/ml) were added followed by 50 μl of 1% triethylamine (freshly prepared) in ethyl acetate. The sample was allowed to stand at room temperature for 1 h. Following reaction, the solvent was removed under a stream of nitrogen at 40°C and the residue was reconstituted in 200 μl of 0.05 M acetic acid containing 30% (v/v) of acetonitrile. The sample was filtered through a microfilterfuge centrifugal filter tube (0.45-μm pore size, nylon 66 membrane) that had been previously washed with 0.5 ml of 0.05 M acetic acid containing 30% (v/v) of acetonitrile. The filtrate was transferred into an autosampler vial and 5–50 μl were injected for HPLC analysis.

Optimization of the precolumn reaction proceeded from the initial conditions described above using a standard solution of racemic fenoldopam. This standard solution was repetitively derivatized using different reagent concentrations and reaction times prior to HPLC separation and analysis. The coulometric response for each diastereomer was monitored by measuring the resulting peak height while keeping the HPLC conditions constant. Using this approach, optimum conditions were determined for maximum coulometric response following precolumn derivatization. The reaction was also monitored for complete conversion of substrate (fenoldopam) to the respective GITC derivatives by measuring the racemic fenoldopam levels in the reaction media according to the method published earlier [4].

High-performance liquid chromatography

The isocratic chromatographic system consisted of an HPLC pump (Model 114; Beckman Instruments, Palo Alto, CA, USA) and an autoinjector (WISP Model 710B; Waters Assoc., Milford, MA, USA). Separations were carried out on an Aqua-

pore butylsilica (7 μm) column (22 cm × 2.1 mm I.D.) (Pierce, Rockford, IL, USA) coupled in-line with a butylsilica guard column (3 cm × 2.1 mm I.D.) (Pierce). The column temperature was maintained at 37°C using a column heater (Rainin Instruments). The mobile phase was pumped at a flow-rate of 0.3 ml/min. Prior to use, the mobile phase was degassed by filtration through a 0.45-μm membrane filter. Following chromatographic separation, the analytes were detected by oxidation of the catechol moiety with a coulometric detector (ESA, Bedford, MA, USA) equipped with three serial electrodes (one guard, G, and two analytical cells, W_1 and W_2). The potential used at these electrodes were G = +0.2 V, W_1 = −0.20 V and W_2 = +0.20 V. Chromatographic peak-height data were collected with a computerized automated laboratory system (Access*Chrom; PE/Nelson, Cupertino, CA, USA).

Validation procedures

Three pools of plasma precision samples containing 0.5, 5 and 50 ng/ml each of (S)- and (R)-fenoldopam were prepared by adding appropriate volumes of standard solutions to drug-free plasma preserved with ascorbic acid (total volume 25 ml). These plasma samples were stored at −20°C until analysis. Five replicate samples from each pool were extracted and analyzed on three separate days. Concentrations were determined by comparison with a calibration graph prepared on the day of analysis. From the data obtained, intra- and interday relative standard deviations (R.S.D.s) and mean accuracies were calculated.

RESULTS AND DISCUSSION

Initial efforts directed toward the development of a direct HPLC separation of (S)- and (R)-fenoldopam compatible with electrochemical detection were not successful. Consequently, an indirect method of analysis was pursued based upon precolumn chiral derivatization followed by chromatographic separation of the diastereomeric products formed. Of the several chiral reagents commercially available, GITC is widely used for precolumn derivatization of primary and secondary amines [8–11] to develop stereospecific HPLC methods for enantiomeric compounds. GITC reacts rapidly with
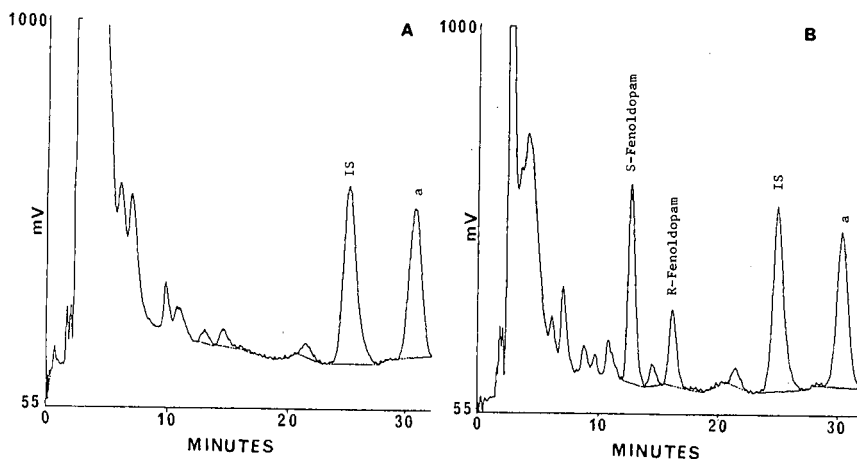
Fig. 2. Chromatogram of plasma extracts from a human subject (A) before and (B) 2 h after intravenous infusion of 1 μg/min · kg of racemic fenoldopam for 2 h. The plasma concentrations of (*S*)- and (*R*)-fenoldopam were 10.06 and 4.95 ng/ml, respectively. The peak labeled a is the other diastereomer of the internal standard. For chromatographic conditions, see the text.

primary and secondary amines, it is commercially available in highly pure form and it is stereochemically stable. The isothiocyanate group of GTIC reacts selectively with secondary amine function of fenoldopam under mild reaction conditions to form corresponding stable thiourea derivative of fenoldopam (Fig. 1). Structures of the derivatives were confirmed by fast atom bombardment mass spectrometry.

The stereospecific plasma assay described here for the determination of (*S*)- and (*R*)-fenoldopam involved ethyl acetate extraction of the drug and the internal standard from alkalinized plasma as a preliminary isolation step, followed by derivatization of the individual enantiomers with GITC. Derivatization of fenoldopam with GITC was carried out in various solvents, such as dimethylformamide, acetonitrile, chloroform and ethyl acetate, with satisfactory results. Ethyl acetate was chosen as the solvent to conduct the derivatization reaction as a higher rate of reaction was observed and, moreover, it was used as the extractions solvent for the isolation of fenoldopam enantiomers from plasma. To facilitate derivatization, a small amount of triethylamine was also added to the reaction media. Further optimization of the precolumn derivatization of fenoldopam with GITC was carried out in ethyl acetate at room temperature by varying the concentration of GITC (20–2000 μg/ml) and reaction time

(30–120 min). The resultes indicated that a GITC concentration of 200 μg/ml and a reaction time of 60 min gave the maximum coulometric response for fenoldopam enantiomers. The diastereomeric thiourea derivatives formed were then analyzed by reversed-phase HPLC–ED. Coulometric detection utilized three electrodes in series so that the catechol moiety of the derivatized analyte would undergo a series of oxidation and reduction reactions (oxidation, reduction, oxidation), with final measurement in the oxidized form. These series of electrochemical reactions can provide additional selectivity for compounds which undergo reversible electrochemical reactions. The use of this technique was necessary in this instance to remove a large negative signal arising from excess of reagent that eluted near the analytes, and to increase the overall sensitivity of detection. The use of narrow-bore HPLC columns (2 mm I.D.) also provided enhanced sensitivity for the detection of GITC-derivatized (*S*)- and (*R*)-fenoldopam.

Typical chromatograms of extracts from a drug-free human plasma sample and a plasma sample obtained from a human subject who had received racemic fenoldopam by intravenous infusion are shown in Fig. 2. The diastereomeric products were well resolved and the retention times were highly reproducible. The assignment of the chromatographic peaks as the diastereomers of (*S*)- and (*R*)-

fenoldopam was accomplished by separate GITC derivatization and chromatographic analysis of standard solutions of the pure S- and R-enantiomers. Endogenous plasma components did not interfere with the quantification of (S)- and (R)-fenoldopam or the internal standard over the plasma concentration range 0.5–50 ng/ml. The recoveries of fenoldopam and the internal standard from plasma was determined previously using the racemic compounds and found to be 89.7 ± 2.96% and 93.4 ± 5.95%, respectively [5]. Recovery of the individual S- and R-enantiomers of fenoldopam from plasma was not conducted owing to non-availability of the pure diastereomers. As the reaction of fenoldopam with GITC was essentially complete, as judged by the disappearance of fenoldopam from the reaction medium, the recovery through the total method was also high. Using 1 ml of plasma, the limit of determination for both (S)- and (R)-fenoldopam in human plasma samples was 0.5 ng/ml (signal-to-noise ratio = 4). There was, however, an interfering chromatographic signal which overlapped as a trailing shoulder on the (S)-fenoldopam peak, and which prevented determination at levels below 0.5 ng/ml. Linear responses of the peak-height ratio of (S)- and (R)-fenoldopam to the internal standard were observed with concentrations of analyte ranging from 0.5 to 50 ng/ml. Correlation coefficients obtained using weighted $(1/y)$ linear regression analysis were typically 0.999.

Results of a 3-day validation study are given in Table I for both enantiomers. The intra-day precision of the method was indicated by the mean of the daily R.S.D. The inter-day precision of the method was indicated by the R.S.D. of the daily means. The inter-day R.S.D.s of the method were also calculated by analysing two pools of quality control plasma samples spiked with 2 and 20 ng/ml of each of (S)- and (R)-fenoldopam over a period of 12 days. The inter-day R.S.D.s, from the analysis of these samples, were found to be 12.1 and 11.7% for (S)-fenoldopam and 16.8 and 11.7% for (R)-fenoldopam, respectively. The mean accuracy of the method, as indicated by the ratio of the actual to theoretical concentration, is also shown in Table I.

In conclusion, we have described a sensitive HPLC–ED method for the determination of (S)- and (R)-fenoldopam in human plasma samples. The limit of determination using 1-ml plasma samples was 0.5 ng/ml for each individual enantiomer. The assay was linear in response over the range 0.5–50 ng/ml. The method was sufficiently sensitive, accu-

TABLE I

ACCURACY AND PRECISION DATA FOR (S)- AND (R)-FENOLDOPAM IN PLASMA

Parameter	Concentration in plasma (ng/ml)					
	0.5 ng/ml		5 ng/ml		50 ng/ml	
	(S)	(R)	(S)	(R	(S)	(R)
R.S.D. (%):						
Day 1	16.5	5.7	3.0	6.1	7.1	6.7
Day 2	15.9	17.9	4.5	4.8	6.8	8.8
Day 3	19.8	6.2	8.0	7.7	6.9	6.8
Error (%)[a]:						
Day 1	−4.0	+26,0	+12.4	+14.0	+10.9	+8.5
Day 2	+14.0	+4.0	+25.8	+14.8	−4.4	−5.3
Day 3	+14.0	+16.0	+8.8	+10.8	+3.9	+6.8
Inter-day R.S.D. (%)[b]	9.3	9.5	7.7	1.9	7.4	7.3
Intra-day R.S.D. (%)[c]	17.4	9.9	5.2	6.2	6.9	7.4
Mean accuracy (%)	106.4	116.2	111.8	104.2	108.9	111.2

[a] [(Calculated concentration − actual concentration)/actual concentration] × 100.
[b] R.S.D. values of daily means.
[c] Mean of the daily R.S.D. values.

rate and precise to support pharmacokinetic studies on (*S*)- and (*R*)-fenoldopam in human subjects. Using this method, plasma concentrations of (*S*)- and (*R*)-fenoldopam could be measured for up to 4 h following intravenous administration of racemic fenoldopam, sufficient to characterize the intravenous pharmacokinetics of fenoldopam diastereomers.

REFERENCES

1 R. M. Stote, J. W. Dubb, R. G. Familiar, B. B. Erb and F. Alexander, *Clin. Pharmacol. Ther.*, 34 (1983) 309.
2 H. O. Ventura, F. H. Messerli, E. D. Frohlich, I. Kobrin, W. Oigman, F. G. Dunn and R. M. Carey, *Circulation*, 69 (1984) 11142.
3 D. M. Ackerman, A. L. Blumberg, J. P. McMafferty, S. S. Sherman, J. Weinstock, C. Kaiser and B. Berkowitz, *Fed. Proc. Fed. Am. Soc. Exp. Biol.*, 42 (1983) 186.
4 V. K. Boppana, F. C. Heineman, R. K. Lynn, W. C. Randolph and J. A. Ziemniak, *J. Chromatogr.*, 317 (1984) 463.
5 V. K. Boppana, K. M. Dolce, M. J. Cyronak and J. A. Ziemniak, *J. Chromatogr.*, 487 (1989) 385.
6 V. K. Boppana, K. L. Fong, J. A. Ziemniak and R. K. Lynn, *J. Chromatogr.*, 353 (1986) 231.
7 V. K. Boppana, R. K. Lynn and J. A. Ziemniak, *J. Pharm. Sci.*, 78 (1989) 127.
8 N. Nimura, H. Ogura and T. Kinoshita, *J. Chromatogr.*, 202 (1980) 375.
9 A. J. Sedman and J. Gal, *J. Chromatogr.*, 278 (1983) 199.
10 N. Nimura, Y. Kasahara and T. Kinoshita, *J. Chromatogr.*, 213 (1981) 327.
11 T. Kinoshita, Y. Kasahara and N. Nimura, *J. Chromatogr.*, 210 (1981) 77.

By-products in the derivatization of amines with the chiral reagent 2,3,4,6-tetra-O-acetyl-β-D-glucopyranosyl isothiocyanate and their elimination

Martin Ahnoff*, Karin Balmér and Yvette Lindman

Bioanalytical Chemistry, Astra Hässle AB, S-431 83 Mölndal (Sweden)

ABSTRACT

The formation of the desired diastereomeric thiourea derivatives did not proceed quantitatively when β-adrenoceptor blocking drugs were allowed to react with 2,3,4,6-tetra-O-acetyl-β-D-glucopyranosyl isothiocyanate (GITC). A competing reaction caused losses, which increased with increasing excess of the reagent (decreasing relative amounts of amine), amounting to as much as 50%. Measurements indicate that the by-products were due to an impurity in the commercial reagent, but also in GITC produced in-house from the corresponding bromide. The side-reaction could be completely eliminated by pretreatment of the reagent solution with a limited amount of another amine. Similar observations of a reactive impurity were made with the chiral reagent α-methylbenzyl isothiocyanate.

INTRODUCTION

Isothiocyanate reagents have been used in peptide sequencing [1] and for amino acid analysis. A number of chiral isothiocyanate reagents have been used as derivatization reagents for the liquid chromatographic separation of amine enantiomers. Neomenthyl isothiocyanate was introduced by Nambara *et al.* [2] and 2,3,4,6-tetra-O-acetyl-β-D-glucopyranosyl isothiocyanate (GITC) and 2,3,4-tri-O-acetyl-α-D-arabinopyranosyl isothiocyanate (AITC) were introduced by Nimura and co-workers [3,4]. GITC has been used for the separation of enantiomers of β-adrenoceptor blocking drugs and related substances [5,6]. α-Methylbenzyl isothiocyanate [7], 1-(1-naphthyl) and 1-(2-naphthylethyl) isothiocyanate [8] and N-fluorenylmethoxycarbonyl-L-*p*-isothiocyanophenylalanine [9] have also been used as chiral derivatization reagents. The typical use of these reagents, including GITC, has been in the assessment of the enantiomeric composition of chiral amines, but applications to the quantitative determination of enantiomers over a wide concentration range have also been reported [5,8,10–12]. Initial attempts in

our laboratory to apply derivatization with GITC to β-blockers in biological samples showed unexpected results and promted us to carry out the present investigation.

EXPERIMENTAL

Chemicals

Metoprolol racemate, (R)-(+)-metoprolol, alprenolol, atenolol, propranolol and H 170/37 (N-isopropylamino-2-propanol) were obtained from Organic Chemistry, Astra Hässle (Mölndal, Sweden). GITC was obtained from Polyscience (Warrington, PA, USA) or was synthesized from 2,3,4,6-tetraacetylglucopyranosyl bromide (acetobromoglucose), obtained from Fluka (Buchs, Switzerland). L-α-Methylbenzyl isothiocyanate (MBITC) was from K&K (Costa Mesa, CA, USA) and (R)-α-methylbenzyl isocyanate (MBIC) from Aldrich (Steinheim, Germany). 2,3,4,6-Tetraacetylglucopyranosyl isocyanate (GIC) was synthesized analogously to GITC [3].

Liquid chromatography

The liquid chromatograph consisted of a Beck-

man 110A pump, a Rheodyne Model 7125 loop injector with a 5-μl loop, a 100 mm × 4.6 mm I.D. column packed with 3-μm octadecylsilica particles (Nucleosil 120-3 C_{18}, Macherey–Nagel, Düren, Germany), a Spectra-Physics SpectraChrom 100 UV detector and a Perkin-Elmer LS-4 spectrofluorimetric detector coupled in series and two Spectra-Physics Model 4270 integrators. Mixtures of acetonitrile and ammonium acetate buffer (50 mmol/l, pH 6.0) were used as mobile phases (see Table I). UV absorbance was measured at 228 nm. The same wavelength was used for fluorescence excitation, while emission was measured at 306 nm (342 nm for propranolol).

Liquid chromatography–mass spectrometry

A Finnigan MAT (San José, CA, USA) TSQ-70 mass spectrometer with a TSP-1 thermospray interface was used. The vaporizer and ion source temperature settings were 100 and 250°C, respectively. The repeller potential was +50 V for positive ions and −50 V for negative ions. Samples (100 μl) were separated on the same column and with the same mobile phase mixtures that were used for UV and fluorescence detection.

Procedures

Solutions of β-blockers (0.50 mmol/l in acetonitrile) were prepared either by direct dissolution of the free base in acetonitrile or by extraction of an aqueous alkaline solution of the salt with diethyl ether–dichloromethane (4:1, v/v), solvent evaporation and reconstitution in acetonitrile. Derivatization was carried out at room temperature by mixing the β-blocker, reagent and triethylamine, all dissolved in acetonitrile. The reaction time was 20 min for GITC, GIC and MBIC and 3 h for MBITC.

RESULTS AND DISCUSSION

Structural formulae of GITC, metoprolol and propranolol and its thiourea derivative are shown in Fig. 1.

Chromatography of reaction products: UV and fluorescence detection

When metoprolol racemate (0.02–10 mmol/l) was allowed to react with GITC (10 mmol/l) in the presence of triethylamine (TEA, 11 mmol/l), the reac-
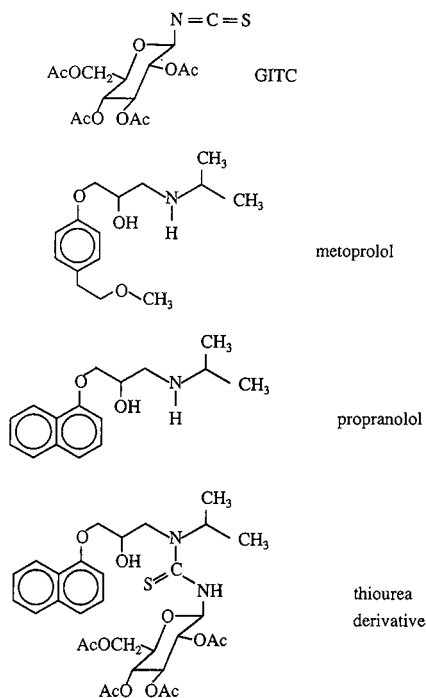

Fig. 1. Structural formulae. Ac = Acetyl.

tion was complete within 10 min at room temperature. Fluorescence detection revealed two pairs of peaks. Derivatization of pure (R)-(+)-metoprolol showed that the last-eluted peak in each pair was a product of this enantiomer. Two pairs of peaks were also obtained from racemates of alprenolol, atenolol and propranolol. Table I lists the retention data for these products.

Fig. 2 shows UV and fluorescence recordings of the separation of the products of propranolol. In comparison with the UV signal, the fluorescence signal was one order of magnitude higher for products X than products D from propranolol. For metoprolol the difference in the fluorescence to UV signal ratio was even greater, and for reactions with low concentrations of β-blocker it was difficult to determine both types of products with the same detector.

Formation of products X and D under various reaction conditions.

When equimolar concentrations (10 mmol/l) of metoprolol and GITC were allowed to react in the presence of TEA, the portion of derivatives X_1 and

TABLE I

SEPARATION OF REACTION PRODUCTS OF FOUR β-BLOCKERS DERIVATIZED WITH GITC

Stationary phase: Nucleosil 120-3 C_{18}. Mobile phase: 30–55% (v/v) acetonitrile in ammonium acetate buffer (pH 6) (0.050 mol/l).

Compound	Acetonitrile (%)	Capacity factor		α	Capacity factor		α
		X_1	X_2		D_1	D_2	
Atenolol	30	5.36	7.18	1.34	19.77	27.74	1.40
Metoprolol	45	6.32	8.38	1.33	15.95	21.64	1.36
Propranolol	55	5.25	6.42	1.22	10.05	12.86	1.28
Alprenolol*	55	6.05	6.92	1.14	11.20	14.03	1.25

X_2 was small. When the added concentration of metoprolol was lowered from 10 to 0.10 mmol/l, the amount of derivatives X_1 and X_2 decreased only slightly, whereas the amount of derivatives D_1 and D_2 decreased more than in proportion to the added metoprolol concentration, so that a straight line fitted to these data had an intercept at about 0.05

mmol/l (Fig. 3). At even lower levels, the amount of X_1 and X_2 formed tended to be proportional to metoprolol, whereas the slope of the D_1 and D_2 curves was lower (*i.e.*, the yield was lower) than at higher levels.

Further, when the added metoprolol concentration was held constant at 0.40 mmol/l and the GITC concentration was increased from 10 to 40 mmol/l (25–100-fold molar excess), the amount of X_1 and X_2 formed increased. The same experiment with 0.040 mmol/l of metoprolol (250–1000-fold molar excess of GITC) gave a more or less constant amount of X_1 and X_2 (Fig. 4).

The findings can be explained by the presence of a reactive impurity in the GITC reagent. The observation that the amounts of the products X_1 and X_2 follow the GITC concentration except for low levels of metoprolol could then be explained by the limited amount of the impurity, together with its much higher reactivity. Thus the impurity will be depleted by the reaction with metoprolol except for very low levels of the latter.

Determination of the amount of reactive impurity in GITC

UV chromatograms of the GITC reagent, recorded using the conditions in Table I (45% acetonitrile), were of little value for detecting the impurity. Preparative chromatography of the impurity was considered difficult also because of its reactivity. Therefore, its presence and properties had to be measured indirectly, via the formation of the products X_1 and X_2.

For the first estimation we make the assumption that X and D are the only reaction products and,
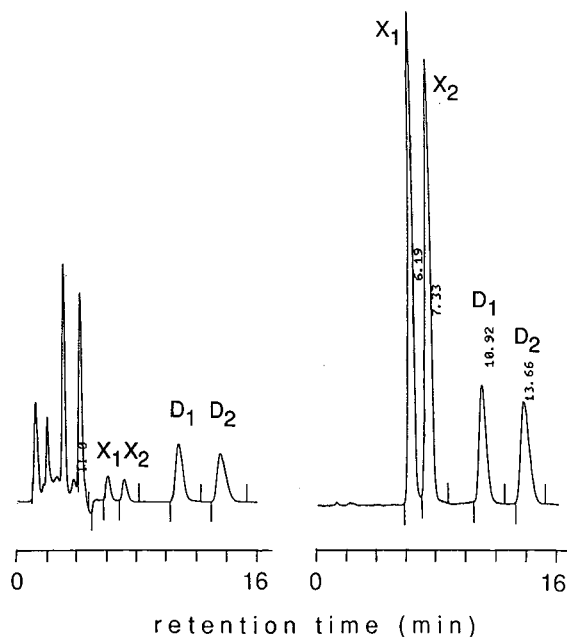

Fig. 2. Separation of products of (*S*)- and (*R*)-propranolol reacted with GITC (0.56 m*M* propranolol racemate, 4 m*M* GITC and 110 m*M* triethylamine in acetonitrile, 20 min at room temperature). Chromatographic conditions as in Table I. Flow-rate, 1.0 ml/min. Left, UV detection (228 nm); right, fluorescence detection (excitation at 228 nm, emission at 342 nm).
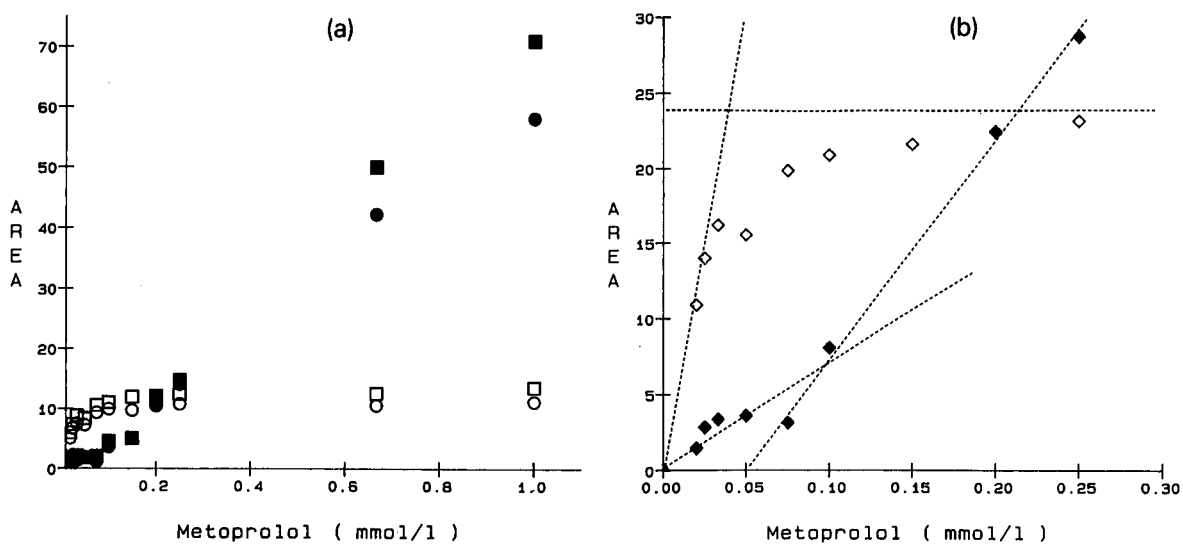
Fig. 3. (a) Amounts of products X and D, measured as fluorescence peak areas, obtained from various amounts of metoprolol racemate (added concentration 0.01–1.0 mmol/l) after rection with GITC (10 mmol/l). $\bigcirc$ = Peak X_1 [by-product from (S)-metoprolol]; $\square$ = peak X_2 [by-product from (R)-metoprolol]; $\bullet$ = peak D_1 [main product from (S)-metoprolol]; $\blacksquare$ = D_2 [main product from (R)-metoprolol]. (b) Expanded plot for low concentrations of metoprolol showing peak areas for ($\Diamond$) X_1 + X_2 and ($\blacklozenge$) D_1 + D_2. Fluorescence excitation and emission wavelengths, 228 and 306 nm, respectively. Chromatographic conditions as in Table I.
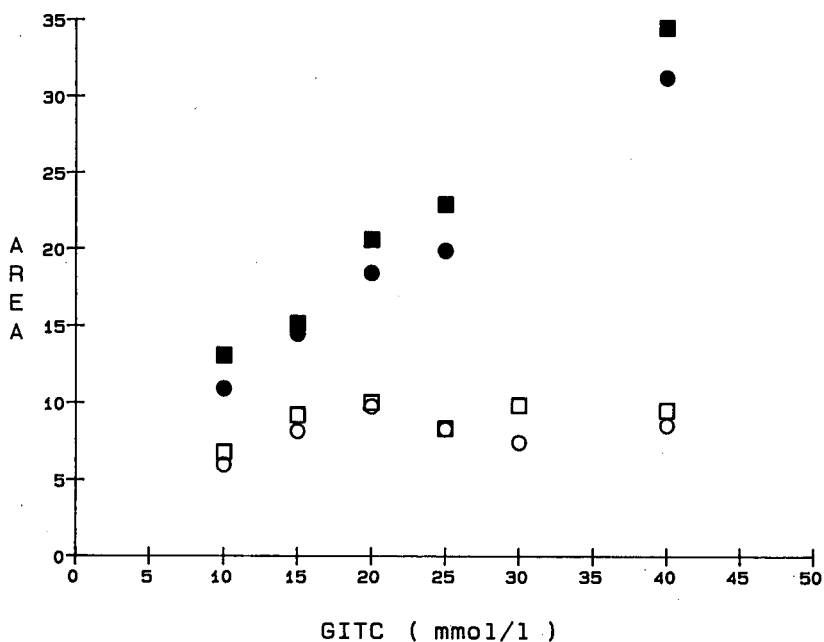
Fig. 4. Amounts of by-product X, measured as fluorescence peak area, obtained from metoprolol racemate after reaction with various amounts of GITC (10–40 mmol/l). ($\bigcirc$) (S)- and ($\square$) (R)-metoprolol 0.04 mmol/l; ($\bullet$) (S)- and ($\blacksquare$) (R)-metoprolol 0.40 mmol/l.

consequently, the sum of their yields is quantitative as long as no unreacted metoprolol is detected. Then the more or less constant level of X for higher concentrations of metoprolol correspond to a loss (z_0) of the main product D, so that peak heights for D (y) *versus* metoprolol concentration (z) follow the relationship.

$$y = k(z - z_0)$$

In Fig. 3, the intercept z_0 can be estimated to be 0.050 ± 0.025 mmol/l. Hence the original concentration of the reactive impurity in GITC would be about 0.050 mmol/l, which is 0.5% of the added GITC concentration, 10 mmol/l.

A second estimation of the amount of reactive impurity can be made from results for low levels of metoprolol, below 0.050 mmol/l. Here, the slopes of the area *versus* concentration curves for X and D as they approach the origin can be estimated. The slope for D is roughly half of the slope for higher concentrations, corresponding to a recovery of about 50% for D. This would imply that the recovery of X at low levels also is about 50% of added metoprolol. The difference in slope for X and D reflects the difference in molar fluorescence response, which would then be about eight times higher for the products X. Now, the constant level of X for high concentrations of added metoprolol can be quantified by dividing peak areas for X by eight and comparing them with the response for D at high levels of added metoprolol. This gives a value of about 0.025 mmol/l, which is lower but still of the same order as the first estimate. To explain why the recoveries of the products X and D are both about 50% at low levels of metoprolol, the impurity must be over two orders of magnitude more reactive than GITC itself under the reaction conditions used.

Avoiding formation of by-products X

It should be possible to remove a small but highly reactive impurity by adding an amount of another amine to the reagent prior to derivatization. N-Isopropylamino-2-propanol (H 170/37) was chosen to check this. When 1 mmol/l of this amine was added to 10 mmol/l of GITC 1 min before metoprolol was allowed to react, only the products D_1 and D_2 were detected (Fig. 5), which is in accordance with our assumption.

Mass spectrometric investigation of reaction products

Propranolol was chosen for liquid chromatographic–mass spectrometric investigations owing to more favourable chromatographic separation of the derivatives from other sample components, especially GITC. The mass spectral fragmentation pattern was also more favourable than for metoprolol and its derivatives. The products D_1 and D_2 gave similar positive-ion mass spectra, one of which is shown in Fig. 6. A molecular ion was not observed, but the ions at m/z 260 and 407, which also are present in the mass spectra of propranolol (M + 1) and GITC (M + 18) confirmed that these peaks were from the thiourea derivatives of GITC and propranolol. X_1 and X_2 gave positive ions at m/z 633 and negative ions at m/z 631, suggesting a molecular weight of 632, which is 16 mass units lower than that of the proper GITC derivatives. A positive ion at m/z 260 showed that the propranolol fragment was present.
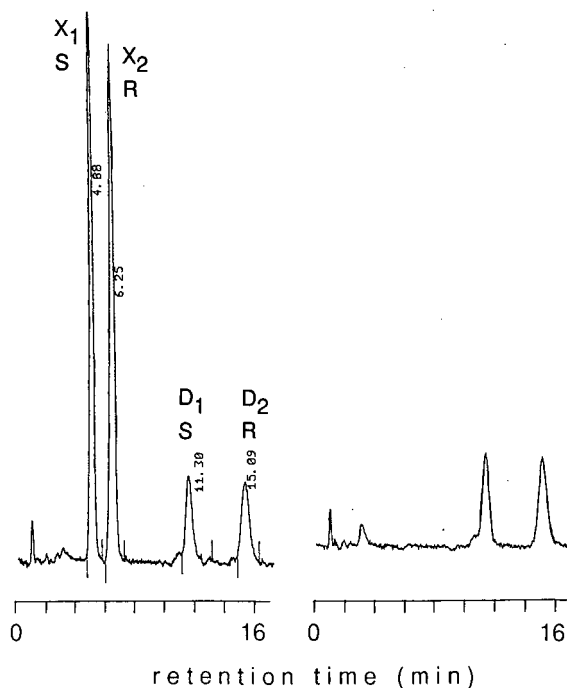

Fig. 5. Separation and fluorescence detection of metoprolol racemate reacted with GITC (0.98 mM metoprolol, 9.8 mM GITC and 10.9 mM triethylamine in acetonitrile). Right: 1.0 mM amine (H 170/37) was added to the reaction mixture 1–2 min before metoprolol was added. Excitation at 228 nm, emission at 306 nm. Chromatographic conditions as in Table I.
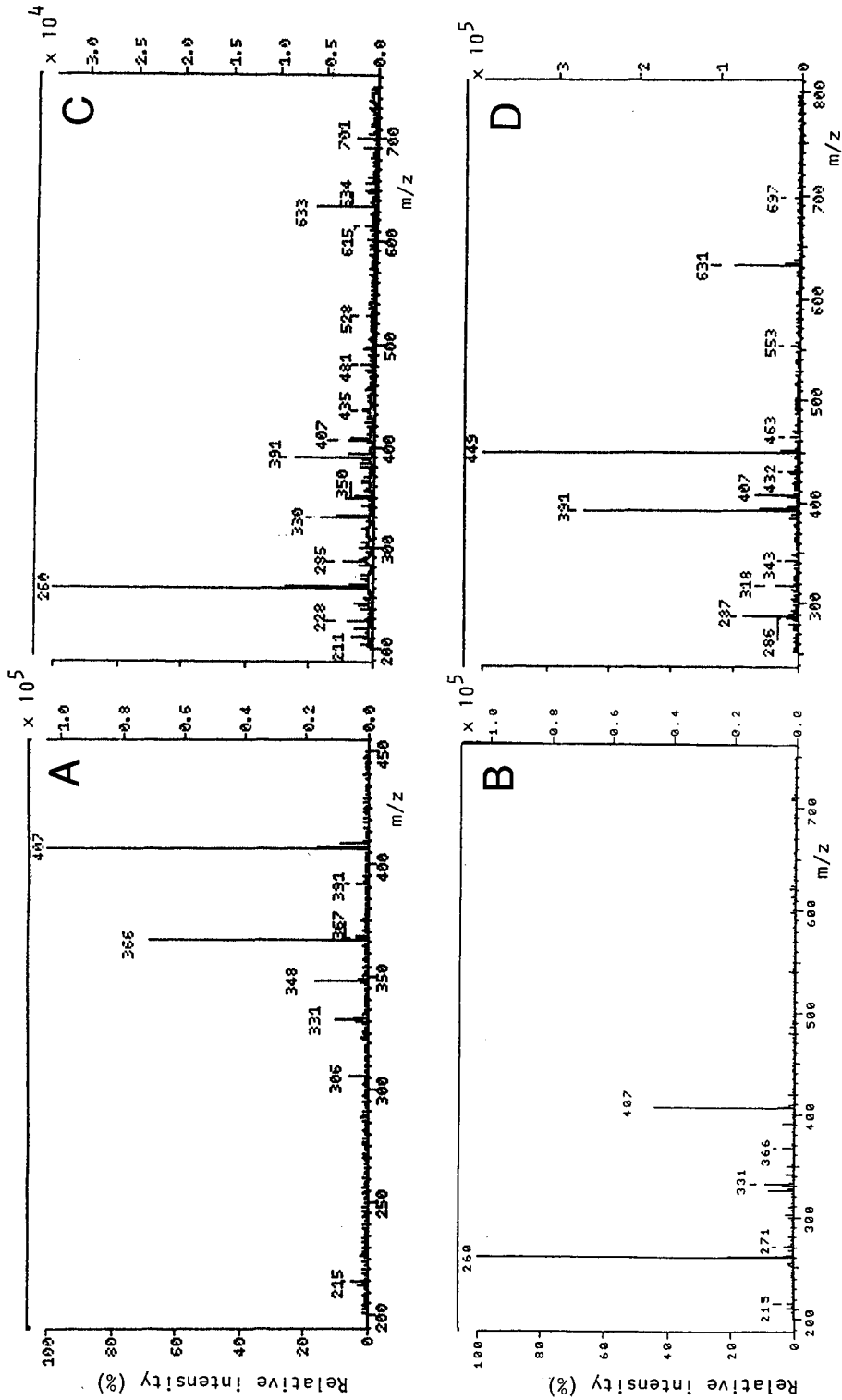
Fig. 6. Thermospray mass spectra of GITC and reaction products with propranolol. Samples (100 μl) of GITC solution (0.50 mmol/l) or reaction mixture (0.17 mM propranolol, 6 mM GITC and 82 mM triethylamine) were separated on an octadecylsilica column (see Table I and Experimental for details). (A) GITC, positive ions; (B) product D₁, positive ions; (C) product X₂, positive ions; (D) product X₂, negative ions. Right hand scales indicate absolute ion intensities (arbitrary units).

Testing possible GITC contaminants

Two substances were considered as possible contaminants of GITC, namely the corresponding bromide and isocyanate. The bromide was tested as a reagent but was found, as could be expected, not to react with β-blockers under the given experimental conditions. The isocyanate was produced from the bromide by reaction with silver cyanate, in analogy with the synthesis of GITC [3]. It was found to react faster than GITC with metoprolol. The diastereomeric derivatives eluted earlier than the GITC derivatives and close to the derivatives X_1 and X_2. They also exhibited fluorescence of similar intensity to X_1 and X_2, but they were eluted as a single peak instead of two separate peaks, and therefore could not be identical with X_1 and X_2. Further, the isocyanate had limited stability in acetonitrile, as opposed to the reactive impurity in GITC.

Reactive impurity in α-methylbenzyl isothiocyanate

α-Methylbenzyl isothiocyanate was studied to see whether a similar competing reaction occurred. When propranolol racemate was allowed to react with this reagent, a pair of peaks was observed and, in addition, one peak with a retention roughly half that of the other two peaks. This peak disappeared when the reagent (13.5 mmol/l) was treated with an amine (H 170/37, 1.7 mmol/l) before propranolol was added. When the isothiocyanate reagent was replaced with the corresponding isocyanate, propranolol racemate gave one peak instead of three. Its retention was virtually the same as that for the early-eluting peak from the isothiocyanate reagent. Also, the fluorescence yield was similar. A chromatogram of the isothiocyanate reagent alone showed a small peak which coincided with that of the isocyanate. However, no final proof was obtained for the identity of the impurity in the α-methylbenzyl isothiocyanate reagent.

CONCLUSION

Derivatization of β-blockers with commercial or in-house prepared GITC and separation of the re-

action products gives two pair of peaks, one pair originating from the expected diastereomeric thiourea derivatives. The products seen as the other two peaks appear to be closely related to the thiourea derivatives, but remain to be identified. With a large excess (250-fold or more) of the reagent, the yield of both types of derivatives was similar, about 50%. With a decreasing excess of reagent, the relative yield of the unidentified products decreased, favouring the formation of the proper thiourea derivatives. The formation of the unidentified products can be avoided by treating the reagent with another amine prior to derivatization. The unidentified products exhibit stronger fluorescence than the thiourea derivatives, which would make them attractive for analytical applications. Identification of their chemical structure might lead to a new chiral reagent that could be an interesting alternative to GITC.

REFERENCES

1 P. Edman, *Acta Chem. Scand.*, 4 (1950) 283.
2 T. Nambara, S. Ikegawa, M. Hasegawa and J. Goto, *Anal. Chim. Acta*, 101 (1978) 111.
3 N. Nimura, H. Ogura and T. Kinoshita, *J. Chromatogr.*, 202 (1980) 375.
4 N. Nimura, Y. Kasahara and T. Kinoshita, *J. Chromatogr.*, 213 (1981) 327.
5 T. Walle, D. D. Christ, U. K. Walle and M. J. Wilson, *J. Chromatogr.*, 341 (1985) 213.
6 J. Gal, *J. Liq. Chromatogr.*, 9 (1990) 673.
7 J. Gal and A. J. Sedman, *J. Chromatogr.*, 314 (1984) 275.
8 J. Gal, D. M. Desai and S. Meyer-Lehnert, *Chirality*, 2 (1990) 43.
9 J. S. Davies and A. K. A. Mohammed, *J. Chem. Soc., Perkin Trans. 2*, (1984) 1723.
10 D. Schuster, M. Woodruff Modi, D. Lalka and F. M. Gengo, *J. Chromatogr.*, 433 (1988) 318.
11 E. J. Eisenberg, W. R. Patterson and G. C. Kahn, *J. Chromatogr.*, 493 (1989) 105.
12 S. E. Rose and E. J. Randinitis, *Pharm. Res.*, 8 (1991) 758.

Reversed retention order and other stereoselective effects in the separation of amino alcohols on Chiralcel OD

Karin Balmér*, Per-Olof Lagerström and Bengt-Arne Persson

Bioanalytical Chemistry, Astra Hässle AB, S-431 83 Mölndal (Sweden)

Göran Schill

Department of Analytical Pharmaceutical Chemistry, University of Uppsala, S-751 23 Uppsala (Sweden)

ABSTRACT

The enantioselective resolution of a series of amino alcohols on Chiralcel OD was studied with respect to the effect of temperature, alcohol additive and water content in a mobile phase of hexane with added diethylamine. The chain length between the hydroxy and the amino groups in the solutes had a considerable influence on the stereoselectivity. For one of the amino alcohols a reversal of the retention order between the antipodes was obtained by varying the above parameters. The amino alcohols are retained by at least two chiral sites, one of which is highly dependent on hydrogen bonding. This bonding ability can be directly controlled by the water content of the mobile phase.

INTRODUCTION

The chiral stationary phase Chiralcel OD contains cellulose tris(3,5-dimethylphenylcarbamate) as a selector coated onto a macroporous silica gel [1]. It has been successfully used in liquid chromatography for the chiral separation of racemic drugs such as a series of amino alcohol derivatives with β-adrenergic blocking activity [2–5].

The chiral recognition is assumed to be due to the formation of inclusion complexes [6] and binding to the polar carbamate groups. The carbamate groups interact with the solute by hydrogen bonding with NH and C=O and dipole–dipole bonding to the C=O moiety [7–9]. The hydroxyl group of the amino alcohol seems to be of importance for the chiral recognition process. The retention and stereoselective effect of the Chiralcel OD column can be influenced by hydrogen bonding modifiers added to the mobile phase [4,5].

The chiral separations are mainly performed with mobile phases containing an alkane, such as hexane, and a lower alcohol. The presence of a small amount of an amine such as diethylamine is needed to improve the peak shape when the solutes are primary or secondary amines [1]. The alcohol additives have a low water content and it has been found that controlling the water content is essential for the optimization of the chiral resolution [10].

This paper reports the effects of the chromatographic conditions, mainly alcohol and water content in the mobile phase and temperature, on the stereoselectivity of Chiralcel OD for amino alcohols related to metoprolol. A model for the chiral recognition is suggested which is based on the assumption of two stereoselective binding sites and a specific effect of water on one of these sites.

EXPERIMENTAL

Chemicals

Metoprolol, H 170/31 and H 170/40 as tartrates, *R*- and *S*-metoprolol as sorbates and H 170/64 were obtained from Organic Chemistry, Astra Hässle AB.

Hexane, 2,2,4-trimethylpentane, propan-2-ol and dichloromethane (HPLC grade), were from Rathburn (Walkerburn, UK), ethanol from Kemetyl (Stockholm, Sweden), propan-1-ol and butan-1-ol from E. Merck (Darmstadt, Germany), butan-2-ol, tertiary butanol and diethylamine from Fluka (Buchs, Switzerland) and diethyl ether from May & Baker (Dagenham, UK). A Milli-Q system (Millipore, Molsheim, France) was used to supply the water.

Instrumentation

The liquid chromatographic system consisted of an LKB 2150 pump (Bromma, Sweden), a Varian 9095 autosampler (Walnut Creek, CA, USA) and a Jasco 821 FP fluorescence detector (Tokyo, Japan) operated at 272 nm (excitation) and 306 nm (emission). A thermostated bath (Lauda RMS, Königshofen, Germany) controlled the water temperature in the column jacket. The chromatograms were recorded on an SP 4400 integrator (Spectra Physics, San Jose, CA, USA). A Metrohm 684 KF Coulometer (Herisau, Switzerland) was used to measure the water content of the mobile phase.

The analytical column (250 × 4.6 mm) was a Chiralcel OD column from Daicel Chemical Industries (Tokyo, Japan), which was used with flow-rates of 0.5–1.0 ml/min at 30°C, unless stated otherwise. The mobile phase contained hexane or 2,2,4-trimethylpentane with the addition of water and various alcohols in the concentrations given for each experiment. All the mobile phases contained 10 mmol/l diethylamine. The mobile phase was prepared in portions of 500 ml and was recirculated during the run. Most of the studies were performed on two different columns to confirm the validity of the observed effects.

Test solutions

Standard solutions of the substances were made up in 0.01 M hydrochloric acid. Test solutions in the organic mobile phase were prepared from alkaline standard solutions by extraction with diethylether–dichloromethane (4:1). After phase separation (freezing of the aqueous phase) and evaporation of the organic phase under nitrogen, the amines were dissolved in the mobile phase. Metoprolol was available in enantiomeric forms. Enantiomers of the other substances were obtained by separation on the

Chiralcel OD column. The absolute configuration was not known. The injected solutions had a concentration between 1 and 10 μmol/l (20-μl injection).

Calculation

The parameters used in the evaluation of retention and stereoselectivity are the capacity factor, k', and the separation factor, α.

$$k' = (t_R - t_0)/t_0$$

$$\alpha = k'_S/k'_R$$

where t_R is the retention time in minutes, and t_0 is the retention time for the interstitial volume (2.5 ml); this was measured for toluene which was assumed to be unretained on the column.

RESULTS AND DISCUSSION

Alcohol modifier

The alcohol additive can affect the retention of the hydrogen bonding solutes in different ways: by improving the solvation in the mobile phase and by competing for the hydrogen bonding sites in the stationary phase. The solutes examined in this study contain amine or hydroxyl groups which can form hydrogen bonds. Their structures are summarized in Fig. 1. Metoprolol, H 170/31 and H 170/40 are closely related and differ only in the length of the carbon chain between the hydroxyl and the amino groups. H 170/64 has no amine function.

The influence of the concentration of propan-1-ol on the stereoselectivity of the column is shown in Fig. 2. Water and diethylamine, which can also

O-CH$_2$-CH(OH)-(CH$_2$)$_n$-R$_1$

CH$_2$-CH$_2$-O-CH$_3$
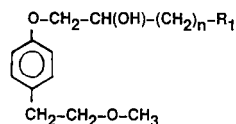
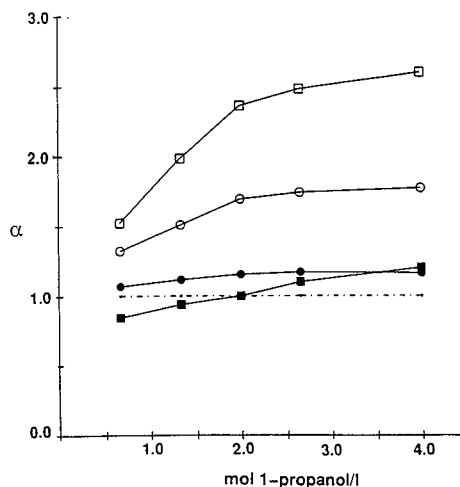| Substance	n	R$_1$
Metoprolol	1	NH–CH(CH$_3$)$_2$
H 170/31	2	"
H 170/40	3	"
H 170/64	4	H

Fig. 1. Structures of the solutes.

Fig. 2. Influence of propan-1-ol concentration on stereoselectivity. Mobile phase: propan-1-ol, 10 mmol/l diethylamine, 0.8 g/l water in hexane. Temperature, 30°C; flow-rate, 0.75 ml/min. □ = H 170/31; ○ = metoprolol; ● = H 170/64; ■ = H 170/40.

affect retention, were held at a constant concentration in the mobile phase. For the amino alcohols, increasing concentrations of propan-1-ol decrease the retention of all the enantiomers in a similar way. The first eluted antipode of each solute is affected to the same extent; an increase of the propan-1-ol content from 0.67 to 4.0 mol/l in the mobile phase decreased the retention by 76–78%. For metoprolol the R-enantiomer was eluted first and it is assumed that the same retention order was followed for the enantiomers of the other solutes.

The retention of the second elute antipode is affected to a different degree, resulting in a change in the stereoselectivity with the concentration of propan-1-ol. The influence of the chain length between the hydroxyl and the amine is remarkable; H 170/31 with a three-carbon chain shows the highest separation factors (α = 1.53–2.65) at all propan-1-ol concentrations, whereas H 170/40 with a four-
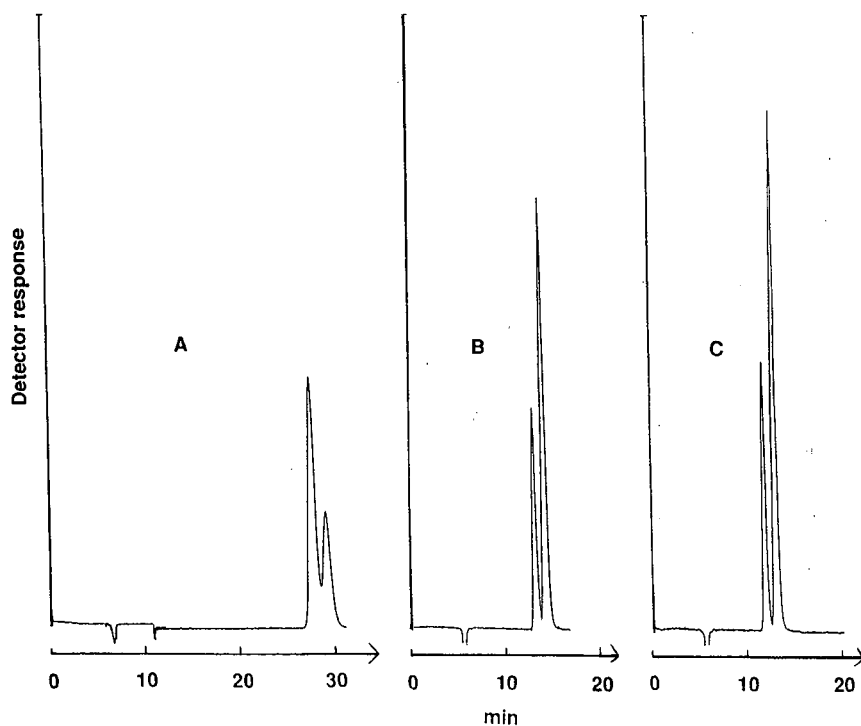

Fig. 3. Effect of propan-1-ol on the resolution of enantiomers of H 170/40. Mobile phase: 1 g/l water, 10 mmol/l diethylamine in hexane and propan-1-ol. Solutes: R- and S-enantiomers in the ratio 1:2. (A) 0.67 mol/l propan-1-ol (α = 0.94); (B) 1.33 mol/l (α = 1.13); (C) 2.0 mol/l (α = 1.17).

carbon chain shows low stereoselectivity and even a change of retention order between the enantiomers at an intermediate propan-1-ol concentration. An example is given in Fig. 3, which shows chromatograms at different propan-1-ol concentrations using samples that contained the *S*-enantiomer in an excess of 100%. The alcohol H 170/64 has a low separation factor but no reversal of the retention order with changes in alcohol content (Fig. 2).

These observations can be used to elucidate the retention processes. The strong influence of the length of the carbon chain might be due to steric effects, *e.g.*, in the binding to the cavities in the stationary phase. The reversal of the retention order indicates that at least two chiral sites take part in the binding and it seems that the binding effect of one of them, the *S*-antipode, is strongly affected when the concentration of propan-1-ol is changed. It is important to remember that the large change in propan-1-ol content will also change the distribution of water between the stationary and mobile phases and it has been observed earlier that a change in the water concentration can have a significant effect on the stereoselectivity of Chiralcel OD for amino alcohols [10]. A reversal of the elution order for the antipodes of 2-phenoxypropanoic methyl ester on changing the alcohol modifiers has also been observed on a Chiralcel OB column [8]. However, no attention was paid to the water content in this study.

The effects of different alcohol modifiers are shown in Table I. The concentrations of water and diethylamine were maintained at the same constant

level as in the previous experiments. The primary and secondary alcohols show rather limited differences in their effects on the retention of the first eluted enantiomer (*R*). In general, ethanol seems to give lower separation factors than the higher alcohols. The peak shape was good for all additives except tertiary butanol.

Water content

It has been emphasized that the water content of the mobile phase has a significant effect on the chiral resolution on the Chiralcel OD phase. This is seen in Fig. 4, which shows the retention of the enantiomers of H 170/40 at different water contents using a constant alcohol concentration. The *S*-enantiomer shows a decreasing value of k' with increasing water content, while k'_R seems to be almost unaffected. The effect of the water content is obvious in the range 0.1–1.0 g/l, but a higher water content does not influence the separation factors or chromatographic properties. For metoprolol, no shift of elution order is obtained as the enantiomers have too high a retention difference at low water contents. On increasing the water concentration, k'_S and the α-value decrease strongly, whereas k'_R is not influenced.

TABLE I

INFLUENCE OF THE ADDITION OF ALCOHOL ON RETENTION OF THE AMINO ALCOHOLS

Mobile phase, 1.33 mol/l alcohol, 10 mmol/l diethylamine, 0.8 g/l water in hexane. Temperature, 30°C; flow-rate, 0.75 ml/min.

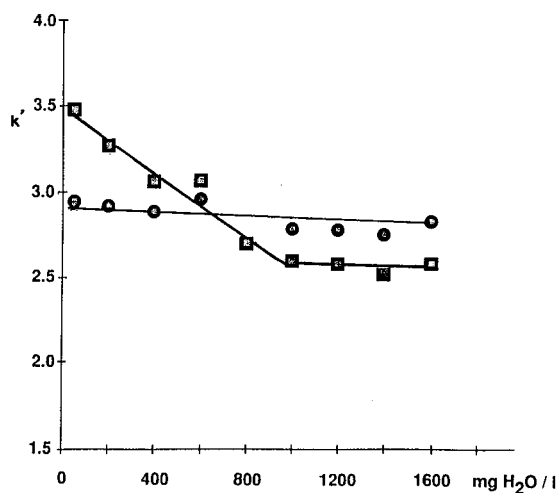| Alcohol	Metoprolol		H 170/31		H 170/40		H 170/64	
	k'_R	α	k'_1	α	k'_1	α	k'_1	α
Ethanol	1.11	1.43	1.42	1.96	1.97	1.04	1.20	1.11
Propan-1-ol	1.07	1.60	1.36	2.12	1.89	1.06	1.35	1.12
Butan-1-ol	0.94	2.15	1.16	2.37	1.77	1.10	1.35	1.14
Propan-2-ol	1.31	1.89	1.81	2.50	2.79	1.20	1.38	1.34
Butan-2-ol	1.25	2.05	1.67	2.72	2.81	1.00	1.56	1.22
tert.-Butanol	2.20	2.16	2.47	2.14	4.37	1.00	2.06	1.25

Fig. 4. Influence of water on the enantiomers of H 170/40. Mobile phase: 1.0 mol/l propan-1-ol, 10 mmol/l diethylamine and water in hexane. Temperature, 30°C; flow-rate, 0.5 ml/min. ■ = *S*-Enantiomer; ● = *R*-enantiomer.
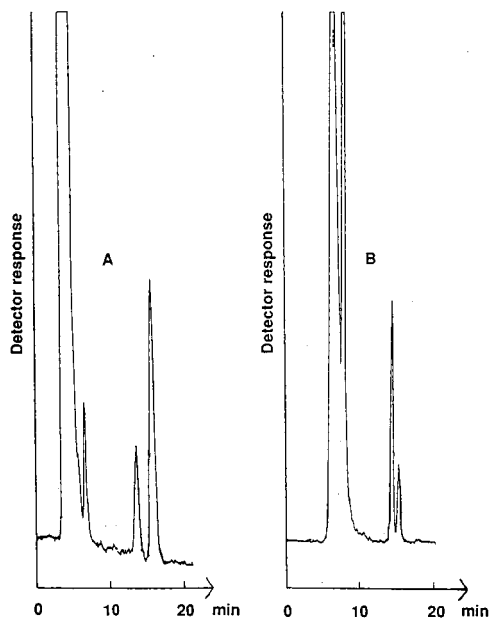
Fig. 5. Effect of temperature on the resolution of the enantiomers of H 170/40 on Chiralcel OD. Mobile phase: 1.0 mol/l propan-1-ol, 10 mmol/l diethylamine and 1 g/l water in 2,2,4-trimethylpentane. Solutes: R- and S-enantiomers in the ratio 2:1. (A) 15°C, flow-rate 1.0 ml/min; (B) 55°C, flow-rate 0.5 ml/min.

Temperature effect

A change in temperature can have a fairly strong effect on the stereoselective separation of amino alcohols on Chiralcel OD. An example is given in Fig. 5, which shows that the retention order for the enantiomers of H 170/40 is reversed when the temperature is changed from 15 to 55°C, if water is added to the mobile phase. 2,2,4-Trimethylpentane was used as the alkane component in the mobile phase to make it work at higher temperature. The injected samples contained the R-enantiomer in a 100% excess.

Van 't Hoff plots for the same substances in the temperature range 8–55°C are shown in Fig. 6. These plots show the highly significant effect of water on the stereoselectivity; a reversal of the retention order is only obtained in the presence of a higher water content. Under identical temperature conditions and across the shared temperature range, the overall reactions, as indicated by the capacity factor, are always less for the R-enantiomer than for the S-enantiomer.

The Gibbs free energy for the solute–stationary phase interaction, ΔG^0, is related to the natural logarithm of the capacity factor by

$$\ln k' = -\Delta G^0/RT + \Phi \qquad (1)$$

where R is the gas constant, T is the absolute temperature and Φ is the natural logarithm of the phase ratio in the column. The equation can be written with the appropriate enthalpy, ΔH^0, and entropy, ΔS^0, as
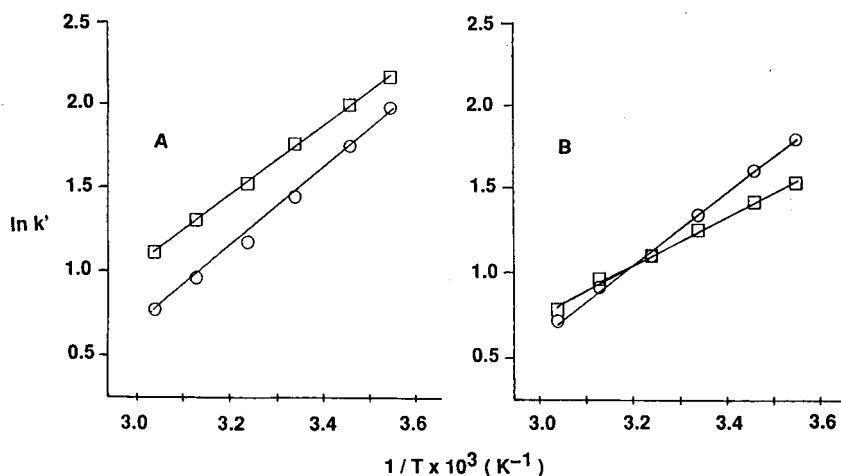

Fig. 6. Van 't Hoff plots for the enantiomers of H 170/40. Temperature range, 8–55°C. Mobile phase, 0.93 mol/l propan-1-ol, 10 mmol/l diethylamine in 2,2,4-trimethylpentane. Flow-rate, 0.5 ml/min. (A) No water added; (B) 1 g/l water added to the system. (□) S-Enantiomer; (○) R -enantiomer.

$$\ln k' = -\Delta H^0/RT + \Delta S^0/R + \Phi \qquad (2)$$

The enthalpy can be estimated from the slope of the Van 't Hoff plot. The values presented in Table II show that the water added to the mobile phase has a different influence on the enantiomers metoprolol, H 170/31 and H 170/40. For the R-antipode the decrease of the slope is fairly low and the change in $-\Delta H^0$ does not exceed 2.1 kJ/mol. The effect on the S-enantiomer is considerably larger and the decrease of $-\Delta H^0$ is in the range 5–8 kJ/mol. For the alcohol H 170/64, the water has about the same effect on both enantiomers.

Contributions of the enthalpy parameter to the enantioselectivity can only be inferred from the differences between values for the individual enantiomers. However, the results of the Van 't Hoff plots support the view that the amino alcohols rather than the alcohol are retained by two chiral sites. The effect of one of these sites seems to be due to hydrogen bonding as its binding ability is highly affected by water. This site has a significantly different influence on the R- and S-enantiomers.

Retention processes

The chiral selective stationary phase Chiralcel can be assumed to consist of different sites, as discussed above and suggested by Gaffney et al. [8]. Our studies on Chiralcel OD show changes in the separation factor, α, by varying the alcohol concentration, temperature or water content. These changes in selectivity also lead to changes in the retention order between the enantiomers of an amino alcohol

TABLE II

ENTHALPY ($-\Delta H^0$ kJ/mol) ESTIMATED FROM THE SLOPE OF VAN 'T HOFF PLOTS

Mobile phase, 0.93 mol/l propan-1-ol, 10 mmol/l diethylamine in 2,2,4-trimethylpentane. Temperature range, 8–55°C. (A) No water added; (B) 1 g/l water added to the system.

Amino alcohol	R-Enantiomer		S-Enantiomer	
	A	B	A	B
Metoprolol	8.6	8.6	15.4	10.1
H 170/31	13.8	12.6	26.4	18.4
H 170/40	19.7	17.6	17.5	12.1
H 170/64	13.6	12.4	14.3	13.0

when the separation factor is fairly low, as for H 170/40.

When the antipodes of a solute are retained by two different kinds of chiral sites, their effects can be illustrated by the partial capacity factors, k'_{S1} and k'_{R1} for one of the sites and k'_{S2} and k'_{R2} for the other. This gives the following expression for the separation factor:

$$\alpha = (k'_{S1} + k'_{S2})/(k'_{R1} + k'_{R2}) \qquad (3)$$

The effects of adding water and alcohol to the mobile phase can be characterized by a simplified retention model based on the following assumptions: (1) the water content in the mobile phase has an influence on the binding effect of only one of the chiral sites; (2) the alcohol has a direct influence on the retention of the enantiomers only by solvation in the mobile phase; and (3) the alcohol binds or solvates water in the mobile phase, thereby influencing the accessible (free) concentration of water. The solvation of water is temperature-dependent.

If the effect of water is due to Langmuir adsorption, the retention of the S-enantiomer can be expressed by

$$k'_S = qK_0K_S/[1 + K_{H_2O}(H_2O)_m] \qquad (4)$$

where q is the phase volume ratio, K_0 the total binding capacity of the site, K_S the binding constant for the solute, K_{H_2O} the binding constant for water and $(H_2O)_m$ the accessible water concentration in the mobile phase.

k' of the S-antipode decreases with increased water content (Fig. 4). The effect levels off at about 1000 mg/l of water, which supports the assumption of adsorption according to a Langmuir isotherm. For the R-antipode there is no significant effect of water, which indicates that the R-antipode is not retained by the site affected by water. Assuming that only k'_{S2} in eqn. 3 changes with the water content, whereas k'_{S1} and k'_{R1} are unchanged and k'_{R2} is negligible, a combination of eqns. 3 and 4 gives

$$\alpha = A + B/[1 + K_{H_2O}(H_2O)_m] \qquad (5)$$

where $A = k'_{S1}/k'_{R1}$ and $B = qK_0K_S/k'_{R1}$ are constant.

Eqn. 5 shows the prerequisites for the reversal of the retention order between the enantiomers. A must be less than 1 whereas $(A + B)$ must be greater than 1. α is controlled by A at high water content and

$(A + B)$ at low water contents. It must be emphasized that eqn. 5 is based on several simplified assumptions. The non-linear relationship between α and $(H_2O)_m$ makes a control of its quantitative validity difficult.

The alcohol in the mobile phase contributes to the transport of the solutes through the column. The elution strength is different for different alcohols, as can be anticipated (Table I), straight-chain alcohols being stronger eluents. An increased alcohol content gives a decreased retention of the solutes, as expected (Fig. 3). However, in a non-polar organic mobile phase, as in the systems studied here, the alcohol is responsible for solvation of the water in the mobile phase. The degree of complexation is dependent on the concentration and the nature of the alcohol. The extent of accessible of free water, $(H_2O)_m$, is a function of this and decreases with increased alcohol content. The effect of the alcohol concentration on the chiral selectivity is thus mediated through water. The influence of the structure of the alcohol on the enantioselectivity is more complex, but is probably related to the accessible water content.

The effect of temperature on the selectivity may be due to the influence on the chiral sites of the stationary phase. However, this effect might be mediated through the free water content by affecting the degree of solvation of water by the alcohol in the mobile organic phase.

CONCLUSIONS

The stereoselectivity of Chiralcel OD for amino alcohols related to metoprolol can be controlled by alcohol additives and the water content of the mobile phase in addition to temperature. For solutes with low separation factors it is even possible to achieve a reversal of the retention order. It has been shown that the amino alcohols are retained by at least two chiral sites. The binding ability of one of these is highly dependent on hydrogen bonding and its effect can be directly controlled by the water content of the mobile phase.

REFERENCES

1 Y. Okamoto, M. Kawashima, R. Aburatani, K. Hatada, T. Nishiyama and M. Masuda, *Chem. Lett.*, (1986) 1237.
2 D. R. Rutledge and C. Garrick, *J. Chromatogr.*, 497 (1989) 181.
3 A. M. Krstulovic, M. H. Fouchet, J. T. Burke, G. Gillet and A. Durand, *J. Chromatogr.*, 452 (1988) 477.
4 H. Y. Aboul-Enein and M. R. Islam, *Anal. Lett.*, 23 (1990) 83.
5 H. Y. Aboul-Enein and M. R. Islam, *J. Chromatogr.*, 511 (1990) 109.
6 I. W. Wainer, R. M. Stiffin and T. Shibata, *J. Chromatogr.*, 411 (1987) 139.
7 Y. Okamoto, M. Kawashima and K. Hatada, *J. Chromatogr.*, 363 (1986) 173.
8 M. H. Gaffney, R. M. Stiffin and I. W. Wainer, *Chromatographia*, 27 (1989) 15.
9 Y. Fukui, A. Ichida, T. Shibata and K. Mori, *J. Chromatogr.*, 515 (1990) 85.
10 K. Balmer, A. Persson, P.-O. Lagerström, B.-A. Persson and G. Schill, *J. Chromatogr.*, 553 (1991) 391.

(2*S*,3*S*)-Dicyclohexyl tartrate as mobile phase additive for the determination of the enantiomeric purity of (*S*)-atropine in tablets

Eva Heldin*, N. Hang Huynh and Curt Pettersson

Department of Analytical Pharmaceutical Chemistry, Biomedical Centre, Uppsala University, Box 574, S-751 23 Uppsala (Sweden)

ABSTRACT

A chromatographic method for the determination of the enantiomeric purity of (*S*)-atropine is presented and has been applied to the analysis of tablets. The (2*S*,3*S*)-enantiomer of the chiral selector, dicyclohexyl tartrate, was used as selector in order to elute the impurity, (*R*)-atropine, before the main component, (*S*)-atropine.

INTRODUCTION

The enantioselective action of atropine was reported in 1904 by Cushny [1]. Later the anticholinergic activity of the two enantiomers was demonstrated in several papers, always with a higher potency for the (*S*)-enantiomer [also called (−)-hyoscyamine] [2]. Some of the drugs containing atropine marketed today contain the racemate, while others consist only of the (*S*)-enantiomer.

Methods are needed for monitoring the enantiomeric purity of (*S*)-atropine, and some reversed-phase chromatographic methods are now available for direct enantioselectivity analysis. Armstrong *et al.* [3] have achieved enantioselectivity using a β-cyclodextrin bonded phase for atropine and analogues. However, the separation factor (α) for atropine was not sufficient to obtain baseline resolution (α = 1.04). High selectivity (α = 3.42) was on the other hand reported using α₁-acid·glycoprotein as the chiral stationary phase [4]. The elution of the (*S*)-enantiomer before the (*R*)-form and the low capacity of the protein column make the method less suitable for the analysis of (*R*)-atropine as an impurity in (*S*)-atropine. A third approach is the use of an enantiomeric form [in ref. 5 the (2*R*,3*R*)-form] of dicyclohexyl tartrate (DCHT) as a mobile phase additive in reversed-phase chromatography

where the support is porous graphitic carbon (Hypercarb). The reproducibility of the method is good, which makes it suitable for routine analysis.

This study demonstrates how the retention order of the enantiomeric forms of a solute can be controlled by the choice of enantiomer of the selector (DCHT). This possibility can give particular advantages in the quantitation of enantiomeric impurities.

EXPERIMENTAL

Chemicals

Racemic atropine sulphate salt, (*S*)-atropine hemisulphate salt and tropic acid were obtained from Sigma (St. Louis, MO, USA). Homatropine and (−)-scopolamine bromide were purchased from Merck (Darmstadt, Germany). Tropine and (*R*)- and (*S*)-mandelic acid were bought from Fluka (Buchs, Switzerland). (1*R*,2*S*)-Norephedrine hydrochloride salt was from Serva (Heidelberg, Germany). (1*S*,2*R*)-Norephedrine hydrochloride salt and (*R*)- and (*S*)-phenyl-1,2-ethanediol were from Janssen (Beerse, Belgium); (*R*)- and (*S*)-ethyl mandelate were from Aldrich (Milwaukee, WI, USA). Belladonine, apoatropine and atropic acid were kind gifts from Astra (Södertälje, Sweden). (2*S*,3*S*)-DCHT was synthesized according to the procedure

previously described [6] for its optical enantiomer, (2R,3R)-DCHT, after exchanging (2R,3R)-tartaric acid for (2S,3S)-tartaric acid. $[\alpha]_D^{22} = -13.3$ ($c = 1.0$ g/100 ml, methanol).

Apparatus

The chromatographic system consisted of a Beckman 114 M pump (Fullerton, CA, USA), a Rheodyne 7120 injector (Berkeley, CA, USA) and a Spectromonitor 3100 detector (Milton Roy, Riviera Beach, CA, USA) connected to a Nelson 2600 chromatography data system (Nelson Analytical, Cupertino, CA, USA) via a Model 762 interface.

Two analytical Hypercarb columns (Shandon, UK) (100 mm × 4.7 mm I.D.) were coupled in series. The columns and solvent reservoir were kept at 25 ± 0.1°C with a Heto type 02 pt 923 TC water bath (Birkerød, Denmark).

Chromatographic technique

The columns were equilibrated with 500 ml of phosphate buffer pH 2.8 before introducing the mobile phase containing the chiral selector. The breakthrough curve for the selector was recorded at 195′ nm and was used to calculate the amount of selector adsorbed onto the support. The determination of atropine enantiomers was performed at 214 nm with a mobile phase consisting of 0.25 mM (2S,3S)-DCHT in phosphate buffer pH 2.8. The flow-rate was 0.4 ml/min and the mobile phase was not recirculated.

Calibration graph

A calibration graph was used for the analysis of the total concentration of atropine in the samples. Injection of racemic atropine gave two peaks of equal area, and the possibility that the (S)- and (R)-enantiomers, owing to interaction with the selector, would give a significant difference in UV absorbance could be excluded. Standard solutions of (S)-atropine (three different weighings) dissolved in the mobile phase in the concentration range $2 \cdot 10^{-7}$ to $5 \cdot 10^{-5}$ M were prepared. (The concentrations used were $2 \cdot 10^{-7}$, $5 \cdot 10^{-7}$, $1 \cdot 10^{-6}$, $5 \cdot 10^{-6}$, $1 \cdot 10^{-5}$, $2 \cdot 10^{-5}$, $3 \cdot 10^{-5}$ and $5 \cdot 10^{-5}$ M.) The areas of the chromatographic peaks were recorded by the Nelson 2600 system using a time constant of 6 s. The calibration graph was constructed by plotting the peak area *versus* the concentration of the standards.

The validity of the graph was checked regularly by injecting a standard solution of a concentration close to the samples.

Assay procedure

The same batch of commercially available (S)-atropine depot tablets, 0.2 mg, was stored for six years in glass bottles sealed with plastic lids, under three different conditions: 25°C; 30°C and 30% relative humidity; and 37°C.

The dissolution of tablets was performed as follows [7]. Ten tablets were dissolved in 25 ml of acetonitrile and put in an ultrasonic bath for 5 min. A 25-ml aliquot of phosphate buffer pH 2.8 was added to the solution and left for another 5 min in the ultrasonic bath. Phosphate buffer pH 2.8 was added to a total volume of about 200 ml. The liquid phase was filtered through a glass fibre filter (Whatman 934-AH) into a volumetric flask of 250 ml and phosphate buffer was added to volume. A 20-μl aliquot of the sample solution was injected into the chromatographic system.

RESULTS AND DISCUSSION

Control of the retention order

The detectability is improved by a low retention, and in studies of impurities the main component is often used in rather high concentrations which might give overloading effects, manifested as an increased tailing. The detectability of an impurity is as a rule improved if it is eluted before the main peak and not after, when the tailing of the main peak will make the definition of the baseline difficult.

The previously used [5] selector, (2R,3R)-DCHT, gave an elution of (S)-atropine before (R)-atropine. For the determination of (R)-atropine as an impurity, the retention order should be reversed. (2S,3S)-DCHT was thus used as chiral selector. Table I presents the retention order and capacity factor of some enantiomeric solutes using the two enantiomers of the selector.

Mobile phase

Besides racemization, (S)-atropine can be degradad by hydrolysis and dehydration. Dehydration gives apoatropine, which may be dimerized to belladonine. The products of hydrolysis are tropine, tropic acid and atropic acid [8].

TABLE I

CONFIGURATION OF DICYCLOHEXYL TARTRATE AND RETENTION ORDER OF SOLUTES

Mobile phase: 0.25 mM DCHT in phosphate buffer pH 2.8; amount of DCHT adsorbed: 0.132 mmol/g.

Solute	(2S,3S)-DCHT			(2R,3R)-DCHT		
		k'_1	α		k'_1	α
2-amino-1-[spiro- (cyclopentane- 1,1'-inden)- 3'-yl]ethanol		15.9	1.60		15.9	1.75
Norephedrine	(1S,2R)	0.24	1.18	(1R,2S)	0.13	1.22
Mandelic acid	(S)	1.67	1.08	(R)	2.60	1.08
Ethyl mandelate	(S)	5.27	1.12	(R)	6.13	1.13
1-Phenyl-1,2- ethanediol	(S)	1.51	1.07	(R)	1.43	1.08
Atropine	(R)	1.39	1.18	(S)	1.42	1.21

As the main aim was to study enantiomeric purity, chromatographic conditions under which the determination of (R)- and (S)-atropine is unaffected by the degradation products had to be found. Previous studies [5] with (2R,3R)-DCHT as selector have shown that the enantioselectivity of atropine is almost independent of pH in the interval pH 2–5, whereas an increase in retention is observed with increasing pH. The acids on the other hand showed a decreased retention with increasing pH. Therefore the analysis was performed at pH 3 to facilitate the separation of atropine from tropic acid. In Fig. 1a the resolution of ($-$)-scopolamine, racemic homatropine, racemic atropine and racemic tropic acid is demonstrated. Tropine does not absorb UV radiation at 214 nm and was not injected. A chromatogram of all solutes except atropine is presented in Fig. 1b. No peaks from apoatropine, atropic acid or belladonine could be detected within 2 h.

Precision in determination of enantiomeric purity

The standard solutions contained a total concentration of atropine enantiomers of about $2.5 \cdot 10^{-5}$ M. They were prepared from (S)-atropine spiked with racemic atropine to contain (R)-atropine in amounts corresponding to 1–10% of the total concentration. The chromatographic system could be used for over 200 injections, but there was a continuous increase in retention (and decrease in peak height), and thus the areas of the peaks were used for quantitation. The increase in capacity factor between the first injection and injection No. 200 was 37%, and as stated in ref. 5 this is probably due to hydrolysis of the selector, giving an acid which may act as a counterion. The precision of the determination of impurity in the range 1–10% is given in Table II. A calibration graph over the interval $2 \cdot 10^{-7}$ to $5 \cdot 10^{-5}$ M was used for the determination of the concentration in the main peak and in the impurity. The graph was linear ($y = 4 \cdot 10^{-8} + 1.829x$) with a correlation coefficient (r^2) of 0.999. As can be seen in Table II the precision of the determination im-
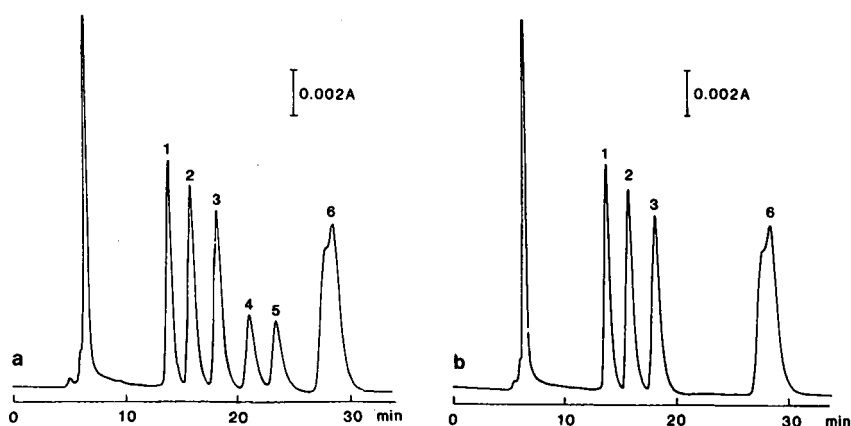

Fig. 1. Separation of atropine and analogues. For chromatographic conditions see Experimental section. (A) Solutes: 1 = ($-$)-scopolamine; 2 = (R)-homatropine; 3 = (S)-homatropine; 4 = (R)-atropine; 5 = (S)-atropine; 6 = racemic tropic acid. (B) Injection lacking atropine.

TABLE II

DETERMINATION OF ENANTIOMERIC PURITY

For chromatographic conditions see Experimental section. Samples: two different weighings of (S)-atropine and two of racemic atropine were used to prepare stock solutions. By mixing the stock solutions in different proportions, two series of samples were prepared. One of the series is marked with an asterisk in the table. The data were obtained on an intra-assay basis.

Proportion of (R)-atropine (%)			Number of injections
Added	Found	R.S.D.	
0.98*	0.92	4.3	5
1.11	1.00	9.5	15
2.00	1.95	5.3	6
2.83*	2.72	4.4	7
3.33	3.25	4.0	8
5.53	5.55	3.1	7
5.55*	5.35	1.5	8
9.99*	9.79	1.9	7
10.9	10.7	0.5	9

proved with increasing proportion of the impurity.

The total amount of atropine was determined by adding the areas for the main peak and the impurity. The total concentration of atropine found in the analysis was close to that expected (Table III).

In order to determine the minimum detectable concentration of (R)-atropine (after 200 injections), a standard curve was made for peak height *versus*

TABLE III

DETERMINATION OF TOTAL ATROPINE

For chromatographic conditions see Experimental section. For samples see Table II.

(R)-Atropine added (%)	Total concentration of atropine $\times 10^5$ (M)			Number of injections
	Added	Found	R.S.D. (%)	
0.98*	2.41	2.45	0.8	5
1.11	2.13	2.14	0.9	15
2.00	2.36	2.40	1.7	6
2.83*	2.51	2.52	0.7	7
3.33	2.13	2.16	0.9	8
5.53	2.14	2.15	2.8	7
5.55*	2.13	2.17	3.2	8
9.99*	2.36	2.36	0.4	7
10.9	2.17	2.23	1.8	9

concentration of (R)-atropine for six different concentrations in the interval 0.118–2.43 μM ($y = 8.6 + 3.1 \cdot 10^8 x$; $r^2 = 0.999$). The minimum detectable concentration, giving a peak height three times the baseline noise, was extrapolated to 59 nM, *i.e.* when injecting 20 μl of a 25 μM solution of atropine the presence of 0.3% (R)-atropine in (S)-atropine could be detected. It may be added that when checking the prepared stock solution of (S)-atropine no (R)-form could be detected.

Analysis of (S)-atropine in tablets

The racemization in commercially available depot tablets when stored under different conditions for six years was monitored. It can be concluded that the preparations are very optically stable during the storage conditions used. Compared with storage at 25°C, storage at 30°C and 30% relative humidity or at 37°C caused only a minor degree of racemization, though increasing significantly ($P = 0.01$) with increasing temperature (Table IV). The original ratio of the two enantiomers is unknown. An example from the analysis of tablets stored at 37°C is shown in Fig. 2.

TABLE IV

ENANTIOMERIC PURITY OF (S)-ATROPINE DEPOT TABLETS

For chromatographic conditions see Experimental section. For sample preparation see *Assay procedure*. The data were obtained on intra-assay basis.

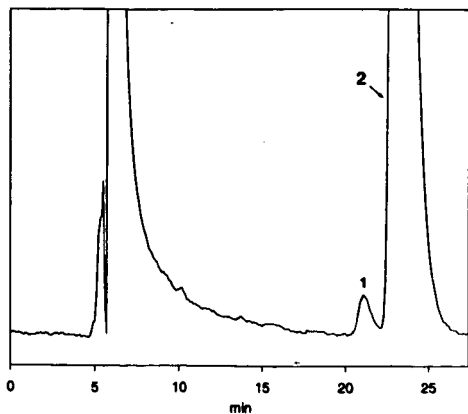| Storage temperature (°C)	Amount of atropine per tablet		(R)-Atropine		n
	mg	R.S.D. (%)	(%)	R.S.D. (%)	
25	0.201	2.5	0.46	15	8
25	0.201	1.5	0.51	5.9	5
25	0.187	0.5	0.44	11	4
30	0.202	1.0	1.08	14	9
30	0.198	2.5	0.99	14	9
30	0.183	1.6	0.95	23	6
37	0.197	1.0	1.52	8.6	11
37	0.190	1.6	1.40	17	7
37	0.190	1.6	1.61	17	6

Fig. 2. Enantiomeric impurity in (S)-atropine depot tablets stored at 37°C. For chromatographic conditions see Experimental section. Peaks: 1 = (R)-atropine, 1.5% of total concentration; 2 = (S)-atropine.

REFERENCES

1 A. R. Cushny, J. Physiol., 30 (1904) 176.
2 D. F. Smith (Editor), CRC Handbook of Stereoisomers: Drugs in Psychopharmacology, CRC Press, Boca Raton, FL, 1984, p. 53.
3 D. W. Armstrong, S. M. Han and Y. I. Han, Anal. Biochem., 167 (1987) 261.
4 E. Arvidsson, S.-O. Jansson and G. Schill, J. Chromatogr., 506 (1990) 579.
5 E. Heldin, N. H. Huynh and C. Pettersson, J. Chromatogr., 585 (1991) 35.
6 E. Heldin, K.-J. Lindner, C. Pettersson, W. Lindner and R. Rao, Chromatographia, 32 (1991) 407.
7 S.-O. Jansson, personal communication.
8 E. Bjerkelund, F. Gram and T. Waaler, Pharm. Acta Helv., 44 (1969) 745.

High-performance ligand-exchange chromatography of some amino acids containing two chiral centres

S. V. Galushko*, I. P. Shishkina and V. A. Soloshonok

Institute of Bioorganic Chemistry and Oil Chemistry, Academy of Sciences of the Ukraine, 253660 Kiev-94 (Ukraine)

ABSTRACT

The separation of 2S,3S-, 2R,3R-, 2S,3R- and 2R,3S-isomers of threonine, phenylserine and the *o*- and *p*-fluoro derivatives of the latter on chiral sorbents was studied. The sorbent ChiralProCu = Si100 gave a complete separation of the four isomers of the amino acids studied.

INTRODUCTION

High-performance ligand-exchange chromatography (HPLEC) is widely used to separate enantiomers of amino acids [1]. Sorbents containing residues of amino acids bonded to the surface of a silica matrix enable enantiomers of different amino acids to be separated [1,2]. Most papers, however, describe the separation of enantiomers that differ in the configuration of only one carbon atom. The separation of enantiomers of amino acids that contain two chiral centres is more complicated but highly desirable. Several methods for the synthesis of such amino acids have been developed [3–5] and the chromatographic separation of two pairs of enantiomers can be very useful for both analytical and preparative usage. The separation of a mixture of four enantiomers of isoleucine on a crown ether-based packing has been demonstrated, but only a very slight resolution of the *threo-* and *allo*-isomer pair was achieved [6]. The enantiomers of threonine were separated by reversed-phase high-performance liquid chromatography (HPLC) with a dynamic coating of a chiral crown ether but no separation of *allo*-threonine enantiomers was obtained [7].

The paper is intended to demonstrate the possibility of separating all four stereoisomers [(2S,3S)-L,L-, (2R,3R)-D,D-, (2R,3S)-D,L- and (2S,3R)-L,D-] of threonine, phenylserine and the *o*- and *p*-fluoro derivatives of the latter.

EXPERIMENTAL

Chromatographic conditions

The experiments were performed on an LKB (Bromma, Sweden) liquid chromatographic system consisting of a Model 2150 HPLC pump, a Model 7410 injector, a Model 2140 rapid spectral detector at 225 nm and a Model 2200 recording integrator. The column used were (1) ChiralProCu = Si100, (2) ChiralValCu = Si100, both 5 μm, 250 × 4.6 mm I.D. (Serva, Heidelberg, Germany), and (3) Nucleosil Chiral-1, 5 μm, 250 × 4.6 mm I.D. (Macherey–Nagel, Düren, Germany). The mobile phases were 1–5 mM copper sulphate solutions at a flow-rate of 0.75 ml/min.

Materials

Stereoisomers of fluorine-containing amino acids were obtained as described [8]. Natural amino acids (threonine and phenylserine) were supplied by Reakhim (Moscow, USSR) and Chemapol (Prague, Czechoslovakia). Copper sulphate (analytical-reagent grade) was used as received. Water was doubly distilled and filtered for HPLC use.

TABLE I

RETENTION (k') OF ISOMERS OF α-AMINO-β-HYDROXY ACIDS ON CHIRAL COLUMNS

Eluent: 5 mM CuSO$_4$.

Compound	2R,3R			2R,3S			2S,3R			2S,3S		
	1[a]	2[a]	3[a]	1	2	3	1	2	3	1	2	3
o-F-PhSer	1.5	1.5	1.6	1.7	1.8	0.9	3.4	2.7	0.85	8.3	4.1	0.9
p-F-PhSer	1.6	1.5	1.3	1.8	1.7	0.9	3.4	2.6	0.88	8.3	4.0	0.85
PhSer	1.4	1.6	1.5	1.6	2.0	1.1	3.4	2.5	1.05	8.6	4.0	1.1
Thr	0.7	0.7	[b]	0.8	0.9	[b]	1.4	1.1	[b]	2.3	1.3	[b]

[a] Columns 1, 2 and 3 as described under Experimental.
[b] The k' values are too low to be determined exactly.

RESULTS AND DISCUSSION

The amino acids studied are α-amino-β-hydroxy acids. They contain two chiral carbon atoms which can be in the S or R configuration:

R–CH–CH–COOH
  | |
 OH NH$_2$
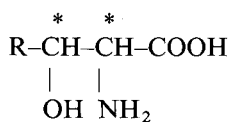
The 2S,3R (S-*threo*) configuration corresponds to natural phenylserine (R = C$_6$H$_5$) and threonine (R = CH$_3$). The configuration and the yield of the isomers of synthetic amino acids depend on the conditions of synthesis [3–5]. In the most complex case all four isomers are present simultaneously.

In searching for the optimum conditions for separation of the isomers, use was made of sorbents that contained residues of (S)-L-proline, (S)-L-hydroxyproline and (S)-L-valine bonded to the surface of the silica matrix.

The experiments showed that a proline column permits the complete separation of all isomers of the amino acids studied with the retention times increasing in the order 2R,3R < 2R,3S < 2S,3R < 2S,3S. It should be noted that the introduction of atoms of fluorine into the *ortho* and *para* positions of the phenyl ring has little effect on the capacity factors (k', Table I) and the selectivity of separation of isomers (Table II). The threonine isomers have much lower retentions than phenylserine isomers. Mobile phases containing 5 mM and 1.25–2.5 mM

TABLE II

SELECTIVITY OF SEPARATION OF α-AMINO-β-HYDROXY ACID ISOMERS ON CHIRAL COLUMNS

Eluent: 5 mM CuSO$_4$.

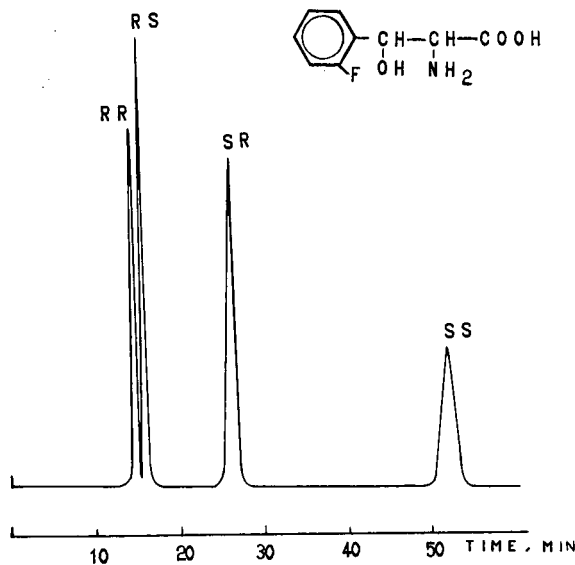| Isomer pairs being separated	o-F-PhSer			p-F-PhSer			PhSer			Thr	
	1[a]	2[a]	3[a]	1	2	3	1	2	3	1	2
$R,R/R,S$	1.1	1.2	1.8	1.1	1.1	1.4	1.1	1.2	1.4	1.1	1.3
$R,R/S,R$	2.3	1.8	1.9	2.1	1.7	1.5	2.4	1.7	1.4	2.0	1.6
$R,R/S,S$	5.5	2.7	1.8	5.2	2.7	1.6	6.1	2.5	1.4	3.2	1.8
$R,S/S,R$	2.0	1.5	1.1	1.9	1.5	1.0	2.1	1.3	1.0	1.8	1.2
$R,S/S,S$	4.9	2.3	1.0	4.6	2.3	1.0	5.3	1.9	1.0	2.9	1.4
$S,R/S,S$	2.4	1.5	1.1	2.4	1.5	1.0	2.5	1.6	1.0	1.6	1.2

[a] Columns 1, 2 and 3 as described under Experimental.

Fig. 1. Separation of isomers of o-fluorophenylserine. Column, ChiralProCu, 5 μm, 250 × 4.6 mm I.D.; eluent, 5 mM CuSO₄; flow-rate, 0.75 ml/min; temperature, 35°C; wavelength, 225 nm.

Fig. 3. Chromatogram of a threonine sample (Chemapol). Column, ChiralProCu, 5 μm, 250 × 4.6 mm I.D.; eluent, 1.5 mM CuSO₄; flow-rate, 0.75 ml/min; temperature, 35°C; wavelength, 225 nm. The order of elution is as in Fig. 2.

copper sulphate are optimum for the separation of isomers of phenylserine and threonine, respectively (Figs. 1–3).

The order of elution of the isomers studied on valine and proline columns is the same whereas the selectivity of the separation of enantiomers on the valine column is much less than that on the proline columns but nevertheless the separation of four
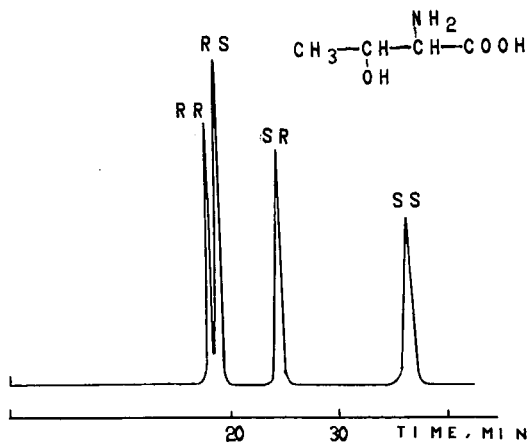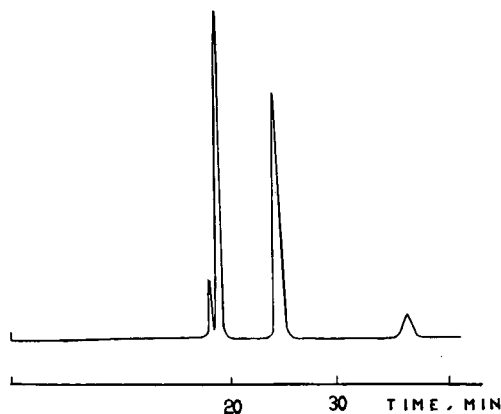
isomers of the aromatic acids can be achieved (Fig. 4). It should be noted that a high column performance is needed for the separation of $2R,3R/2R,3S$ pairs on both the proline and valine columns. It is also interesting that the decrease in the selectivity of separation of enantiomers on the valine column as compared with the proline column is the result of a decrease in retention mainly of the $2S,3R$ and $2S,3S$ isomers (Tables I and II). The optimum concentrations of copper sulphate in the eluent are 4–5 mM for

Fig. 2. Separation of isomers of threonine. Column, ChiralProCu, 5 μm, 250 × 4.6 mm I.D.; eluent, 2.5 mM CuSO₄; flow-rate, 0.75 ml/min; temperature, 35°C; wavelength, 225 nm.
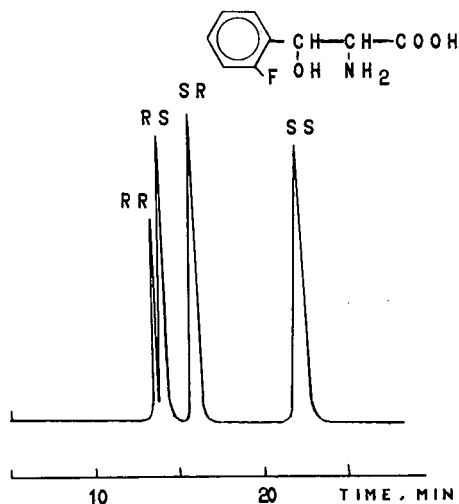

Fig. 4. Separation of isomers of o-fluorophenylserine. Column, ChiralValCu, 5 μm, 250 × 4.6 mm I.D.; eluent, 5 mM CuSO₄; flow-rate, 0.75 ml/min; temperature, 35°C; wavelength, 225 nm.

separation of isomers of phenylserine on the valine column. The retention and selectivity of the separation of threonine isomers on this column were not high enough for complete resolution to be obtained.

As can be seen from the results in Table I, the $3S$ isomers have the highest retention on the proline and valine sorbents. Moreover, if we consider the selectivity of separation of the $2R,3R/2R,3S$ and $2R, 3R/2S,3R$ and also the $2S,3S/2R,3S$ and $2S,3S/2S, 3R$ pairs (Table II), it can be seen that a change in the configuration of the α-carbon atom has a much greater effect on the selectivity of separation than that of the β-carbon atom. It can therefore be concluded that coordination interactions make a considerable contribution to the selectivity of separation of the isomers.

The order of elution and the selectivity of separation of enantiomers on the Nucleosil Chiral-1 hydroxyproline column are entirely different from those on the other two columns (Tables I and II). The capacity factors of isomers of aromatic amino acids increase in the order $2S,3R < 2S,3S = 2R, 3S < 2R,3R$. In this instance it is impossible to separate all four isomers. The selectivity of the separation of the pairs $2S,3R/2R,3S$ and $2S,3R/2S, 3S$ is not high, but the selectivity of the separation of the pair $2R,3S/2R,3R$ is higher than that on the proline and valine columns. The replacement of hydrogen in the phenyl ring with fluorine has a weak effect on the retention of enantiomers on the hydroxyproline column. The retention times and selectivity of separation threonine isomers on this column were insufficient to obtain the resolution needed.

It is concluded that ChiralProCu = Si100 is an excellent sorbent for the simultaneous separation of all four isomers of amino acids containing two chiral centres. ChiralValCu = Si100 has similar possibilities for the separation of isomers of aromatic α-amino-β-hydroxy acids. The Nucleosil Chiral-1 hydroxyproline column is to be preferred for the separation of the $2R,3R/2R,3S$ pair. It should be noted that the possibility of separating all four isomers of such amino acids with two chiral centres has other useful applications in addition to analytical and preparative usages. As the capacity factors for enantiomers on ChiralProCu differ greatly and are weakly dependent on substituents in the phenyl ring, HPLEC may be effective in establishing the absolute configuration of the molecules. In many instances this problem is difficult to solve and needs expensive instrumentation and much effort.

REFERENCES

1 V. A. Davankov, J. D. Navratil and H. F. Walton, *Ligand-Exchange Chromatography*, CRC Press, Boca Raton, FL, 1988.
2 G. Gubitz and W. Jellens, *J. Chromatogr.*, 203 (1981) 377.
3 Yu. N. Belokon, A. G. Bulychev, S. V. Vitt, Yu. T. Struchkov, A. S. Batsanov, T. V. Timofeeva, V. A. Tsyryapkin, M. G. Ryzhov, L. A. Lysova, V. I. Bakhmutov and V. M. Belikov, *J. Am. Chem. Soc.*, 107 (1985) 4252.
4 M. J. O'Donnell (Editor), *Synthesis of α-Amino Acids, Tetrahedron*, Symp. Vol. 44 N17 (1988).
5 D. Pons, M. Savignac and J. P. Genet, *Tetrahedron Lett.*, 31 (1990) 5023.
6 *Application Guide for Chiral Column Selection*, Daicel, Tokyo, Japan, 1989, p. 34.
7 T. Shinbo, T. Yamaguchi, K. Nishimura and N. Sugiura, *J. Chromatogr.*, 405 (1987) 145.
8 V. A. Soloshonok, V. P. Kukhar and S. V. Galushko, *Izv. Akad. Nauk. SSSR, Ser. Khim.*, N5 (1991) 1166 and N8 (1991) 1906.

PUBLICATION SCHEDULE FOR 1992

Journal of Chromatography and *Journal of Chromatography, Biomedical Applications*

MONTH	O 1991	N 1991	D 1991	J	F	M	
Journal of Chromatography	585/1	585/2 586/1 586/2 587/1	587/2 588/1 + 2	589/1 + 2 590/1 590/2	591/1 + 2 592/1 + 2 593/1 + 2	594/1 + 2 595/1	The publication schedule for further issues will be published later
Cumulative Indexes, Vols. 551–600							
Bibliography Section						610/1	
Biomedical Applications				573/1 573/2 574/1	574/2	575/1 575/2	

INFORMATION FOR AUTHORS

Types of Contributions. The following types of papers are published in the *Journal of Chromatography* and the section on *Biomedical Applications:* Regular research papers (Full-length papers), Review articles and Short Communications. Short Communications are usually descriptions of short investigations, or they can report minor technical improvements of previously published procedures; they reflect the same quality of research as Full-length papers, but should preferably not exceed five printed pages. For Review articles, see inside front cover under Submission of Papers.

Submission. Every paper must be accompanied by a letter from the senior author, stating that he/she is submitting the paper for publication in the *Journal of Chromatography*.

Manuscripts. Manuscripts should be typed in double spacing on consecutively numbered pages of uniform size. The manuscript should be preceded by a sheet of manuscript paper carrying the title of the paper and the name and full postal address of the person to whom the proofs are to be sent. As a rule, papers should be divided into sections, headed by a caption (*e.g.*, Abstract, Introduction, Experimental, Results, Discussion, etc.). All illustrations, photographs, tables, etc., should be on separate sheets.

Introduction. Every paper must have a concise introduction mentioning what has been done before on the topic described, and stating clearly what is new in the paper now submitted.

Abstract. All articles should have an abstract of 50–100 words which clearly and briefly indicates what is new, different and significant.

Illustrations. The figures should be submitted in a form suitable for reproduction, drawn in Indian ink on drawing or tracing paper. Each illustration should have a legend, all the *legends* being typed (with double spacing) together on a *separate sheet*. If structures are given in the text, the original drawings should be supplied. Coloured illustrations are reproduced at the author's expense, the cost being determined by the number of pages and by the number of colours needed. The written permission of the author and publisher must be obtained for the use of any figure already published. Its source must be indicated in the legend.

References. References should be numbered in the order in which they are cited in the text, and listed in numerical sequence on a separate sheet at the end of the article. Please check a recent issue for the layout of the reference list. Abbreviations for the titles of journals should follow the system used by *Chemical Abstracts*. Articles not yet published should be given as "in press" (journal should be specified), "submitted for publication" (journal should be specified), "in preparation" or "personal communication".

Dispatch. Before sending the manuscript to the Editor please check that the envelope contains four copies of the paper complete with references, legends and figures. One of the sets of figures must be the originals suitable for direct reproduction. Please also ensure that permission to publish has been obtained from your institute.

Proofs. One set of proofs will be sent to the author to be carefully checked for printer's errors. Corrections must be restricted to instances in which the proof is at variance with the manuscript. "Extra corrections" will be inserted at the author's expense.

Reprints. Fifty reprints of Full-length papers and Short Communications will be supplied free of charge. Additional reprints can be ordered by the authors. An order form containing price quotations will be sent to the authors together with the proofs of their article.
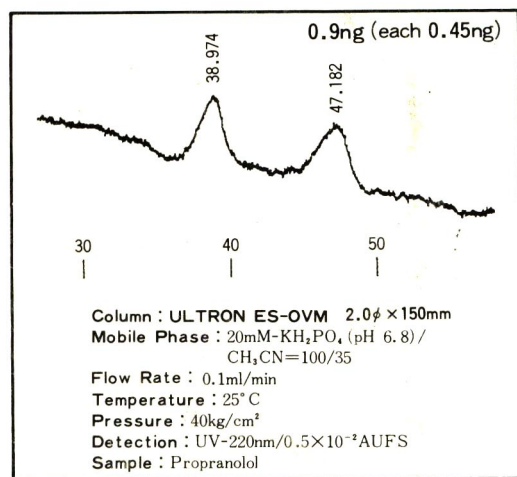
Advertisements. The Editors of the journal accept no responsibility for the contents of the advertisements. Advertisement rates are available on request. Advertising orders and enquiries can be sent to the Advertising Manager, Elsevier Science Publishers B.V., Advertising Department, P.O. Box 211, 1000 AE Amsterdam, Netherlands; courier shipments to: Van de Sande Bakhuyzenstraat 4, 1061 AG Amsterdam, Netherlands; Tel. (+31-20) 515 3220/515 3222, Telefax (+31-20) 6833 041, Telex 16479 els vi nl. *UK*: T. G. Scott & Son Ltd., Tim Blake, Portland House, 21 Narborough Road, Cosby, Leics. LE9 5TA, UK; Tel. (+44-533) 753 333, Telefax (+44-533) 750 522. *USA and Canada*: Weston Media Associates, Daniel S. Lipner, P.O. Box 1110, Greens Farms, CT 06436-1110, USA; Tel. (+1-203) 261 2500, Telefax (+1-203) 261 0101.

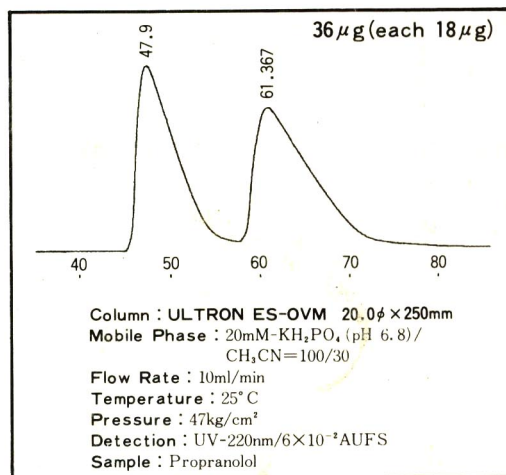# The most useful chiral separation column,

ULTRON ES-OVM, for enantiomeric drug

Substance	Rs	Substance	Rs	Substance	Rs
Acetylpheneturide	2.74	Disopyramid	2.04	Nisoldipine	2.36
Alimemazine	6.06	Eperisone	1.15	Nitrendipine	1.80
Alprenolol	1.09[1]	Ethiazide	1.42	Oxazepan	2.65[2]
Arotinolol	1.95	Fenoprofen	0.80	Oxprenolol	1.38
Bay K 8644	5.92	Flurbiprofen	1.27	Pindolol	2.04
Benproperine	3.27	Glutethimide	1.36	2-Phenylpropionic acid	0.80
Benzoin	8.41	Glycopyrronium	1.73	Pranoprofen	0.63
Biperiden	3.17	Hexobarbital	1.70	Prenylamine	0.86
Bunitrolol	3.08	Homochlorcyclizine	3.04	Profenamine	3.31
Bupivacaine	1.26	Hydroxyzine	2.15	Promethazine	1.42
Chlormezanone	6.48	Ibuprofen	1.72	Propranolol	1.24
Chlorphenesin	2.23	Ketoprofen	1.37	Terfenadine	2.22
Chlorpheniramine	2.36	Lorazepam	2.55[2]	Thioridazine	0.72
Chlorprenaline	2.34	Meclizine	3.71	Tolperisone	1.50
Cloperastin	2.85	Mepenzolate	1.40	Trihexyphenidyl	5.16
Dimethindene	4.33	Mephobarbital	1.70	Trimipramine	3.69
1,2-Diphenylethylamine	1.74	Methylphenidate	1.13[1]	Verapamil	1.4

NOTE: 4.6×150mm column at room temp. except[1] 6.0×150mm at room temp. and[2] 6.0×150mm at 10°C

From trace analysis for metabolites   **to preparative scale**

0.9ng (each 0.45ng)

38.974
47.182

30   40   50

Column : ULTRON ES-OVM 2.0φ×150mm
Mobile Phase : 20mM-KH₂PO₄ (pH 6.8)/
              CH₃CN=100/35
Flow Rate : 0.1ml/min
Temperature : 25°C
Pressure : 40kg/cm²
Detection : UV-220nm/0.5×10⁻²AUFS
Sample : Propranolol

36μg (each 18μg)

47.9
61.367

40   50   60   70   80

Column : ULTRON ES-OVM 20.0φ×250mm
Mobile Phase : 20mM-KH₂PO₄ (pH 6.8)/
              CH₃CN=100/30
Flow Rate : 10ml/min
Temperature : 25°C
Pressure : 47kg/cm²
Detection : UV-220nm/6×10⁻²AUFS
Sample : Propranolol

SHINWA CHEMICAL INDUSTRIES, LTD

50 Kagekatsu-cho, Fushimi-ku, Kyoto 612, JAPAN
Phone: 80-75-621-2360 Fax : 80-75-602-2660

Please contact in United States of America and Europe to :

Rockland Technologies, Inc. 538 First State Boulevard, Newport, DE 19804, U.S.A.
Phone : 302-633-5880, Fax : 302-633-5893

This product is licenced by Eisai Co., Ltd.